MOLECULAR MECHANISMS OF SENESCENCE RESPONSE TO TRANSFORMING GROWTH FACTOR-BETA IN LIVER CANCER

A THESIS SUBMITTED TO
THE DEPARTMENT OF MOLECULAR BIOLOGY AND GENETICS
AND THE INSTITUTE OF ENGINEERING AND SCIENCE OF
BILKENT UNIVERSITY
IN PARTIAL FULFILLMENT OF THE REQUIREMENTS FOR
THE DEGREE OF DOCTOR OF PHILOSOPHY

BY
ŞERİF ŞENTÜRK
AUGUST 2010

I certify that I have read this thesis and that in my opinion it is fully adequate, in scope and in quality, as a thesis for the degree of Doctor of Philosophy.

Prof. Dr. Mehmet Öztürk

I certify that I have read this thesis and that in my opinion it is fully adequate, in scope and in quality, as a thesis for the degree of Doctor of Philosophy.

Prof. Dr. Neşe Atabey

I certify that I have read this thesis and that in my opinion it is fully adequate, in scope and in quality, as a thesis for the degree of Doctor of Philosophy.

Prof. Dr. Nazmi Özer

I certify that I have read this thesis and that in my opinion it is fully adequate, in scope and in quality, as a thesis for the degree of Doctor of Philosophy.

Assoc. Prof. Dr. Işık Yuluğ

I certify that I have read this thesis and that in my opinion it is fully adequate, in scope and in quality, as a thesis for the degree of Doctor of Philosophy.

Assist. Prof. Dr. Uygar Tazebay

Approved for the Institute of Engineering and Science

Director of Institute of Engineering and Science
Prof. Dr. Levent Onural

ABSTRACT

MOLECULAR MECHANISMS OF SENESCENCE RESPONSE TO TRANSFORMING GROWTH FACTOR-BETA IN LIVER CANCER

Şerif Şentürk
Ph.D. in Molecular Biology and Genetics
Supervisor: Prof. Dr. Mehmet ÖZTÜRK
August 2010, 250 Pages

Hepatocellular carcinoma (HCC) is the fifth most common cancer in the world. HCC is associated with several etiological factors including infections with hepatitis B and C viruses, heavy alcohol consumption and chronic aflatoxin B1 exposure. Due to its multi-step disease hallmark characterized with genetic heterogeneity, liver cancer has very limited therapeutic options. In light of many previous findings, cellular senescence acts as a barrier against immortalization and prohibits the proliferation of premalignant cells in various tumors including HCCs. However, implications of this anti-tumor mechanism in hepatic tissues are not well-known.

TGF-β is a multifunctional cytokine implicated in diverse cellular processes including senescence arrest as well as liver physiology and pathophysiology. Although TGF-β-induced senescence has been described in different cell types, this issue has never been addressed for hepatic cells. According to our recent data, TGF-β1 expression pattern in various HCC malignancies closely correlated with reported frequencies of SABG activities in these corresponding disease stages. Therefore, we hypothesized that TGF-β signaling might play key role in hepatocellular senescence. Well-differentiated (WD) five cell lines characterized with epithelial-like morphology displayed TGF-β-induced growth inhibition associated with SABG activity, with lack of evidence of apoptosis induction. Even a brief exposure to TGF-β was sufficient to trigger a massive senescence response. Senescence arrest in WD cell lines was linked to c-myc down-regulation and a reciprocal increase in $p21^{Cip1}$

and $p15^{Ink4b}$ protein levels. In addition, TGF-β-induced senescence was correlated with Nox4 induction, intracellular accumulation of reactive oxygen species (ROS) and sustained 53BP1 foci formation as a mark of DNA-damage response. Moreover, intratumoral injection of TGF-β in human HCC tumors, generated subcutaneously in immunodeficient mice, induced expanded SABG that was associated with a strong anti-tumor response activity.

On the other hand, poorly differentiated (PD) HCC cell lines with mesenchymal-like characteristics appeared to be resistant to TGF−β-induced senescence. However, PD cell lines had intact TGF-β signaling from cell membrane to nucleus. Resistance of PD cell lines was partially due to zeb2 overexpression, homozygous $p15^{Ink4b}$ deletion and lack of pRb expression. Besides, PD cells did not display Nox4 upregulation and also lacked ROS accumulation upon TGF-β stimulation.

In addition, we demonstrated that sustained exposure to TGF-β established resistant Huh7 subclone. The resistance was partially attributed to deregulated Smad signaling, permanent epithelial-mesenchymal transition-like transformation. Surprisingly enough, removal of TGF-β from culture medium of continuously treated Huh7 subclone did not resolve the resistance phenotype in the rescued subclone. Epigenetic regulations mainly histone modifications are considered as candidate mechanisms responsible for irreversible TGF-β-resistance and maintenance of mesenchymal-like phenotype. Taken together, our results establish a close link between senescence arrest and anti-tumor activity of TGF-β signaling pathway in WD cell lines by delineating the mechanisms underlying TGF-β-induced growth arrest. Moreover, we propose partial explanation for the resistance to TGF-β-mediated growth arrest in PD cell lines and thoroughly signify the potential mechanisms of acquired resistance to TGF-β in continuously treated cultures. Further studies to enlighten our knowledge about implications of TGF-β signaling in less differentiated HCCs are necessary. As a conclusion, we identify TGF-β signaling as a potent therapeutic option for well-differentiated early HCCs.

ÖZET

KARACİĞER KANSERİNDE BAŞKALAŞTIRICI BÜYÜME ETMENİ-BETA'YA BAĞLI YAŞLANMA YANITININ MOLEKÜLER MEKANİZMALARI

Şerif Şentürk
Moleküler Biyoloji ve Genetik Doktorasi
Tez Yöneticisi: Prof. Dr. Mehmet Öztürk
Ağustos 2010, 250 Sayfa

Hepatoselüler kanser dünyada beşinci sıklıkta görülen kanser türüdür ve hepatit b ve c virüsü enfeksiyonlarına, yüksek alkol tüketimine ve aflatoksin b1'e maruz kalmak gibi etiyolojik faktörlere bağlı olarak gelişir. Genetik heterojenlik özelliği ile karakterize edilen karaciğer kanseri çok basamaklı bir hastalık olması özelliği ile de tedavi edici opsiyonlar bakımından sınırlıdır. Daha önce elde edilen bilgiler ışığında, hücre yaşlanmasının ölümsüzleşme karşıtı bir mekanizma olduğu ve bu yönüyle de karaciğer kanserleri de dahil olmak üzere birçok kanser türünde habis oluşuma engel olan bir bariyer olduğu düşünülmektedir. Ancak tümör karşıtı bu mekanizmanın karaciğer kanserindeki rolü tam olarak bilinmemektedir.

TGF-β çok yönlü bir sitokin olup, hücre yaşlanması ve karaciğer hastalıkları da dahil olmak üzere birçok hücresel işlemde rol aldığı belirtilmektedir. Daha önceleri, TGF-β'ya bağlı yaşlanma gözlemleri birçok hücre için belirtilmiş olduğu halde bu konu karaciğer hücreleri için çalışılmamıştır. Yeni elde ettiğimiz bulgulara göre, farklı karaciğer hastalık dokularında görülen TGF-β ifadesi, yine aynı dokularda tespit edilen hücre yaşlanması sıklığıyla benzerlik göstermektedir. Bundan yola çıkarak, TGF-β sitokininin karaciğer rahatsızlıklarında görülen yaşlanma ile ilintili olabileceğini düşündük. Epitel kökenli iyi diferansiye beş karaciğer kanseri hücre hattı TGF-β muamelesi ile birlikte yaşlanma belirtgeci için pozitif aktivite ile karakterize olan hücre bölünmesinde inhibisyon göstermiştir. TGF-β ile bir dakikadan daha az muamele bile çok belirgin bir yaşlanma yanıtı oluşturmak için

yeterli olmuştur. Iyi diferansiye hücrelerde görülen yaşlanma yanıtı c-myc düşüşü ve karşıt $p15^{Ink4b}$ ve $p21^{Cip1}$ protein artışı ile ilintilidir. Öte yandan TGF-β tarafından tetiklenen yaşlanma yanıtı Nox4 artışı, hücre içi reaktif oksijen türleri birikimi ve kalıcı dna hasarı yanıtı olarak nükleer 53BP1 odaklarının oluşmasıyla ilişkilidir. Dahası, deri altı tümörlerinde, tumor içi TGF-β enjeksiyonu çok belirgin yaşlanma yanıtı geliştirmiş ve bu yanıt tümör engelleyici sonuçlar doğurmuştur.

Diğer taraftan, mezenkimal kökenli kötü diferansiye hücre hatları TGF-β'ya bağlı yaşlanma yanıtına direnç göstermektedirler. Bu hücre hatlarında TGF-β sinyal yolağında herhangi bir sorun olmadığını tespit ettik. Direnç mekanizmasının kısmen zeb2 protein miktarındaki artışa, $p15^{Ink4b}$ delesyonuna ve pRb eksikliğine bağlı olduğu gösterildi. Bununla birlikte bu hücrelerde Nox4 artışı ve reaktif oksijen türlerinde birikimi gözlemleyemedik. Öte yandan Huh7 hücrelerini devamlı TGF-β muamelesine maruz bıraktığımızda dirençli klonlar elde ettik. Direnç mekanizmasının kısmen Smad yolağındaki bozukluklara ve kalıcı epitel-mezenkimal dönüşüme bağlı olduğu tespit edilmiştir.

İlginç olarak, devamlı muamele edilen dirençli klonları TGF-β'dan kurtarıp elde ettiğimiz ikincil klonda TGF-β yanıtının geri gelmediğini gözlemledik. Bu geri dönüşümsüz direnç mekanizmalarının temelinde olası epigenetik regülasyonların rol aldığıyla ilgili sonuçlar elde ettik.

Sonuç olarak, bu çalışmada elde edilen bulgular yaşlanma yanıtı oluşturan mekanizmalarla TGF-β'nın tümör karşıtı özelliği arasında yakın bir bağlantı kurmaktadır. Bundan başka, kötü diferansiye hücre hatlarındaki direnç için kısmi açıklama da getirmiş bulunuyoruz. Uzun dönem TGF-β muamelesi sonucunda oluşan direnç için de mekanizmalar üzerinde detaylı çalışmalar yürütmüş bulunuyoruz. Netice itibari ile, TGF-β sinyal yolağının iyi diferansiye karaciğer kanserlerinde tümör karşıtı tedavi edici özelliği konusunda önemli ipuçları sunuyoruz.

TO MY PARENTS GÜLTEN and İSMAİL ŞENTÜRK
And TO MY LOVELY SISTER ASLI ŞENTÜRK FOR THEIR ENDLESS LOVE and SUPPORT

AİLEME

ACKNOWLEDGEMENTS

It is of great pleasure for me to thank many people who have made this thesis possible.

First and foremost, I wish to express my greatest thanks to my thesis advisor and mentor Prof. Dr. Mehmet Öztürk for his invaluable supervision and guidance throughout this study. I am grateful for his endless patience, motivation, enthusiasm, inspiring comments and immense knowledge in molecular biology and encouragement for personal development in this research field.

I would like to thank the entire MBG faculty. I am grateful to Assoc. Prof. Rengül Çetin-Atalay, Assoc. Prof. Kamil Can Akçalı and Assoc. Prof. Uygar Tazebay for their efforts and help in providing me with experimental support and inspiration. It was always a great pleasure to work with Assoc. Prof. Işık Yuluğ, Assoc. Prof. Özlen Konu and Prof. Tayfun Özçelik in the same environment.

Many thanks will go to all the members of the Molecular Oncology Group, especially to Mine Mumcuoğlu, Gökhan Yıldız, Çiğdem Özen, Eylül Harputlugil, Mustafa Yılmaz and of course to Haluk and Özge Yüzügüllü who have always been so much more than just lab colleagues. Of course, many thanks to all the past members including Nuri Öztürk, Nilgün Taşdemir, Ayça Arslan-Ergül, Sevgi Bağışlar, M. Ender Avcı and Dr. Hani Alotaibi who are long gone but never forgotten. I have learned from them and shared a lot and most importantly had the chance to work together.

I would also like to thank all the members of the MBG lab, especially to Koray Doğan Kaya, İbrahim Fırat Taş and Tamer Kahraman, Tülin Erşahin, Ebru Bilget Güven for their friendship and support.

I was delighted to interact with Füsun Elvan, Sevim Baran, Abdullah Ünnü, Turan Daştandır, Bilge Kılıç, Burcu Cingöz, Emre Buğdaycı and Yavuz Ceylan during my research period at Bilkent University. I am indebted to them for their help in or outside the lab.

Last but not the least, my deepest gratitude goes to my family for their unconditional love and support throughout my life; I would like to dedicate this dissertation to them.

This work was supported by the KANILTEK project from State Planning Office, and partially by a grant from TUBITAK.

TABLE OF CONTENTS

LIST OF TABLES

LIST OF FIGURES

ABBREVIATIONS

ACTB	b-actin
AFB1	AflotoxinB1
AFP	Alpha-feto Protein
AI	Allelic Imbalance
Amp	Ampicillin
ALT	Alternative Mechanism of Telomere Lengthening
AP	Alkaline Phosphatase
APS	Ammonium Persulphate
ARF	Alternative Reading Frame
ASMA	Alpha-smooth Muscle Actin
BMP	Bone Morphogenetic Protein
bp	Base Pairs
BrdU	Bromodeoxyuridine
BSA	Bovine Serum Albumin
cDNA	Complementary DNA
C/EBP	CCAAT enhancer binding protein
CDK	Cyclin Dependent Kinase
CK19	Cytokeratin 19
Co-IP	Co-Immunoprecipitation
CO2	Carbon Dioxide
CRC	Colorectal Cancer
CSC	Cancer stem cell
Ct	Cycle Threshold
C-terminus	Carboxy Terminus
ddH2O	Double Distilled Water
DMEM	Dulbecco's Modified Eagle's Medium
DMSO	Dimethyl Sulphoxide

DNA	Deoxyribonucleic Acid
dNTP	Deoxyribonucleotide Triphosphate
ds	Double Strand
EDTA	Ethylenediaminetetraacetic Acid
EMT	Epithelial-Mesenchymal Transition
EtBr	Ethidium Bromide
FBS	Fetal Bovine Serum
g	Gram
GAPDH	Glyceraldehyde-3-phosphate Dehydrogenase
GSK3β	Glycogen Synthase Kinase 3-beta
HB	Hepatoblastoma
HBV	Hepatitis B Virus
HBX	Hepatitis B virus X protein
HBXAg	Hepatitis B virus X antigen
HCC	Hepatocellular Carcinoma
HCV	Hepatitis C Virus
HDAC	Histone Deacetylase
HGF	Hepatocyte Growth Factor
HRP	Horse Radish Peroxidase
HSC	Hepatic Stellate Cell
HT	Hypoxanthine-Thymidine
hTERT	human Telomerase Reverse Transcriptase
hTR	human telomerase RNA
I	Immortal
Ig	Immunoglobulin
i.p	Intraperitoneal
IP	Immunoprecipitation
i.t	Intratumoral
i.v	Intravenous
Kan	Kanamycin
Kb	Kilobase
kDa	kilo Dalton

LAP	Latent Associated Protein
LB	Luria-Bertani media
LCD	Large Cell-dysplasia
LOH	Loss of Heterozygosity
LTBP	Latent TGF-β Binding Protein
MAb	Monoclonal Antibody
MAPK	Mitogen Activated Protein Kinase
mg	Milligram
µg	Microgram
MgSO4	Magnesium Sulfate
Min	Minute
ml	Milliliter
mRNA	Messenger RNA
µl	Microliter
MQ	MilliQ Water
NaCl	Sodium Chloride
NADPH	Nicotinamide Adenine Dinucleotide Phosphate
NaF	Sodium Fluoride
NaOH	Sodium Hydroxide
Na3VO4	Sodium Ortho-vanadate
NEAA	Non-essential Amino Acid
ng	Nanogram
nm	Nanometer
nM	Nanomolar
N-terminus	Amino Terminus
NOD/SCID	Non-obese diabetic/severe combined
NOX	NADPH oxidase
O/N	Over Night
Oligo(dT)	Oligodeoxythymidylic Acid
OD	Optical Density
PAb	Polyclonal Antibody
PAGE	Polyacrylamide Gel Electrophoresis

PBS	Phosphate Buffered Saline
PBS-T	Phosphate Buffered Saline with Tween-20
PCR	Polymearase chain reaction
PD	Poorly-differentiated
PD	Population Doubling
PI-3 kinase	Phosphatidylinositol 3-kinase
PMSF	Phenylmethylsulphonylfluoride
pRb	Retinoblastoma Protein
qRT-PCR	Quantitative Reverse Transcription PCR
RE	Restriction Enzyme
RNA	Ribonucleic acid
ROS	Reactive Oxygen Species
rpm	Revolutions per Minute
RT-PCR	Reverse Transcription PCR
S	Senescent
s.c	Subcutaneous
S/N	Supernatant
SABG	Senescence Associated beta Galactosidase
SAP	Shrimp Alkaline Phosphatase
SCD	Small Cell-dysplasia
SDS	Sodium Dodecyl Sulfate
SDS-PAGE	SDS- Polyacrylamide Gel Electrophoresis
Sec	Second
shRNA	Short Hairpin RNA
SIP1	Smad Interacting Protein 1
siRNA	Small Interfering RNA
Smad	Homolog of Mothers against Decapentaplegic (MAD)
TAE	Tris-Acetate-EDTA Buffer
TBS	Tris Buffered Saline
TBS-T	Tris Buffered Saline with Tween-20
TEMED	N, N, N, N-tetramethyl-1, 2 diaminoethane
TGF-α	Transforming Growth Factor Alpha

TGF-β	Transforming Growth Factor Beta
Tm	Melting Temperature
TNF	Tumor Necrosis Factor
Tris	Tris (hydroxymethyl)-methylamine
UV	Ultraviolet
v/v	Volume/volume
w/v	Weight/volume
WD	Well-Differentiated
WIF-1	Wnt-inhibitory factor-1
X-Gal	5-bromo-4-chloro-3-indolyl-b-D-galactoside
ZFHX1B	Zinc finger homeobox 1B

CHAPTER 1. INTRODUCTION

1.1. Liver Homeostasis

Animals are in constant battle efforts with many different sources of danger, in order to reach to enough food sources to prevent dehydration, overheating and/or freezing, and to run away from a certain predator, and so forth. Therefore, to survive and reproduce in this hostile environment, animals have adapted well-organized behaviors and evolutionized bodily features.

For survival, animal kingdom has to maintain critical parameters within a certain range. For instance, a certain animal must regulate its body temperature, energy levels and amount of fluids. Maintenance of these critical parameters necessitates that the animal might come into direct or indirect contact with the corresponding satisfactory stimulus. In a simplified manner, each stimulus can be viewed as a native specified requirement. The physiological mechanisms which work for the regulation of these requirements are extremely complex and distinct. Such physiological mechanisms are entirely carried out in the body of the animals. Cells situated at different target organs of the entire body, work for their best to regulate body temperature, glucose levels, and bodily fluids at optimum survival levels.

Maintenance of such a constant environment in the body is referred to as homeostasis. Homeostatic regulation is referred to the process of maintaining critical parameters regulated by certain cell types. All animals have a sustained body temperature that is 37^0C for humans which is absolutely constant in hot or cold environments. Animals also have to maintain a certain range of glucose levels. Humans have an exact level of glucose in the blood necessitated by the cells. In

addition, water levels in the body are controlled to maintain the necessary amount of the water in the body.

Such maintenance of homeostasis under constant composition of the fluids, glucose and body temperature is under the control of different body systems. Each system is composed of different organs and each organ has its own contribution in maintaining the body homeostasis.

Liver is one of the most important organs safeguarding the maintenance of homeostasis. Liver is the largest internal organ weighing 1.5 kg in the human body and is present in vertebrates and some other animals. It fills the upper right costal margin of the human abdomen just beneath the rib cage. The main liver functions involve metabolism, excretion, secretion, interconversion, synthesis, storage and body defense (Fan et al., 2009; Francini et al., 2009; Jourdan et al., 2009).

Hepatocytes are the functional cells of the liver and consist of almost over 90% of the total liver mass. Ito cells, also known as hepatic stellate cells, are unique to this organ. Kupffer cells are macrophages specified to function in the liver. Bile duct cells occupy approximately 5% of the total cell population in the liver (Fan et al., 2009).

Liver receives all exiting circulation from the small and the large intestine, as well as spleen and pancreas, through the portal vein. In addition, the strategic location of liver allows it to function as a biochemical defense mechanism against toxic chemicals entering the body through food ingredients. Nutrients which enter the liver are generally converted into secreted proteins namely, albumin, coagulation and plasma carrier proteins, lipids which are sent as lipoproteins to other tissues, and carbohydrates that are stored in the liver as glycogen. Liver is the major regulator of plasma glucose levels therefore, is essential for optimal function of the whole body.

The functions performed by liver towards the rest of the body have been devoted by evolutionary events which attributed to liver with an incredible capacity to regenerate. Liver is an interesting organ with high regenerative capacity (Chu and Sadler, 2009; Mishra et al., 2009; Sawitza et al., 2009). This process allows liver to

recover lost mass without disturbing functionality of the entire body. The capacity of liver regeneration following loss of liver mass is quite similar in all vertebrate organisms, from humans to fish. Regeneration is also stimulated when livers from small animals (e.g., dogs) are transplanted to large recipients of the same species.

Liver homeostasis is lost in many different conditions among which are various sources of pathological conditions as briefly described in the following sentences;

- Wilson's disease is a hereditary disorder in which the liver to detain copper (Schilsky, 2009).
- Haemochromatosis is a hereditary disorder which leads to the accumulation of iron in the liver and thereby causes hepatocyte damage (Janssen and Swinkels, 2009).
- Hepatitis is characterized with by inflammation of the liver by various viral infections but also by several poisons, autoimmunity or genetic conditions (Iadonato and Katze, 2009).
- Cirrhosis replaces dead liver cells through the formation of fibrous scar tissue. Such pathological conditions are typically caused by viral hepatitis, alcohol consumption or contact with carcinogenic chemicals (Cavazza et al., 2009; Hirschfield and Siminovitch, 2009).
- Primary sclerosing cholangitis is characterized by inflammation of the bile duct which makes this disease likely to be autoimmune (Tischendorf and Schirin-Sokhan, 2009).
- Primary biliary cirrhosis is associated with autoimmunity of bile ducts (Lindor et al., 2009).

1.2. Hepatocellular Carcinoma

Liver cancer is comprised of various primary hepatic neoplasms including hepatocellular carcinoma (HCC), intrahepatic bile duct carcinoma (cholangiocarcinoma), hepatoblastoma, haemangiosarcoma (Di Bisceglie, 2009; Dufour and Johnson; Kirk et al., 2006). Among these, HCC is the most common type of liver neoplasms, representing 83% of all cases (Hernandez-Alcoceba et al., 2007; Hoffmann et al., 2007). It is also the 3rd most lethal cancer with lack of biomarkers and potentially curative treatment options, affects many of the world's populations (Farazi and DePinho, 2006) with more than 600,000 annual deaths (Bruix and Llovet, 2009; Minguez et al., 2009) and continues to increase in incidence rate in several regions of the world and is associated with poor overall survival. Hepatocellular carcinoma is usually diagnosed at late stages of the disease characterized with heterogeneous phenotypic and genetic malformations of patients with poor prognosis. Therefore, hepatocellular carcinoma has been classified as a heterogeneous disease.

1.3 Pathogenesis of Hepatocellular Carcinoma

Hepatocellular carcinoma has different epidemiologic features including dynamic and well-documented variations among geographic regions and between men and women (El-Serag and Rudolph, 2007). Various host and environmental factors interact at molecular level to cause hepatocyte damage that is accompanied with hepatocyte proliferation. Continuous rounds of hepatocyte regeneration develops into pathological liver diseases from normal liver through fibrosis to chronic hepatitis/cirrhosis and dysplastic nodules to HCC (Azam and Koulaouzidis, 2008; Bartosch et al., 2009; Schlaeger et al., 2008). The progression of HCC, however, is not well-defined as other cancer types (Figure 1.1).

Liver fibrosis is a condition in which the liver gradually deteriorates and malfunctions due to chronic hepatocyte injury, stellate cell activation and collagen deposition. Scar tissue surrounded by collagen deposition replaces healthy liver

tissue, partially blocking the flow of blood throughout the liver and manifesting hepatocyte loss associated with apoptotic cell death (Cavazza et al., 2009).

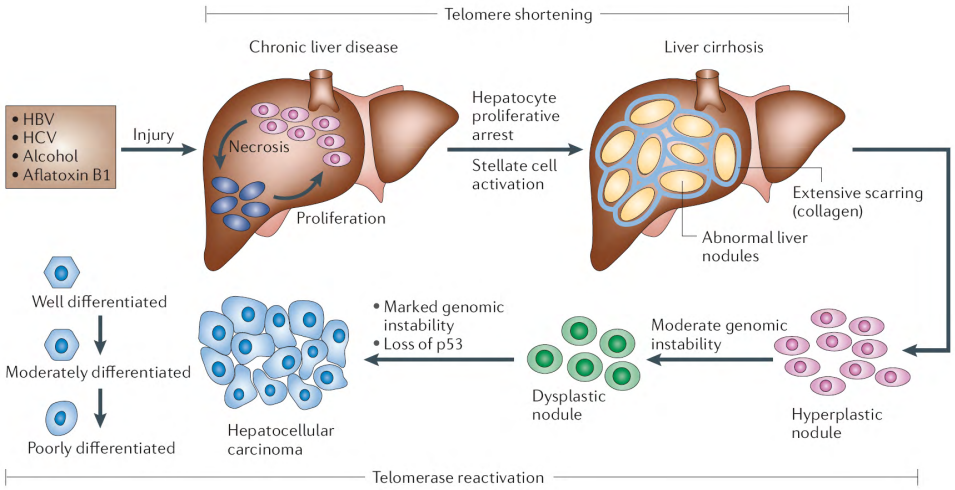

Figure 1.1: Molecular pathogenesis of hepatocellular carcinoma. Hepatocyte injury is provoked by several factors incuding HBV and HCV infections, heavy alcohol consumption and aflatoxin B1 contamination. Necrosis, apoptosis and replicative senescence are major cellular mechanisms followed by hepatocyte damage (Farazi and DePinho, 2006).

Liver cirrhosis is one of the most important pathological conditions that lead to hepatocarcinogenesis. Cirrhosis is strongly characterized by increased chromosomal aberrations, gene mutations, allelic losses, epigenetic alterations and deregulations in various signaling pathways. Some of these alterations are accompanied by a stepwise increase in different pathological disease stages during hepatocarcinogenesis. Abnormal liver nodules observed in cirrhotic livers often develop into precancerous hyperplastic nodules with moderate genomic instability. The distinction between precancerous and cancerous lesions remains elusive, and the developmental process with clear evidence of molecular pathogenesis from preneoplastic lesions to manifest HCC is still not well-known.

Nonetheless, what is known so far is that pre-neoplastic nodules that are in an intermediate stage between non-neoplastic regenerating nodules and HCC evolve into dysplastic nodules with high regeneration capacity. HCC usually develops on the background of dysplastic nodules with genomic instability, telomerase

reactivation and loss of p53 function characterized by hotspot mutations and micro-deletions (Gouas et al., 2010). Moreover, HCC can be classified into three distinct histological groups which are generally defined as well-differentiated (WD), moderately differentiated (MD), poorly differentiated (PD) or undifferentiated types of HCC (Nam et al., 2005).

1.3.1. Viral Hepatocarcinogenesis

Hepatocarcinogenesis in humans has various aetiologies. Heavy alcohol consumption and chronic infections with HBV and HCV, as well as naturally occurring aflatoxins and hereditary disorders have been the most common causes of chronic liver diseases (Fung et al., 2009; Kuniholm et al., 2008; Marcellin, 2009). Cirrhosis usually precedes the multistep tumor development, in which viral carcinogenesis can be identified (Raoul, 2008).

HCC evolves during a process that usually takes more than 30 years after infections with HBV and HCV. Such chronic infections provoke active immune response activation followed by inflammation and fibrosis, which progresses to cirrhosis and ultimately unfold into HCC (Thorgeirsson and Grisham, 2002). The incidence rate of hepatocellular carcinoma is usually correlated with the incidence rate of chronic hepatitis B virus infection. For chronic hepatitis B carriers who were characterized by high serum HBsAg, the HCC risk has been estimated to be up to 40-50% (Marcellin, 2009).

Although both viruses cause hepatotropic infections; there are significant differences in their oncogenic mechanisms. HBV belongs to the Hepadnavirus family and has an estimated number of 350 million human infections in the world (Zuckerman, 1999). Viruses in this family have very small (approximately 3200 kb) and partially double-stranded relaxed DNA molecule with two uneven strands consisting of a full length of negative strand and a shorter positive strand. Viruses in this family replicate through an RNA intermediate, which they translate back into DNA using reverse transcriptase. Most common clinical course of infection, on the

other hand, is vertical transmission meaning that from mother to neonate which is followed by childhood infection (Rehermann and Nascimbeni, 2005). HBV genomic integration has been demonstrated in many cases that is not solely restricted to transformed hepatocytes but normal hepatocytes in non-tumor tissues also carry HBV genome after chronic infections (Tsai and Chung, 2010). Integration of HBV genome into human genomic DNA has various effects such as; genomic instability associated with chromosomal abnormalities as deletions and translocations, amplification of cellular DNA and alterations in the expression patterns of various oncogenes, tumor suppressor genes and miRNAs (Feitelson and Lee, 2007)(Figure 1.2).

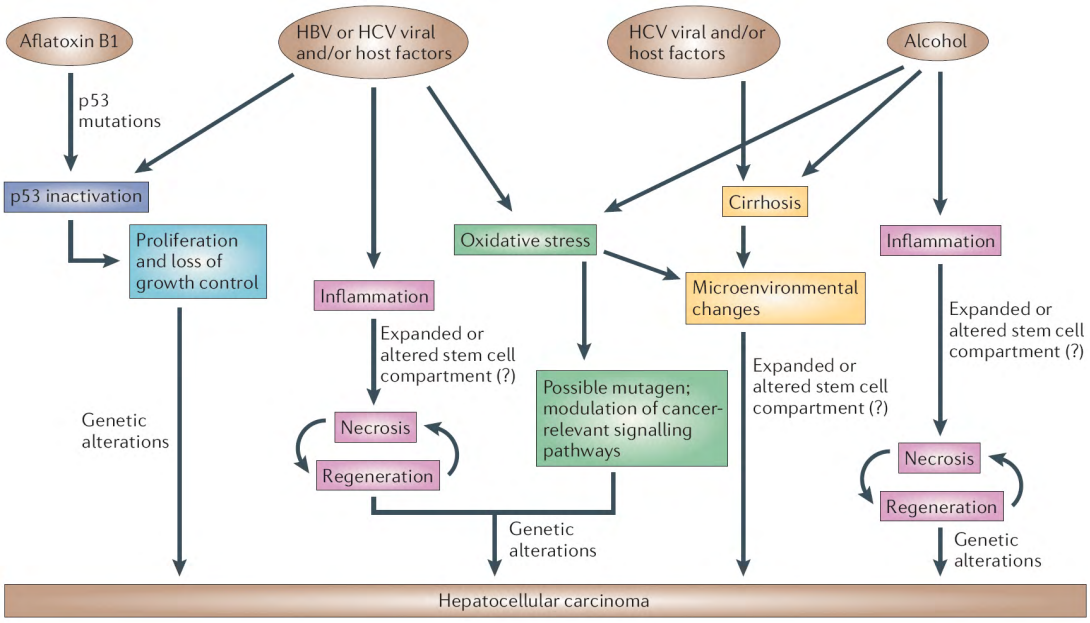

Figure 1.2: Molecular mechanisms of liver cancer development (Farazi and DePinho, 2006).

A large proportion of HCC cases with HBV genome integration have HBV X (HBx) protein expression which affects various cellular processes and functions of molecular signaling pathways (Figure 1.3). HBx physically binds to and inactivates

the wild-type p53 tumor suppressor protein as well as proteasome subunits and UV-damaged DNA binding proteins (Zhang et al., 2006b).

Furthermore, HBx protein has been implicated in activation of NF-kB and TGF-β signaling. Together with that, sevaral growth regulatory genes including c-myc and EGF were associated with HBV infection and HBx protein (Brechot et al., 2000).

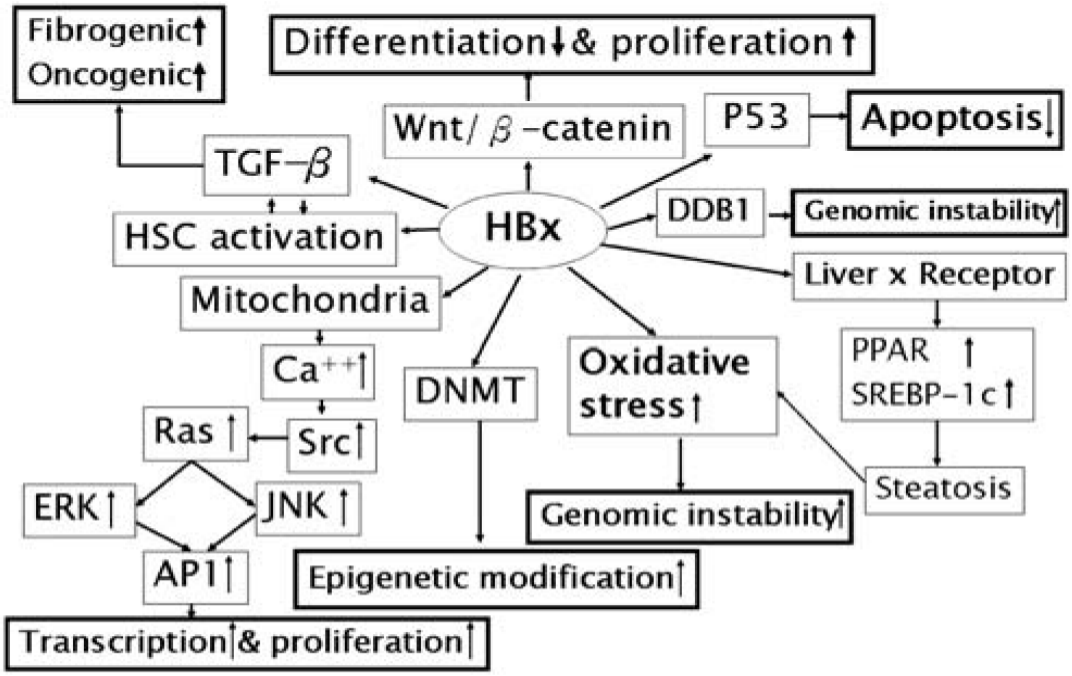

Figure 1.3: Cellular signaling pathways impicated in HBV X related hepatocarcinogenesis (Tsai and Chung, 2010).

HCV, on the other hand, is classified in Flaviviridae family with more than 170 million infections reported by World Health Organization. Notably, patients with the background of persistent HCV infection usually develop liver cirrhosis in approximately 30 years. In addition, HCV is an enveloped, single stranded, positive sense RNA virus which consists of a 10-kb genome that contains a large open reading frame encoding several structural proteins as core protein, envelope protein 1

and 2, p7 and non-structural proteins NS2, -3, -4A, -4B, -5A, -5B (Lindenbach et al., 2005). In contrast to HBV, HCV does not enter the nucleus of host cells. Instead, RNA genome of HCV functions in the cytoplasm of the infected cell. HCV core protein interacts with many intracellular proteins including p53, p73 and pRb and thus affects diverse range of functions in the cell (Majumder et al., 2001; Ray et al., 1997).

1.3.2. Alcohol-induced Hepatocarcinogenesis

Chronic heavy alcohol consumption is closely associated with hepatocarcinogenesis. Numerous studies established a causal link between high incidence rate of HCC and alcohol abuse (Hassan et al., 2002; Horie et al., 2003; Kew, 1986). However, the exact contribution of alcohol abuse to liver cancer compared to HBV and HCV infections is still not well-defined largely due to the contribution of other risk factors that can affect the systemic and intrahepatic effects of alcohol. Persistent exposure of the liver to alcohol elicits hepatocyte hyper regeneration due to activation of several survival factors, interference with hepatic metabolisms and direct DNA damage mostly associated with increased production of intracellular reactive oxygen species (Gao et al., 2004; Wu and Cederbaum, 2003; Wu et al., 2006). Furthermore, alcohol-induced hepatocellular injury can lead to fibrosis and finally cirrhosis, the latter being per se associated with an increasing risk of HCC development.

1.3.3. Aflatoxin-induced Hepatocarcinogenesis

Aflatoxin B1 is one of the most potent naturally occurring hepatocarcinogens, and a metabolic byproduct, mycotoxin of fungi, *Aspergillus Flavus* and *Aspergillus Parasiticus*. Aflatoxin B1 can contaminate the food supply such as rice, nuts, spices, corns at any time during production, processing, transport and storage (Picco et al., 1999). Data on aflatoxin exposure by contamination of food correlates well with

incidence rates in Africa and to some extent in China. Chronic exposure of the liver to aflatoxins is associated with a specific AGG to AGT transversion mutation at codon 249 of the p53 gene specifically in human HCC, providing mechanistic support to a causal link between exposure and liver disease (Bressac et al., 1991; Puisieux et al., 1991).

1.3.4. Other Aetiological Factors Associated With HCC

In addition to most common factors associated with HCC, other factors have been proposed to play role in liver cancer development with a lower frequency. Several common conditions or diseases were associated with high risk of developing HCC. Those include inherited genetic diseases antitrypsin deficiency, glycogen storage disease, heamochromatosis and hereditary tyrosinemia type. Several other diseases were also implicated in increased risk of hepatocarcinoma development. Hereditary heamochromatosis is a common genetic disorder that is associated with increased iron absorption by hepatocytes which then hasten hepatocellular damage (Pietrangelo, 2009). Alpha1-antitrypsin deficiency (AATD) is an autosomal co-dominantly inherited disease which affects about 1 in 2000 to 5000 people. AATD affects the liver predominantly through appearance of increased antitrypsin polymers in hepatocytes provoking hepatocyte death and cirrhosis (Kaplan and Cosentino; Parfrey et al., 2003).

HCC has also been described in patients with obesity and diabetes with no previous history of liver disease associated with other risk factors (Chuang et al., 2009; Polesel et al., 2009). This predisposition has been well-correlated with insulin resistance and elevated free fatty acid production in the liver (Maclaren et al., 2007; Ooi et al., 2005). Lipid accumulation in the liver can subsequently provoke hepatocyte damage mostly characterized by apoptosis, senescence and cytokine production, and reactive oxygen species generation due to high rates of oxidation of fatty acids and ultimately the development of fibrosis (Farrell and Larter, 2006).

1.4. Genetics of Hepatocellular Carcinoma

Human cancers arise as a result of genetic changes that impact on cell proliferation through diverse mechanisms. Cancers, in addition, are usually associated with the presence and accumulation of genetic alterations which mainly target various chromosomal locations. Tumor development usually takes long periods which indicates that different genetic variations may be necessary to evolve the malignant transformation (Fearon and Vogelstein, 1990). It is believed that hepatocarcinogenesis shares this common molecular pathogenesis as other solid tumors. HCC has been extensively studied in terms of genetic abnormalities.

Hepatocarcinogenesis involves complex combinations of molecular events, such as genetic aberrations, epigenetic changes and altered gene expression profiles. Hepatocellular cancers display many chromosomal changes such as polyploidy, loss of heterozygosity (LOH), allelic imbalance (AI), amplifications as well as translocations. Likewise in other solid tumors, a large number of genetic variations such as activating mutations of proto-oncogenes as well as inactivating mutations of many tumor suppressor genes have been reported to accumulate during the course of hepatocarcinogenesis.

After the development of Comperative Genomic Hybridization (CGH), Restriction Fragment Length Polymorphism (RFLP) and Micro Satellite Analysis (MSA) techniques along with new publicly available genomic data obtained with the efforts of the Human Genome Project, important molecular pathways involved in hepatocellular carcinoma, and several chromosomal and genetic aberrations have been identified to be altered during the carcinogenic process.

1.4.1. Genetic Aberrations in Hepatocellular Carcinoma

Chromosomal aberrations are alterations in chromosome structure and morphology and have been reported frequently in HCC (Kishnani et al., 2009; Midorikawa et al., 2009). Common chromosomal copy number losses associated

with HCC are 1p, 2q, 4q, 6q, 8p, 9p, 10q, 13q, 16p, 16q and 17p (Chochi et al., 2009). These chromosomal regions contain key players in hepatocarcinogenesis such as TP53, RB1 (retinoblastoma 1), AXIN1 (axis inhibition protein 1), CDKN2A (cyclin-dependent kinase inhibitor 2A). Originally identified as an oncogene TP53, the most frequently altered gene in human cancers, is located at 17p, a common site for deletion (Hanahan and Weinberg, 2000; Hollstein et al., 1991).

The frequency of p53 mutations, mostly associated with Aflatoxin B1 ingestion in HCC, has been reported to be around 30% worldwide (Bressac et al., 1991). Strong correlation between p53 mutations and large tumor size as well as poor differentiation state has been reported (Qin et al., 1997). The retinoblastoma protein is the universal inhibitor of the cell cycle progression and a gatekeeper at G1 phase (Nevins, 2001). The Rb gene is localized to 13q, which is a common LOH site for different cancer types including HCCs. In addition, inactivating RB1 mutations were observed with more than 15% reported frequency (Ozturk, 1999).

Cyclin-dependent kinase inhibitors have been reported to be inactivated in many cancers including HCC. Two closely located cdk-inhibitor genes at chromosome 9p, CDKN2A and CDKN2B, display genomic alterations such homozygous deletions. Expression patterns of these genes are also modulated through *de novo* methylation. Recently, β-catenin gene has been identified as one of the most frequently mutated genes in both hepatocellular carcinomas and hepatoblastomas. Both missense mutations and in-frame deletions affect the function of this gene product thereby deregulating Wnt signaling (Yam et al., 2010). Common amplifications, on the other hand, have been reported to be mainly located on 1q, 7q, 8q and 17q (Midorikawa et al., 2009). These regions are likely to harbor genes that are implicated in tumor progression. In many cases, amplification of myc and cyclin genes have been reported (Ozturk, 1999).

1.5. Liver Cirrhosis and senescence

Liver cirrhosis is a well-defined pathological condition characterized by abnormal liver nodule generation and widespread fibrous scarring induced by many intrinsic and extrinsic factors such as viral hepatitis, heavy alcohol consumption, prolonged biliary obstruction, genetically transmitted disorders, and others. Independent of its etiology, cirrhosis is considered a major clinical and histopathological risk factor for hepatocarcinogenesis. Regenerative nodules are characteristic complications of liver cirrhosis. Such lesions lack bile ducts and exhibit poorly organized hepatocytes surrounded by fibrotic tissue.

Chronic liver diseases are associated with progressive telomere shortening during excessive proliferation of hepatocytes. Hepatocyte telomeres undergo shortening during progression of chronic liver diseases which is accompanied by decline of hepatocyte proliferation. Hepatocyte telomere shortening and senescence are general markers of human liver cirrhosis, and correlate with progression of fibrosis in cirrhosis samples (Wiemann et al., 2002).

Telomere shortening in cirrhosis has been demonstrated to be hepatocyte specific, although stellate cells have been reported to undergo senescence arrest *in vivo* as well (Krizhanovsky et al., 2008).

1.5.1. Cellular senescence

Most of the primary cells have a limited number of population doublings as proposed by Hayflick and Moorhead that when normal human fibroblast cells are explanted from embryonic tissues into culture they have limited capacity to proliferate (Hayflick and Moorhead, 1961). Such cells, after around 50 to 70 population doublings are irreversibly arrested in G1 phase of the cell cycle and become unresponsive to proliferative mitogenic stimuli (Harley et al., 1990).

Cellular senescence is a condition in which cells, despite being alive, are unable to proliferate further. Cellular senescence is a stable proliferative arrest in

response to diverse intrinsic and extrinsic factors such as dysfunctional telomeres, DNA damage, oncogenic signaling such activated Ras or Raf, and lack of growth stimulating signals and disrupted chromatin and therefore it is different from quiescence or terminal differentiation (Serrano et al., 1997)(Figure 1.4).

Upon entering senescence, cells undergo dramatic changes. Such cells acquire large volume, flattened cytoplasm morphology accompanied by changes in nuclear structure, gene expression, protein processing and metabolism and senescence associated β-galactosidase activity (Campisi, 2000; Dimri et al., 1995; Narita et al., 2003).

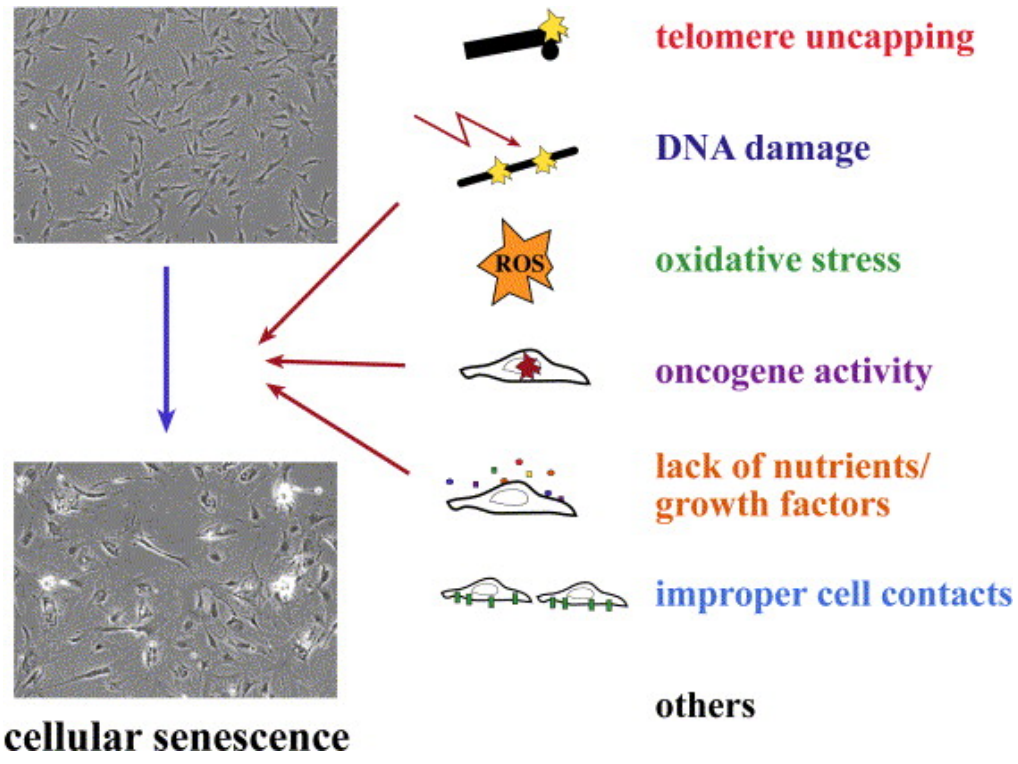

Figure 1.4: Various signals that provoke cellular senescence (Ben-Porath and Weinberg, 2005).

1.5.2. Replicative senescence

Human chromosome telomere ends are special structures composed of stretches of repetitive tandem hexameric units-TTAGGG in vertebrates and associated telomeric proteins that cap the ends of linear chromosomes. The length of human telomeres range from a few kilobases to 10–15 kbs. Telomere specific proteins protect chromosome from degradation or chromosomal end-to-end fusion during DNA-repair process (Reaper et al., 2004).

In the absence of maintenance mechanism, progressive erosion of telomeres at each replicative round limits the continuous replication. During every S-phase, due to the end-replication problem of DNA polymerase, telomeres shorten during each DNA replication cycle by 50-100 base pairs (bp).

In summary, when the length of one or more telomeres gets below a certain threshold, usually characterized with the single-strand overhang erosion, the exposed telomeric DNA ends are recognized as double-strand breaks (DSBs) by the DNA damage response (DDR) mechanism to release a senescence inducing signal to the cell (Figure 1.5).

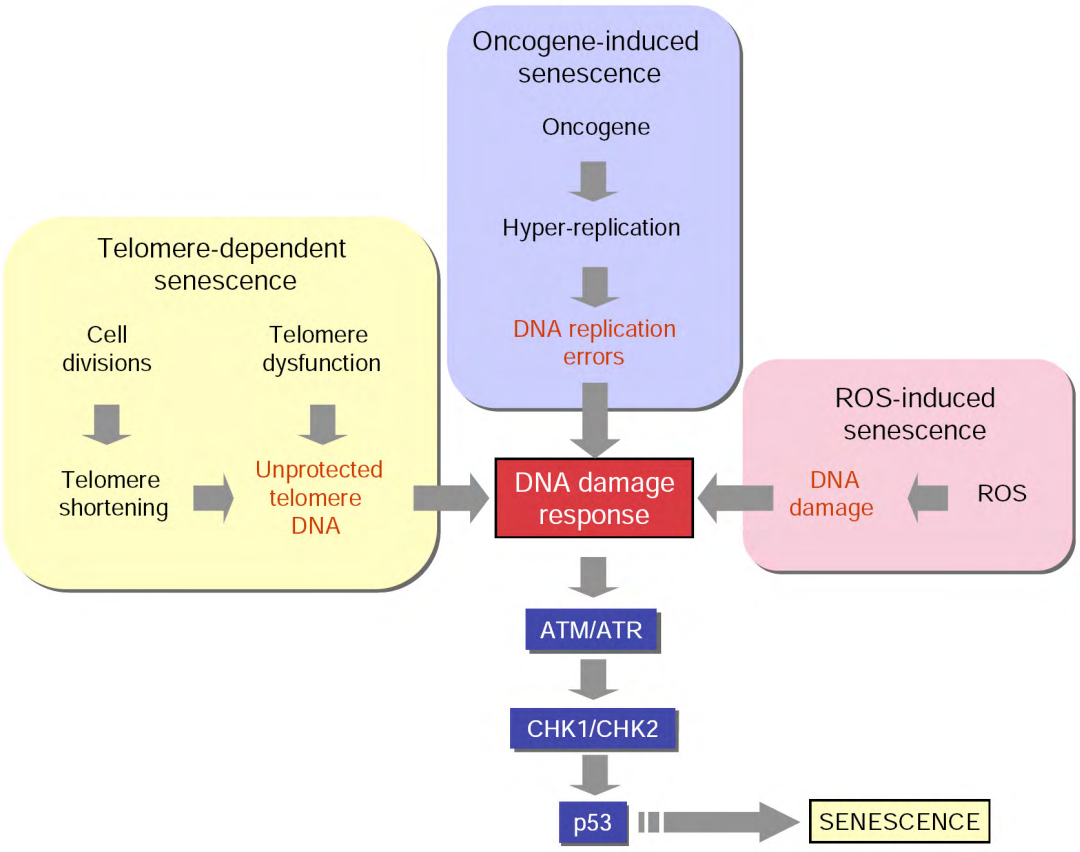

Figure 1.5: Senescence as a general stress response program. DNA damage response and activation of p53 through ATM/ATR and CHK1/CHK2 play central roles in all indicated pathways (Ozturk et al., 2009).

DNA-damage is dangerous because it compromises the structural integrity of chromosomes. DNA-damage response checkpoint is a safety mechanism that prohibits proliferation of damaged cells under such conditions and thereby provokes replicative senescence (also referred to as telomere-initiated or telomere-dependent senescence) which is the inevitable consequence of this end-replication problem.

Specialized complexes on single-stranded DNA and DSBs recruit and activate apical local kinases such as ATM and ATR. Activation of these specialized kinases at the DNA-damage site in senescent cells is usually mediated through autophosphorylation of ATM that is usually associated with nuclear foci formation

by phosphorylated H2AX. Nuclear foci accumulation is also characterized with DNA repair damage checkpoint factors such as MREII, MDC1, RAD9 and NBS1 as well as the activation of CHK1 and CHK2 kinases. Ultimately, DNA-damage checkpoint machinery often responds with activation of signaling pathways that eventually converge on key decision making factors such as p53 and the cell-division cycle 25 (CDC25) phosphatases (d'Adda di Fagagna, 2008). Finally, the CDC25 phosphatases along with p53 interface DNA-damage response with the core of the cell-cycle progression machinery (Figure 1.6).

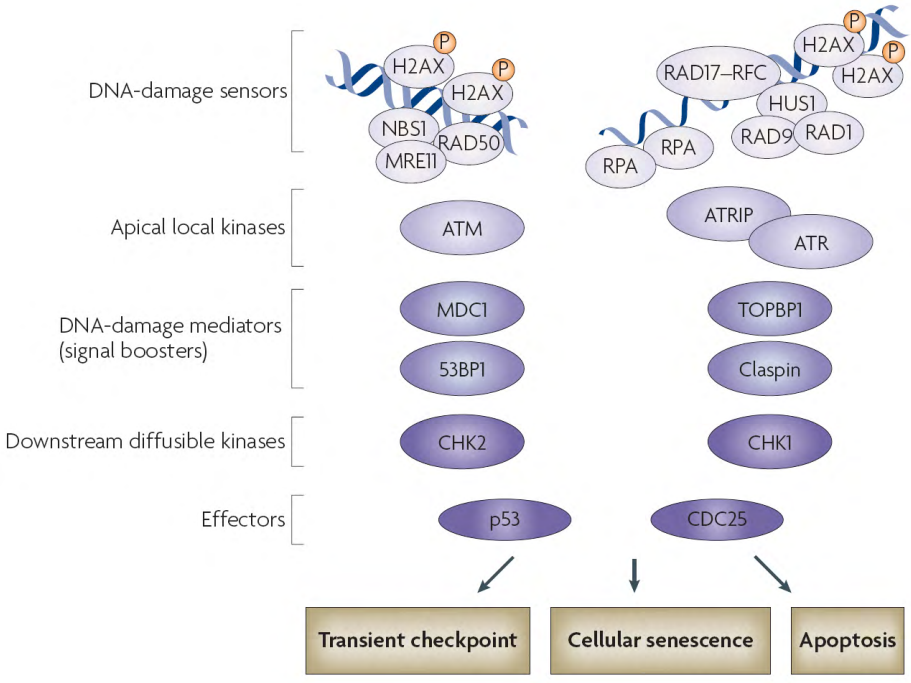

Figure 1.6: Activation of DNA-damage response (DDR) machinery. Increased local ATM and ATR activity above a threshold engages DDR factors that may function far from the damaged site (d'Adda di Fagagna, 2008).

The signaling pathways leading to permanent growth arrest in relation to shortened telomeres has been well-characterized. In this regard, a role for reactive oxygen species (ROS) in telomere shortening and uncapping has also been defined (Cattan et al., 2008; von Zglinicki, 2002).

In summary, senescence is not simply the end result of telomere shortening as the rate of shortening varies between cells during in vitro culture and there is not such a strict threshold of shortened telomere length at which the mechanism would be provoked (Lundberg et al., 2000).

1.5.3. Oncogene-induced senescence (OIS)

Telomere attrition is clearly not the only stimulus for senescence since mouse cells possess very long telomeres but still undergo senescence arrest in vivo (Kim et al., 2009b; Kortlever et al., 2006; Murga et al., 2009). Although, various physiologic stress conditions could hasten the onset of senescence. Induction of senescence is also the frequent outcome of oncogene activation in normal cells. Like oncogene-induced apoptosis, OIS has been implicated as a powerful tumor suppressive mechanism that impedes the proliferation of cells with high expression of an aggressive oncogene.

OIS can be triggered by activated onco-proteins like *E2F1*, *MYC* and Ras^{V12} (Courtois-Cox et al., 2006; Grandori et al., 2003; Lazzerini Denchi et al., 2005). Ras overexpression triggers a hyper replicative phase in which cells proliferate faster than control cells. However, this transient hyperproliferation state is quickly restrained by aberrant activation of DDR checkpoint pathways along with engagement of negative cell-cycle regulators that eventually establish cellular senescence (Di Micco et al., 2006; Mallette et al., 2007). Therefore, OIS is primarily a DNA-damage response as demonstrated by recent findings that senescent cells in response to oncogene expression depict increased appearance of DNA damage sites together with the accumulation of heterochromatin foci that lead to silencing of proliferative genes (Figure 1.5).

Expression of other onco-proteins downstream of Ras, like $BRAF^{E600}$, has also been shown to trigger cell cycle arrest (Michaloglou et al., 2005). Conversely, the loss of PTEN, which is an inhibitor of the same pathway, also leads to senescence (Alimonti et al., 2010). Oncogene-induced senescence appears to be engaged by a

variety of intrinsic and extrinsic signals. Nevertheless, OIS is not clearly associated with telomere shortening, although established independently of any telomere attrition or dysfunction (Hornsby, 2007). Independent of the mechanism, cells that have undergone OIS and replicative senescence share common features such as flat morphology, SABG activity and induction of cell cycle inhibitory proteins such as p53 and $p16^{Ink4a}$ (Ferbeyre et al., 2002; Serrano et al., 1997).

Additionally, similar to replicative senescence, oncogene-induced senescence has a causal link to reactive oxygen species (ROS) accumulation and can be abrogated by culturing cells in the presence of antioxidants (Lee et al., 1999).

1.5.4. Reactive oxygen species (ROS)-induced senescence

Respiratory chain processes in the mitochondria are the major sources of intracellular oxygen radicals. Reactive oxygen species are also produced by intracellular NOX enzymes. Experimental induction of ROS accumulation in cells through H_2O_2 treatment or glutathione depletion provokes senescence-like growth arrest in various cell types (Blanchetot and Boonstra, 2008). Besides, several studies have linked intracellular accumulation of ROS to telomere shortening. On the other hand, depending on the level of stress such free radicals may also lead to telomere-independent senescence response (Lu and Finkel, 2008). Thus, ROS-dependent senescence shall be raised as a process to limit the ROS-induced mutation by removing damaged cells. Therefore, any disturbance in the physiologic intracellular levels of ROS would be expected to provoke senescence induction (Colavitti and Finkel, 2005).

Nevertheless, the mechanisms of ROS-initiated senescence are still not well-known. However, the issues discussed above thus suggest that cellular senescence, whether induced by telomere attrition, DNA replication stress provoked by oncogene activation, or ROS accumulation, share a common underlying reason, which is the DNA-damage response. In view of this, reactive oxygen species are the major agents responsible for endogenous oxidative DNA damage in the cells and DNA-damage

response is the critical mediator in triggering senescence. The signaling pathways activated by these responses eventually converge on p53 (Figure 1.5).

1.5.5. DNA-damage-independent senescence

DNA-damage mediated activation of p53 induces the upregulation of the cyclin-dependent kinase (CDK) inhibitor $p21^{Cip1}$, a factor known to have a direct inhibitory link to cell-cycle progression. However, absence of $p21^{Cip1}$ in mouse embryonic fibroblasts does not overcome senescence induction. This would suggest a prominent role for other senescence relaying signals as well. Other mechanisms of senescence mainly focus on the 35 kilobases INK4/Arf locus encoded tumor suppressors, namely ARF, $p16^{Ink4a}$ and $p15^{Ink4b}$. These cyclin-dependent kinase inhibitors (CDKIs) represent the most important regulatory factors in senescence and immortality. Activation of these CDKIs promotes growth arrest and/or senescence, and inhibits entry into S-phase of the cell cycle depending on the cellular context.

Independent of p53 activation, driven by DNA-damage checkpoint machinery, these tumor suppressors oppose aberrant mitogenic stimuli and engage senescence inducing signals to retinoblastoma (pRb) pathway (Takahashi et al., 2006). Activity of pRb, a crucial gatekeeper of cell cycle progression, is controlled by various post-translational modifications such as phosphorylation, acetylations and ubiquitination (Chen et al., 2003; Markham et al., 2006). Several lines of evidence suggested the phosphorylation event to be the key step in imposing the G1 arrest (Sherr and McCormick, 2002). In particular CDK2, CDK4 and CDK6, a series of cyclin-dependent kinases, have been implicated to play prominent role in pRb phosphorylation (Malumbres and Barbacid, 2007). By phosphorylating the retinoblastoma (pRb) family members, CDKs enable the transcription of cell-cycle regulatory genes that are under the control of transcription factors belonging to E2F family proteins. Cyclin-dependent kinase activities, on the other hand, are tightly controlled by INK4 proteins. Through direct association with CDK4 and CDK6, these INK4 proteins block the assembly of catalytically active cyclin-CDK

complexes. The association of the INK4 proteins to CDK4 and CDK6 induces an allosteric change that inhibits the binding of these kinases to D-type cyclins, abrogating CDK4/6-mediated phosphorylation of retinoblastoma (Rb) family members (Kim and Sharpless, 2006). Thus, the net result of elevated expression of INK4 proteins; maintains Rb-family proteins in hypophoshorylated state which promotes inhibitory binding to E2F and therefore causes a G1-phase cell-cycle arrest (Gil and Peters, 2006).

Given the importance of factors expressed from INK4 locus in tumor suppression and aging, several intensive studies have been conducted on regulation of this particular locus. Thus, work in this field enhanced the understanding of the regulation of INK4 locus. Consequently, several factors were identified in the last decade with evidenced implications on the control of expression of these tumor suppressors (Figure 1.7).

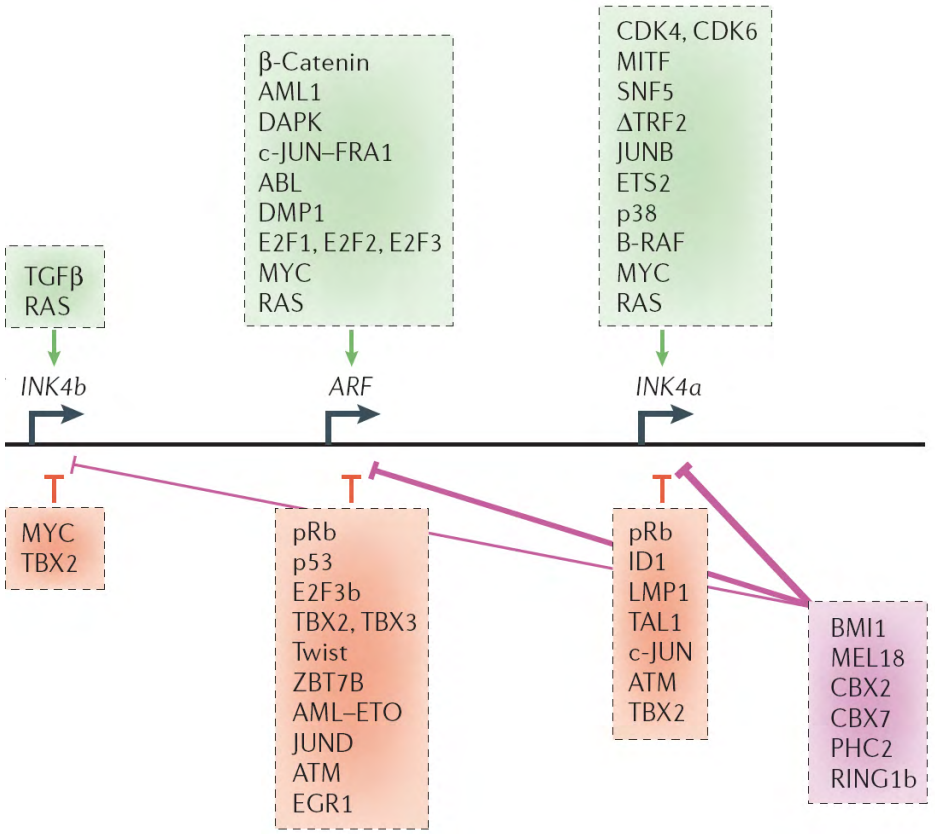

Figure 1.7: Regulation of the INK4/Arf locus. Activators and repressors of the locus are indicated above and below each gene, respectively (modified from (Gil and Peters, 2006)).

1.5.6. Cancer Cell Senescence

Senescence is now considered as an anti-tumor program to limit proliferation of transformed cells *in vivo*. Since senescent cells can no longer proliferate, cancer cell senescence acts as a barrier against tumor progression. Although senescent cells are absent in malignant tumors, there are examples of cellular senescence in pre-malignant tumors suggesting senescence as a limiting factor for malignant transformation. Senescence tumor cells were initially identified in pre-malignant lung adenomas, pancreatic neoplasias and melanocytic nevi (Collado et al., 2005). Unfortunately, such senescent cells were not detected in corresponding malignant adenocarcinoma tumors.

Several lines of evidence demonstrated senescence in diverse liver diseases, with most striking outcomes implicated in liver cirrhosis samples which are closely associated with hepatocyte specific telomere shortening. Some HCC samples were also demonstrated to harbor cell populations with SABG activity. All these observations implicated senescence as a tumor suppressive mechanism. Supporting evidence came from the studies performed with genetically well-defined mouse models. Murine HCC tumors generated through mutant Ras overexpression in p53-deficient hepatoblasts were efficiently cleared by reactivation of p53 expression (Xue et al., 2007).

Surprisingly enough, restoration of the tumor suppressive function of p53 in a similar study triggered a senescence response for tumor regression only in tumor cells leaving normal cells unaffected (Ventura et al., 2007). In this experimental setting tumor regression was closely associated with infiltration of neutrophils, macrophages and natural killer cells suggesting a functional role for immune system in tumor cell clearance.

Other studies with particular interest in titrated activation of Nras oncogene or ablation of tumor suppressor Pten also contributed to the field by describing experimental evidence for oncogene-induced senescence in vivo (Alimonti et al., 2010; Braig et al., 2005). Of note, all these senescence programs described so far converge on p53 and $p21^{Cip1}$ activation as well as a contribution from $p27^{Kip1}$. Since these factors monitor the presence of oncogenic signaling; abrogation of single one of them contributes well to malignant transformation.

However, senescence observed in pre-malignant tumors is not solely modulated by INK4 locus proteins, $p21^{Cip1}$ or p53. β-catenin overexpression as well as BRAF activation in the absence of p53 or $p16^{Ink4a}$ resulted in senescent cells in melanomas (Dhomen et al., 2009; Xu et al., 2008). All these data support the hypothesis that other cell cycle regulators might also be engaged in senescence initiation and maintenance in pre-malignant tumors and their loss of function is one of the mechanisms to escape from redundant senescence program and progress to a more malignant phenotype.

Taken together, induction of senescence program in pre-malignant tumors as well as in some malignant stage cancers may be considered as an anti-tumor therapy as an alternative development to current strategies. Currently available targeted therapies are mainly designed to kill malignant cells, although they are often prohibited by pro-survival factors present in cancer cells. Therefore, attacking tumor cells by senescence-inducing strategies alone or in combination with currently available therapies might prove effective in an alternative intervention perspective in various malignant lesions including some forms of HCC.

1.6. Transforming growth factor-beta signaling

Transforming growth factor-beta (TGF-β) signaling controls a diverse set of functions mainly those related to cell proliferation, development, differentiation, adult homeostasis and disease. TGF-β superfamily cytokines are virtually secreted by all type of cells and have overlapping receptor usage (Massague, 1998).

1.6.1. TGF-β ligands and receptors

Cytokines belonging to this superfamily are initially secreted as precursor proteins which undergo proteolytic cleavage and reach maturation. The functional form of TGF-β ligand is a 12-15 kDa homo-dimer stabilized by hydrophobic disulfide-rich core characteristic of a tight structure known as “cysteine knot” (Sun and Davies, 1995). The cleavage of covalent bonds between the pro-peptide and the mature ligand is facilitated via a furin-like convertase (Derynck et al., 1985; Miyazono et al., 1988).

The two dimeric polypeptides formed by cleavage remain intact through non-covalent interactions, and they are secreted as a latent complex. Latency-associated protein (LAP), the propeptide portion of this complex keeps the mature propeptide biologically inactive by preventing accessibility to membrane receptors (Lee and McPherron, 2001). In some cases, LAP may remain as the noncovalently bound

predominant extracellular partner in the secretory pathway of the TGF-β ligand. Alternatively, LAP complex may bind to large secretory glycoproteins known as latent TGF-β binding proteins (LTBPs). LTBPs are known to aid the secretion or activation of LAP-ligand complexes. The release of biologically active TGF-β ligands from latent complexes is mediated through proteolytic processing of LAP (Massague and Chen, 2000).

Pleiotropic cytokine, TGF-β, initiates signal transduction through direct contact with a membrane-anchored proteoglycan, known as type III receptor or betaglycan (Wrana et al., 1992). This process then facilitates the formation of a bi-dimeric receptor complex. Binding of TGF-β to receptor type I (TGFβRI, also known as ALK5) brings together receptor type II family forming a complex of two serine/threonine kinase receptors which initiate intracellular signaling (Shi and Massague, 2003).

TGF-β superfamily receptors consist of 12 members, namely seven type I receptors and five type II receptors, all belonging to TGF-β signaling pathway (Figure 1.8)(Manning et al., 2002).

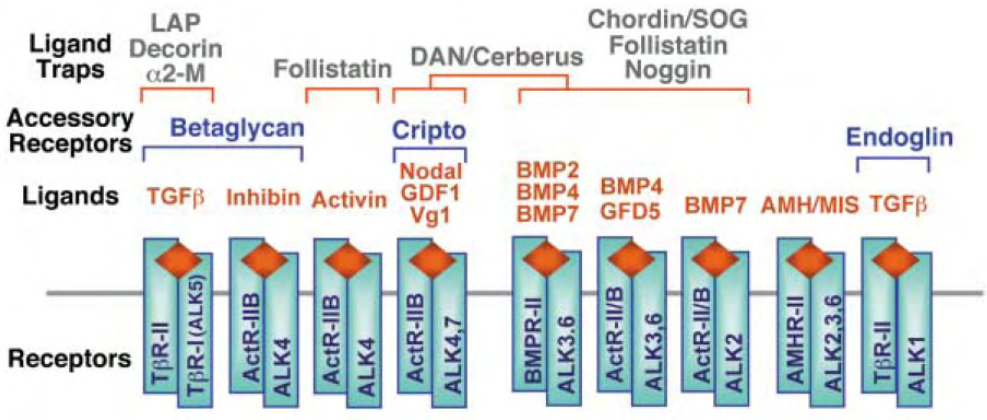

Figure 1.8: TGF-β superfamily ligands and receptors in vertebrates (adapted from (Shi and Massague, 2003)).

1.6.2. Mechanisms of receptor and Smad activation

Ligand binding to the extracellular domains of both types of the transmembrane receptors promotes direct contact and induces conformational change at the intracellular kinase interface of receptors thereby forming a heterotetrameric complex. This close proximity promotes phosphorylation of type I receptor at multiple serine and threonine residues at the cytoplasmic GS region by constitutively active type II receptor (Attisano and Wrana, 2002).

Subsequent activation of receptor type I is mediated through autophosphorylation. Activated TGFβ-RI then specifically recognizes intracellular receptor-regulated Smad proteins (R-Smads) with the aid of adaptor protein SARA (Smad anchor for receptor activation) (Wu et al., 2000), and subsequently transmits the signal through direct phosphorylation at serine residues located at the extreme carboxy terminus (Attisano and Wrana, 2000).

Once activated by phosphorylation, Smad2 and/or Smad3 form a heterodimeric or heterotrimeric complex with a common signaling partner Smad4, also known as cooperating-Smad (Co-Smad), and translocate into the nucleus and in concert with adaptor transcription factors regulate the transcription of a large set of target genes (Figure 1.9)(Chen et al., 2002; Derynck et al., 1998; Derynck and Zhang, 2003; Gomis et al., 2006).

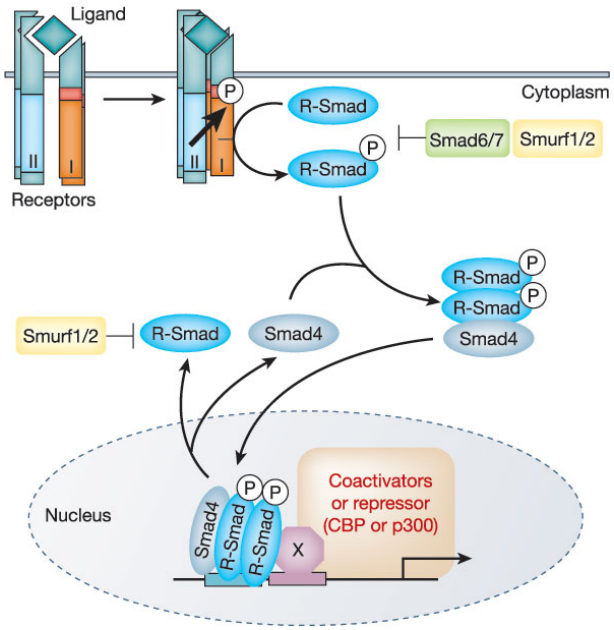

Figure 1.9: Simple diagram of TGF-β signaling from cell membrane to nucleus (Derynck and Zhang, 2003).

The R-Smads are composed of two conserved domains separated from each other by a proline-rich less-conserved linker region (Shi et al., 1998). MH1 domain located at the far N-terminus has DNA-interaction domain, whereas subcellular localization and transcription regulatory activity is mediated by MH2 domain situated at the C-terminus (Figure 1.10) (Hill, 2009; Wu et al., 2000).

Figure 1.10: Conserved domain structures in receptor-regulated Smads in vertebrates. S: serine, V: valine, M: methionine, P: mark of phosphorylation (Hill, 2009).

1.6.3. Dynamic Smad nucleocytoplasmic shuttling for proper signal transduction

Receptor mediated activation of R-Smads mediates their subsequent translocation into the nucleus. At steady-state, R-Smads are predominantly in the cytoplasm in their inactive forms, whereas Smad4 is distributed through the cytoplasm and the nucleus. Unlike R-Smads, inhibitory-Smads (I-Smads, Smad6 and Smad7) which block TGF-β signaling by recruiting ubiquitin ligases-Smurfs to the receptors and ensuring their internalization and degradation (Kavsak et al., 2000), are nuclear and upon initiation of TGF-β signal propagation tend to move to the cytoplasm (Hanyu et al., 2001; Itoh et al., 1998).

Upon activation, R-Smads and Smad4 translocate into the nucleus. Shuttling between the nucleus and cytoplasm is controlled by reciprocal functions of importin, a transporter that binds to nuclear localization sequences (NLS) and carries the cargo into the nucleus, and CRM1, an importin-like adaptor protein which binds to nuclear export sequences on Smads mediates their export from the nucleus (Xiao et al., 2003; Xiao et al., 2000).

1.6.4. Target gene activation by Smads

Recruitment of activated R-Smads to DNA is the key step in modulation of gene expression in response to TGF-β stimulation. The presence of additional amino acids encoded from exon 3 (Ex3) on MH1 domain in the most common splice form of Smad2 interferes with its DNA-interaction feature which renders Smad2 different from Smad3 and Smad4. Direct contact with DNA located on regulatory regions of target genes is ensured by 5 bp sequence CAGAC, referred as Smad-binding element, although CAGA has been reported to suffice for optimal binding (Kim et al., 1997).

Smad-binding element can be found on average once every ~1 kb on human genome (Massague and Wotton, 2000). This also corresponds to one CAGA

sequence on every candidate gene with the similar average size. However, all these sequences do not bind Smad factors and association of Smads with DNA is quite unstable to solely provide an effective binding *in vivo* and explain target gene selection by TGF-β (ten Dijke et al., 2000). Selectivity and high affinity for target gene activation is achieved through direct association of R-Smads and Co-Smads with more that one SBE together with additional DNA contacts mediated by DNA-binding partners and transcriptional co-activators and co-repressors (Zawel et al., 1998).

Smad interactions with other transcription factors can be mediated by MH1 and/or MH2 domains. In addition, selective gene responses either transcriptional activation or repression could be direct which involves contact of Smads with DNA, or "self enabled" in which product of a direct target subsequently associates with Smads to control another set of gene regulations (Kang et al., 2003). A list of Smad co-activators and co-repressors is depicted below which explains Smad signaling through protein and DNA interactions (Table 1.1).

Smad-interacting component	Smad	Interacting Smad domain	Functional properties of Smad-interacting component
SARA	Smad2, Smad3	MH2	Recruitment of Smad to receptor
TβR-I, ActR-IB, ALK7	Smad2, Smad3	L3 loop in MH2	Phosphorylation of Smad at C terminus
ALK1, ALK2, BMPR-IA, BMPR-IB	Smad1, Smad5, Smad8	L3 loop (and H1 α helix) in MH2	Phosphorylation of Smad at C terminus
R- and Co-Smads	R- and Co-Smads	MH2	Cooperation in nuclear translocation and transcriptional regulation
Smad6	Smad1	MH2	Competition with Smad4 for Smad1 interaction
Smurf1	Smad1, Smad5	PY motif in linker	E3 ubiquitin ligase; targets Smads for ubiquitin-mediated degradation
FAST1	Smad2, Smad3	αH2 in MH2	Winged-helix transcription factor; functionally cooperates with Smads
c-Jun, JunB, JunD	Smad3	MH1 and linker	AP-1 transcription factor family members; functionally cooperate with Smad3
c-Fos	Smad3	MH2	AP-1 transcription factor family members; functionally cooperate with Smad3
ATF-2	Smad3	MH1	ATF/CREB family member; functionally cooperates with Smad3
Evi-1	Smad3	MH2	Zinc-finger transcriptional regulator; inhibits binding of Smad3 to DNA
PEBP2/CBFA/AML	R-Smads	MH1, MH2	Runt-domain-containing transcription factor; functionally cooperates with Smads
C-terminally truncated Gli3	Smad1, Smad2, Smad3, Smad4	Not determined	Zinc-finger transcription factors
VDR	Smad3	MH1	Vitamin D receptor; functionally cooperates with Smad3
Hoxc-8	Smad1	Not determined	Homeodomain transcriptional repressor
SIP1	R-Smads	MH2	Zinc-finger/homeodomain transcriptional repressor
GR	Smad3, Smad4	MH2	Glucocorticoid receptor; Smad repressor
CBP/p300	Smad2, Smad3	MH2	Transcriptional co-activator with intrinsic histone acetyl transferase activity
MSG1	Smad4	MH2	Transcriptional co-activator
TGIF	Smad2	MH2	Transcriptional co-repressor; recruits histone deacetylase activity
Ski/SnoN	Smad2, Smad3, Smad4	MH2	Transcriptional co-repressor
5′-AGAC-3′	Smad3, Smad4	β-hairpin loop in MH1	DNA

Table 1.1: Smad co-activators and co-repressors (ten Dijke et al., 2000)

1.6.5. Regulation of cell cycle progression and apoptosis by Smad proteins

TGF-β pathway has been demonstrated to regulate many intracellular processes along with proliferation and apoptosis in many cell types. Cell cycle inhibition manifested by TGF-β is predominantly a G1-phase arrest (Ewen et al., 1995; Geng and Weinberg, 1993; Herrera et al., 1996; Zhang et al., 1999), although G2-arrest has also been reported (Hashimoto et al., 2003). TGF-β-mediated anti-proliferative responses are controlled by multiple mechanisms and depend on the cellular context. Several studies have implicated TGF-β in growth arrest of various through upregulation of $p15^{Ink4b}$ and $p21^{Cip1}$ (Polyak et al., 1994; Senturk et al., 2010), which then inhibit cyclin-dependent kinase (CDK)-mediated phosphorylation

of retinoblastoma protein (pRb) (Florenes et al., 1996; Rich et al., 1999; Robson et al., 1999). TGF-β-induced upregulation of $p21^{Cip1}$ is in most cases p53-independent (Datto et al., 1995). TGF-β can also induce cell cycle arrest in $p15^{Ink4b}$-deficient cells by upregulation of $p27^{Kip1}$ expression as well as inhibition of the expression of CDK tyrosine phosphatase cdc25A (Iavarone and Massague, 1997).

TGF-β inhibits the expression of c-Myc proto-oncogene through direct interaction of Smad3 and Smad4 to regulatory regions located in the Myc promoter (Chen et al., 2001). Although E2F4/5, p107 and p130 were demonstrated to be direct targets of TGF-β (Belbrahem et al., 1996), they were also implicated as Smad cofactors in c-myc down regulation mechanism (Chen et al., 2002). TGF-β-induced c-myc downregulation has also been shown to regulate TGF-β-mediated activation of $p15^{Ink4b}$ (Seoane et al., 2001).

TGF-β family factors can also induce apoptotic cell death in many cell types which is typically accompanied by growth arrest. Several lines of evidence implicated JNK and p38 pathways in TGF-β-induced apoptosis which is mediated by the adaptor protein Daxx (Edlund et al., 2003; Perlman et al., 2001). Programmed cell death induced by TGF-β is usually accompanied by reactive oxygen species accumulation (Langer et al., 1996), decreased expression of Id2 (Cao et al., 2009) and transcriptional modulation of BIK and BCL-XL proteins (Spender et al., 2009).

1.6.6. Role of TGF-β signaling in epithelial-mesenchymal transition

TGF-β signaling pathway is also a potent inducer of epithelial mesenchymal transition. EMT is a complex machinery which involves break-down of polarized epithelial morphology and transformation into spindle shaped cells together with reduced adhesion at cellular junctions. These phenotypic alterations are mainly accompanied by loss of apical-basolateral cell polarity, actin reorganization and down regulation and internalization of E-cadherin and ZO-1 and increased cell motility (Levayer and Lecuit, 2008). TGF-β-induced EMT has been demonstrated in

many different cell types including keratinocytes, mammary epithelial cells and hepatocytes (Cui et al., 1996; Davies et al., 2005; Miettinen et al., 1994; Sheahan et al., 2008). Several lines of evidence implicated the combinatorial action of transcriptional factors during TGF-β-induced mesenchymal transdifferentiation. These factors function in a tissue- and developmental stage-specific manner associated with their expression patterns (Peinado et al., 2007). These factors belong to Snail family, ZEB family and helix-loop-helix transcription factors including Twist transcription factors (Xu et al., 2009). Snail and Zeb family transcription factors bind to regulatory E-box elements found on various target genes (Figure 1.11).

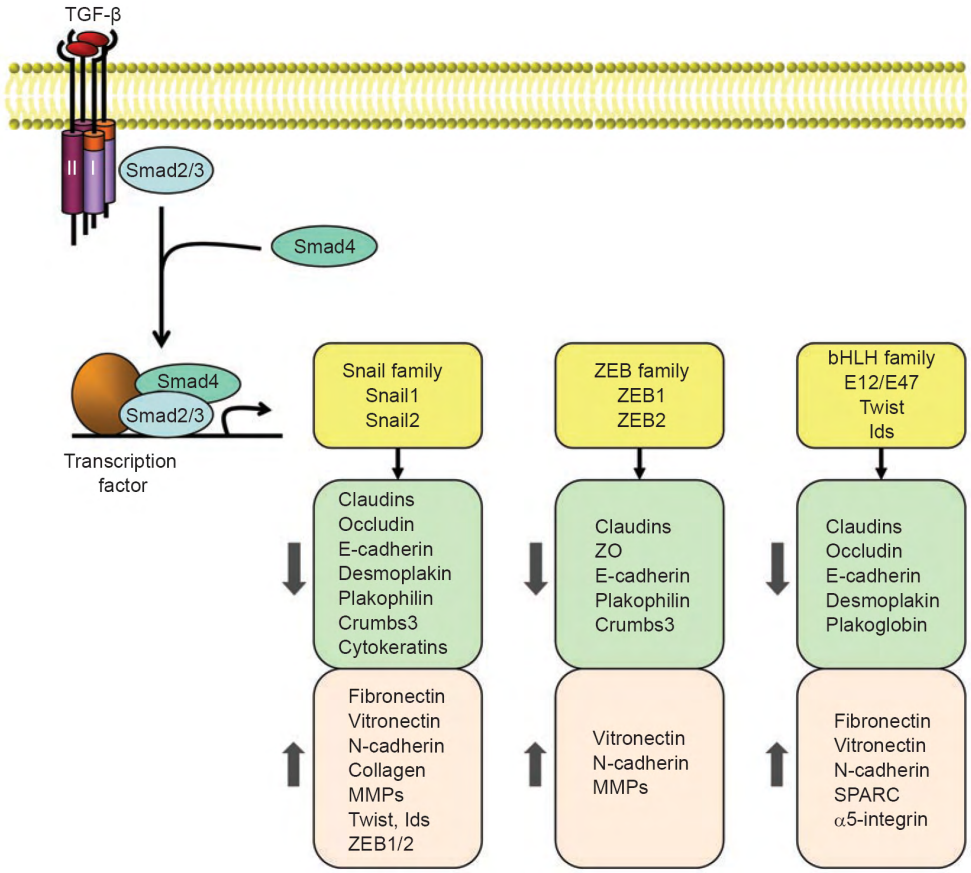

Figure 1.11: Expression of epithelial mesenchymal markers by TGF-β-regulated transcription factors. (Xu et al., 2009).

Through direct association with DNA together with recruitment of a complex consisting of HDAC, TGF-β-induced Snail family transcription factors regulate the expression of various target genes including E-cadherin (Dhasarathy et al., 2007; Zavadil and Bottinger, 2005). Similarly, Zeb family factors recognize E-box elements on regulatory regions of targets genes and repress transcription of E-cadherin by recruiting transcriptional co-repressor C-terminal binding protein (CtBP) (Vandewalle et al., 2005). Smad-interacting protein-1 (SIP1), member of Zeb family transcription factors, is a downstream target of TGF-β signaling pathway (Kojima et al., 2008). Interestingly sip1, hereafter termed as zeb2, interacts predominantly with activated Smad3 and inhibits expression of epithelial marker genes (Postigo et al., 2003). The HLH factors Twist1 and Twist2 and high mobility group A2 (HMGA2) proteins are other downstream effectors of TGF-β during EMT (Mani et al., 2007; Thuault et al., 2006).

1.6.7. TGF-β signaling pathway in cancer

TGF-β signaling perturbations are frequently observed during carcinogenesis. Genetically unstable cancer cells have the capacity to escape the suppressive functions of TGF-β pathway through accumulation of inactivating mutations in major components. Mutations and allelic loss of heterozygosity (LOH) are frequently detected in receptor type II (TGFBR2) in various types of cancers (Levy and Hill, 2006). Truncating mutations on both alleles of TGFBR2 frequently occur in colon, gastric, head and neck carcinomas. Such mutations are typically associated with replication errors in tumors with microsatellite instability. On the other hand, infrequent mutations such as frameshift and missense mutations have been reported for receptor type I (TGFBRI) coding region in ovarian and esophageal cancers (Kaklamani et al., 2004). In addition, deregulated expression of both types of receptors through epigenetic alterations have been identified in prostate and bladder cancers (Kim et al., 2000).

In sharp contrast to R-Smads, Smad4 inactivating mutations are more frequent in cancers (Levy and Hill, 2006). Smad4 has been demonstrated to be inactivated in most of the pancreatic and gastric carcinomas, juvenile polyposis, and biliary tract carcinomas (Hahn et al., 1998; Howe et al., 1998; Powell et al., 1997). Smad2 and Smad3 mutations were very rare in colorectal, esophageal and hepatocellular carcinomas (Kawate et al., 1999; Osawa et al., 2000; Yakicier et al., 1999). Nevertheless, TGF-β pathway disruption in hepatocarcinomas is frequently associated with perturbed expression of adaptor protein embryonic liver fodrin (ELF) (Baek et al., 2008; Mishra et al., 2004).

Several lines of evidence presented above implicated TGF-β pathway as a potent tumor-inhibitory mechanism. Frequent inactivations observed with receptors and Co-Smad supports this notion. Loss of TGF-β-mediated cytostatic response in various tumors is achieved through perturbation of $p15^{Ink4b}$ and $p16^{Ink4a}$ expression by epigenetic silencing of INK4 locus as well as homozygous deletions (Herman et al., 1996; Krimpenfort et al., 2007; Krimpenfort et al., 2001). Loss of TGF-β responsiveness could also be related to oncogene activation.

Cancer cells that loose tumor-suppressive arm of TGF-β pathway usually acquire ability to interpret TGF-β signals as tumorigenic to enhance tumor growth, invasion and distal metastasis (Gupta and Massague, 2006). Recently, much attention has been paid on linker region phosphorylation of R-Smads as a candidate mechanism to switch tumor-suppressive function of TGF-β pathway into tumor-promoter role. For instance oncogenic Ras can suppress inhibitory functions of TGF-β pathway through linker phosphorylation of Smads (Sekimoto et al., 2007). GSK3β is one of the factors identified to directly phosphorylate several residues situated in the linker region and perturb TGF-β signal (Lu et al., 2008; Wang et al., 2009). In addition, HCV core protein expression in the liver inhibits TGF-β cytostatic responses (Battaglia et al., 2009). Direct crosstalk between hyperactive PI3K and TGF-β pathways is also implicated in suppression of TGF-β cytostatic responses (Conery et al., 2004; Danielpour and Song, 2006; Song et al., 2006).

Tumor-promoting activities of TGF-β pathway is typically linked to epithelial mesenchymal transition by which contributes to tumor invasion and dissemination (Giampieri et al., 2009; Moutsopoulos et al., 2008). In addition to that, cancer cells resistant to cytostatic responses benefit from immunosuppressive functions of TGF-β to evade immunity (Gorelik and Flavell, 2001).

1.7. Reactive oxygen species (ROS) and NADPH oxidase system

Oxygen-derived small molecules produced by cells are, in general, termed as reactive oxygen species (ROS). Intracellular ROS generation is usually initiated by formation of superoxide which is then converted to hydrogen peroxide by superoxide dismutases. ROS molecules interact with a diverse set of intracellular macromolecules and may therefore irreversibly destroy their functions.

The physiological ROS generation is usually considered as generation of byproducts of several other biological functions. Intracellular ROS generation occurs in several intracellular organelles by endogenous sources including mitochondria, peroxisomes, cytochrome p-450, cell membrane and other cellular entities (Balaban et al., 2005; Gonzalez, 2005; Pritchard et al., 2001). ROS can also be produced by exogenous sources including environmental agents, pharmaceuticals (Klaunig and Kamendulis, 2004). Such reactive oxygen species may then influence many biological processes by inducing DNA and protein-damage, damage to protein-coding and non-coding RNA, and chromosomal instability together with loss of tumor-suppressor genes and finally oxidative damage on other biological systems that may provoke carcinogenesis (Ishikawa et al., 2008; Kumar et al., 2008; Tanaka et al., 1999).

Oxidative DNA-damage has been proposed as a major source of DNA mutations with a diverse array of DNA adducts (Dizdaroglu, 1992; Lu et al., 2001). Much effort has been made on studies with most abundant oxidative DNA lesion 8-hydorxydeoxy guanosine (8-OHdG) showing elevated levels in various human

cancers, including hepatocarcinomas (Diakowska et al., 2007; Miyake et al., 2004) and *in vivo* hepatocarcinogenesis models (Muguruma et al., 2007).

1.7.1. NADPH (reduced nicotineamide adenine dinucleotide phosphate) oxidase system

The NOX family members are transmembrane proteins that control the transfer of electrons in various biological membranes found in virtually all cell types. In this system, the electron acceptor is oxygen and superoxide ($O_2^{\cdot-}$) is the end product of this reaction. Therefore, the ultimate biological function of NOX family NADPH oxidases is the generation of ROS. Several Nox homologs have been identified in the last few decades. In accordance with conservation, all members have been demonstrated to have preserved structural and functional features together with known regulatory factors (Table 1.2). Phox, gp91phox, is the first super-oxide generating NADPH oxidase identified in macrophages and neutrophils (Han et al., 2001).

Enzyme	Highest level of expression
gp91phox (NOX2)	Phagocytes
NOX1	Inducible: colon and vascular smooth muscle
NOX3	Fetal kidney
NOX4	Kidney, osteoclasts, ovary and eye; widespread
NOX5	Spleen, sperm, mammary glands and cerebrum
DUOX1	Thyroid, cerebellum and lungs
DUOX2	Thyroid, colon, pancreatic islets and prostate

Table 1.2: Human Nox/Duox enzymes and tissues with highest level of expression. (adapted from (Lambeth, 2004)).

The Nox family members were grouped into three in accordance with their common domain gp91phox and additional domains necessary for complete functionality (Lambeth et al., 2000). The first group includes Nox1, Nox3 and Nox4 enzymes which are almost identical in structure and size to gp91phox. Nox5 presents

high identity to gp91phox with an additional calmodulin-like domain which consists of four binding sites for calcium which makes this unique among previous enzymes to be regulated by other factors (Banfi et al., 2001). Along with preserved similarity to Nox5, Duox1 and Duox2 enzymes constitute the third group with an additional peroxidase-homology domain (Edens et al., 2001; Ritsick et al., 2004). Function of these two enzymes is also modulated by calcium.

Regulation of Nox family members is also modulated by other identified factors, namely membrane-associated p22phox and the cytosolic subunits p47phox, p67phox and p40phox and small GTPase RAC (Vignais, 2002).

1.8. Objectives and rationale

Hepatocellular carcinoma (HCC) is among the most frequent cancers in the human population. Despite its high incidence rate in the world, there is only little understanding of the molecular mechanisms leading to the onset of hepatocarcinogenesis. Owing to genetic heterogeneity of HCCs, development of therapeutic options are very limited (Farazi and DePinho, 2006). Therefore, it is of ultimate importance to delineate the mechanisms leading to transformation of hepatocytes and develop new strategies to implement novel tumor-suppressive therapeutics.

Somatic cells have a limited proliferative potential in culture. Following a number of divisions they cease proliferation due to end-replication problem of telomeric regions and terminally enter a cellular state referred to as replicative senescence. Nevertheless, replicative immortality is a hallmark of cancers (Hanahan and Weinberg, 2000). Recently, senescent cells have been identified in various premalignant tumors and multiple liver disease stages; therefore senescence has been implicated as an anticarcinogenic program against malignant transformation and immortalization. In hepatocellular carcinoma, senescence inducing factors $p16^{Ink4a}$ and p53 are usually inactivated through epigenetic and genetic mechanisms (Ozturk, 1999). Nonetheless, a few recent reports have provided strong evidence that the

senescence machinery could be utilized as an anti-tumor barrier in HCCs (Ozturk et al., 2006; Wu et al., 2007; Xue et al., 2007).

Transforming growth factor-beta (TGF-β) has been implicated in senescence induction in various cell types as well as liver diseases (Nagasue et al., 1996; Reimann et al., 2010; Sacco et al., 2000; Sugano et al., 2003; Vijayachandra et al., 2009). We demonstrated close correlation between TGF-β expression patterns and senescence frequencies of various liver disease stages. Therefore, we hypothesized that TGF-β could be used as a senescence-inducing agent in hepatocellular carcinomas.

In the framework of this study, we aimed to study implications of TGF-β signaling in a set of HCC cell lines. Screening of HCC cell lines for TGF-β responsiveness demonstrated senescence-induction in only epithelial-like well-differentiated (WD) cell lines, while those with high mesenchymal marker expression referred to as poorly-differentiated (PD) were typically resistant to TGF-β-induced senescence. In this regard, we divided the study into two and aimed to characterize the senescence induction in WD cell lines and address the potential implications of senescence in vivo. In addition, we further aimed to study the mechanisms underlying resistance to TGF-β-induced growth arrest in mesenchymal-like cell lines.

Having elucidated the rapid onset of permanent senescence arrest after very brief stimulation with TGF-β, we also aimed to investigate the implications of sustained exposure of Huh7 cells to TGF-β treatment.

CHAPTER 2. MATERIALS AND METHODS

2.1. MATERIALS

2.1.1. General reagents

Most of the chemicals used in the laboratory including bradford reagent, haematoxylin, ethanol and methanol were from Sigma-Aldrich (St. Louis, USA) and Merck (Darmstadt, Germany). Additionally, ECL+ Western blot detection kit was from Amersham GE Healthcare Life Sciences (Buckinghamshire, UK). Fluorescent mounting medium was from Dako (Denmark). Ponceau S and DMSO were from Applichem Biochemica (Darmstadt, Germany). X-Gal was from Fermentas GmbH (Germany). Total RNA isolation kit: Nucleospin RNA II was from Macherey-Nagel (Duren, Germany). Standard agarose was from Sigma Biosciences (St. Louis, USA). Purified recombinant human TGF-β1 was from R&D Systems (Minneapolis, USA). Maxi-prep kit (for large scale plasmid isolation) and Gel-extraction kit (for recovery and extraction of DNA from agarose gel) were from Qiagen (Chatsworth, CA, USA). Agar, tryptone and yeast extract were obtained from Gibco, BRL Life Technology Inc. (Gaithersburgs, MD, USA). Doxocycline was purchased from Appligene (France).

2.1.2. Bacterial Strains

The bacterial strain used in this study was E.Coli DH5a.

2.1.3. cDNA synthesis and polymerase chain reaction (PCR) reagents

Fermentas RevertAid First Strand cDNA synthesis kit was from Fermentas (Leon-Rot, Germany). Polymerase Chain Reaction (PCR) reagents were also

purchased from Fermentas. Master Mix for qPCR reactions, DyNAmo HS SYBR Green qPCR Kit F-410L, was purchased from Finnzymes (Finland).

2.1.4. Nucleic acids

DNA molecular weight markers and ultrapure deoxyribonucleotides were purchased from MBI Fermentas. pEGFP-N2 (Clontech) and pcDNA-3.1C (Invitrogen) were obtained commercially. pSBE4-luc and p3TP-lux constructs were kindly provided by Edward B. Leof (Mayo Clinic Cancer Center, MN, USA). The Nox4 and control siRNAs were synthesized by Metabion (Martinsried, Germany).

2.1.5. Oligonucleotides

Oligonucleotides used in this study were synthesized by İONTEK (Istanbul, Turkey). The complete list of oligonuclotides is given in Table 2.1.

Primer ID	Sequence (5' → 3')	Product Size (bp)
c-Myc-F	CCTACCCTCTCAACGACAGC	248
c-Myc-R	CTCTGACCTTTTGCCAGGAG	
PAI-1-F	CACCCTCAGCATGTTCATTG	188
PAI-1-R	CCAGGTTCTCTAGGGGCTTC	
Nox4-RT-F	TCCTCGGTGGAAACTTTTGT	136
Nox4-RT-R	TGTCCCATATGAGTTGTTCTGG	
Nox4-Ex1-F	GCCAACGAAGGGGTTAAACA	733
Nox4-Ex2-R	CTGGCCCTTGGTTATACAGC	
Nox4-Ex9-F	CGGCTGCATCAGTCTTAACC	163

Nox4-Ex9-R	AGCTTGGAATCTGGGCTCTT	
Smad2-F	CGAAATGCCACGGTAGAAAT	130
Smad2-R	GATTACAATTGGGGCTCTGC	
Smad3-F	CAGAGTGCCTCAGTGACAGC	134
Smad3-R	AGCGAACTCCTGGTTGTTGA	
Smad4-F	TTTGGGTCAGGTGCCTTAGT	142
Smad4-R	TGACACTGACGCAAATCAAAG	
$p27^{Kip1}$-F	GGCCTCAGAAGACGTCAAAC	147
$p27^{Kip1}$-R	ACAGGATGTCCATTCCATGA	
$p15^{Ink4b}$-RT-F	ATGCGCGAGGAGAACAAG	138
$p15^{Ink4b}$-RT-R	GAAACGGTTGACTCCGTTG	
$p15^{Ink4b}$-Ex1-F	CGGGGACTAGTGGAGAAGGT	174(cDNA)-297(gDNA)
$p15^{Ink4b}$-Ex2-R	GGTGAGAGTGGCAGGGTCT	
$p16^{Ink4a}$-F	GGGTCCCAGTCTGCAGTTA	131
$p16^{Ink4a}$-R	GGAGGGTCACCAAGAACCT	
GFP-F	ACTACCTGAGCACCCAGTCC	
GFP-R	CTTGTACAGCTCGTCCATGC	
GAPDH-F	GGCTGAGAACGGGAAGCTTGTCAT	169 (cDNA)
GAPDH-R	CAGCCTTCTCCATGGTGGTGAAGA	272 (gDNA)
Alk4-RT-F	CGTGAAGAACGGTCTTGGTT	153
Alk4-RT-R	GGACCCGTGCTCATGATAGT	
p15-Clon-Iso1&2-F	GATGCCAAGCTTATGCGCGAGGAGAACAAGG	441
p15-Clon-Iso1-R	TTGTCAGAATTCTCAGTCCCCCGTGGCTGTG	

p15-Clon-Iso2-R	ATGCCAGAATTCCTAGGTTCCAGCCCCGATC	261
p21-Clon-F	GATGCCAAGCTTATGTCAGAACCGGCTGGGG	519
p21-Clon-R	AGTCGCGGATCCTTAGGGCTTCCTCTTGGAG	
p15-Seq-Ex1-F	CGTTAAGTTTACGGCCAACG	307
p15-Seq-Ex1-R	ACATCGGCGATCTAGGTTCC	
p15-Seq-Ex2-F	GGGTGAAAACTTTGCAATTAGG	461
p15-Seq-Ex2-R	TGGCAGCCTTCATCGAATTA	
Cdh1-F	AGCGTGTGTGACTGTGAAGG	240
Cdh1-R	CTCTTCTCCGCCTCCTTCTT	
Zeb2-F	TCCTGTCTGTCTCGCAAAAA	193
Zeb2-R	GCCTTGAGTGCTCGATAAGG	
Vimentin-F	CGTCACCTTCGTGAATACCA	169
Vimentin-R	CCAGAGGGAGTGAATCCAGA	
Alk5-F	TGAATCCTTCAAACGTGCTG	207
Alk5-R	TCACAGCTCTGCCATCTGTT	
TGF-betaRI-F	TTGTGGCACGGTGAGAGTGT	865
TGF-betaRI-R	TGCTCCTGGGCTATTGAATCA	
TGF-betaRII-F	GTTAACCGGCAGCAGAAGCT	401
TGF-betaRII-R	ATCAGCCAGTATTGTTTCCC	

Table 2.1: Primer list

2.1.6. Electrophoresis, luciferase assay, spectrophotometer and ELISA readings

Horizontal electrophoresis equipment was from Thermo Scientific (Wilmington, USA). Power supplies Power-PAC200 and Power-PAC300 were from Bio-Rad Laboratories (CA, USA). Protein concentrations were measured by Bradford Assay with the aid of spectrophotometer Beckman Du640, from Beckman Instruments Inc. (CA, USA). Nucleic acid measurements were performed with NanoDrop from Thermo Scientific. Luciferase reporter assay reagents were from Promega. The Reporter Microplate Luminometer Reader was from Turner Bio-Systems (Sunnyvale, USA). ELISA reader was from Beckman Instruments.

2.1.7. Tissue culture materials and reagents

Dulbecco's modified Eagle's medium (DMEM) and Roswell Park Memorial Institute (RPMI) 1640 medium were purchased from GIBCO (Invitrogen, Carlsbad, CA, USA). Opti-MEM medium, penicillin/streptomycin solution, trypsin-EDTA, fetal calf serum (FCS) and Geneticin-sulphate (G418, neomycin) were also from GIBCO. Tissue culture flasks, petri dishes, plates, cryovials were obtained from Corning Life Sciences Incorporated (USA). Serological pipettes were from Costar Corporation (Cambridge, UK). Transfection reagents, namely Oligofectamine, Lipofectamine 2000, and Lipofectamine RNAiMax were purchased from Invitrogen.

2.1.8. Antibodies

Primary and secondary antibodies used throughout the study were commercially obtained from various sources. Working dilutions of primary antibodies are depicted in Table 2.2.

Primary/Secondary Antibody	Company and catalog number	Western Blot (tested dilution)	Immunostaining working dilution
$p15^{Ink4b}$	Santa Cruz, sc612	1:400 (RT) 1:1000 (O/N)	1:1000 (IP)
$p21^{Cip1}$	Calbiochem, OP64	1:100 (RT) 1:250 (O/N)	1:100 (IF, IP)
$p27^{Kip1}$	BD Biosciences, 554069	1:250	1:100 (IF)
p53	BD Biosciences, 554293	1:500 (RT)	-
p-p53	Cell Signaling, 9284	1:500 (O/N)	-
c-myc	Calbiochem, OP10	1:1000 (O/N)	1:150 (IP)
α-tubulin	Calbiochem, CP06	1:10000 (RT) 1:25000 (O/N)	-
Calnexin	Sigma, C4731	1:10000 (RT)	-
$p16^{Ink4a}$	Calbiochem, NA29	1:250 (RT)	-
pRb	BD Biosciences, 554136	1:500 (O/N)	-
Vimentin	Dako, M7020	1:5000 (O/N)	1:500 (IF, IP)
ZO-1	Transduction, 610966	1:2500 (O/N)	1:500 (IF)
p-Smad2	Cell Signaling, 3101	1:1000 (O/N)	1:200 (IF)
p-Smad3	Cell Signaling, 9514	1:1000 (O/N)	1:150 (IF, IP)
Smad2/3	BD Biosciences 610843	1:1000 (O/N)	1:250 (IF)
Smad3	Santa Cruz, sc8332	1:1000 (O/N)	1:200 (IF)
Smad4	Santa Cruz, sc7966	1:1000 (O/N)	1:250 (IF)
GSK3β	Transduction, G22320	1:2500 (O/N)	-

Actin	Santa Cruz, sc1616	1:2000 (O/N)	-
PARP	Santa Cruz, sc8007	1:1000 (O/N)	-
Cleaved Caspase-3 (Asp 175)	Cell Signaling, 9664	1:500 (O/N)	1:150 (IP)
Phospho-pRb	Cell Signaling, 9308	1:1000 (O/N)	-
e-cadherin	Santa Cruz, sc7208	1:2000 (O/N)	-
CK19	Santa Cruz, sc6278	-	1:250 (IF)
PAI-1	Santa Cruz, sc5297	1:500 (O/N)	-
p107, p130	Santa Cruz, sc318 sc317	1:200 (O/N)	-
β-catenin	Santa Cruz, sc7963	1:2000 (O/N)	1:350 (IF)
Nox4	Santa Cruz, sc30141	1:2500 (O/N) 1:750 (RT)	1:250 (IF)
H3K9me1 (rabbit antiserum)	Abcam, Ab9045	-	1:350 (IF)
H3K9me3 (rabbit antiserum)	Upstate, 07-523	-	1:350 (IF)
H3K27me1 (rabbit polyclonal)	Upstate, 07-448	-	1:350 (IF)
H3K27me3 (rabbit polyclonal)	Upstate, 07-449	-	1:350 (IF)
H3K36me3 (rabbit polyclonal)	Abcam, ab9050	-	1:350 (IF)
BrdU	DAKO, M0744	-	1:500 (IF, IP)
Anti-mouse-HRP	Sigma, A0168	1:5000	-
Anti-rabbit-HRP	Sigma, 6154	1:5000	-
Anti-mouse/rabbit-Alexa Fluor 488	Invitrogen, A11034	-	1:750 (IF)

Anti-mouse/rabbit-Alexa Fluor 568	Invitrogen, A11031	-	1:600 (IF)
WHSC1	Abcam, 75359	1:5000 (O/N)	1:1000 (IF)

Table 2.2: Antibody dilutions and working conditions

2.1.9. Restriction endonucleases

All restriction enzymes used in this study were purchased from Fermentas. T4 DNA ligase was from Promega.

2.1.10. Immunoperoxidase staining reagent

In immuno-peroxidase staining experiments; DAKO EnVision+ System was used, DAKO (Glostrup, Denmark).

2.2. SOLUTIONS AND MEDIA

2.2.1. Electrophoresis buffers

50X Tris-acetic acid-EDTA (TAE)	2 M Tris-acetate, 50 mM EDTA pH 8.5 Diluted to 1X for working solution.
Ethidium bromide	10 mg/mL in water (stock solution), 30 ng/mL (working solution)

6X Gel loading dye solution	10 mM Tris-HCl (pH 7.6), 0.03% bromophenol blue, 0.03% xylene cyanol**,** 60% glycerol, 60mM EDTA (0.5M pH8.0)

2.2.2. Reagents used in bacteria experiments

Luria-Bertani medium (LB)	10 g bacto-tryptone, 5 g bacto yeast extract, 10 g NaCl. For agar plates, add 15 g/L bacto agar.
Ampicillin	100 mg/mL solution in double distilled water, sterilized by filtration and stored at -20°C (stock solution). 100 μg/mL (working solution)
Kanamycin	300 mg/mL solution in double-distilled water sterilized by filtration and stored at -20°C (stock solution). Working solution was 30 μg/mL.

SOB medium	20 g tryptone (2%), 5 g yeast extract (0.5%), 0.584 gr NaCl (10 mM), 0.1864 g KCl (2.5 mM) autoclaved to sterilize. Then, 2.46 g MgSO4 and 2.03 g $MgCl_2$ (10 mM) are added.
SOC medium	SOB + 20 mM glucose from filter sterilized 1M glucose stock solution in ddH2O.
Transformation Buffer (TB)	10 mM K.PIPES, 55 mM $MnCl_2$, 15 mM $CaCl_2$, 250 mM KCl. Filter sterilize and store at 4^oC.

2.2.3. Cell culture solutions

DMEM/RPMI working medium	10% FBS/FCS, 1% penicillin/ streptomycin, 1% non-essential amino acid. Store at 4^oC.
10X Phosphate-buffered saline (PBS)	80 g NaCl, 2 g KCl, 14.4 g Na_2HPO_4, 2.4 g KH_2PO_4, pH 7.4. Store at 4^oC.

2.2.3.1. Antibiotics and reconstitution of TGF-β1

Geneticin-G418 (Sulfate)	500 mg/mL solution in double-distilled water. Sterilized by filtration and stored at -20°C (stock solution).
Puromycin	2 mg/mL in double-distilled water (stock solution). Sterilized by filtration (0.2 μm pores) and stored at -20°C.
Doxocycline	1 mg/mL stock solution in 70% ethanol, sterilized by filtration (0.2 μm pores) and stored at -20°C.

2.2.3.2. Reconstitution of TGF-β1

Reconstitute at a concentration of no more than 10 μg/mL in filter sterilized 4 mM HCl containing 1 mg/mL bovine serum albumin to ensure complete recovery from glass surfaces. Reconstitute TGF-β1 antibody (monoclonal mouse IgG_1) at 0.5 mg/mL in sterile PBS.

2.2.4. Western blotting reagents

NuPAGE pre-cast 4-12% gradient or 10% Bis-Tris mini gels were purchased from Invitrogen. MES and MOPS running buffers and 20X transfer buffer were also

obtained commercially from Invitrogen. 4X sample loading buffer, 10X denaturing agent and antioxidant used in immunoblotting were also from Invitrogen.

NP-40 lysis buffer	150 mM NaCl, 50 mM TrisHCl (pH 8.0), 1% NP-40, 1x protease inhibitor (from 25X conctail) in double-distilled water.
Modified RIPA lysis buffer	10 mM Tris-HCl (pH 7.6), 5 mM EDTA, 50 mM NaCl, 30 mM sodium pyrophosphate, 50 mM sodium fluoride, 100 μM sodium orthovanadate, 1% TritonX-100 and 1X protease inhibitor complex in double-distilled water.
10X Tris buffered saline (TBS)	12.2 g Trisma base, 87.8 g NaCl in 1 liter ddH_2O, pH 7.8.
TBS-tween (TBS-T)	0.2% Tween-20 was dissolved in 1x TBS.
Ponceau S	0.1% (w/v) Ponceau, 5 % (v/v) acetic acid in double-distilled water.

Blocking solution	5% (w/v) non-fat dry milk/bovine serum albumin in 0.2% TBS-T.

2.2.5. Immunohistochemistry solutions

Blocking solution	10% FBS, 0.1% Triton-X in 1x PBS.
DAPI (4', 6-diamino-2-phenylindole)	0.1-1 μg/mL working solution in double-distilled water.

2.2.6. Senescence associated β-galactosidase (SABG) assay solution

SABG buffer	40 mM citric acid/sodium phosphate buffer (pH 6.0), 5 mM potassium ferrocyanide, 5 mM potassium ferricyanide, 150 mM NaCl, 2 mM $MgCl_2$, 1 mg/mL X-gal (from 40 mg/mL stock solution) in ddH_2O. Adjust pH to 6.0, and filter the solution before use.

2.2.7. BrdU stock preparation

BrdU stock solution	Stock: 10 mg/mL BrdU in ddH_2O. (Working solution is 30 μM, 9.2 μl in 10 mL culture medium).

2.2.8. Cell cycle analysis solutions

Propidium Iodide staining solution	50 µg/mL propidium iodide, 0.1 mg/mL RNase A and 0.05% TritonX-100 in 1X PBS.

2.3. METHODS

2.3.1. General laboratory methods

2.3.1.1. Agarose gel electrophoresis of DNA

DNA fragments were separated by horizontal electrophoresis using standard running buffers and loading solutions. DNA fragments less than 1 kb were generally separated on 2.0% agarose gel, whereas those larger than 1 kb were typically run on 0.8 or 1.0% agarose gels. Agarose gels were completely dissolved in 1X TAE buffer in microwave. Ethidium bromide was added to a final concentration of 30 µg/mL. The DNA samples were mixed either with 6X bromo-phenol blue or 6X xylene cyanol loading buffer and loaded onto gels. The gel was usually run at 100-120 V at room temperature until the fragments were spatially separated. Nucleic acids were visualized under ultraviolet light and size was estimated in comparison to standard DNA size markers (100 bp ladder and 1 kb ladder).

2.3.1.2. Restriction enzyme digestion of DNA

These reactions were routinely performed in 20 or 50 µl reaction volume depending on the quantity of the DNA material to be digested. Generally the reaction

was carried out for 2-3 hr or sometimes for large quantities like 5-10 µg of plasmid DNA for O/N, supplemented with 5-15 units of restriction enzymes at 37^0C. Appropriate reaction buffers were utilized for digestion reactions according to manufacturer's recommendations. In case of double digestion with two different restriction enzymes, web page (http://www.fermentas.com/doubledigest/index.html) was visited in order to determine the recommended buffer for the reaction.

2.3.1.3. Databases and software tools

All the necessary information regarding the gene of interest was deduced from NCBI and Ensembl Genome Browser. Primers were designed according to the instructions given in the online web tool Primer3 (http://frodo.wi.mit.edu/primer3/). Promoter prediction tools and corresponding web pages were given throughout the following pages.

2.3.2. Cell culture methods

All cell lines used in this study were grown in media supplemented with 10% fetal calf serum (FCS), 1% non-essential amino acids, 100 mg/mL penicillin/streptomycin at 37^0C and 5% CO_2. Huh7, HepG2, Hep3B, Hep3B-TR, Hep40, PLC/PRF-5, Mahlavu, Focus,SkHep1 and A431 cell lines were cultured in DMEM, whereas the rest of the cell lines including SNU182, SNU387, SNU398, SNU423, SNU449, SNU475 were cultivated in RPMI growing media.

2.3.2.1. Cryopreservation of stock cells

Cells were recovered by 5 mL of DMEM/RPMI after trypsin treatment. They were the centrifuged at 1500 rpm for 3-5 minutes. After washing with 5 mL 1X PBS, cells were again spinned down at 1500 rpm for 3-5 minutes. The pellet was then resuspended in 1 mL of ice cold Freezing medium containing complete growth

medium supplemented with 10% FCS and 8% DMSO after which the cell suspension was transferred to freezing vials. Cells were left at -20^{0}C for 1 hour and transferred to -80^{0}C for long term storage. In case of availability cells were transferred to nitrogen tank after O/N storage at -80^{0}C.

2.3.2.2. Thawing of frozen cells

One vial of the frozen cell line was taken from the nitrogen tank or -80^{0}C fridge and put into ice immediately. The vial was then placed into water bath at 37^{0}C until the ice became a cell suspension. The cells were resuspended gently using a pipette and transferred to 15 mL falcon tube with 5 mL of medium. Cells were then centrifuged at 1500 rpm for 3-4 minutes to get rid of the DMSO which was discarded following centrifugation by removing the supernatant. The pellet was then resuspended in complete culture medium with 20% FCS to be plated into suitable culture disk and/or flask. Cells were left O/N in culture and the following morning culture medium was refreshed.

2.3.2.3. Transfection of cell lines

2.3.2.3.1. Transfection of cell lines using Lipofectamine2000

In general, transfections were carried out in 6-well plates with a 3:1 Lipo2000:DNA ratio. One day before transfection, subconfluent cells (4 x 10^5 cells) were plated into 6-well plates in 2.5 mL of growth medium without antibiotics so that the cells would be 90-95% confluent at the time of transfection. For each transfection sample, plasmid DNA (4 µg) was diluted in 250 µL of Opti-MEM Reduced Serum Medium and mixed gently. Meanwhile, 12 µL mixed Lipofectamine2000 was diluted in 250 µl Opti-MEM medium and incubated for 5-10 minutes at room temperature. After incubation period, the diluted plasmid DNA was combined with diluted Lipofectamine2000 (total volume = 500 µl). Afterwards, the complex was mixed very gently and incubated for another 20-25 minutes at room

temperature. During this incubation period, cells were rinsed twice with 1X PBS and supplemented with 2 ml Opti-MEM growth medium. Finally, after incubation was over, the complex was added to each well and the plates were incubated at 37^0C in the CO_2 incubator. Six to eight hr later, the transfection medium was replaced with normal growth medium without antibiotics until the assay to be performed.

2.3.2.3.2. Transfection of cell lines using FuGene-6

Transfections with Fugene-6 Transfection Reagent were performed in 6-well plates with optimized Fugene-6:DNA ratios (3:1) and desired cell density. In brief; one day prior to transfection, cells were trypsinized, counted manually and seeded at a density of 2 x 10^5/per well to achieve the desired density of confluency at the day of transfection. During transfection procedure, 3 µL Fugene-6 Transfection Reagent was diluted with 97 µL serum-free medium (without antibiotics). The tube was vortexed or flicked for one second and incubated at room temperature for 5 minutes. Meanwhile, 1 µg of plasmid DNA was added directly into the medium without allowing contact with the tube wall. Then, the transfection reagent:DNA mixture was allowed to incubate at room temperature for 20-30 minutes which was followed by addition of the complex to the cells in a drop-wise fashion. Finally, 6-well plates were cultivated in the incubator for 12-48 hr until the time of assay.

2.3.2.3.3. Transfection of cell lines using Lipofectamine RNAiMax

Scrambled (unsilencing) and human Nox4 RNAi duplexes were obtained commercially from Metabion (Martinsried, Germany). The sense oligo sequences were as follows: 5'-GUAAGACACGACUUAUCGC-3' (unsilencing), and 5'-GCCUCUACAUAUGCAAUAA-3' (Nox4 specific). For transient siRNA transfection, Huh7 cells, at 30-50 % of confluency in 6-well plate were transfected using Lipofectamine RNAiMAX in Opti-MEM Medium as recommended by the manufacturer, with a final siRNA duplex concentration of 10 nM. Cells were left in

culture for 24h, then trypsinized and seeded in 24-well and/or 6-well plates. Effects of TGF-β (5 ng/mL) were analyzed after 72 h of treatment.

2.3.3. Luciferase reporter assay

pSBE4-luc and/or p3TP-lux reporter constructs were co-transfected with pRL-TK (Promega) that contains the herpes simplex virus thymidine kinase promoter to provide Renilla luciferase expression as an internal control. Transfection experiments were performed in triplicates in 24-well plates using Lipofectamine2000 in accordance with manufacturer's instructions. Transfection was done with 200 ng of reporter vector plus 3 ng of pRL-TK. Six-hour post-transfection, cells were supplemented with 5 ng/mL TGF-β1-containing growth medium and incubated for an additional 24 hr in culture before reporter assay. The luciferase reporter assay was performed using Dual-Glo Luciferase assay kit (Promega) as instructed by the manufacturer. The luminescence intensity of Firefly luciferase was normalized to Renilla luciferase.

2.3.4. Bromodeoxyuridine (BrdU) labelling

To identify cells with permanent cell cycle arrest associated with senescence, subconfluent cells treated with different doses of TGF-β in triplicate were incubated with 30 μM bromodeoxyuridine (BrdU) for 24 hr in freshly added TGF-β-containing culture medium, then fixed with ice-cold 70% ethanol for 10 min at -20°C. After DNA denaturation in 2N HCl for 20 minutes, cells were incubated with monoclonal anti-BrdU antibody (1 hr) and followed by incubation with 1:1000 dilution anti-mouse Alexa Fluor 488 (1 hr) and DAPI counterstaining (60 sec).

2.3.5. RNA extraction and cDNA synthesis

Total RNAs from cultured cells were isolated using the NucleoSpin RNA II Kit (Macherey-Nagel) according to the manufacturer's protocol. First-strand cDNA

synthesis was carried out using 2 µg of DNase I-treated total RNA as a template utilizing the RevertAid First Strand cDNA synthesis kit (Fermentas). cDNAs were stored at -20°C. Corresponding cDNAs were subjected to semi-quantitative reverse transcriptase PCR (RT-PCR) and quantitative PCR (qRT-PCR) amplification using specific primers.

2.3.6. Semi-quantitative and quantitative real-time RT-PCR assays

PCR assays were performed using appropriate primers. Thermal cycler conditions were an initial denaturation step at 95°C for 5 min; a loop cycle of 95°C for 30 sec, at 60^0C for 30 sec, at 70^0C for 30sec; and a final extension at 72°C for 5 minutes. All primers used for PCR amplifications in this study work at 60^0C.

Quantitative expression analyses were performed using SYBR Green I (Invitrogen) and DyNAmo HS SYBR Green qPCR Kit F-410 (Finnzymes) on iCycler iQ real-time RT-PCR machine (Bio-Rad) and Mx 3005P (Stratagene). The PCR reaction was performed according to the manufacturer's instructions.

Reactions were set up in a total volume of 20 µl with 1-2 µl cDNA for each sample. Reactions were initiated with 10 minutes initial denaturation at 95ºC, then amplification was run for 45 cycles (30 seconds at 95ºC, 30 seconds at 60^0C, 30 seconds at 72ºC) Expression levels were calculated using the following formula:

$R = (E_{target})^{\Delta Ct_{target}(control-sample)} / (E_{ref})^{\Delta Ct_{ref}(control-sample)}$. In the above formula E_{target} and E_{ref} represent the primer efficiencies for target and reference genes, respectively. PCR amplification efficiencies for the genes range between 1.9 and 2.0. All experiments were performed in triplicates. GAPDH and β-actin were used as internal controls in qRT-PCR experiments.

2.3.7. Western blotting

Cells treated with different doses of TGF-β for 72 hr were lysed with a slightly modified Radio-Immunoprecipitation Assay (RIPA) Buffer (10 mM Tris-HCl, pH 7.6, 5 mM EDTA, 50 mM NaCl, 30 mM sodium pyrophosphate, 50 mM sodium fluoride, 100 μM sodium orthovanadate, 1% TritonX-100 and 1X protease inhibitor complex (Roche, Indianapolis, USA). Cconcentrations of protein lysates were measured by the conventional Bradford assay utilizing spectrophotometer at 595 nm. Sample protein concentrations were normalized in accordance with bovine serum albumin (BSA) protein of a known concentration.

25 μg of total protein was subjected to gel electrophoresis using NuPAGE system with MES and/or MOPS buffers. Proteins were wet-transferred onto HyBond ECL nitrocellulose or PVDF membranes, depending on the protein of interest. The membranes were blocked for 1 hr at room temperature with either 5% non fat dry milk or BSA in TBS-T, depending on the specific antibodies used. Membranes were incubated with the primary antibodies either at room temperature for 1 hr, or overnight at +4ºC. Following primary antibody incubations and extensive washing with TBS-T, secondary antibodies conjugated with horse-radish peroxidase (HRP) were incubated 1 hour at room temperature. After an additional wash of half an hour, chemiluminescent reaction was detected using ECL+ western blot detection kit (Amersham, UK), according to the manufacturer's protocols. X-ray films were exposed to the emitted chemiluminescence, duration depends on the specific antibody.

2.3.8. Enzyme-linked immunosorbent assay

Coating of Immulon 2HB plates (Thermo, USA) was done with monoclonal antibodies against human cytokines IL-6 and IL-8. Coating incubations were essentially run at +4°C overnight with 1-5 μg/mL antibody concentrations in 1x PBS. For coating, 50 μL of the antibody dilutions were distributed in wells. Following O/N coating, anti-cytokine solution was discarded and wells were blocked with 200

μL blocking buffer O/N at +4°C. Washing step was performed 5 times for 5 min each. Following washing, plates were rinsed twice with distilled water and dried by tapping. Next, collected supernatants were incubated in 96-well plates at a final volume of 50 μL/well for each cytokine. Corresponding recombinant cytokines were serially distributed. Corresponding recombinant cytokine standards were serially diluted by two-fold starting from 1000 ng/mL concentration in 1x PBS for 11 times. Plates were incubated at +4°C overnight. Following cytokine and supernatant incubations, plates were rinsed and dried as previous washing steps. Meanwhile, biotin-conjugated anti-cytokine antibodies were freshly prepared in T-cell buffer with a 1:1000 dilution, added in the wells with a final volume of 50 μL/well and incubated for another 2 hr at RT. After a series of washing steps, 50 μL of streptavidin-conjugated alkaline-phosphatase solution (SA-AKP, Pierce, USA) diluted in T-cell buffer was administered to the wells. After 1 hr of incubation at RT, washing and drying steps were repeated. Finally, 1 tablet fresh PNPP substrate (Pierce, USA) was dissolved in 4 mL ddH_2O + 1 mL buffer and distributed onto the wells as 50 μL aliquots. Development of yellow color was followed continuously and multiple OD readings (at 405 nm) were recorded by ELISA reader (Molecular Devices). The OD measurements were analyzed at SoftMax Pro v5 software. The OD readings were terminated when 4-parameter standard curve was reached. Amount of released cytokines were calculated with respect to control recombinant standards.

2.3.9. Plasmid construction and transient antibiotic selection

Human $p15^{Ink4b}$ and $p21^{Cip1}$ were reverse transcribed from total RNA of Hep40 and HepG2 cells, respectively, using the unique Phusion DNA polymerase (Finnzymes). Both $p15^{Ink4b}$ isoform sequences were reverse transcribed with primers (5'-ATGCCAAGCTTATGCGCGAGGAGAACAAGG-3' and

5'-TTGTCAGAATTCTCAGTCCCCCGTGGCTGTG-3') and cloned into pcDNA-3.1-C/Neomycin (Invitrogen) using the *Hind*III and *Eco*RI restriction enzymes and

sequence verified. $p21^{Cip1}$ cDNA was amplified using primers (5'-GATGCCAAGCTTATGTCAGAACCGGCTGGGG-3' and 5'-AGTCGCGGATCCTTAGGGCTTCCTCTTGGAG-3'), cloned into pcDNA3.1(+)/Hygromycin (Invitrogen) harboring *Hind*III and *Bam*HI restriction enzymes and sequence verified. For transfection, empty vectors and $p15^{Ink4b}$ and $p21^{Cip1}$ gene expressing plasmids were transfected into Huh7 cells using Lipofectamine2000 as stated previously. Huh7 cells transfected with $p15^{Ink4b}$ and $p21^{Cip1}$ expression plasmids, along with corresponding empty vectors, were selected with 700 μg/mL Geneticin-G418 (Gibco, USA) and/or 200 μg/mL Hygromycin-B (Roche, Indianapolis, USA), respectively, for eight days in culture.

2.3.10. Immunoperoxidase and immunofluorescence staining

Both methods were performed essentially similar. Except that secondary antibody incubations and visualizations were different. For immunoperoxidase staining, cells were fixed with 4% formaldehyde and permeabilized with phosphate-buffered saline (PBS) supplemented with 0.5% saponin (Sigma) and 0.3% TritonX-100 (Sigma). After blocking for 1 hour in blocking solution (10% fetal calf serum and 0.1% TritonX-100 in PBS), cells were incubated with primary antibodies for 1 hour in PBS containing 2% fetal calf serum and 0.1% TritonX-100 solution. After washing with PBS, cells were incubated for 30 min with Cytomation Envision+Dual link system-HRP (Dako), and eventually the staining was performed with DAB detection solution (Dako). Cover slips were then rinsed with distilled water and counterstained with haematoxylin (Sigma) for 3-4 min, mounted on glass microscopic slides using 90% (v/v) glycerol and examined under light microscope.

For immunofluorescence staining, fixed and permeabilized cells were incubated 1 hr with anti-mouse or anti-rabbit Alexa Fluor 488 and Alexa Fluor 568 secondary antibodies. Following secondary antibody incubations, cells were counterstained using 1:10000 4', 6-diamidino-2-phenylindole, DAPI for 1 min.

Coverslips were mounted onto glass slides with ProLong Gold antifade reagent (Invitrogen).

2.3.11. Fluorescent-activated flow cytometry analysis of cell cycle distribution

Cells were treated with TGF-β for indicated time points and harvested respectively. Post incubation with TGF-β, cells were rinsed with PBS and collected by trypsinization. Cells were pelleted and resuspended in 1 mL 1XPBS and added up to 3.5 mL and fixed for 15 min with 70% ice-cold ethanol on ice. Fixed cells were collected by centrifugation and resuspended in PI-solution (50 μg/mL propidium iodide, 0.1 mg/mL RNase A and 0.05% TritonX-100), and incubated 40 min at 37°C. Following centrifugation at 1500 rpm for 3 min, fluorescently stained cells were transferred to polystyrene tubes with 600 μL PBS and analyzed using FACSCalibur Flow Cytometer (BD Biosciences). Cell cycle arrest was assessed through analysis of the proportion of cells in the G1, S, and G2/M fraction of the cell cycle using Cell Quest 3.2.

2.3.12. Measurement of intracellular ROS production

Endogenous amounts of ROS were qualified with 2', 7'-dichlorofluorescein diacetate (DCFH-DA, Fluka). Cellular fluorescence staining and intensity was visualized with fluorescence microscope after 30 min of incubation with 10 μM DCFH-DA. 100-150 nM MitoTracker Red was used as a counterstain (Molecular Probes).

2.3.13. Senescence-associated β-galactosidase (SA-β-Gal) assay

Cells were rinsed twice with 1XPBS and fixed with 4% formaldehyde (diluted in 1XPBS from 37% stock solution) for 10 min at room temperature. After

two additional washes with PBS, cells were allowed to stain in SABG buffer. Blue staining was visible under the light microscope after incubation for 12-16 hr at 37°C in CO_2-free incubator.

2.3.14. In vivo tumor assays

Huh7, Hep3B and Hep3B-TR cells (5 million) were suspended in 250 μL PBS, and injected subcutaneously on the back shoulders of Balb/c *nude* mice and animals were examined for palpable tumors on a weekly basis. Intratumoral injection of ~50 μL of 10 ng/mL TGF-β1 solution was initiated when Huh7 tumors reached easily palpable sizes. Control Huh7 tumors were treated similarly with vehicle.

CHAPTER 3. RESULTS

3.1. Differential expression of TGF-β1 in normal liver, cirrhosis, and hepatocellular carcinoma

Recently, TGF-β1 has been implicated in liver disease processes. Based on earlier findings on increased hepatic levels of TGF-β in cirrhosis and HCC, we first analyzed TGF-β1 expression in normal liver, cirrhosis and HCC, using the publicly available dataset generated by Wurmbach et al. (Wurmbach et al., 2007). This microarray dataset was established during a study in which the main concept was to define the molecular mechanisms of hepatocarcinogenesis and designate novel therapeutic candidates for liver cancer. In this microarray analyses, the gene expression profiles of 75 tissue samples were conducted. These samples represent the gradual hepatocarcinogenesis process. Sample pathological grades start from preneoplastic lesions such as cirrhosis and dysplasia and eventually evolve into neoplastic lesions including 4 different stages characterized with metastatic tumors from patients with HCV infection, namely very early HCC, early HCC, advanced HCC and very advanced HCC.

In order to analyze the differential expression pattern of TGF-β1 among various disease stages of liver, we queried TGFB1 gene in Wurmbach et. al. microarray data. Of two probe-sets reported to represent TGF-β1 (203084_at, 203085_s_at), 203085_s_at demonstrated statistically significant values between different paired disease stages, hence was used for further analyses. TGF-β1 expression displayed a bell-shaped distribution with a sharp increase in cirrhosis (cirrhosis versus normal liver, $P < 0.001$), followed by a progressive decrease in early HCC (early HCC versus cirrhosis, $P < 0.02$) and advanced HCCs (Figure 3.1).

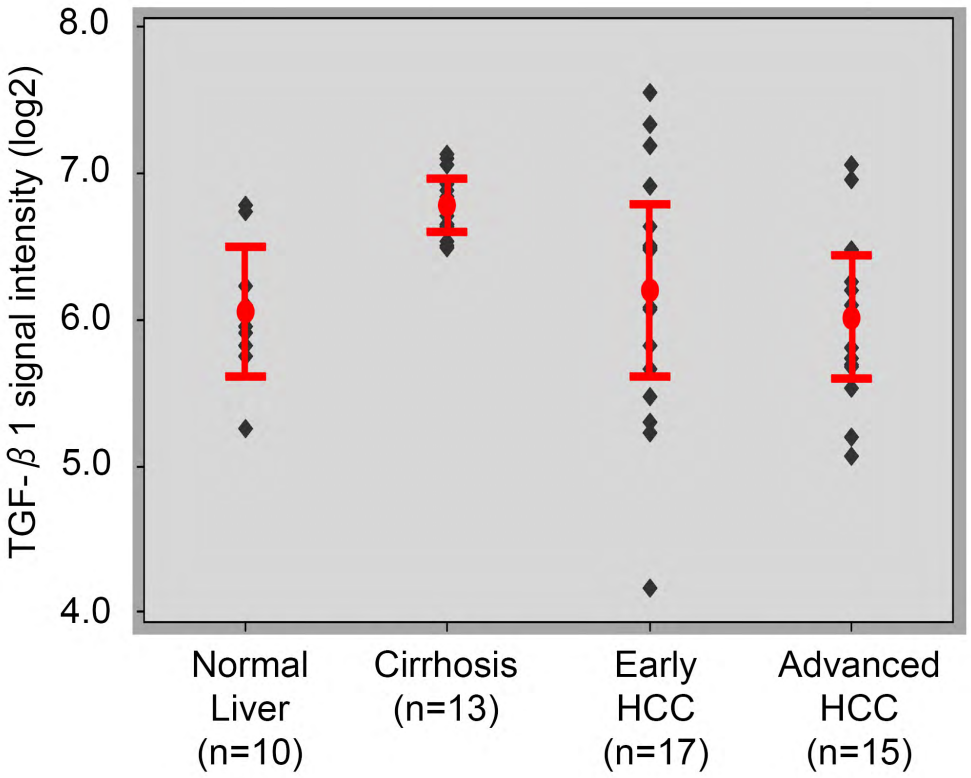

Figure 3.1: Expression analysis of TGF-β1 in liver diseases. Regrouped samples were categorized into four; representing each liver tissue stage as normal liver (n=10), cirrhosis (n=13), early HCC (n=17) and advanced HCC (n=15). Distribution of normalized and log(2) transformed TGF-β1 probe-set signal intensity for each relavant-sample was drawn to scale. Mean values obtained for different samples were indicated with a red full-circle. Two-sided interval bars were drawn with a 95% confidence interval for the mean. TGF-β1 expression was substantially increased in cirrhosis samples as compared to normal liver samples ($P < 0.001$). Thereafter, the expression of TGF-β1 displayed a significant decrease between cirrhosis and early HCC samples ($P < 0.02$). Expression change of TGF-β1 was not significant between early and advanced HCC samples ($P = 0.485$) (Senturk et al., 2010).

Curiously, this expression pattern displayed almost a perfect correlation with reported frequencies of SA-β-Gal activities in normal liver, cirrhosis and HCC with lowest and highest rates in normal liver and cirrhosis, respectively (Ikeda et al., 2009a; Ikeda et al., 2009b; Kim et al., 2009a; Paradis et al., 2001; Wiemann et al., 2002).

3.2. TGF-β signaling pathway in well-differentiated (WD) HCC cell lines

3.2.1. Expression of critical TGF-β signaling components

Based on this co-occurrence of TGF-β expression pattern and senescence in liver diseases, we hypothesized that this cytokine would be causally implicated in hepatocellular senescence. In order to test this hypothesis, we initialized our studies on a panel of "well-differentiated" HCC cell lines, including Huh7, Hep40, HepG2, PLC and Hep3B. Well-differentiated HCC cell lines display e-cadherin expression and epithelial-like morphology and share many features with normal hepatocytes (Yuzugullu et al., 2009). They also share the same TGF-β early response gene expression patterns with normal hepatocytes (Coulouarn et al., 2008). All five cell lines, based on studies with semi-quantitative RT-PCR, expressed TGF-β1 ligand, and all critical components of TGF-β signaling pathway including its receptors (*TGFBR1* and *TGFBR2*) and SMADs (Figure 3.2).

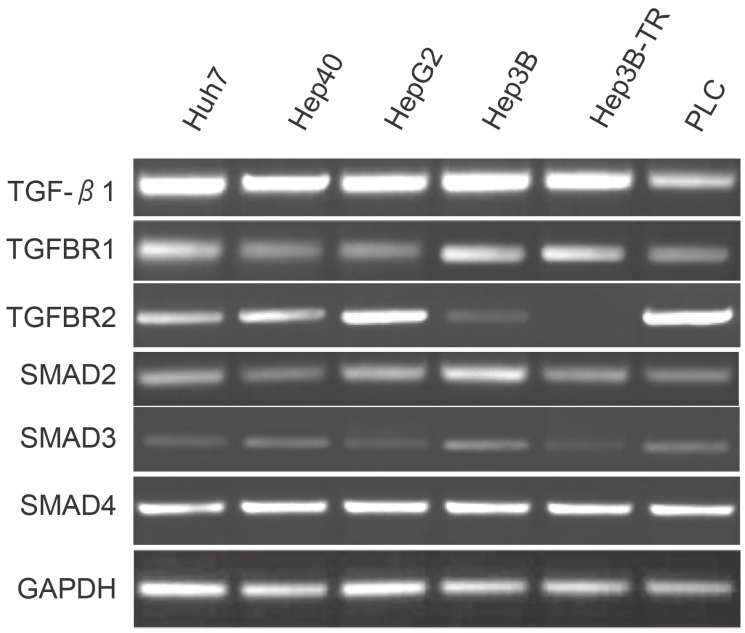

Figure 3.2: Expression of TGF-β signaling pathway components in well-differentiated HCC cell lines. Expression levels of these particular genes ware studied by RT-PCR analysis of cDNAs extracted from different cell lines. Hep3B-TR lacked TGFBR2 expression.

Hep3B-TR (TR: TGF-β resistant) cell line which displayed a loss of *TGFBR2* expression and was used for control experiments. This cell line was originally derived from Hep3B cell line through sustained exposure to increasing doses of TGF-β1 and has been reported to harbor a homozygous deletion as we also confirmed through PCR-based amplification of this particular locus with genomic oligo-pairs (Figure 3.3) (Hasegawa et al., 1995; Inagaki et al., 1993).

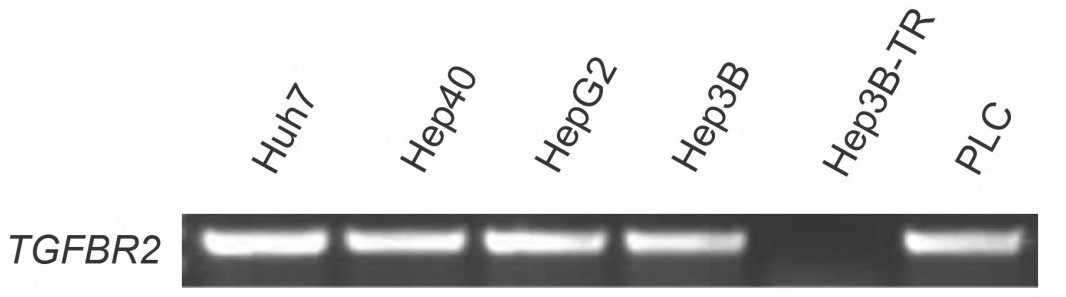

Figure 3.3: PCR analysis of TGFBR2 in genomic DNAs displayed no amplification in Hep3B-TR cells indicating homozygous deletion.

3.2.2. Intact TGF-β signaling in well-differentiated HCC cell lines

There are several ways to analyze intactness of a growth factor stimulated signal transduction pathway. Expression patterns of growth factor regulated target genes, as well as promoter activities using luciferase reporter-based systems shall be explored in this regard. Here, we used a firefly luciferase-based assay to assess the intactness of the signaling pathway as well as responsiveness of WD cell lines to TGF-β treatment. All five HCC cell lines displayed intact TGF-β signaling activity, as tested by pSBE4-Luc reporter activity. pSBE4-Luc plasmid is an artificial mammalian TGF-beta-inducible Smad2/3-responsive construct which contains four tandem copies of human SMAD3 and SMAD4 binding elements (5 bp sequence CAGAC, however 4 bp CAGA suffices for activation) upstream of a minimal promoter adjoining a luciferase reporter (Zawel et al., 1998). Such SBEs are often present in TGF-β-responsive regions of target genes. Inserts containing 8 bp palindromic SBE sequences were generated by ligation of concatamerized oligonucleotides to pGL3-basic. The complementary oligonucleotides used for

reporter construction were 5'-TAAGTCTAGACGGCAGTCTAGACGTAC-3' and 5'-GTCTAGACTGCCGTCTAGACTTAGTAC-3'.

Following 6 hr post Lipofectamine-based transfection of all cell lines with pSBE4-Luc in 24-well plates, together with pRL-TK (a vector developed for internal control, encodes Renilla luciferase under the control of herpex simplex virus thymidine kinase promoter), the transfection medium containing OPTI-MEM was replaced with standard growth medium supplied with TGF-β1. After performing Dual-Glo luciferase assay measurements using luminometer firefly luciferase signal intensities were normalized with similarly obtained renilla luciferase signals. Therefore, 24 hr 5 ng/mL (200 pM) TGF-β1 treatment of cells yielded 9 to 19-fold induction of pSBE4-Luc reporter activity in all cell lines with the exception of non-responsive Hep3B-TR cells (Figure 3.4).

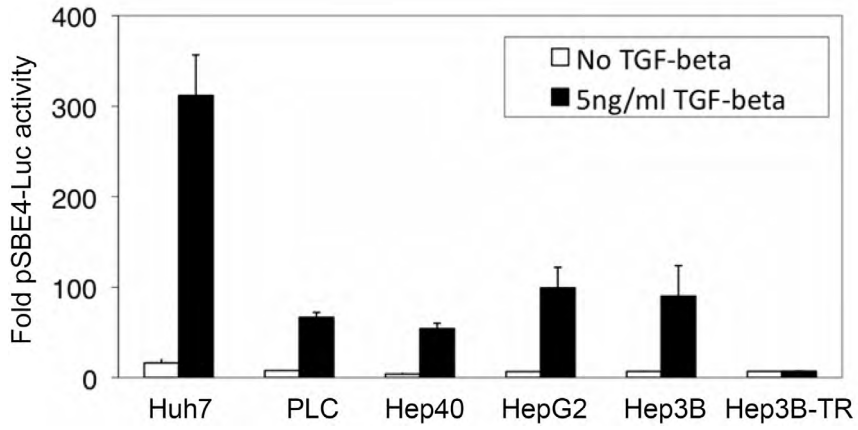

Figure 3.4: Well-differentiated HCC cell lines are competent for TGF-β-signaling activity. Cells were co-transfected with pSBE4-Luc and control pRL-TK plasmids, and treated with or without TGF-β1 (5 ng/mL) for 24 hr. The luciferase activity was measured and expressed as fold activity of pSBE4-Luc/pRL-TK (mean ± SD; n=3).

3.2.3. TGF-β stimulated transcriptional responsiveness in well-differentiated HCC cell lines

Similarly, we also did another luciferase reporter-based study using p3TP-lux, a reporter that is empirically designed to obtain maximal TGF-β responsiveness.

Along intactness of the pathway, it simply measures transcriptional responsiveness of cells to TGF-β and Activin growth factors as well. p3TP-lux contains a portion of the TGF-β–response element of plasminogen activator inhibitor-1 (*PAI-1*) gene promoter along with three repeats of the collagenase I AP-1 site in front of a luciferase reporter (Wrana et al., 1992). Accordingly, upon TGF-β1 stimulation, the signal intensity obtained from p3TP-lux response is anticipated to be quite different form pSBE4-luc reporter. As expected, p3TP-lux reporter analyses displayed different results when compared to pSBE4-luc (Figure 3.5). Unlike very high and similar endogenous pSBE4-luc reporter activity among untreated controls, p3TP-Lux reporter activity has very low and incomparably distinct values which make it difficult to draw in an "in-scale" figure. Thereby, for simplicity the results for p3TP-Lux are depicted as "fold change" instead of "fold activity".

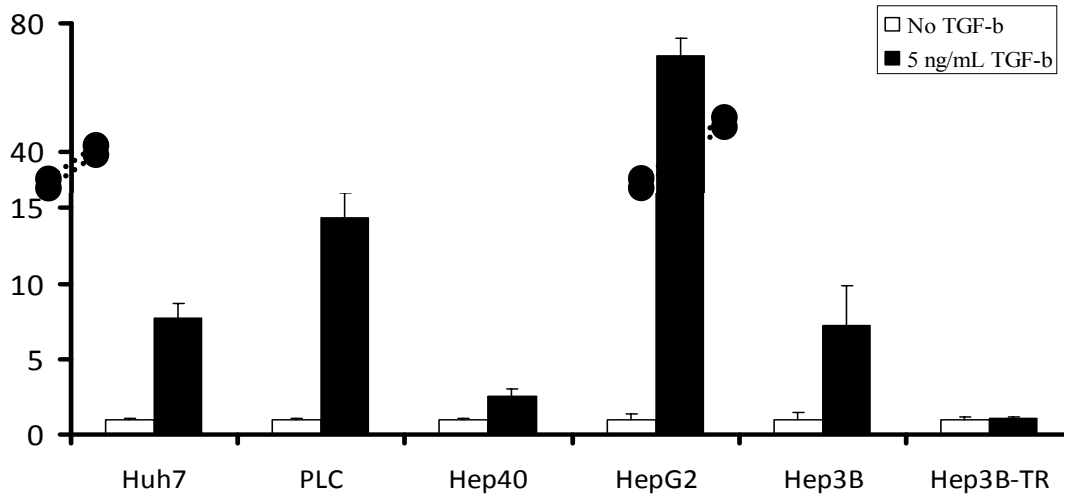

Figure 3.5: Well-differentiated HCC cell lines demonstrate differential transcriptional responses to TGF-β treatment. Cells were co-transfected with p3TP-Lux and control pRL-TK plasmids, and treated with or without TGF-β1 (5 ng/mL) for 24 hr. The luciferase activity was measured and expressed as fold change of p3TP-Lux/pRL-TK (mean ± SD; n=3).

Following reporter assays, we also analyzed TGF-β1-regulated expression of plasminogen activator inhibitor-1 (*PAI-1*), a well characterized TGF-β target gene

(Sandler et al., 1994) in selected three cell lines. TGF-β1 treatment induced PAI-1 protein expression in Huh7 and Hep3B cells, but not in Hep3B-TR cell line (Figure 3.6-A) and this was associated with induced expression of PAI-1 transcripts (Figure 3.6-B and 3.6-C).

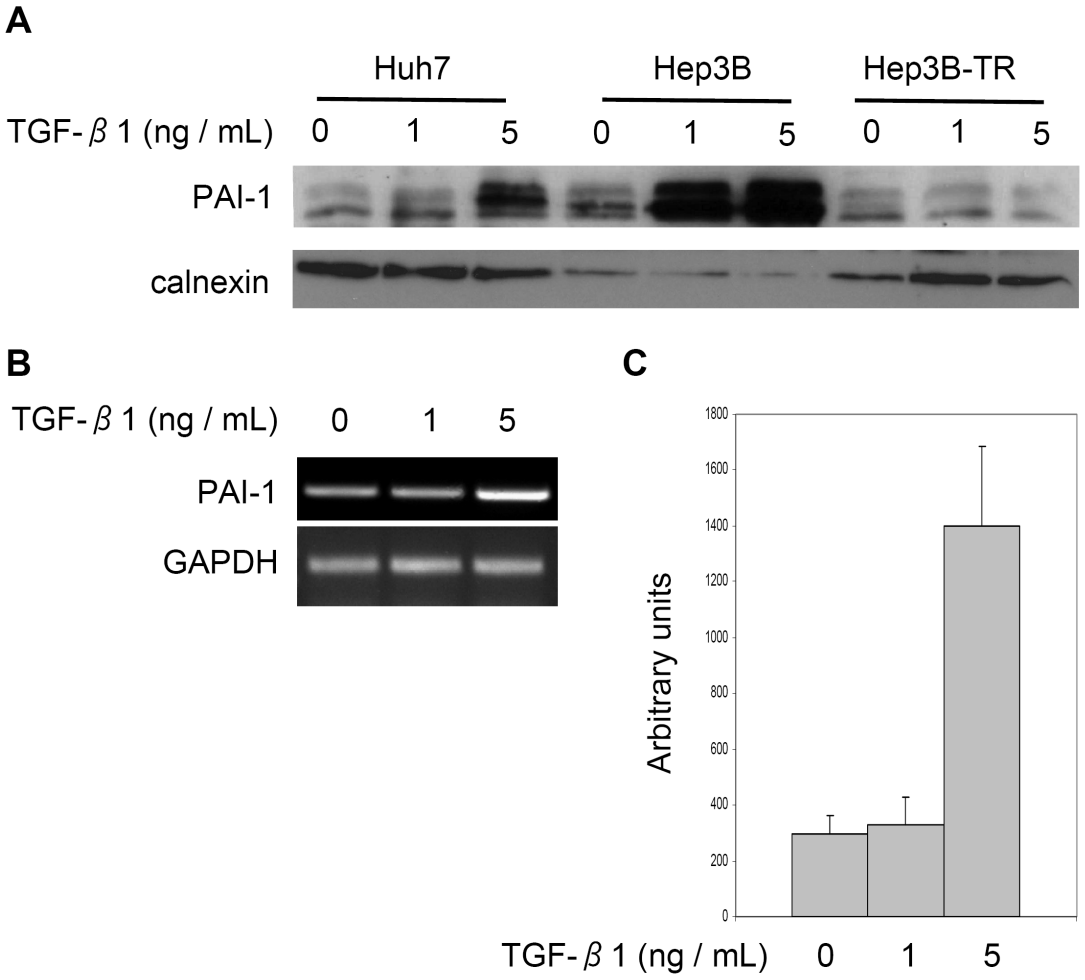

Figure 3.6: Upregulation of TGF-β target gene PAI-1 in different cell lines upon TGF-β1 exposure. (*A*) The expression of PAI-1 was tested by western blotting. Huh7 and Hep3B cell lines displayed a substantial increase in PAI-1 protein levels with increasing TGF-β1 concentrations after 72 hr of treatment. As expected, TGFBR2-deleted Hep3B-TR cell line was non-responsive. Calnexin was used as a control to normalize expression levels in western blots. (*B, C*) RT-PCR (*B*) and qRT-PCR (*C*) analyses indicated that TGF-β1 induced the transcription of PAI-1 in Huh7 cells. GAPDH (*B*) and β-actin (*C*) were used as internal controls for RT-PCR and qRT-PCR experiments, respectively.

Thus, Huh7, PLC, Hep40, Hep3B and HepG2 cell lines not only produced TGF-β1, but also displayed intact TGF-β signaling activity as well as transcriptional responses both at the mRNA and protein levels.

3.3. TGF-β1 induced senescence in well-differentiated HCC cell lines

TGF-β signaling pathway has been linked to different cellular processes including senescence. The interplay between TGF-β and senescence observed in liver tissues has never been addressed in HCC cell lines. To test our hypothesis, we treated all these WD cell lines with different doses of TGF-β1 (1-5 ng/mL) in standard serum-containing cell culture medium (on cover-slips) and kept them in culture up to 12 days with medium change (without TGF-β1) every three days.

After initiation of treatment, we examined all cell lines in culture on a daily based follow-up. All cell lines displayed morphological changes after 12-16 hr (our observations, unpublished data) which became robust after 48 hr. In order to test senescence induction upon TGF-β1 exposure, we subjected the cells to SA-β-Gal assay at different time points (Figure 3.7).

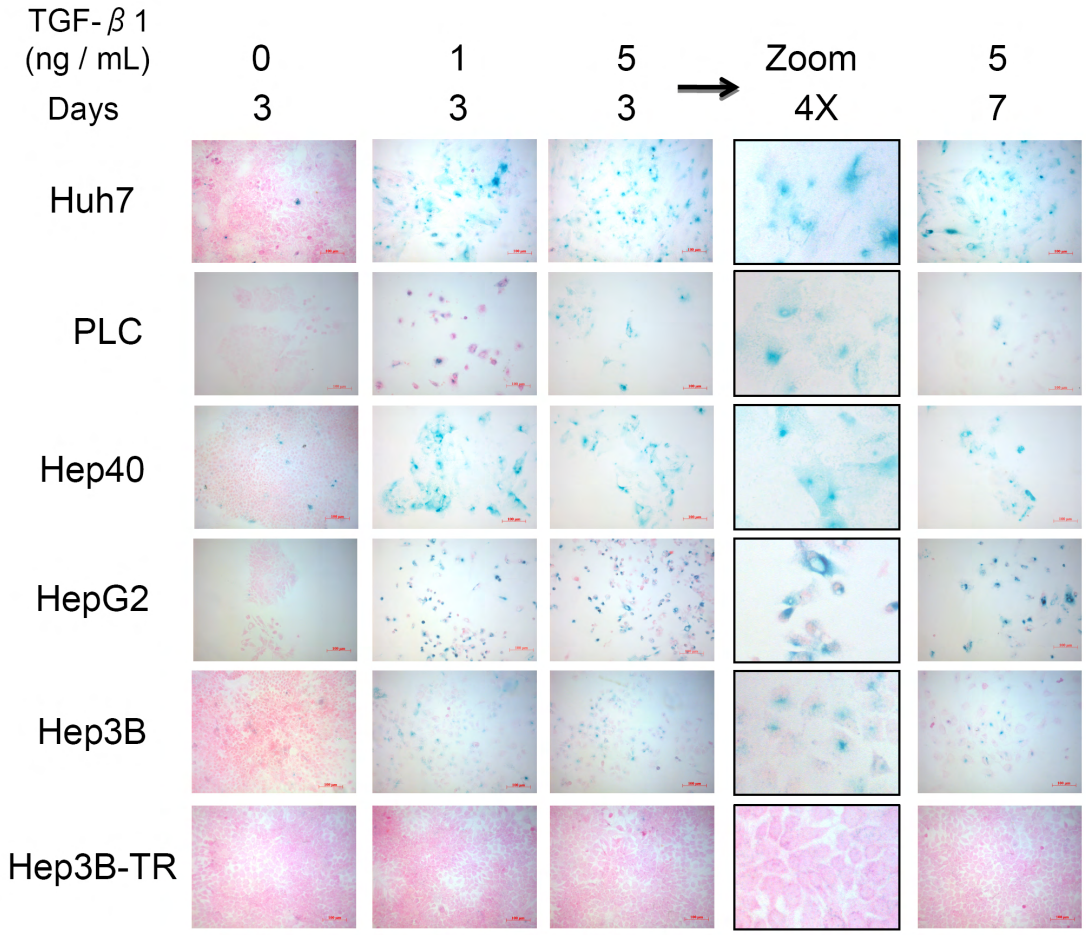

Figure 3.7: Growth inhibition associated with potent senescence-like response. Cells were plated at low density and treated with 1 or 5 ng/mL TGF-β1 for 72 hr, and tested for SA-β-Gal activity (blue) at days 3 and 7. 0: no treatment. Counterstain: Fast Red. TGFBR2-deleted Hep3B-TR cells were used as negative control.

All cell lines tested, except Hep3B-TR, displayed growth inhibition associated with flattened cell morphology and > 50%-positive SA-β-Gal activity, as early as three days after TGF-β1 treatment (Figure 3.8).

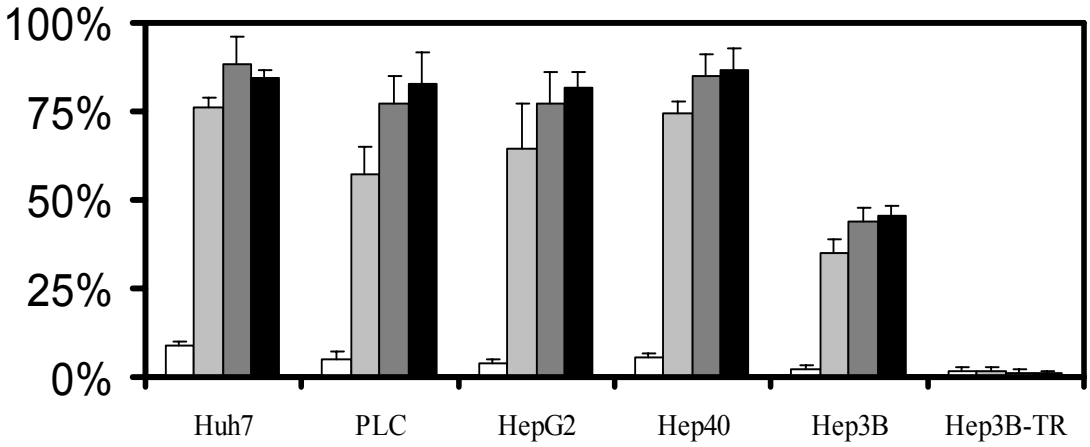

Figure 3.8: Percent of senescent cells after TGF-β1-treatment. (Counts for White bars: No TGF-β1 treatment after 3 days; Grey bars in order: 1 ng/mL and 5 ng/mL after 3 days of treatment; Black bars: 5 ng/mL TGF-β1 treatment after 7 days).

Senescence phenotype was still detectable seven days after TGF-β1 exposure (Figure 3.7) and remained stable for at least 12 days (data not shown).

3.4. TGF-β-induced senescence was correlated with loss of BrdU incorporation

To confirm the specificity of senescence response, we also tested the ability of selected cell lines to incorporate BrdU (bromodeoxyuridine) into cellular DNA after TGF-β1 exposure. BrdU is a synthetic thymine analog which is incorporated into DNA in replicating cells during S-phase progression. Antibodies specific for BrdU can be used to detect positive cells by immunocytochemical staining procedures. Of note, detection of BrdU in such methods requires denaturation of DNA, usually by exposing cells to acidic buffers. In this experimental setting, analysis of 24 hr BrdU incorporation into cellular DNA in Huh7 and PLC cell lines displayed time- and dose-dependent gradual decrease as demonstrated in Figure 3.9.

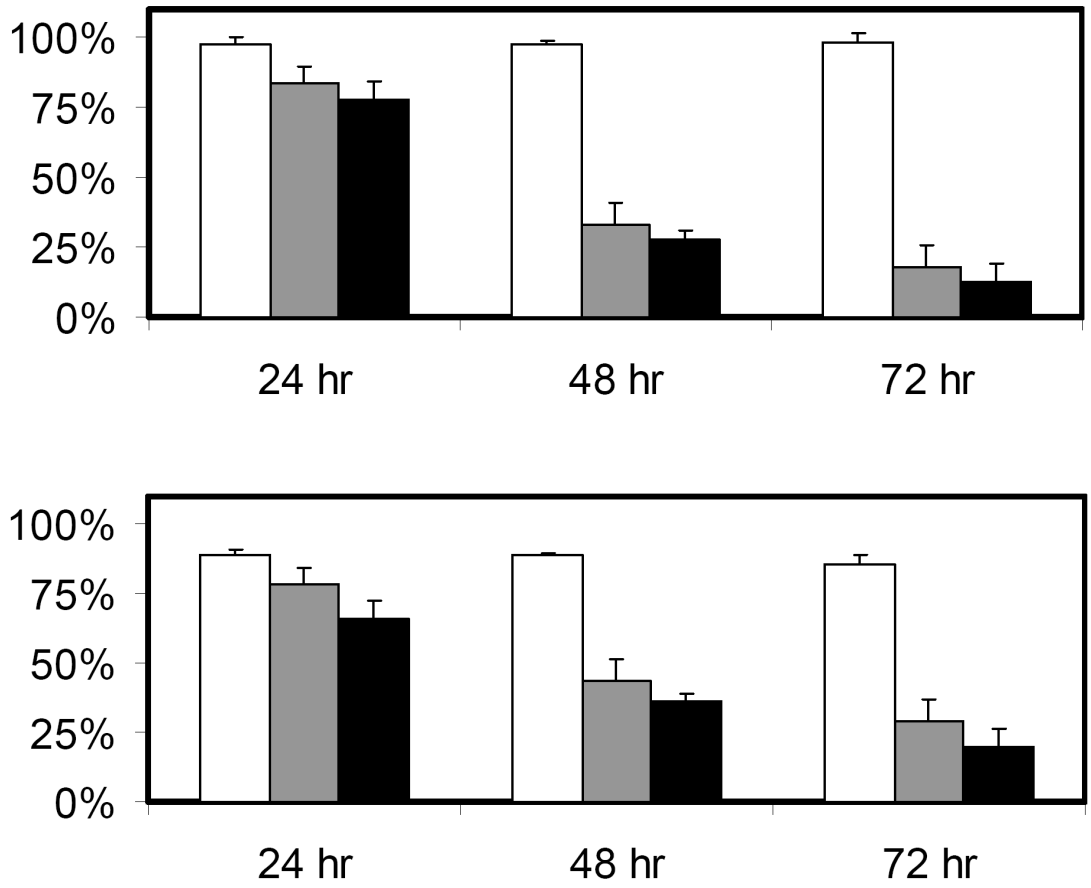

Figure 3.9: Time- and dose-dependent changes in percent BrdU incorporation in Huh7 (upper graph) and PLC (lower graph). Y-axis: BrdU + cells. (White bars: No TGF-β1 treatment; Grey bars: 1 ng/mL; Black bars: 5 ng/mL).

Parental Huh7 cells usually have >95% positive cells after 24 hr of BrdU incorporation. Following 1 ng/mL or 5 ng/mL TGF-β1 treatment, the number of BrdU positive cells decreased by 15-25% after 24 hr, whereas this decrease became robust after 48 hr and reached to a maximal inhibition at 72 hr (Figure 3.9) where more than 80-85% of cells lost their ability to incorporate BrdU into cellular DNA suggesting a strong prohibition of proliferation (Figure 3.10).

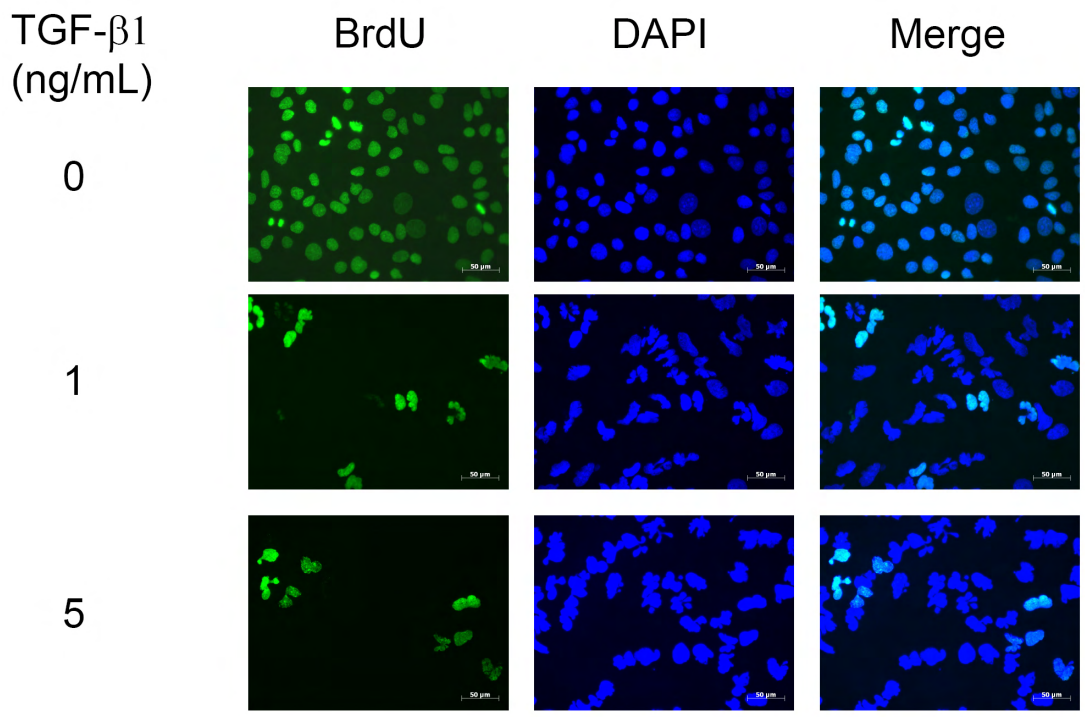

Figure 3.10: Dose-dependent decrease in BrdU incorporation in Huh7 cells. After 24 hr of incorporation, cells positively labeled for BrdU were stained with immunofluorescence technique using anti-BrdU (mouse) primary antibody which was followed by anti-mouse alexa-488 secondary antibody incubation. DAPI was used for nuclear counter-staining. (See Figure 3.9 for statistical results). At least 5 areas were counted on each triplicate assay.

PLC cells, on the other hand, have a total of approximately 90% BrdU positive cells in untreated conditions. After exposure to different doses of TGF-beta, proliferation of PLC cells also decreased gradually (Figure 3.11). Only 20-25% of cells were able to incorporate BrdU into cellular DNA after 72 hr of treatment.

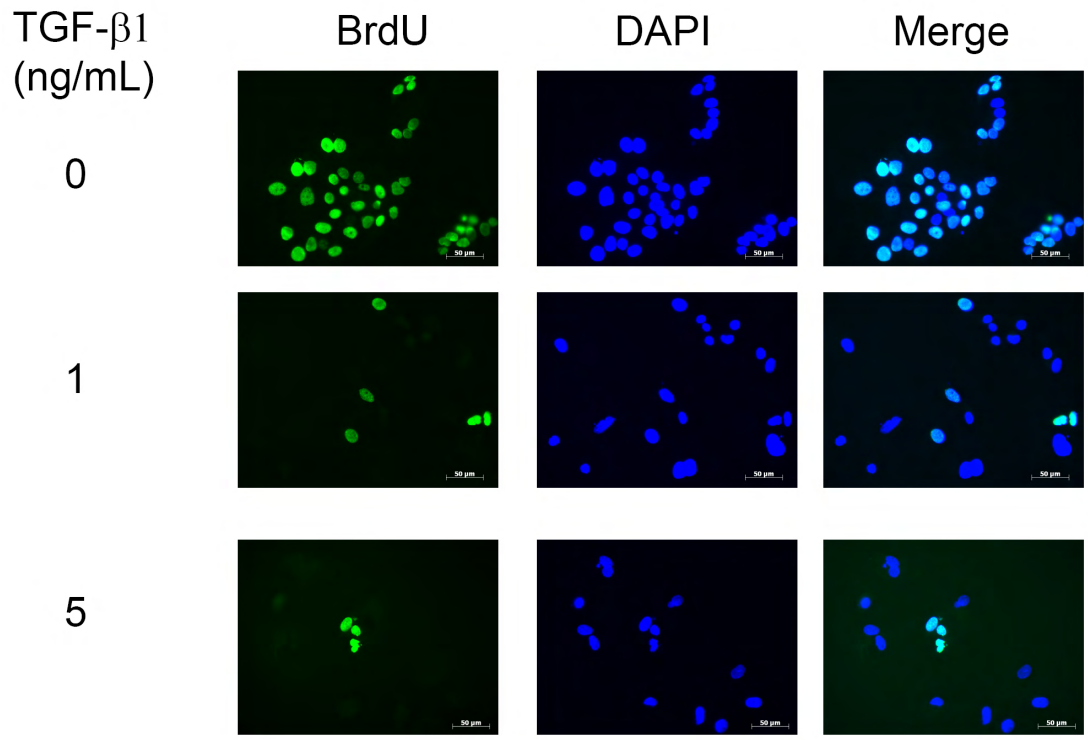

Figure 3.11: Dose-dependent decrease in BrdU incorporation in PLC cells. After 24 hr of incorporation, cells positively labeled for BrdU were stained with immunofluorescence technique using anti-BrdU (mouse) primary antibody which was followed by anti-mouse alexa-488 secondary antibody incubation. DAPI was used for nuclear counter-staining. (See Figure 3.9 for statistical results). At least 5 areas were counted on each triplicate assay.

These observations suggested a dose-dependent late occurring proliferation arrest by TGF-β1.

3.5. Cell cycle arrest provoked by TGF-β1

Decreased proliferation as tested by BrdU incorporation is typically associated with inhibition of cell cycle progression. Propidium iodide is a DNA intercalating agent and a fluorescence molecule that is frequently used to stain DNA in various techniques (Senturk et al., 2010). Therefore, we utilized propidium iodide labeling in TGF-β-treated cells in order to evaluate cell viability and cell cycle progression using flow cytometry. As reported in BrdU incorporation experiments

cells treated with TGF-β1 for 72 hr similarly displayed a dose-dependent decrease in S-phase cells and a concomitant increase in G1-phase cells (Figure 3.12).

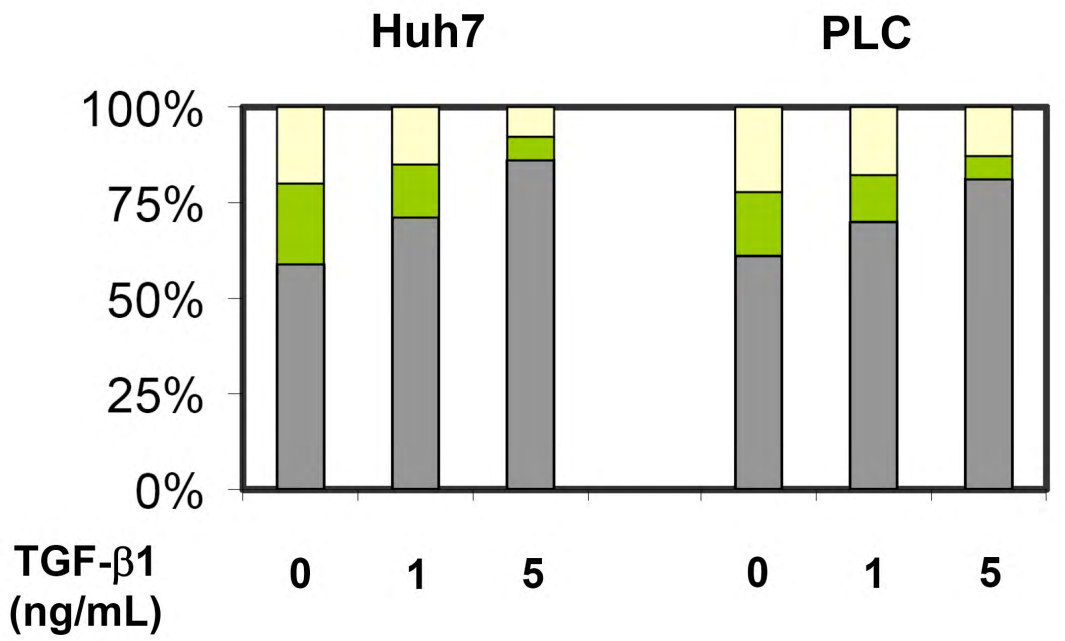

Figure 3.12: Cell cycle distribution in Huh7 and PLC cells after 72 hr TGF-β1-treatment. (Grey bars: G1-phase; Green bars: S-phase; Yellow: G2-phase).

Well-differentiated HCC cell lines under normal culture conditions usually have a 60% G1, 20% S, and 20% G2-M cell-cycle distribution with slight variations depending on the experimentation. Nevertheless, TGF-β1 treatment in Huh7 cells induced a G1-phase accumulation in a dose-dependent manner (72% with 1 ng/mL and 90% with 5 ng/mL), accompanied by a reciprocal decrease in S-phase cells (11% with 1 ng/mL and 5% with 5 ng/mL). PLC cells also displayed a quite similar pattern of cell-cycle distribution in TGF-β1 treated and non-treated conditions. The increase in G1-phase was moderately lower when compared to Huh7 cells. However, this response was in support of BrdU incorporation results (Figure 3.9, lower panel).

Similar to time-dependent experiments for BrdU incorporation assay, we also performed a cell-cycle distribution analysis in a time-dependent manner; this time treatment was done with single 5 ng/mL dose TGF-β1. As the report given in the

Figure 3.13, Huh7 cells displayed a gradual increase in G1-phase cells from 63% to over 80% after 48 hr together with a maximum after 72 hr and slight increases after 96 and 120 hr. Please note that, treatments were initiated accordingly as to perform measurements at the same time to minimize experimental variations in flow cytometry readings. The table shows percentage of cell-cycle distributions in indicated time points. To the right, gated cell populations obtained from the readings in FL2-channel are depicted.

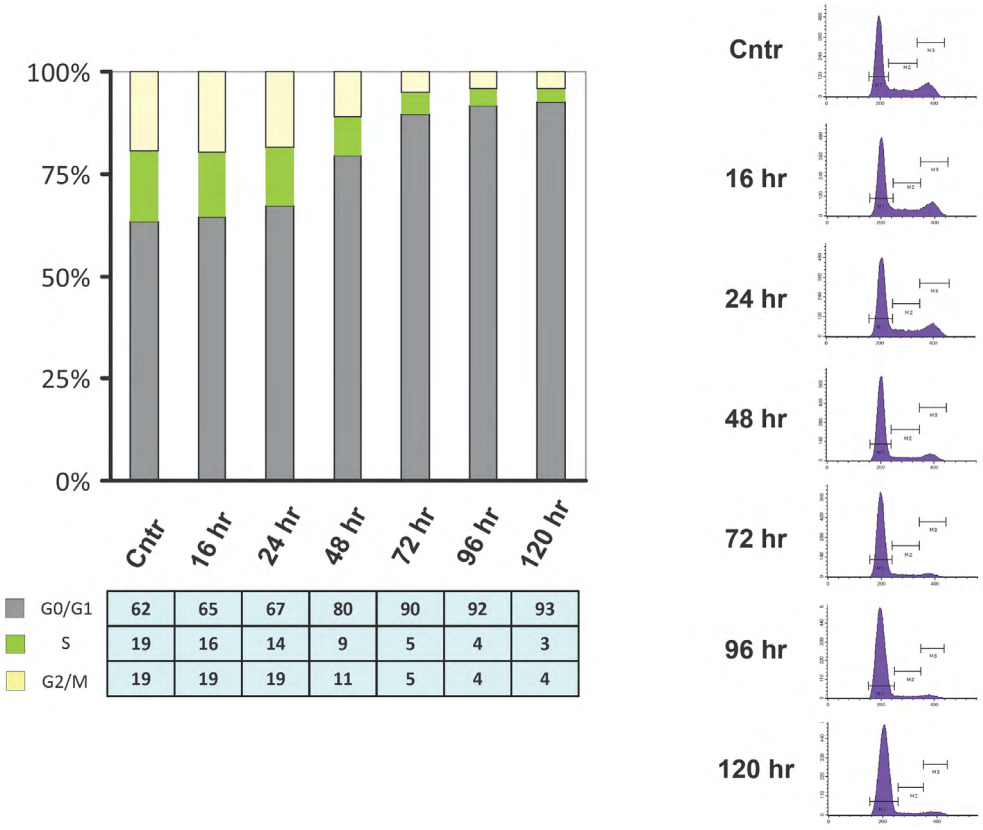

	Cntr	16 hr	24 hr	48 hr	72 hr	96 hr	120 hr
G0/G1	62	65	67	80	90	92	93
S	19	16	14	9	5	4	3
G2/M	19	19	19	11	5	4	4

Figure 3.13: Cell cycle distribution in Huh7 cells after time-dependent TGF-β1-treatment. Control cells were obtained from untreated samples at 120 hr.

In this outcome, please note that the higher peak on the far left, displays 2N cells which are G1, far right 4N cells which are G2-M and in between are the S-phase cells which are usually 2N-4N. For simplicity, gating was done accordingly to

exclude >4N cells from the results, which did not display variations between treated and non-treated samples.

3.6. TGF-β is an autocrine senescence-inducing cytokine in HCC cells

Autocrine signaling is a form of signaling in which chemokines or cytokines released from a cell act on the same cell through autocrine receptors to create a loop of signaling events. Expression of TGF-β1 in all tested cell lines implicated that it could act as an autocrine cytokine. Therefore, to test this hypothesis and confirm the TGF-β-mediated specificity of senescence response, Huh7 cells were plated at low-density (day zero), exposed to either TGF-β1 (5 ng/mL) or anti-TGF-β1 antibody (5 µg/mL) on day one in regular medium, incubated with repeated treatments on days four and seven, and total and SA-β-Gal-positive cells in isolated colonies were counted on day 10, as described previously (Ozturk et al., 2006). TGF-β1 caused 7-fold decrease in colony size ($P < 0.005$) (Figure 3.14) and 5-fold increase in SA-β-Gal activity ($P < 0.0001$) (Figure 3.15).

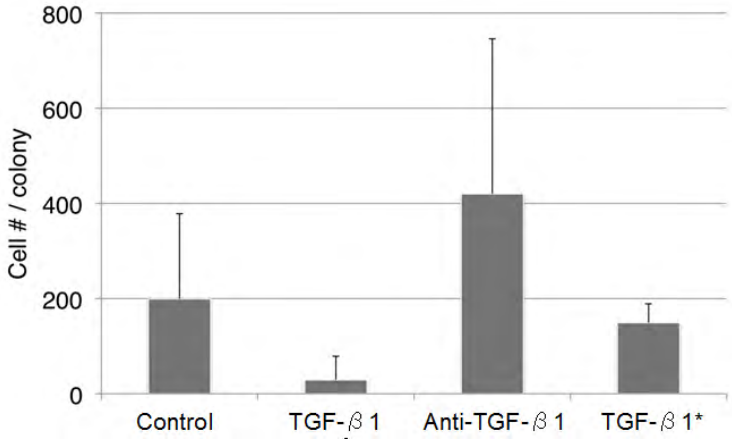

Figure 3.14: Colony formation in Huh7 cells after TGF-β1 and anti-TGF-β1 antibody treatment. Huh7 cells were seeded at low density in 6-well plates. Cells were either left untreated or treated with 5 ng/mL TGF-β1 or 5 µg/mL neutralizing anti-TGF-β1 antibody for 10 days by refreshing the medium with three days intervals. Cell numbers per colony were determined on day 10 by manual counting of at least 10 colonies per treatment. TGF-β1 treatment significantly reduced colony size ($P < 0.005$) when used at three day intervals (TGF-β1), but not when used only once three days before the analysis (TGF-β1*). Conversely, cells treated with neutralizing anti-TGF-β1 antibody displayed significantly increased colony size ($P < 0.04$).

When cells were treated with TGF-β1 just once three days prior to cell counting, colony size did not change significantly, but again there was 3-fold increase in SA-β-Gal activity ($P < 0.0001$). Conversely, cells treated with neutralizing anti-TGF-β1 antibody displayed 2-fold increased colony size ($P < 0.04$), and SA-β-Gal activity was decreased by 50% ($P < 0.02$).

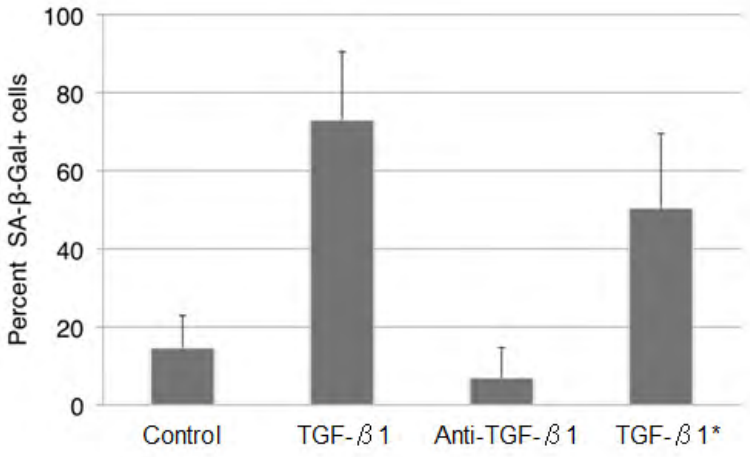

Figure 3.15: Modulation of spontaneous senescence in Huh7 cells by TGF-β1 and anti-TGF-β1 antibody treatment. Huh7 cells were seeded at low density in 6-well plates. Cells were either left untreated or treated with 5 ng/mL TGF-β1 or 5 µg/mL neutralizing anti-TGF-β1 antibodies for 10 days by refreshing the medium with three days intervals. Cell numbers per percent SA-β-Gal positive cells were determined on day 10 by manual counting of at least 10 colonies per treatment. TGF-β1 caused significant increase in SA-β-Gal activity, when tested after one (TGF-β1*) or three-cycles (TGF-β1) of three-day treatment ($P < 0.0001$). Conversely, cells treated with neutralizing anti-TGF-β1 antibody displayed 50% decrease in SA-β-Gal activity ($P < 0.02$).

Collectively, these findings indicated that ectopic TGF-β1 is able to induce a senescence-like growth arrest response in well-differentiated HCC cell lines. Furthermore, Huh7 cell line produced TGF-β1 that acted as a weak autocrine senescence-inducing signal that was inhibited by neutralizing antibody treatment and amplified by ectopic TGF-β1.

3.7. Brief exposure to TGF-β1 for a robust senescence response

To test the shortest time of exposure to TGF-β1 for a full senescence response, three cell lines were treated with TGF-β1 between < 1 minute (~20 seconds) and 72 hr, and subjected to SA-β-Gal staining after 3 days incubation in culture. To our surprise, < 1 minute (~20 seconds) exposure was sufficient for a robust senescence response (Figure 3.16). Of note, quite similar results were obtained when cells were continuously cultured until Day 8 (data not shown). Thus, the senescence-initiating effect of TGF-β1 was immediate, even though the senescence phenotype (>50% SA-β-Gal positive and flattened cells) was manifested three days later.

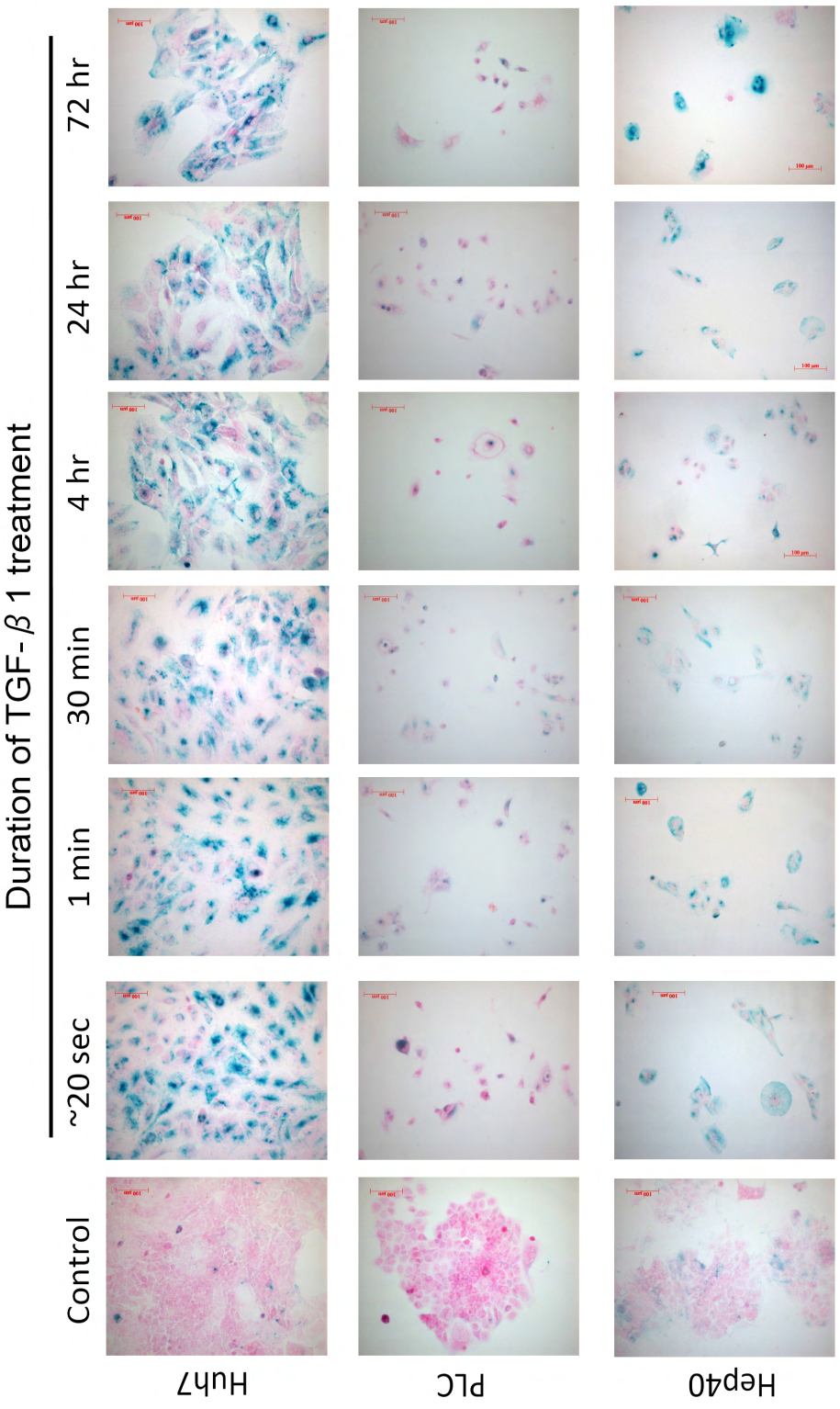

Figure 3.16: Induction of a strong senescence-like response by TGF-β1 even after a very short treatment. Cells were plated at low density and treated with TGF-β1 (5 ng/mL) for indicated times, ranging from less than 1 minute to 72 hrs. SA-β-Gal activity (blue) was tested at 72 hr. Control: no TGF-β1 treatment. Counterstain: Fast Red.

To investigate the robust senescence response mechanism underlying the high impact of brief exposure to TGF-β1, we performed a series of analysis with Huh7

cells. First, we analyzed the amplitude of shuttling of TGF-β1 signal from cell membrane to nucleus by activated Smad proteins using phospho-specific Smad3 antibody in immunofluorescence experiments. Surprisingly, a very short exposure to TGF-β (~20 seconds) was able to induce a time-dependent translocation and sustained retainment for p-Smad3 in the nucleus (Figure 3.17).

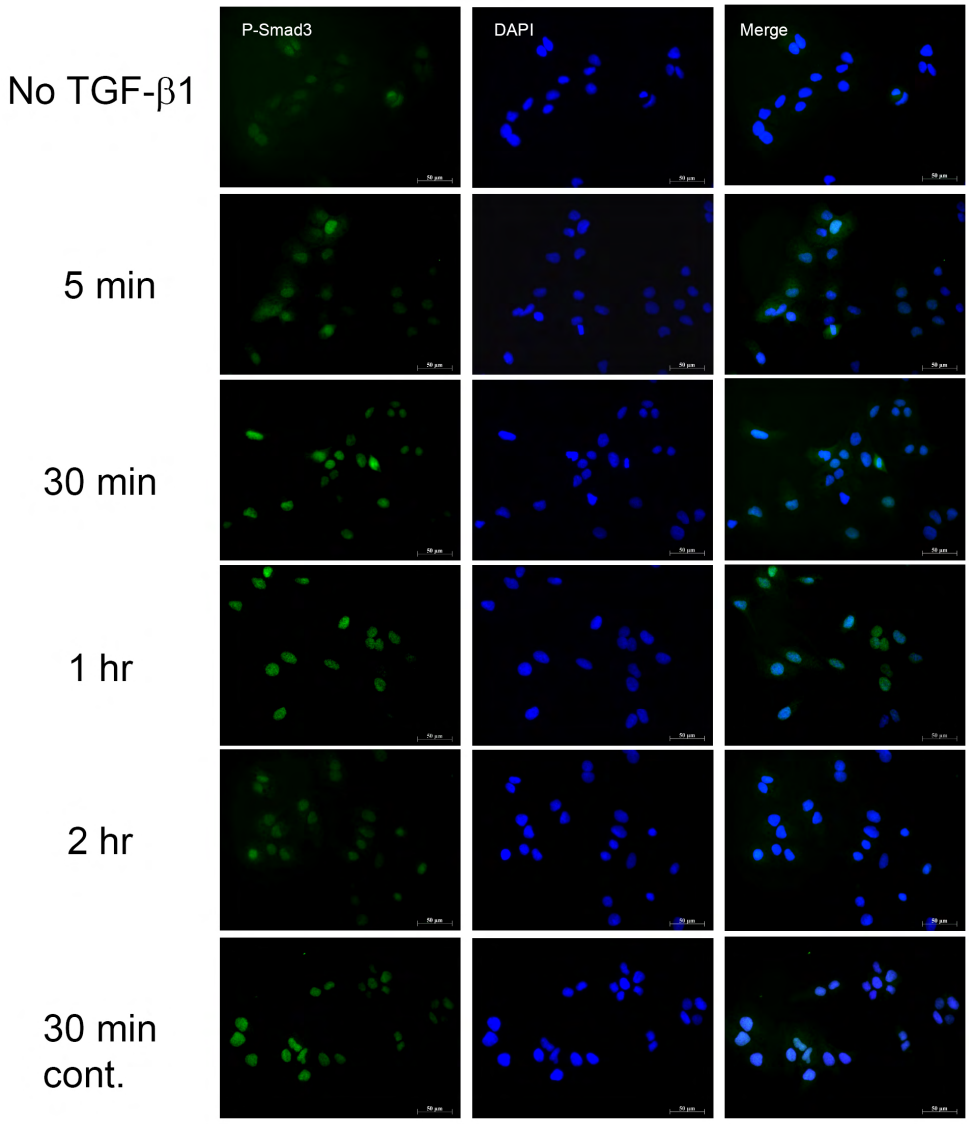

Figure 3.17: Localization of p-smad3 even after a very short stimulation by TGF-β1. Huh7 cells were treated with 5 ng/mL TGF-β1 for less than 1 min and tested for p-smad3 localization by immunofluorescence at indicated time points. 30 min continuous treatment served as positive control. DAPI was used for counterstaining.

Second, we tested activation of pSBE4-luc luciferase reporter after brief exposure to TGF-β1, and demonstrated that even a very short treatment was able to produce a similar response as compared to 5 min and 24 hr treatment (Figure 3.18).

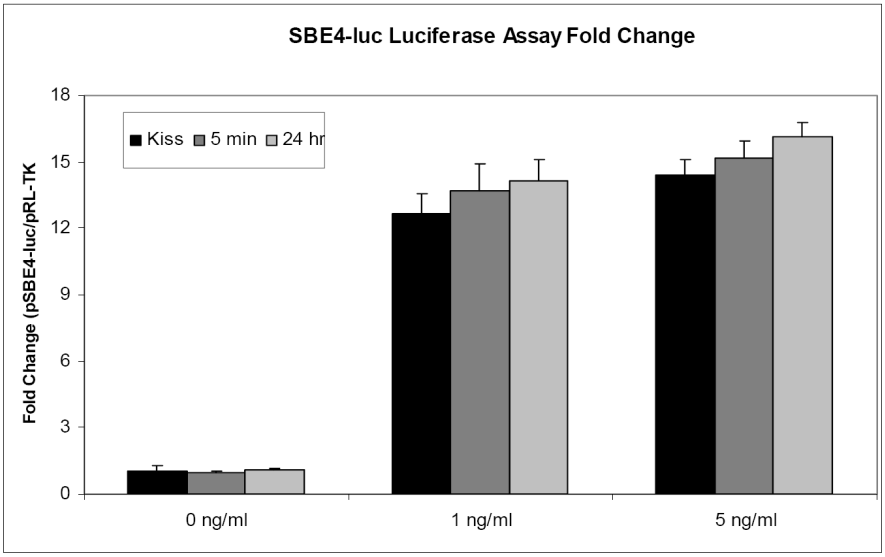

Figure 3.18: Brief exposure to TGF-β1 for a sustained reporter activation. Cells were co-transfected with pSBE4-Luc and control pRL-TK plasmids, and treated with or without TGF-β1 (1 ng/mL and 5 ng/mL) for ~20 sec, 5 min and 24 hr. The luciferase activity was measured and expressed as fold change of pSBE4-Luc/pRL-TK compared to non-treated controls (mean ± SD; n=3).

3.7.1. Implications of autocrine positive-feedback loops in senescence secretome

Recent findings identified many cytokine factors implicated in oncogene-induced and replicative senescence (Acosta et al., 2008; Kuilman et al., 2008). However, the most striking outcome of such studies was the identification of positive-feedback loops modulated by senescence-driving factors as well as autocrine contribution of cytokines released from senescent cells.

On the other hand, we and others have demonstrated the growth inhibitory functions of autocrine loops of several cytokines including TGF-β (Gressner, 1995; Hov et al., 2004; Matsuzaki et al., 2000). TGF-β signaling pathway has also been implicated in control of a subset of cellular processes associated with cellular secretome (Bierie et al., 2009; Xu et al., 2010).

Therefore, we hypothesized a potential involvement of a positive-feedback loop in senescent Huh7 cells after a very brief exposure to TGF-β. In this respect, we tested the expression of TGF-β1 at the mRNA level in Huh7 cells which were stimulated to undergo senescence arrest after 3 days, only with a short pulse of TGF-β1 exposure. Surprisingly enough, this very brief exposure to ectopic TGF-β caused a robust increase in its own endogenous transcript levels in a dose-dependent manner (Figure 3.19).

DNA-damaging agents were also implicated in premature senescence induction as well as cytokine secretory phenotype (Novakova et al., 2010). The onset of senescence induced by DNA-damaging agents is quite different from TGF-β-induced senescence. There are major differences in morphological changes and cell cycle distributions (our own observations) as well as senescence-messaging secretome (Kuilman and Peeper, 2009). Therefore, we also tested the TGF-β1 expression in doxorubicin- and cisplatin-induced senescence. Of note, DNA-damaging compounds did not induce senescence in brief exposure conditions, hence the treatment with these chemicals was performed for 72 hr.

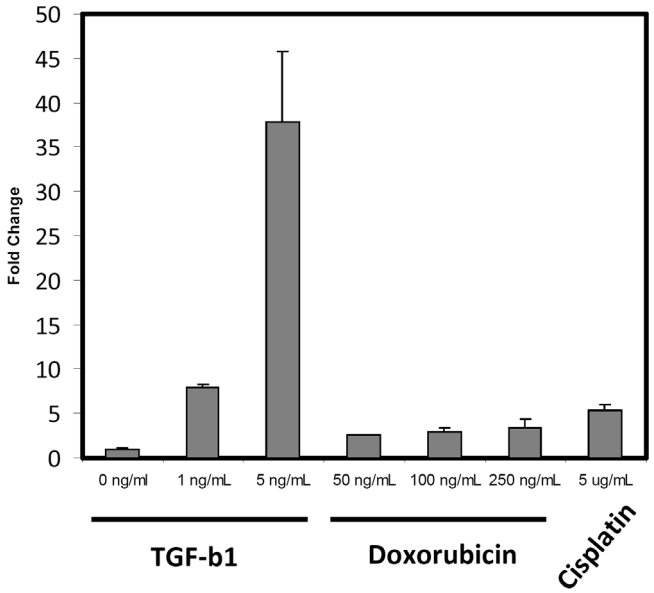

Figure 3.19: Brief exposure to TGF-β induces its own endogenous expression. Huh7 cells were treated with 1 ng/mL and 5 ng/mL TGF-β1 for ~20 seconds and analyzed for TGF-β1 expression after 3 days in culture by qRT-PCR. Results were indicated as fold change (treated/non-treated). Experiments were performed in triplicate. Doxorubicin and Cisplatin were used as senescence inducers by DNA-damage (72 hr).

Taken together, TGF-β1 induced its own expression even when treated for a very short time. DNA-damage causing compounds also increased TGF-β1 expression but to a lesser extent (~ 3 to 5 fold).

In addition, we also performed experiments with other cytokines which were recently identified as mediators of senescence in different cellular models, namely IL-6 and IL-8 (Orjalo et al., 2009). As tested by real-time PCR, we demonstrated increased levels of expression for IL-6 (Figure 3.20) and IL-8 (Figure 3.21).

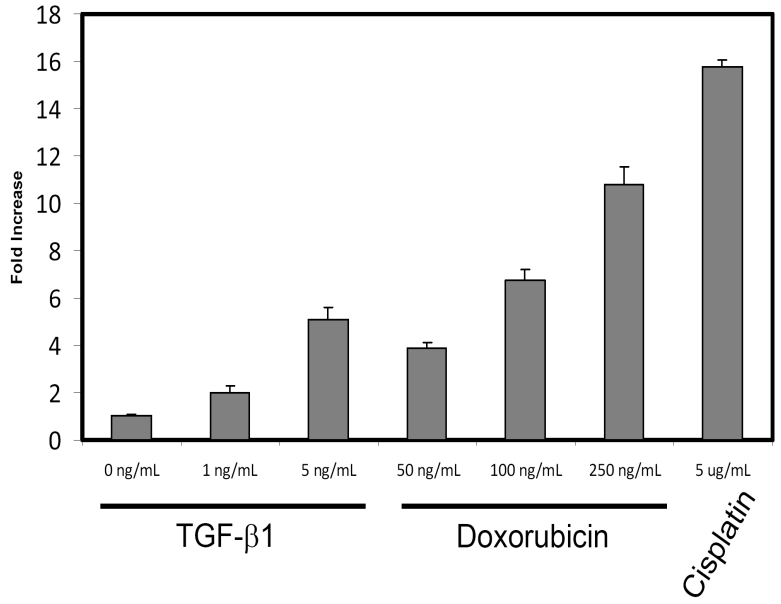

Figure 3.20: Brief exposure to TGF-β1 induces IL-6 expression. Huh7 cells were treated with 1 ng/mL and 5 ng/mL TGF-β for ~20 seconds and analyzed for IL-6 expression after 3 days in culture by qRT-PCR. Results were indicated as fold increase (treated/non-treated). Experiments were performed in triplicate. Doxorubicin and Cisplatin were used as senescence inducers by DNA-damage (72 hr).

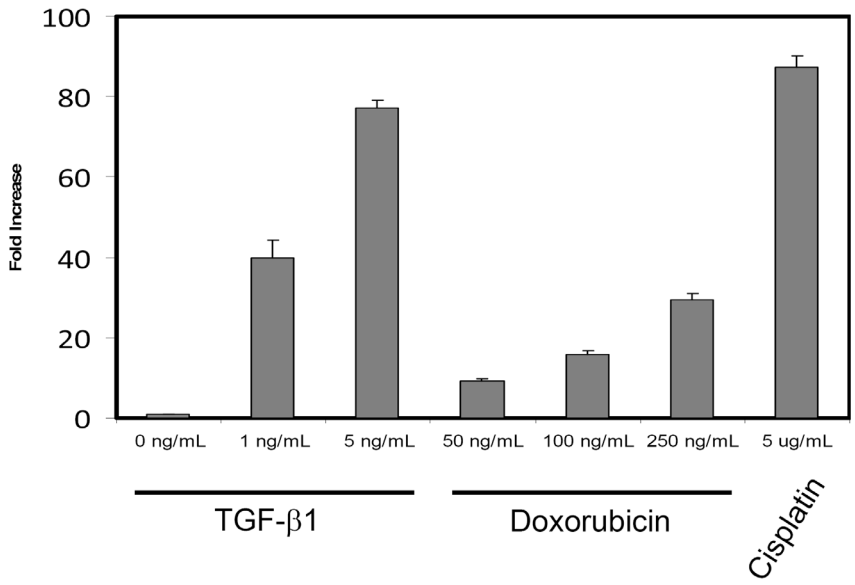

Figure 3.21: Brief exposure to TGF-β1 induces IL-8 expression. Huh7 cells were treated with 1 ng/mL and 5 ng/mL TGF-β for ~20 seconds and analyzed for IL-8 expression after 3 days in culture by qRT-PCR. Results were indicated as fold increase (treated/non-treated). Experiments were performed in triplicate. Doxorubicin and Cisplatin were used as senescence inducers by DNA-damage (72 hr).

Moreover, elevations in levels of IL-6 expression were moderately low compared to IL-8; therefore we were not able to detect any increase in the amount of released form of IL-6 when tested with ELISA (data not shown). Nevertheless, we detected that parental Huh7 cells secrete significant amount of IL-8 with substantially increased levels in TGF-β1 ($p < 0.01$) and doxorubicin ($p = 0.05$) treated samples as assessed by ELISA (Figure 3.22).

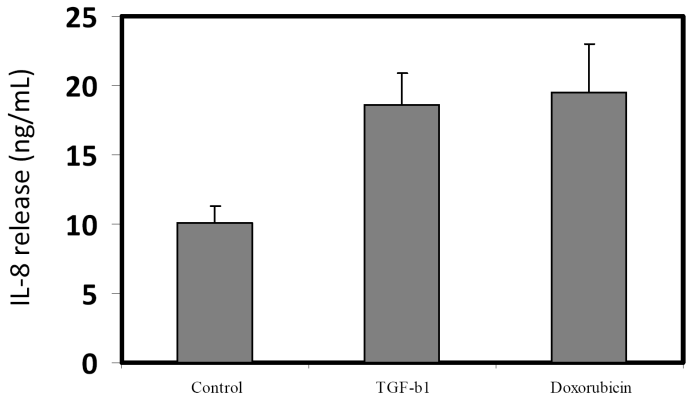

Figure 3.22: Brief exposure to TGF-β induces IL-8 secretion. Huh7 cells were treated with 5 ng/mL TGF-β for ~20 seconds and conditioned media was analyzed for IL-8 secretion after 3 days in culture. Experiments were performed in triplicate.

Taken together, robust senescence induction even after a very short TGF-β1 exposure might be modulated through amplification of an autocrine positive feedback loop. qRT-PCR and ELISA assays performed to analyze IL-6 and IL-8 involvement in TGF-β-induced growth arrest also implicated a potential role for IL-8 secretion in maintenance of senescence response. However, these results shall require further investigation to understand the details underlying the unnecessity for sustained exposure to TGF-β1 during permanent senescence arrest.

3.8. Lack of evidence for TGF-β1-induced apoptosis

Earlier studies indicated that TGF-β induces apoptosis in hepatocytes and HCC cell lines under serum-free conditions (Fan et al., 1996; Fan et al., 2002; Lamboley et al., 2000). However, it remains elusive whether the apoptotic response is also induced under serum-containing standard cell culture conditions. Under our culture conditions with 10% fetal calf serum-containing medium, all tested cell lines failed to undergo apoptotic cell death as tested by using NAPO (Negative in Apoptosis) antibody (Sayan et al., 2001) and active caspase-3 antibody assays. Cells

maintained NAPO expression when tested at 24 hr (Figure 3.23), and at day 7 (Hep3B; Figure 3.24).

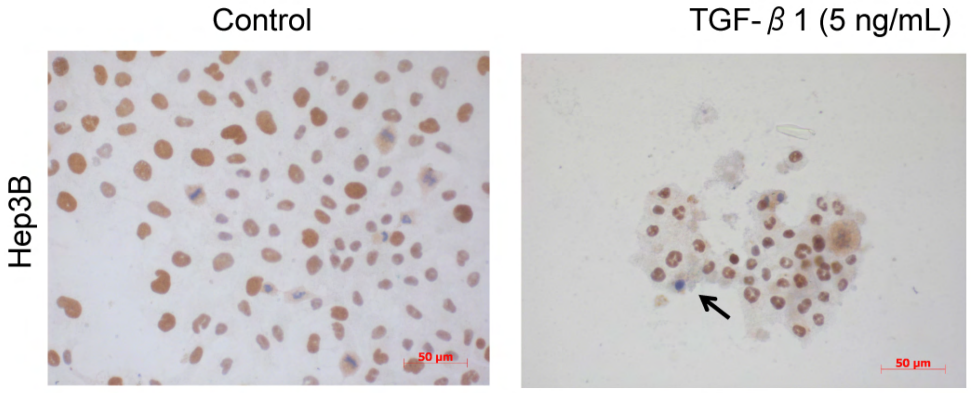

Figure 3.24: There was no change in NAPO expression under TGF-β1 treatment. Hep3B cells were treated with TGF-β1 (5 ng/mL) for 72 hr and subjected to NAPO immunoperoxidase staining (Sayan et al., 2001) on day seven. Arrow: Negative nucleus for NAPO.

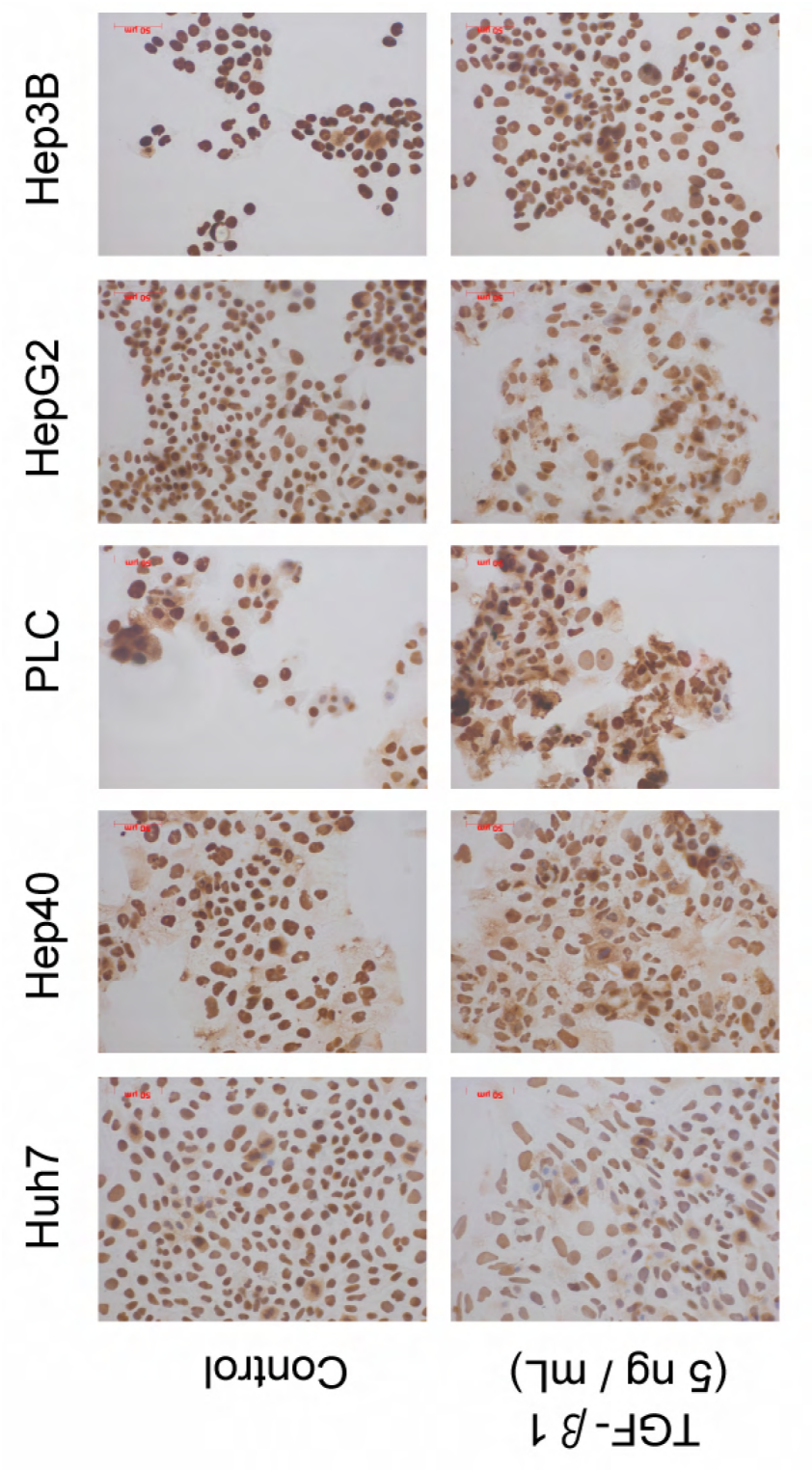

Figure 3.23: No change in NAPO expression under TGF-β1 treatment. Cells were treated with TGF-β1 (5 ng/mL) for 72 hr and subjected to NAPO immunoperoxidase staining.

Furthermore, activated caspase-3 immunoreactivity did not increase following TGF-β1 treatment (Figure 3.25 and 3.26).

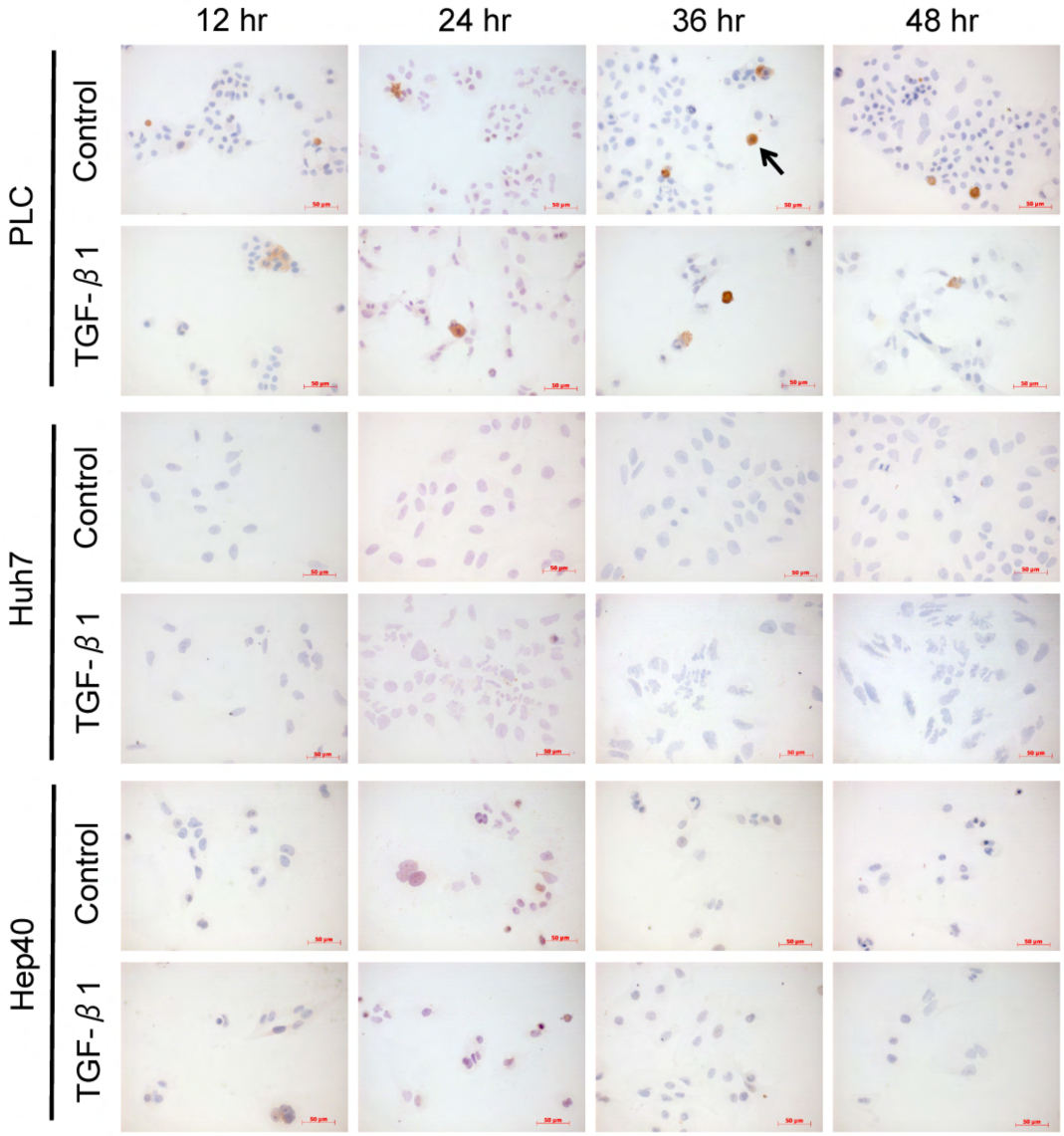

Figure 3.25: There was no change in NAPO expression after TGF-β1 treatment. Active caspase-3 immunoreactivity was assessed by immunoperoxidase staining. Cells were exposed to 5 ng/mL TGF-β1 for indicated time periods and stained with an anti-activated caspase-3 (Asp175) antibody. There was no discernible increase in the number of caspase-3-positive cells under TGF-β treatment. Arrow indicates a cell that displayed positive caspase-3 staining.

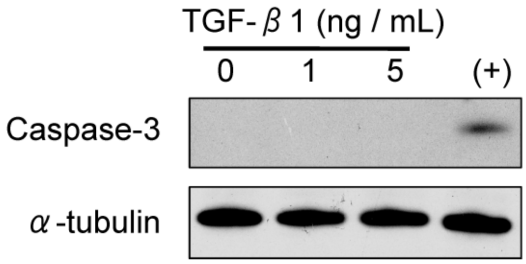

Figure 3.26: Lack of Caspase-3 activation during TGF-β1 treatment. Hep40 cells were treated with different doses of TGF-β1 for 72 hr and assayed by western blotting. Etoposide-treated (25 μM) Jurkat cell line extracts were used as positive control (+) for cleaved caspase-3 immunoblotting. The α-tubulin was used as an internal control.

Concusively, under our experimental conditions, we did not detect any significant apoptotic response in well-differentiated HCC cell lines. Of particular interest, Hep3B which has been used as a model for TGF-β1-induced apoptosis under serum-free conditions by others did not display such a response under serum-containing conditions (Carmona-Cuenca et al., 2008).

3.9. Molecular Mechanisms of TGF-β-induced Senescence

3.9.1. TGF-β-induced senescence is associated with sustained induction of $p21^{Cip1}$ and $p15^{Ink4b}$

Cellular senescence is usually associated with cell cycle arrest induced by p53, $p21^{Cip1}$, $p16^{Ink4a}$ and/or $p15^{Ink4b}$, leading to the accumulation of underphosphorylated pRb protein (Campisi and d'Adda di Fagagna, 2007; Gil and Peters, 2006). In all cell lines tested, 72 hr of TGF-β1 treatment caused an upregulation of $p15^{Ink4b}$ and $p21^{Cip1}$, in association with c-myc downregulation (Figure 3.27).

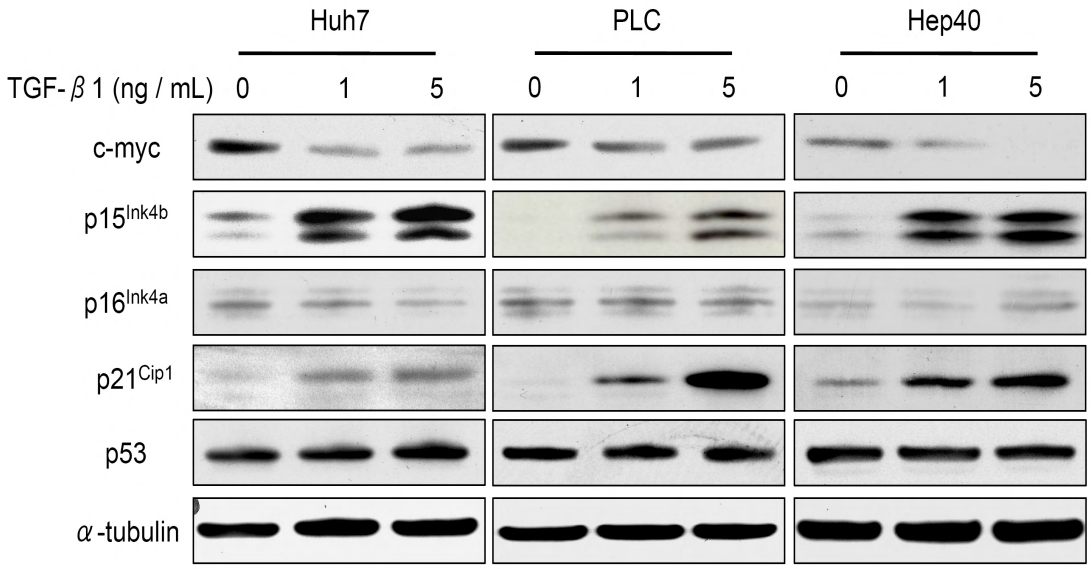

Figure 3.27: Protein expression patterns after TGF-β1 treatment. TGF-β1 treatment (72 hr) of HCC cell lines led to the induction of senescence markers $p15^{Ink4b}$ and $p21^{Cip1}$ that was associated with c-myc downregulation. $p16^{Ink4a}$ blots were overexposed to visualize weak expression. α-tubulin served as equal loading control.

In addition, $p15^{Ink4b}$ and $p21^{Cip1}$ accumulation in protein levels was associated with transcriptional upregulation (Figure 3.28).

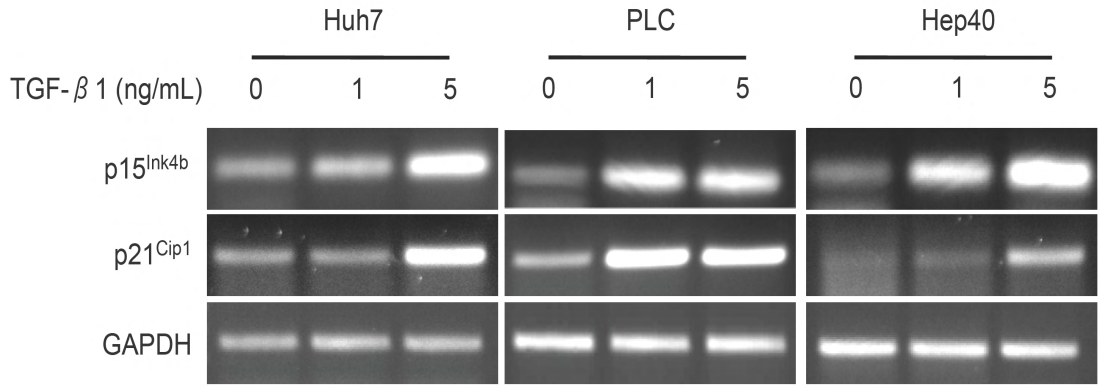

Figure 3.28: mRNA expression patterns after TGF-β1 treatment. TGF-β1 treatment (3 days) of HCC cell lines induced transcriptional upregulation of senescence markers $p15^{Ink4b}$ and $p21^{Cip1}$ as tested by semi-quantitative RT-PCR. GAPDH was used as equal loading control.

3.9.2. Sustained changes in c-Myc and p21^{Cip1} transcript levels

TGF-β-induced senescence observed in well-differentiated cell lines was associated with activation of cyclin-dependent kinase inhibitors as well as downregulation in c-myc protein and transcript levels. On the other hand, TGF-β-induced senescence was a sustained event. Three days of incubation was adequate to promote a permanent senescence arrest even after 12 days of incubation in culture. In this respect, we studied the expression levels of two genes implicated in senescence arrest after 12 days of incubation. As demonstrated in Figure 3.29, p21^{Cip1} mRNA levels were maintained even after the removal of TGF-β1 from the culture medium.

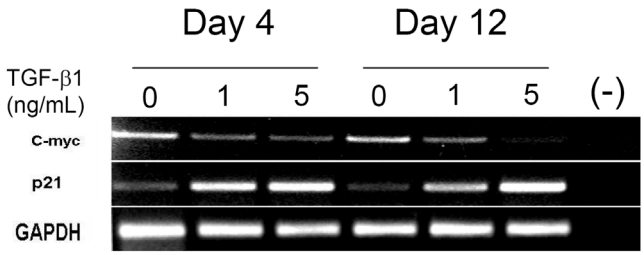

Figure 3.29: Sustained changes in c-myc and p21^{Cip1} transcript levels. TGF-β treatment (3 days) of HCC cell lines induced transcriptional regulation of p21^{Cip1} and c-myc as tested by semi-quantitative RT-PCR. Expression changes in these particular genes were maintained even after 8 days following removal of TGF-β1 from growth medium. GAPDH; equal loading control.

This observation was also supported with the decrease in relative levels of c-myc expression when compared to control samples. Taken together, we can conclude that TGF-β1 provokes a sustained cytostatic response, as well as maintained expression levels for genes responsible for TGF-β1-induced senescence.

3.9.3. Loss of pRb phosphorylation in TGF-β-induced senescence

Additionally, TGF-β-treatment led to a decrease in pRb phosphorylation status, together with a decrease in p107 and reciprocal increase in p130 protein levels (Figure 3.30).

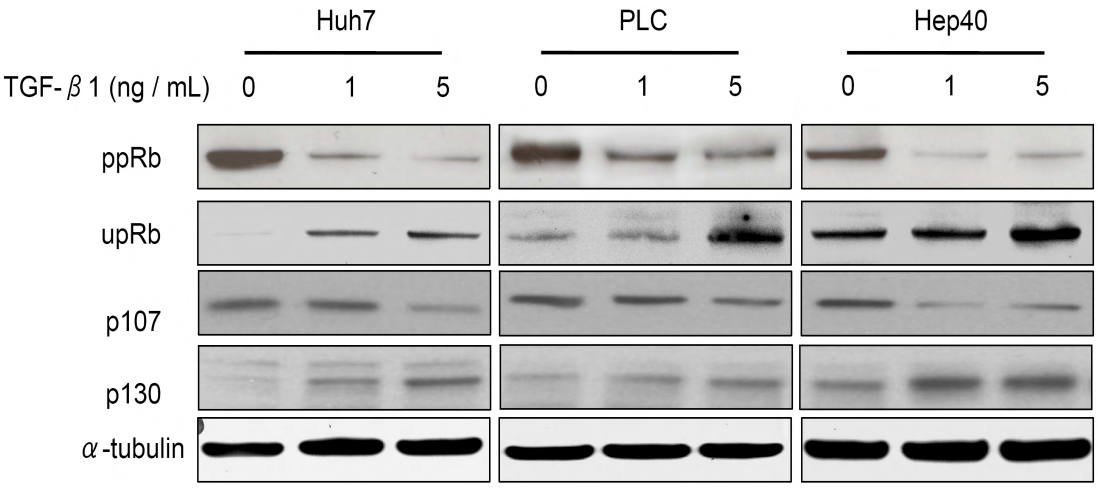

Figure 3.30: RB family proteins in TGF-β1-induced senescence. TGF-β1 treatment (72 hr) of HCC cell lines decreased phosphorylated pRb (ppRb) levels, together with a reciprocal increase in underphosphorylated pRb (upRb) levels. Also, p107 levels were decreased and p130 increased. α-tubulin served as equal loading control.

These changes in the retinoblastoma family proteins correlate well with exit from the cell cycle (Classon and Dyson, 2001).

3.9.4. TGF-β-induced senescence is $p16^{Ink4a}$ and p53-independent

All cell lines used in this study, except HepG2, harbor p53 mutations, therefore express mutant p53 proteins (Erdal et al., 2005). This data suggested a p53-independent upregulation of $p21^{Cip1}$ protein and mRNA levels.

Moreover, we did not observe any change in the phosphorylation status of p53 protein (Figure 3.31), a modification that marks activation of p53, in p53 wild type HepG2 cells. HepG2 cells were treated with TGF-β1 to test p53 protein expression, as well as activation of p53 function through p53 (Ser15) phosphorylation. We used a previously tested DNA-damaging chemical (Doxorubicin) known to increase p53 expression and phosphorylation under genotoxic stress conditions (Liu et al., 2008; Vassilev et al., 2004). We treated HepG2 cells with 10 ng/mL doxorubicin for 72 hr and analyzed p53 expression as

well as phosphorylation status with western immunoblotting. Doxorubicin treatment substantially increased p53 expression as well as modulated p53 (Ser15) phosphorylation. This effect demonstrated a causal link in $p21^{Cip1}$ induction. As opposed to doxorubicin-induced changes in p53, TGF-β-treatment did not alter p53 protein levels or phosphorylation status (Figure 3.31, left).

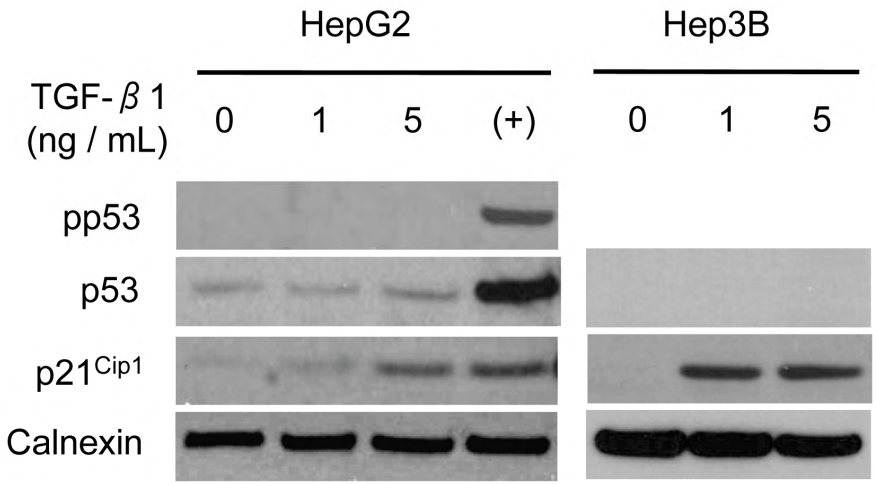

Figure 3.31: The induction of $p21^{Cip1}$ by TGF-β was independent of p53. HepG2 cells with wild-type *TP53* gene (left) responded to TGF-β1 treatment by $p21^{Cip1}$ accumulation, without an increase in $p53^{ser15}$ phosphorylation (pp53) or in total p53 levels (p53). Doxorubicine (10 ng/mL)-treated cells were used as a positive control (+) for p53 phosphorylation and accumulation. Calnexin was used as loading control. *TP53*-deleted Hep3B cells (right) also responded to TGF-β1 treatment by $p21^{Cip1}$ accumulation, despite the lack of p53 protein. The α-tubulin was used as loading control for Hep3B cells. Cell lysates were tested by western blotting at day three, following TGF-β1 or doxorubicin treatment.

For control studies we used Hep3B cell line which has mutant p53 gene due to a large deletion (7-kbp), thereby lack p53 transcript and protein expression (Bressac et al., 1990). Like HepG2 cells, TGF-β-treatment substantially increased $p21^{Cip1}$ protein expression in Hep3B cells independent of p53 status (Figure 3.31, right).

Moreover, TGF-β treatment did not change $p16^{Ink4a}$ levels. Indeed, the *CDKN2A* gene is frequently silenced in HCC (Roncalli et al., 2002). Accordingly,

p16^{Ink4a} protein levels were extremely low in all tested cell lines, except Hep3B and Hep3B-TR cells (Figure 3.32).

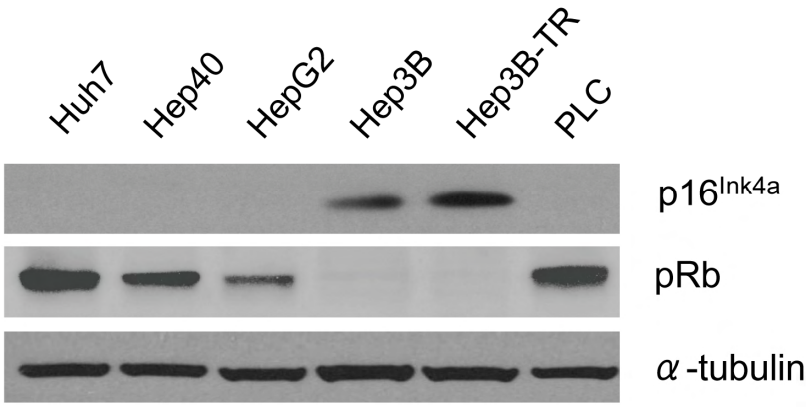

Figure 3.32: HCC cell lines expressed little or no p16^{Ink4a} protein, except pRb-deficient Hep3B and Hep3B-TR cell lines.

On the other hand, our observations for senescence arrest in Hep3B cells suggested that pRb expression was also dispensable for TGF-β1-induced senescence in HCC cells. Taken together, these findings suggested that TGF-β was able to induce senescence arrest in HCC cells independent of p53, p16^{Ink4a} and pRb status.

3.9.5. TGF-β-induced senescence can be reproduced by p21^{Cip1} or p15^{Ink4b} overexpression

Cellular senescence is defined as an irreversible arrest of mitotic cells at G1-phase, but some genetically deficient tumor cells can also senesce at G2 or S phases (Campisi and d'Adda di Fagagna, 2007) (our unpublished observations).

Control and TGF-β1-treated (5 ng/mL) Huh7 cells were analyzed by flow cytometry. Cells exposed to TGF-β1 were examined three days later at the time of senescence. TGF-β1 treatment caused an increase of G1 phase cells from 59% to 81% with a concomitant decrease of S phase cells from 23% to 8% in Huh7 cells

(Figure 3.33-A). Next we tested respective contributions of $p21^{Cip1}$ and $p15^{Ink4b}$ to senescence arrest in Huh-7 cells by transient transfection with corresponding expression vectors. Transfected cells were selected with antibiotic treatment for eight days and subjected to following analyses. $p21^{Cip1}$-overexpressing cells displayed an increase in G1 phase from 61% to 78%, together with a decrease of S phase from 26% to 12% (Figure 3.33-B). Overexpression of $p15^{Ink4b}$, on the other hand, increased G1 cells from 59% to 66% and decreased S phase cells from 22% to 15% (Figure 3.33-C).

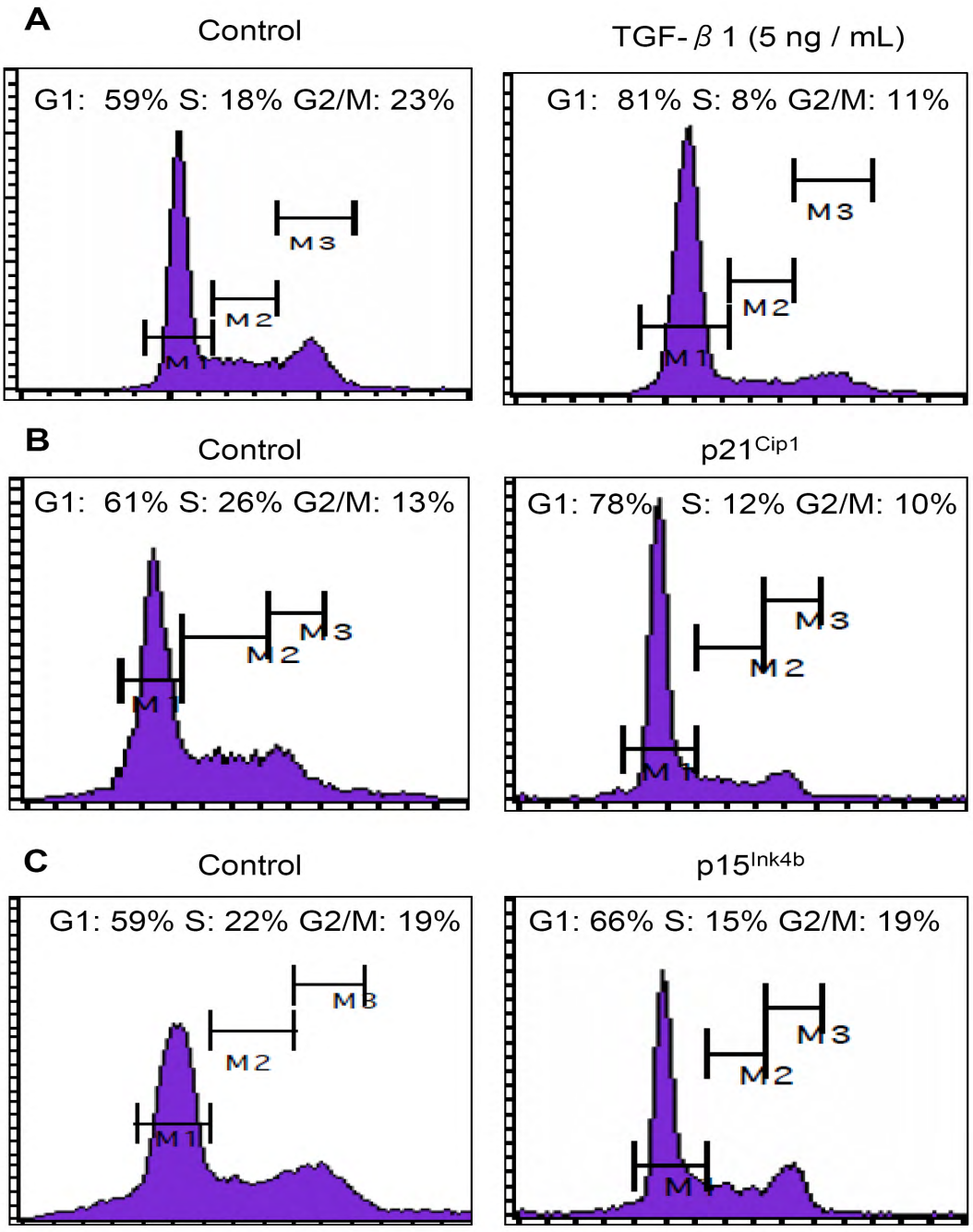

Figure 3.33: The G1-arrest induced by TGF-β treatment can be recapitulated by ectopic expression of $p21^{Cip1}$ and $p15^{Ink4b}$. (*A*) Untreated and TGF-β1-treated Huh7 cells were subjected to cell cycle analysis after three days of culture. G1 phase cells were increased from 59% to 81% together with a decrease in S phase cells from 18% to 8%. (*B*, *C*) Huh7 cells were transiently transfected with $p21^{Cip1}$ and $p15^{Ink4b}$ expression vectors, and subjected to cell cycle analysis after eight days of culture under antibiotic selection. $p21^{Cip1}$-transfected cells displayed an increase in G1 phase cells from 61% to 78% accompanied with a decrease of S phase cells from 26% to 12% (*B*). Similarly, $p15^{Ink4b}$-transfected cells showed an increase of G1 phase cells from 59% to 66% together with a decrease of S-phase cells from 22% to 15% (*C*). Compared to $p15^{Ink4b}$, $p21^{Cip1}$ expression provoked a more pronounced G1-arrest.

p21^{Cip1}-transfected cells demonstrated highly increased p21^{Cip1} protein expression (Figure 3.34-A). p15^{Ink4b}-transfected cells displayed moderately increased expression of the short form of p15^{Ink4b}, partly because of endogenous expression of p15^{Ink4b} (Figure 3.34-B).

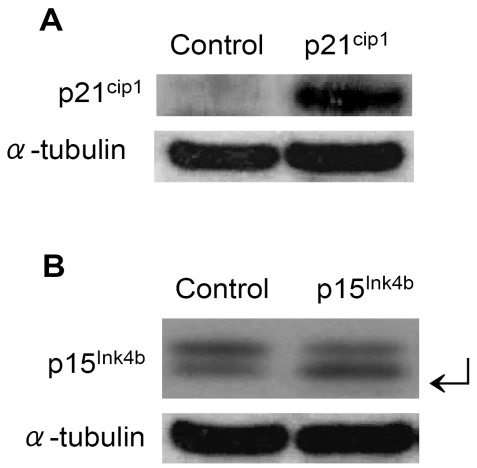

Figure 3.34: Overexpression of p21^{Cip1} (*A*) and p15^{Ink4b} (*B*) in transiently transfected Huh7 cells. Cells were transfected with expression plasmids encoding p21^{Cip1} (***A***) or p15^{Ink4b} (***B***), selected for eight days in the presence of antibiotics, and cell extracts were analyzed by western immunoblotting. The α-tubulin was used as loading control. Only short form of p15^{Ink4b} displayed increased expression (arrow in ***B***), as we used a plasmid encoding this form.

To support previous findings, we also performed senescence and BrdU incorporation assays. As expected, p21^{Cip1}-induced changes were associated with increased SA-β-Gal activity (Figure 3.35, upper panel) and flattened cell morphology (Figure 3.35, lower panel), and decreased BrdU incorporation into cellular DNA ($P < 0.001$; Figure 3.36).

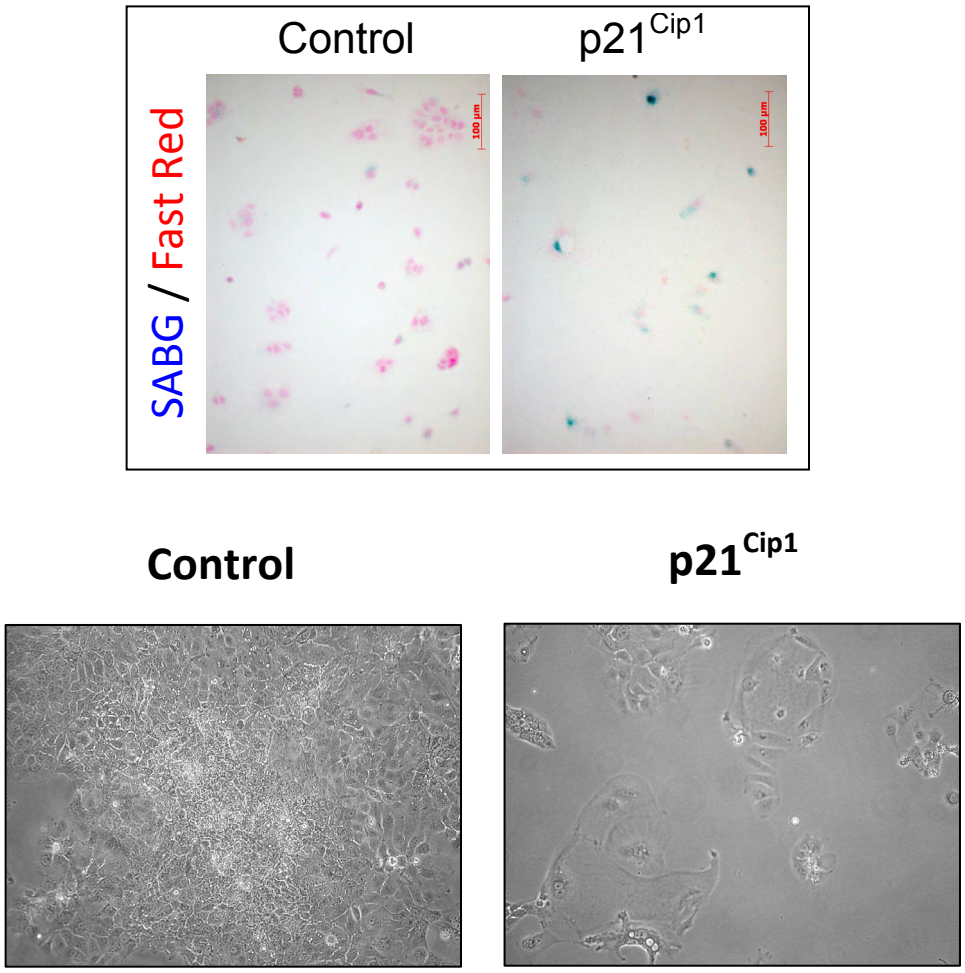

Figure 3.35: Changes in p21^{Cip1} overexpressing cells. Transiently transfected p21^{Cip1} overexpressing Huh7 cells displayed increased SA-β-Gal activity (upper panel), as well as flattened cell morphology (lower panel) at day eigth. Nuclear Fast Red was used for counterstaining in SA-β-Gal staining experiments.

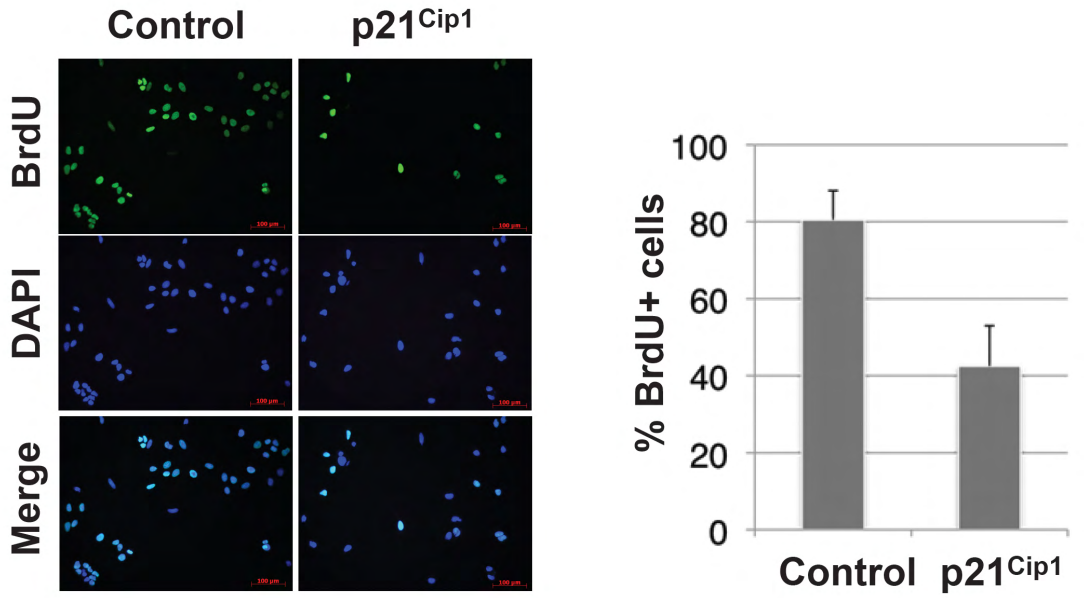

Figure 3.36: BrdU incorporation in $p21^{Cip1}$ overexpressing cells. Transiently transfected $p21^{Cip1}$ overexpressing Huh7 cells displayed decreased anti-BrdU immunofluorescence at day eight ($p < 0.001$). DAPI was used for counterstaining.

Transient overexpression of p15Ink4b induced similar changes when compared to p21Cip1. $p15^{Ink4b}$-transfected cells displayed moderately increased expression of the short form of $p15^{Ink4b}$, partly because of endogenous expression of $p15^{Ink4b}$ (Figure 3.34-B). Overexpression of $p15^{Ink4b}$ increased G1 cells from 59% to 66% and decreased S phase cells from 22% to 15% (Figure 3.33-C). These changes also were associated with increased SA-β-Gal activity (Figure 3.37), and decreased BrdU incorporation into cellular DNA ($P < 0.001$; Figure 3.38).

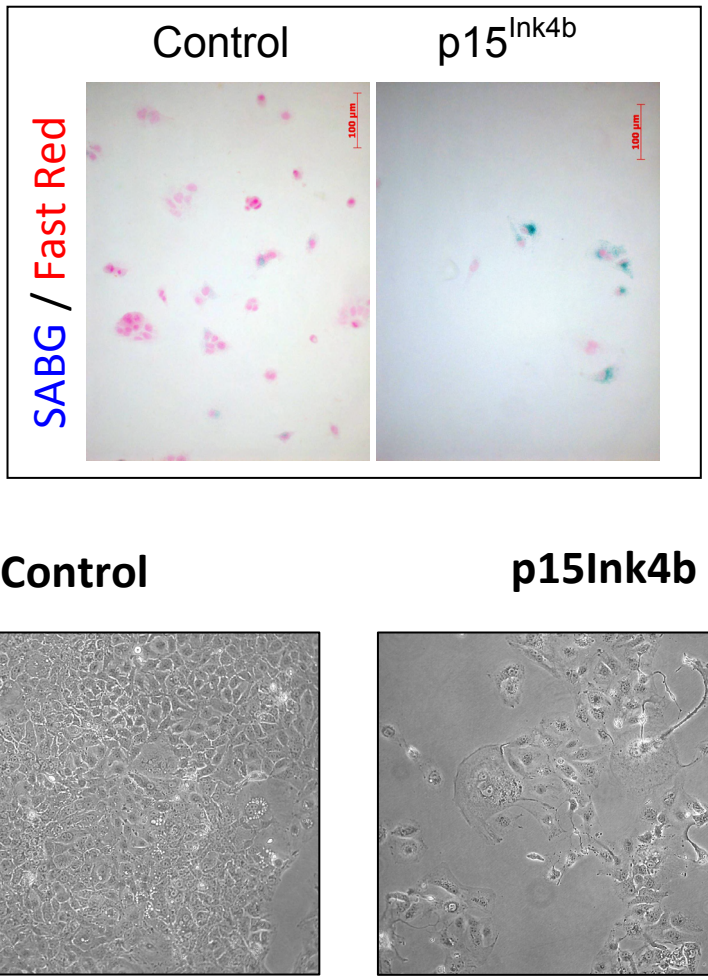

Figure 3.37: Changes in p15^{Ink4b} overexpressing cells. Transiently transfected p15^{Ink4b} overexpressing Huh7 cells displayed increased SA-β-Gal activity (upper panel) as well as flattened cell morphology (lower panel) at day eigth. Nuclear Fast Red was used for counterstaining in SA-β-Gal staining experiments.

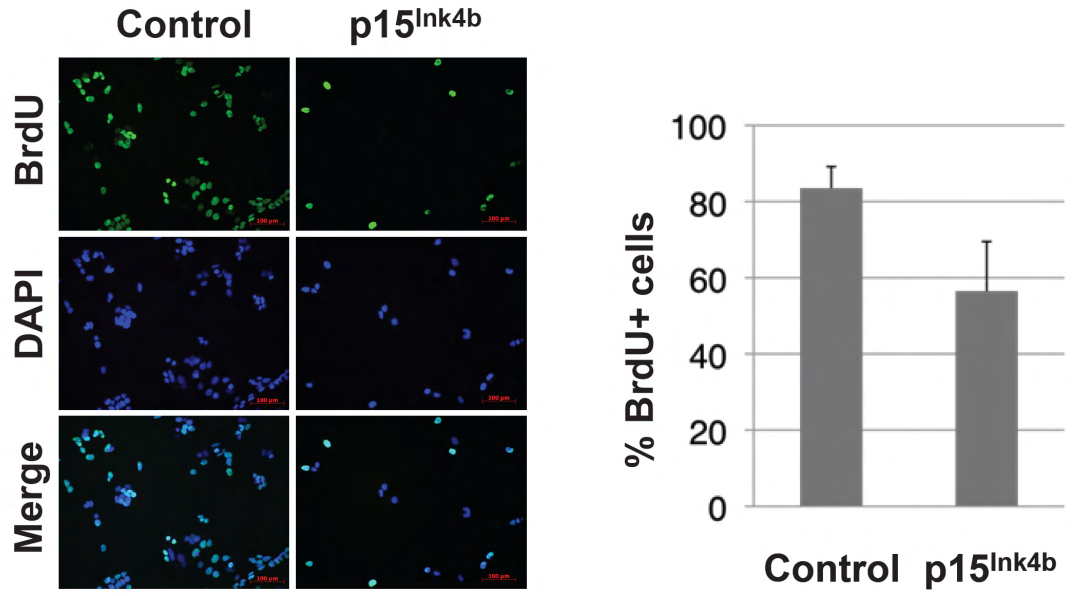

Figure 3.38: BrdU incorporation in $p15^{Ink4b}$ overexpressing cells. Transiently transfected $p15^{Ink4b}$ overexpressing Huh7 cells displayed decreased anti-BrdU immunofluorescence at day eight ($p < 0.001$). DAPI was used for counterstaining.

Senescence-related effects of $p21^{Cip1}$ were more dramatic than those induced by $p15^{Ink4b}$. Collectively, these findings demonstrated that TGF-β-induced senescence in HCC cells was associated with G1-phase arrest and significant reduction in the ability to reinitiate DNA synthesis. These effects appeared to be mediated mostly by $p21^{Cip1}$ with a significant contribution from $p15^{Ink4b}$ in Huh7 cell line.

3.9.6. TGF-β-induced senescence is linked to Nox4 induction and intracellular accumulation of reactive oxygen species

Several lines of evidence have implicated ROS in limiting longevity and organism life. However, exact implications of biochemical ROS mechanisms in physiologic basis of aging are not known. On the other hand, there are studies indicating that ROS accumulation contributes to senescence induced by Ras

oncoprotein in fibroblasts (Lee et al., 1999) as well as INF-gamma induced senescence in human umbilical vascular endothelial cells (HUVEC) (Kim et al., 2009b).

The generation of reactive oxygen species can be monitored by the aid of luminescence analyses or fluorescence methods. The intracellular generation of ROS can be investigated using DCFH-DA which is a well-established compound to detect intracellular reactive oxygen species, particularly hydroxyl radical, nitric oxide, peroxyl radical, singlet oxygen and superoxide anion. Non-fluorescent probe DCFH-DA is hydrolyzed inside the cell by nonspecific esterases to form DCFH. This compound is then oxidized by intracellular ROS to generate the highly fluorescent product DCF. In order to optimize intracellular ROS staining by DCFH-DA, we cultured Huh7 and Snu387 cells in serum-free growth conditions (data not shown), as oxidative stress inducing conditions (Osborne et al., 1998). Following these initial experiments, we decided on the concentration of DCFH-DA and the duration of the staining. Similar to DCFH-DA, we also utilized another compound MitoTracker Red CMXRos, a reduced and nonfluorescent version of MitoTracker Red. CMXRos diffuses across the plasma membrane, accumulates in active mitochondria and fluoresces upon oxidation; an event which is dependent on the membrane potential.

Treatment of hepatocytes with TGF-β provokes ROS accumulation (Sanchez et al., 1996) most probably by activating a NADPH-oxidase (Nox)-like system (Herrera et al., 2004) via Nox4 induction (Carmona-Cuenca et al., 2006). In addition, Nox family members have recently been identified as candidates to promote ROS accumulation in human endothelial cells (Schilder et al., 2009). Therefore, we investigated the potential role of reactive oxygen species in TGF-β-induced senescence with a particular interest in the contribution of Nox4 induction.

We first demonstrated that TGF-β regulated Nox4 expression in a dose-dependent manner both at the mRNA and protein level (Figure 3.39).

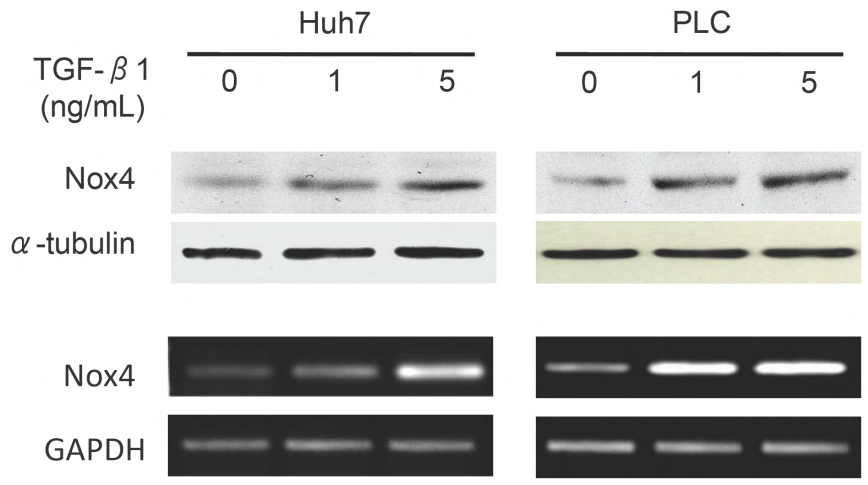

Figure 3.39: TGF-β-regulated Nox4 expression in Huh7 and PLC cells. Both cell lines were treated with indicated doses of TGF-β1 for 72 hr and tested for Nox4 expression at RNA and protein level. A-tubulin and GAPDH served as internal controls in western blotting and RT-PCR experiments, respectively.

We then tested ROS accumulation in selected well-differentiated cell lines upon TGF-β1-treatment in a similar experimental set-up used in senescence experiments. We observed high levels of intracellular ROS signals in TGF-β-treated cells, but not in non-treated cells (Figure 3.40).

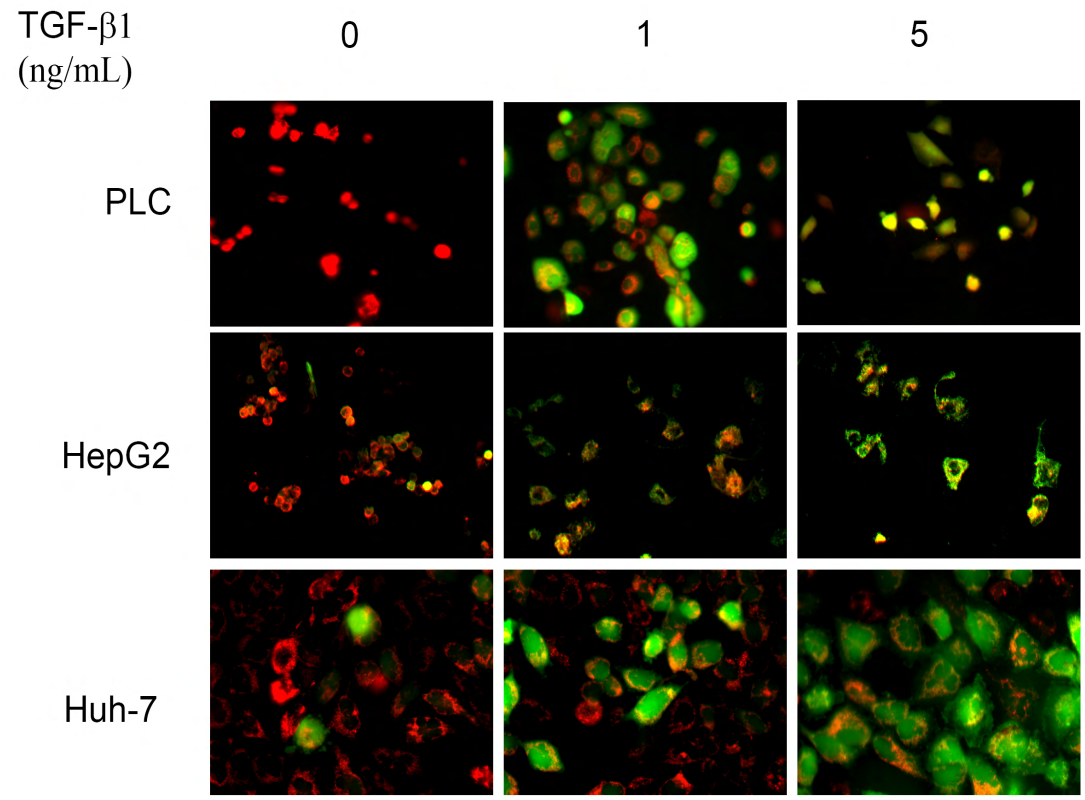

Figure 3.40: TGF-β1 induced ROS accumulation in WD cell lines. WD cell lines were treated with different doses of TGF-β1 for 72 hr. DCFH-DA (green) staining indicates ROS accumulation inside the cell. Mitochondrial dye MitoTracker (red) was used as mitochondrial ROS probe. Pictures were taken at 20X.

From these results, we excluded the possible involvement of TGF-β in mitochondrial ROS production in WD cell lines, as we were not able to detect a significant change in the mitochondrial signal after staining with MitoTracker CMXRos with IF technique.

On the other hand, if ROS played a critical role in TGF-β1 induced senescence response, we should be able to interfere with this response by preventing ROS accumulation in TGF-β1-treated cells. We, therefore, used N-acetyl-L-cysteine (NAC) as a physiological ROS scavenger (Droge, 2002) to test this hypothesis. The co-treatment of 5 ng/mL TGF-β1-treated cells together with 10 mM NAC completely suppressed the accumulation of ROS in Huh7 and PLC cell lines (Figure 3.41), as well as the accumulation of SA-β-Gal-positive cells (Figure 3.42).

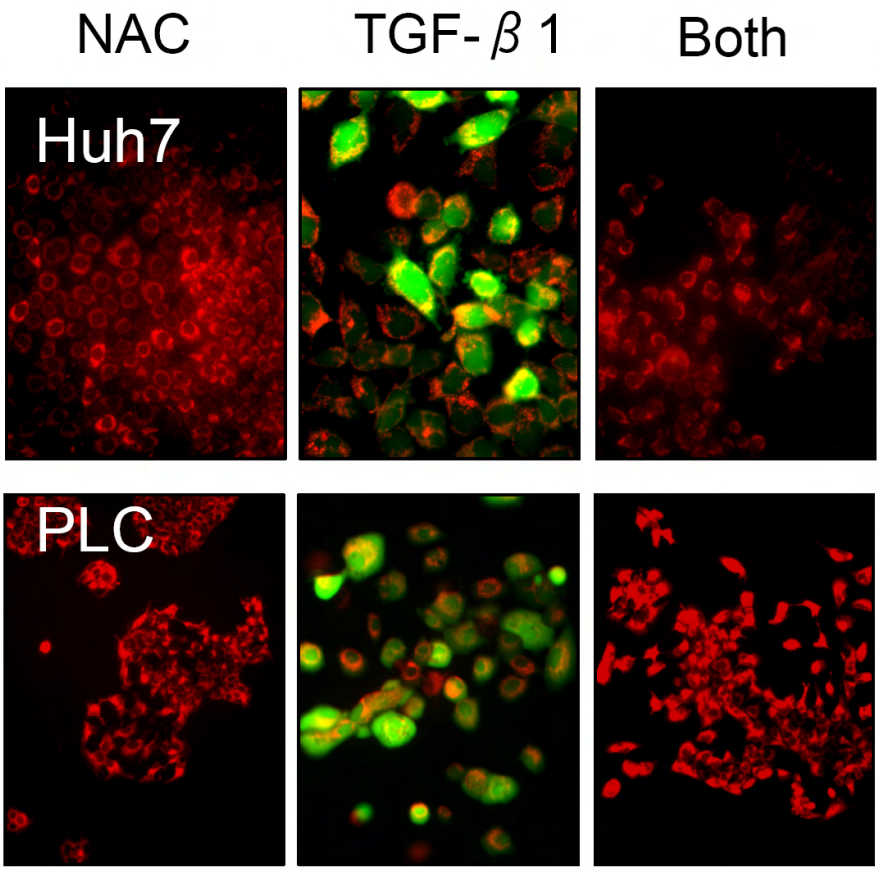

Figure 3.41: TGF-β1 induced ROS accumulation in WD cell lines after NAC treatment. WD cell lines were treated with 5 ng/mL TGF-β1 alone or together with 10 mM NAC for 72 hr. DCFH-DA (green) staining indicates ROS accumulation inside the cell. Mitochondrial dye MitoTracker (red) was used as mitochondrial ROS probe. Pictures were taken at 20X.

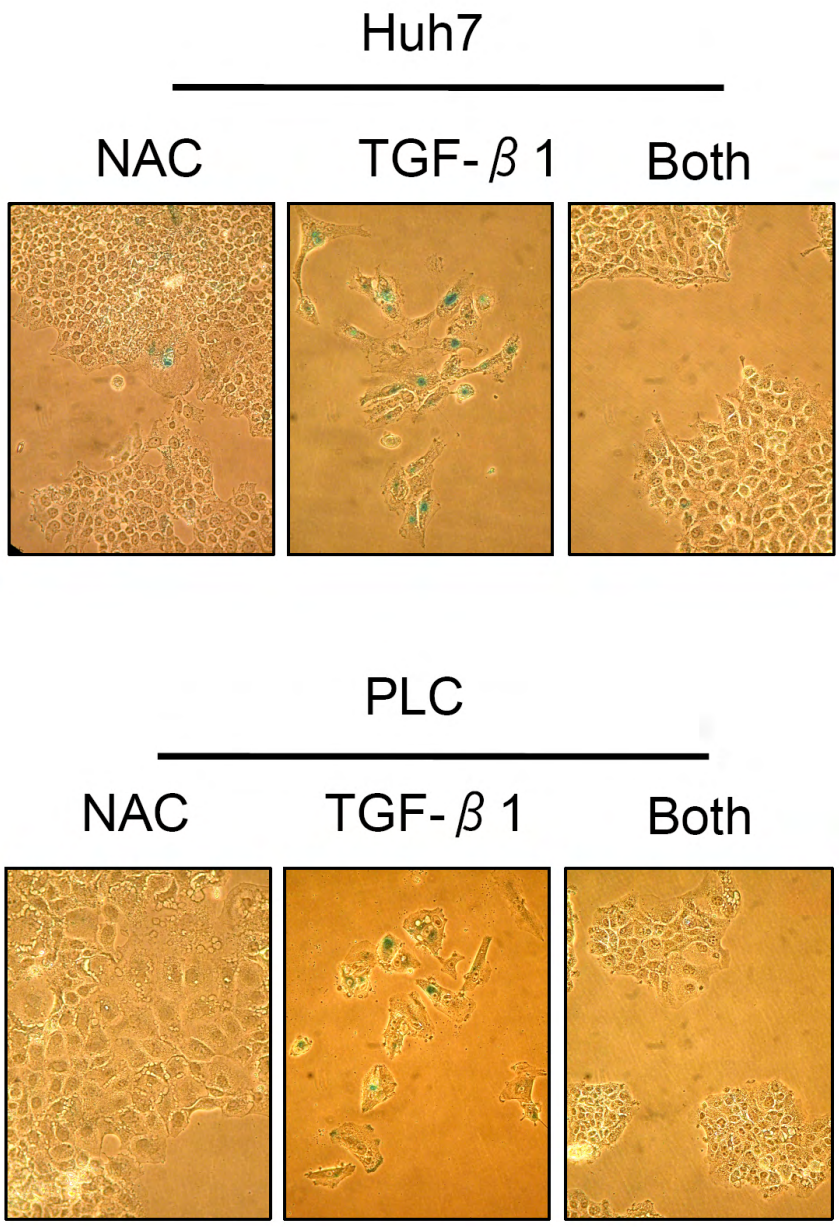

Figure 3.42: Rescue of senescence after NAC treatment. Co-treatment of TGF-β1 (5 ng/mL)-treated cells with ROS scavenger NAC (10 mM) for 72 hr rescued senescence arrest as tested by SA-β-Gal assay. Pictures were taken at 20X.

Co-treatment with NAC treatment also strongly inhibited TGF-β1-induced expression of $p15^{Ink4b}$ and $p21^{Cip1}$, and restored pRb phosphorylation, without affecting Nox4 levels in PLC cells (Figure 3.43). Similar results were obtained with Huh7 (data not shown).

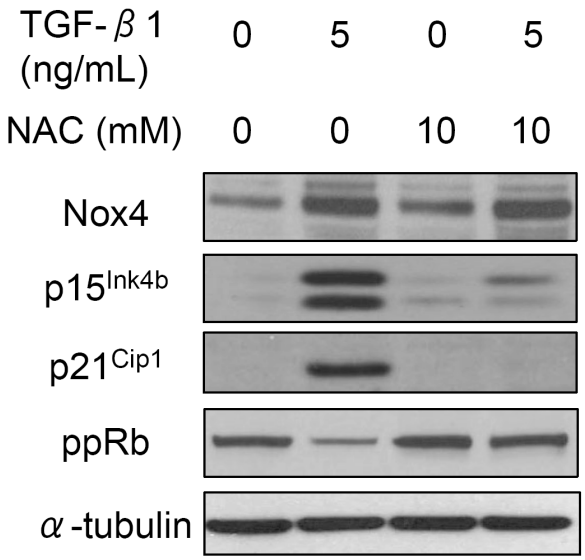

Figure 3.43: Implication of ROS in TGF-β-induced gene expression regulation. Co-treatment of TGF-β1 (5 ng/mL)-treated PLC cells with ROS scavenger NAC (10 mM) for 72 hr reversed TGF-β1 mediated expression effects. ppRb (ser807/811). α-tubulin was used for equal loading.

Nevertheless, the prevention of ROS accumulation and the inhibition of $p15^{Ink4b}$ and $p21^{Cip1}$ induction by NAC were sufficient to rescue TGF-β1-induced growth arrest as tested by BrdU incorporation (Figure 3.44, left) and cell cycle analysis in Huh7 and PLC cell lines (Figure 3.44, right).

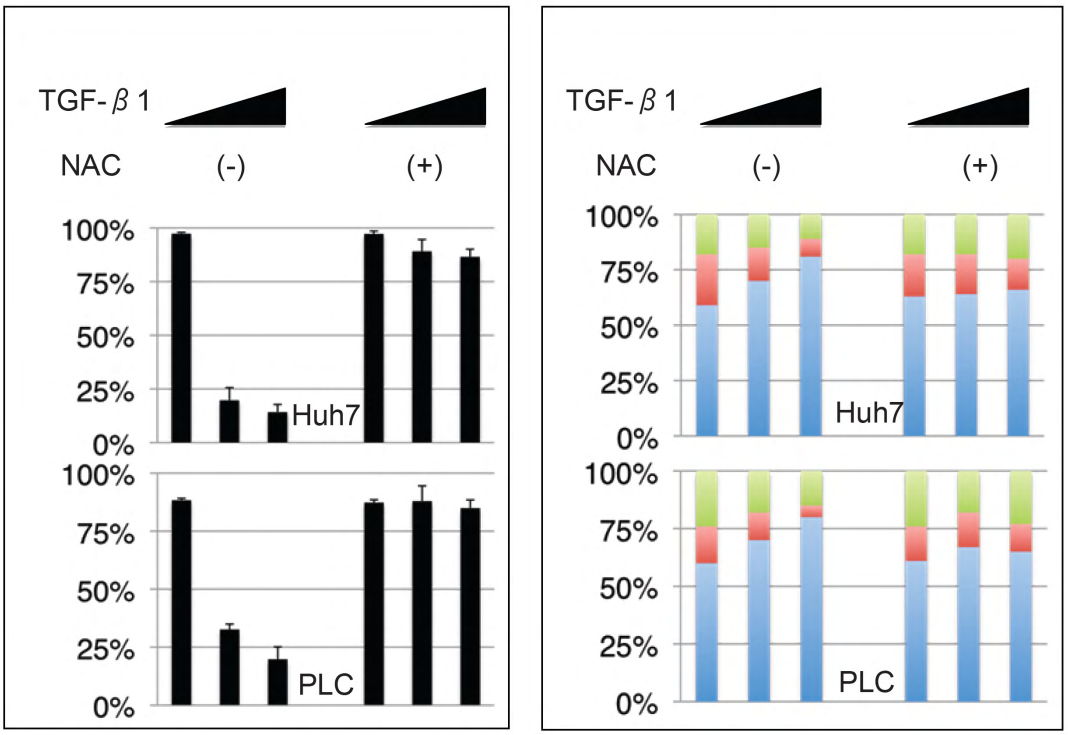

Figure 3.44: Implication of ROS in TGF-β-induced growth arrest. Co-treatment of TGF-β1 (1 ng/mL and 5 ng/mL)-treated Huh7 and PLC cells with ROS scavenger NAC (10 mM) for 72 hr reversed TGF-β1 mediated growth arrest effects.

Taken together, all these effects exerted by NAC demonstrate a causal link between reactive oxygen species accumulation and the stimulation of TGF-β-induced growth arrest and the onset of senescence. Moreover, the inhibitory mechanism of NAC activity does not involve any interference with TGF-β signal transduction as we demonstrated by immunofluorescence experiment with activated Smad3 (Figure 3.45). In this setting, we showed that treatment of PLC cells with 5 ng/mL TGF-β1 for 30 min provoked nuclear localization of phospho-Smad3 and moreover this effect was not interrupted by 10 mM NAC co-treatment. We observed similar results when treatments were performed for 2 hr (data not shown).

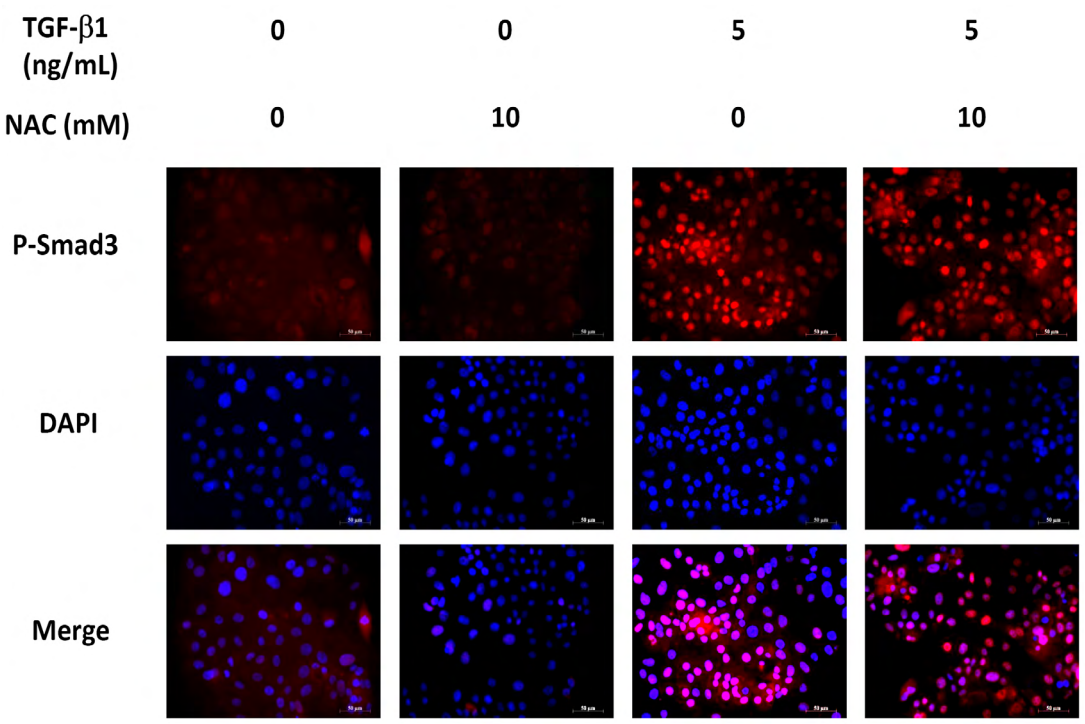

Figure 3.45: TGF-β1 induced nuclear p-Smad3 accumulation in PLC cell line. PLC cells were treated with 5 ng/mL TGF-β1 alone or together with 10 mM NAC for 30 min. Cells were stained with primary abs against p-Smad3 which was followed by Alexa 568 secondary antibody. DAPI served as nuclear counterstaining. Pictures were taken at 40X (scale bar: 50 μM).

3.9.7. NOX4 gene silencing interferes with TGF-β-induced $p21^{Cip1}$ accumulation and growth arrest

The correlation between Nox4 induction, ROS accumulation and senescence arrest, suggested that the Nox protein might serve as a key intermediate in TGF-β-induced senescence. In order to test whether Nox4 was indeed involved in TGF-β-induced senescence, we performed NOX4 gene silencing by siRNA. Huh7 cells were first transfected with NOX4 specific siRNA and a scrambled siRNA, as control. Cells were trypsinized and divided into two fractions following 24 hr post-transfection. This was followed by treatment with either 5 ng/mL TGF-β1 or vehicle only for 72 hr. At this time-point, we tested the expression of NOX4 RNA and protein levels by qPCR and western blot, respectively.

We demonstrated that TGF-β-induced accumulation was inhibited by ~75% by NOX4-specific siRNA, but not scrambled siRNA (Figure 3.46).

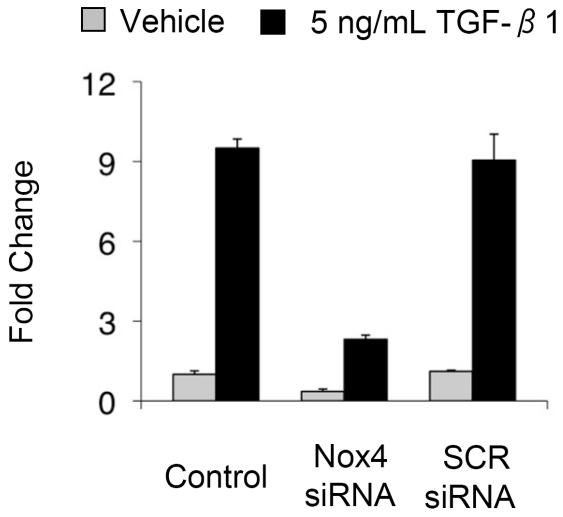

Figure 3.46: Inhibition of TGF-β-induced accumulation of Nox4 transcripts by siRNA transfection. Huh7 cells were transfected with 10 nM Nox4-specific siRNA and corresponding scrambled siRNA. Cells were treated with 5 ng/mL TGF-β for 72 hr and subjected to qRT-PCR analysis. Experiments were performed in triplicate. GAPDH was used as normalization control.

Under these conditions, we also detected a substantial inhibition in TGF-β-induced NOX4 protein accumulation after NOX4-specific siRNA transfection (Figure 3.47).

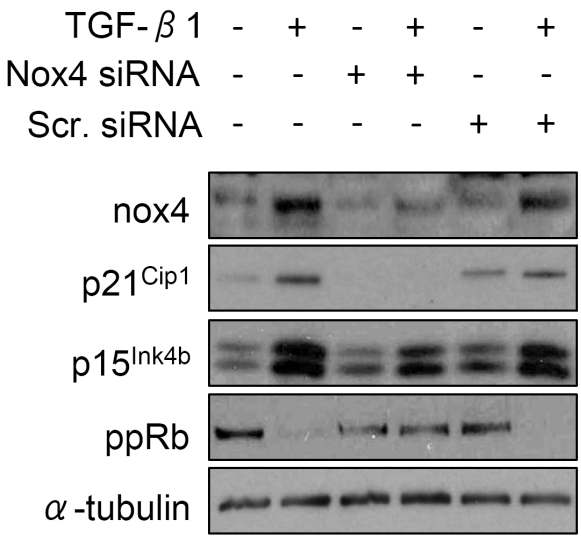

Figure 3.47: NOX4 gene silencing rescued TGF-β-induced Nox4, $p21^{Cip1}$ and $p15^{Ink4b}$ protein accumulation and the inhibition of pRb phosphorylation. Huh7 cells were transfected with 10 nM Nox4-specific siRNA and corresponding scrambled siRNA. Cells were treated with 5 ng/mL TGF-β1 for 72 hr and subjected to western blotting analysis. α-tubulin was used as control loading.

Moreover, the inhibition of Nox4 protein expression resulted in strong inhibition of $p21^{Cip1}$ accumulation, but $p15^{Ink4b}$ levels were affected mildly. More interestingly, the loss of phosphorylated pRb (ppRb) in TGF-β-treated cells was restored in association with Nox4 inhibition.

The effects of siRNA-mediated Nox4 inhibition on cell proliferation were intriguing. The incorporation of BrdU into cellular DNA was inhibited by more than 85% in TGF-β-treated cells in the absence of Nox4 siRNA. NOX4 gene silencing restored this effect, almost completely (Figure 3.48).

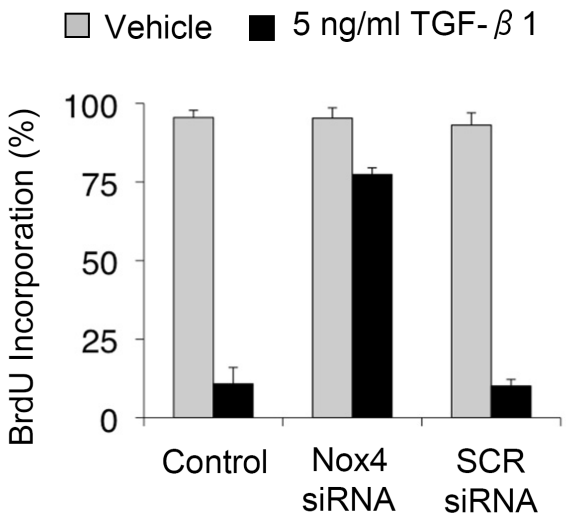

Figure 3.48: Nox4 gene silencing rescued TGF-β-induced growth arrest. Huh7 cells were transfected with 10 nM Nox4-specific siRNA and corresponding scrambled siRNA. Cells were treated with 5 ng/mL TGF-β for 72 hr and subjected to BrdU immunostaining. Cells were labelled with BrdU for 24 hr prior to day 3, and percent BrdU-positive cells were counted manually.

In conclusion, growth arrest induced by TGF-β in Huh7 cells was restored upon inhibition of Nox4 induction.

3.9.8. Implications of DNA-damage response in TGF-β-induced senescence arrest

3.9.8.1. 53BP1 foci formation

Intracellular as well as mitochondrial reactive oxygen species have been implicated in DNA-damage response (Courtois-Cox et al., 2008). Moreover, both telomere-dependent and telomere-independent senescence is now recognized as a DNA damage response (DDR), and such response can be quantitatively examined by analyzing DNA foci formation with DDR proteins such as 53BP1 (d'Adda di Fagagna, 2008). In development of such a hypothesis, we exposed Huh7 cell line to

1 and 5 ng/mL TGF-β1 for a short period (~ 20 seconds), and examined for nuclear 53BP1 foci formation by an immunofluorescence assay (Figure 3.49).

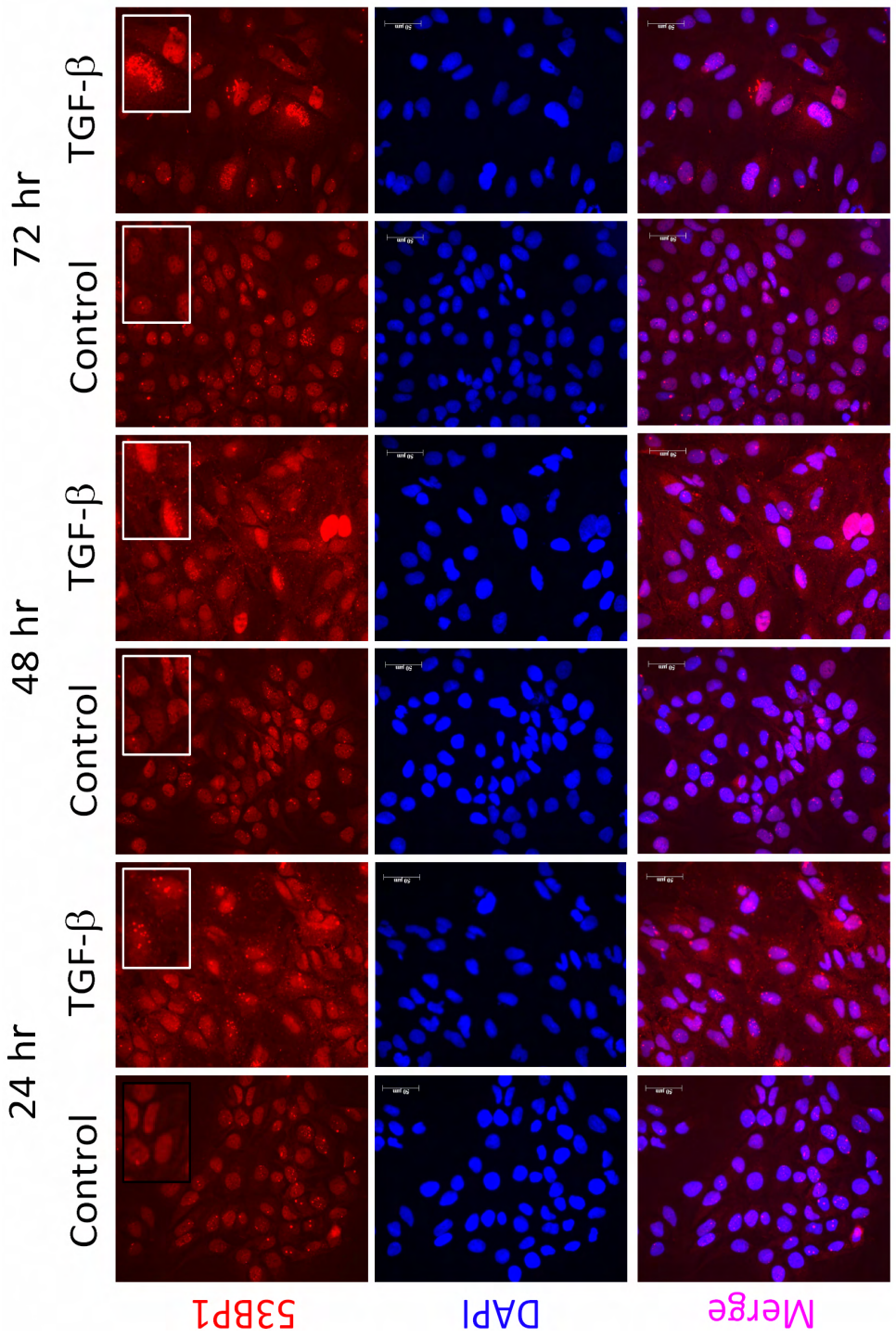

Figure 3.49: DNA damage response in TGF-β-treated cells. 53BP1 foci in TGF-β1-treated cells. Control and TGF-β1-treated (~ 20 seconds) cells were subjected to 53BP1 immunofluorescence assay after 24, 48 and 72 hours of culture. Pictures shown were taken from control and 1 ng/mL TGF-β1-treated cells.

Mean values for 53BP1 foci (> 4 foci/nucleus) were calculated by manual counting (Figure 3.50).

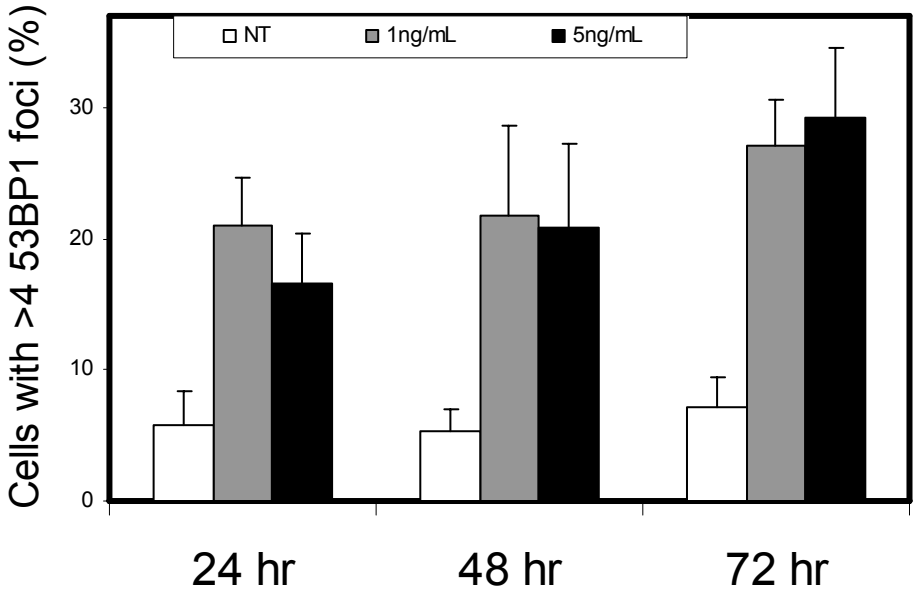

Figure 3.50: DNA damage response in TGF-β-treated cells. Histograms indicate the percentage of cells with at least 5 clearly detectable foci (mean ± SD). More than 100 cells were screened per point in independent experiments. Compared to control cells, 1 ng/mL and 5 ng/mL TGF-β1 treatment significantly increased the percentage of 53BP1-positive cells ($P < 0.001$ for both doses and all time points tested).

53BP1 foci were 6%, 5% and 7% in untreated cells at 24, 48 and 72 hr, respectively. With 1 ng/mL TGF-β1, 21%, 21% and 27% of cells displayed increased 53BP1 foci formation at 24, 48 and 72 hr, respectively ~4-fold increase; $P < 0.001$. Similarly, with 5 ng/mL TGF-β1, 17%, 21% and 29% of cells displayed increased foci formation at 24, 48, and 72 hr, respectively ~4-fold increase; $P < 0.001$.

3.9.8.2. Ataxia telangiectasia mutated (ATM) activation

ATM activation is a central event in DNA-damage response in double strand-breaks. However, activation of ATM was also reported in various other studies which implicated a potential role for TGF-β signaling (Wiegman et al., 2007; Zhang et al., 2006a). Therefore, we tested TGF-β-stimulated ATM activation in Huh7 cells after exposure to commonly used doses 1 ng/mL and 5 ng/mL for less than 1 min. In an effort to assess time-dependent stimulation of ATM, we performed immunofluorescence staining at different time points (Figure 3.51).

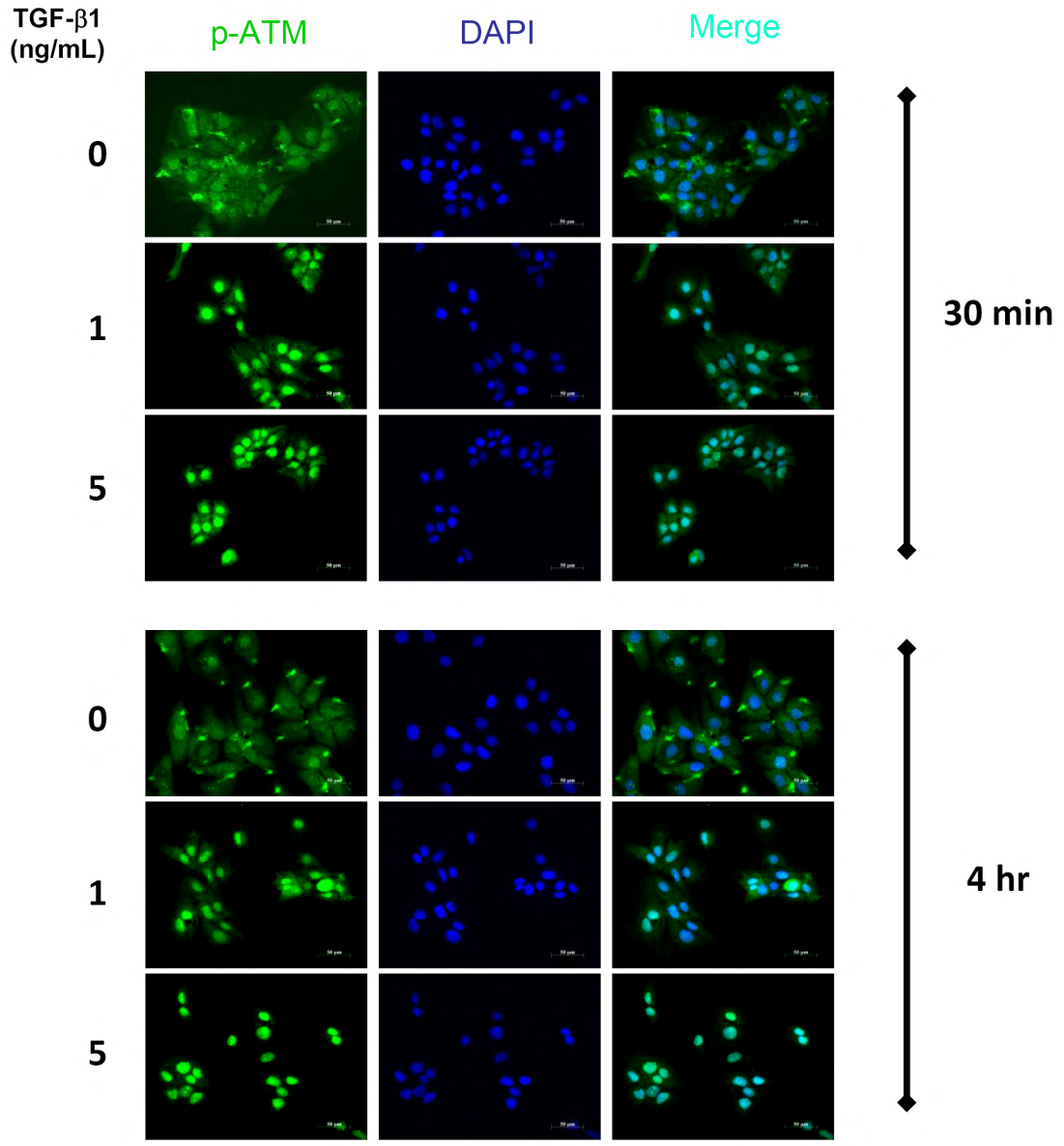

Figure 3.51-A: ATM activation after brief exposure to TGF-β1. Huh7 cells were treated with 1 ng/mL and 5 ng/mL TGF-β for less than 1 min. Immunofluorescence analysis was performed after 30 min and 4 hr, respectively. DAPI was used to stain the nuclei.

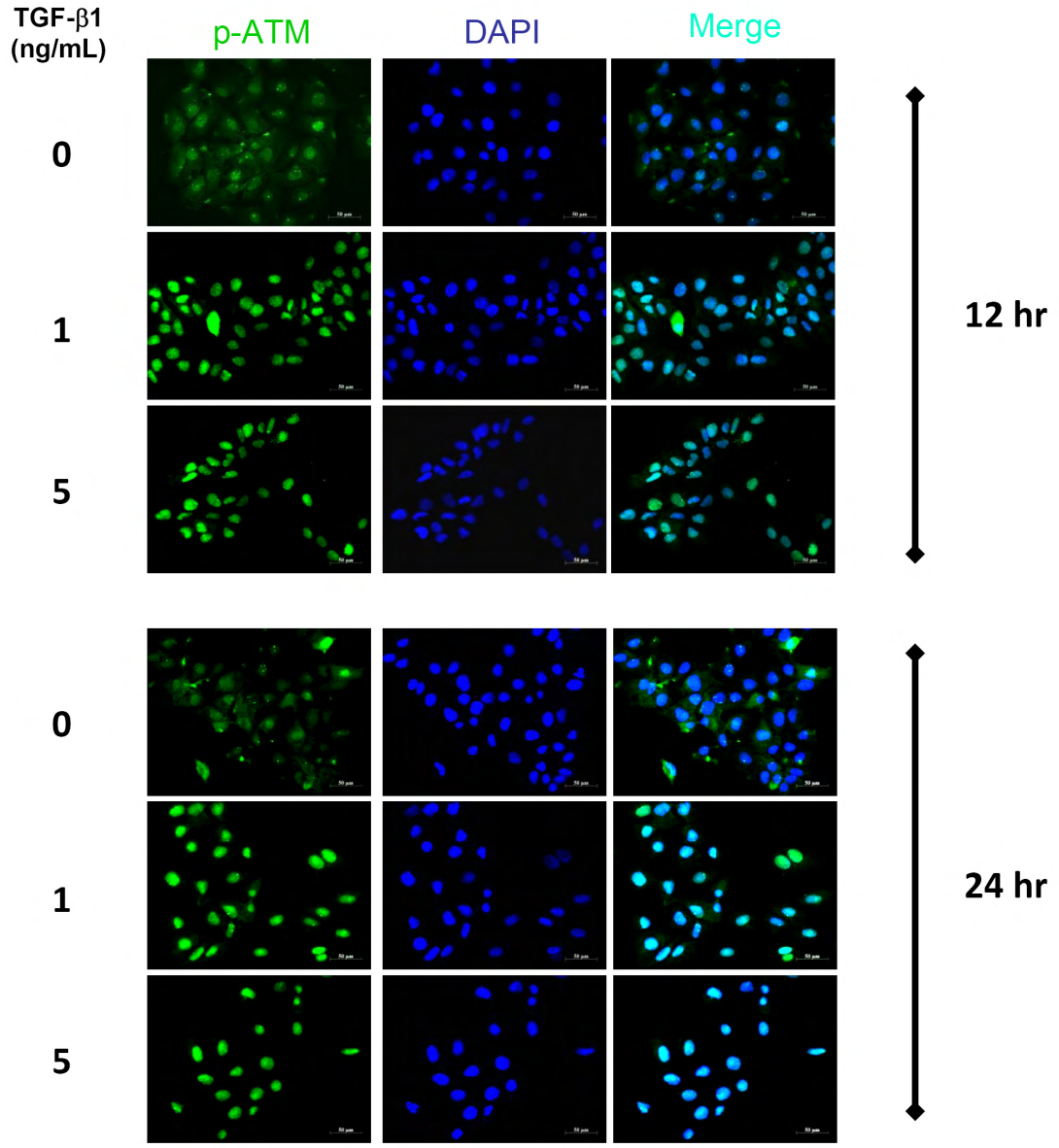

Figure 3.51-B: ATM activation after brief exposure to TGF-β1. Huh7 cells were treated with 1 ng/mL and 5 ng/mL TGF-β for less than 1 min. Immunofluorescence analysis was performed after 12 hr and 24 hr, respectively. DAPI was used to stain the nuclei.

In control cells, p-ATM showed intracellular diffuse staining. Whereas, the treatment with TGF-β caused dense nuclear staining with detectable increase at the first time-point tested. The staining was also dose-dependent. Nuclear staining reached a peak level at 4 hr and maintained high until 24 hr. At 48 hr and 72 hr, nuclear staining density decreased with immense cytoplasmic staining.

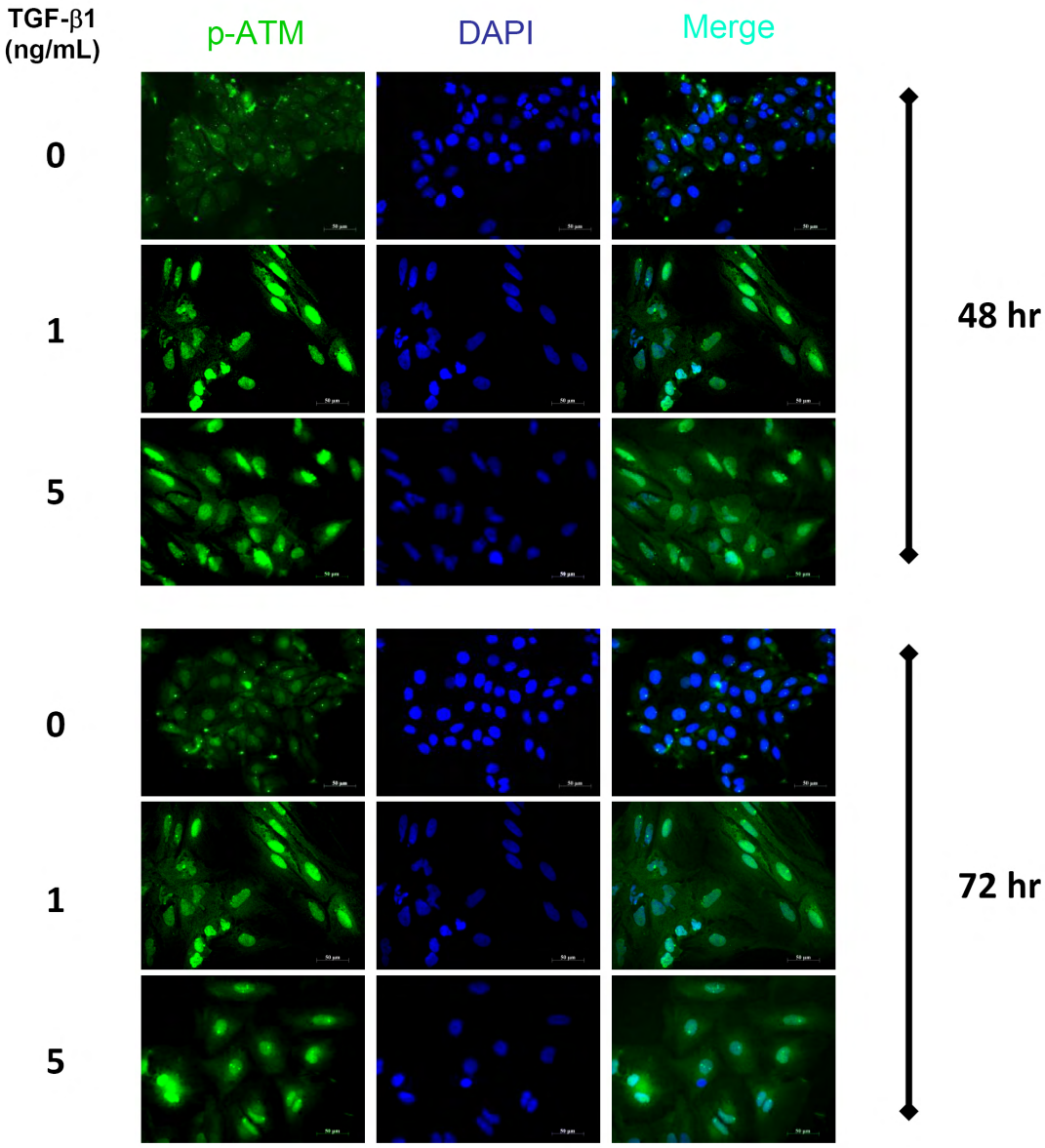

Figure 3.51-C: ATM activation after brief exposure to TGF-β1. Huh7 cells were treated with 1 ng/mL and 5 ng/mL TGF-β for less than 1 min. Immunofluorescence analysis was performed after 48 hr and 72 hr, respectively. DAPI was used to stain the nuclei.

Taken together, these results demonstrated a potential involvement of TGF-β signaling pathway in ATM activation and nuclear translocation of p-ATM. These findings also suggested a potential role for TGF-β in the onset of DNA-damage response.

3.10. TGF-beta-induced senescence and anti-tumor activity in vivo

Collectively, our *in vitro* studies provided strong evidence for a major senescence-inducing role for TGF-β in well-differentiated HCC cells. Additionally, we tested *in vivo* relevance of these findings by a series of animal experiments. In an effort to test this issue, we established human HCC tumors in immunodeficient mice.

First, we tested whether TGF-β1 induces senescence in Huh7 tumors. TGF-β1 (~ 50 µL of a 10 ng/mL solution) was injected into subcutaneous Huh7 tumors. Control experiments were performed using solution vehicle only, under parallel conditions. Tumors were removed one week later (Figure 3.52) and subjected to SA-β-Gal staining.

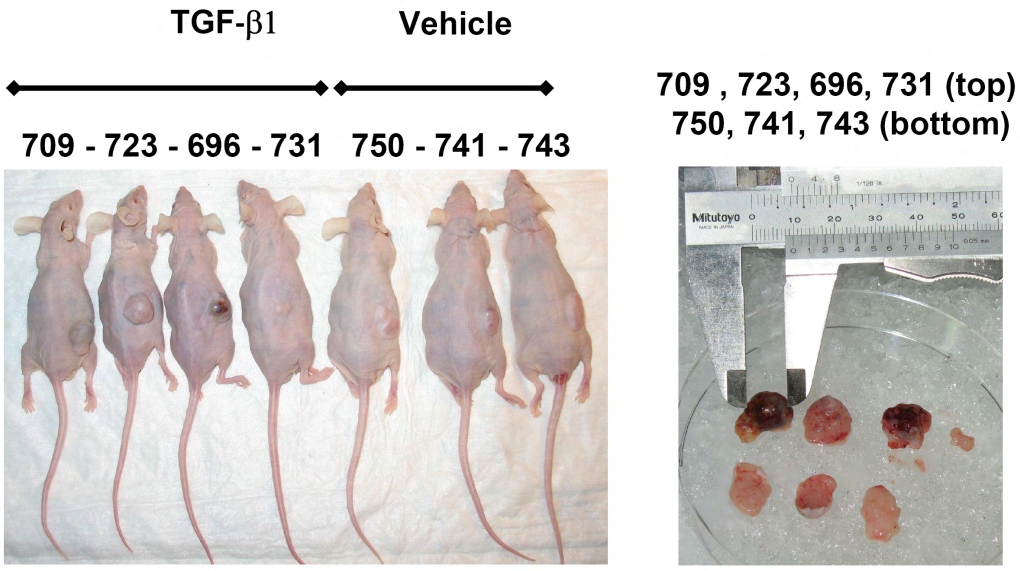

Figure 3.52: Nude mice and extracted Huh7 tumors

Intratumoral injection of TGF-β1 (~ 0.5 ng) induced local but expanded SA-β-Gal activity in three of four tumors tested; whereas three tumors treated with vehicle only were completely negative (Figure 3.53).

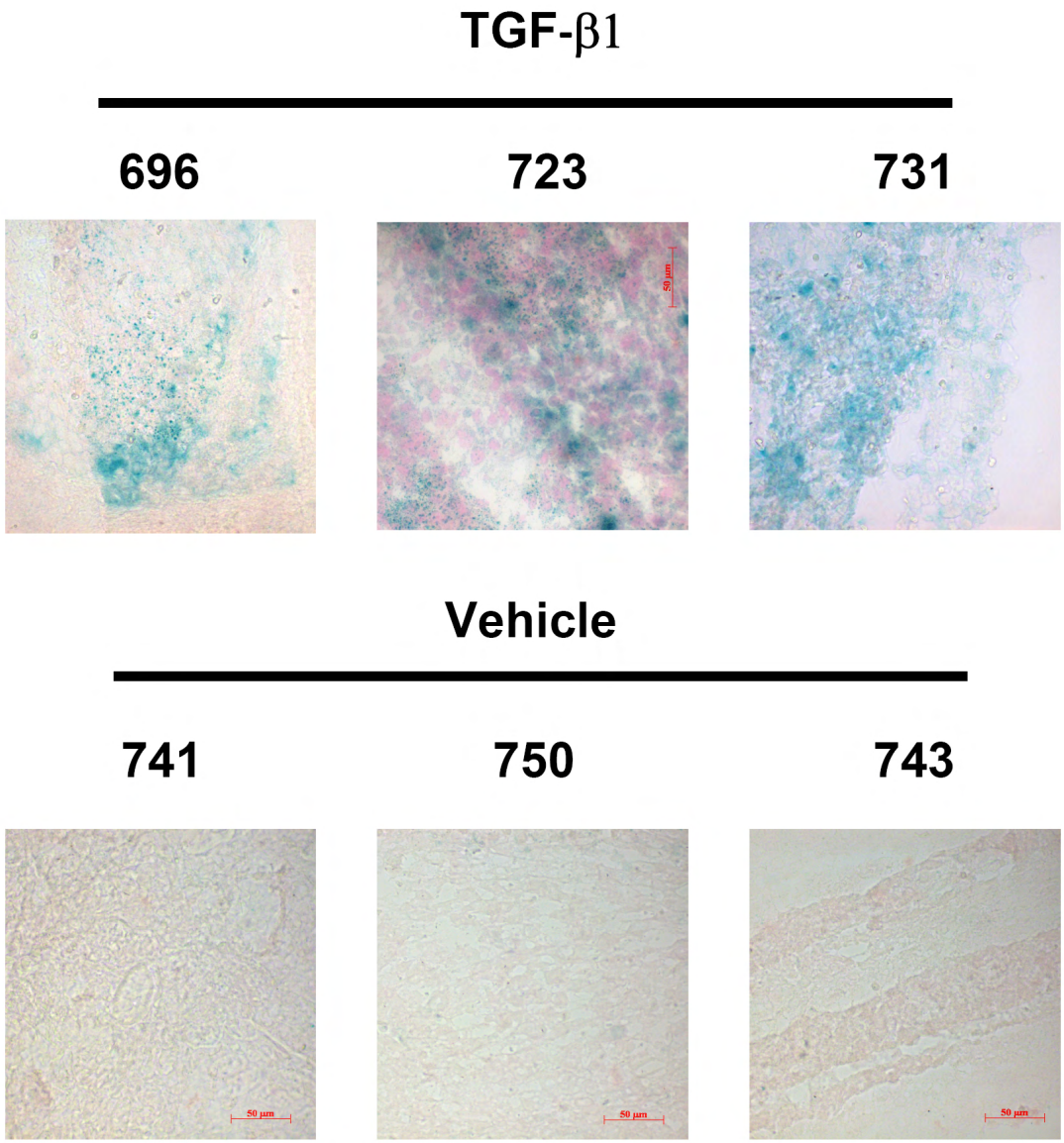

Figure 3.53: TGF-β1-induced SA-β-Gal activity in Huh7 tumors. Huh7 cells were injected subcutaneously to *nude* mice to obtain tumors that were then injected with TGF-β1 (~50 ul of 10 ng/mL solution) or a vehicle control by intratumoral injection, and animals were sacrificed seven days later to collect tumor tissues. Cryostat sections were prepared from freshly frozen tumors and subjected to SA-β-Gal staining (blue). Counterstain: Nuclear Fast Red.

Next, we tested whether TGF-β treatment exerts any anti-tumor activity against Huh7 tumors raised in immunodeficient mice. Early subcutaneous tumors were subjected to either TGF-β1 (2 ng per peritumoral injection, ~ 50 ul of 10 ng/mL

solution) or vehicle treatment with four days of intervals. TGF-β1 treatment lasted 24 days and tumor sizes were measured prior to each injection. As shown in Figure 3.54, vehicle-treated tumors displayed exponential growth to reach 4 cm^3 volume on average within 24 days. In contrast, TGF-β-treated tumors were growth arrested throughout the experiment and remained less than 1 cm^3 on average at the same time period.

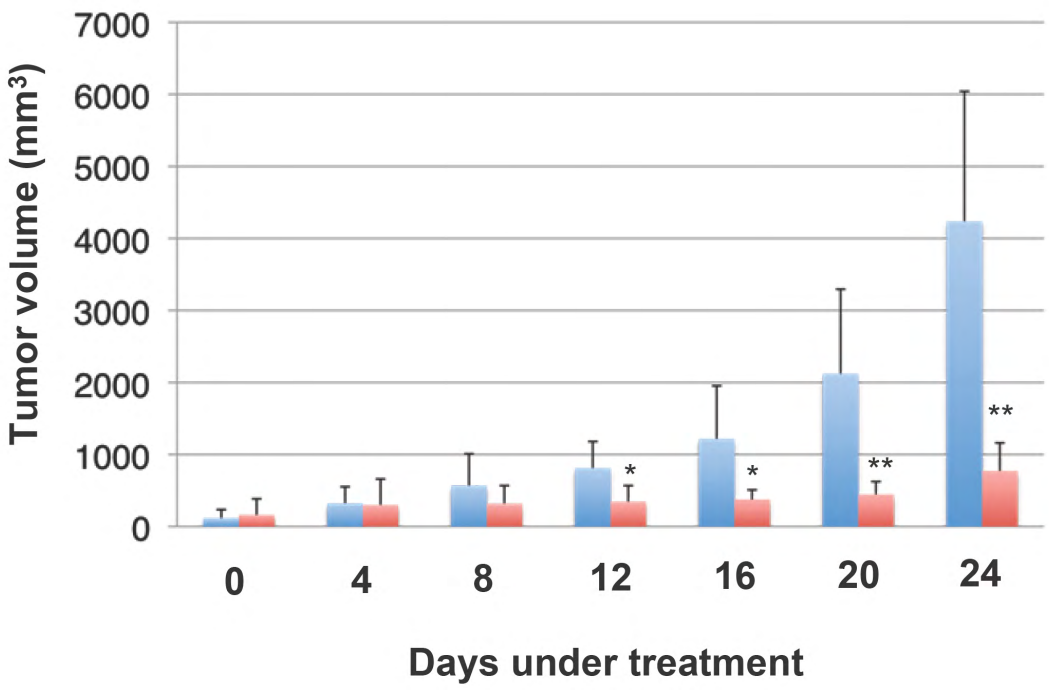

Figure 3.54: Inhibition of tumor growth by TGF-β. Huh7 tumors were treated with 2 ng TGF-β or vehicle control only at 4-day intervals and tumor sizes were measured accordingly. TGF-β treated tumors were growth arrested, resulting in > 75% inhibition of tumor growth. * $P < 0.05$, ** $P < 0.01$.

This inhibition of preexisting tumor growth by TGF-β treatment was statistically significant after 12 days of treatment or after three doses ($P < 0.05$) Tumor inhibition remained significant at least 24 days or after six doses ($P < 0.01$ to < 0.05). However, TGF-β treatment did not completely eliminate the tumor mass, even though two tumors totally regressed and disappeared. As an additional test for anti-tumor activity of TGF-β signaling, we compared the tumorigenicity of

TFGBR2-deleted Hep3B-TR cells (Inagaki et al., 1993) with parental Hep3B cells. Hep3B and Hep3B-TR cells were injected subcutaneously ($5x10^6$ cells/animal). Three animals injected with Hep3B-TR cells developed palpable tumors within two weeks of injection and died within 4-6 weeks. Three other animals injected with Hep3B cells also developed tumors, but with a latency of 6-7 weeks (Figure 3.55).

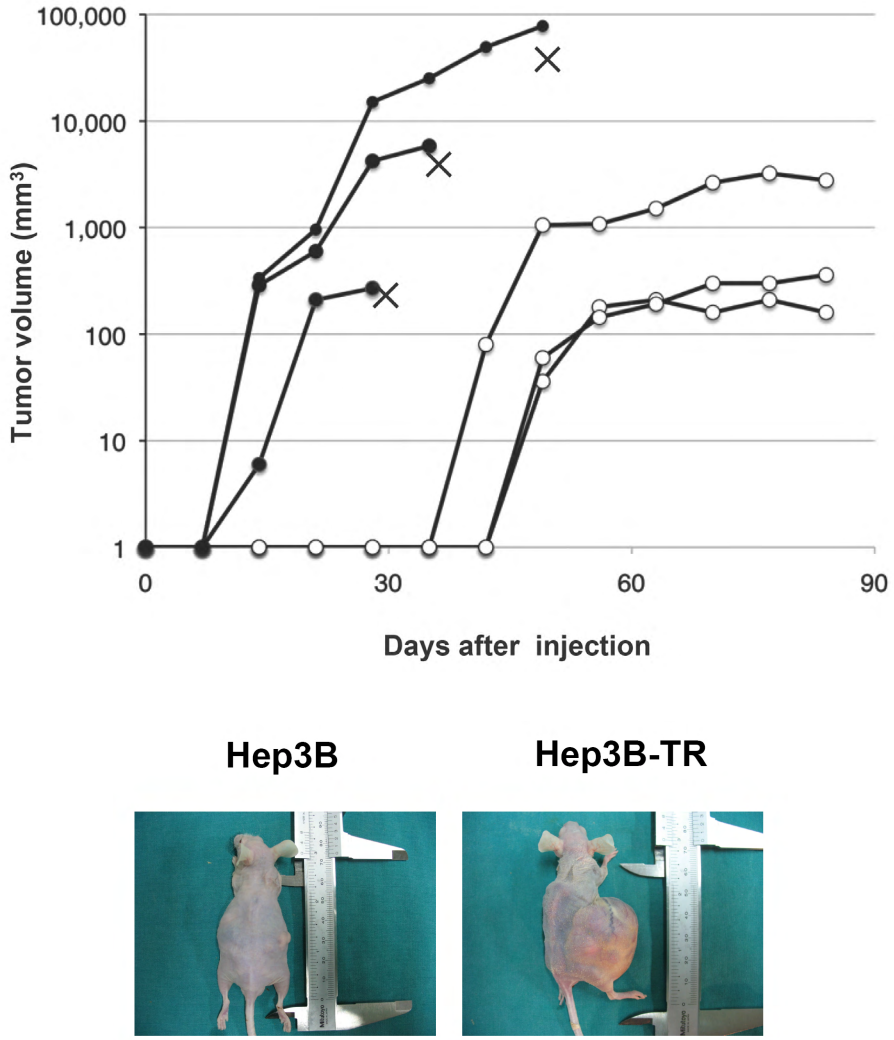

Figure 3.55: Hep3B-TR cells that display homozygous TGFBR2 deletion displayed accelerated tumorigenicity, as compared to parental Hep3B cells. Cells ($5x10^6$) were injected subcutaneously to *nude* mice and tumor sizes were measured on a weekly basis. X indicates animal death. Pictures were taken from representative animals with tumors at day 35.

As increased tumorigenicity of Hep3B-TR cells has been reported by others during these studies (Zimonjic et al., 2009), we discontinued our animal experiments for ethical reasons and concluded that the genetic disruption of TGF-β signaling in HCC cells may lead to increased tumorigenicity.

3.11. Resistance mechanisms to TGF-β-induced growth arrest in poorly differentiated cell lines

As previously stated, we classified human HCC cell lines into "well-differentiated" (WD) and "poorly differentiated" (PD) subtypes based on the expression of hepatocyte lineage, epithelial and mesenchymal markers (Yuzugullu et al., 2009).

3.11.1. TGF-β receptor expression in poorly differentiated (PD) cell lines

After we performed studies with well-differentiated cell lines to understand the relevance of senescence induction and mechanisms, we then moved on to evaluate poorly differentiated cell lines. In this context, we investigated nine PD cell lines to investigate their ability to undergo senescence arrest following TGF-β treatment.

Prior to these studies, we explored the status of TGF-β1 ligand and TGF-β receptor and intracellular signaling components expression in these cell lines by RT-PCR analysis of the relevant transcripts (Figure 3.56). Our studies demonstrated that almost all HCC cell lines tested expressed TGF-β1 ligand and receptors and intracellular signaling components. Of note, Snu398 cells had markedly decreased TGFβRII expression, as reported previously (Kitisin et al., 2007). SMAD genes located downstream to TGF-β receptors display mutations only rarely in primary HCC, but not in HCC cell lines (Yakicier et al., 1999). Thus, it appears that the main components of TGF-β signaling are intact and present in most HCC cell lines.

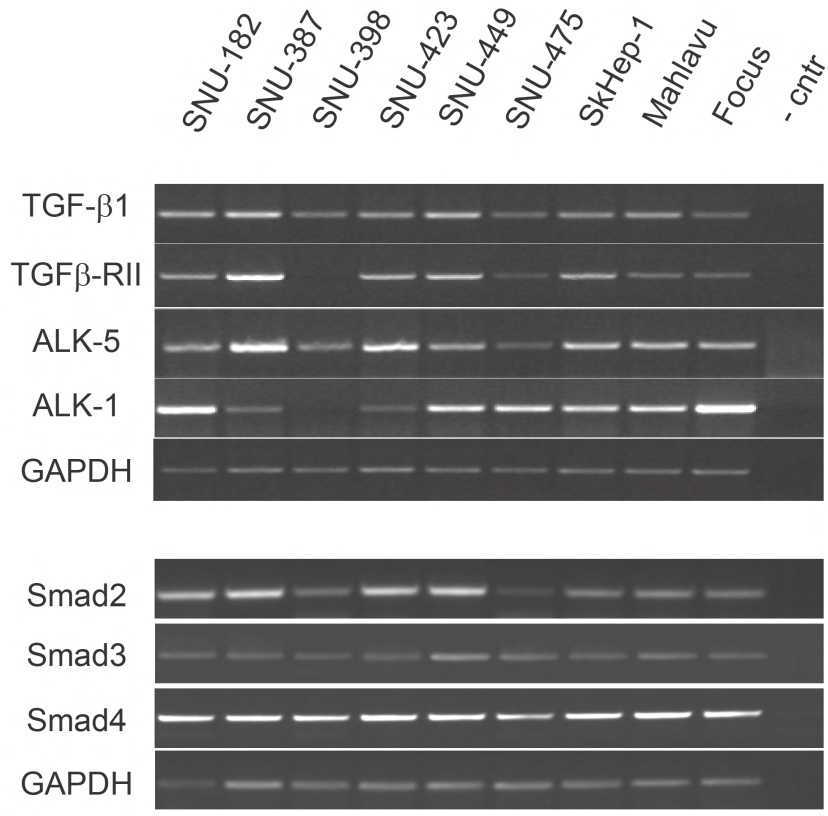

Figure 3.56: Expression of TGF-β1 ligand, receptors and intracellular signaling components.

3.11.2. Lack of TGF-β1-induced senescence in poorly differentiated HCC cell lines

TGF-β-induced senescence has been extensively studied for well-differentiated cell lines. WD cell lines responded to TGF-β1 by massive senescence induction of SABG staining within three days following treatment. However, this effect appeared to be limited to WD cell lines, as PD cell lines were completely resistant to senescence induction.

PD cells were seeded at low density and subjected to TGF-β treatment effective 24 hr of post-seeding. After three days of incubation, cells were stained for senescence associated β-galactosidase activity (Figure 3.57).

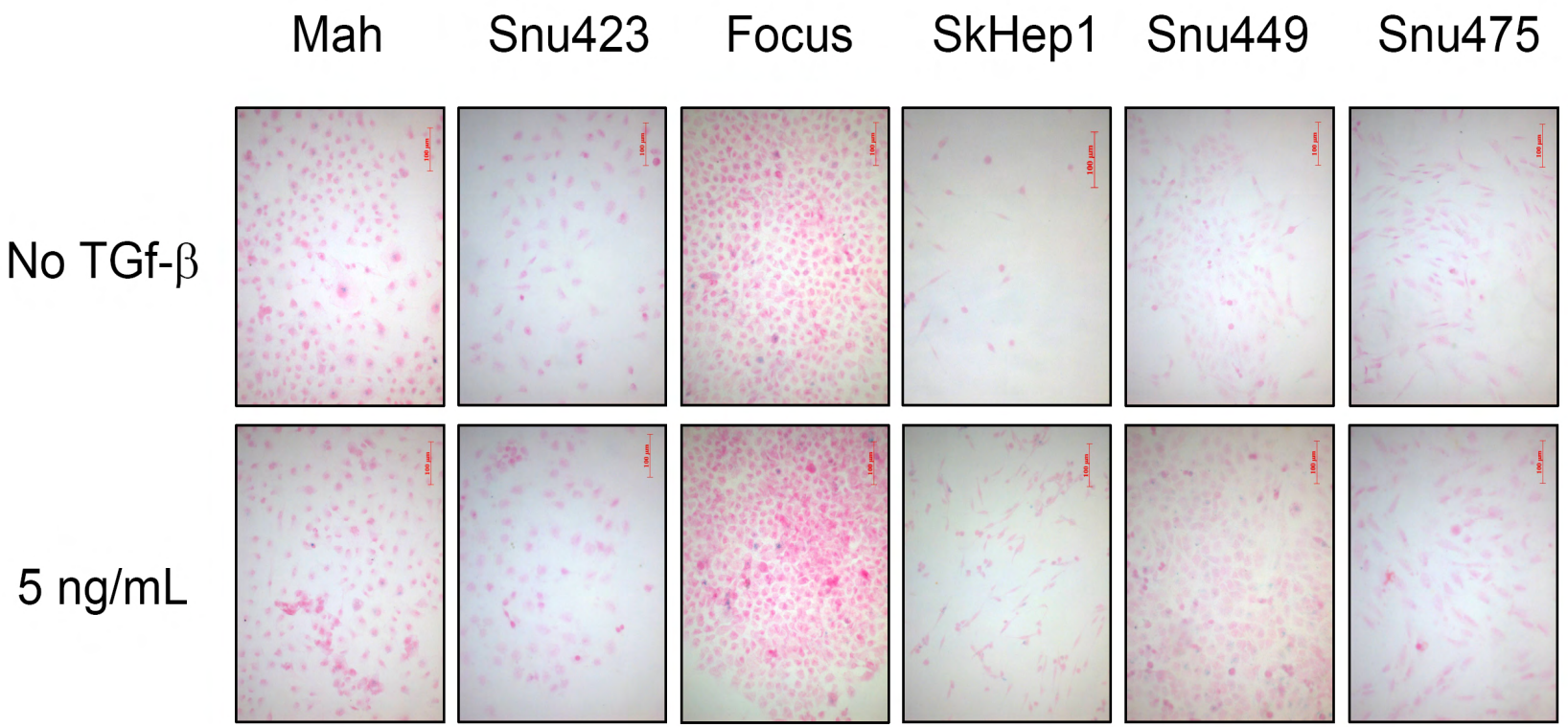

Figure 3.57: Lack of senescence-like response in PD cell lines. Cells were plated at low density and treated with TGF-β1 (5 ng/mL) for 72 hr. SA-β-Gal activity (blue) was tested at 72 hr. Control: no TGF-β1 treatment. Counterstain: Fast Red.

We tested nine PD cell lines, only six of them were depicted in the figure, and all of them were negative for SABG staining after three days and even after five days following removal of TGF-β1 (data not shown).

3.11.3. TGF-β treatment does not alter BrdU incorporation in PD cell lines

Following SABG experiments, we assessed proliferation assays with Snu387 and Snu449 cell lines. These cells were treated with TGF-β1 for three days and incubated for 24 hr with BrdU prior to staining (Figure 3.58).

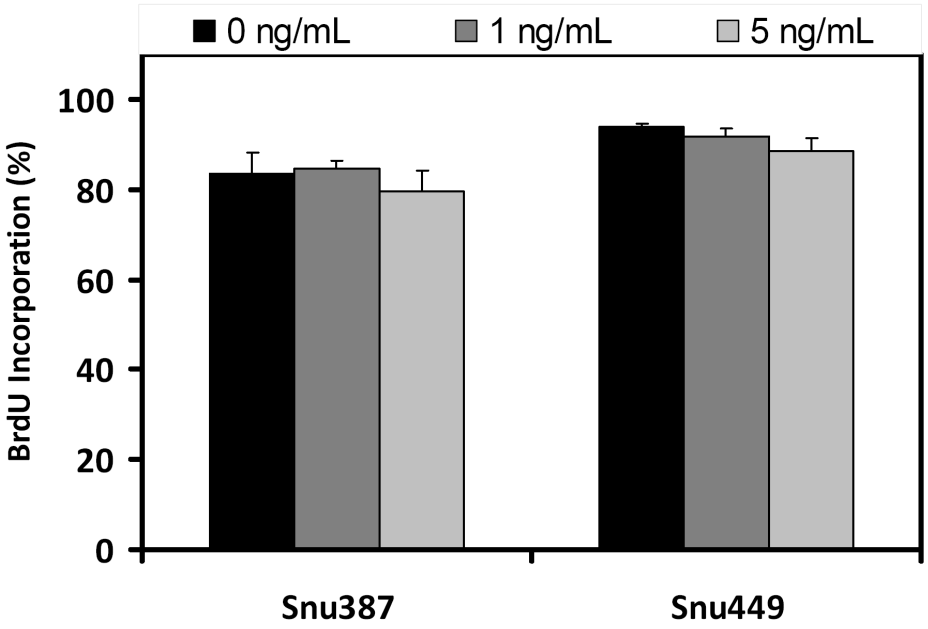

Figure 3.58: Cells were treated with 1 ng/mL and 5 ng/mL TGF-β1 for three days and subjected to immunofluorescence assay with anti-BrdU antibody. Positive cells in at least 5 areas for each triplicate were manually counted with reference to DAPI positive nuclei.

Proliferation capacity of these two cell lines were not influenced by TGF-β treatment suggesting a marked resistance against TGF-β-induced cytostatic responses.

3.12. Target gene expression profiles in poorly differentiated hepatocellular carcinoma cell lines

TGF-β-treated well-differentiated cells were growth arrested by upregulation of senescence markers such as $p21^{Cip1}$ and $p15^{Ink4b}$, with a reciprocal decrease of c-myc and phosphorylated-Rb. In order to assess the mechanisms underlying resistance to TGF-β-induced growth arrest in poorly differentiated cells, we initially studied gene expression profiles controlled by TGF-β. Tested cell lines were treated with 1 and 5 ng/mL TGF-β for three days and expression changes were studied with western blotting and RT-PCR assays. By western blotting technique, we detected no change in the expression levels of $p21^{Cip1}$ and $p15^{Ink4b}$ upon TGF-β treatment. In all cell lines tested except Snu387, we reported no change in the status pRb phosphorylation (Figure 3.59).

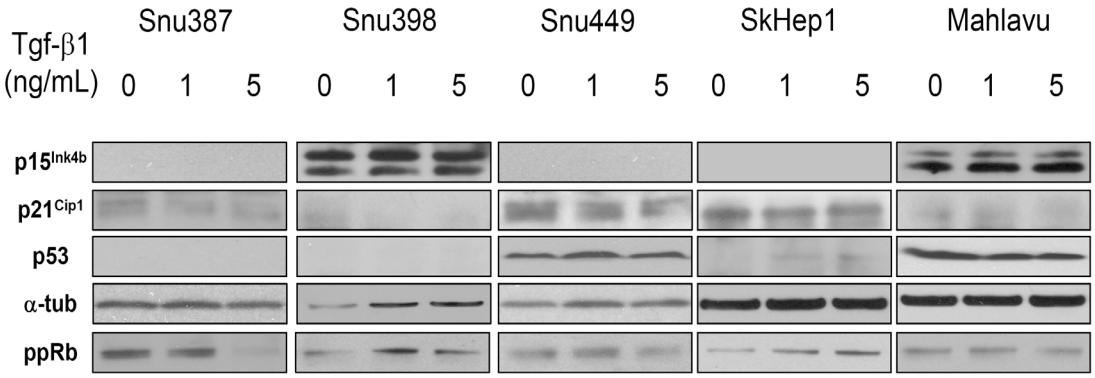

Figure 3.59: Gene expression profiles by western blot in TGF-β-treated of PD cell lines. Cells were treated with different doses of TGF-β1 and assayed for gene expression by western blotting. All incubations were essentially performed at room temperature. α-tubulin served as internal control.

Besides, we were not able to observe any change in PAI-1, a well-known TGF-β target gene, and as well as in $p21^{Cip1}$ transcript levels in Snu387, Snu449 and Mahlavu cells (Figure 3.60).

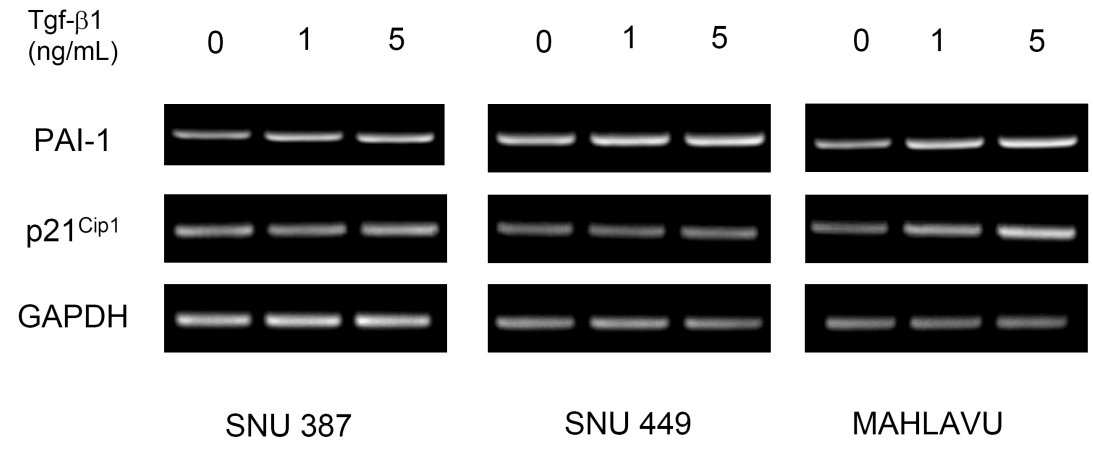

Figure 3.60: Gene expression profiles by RT-PCR in TGF-β-treated PD cell lines. Cells were treated with different doses of TGF-β1 and assayed for gene expression by semiquantitative RT-PCR. GAPDH served as internal control.

In order to confirm lack of expression in western blot, we also studied the expression of $p15^{Ink4b}$ at transcript level in all HCC cell lines. Three cell lines did not display any amplification (Figure 3.61-A). Then we performed genomic PCR experiments with cell lines that lack $p15^{Ink4b}$ expression at transcript level using specific primers amplifying INK4 locus. As shown in Figure 3.61-B, Snu387, Snu449 and SkHep1 cell lines have deletion at INK4 locus.

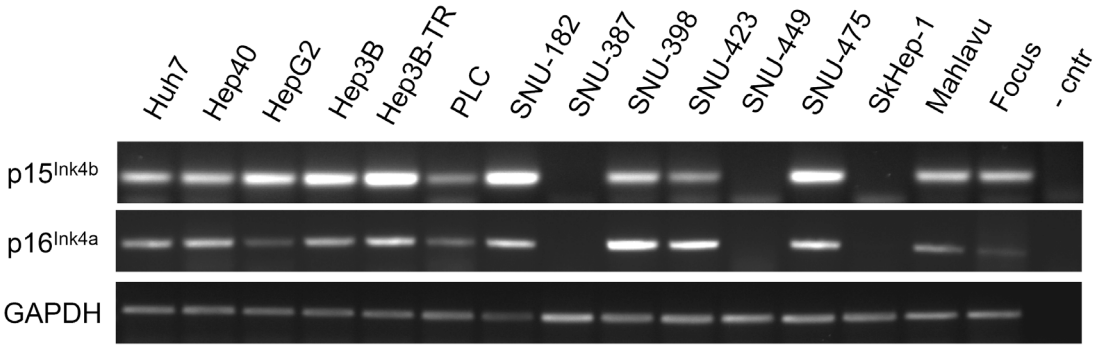

Figure 3.61-A: RT-PCR analysis for selected genes in all HCC cell lines.

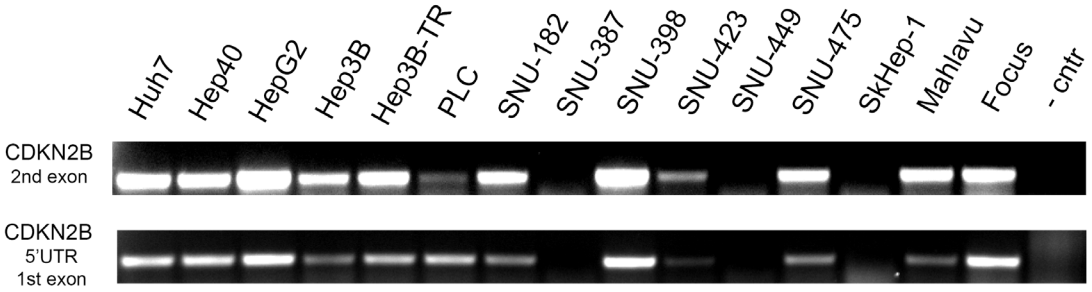

Figure 3.61-B: genomic-PCR analysis for selected regions on CDKN2B gene in all HCC cell lines.

INK4 locus also harbors ARF and CDKN2A and those cell lines with deletion do not express $p14^{Arf}$ and $p16^{Ink4a}$ protein either (Figure 3.62).

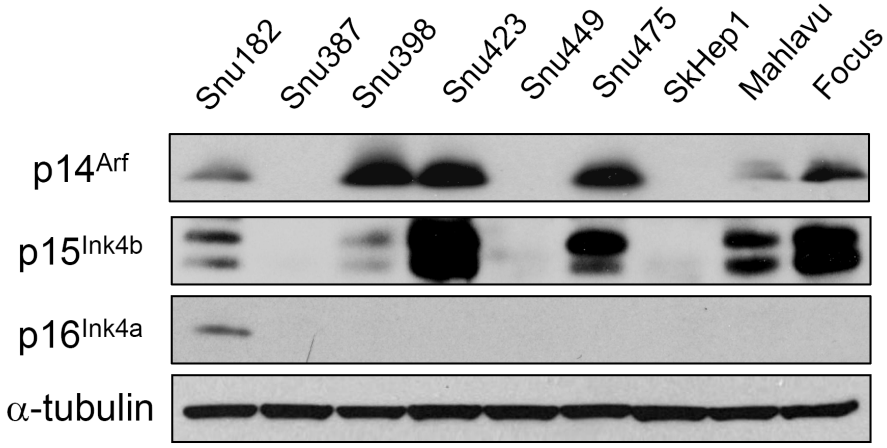

Figure 3.62: Western blot analysis for selected gene products in PD HCC cell lines. A-tubulin served as internal control.

Homozygous deletion for this locus in HCC tumors has been reported in other studies as well (Liew et al., 1999; Tannapfel et al., 2001).

3.13. TGF-β signaling is functional in poorly differentiated hepatocellular carcinoma cell lines

Several reasons may underlie the resistance to TGF-β-induced senescence as well as lack of activation of senescence marker genes. TGF-β signaling components were determined to be expressed at transcript level. In the context of identification of candidate resistance mechanisms, we tested functional TGF-β signal transduction from cell membrane to nucleus. TGF-β-mediated Smad activation in cytostatic responses is modulated through post-translational phosphorylation on serine residues located on the C-terminus. Therefore, we first tested the functionality of TGF-β receptors. In this respect, all poorly differentiated cell lines were treated with 5 ng/mL TGF-β1 for 30 min. Cell lysates were subjected to western blotting against activated Smad. Here, we used Smad2 to perform functional assays. All cell lines, except Snu398, had substantially increased phosphorylated-Smad2 (Figure 3.63).

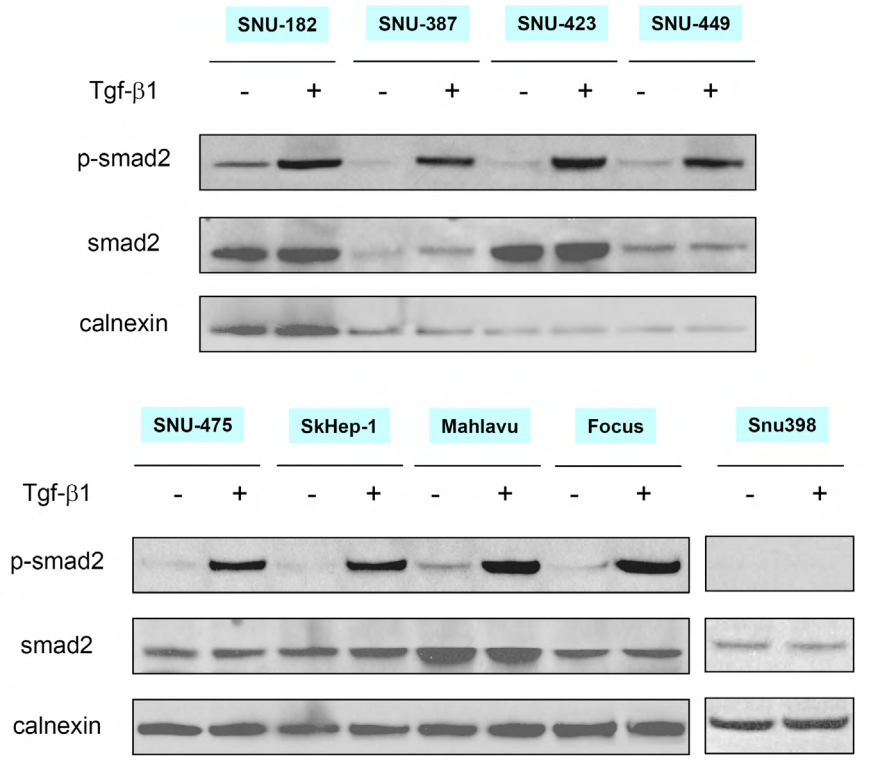

Figure 3.63: TGF-β leads to early phosphorylation of Smad2 in PD cell lines. Cells were treated with 5 ng/mL TGF-β1 for 30 min under normal culture conditions and cell lysates were subjected to western blotting with specific p-Smad2 antibody. Calnexin was used as equal loading control.

Next we studied effective signal transduction from cell membrane to nucleus using phospho-Smad3 specific antibody in immunoperoxidase assays. Similar to previous experiment, cells were seeded on 12-well plate coverslips at moderate density, and treated for 30 min with 5 ng/mL TGF-β1 24 hr post-seeding (Figure 3.64 and 3.65).

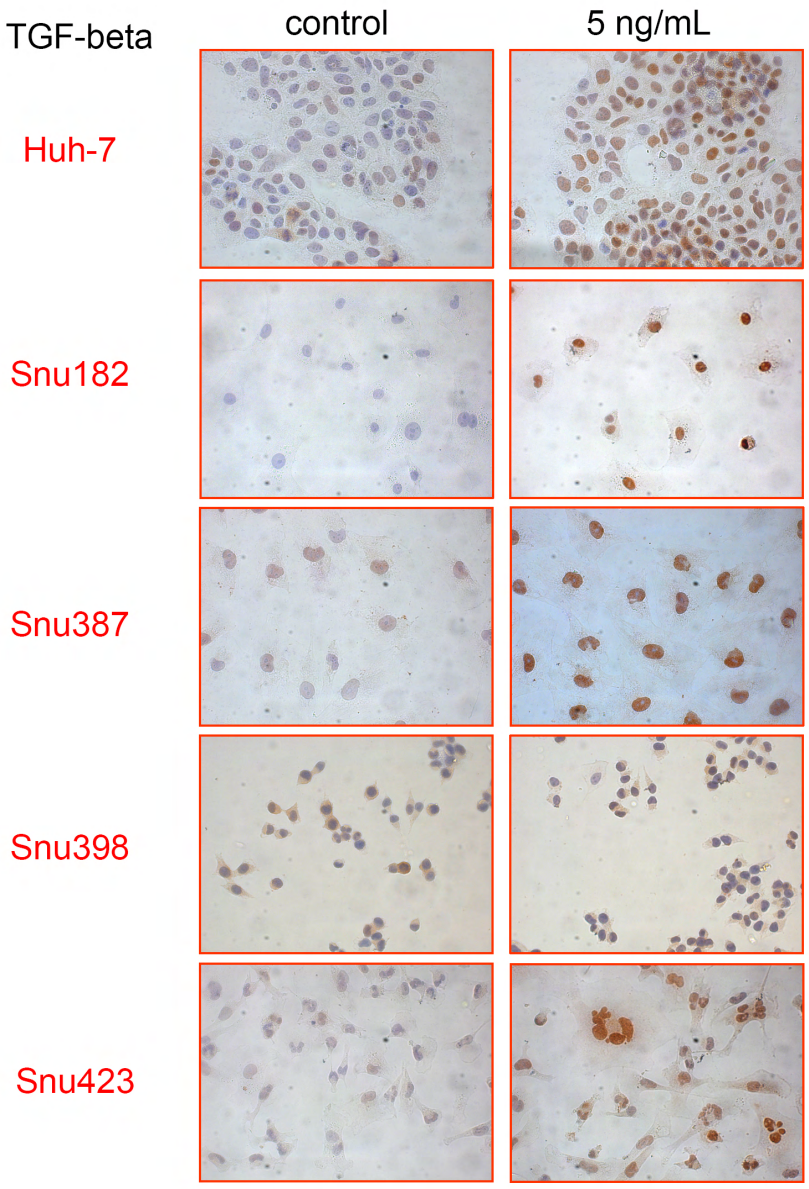

Figure 3.64: p-Smad3 localization in PD cell lines. All cell lines were treated with 5 ng/mL TGF-β1 for 30 min and stained with p-Smad3 specific antibody. Huh7 was used as positive control. Haemotxylin was used as nuclear counterstain.

We used Huh7 cells as positive control with active and intact TGF-β signal transduction. Hep3B-TR cell line was utilized as negative control for the specificity of the primary antibody, since we expected no or very faint nuclear staining.

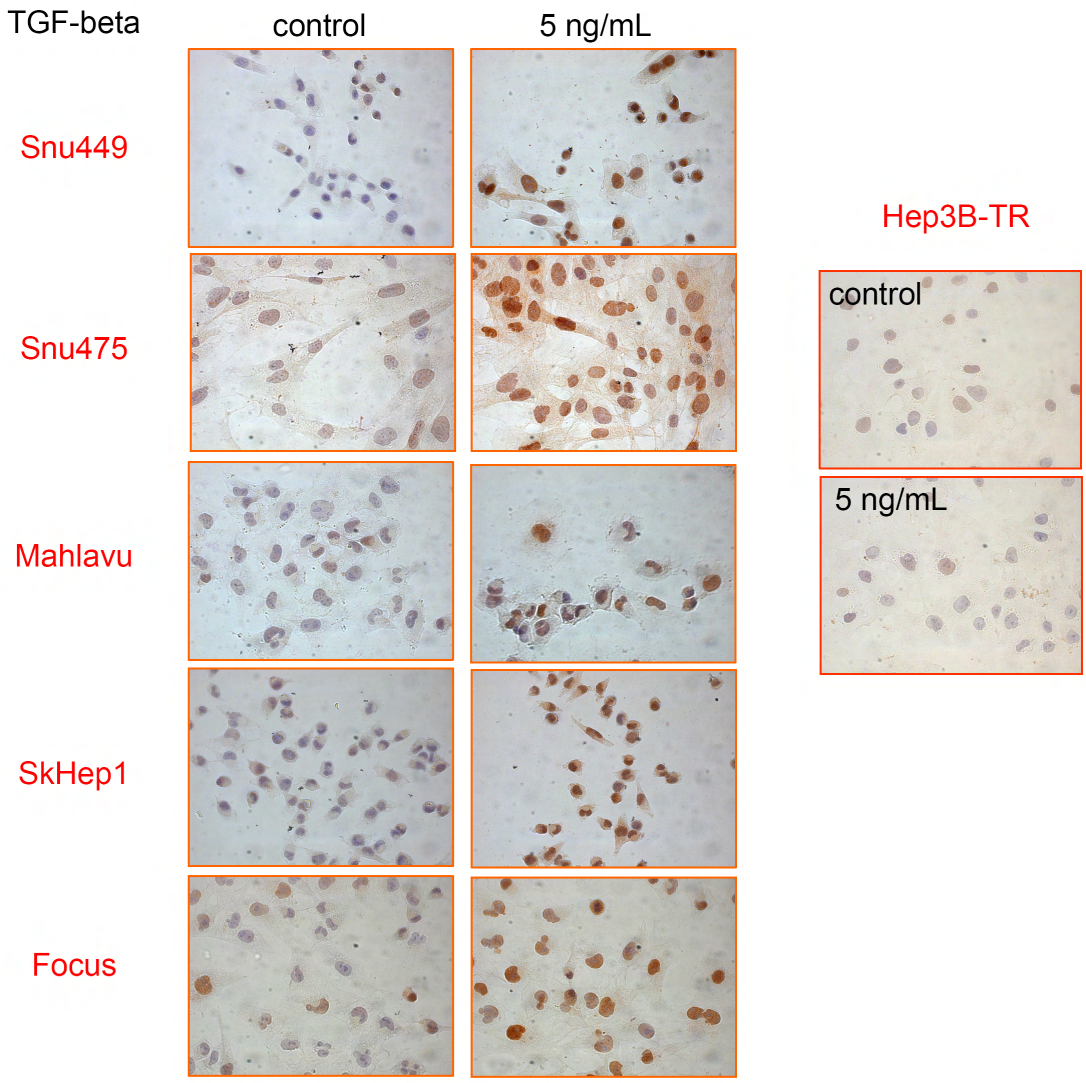

Figure 3.65: p-Smad3 localization in PD cell lines. All cell lines were treated with 5 ng/mL TGF-β1 for 30 min and stained with p-Smad3 specific antibody. Hep3B-TR was used as negative control. Haemotxylin was used as nuclear counterstain.

After fixation, cells were stained with p-Smad3 primary antibody and nuclei positive for p-Smad3 staining were determined by manual counting (Figure 3.66).

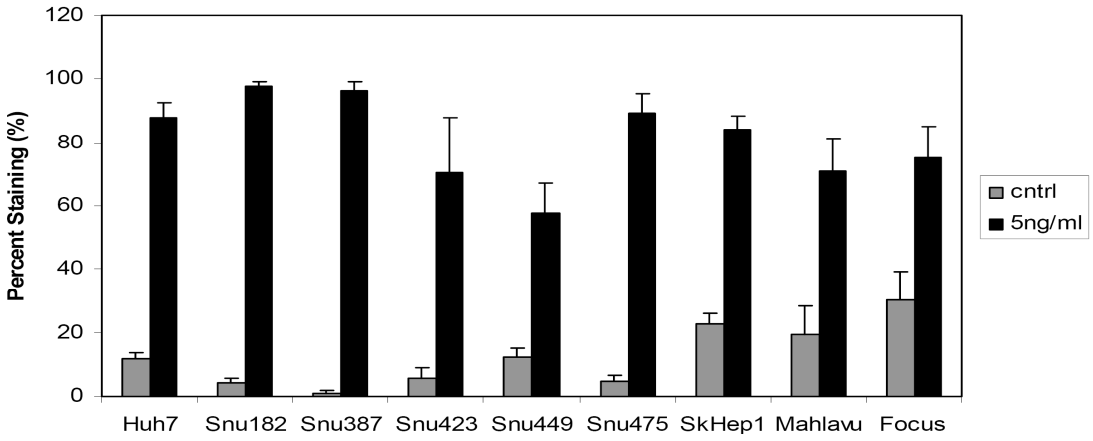

Figure 3.66: Positive nuclear staining in PD cell lines.

All cell lines tested displayed distinctively increased nuclear staining upon TGF-β treatment. Besides, almost all cell lines displayed endogenous nuclear p-Smad3 staining under normal culture conditions suggesting functional autocrine TGF-β signaling in PD cell lines similar to WD cells. Snu398 cells, on the other hand, were negative for p-Smad3 staining under TGF-β-treated and non-treated conditions, probably owing to diminished expression of TGFβRII (Kitisin et al., 2007).

3.14. TGF-β responsiveness of PD HCC cell lines

In order to analyze differential response of HCC cell lines to TGF-β treatment, we employed luciferase assay system similar to those performed with WD cell lines. To monitor responsiveness of PD HCC cell lines, we used two well-known TGF-β-responsive luciferase reporter constructs namely pSBE4-luc and p3TP-lux. Transfection efficiency was monitored with pEGFP vector.

All cell lines had ~60-90% transfection efficiency. As evidenced in Figure 3.67, all cell lines except Snu398 differentially responded to TGF-β with elevated pSBE4-luc reporter activity. All cell lines displayed 2 to 6 fold increase in luciferase

activity after treatment with TGF-β. Snu398 cells were completely unresponsive to treatment.

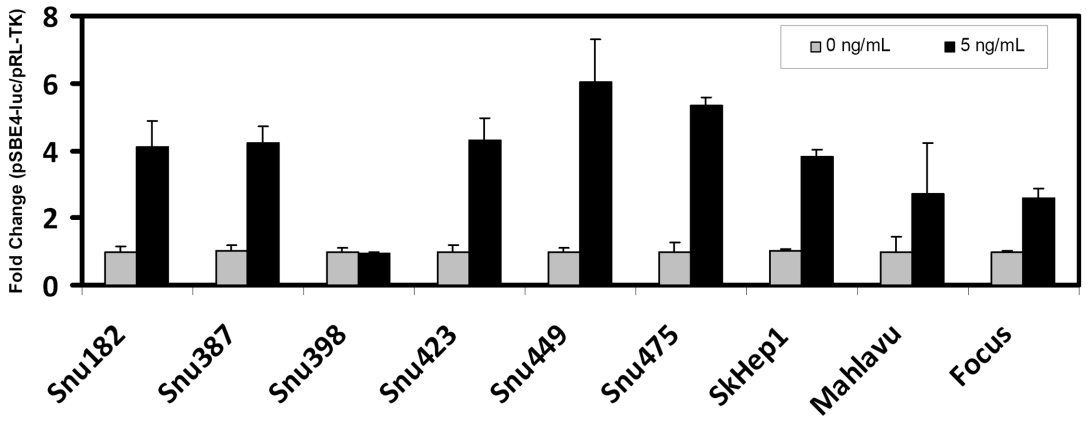

Figure 3.67: Intactness of TGF-β signaling in PD cell lines by pSBE4-luc activation. All cell lines were co-transfected with pSBE4-luc and pRL-TK renilla luciferase vectors. Six hours post-transfection, cells were supplemented with 5 ng/mL TGF-β1 for 24 hr and assayed for luciferase activity. Luciferase activity of reporter constructs was normalized to renilla luciferase. All experiments were performed in triplicate. All non-treated controls were normalized to a value of "1 (One)".

On the other hand, p3TP-lux transfection also demonstrated that all tested PD cell lines, except Snu182 and Snu398, responded to TGF-β with varying amplitudes (Figure 3.68).

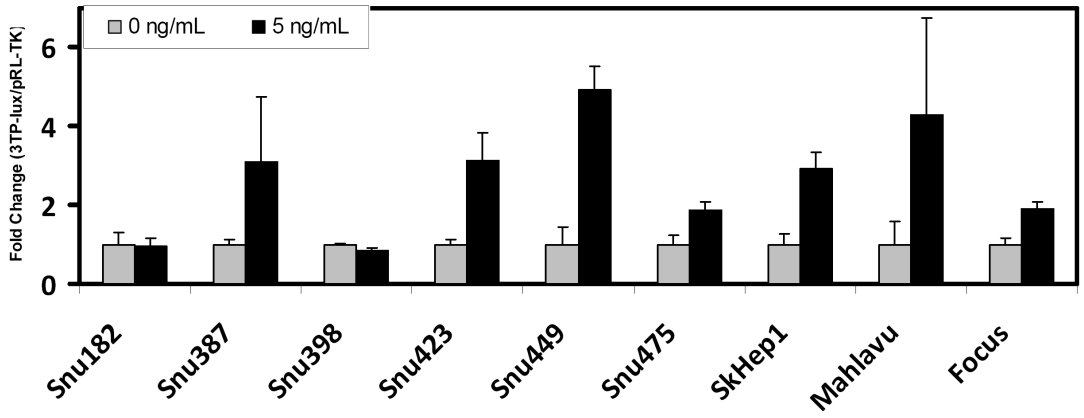

Figure 3.68: Responsiveness of PD cell lines by p3TP-lux activation. All cell lines were co-transfected with p3TP-lux and pRL-TK renilla luciferase vectors. Six hours post-transfection, cells were supplemented with 5 ng/mL TGF-β1 for 24 hr and assayed for luciferase activity. Luciferase activity of reporter constructs was normalized to renilla luciferase. All experiments were performed in triplicate. All negative controls were normalized to a value of "1 (One)".

These data clearly demonstrated that, most of the cell lines differentially responded to TGF-β treatment. However, the response of PD cell lines obtained with both vectors was comparably less than WD cell lines.

3.15. Lack of reactive oxygen species accumulation in PD cell lines

TGF-β-induced senescence in well-differentiated cell lines was closely associated with reactive oxygen species accumulation and Nox4 upregulation. As evidenced from previous experiments, we did not detect any senescence signal in PD cells upon TGF-β1 exposure. When compared to WD cell lines, we wanted to study a potential involvement of ROS accumulation and Nox4 upregulation in these cells. When cells were cultured with 5 ng/mL TGF-β1 for three days under normal culture conditions, no increase was detectable in production of intracellular ROS, except some endogenously positive cells (Figure 3.69).

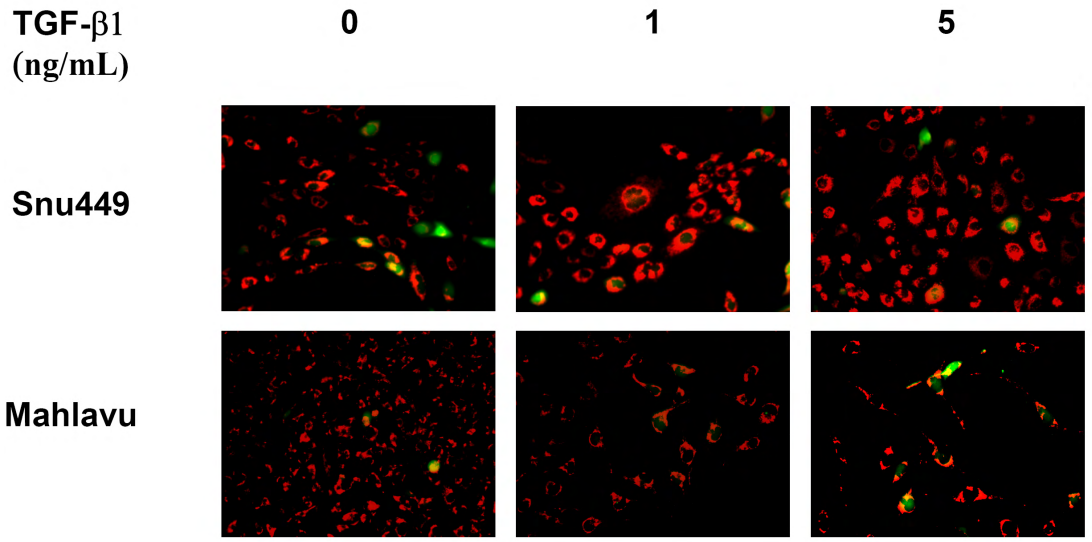

Figure 3.69: TGF-β1 failed to induce ROS accumulation in PD cell lines. PD cell lines were treated with 1 ng/mL and 5 ng/mL TGF-β1 for 72 hr. DCFH (green) staining indicates ROS accumulation inside the cell. Mitochondrial dye MitoTracker (red) was used as counterstain. Pictures: 20X with objective lens. Huh7 cell were used positive control for staining but not depicted here.

Nox4 accumulation has been linked to senescence arrest provoked by TGF-β in WD cell lines. Therefore, we similarly analyzed Nox4 mRNA expression after 72 hr TGF-β treatment. Unlike well-differentiated cell lines, we failed to observe neither endogenous expression in Nox4 transcripts nor upregulation in the presence of TGF-β (Figure 3.70).

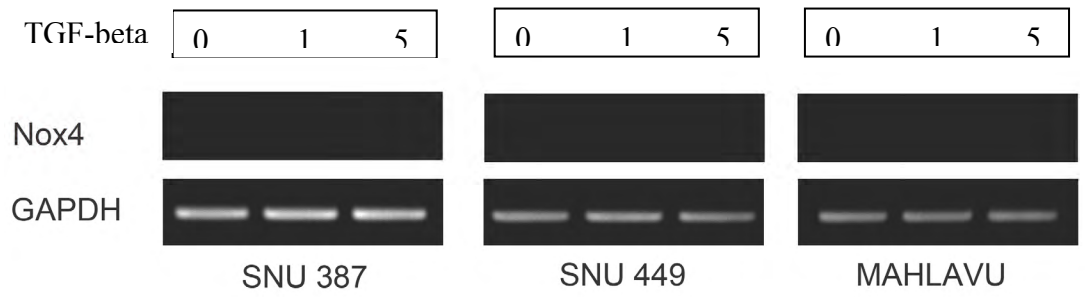

Figure 3.70: Nox4 is not expressed in PD cell lines. TGF-β did not induce Nox4 expression as well. GAPDH was used as internal control. Huh7 mRNA was used as positive control for Nox4 expression, not included here.

There are several reasons underlying the lack of expression of a specific gene under normal conditions including genetic and/or epigenetic impairment. Similar to INK4 locus deletion observed in PD cell lines, we wanted to assess the possibility of a deletion present in this locus. When we performed genomic PCR, we observed no deletion at two genomic regions of the *NOX4* gene (Figure 3.71).

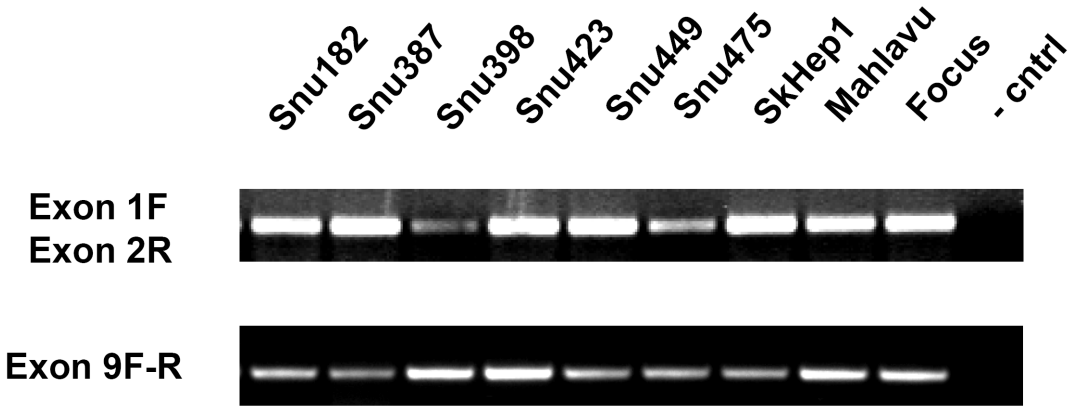

Figure 3.71: Genomic PCR to amplify different regions on *NOX4* gene.

In addition, we also performed a bioinformatics search to check out putative Nox4 promoter methylations. Using different tools, we identified putative Nox4 promoter over a 5.3 kb region (Figure 3.72).

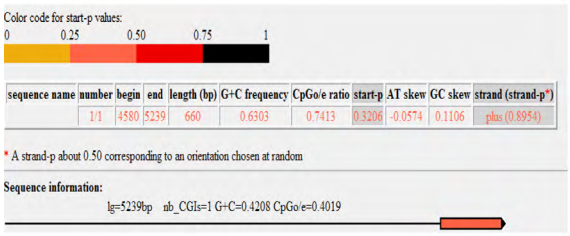

CpGProD (CpG Island Promoter Detection)

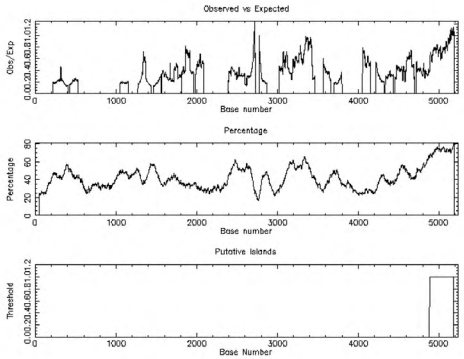

EMBOSS CpGPlot Results

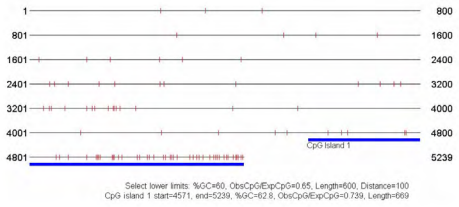

http://www.cpgislands.com/

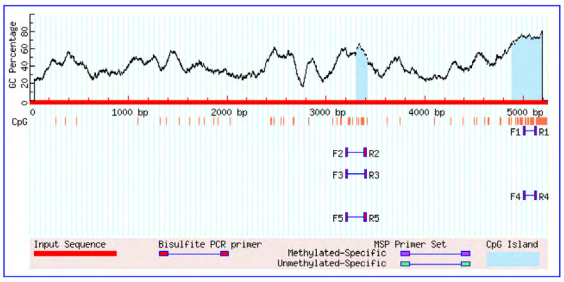

MethPrimer - Design Primers for Methylation PCRs

http://www.urogene.org/methprimer/index1.html

Figure 3.72: CpG island prediction on putative *NOX4* gene promoter.

This region harbors a putative CpG island covering upstream of the transcription start site and ~200 bp downstream of the transcription start site through 5'-UTR. Obviously these encouraging results need further exploration to determine the mechanisms that regulate endogenous Nox4 expression in PD cell lines.

3.16. Smad-interacting protein-1 (Sip-1, Zeb2) in hepatocellular carcinoma

Having elucidated the intactness and differential responsiveness of PD HCC cell lines to TGF-β, we further hypothesized that diminished senescence response of PD cell lines to this cytokine might be mediated through another mechanism independent of intracellular signal transduction. We concentrated on mesenchymal-like phenotype hallmark of these cell lines.

Epithelial and mesenchymal markers expression analysis of HCC cell lines revealed differential expression of Zeb2 (sip1, smad-interacting protein 1) mRNA together with others (Yuzugullu et al., 2009). Zeb2 was highly expressed in PD cell lines whereas WD cell lines have diminished expression at the transcript level (Figure 3.73).

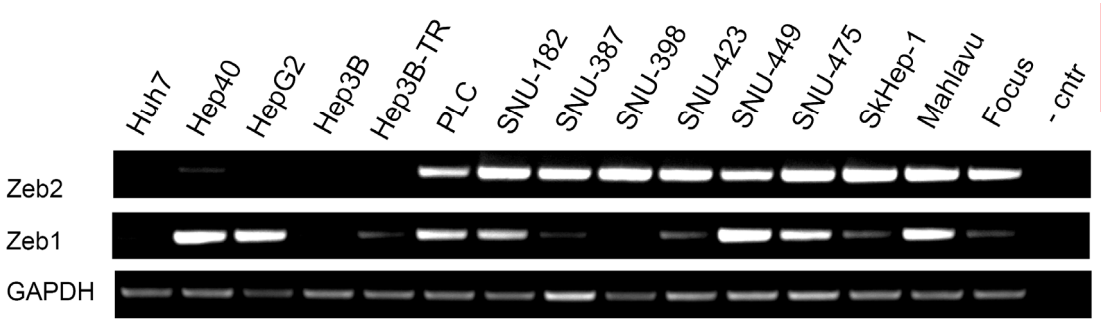

Figure 3.73: Expression of zeb2 and zeb1 in HCC cell lines by RT-PCR. GAPDH served as internal control, negative control lane: without template.

Zeb2 is a transcriptional repressor of e-cad (Vandewalle et al., 2005), cyclin-D1 (Mejlvang et al., 2007) and human telomerase reverse transcriptase (hTERT) (Ozturk et al., 2006). Recently, zeb2 has been suggested as a downstream target of TGF-β signaling pathway, as well as a modulator of signal transmission and a repressor for certain TGF-β pathway target genes (Postigo, 2003; Postigo et al., 2003). Recently, zeb2 has been proposed to play a prominent role in the interplay between EMT modulation and the onset of senescence (Ohashi et al., 2010). Nevertheless, its role in HCC is elusive. Whereas Zeb1, another two-handed zinc finger protein known to interact with Smads and activate transcription (Postigo, 2003), did not exhibit a differential expression towards PD cell lines (Figure 3.73).

We then investigated the expression and intracellular localization of zeb2 in HCC cell lines by immunostaining with a home made zeb2 antibody, namely 6E5. All WD cell lines had faint cytoplasmic staining and lacked nuclear zeb2 expression (Figure 3.74).

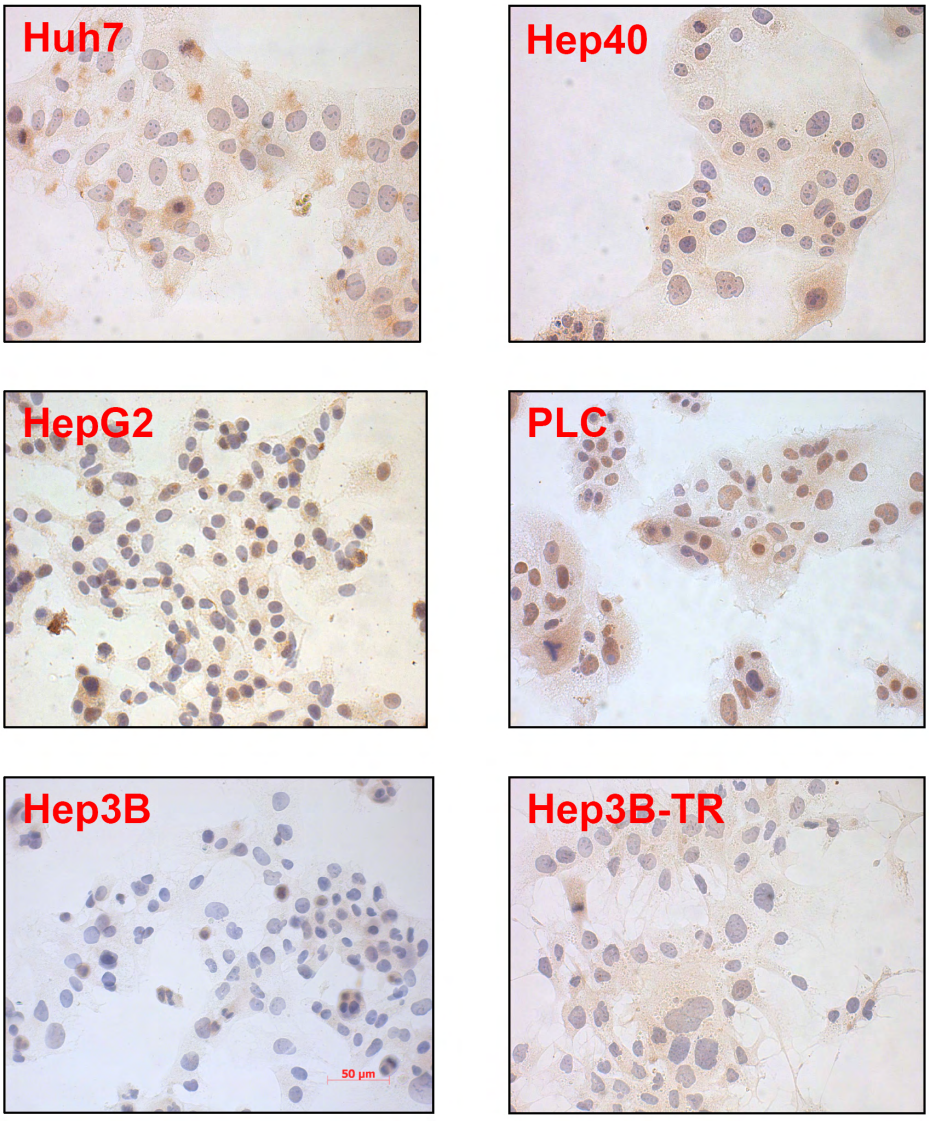

Figure 3.74: Expression and localization of zeb2 protein in WD HCC cell lines by immunoperoxidase staining. Zeb2 expression (brown staining). Haematoxylin was used as nuclear counterstain (blue).

On the other hand, all PD cell lines presented intense nuclear staining with very faint cytoplasmic zeb2 expression (Figure 3.75).

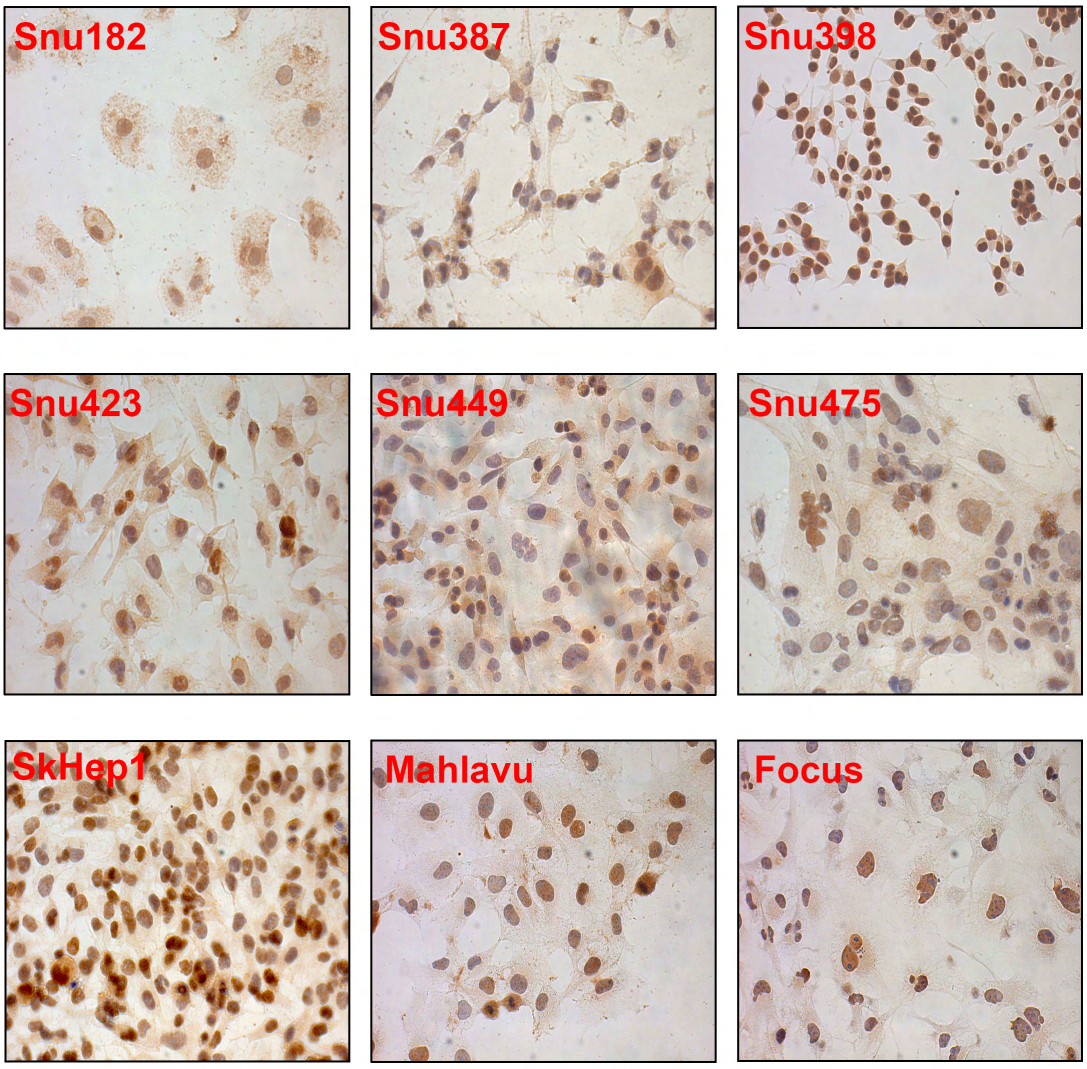

Figure 3.75: Expression and localization of zeb2 protein in PD HCC cell lines by immunoperoxidase staining. Zeb2 expression (brown staining). Haematoxylin was used as nuclear counterstain (blue).

Snu398 and SkHep1 exhibit the highest expression whereas Snu387 and Snu449 had comparably low levels of expression.

ZEB family proteins, zeb1 and zeb2, harbor two-handed zinc fingers with a high aminoacid sequence homology and have opposing functions on TGF-β signaling. Zeb1 synergizes with Smads and acts as an activator of TGF-β signaling to regulate a number of functions by promoting p300-Smad complex formation. On the

other hand, zeb2 has been demonstrated to act as a repressor of TGF-β signaling by recruiting CtBP corepressor along with Smads at certain target genes (Postigo, 2003). Therefore we hypothesized that high nuclear zeb2 expression in PD cell lines may block cytostatic functions of TGF-β signaling pathway by deregulating the activation of target genes such as $p21^{Cip1}$ and $p15^{Ink4b}$. To test our hypothesis, we used a Tet ON/OFF system controlling stable zeb2 expression generated in A431 cell line, a human epithelial skin carcinoma cell line with intact TGF-β signaling.

Therefore, we asked the effects of zeb2 reexpression in A431 carcinoma cell. We initially co-transfected A431 cells with luciferase reporter p3TP-lux and pRL-TK and analyzed activation of the reporter by TGF-β1 in the presence of wild-type zeb2 expression controlled by doxocyline. As demonstrated in Figure 3.76, reexpression of zeb2 inhibited TGF-β-induced activation of p3TP-lux reporter by more that 50%. This inhibition was also detectable in the absence of TGF-β.

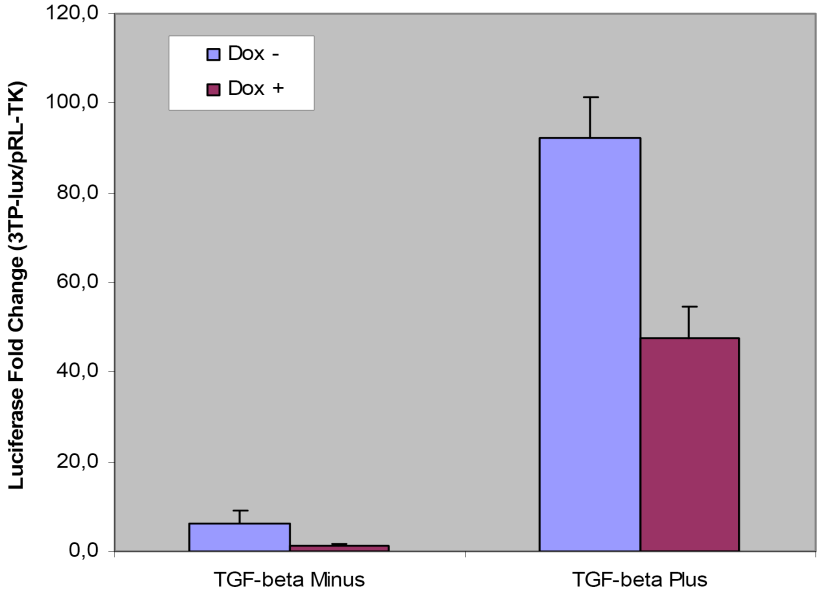

Figure 3.76: Inhibition of p3TP-lux activation by zeb2 protein in A431 cell line. p3TP-lux was co-transfected with pRL-TK. Six hour post-transfection, transfection medium was replaced by growth medium supplemented with 5 ng/mL TGF-β1 and 2 µg/mL doxocycline. Luciferase assay was performed in triplicate 24 hr post-addition of TGF-β1 and Dox.

Next, we tested target gene activation by TGF-β. Similar to luciferase assay, we treated A431 cell line with TGF-β in the presence and absence of doxocycline for 48 hr (Figure 3.77). Re-expression of wild-type zeb2 inhibited TGF-β-mediated $p21^{Cip1}$ upregulation. All these effects were diminished in CtBP-interacting (transcriptional repressor) domain mutant zeb2 (mt CID). Similar results were obtained when treatments were performed for 24 hr.

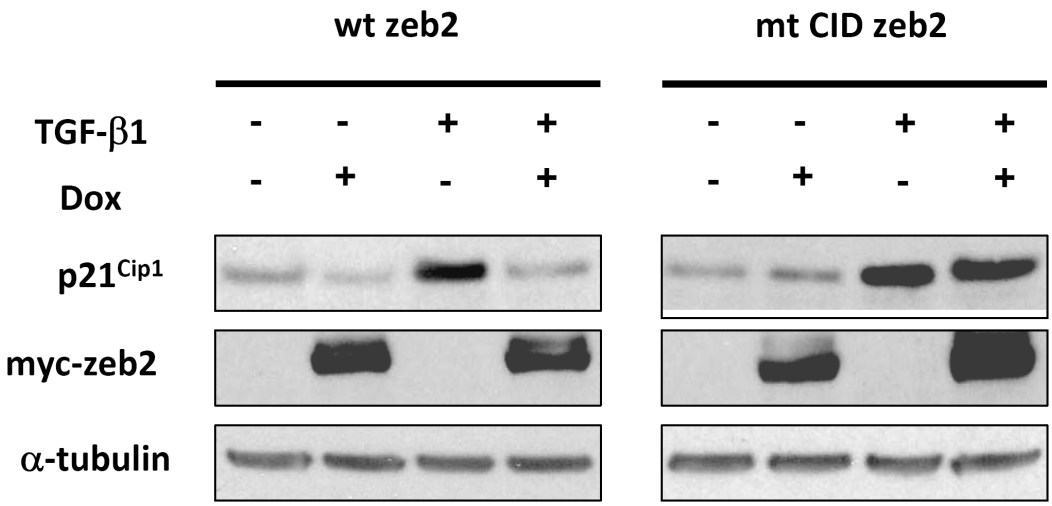

Figure 3.77: Inhibition of p21Cip1 upregulation in A431 cell line by wild-type zeb2 protein, but not by mutant zeb2. Cells were treated with/without 5 ng/mL TGF-β1 and/or 2 μg/mL doxocycline. 48 hr later, cell lysates were subjected to western blotting with specific antibodies. Myc-tagged zeb2 expression was detected with a myc-epitope specific antibody. α-tubulin was used to quantify equal loading.

Similar to western blotting assays, we performed immunoperoxidase staining analyses to determine the effects of zeb2 re-expression on $p21^{Cip1}$ nuclear accumulation using $p21^{Cip1}$-specific monoclonal antibody along with myc-epitope-specific primary antibody. As pictured in Figure 3.78, re-expression of zeb2 by doxocycline inhibited nuclear $p21^{Cip1}$ accumulation in A431 cells.

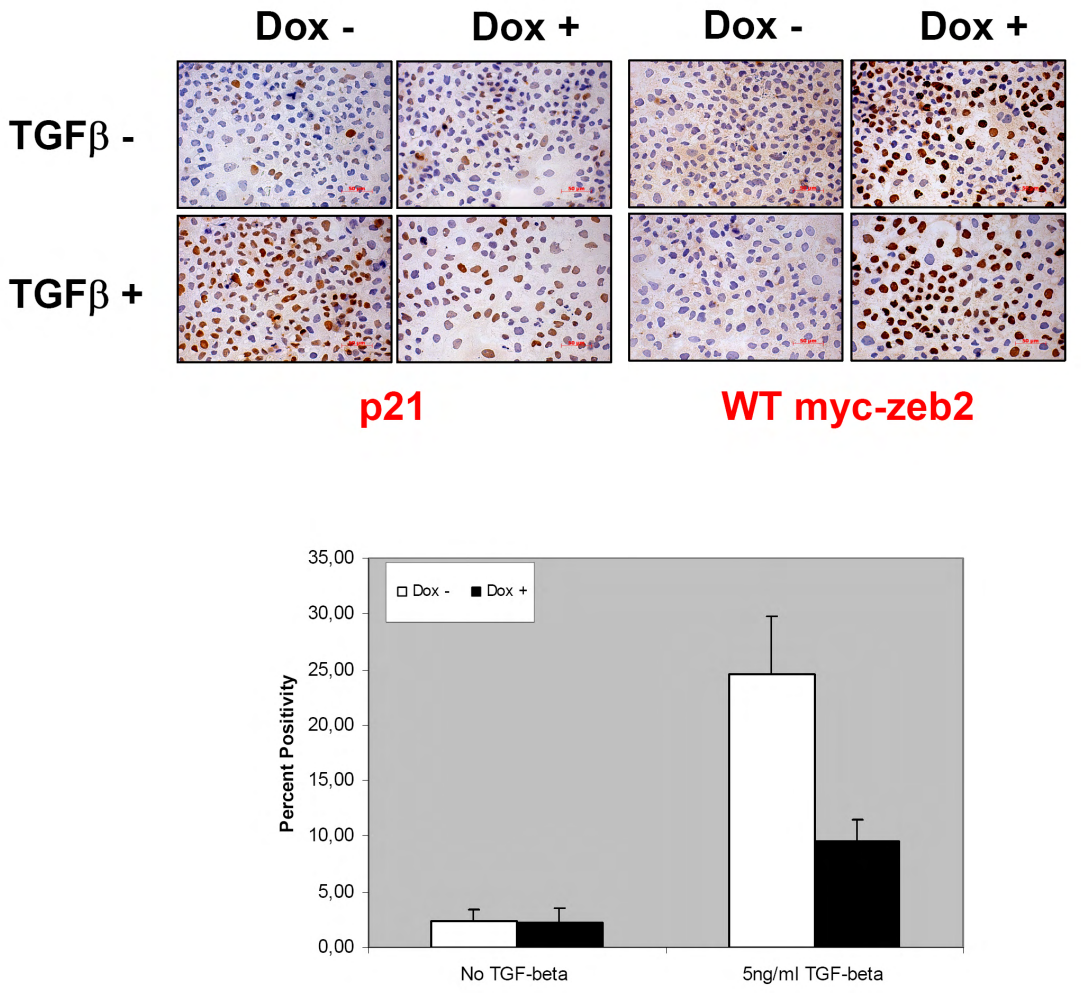

Figure 3.78: Inhibition of p21^{Cip1} nuclear upregulation in A431 cell line by wild-type zeb2 protein. Cells were treated with/without 5 ng/mL TGF-β and/or 2 ug/mL doxocycline. 48 hr later, cell were subjected to immunoperoxidase staining with specific antibodies. Myc-tagged zeb2 expression was detected with a myc-epitope specific antibody. Percent nuclear staining (bottom panel) was calculated by manual counting of at least 4 areas in each of the triplicate experiments.

Similar to those results obtained with mt CID zeb2 in western blotting experiments, we observed no significant change in nuclear p21^{Cip1} expression (Figure 3.79). Please note that, zeb2 re-expression was not at same detectable level in all nuclei after 48 hr of doxocycline addition. Similar results were obtained in another study (Sayan et al., 2009).

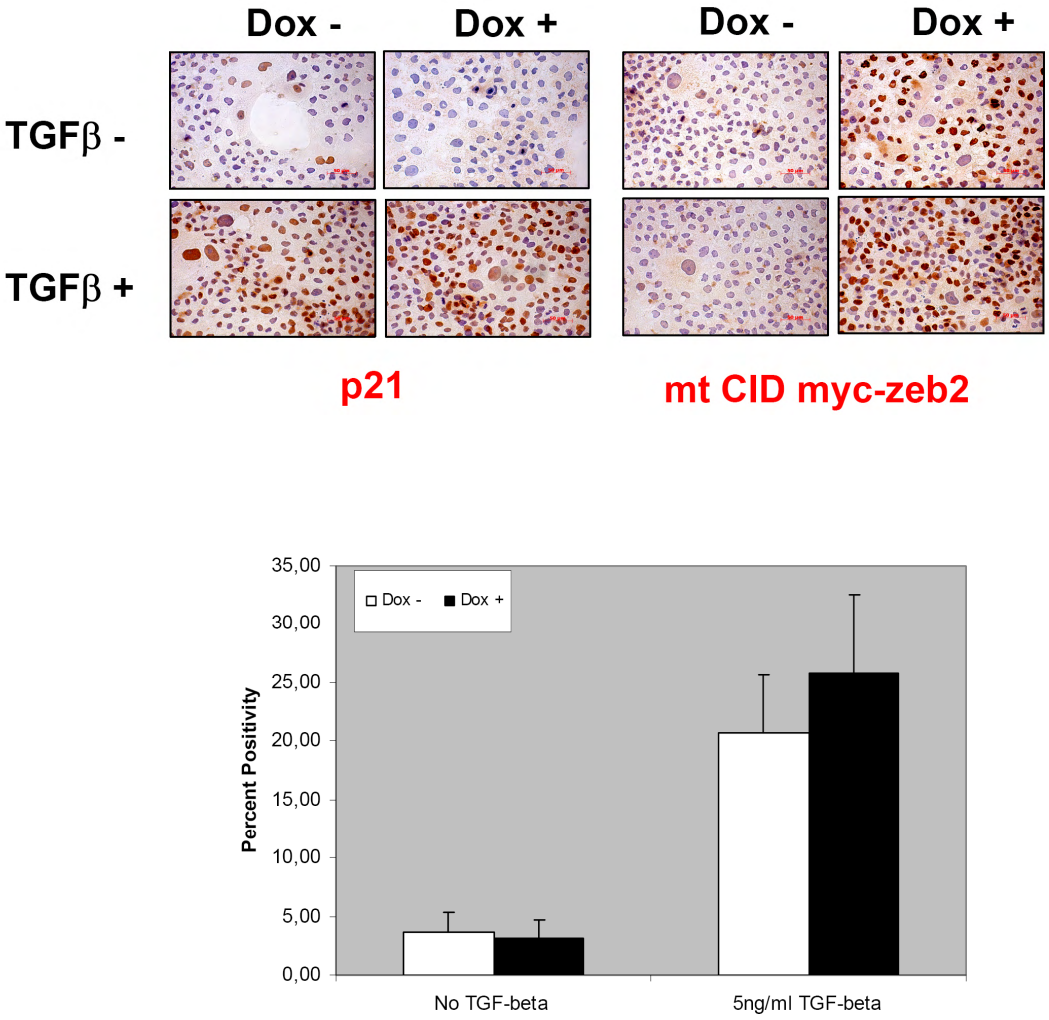

Figure 3.79: Lack of inhibition of p21^{Cip1} nuclear upregulation by mutant zeb2 protein in A431 cell line. Cells were treated with/without 5 ng/mL TGF-β and/or 2 µg/mL doxocycline. 48 hr later, cell were subjected to immunoperoxidase staining with specific antibodies. Myc-tagged zeb2 expression was detected with a myc-epitope specific antibody. Percent nuclear staining (bottom panel) was calculated by manual counting of at least 4 areas in each of the triplicate experiments.

Following these experiments we performed similar assays with PLC cell line, an epithelial-like HCC cell line. Ectopic Zeb2 overexpression presented a similar response in PLC cells under TGF-β treatment conditions (Figure 3.80).

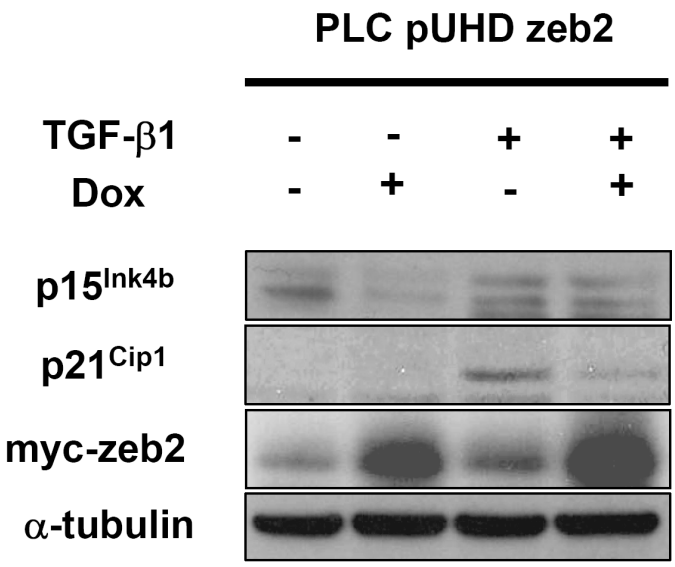

Figure 3.80: TGF-β-mediated p15Ink4b and p21Cip1 upregulation was inhibited by ectopic zeb2 expression in PLC cells. Cells were cotransfected with pUHD10.3/wt-zeb2 and reverse tetracycline-dependent transactivator (rtTA) expressing pUHD172-1 plasmids. Cells were supplied with 5 ng/mL TGF-β1 and 2 μg/mL doxocycline for 24 hr prior to immunoblotting. α-tubulin was used as equal loading.

All PD cell lines expressed high levels of Zeb2 protein as evidenced by RT-PCR and immunoperoxidase staining procedures. Hence, we hypothesized that downregulation of zeb2 using siRNA technology could enhance TGF-β-mediated target gene activation. Therefore, we silenced zeb2 expression in Mahlavu and Snu449 cells using 10 nM zeb2 siRNA. Initially, we detected more that 75% decrease in zeb2 expression with a reciprocal ~7 fold increase in the expression of $p21^{Cip1}$ in Mahlavu, by qRT-PCR (Figure 3.81).

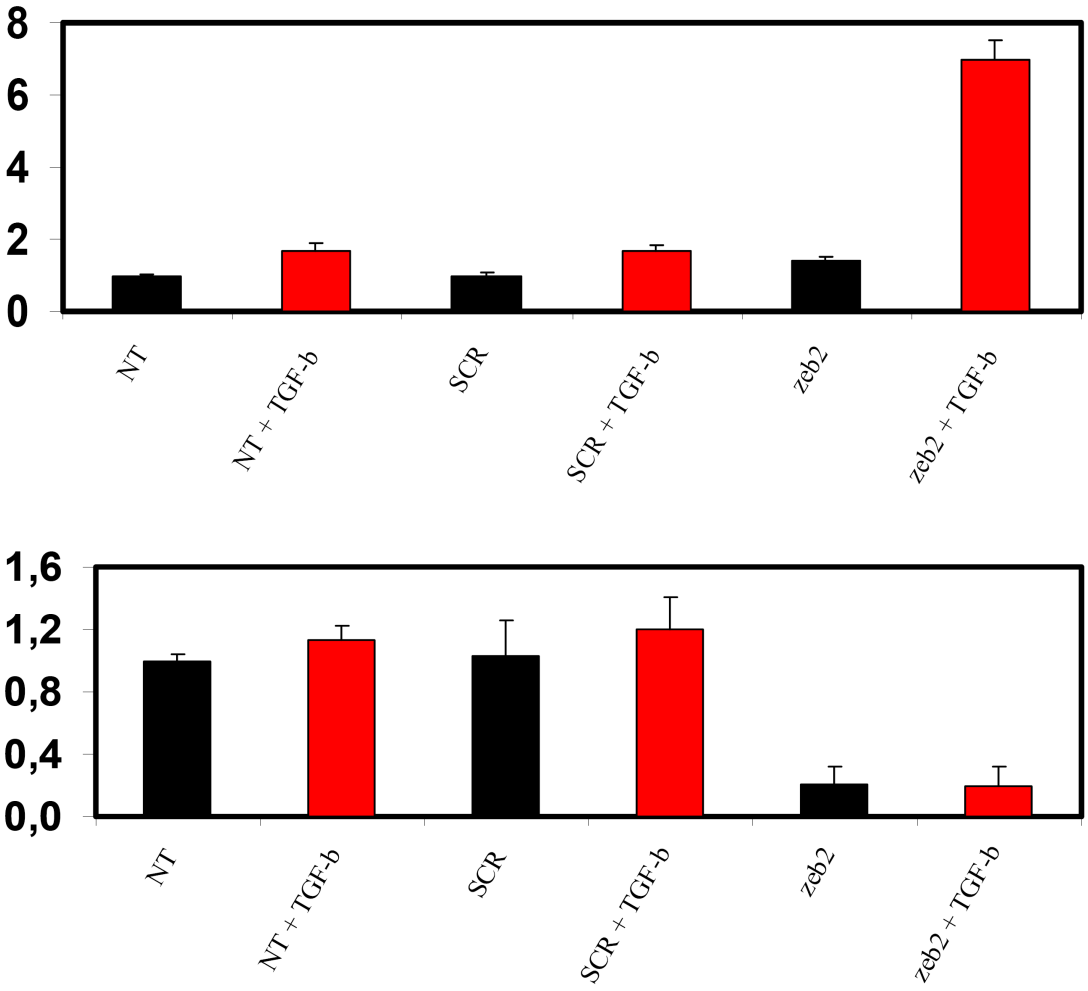

Figure 3.81: p21^{Cip1} expression following knockdown of zeb2 in Mahlavu cells. Cells were transfected with 10 nM zeb2 siRNA and a corresponding scrambled siRNA sequence using RNAiMax Lipofectamine. Six hrs post-transfection, cells were supplied with 5 ng/mL TGF-β1 for 48 hr prior to real-time pcr. All zeb2 values were normalized with GAPDH calues accordingly. Red bars indicate TGF-β addition. **Y-axis: Fold difference, Upper graph: p21^{Cip1} expression, lower graph: zeb2 expression**

In addition to that, we also studied same effects of zeb2 knockdown in Snu449 cells. Unlike Mahlavu cells, upregulation of p21^{Cip1} in zeb siRNA transfected samples after TGF-β addition was moderately low but still detectable (Figure 3.82).

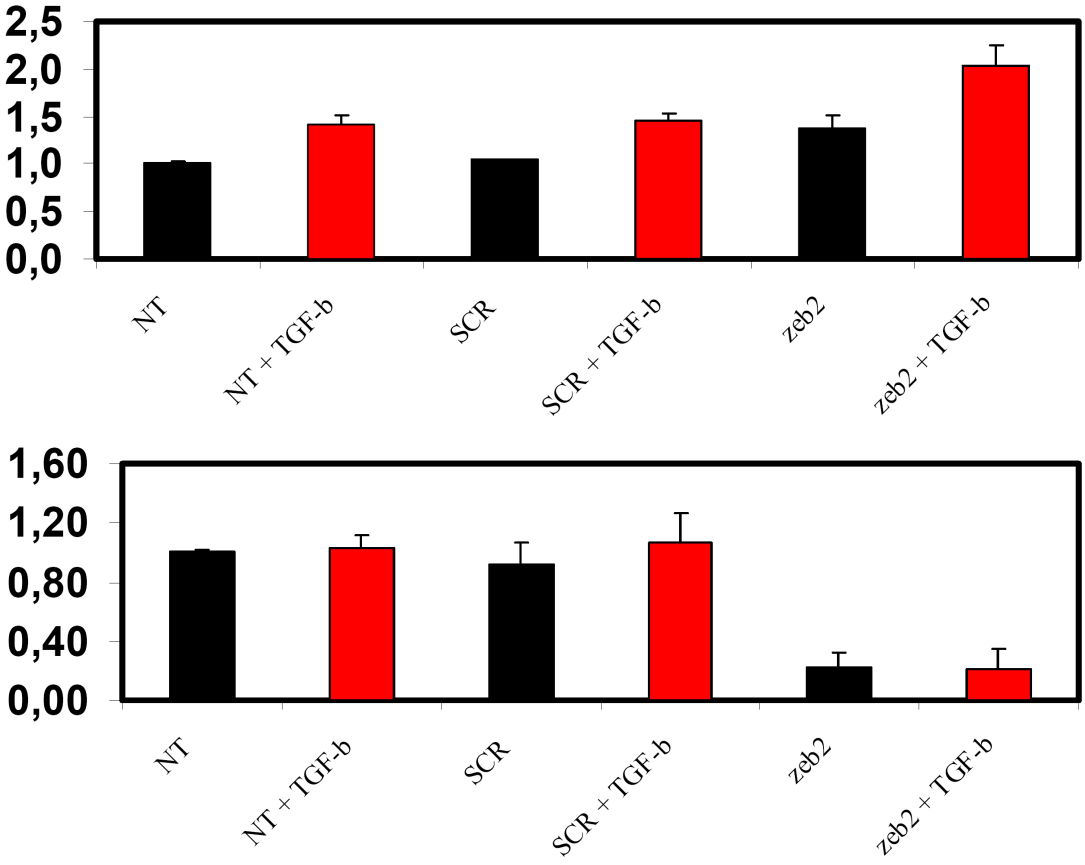

Figure 3.82: p21^{Cip1} expression following knockdown of zeb2 in Snu449 cells. Cells were transfected with 10 nM zeb2 siRNA and a corresponding scrambled siRNA sequence using RNAiMax Lipofectamine. Six hrs post-transfection, cells were supplied with 5 ng/mL TGF-β for 48 hr prior to real-time pcr. All zeb2 values were normalized with GAPDH calues accordingly. Red bars indicate TGF-β addition. **Y-axis: Fold difference, Upper graph: p21^{Cip1} expression, lower graph: zeb2 expression**

These initial experiments with major interest in knocking down zeb2 expression have clearly demonstrated a prominent role for zeb2 in conferring partial TGF-β resistance in poorly differentiated cell lines.

3.17. Prolonged exposure to TGF-β generates resistant clones in Huh7 cell line

TGF-β-induced growth arrest in well-differentiated cell lines was studied in three days intervals. Initial experiments for SABG activity were studied after three

days of exposure to TGF-β. Later experiments were performed with cells which were stimulated with TGF-β for 72 hr and left untreated until day 12. As previously stated, we determined SABG positive cells in three days culture as well as 12 days culture. Up to this point, we demonstrated sustained senescence response in well-differentiated cell lines. We next wanted to test the effects of TGF-β in long-term cultures. Thus, we initiated 5 ng/mL TGF-β1 treatment with parental Huh7 cells in a low-density clonogenicity based manner in 10 cm dishes. TGF-β1 was administered into cell culture medium on every three-four days period.

In this low density setting, non-treated control Huh7 cells were split every three days. Whereas, TGF-β1 treated cells were split whenever they reached confluency. Depending on the number of cells the experiment was initiated and the flattened morphology they obtain in sustained culture, they were split in 5-6 days intervals until all cells completely cease proliferation which is typically 2 passages. Together with live non-proliferating cells attached at the bottom of the dish, we observed a high population of unviable floating cells. Following prolonged senescence and proliferative decline due to various stress stimuli, the floating cells probably at the state of crisis (Macera-Bloch et al., 2002; Stein, 1985), were completely eliminated from cell culture after approximately 25 days. Surprisingly enough, approximately following 40 days from the initiation of first TGF-β addition, we observed few colonies with slow growing potential. We obtained a clone approximately after 50 days. Initial cell freezing was performed after ~60 days in culture when we reached a high number of proliferating cells. In the meantime, we continuously introduced TGF-β into the cell culture medium. The subclone established from Huh7 by prolonged TGF-β treatment was morphologically distinct from parental Huh7. Cells had fibroblast like outgrowing extensions with flattened cytoplasmic structure. Such clones were most likely delineated as mesenchymal-like cells.

Recently, epithelial mesenchymal transition has been defined as an alternative mechanism to alleviate the pressure of senescence inducing stress signals (Ansieau et al., 2008; Weinberg, 2008). Thus, we decided to perform a series of

analyses with the established subclone to delineate the structure-function interplays between resistance to TGF-β and escape from senescence arrest.

3.17.1. Loss of TGF-β responsiveness in the established clone, Huh7-5

As an initial experiment, we performed analysis with a primary goal to evaluate the current responsiveness of this ~60 days TGF-β treated subclone. As previously performed, we used luciferase reporters to investigate the response of Huh7 subclone to our cytokine. Parental Huh7 cells had ~10 fold increase in pSBE4-luc activity after 24 hr TGF-β treatment, whereas the response of Huh7-5 (5 designates the new clone with continuous treatment of 5 ng/mL TGF-β) was completely diminished (Figure 3.83). We also did a similar experiment with p3TP-lux and reporter a quite similar outcome (Figure 3.76).

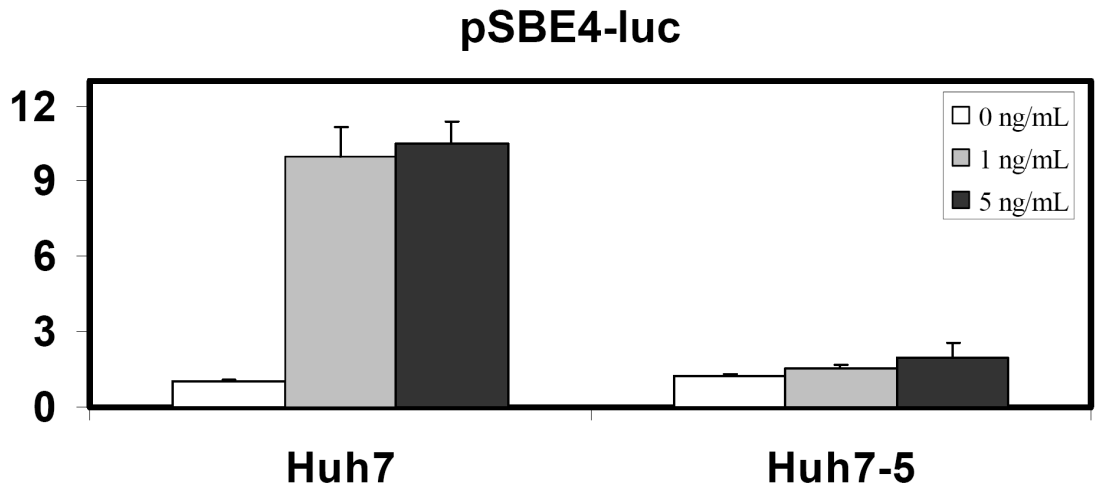

Figure 3.83: Diminished response to TGF-β treatment with pSBE4-luc in Huh7-5 clone after ~60 days. Cells were co-transfected with pSBE4-Luc and control pRL-TK plasmids, and treated with or without TGF-β1 (1 ng/mL and 5 ng/mL) for 24 hr. The luciferase activity was measured and expressed as fold change of Reporter/pRL-TK (mean ± SD; n=3). **Y-axis: Fold Change**

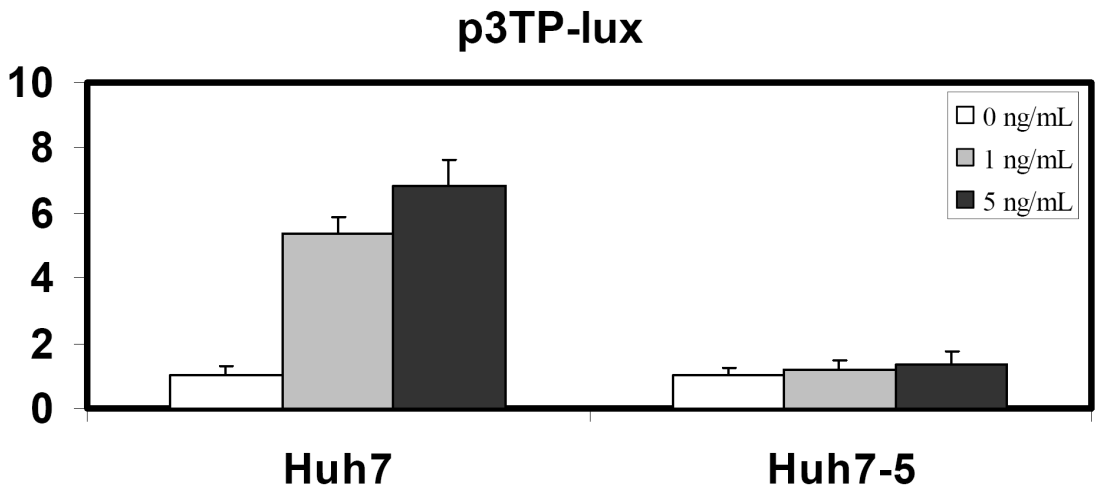

Figure 3.84: Diminished response to TGF-β treatment with p3TP-lux in Huh7-5 clone after ~60 days. Cells were co-transfected with p3TP-lux and control pRL-TK plasmids, and treated with or without TGF-β1 (1 ng/mL and 5 ng/mL) for 24 hr. The luciferase activity was measured and expressed as fold change of Reporter/pRL-TK (mean ± SD; n=3). **Y-axis: Fold Change**

These results clearly indicated a virtually complete loss of response to TGF-β treatment in the established subclone Huh7-5.

3.17.2. Escape from TGF-β-induced loss of BrdU incorporation in the established subclone Huh7-5

Senescence arrest provoked by TGF-β treatment in Huh7 cells is always characterized with loss of BrdU incorporation reaching a peak after three days of stimulation. Similar to that, we therefore decided to study the effects of TGF-β on BrdU incorporation in Huh7-5 clone. Parental Huh7 and subclone Huh7-5 were treated with increasing doses of TGF-β and supplied with BrdU 24 hr prior to detection and subjected to immunofluorescence assay after a total of 72 hr. Parental Huh7 had over 80% decrease in BrdU incorporating cells in both doses applied, whereas Huh7-5 subclone had complete resistance to TGF-β cytostatic responses with no inhibition in BrdU incorporation into cellular DNA (Figure 3.85).

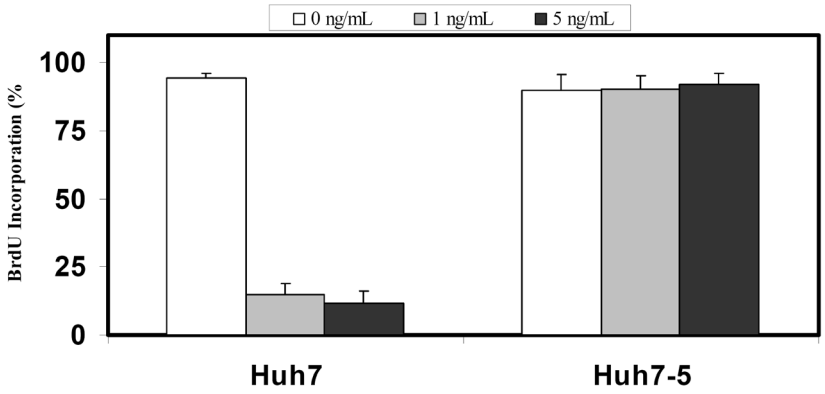

Figure 3.85: Resistance to inhibition of BrdU incorporation in ~60 days TGF-β treated Huh7-5 cells. After 24 hr of incorporation, cells positively labeled for BrdU were stained with immunofluorescence technique using anti-BrdU (mouse) antibody. DAPI was used for nuclear counter-staining in IF experiments. At least 5 areas were manually counted in triplicate assays.

3.17.3. The resistant subclone did not respond to TGF-β

Cytostatic responses controlled by $p21^{Cip1}$ and $p15^{Ink4b}$ seemed to be unaffected by TGF-β in Huh7-5 subclone (Figure 3.86). As previously described, we detected complete loss in phosphorylated Rb in parental Huh7 cells, while in Huh7-5 subclone we almost detected no change. In addition, Nox4 expression was not induced by TGF-β in resistant clone.

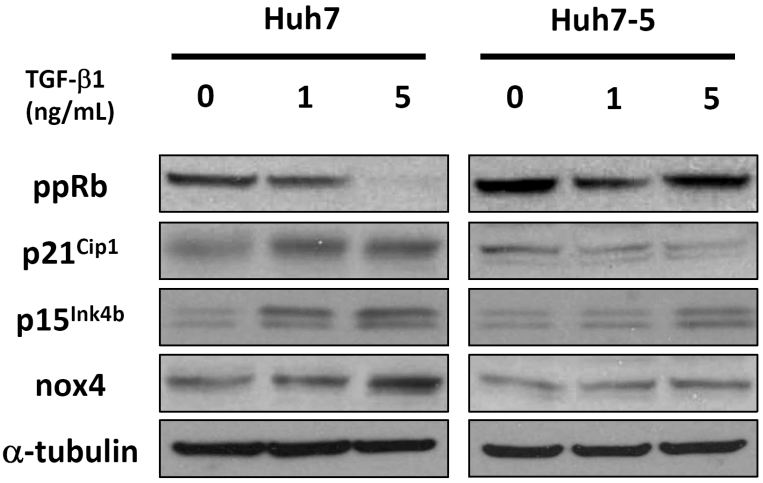

Figure 3.86: TGF-β treatment (72 hr) of parental Huh7 and Huh7-5 subclone cells. α-tubulin served as equal loading control.

3.17.4. Lack of responsiveness in rescued subclones

During the period of above experiments, we continued TGF-β treatment. At the day of ~70 of sustained treatment, we decided to generate another subclone of Huh7-5 which was rescued from TGF-β treatment. When reached at Day 100, we again performed a series of experiments in order to compare TGF-β responsiveness in parental Huh7, TGF-β-treated Huh7-5 subclone (continuously for 100 days) and rescued subclone Huh7-5-0 with no TGF-β treatment in the following 30 days. Therefore, the Huh7-5-0 subclone was designated as 70 days ON and 30 days OFF. We initially tested TGF-β response in the established subclones using luciferase based reporter systems. Parental Huh7, permanently TGF-β-treated subclone Huh7-5 and rescued clone Huh7-5-0 were accordingly transfected with pSBE4-luc to investigate intactness of TGF-β signaling and with p3TP-lux to analyze TGF-β responsiveness. As depicted in Figure 3.87 and 3.88, two established subclones had diminished response to TGF-β treatment. Parental Huh7 cells served as control and had intact signaling.

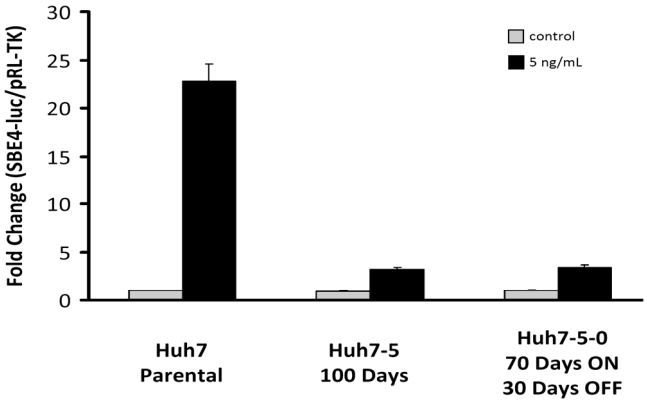

Figure 3.87: Diminished response to TGF-β treatment with pSBE4-luc in Huh7 clones after ~100 days. Cells were co-transfected with pSBE4-Luc and control pRL-TK plasmids, and treated with or without TGF-β1 (5 ng/mL) for 24 hr. The luciferase activity was measured and expressed as fold change of Reporter/pRL-TK (mean ± SD; n=3).

Parental Huh7 had over 20 fold increase in pSBE4-luc reporter activity under TGF-β treatment conditions. However, resistant subclone Huh7-5 and rescued Huh7-

5-0 subclone were not responsive to TGF-β treatment and showed only ~2-3 fold increase which was negligible under these conditions.

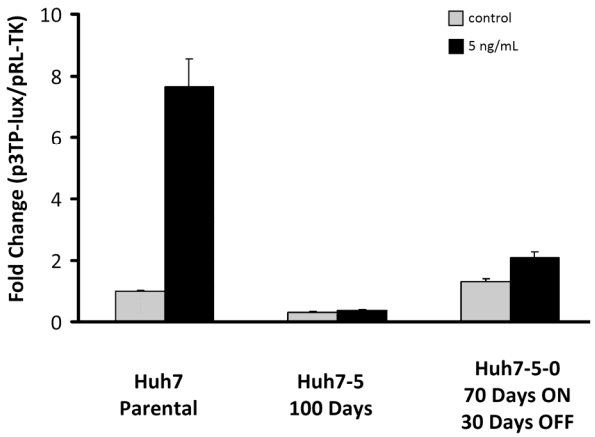

Figure 3.88: Diminished response to TGF-β treatment with p3TP-lux in Huh7 clones after ~100 days. Cells were co-transfected with p3TP-Lux and control pRL-TK plasmids, and treated with or without TGF-β1 (5 ng/mL) for 24 hr. The luciferase activity was measured and expressed as fold change of Reporter/pRL-TK (mean ± SD; n=3).

Parental Huh7 responded to 24 hr TGF-β treatment by a ~8 fold increase in p3TP-lux reporter activity. On the other hand, resistant subclone Huh7-5 displayed diminished reporter activity both in the presence and absence of TGF-β. In contrast to that, the rescued clone Huh7-5-0 had ~1.5 fold increased endogenous reporter activity with ~2 fold increased reporter response under TGF-β treatment conditions when compared to non-treated parental Huh7.

Next, we explored TGF-β-induced inhibition of BrdU incorporation. We found out that both resistant and rescued clones did not respond to TGF-β with a decrease in BrdU incorporation after 72 hr of treatment (Figure 3.89).

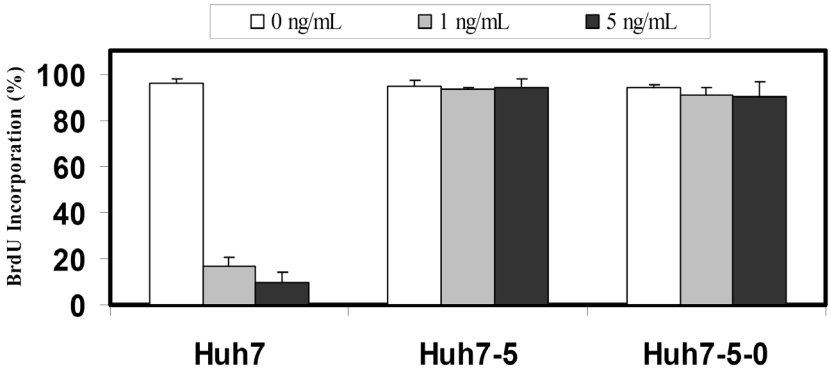

Figure 3.89: Resistance to inhibition of BrdU incorporation in ~100 days TGF-β-treated Huh7-5 and rescued Huh7-5-0 cells following 72 hr treatment. After 24 hr of incorporation, cells positively labeled for BrdU were stained by immunofluorescence (IF) technique using anti-BrdU (mouse) antibody. DAPI was used for nuclear counter-staining in IF experiments. At least 5 areas were manually counted in triplicate assays.

The subclones seemed to be completely resistant to TGF-β-induced cytostatic responses. In addition, we performed cell cycle analysis in there clones. Similar to BrdU incorporation results, we determined no change in cell cycle pattern in resistant and rescued clones (Figure 3.90). Parental Huh7 had around 60% G1 cells and 20% S-phase cells. After treatment with increasing doses of TGF-β1, G1-phase cells reached to ~75% and ~90% distribution in parental Huh7 with 1 ng/mL and 5 ng/mL TGF-β1, respectively.

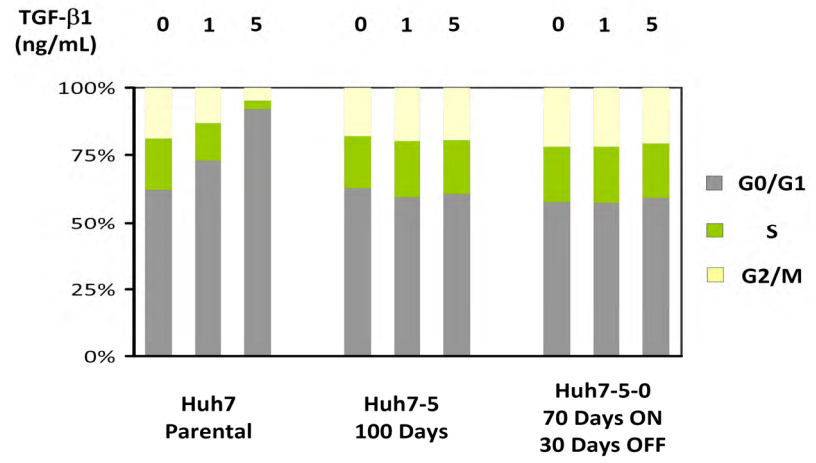

Figure 3.90: Cell cycle distribution in Huh7, resistant Huh7-5 and rescued Huh7-5-0 cells after 72 hr TGF-β1-treatment.

3.17.5. Intactness of TGF-β signaling pathway in resistant Huh7-5 and rescued Huh7-5-0 subclones

There might be several reasons behind the resistance to TGF-β cytostatic response along with loss of responsiveness to TGF-β tested by luciferase reporters. In order to delineate possible mechanisms conferring resistance to TGF-β, we initially performed a series of analyses in TGF-β pathway integrity to assess the possibility of a disruption in signal transduction. Parental Huh7, resistant Huh7-5 subclone and rescued Huh7-5-0 subclone cells were treated with TGF-β for 60 min under normal culture conditions. We then tested Smad2 activation by TGF-β receptors using phospho-specific Smad2 antibody (Figure 3.91).

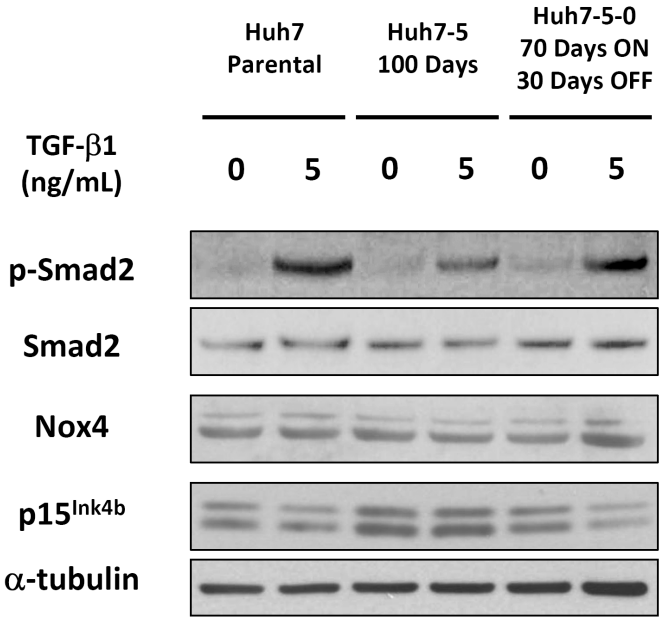

Figure 3.91: Slightly decreased activation of Smad2 in resistant clone. Cells were treated with 5 ng/mL TGF-β for 60 min under normal culture conditions.

Treatment of cells with 5 ng/mL TGF-β for 60 min resulted in substantial activation of Smad2 as demonstrated by increase in the phosphorylated form of Smad2. Resistant subclone Huh7-5 had a slightly decreased but still detectable phosphorylation in Smad2 suggesting a possible desensitization to TGF-β after

prolonged exposure. On the other hand, we tested possible early activation of Nox4 and $p15^{Ink4b}$ in all Huh7 clones but detected no change in 1 hr treatment indicating that these genes may not be early-response targets in HCC cells.

Since we determined active receptor status with very low impairment in resistant Huh7-5 clone but intact signaling in parental Huh7 and rescued Huh7-5-0, we moved on to analyze the status of signal transduction from cell membrane to nucleus. We initially tested p-Smad3 localization after 60 min of TGF-β treatment. As depicted in Figure 3.92, p-smad3 was localized to nucleus upon TGF-β exposure with a bit of deregulation in resistant and rescued subclones. So that signal intensity in resistant and rescued clones was comparably less.

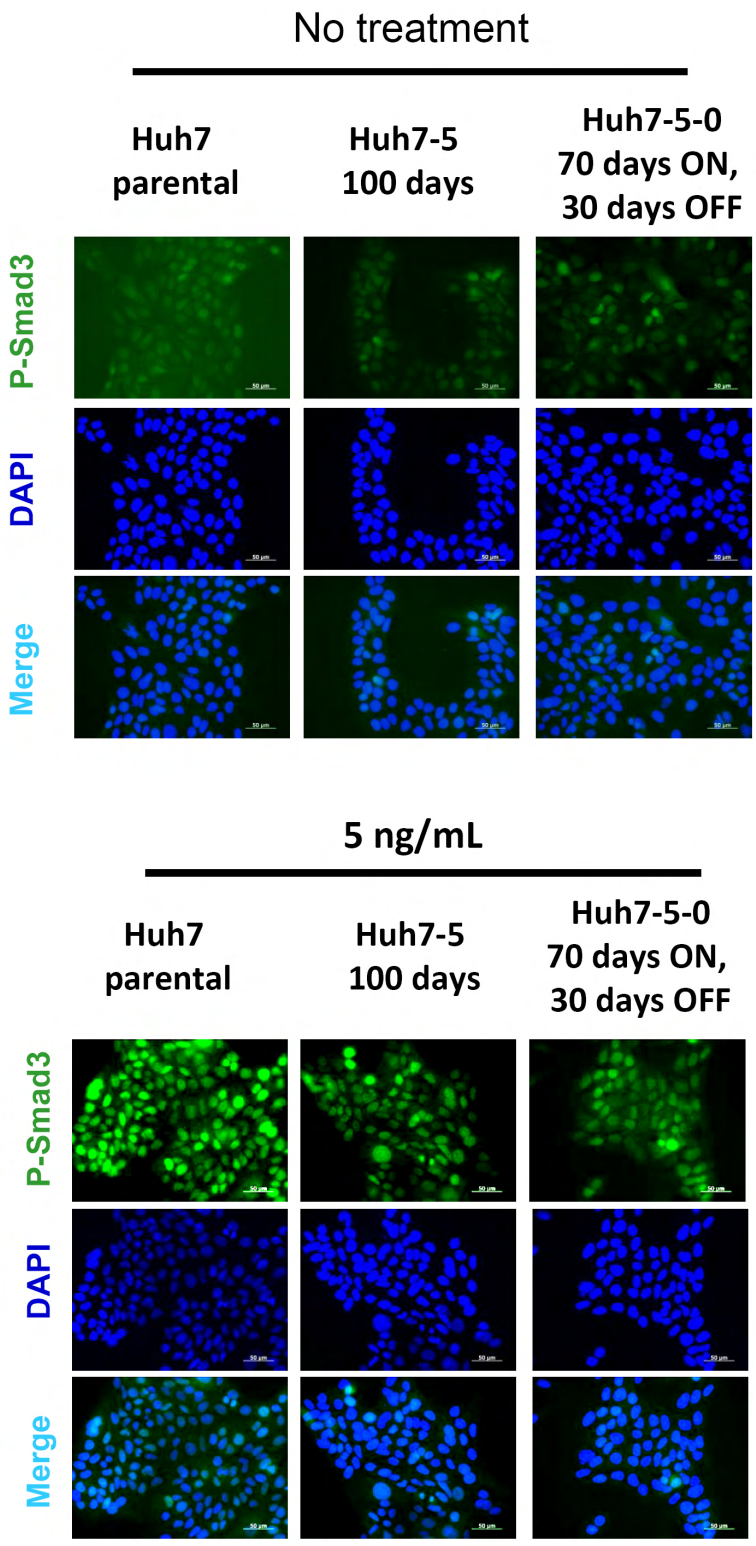

Figure 3.92: Decreased nuclear accumulation of activated p-Smad3 in resistant and rescued clones. Cells were treated with 5 ng/mL TGF-β for 60 min under normal culture conditions. Pictures taken at 40X objective lens.

On the other hand, we also studied nuclear localization of Smad4 and Smad2/3 by immunofluorescence experiments. Two primary antibodies against Smad2/3 were predominantly recognizing either Smad2 or Smad3. Due to high aminoacid sequence homology between Smad2 and Smad3, the antibodies generated against each of these proteins usually recognize the other partner as well, but with less affinity.

TGF-β treatment, in parental Huh7, induced nuclear transduction of Smad3 in 60 min. Nuclear smad3 was also detectable in resistant Huh7-5 and rescued Huh7-5-0 subclones with additional positive cytoplasmic smad3 staining. However, the nuclear intensity was less when compared to parental Huh7 (Figure 3.93).

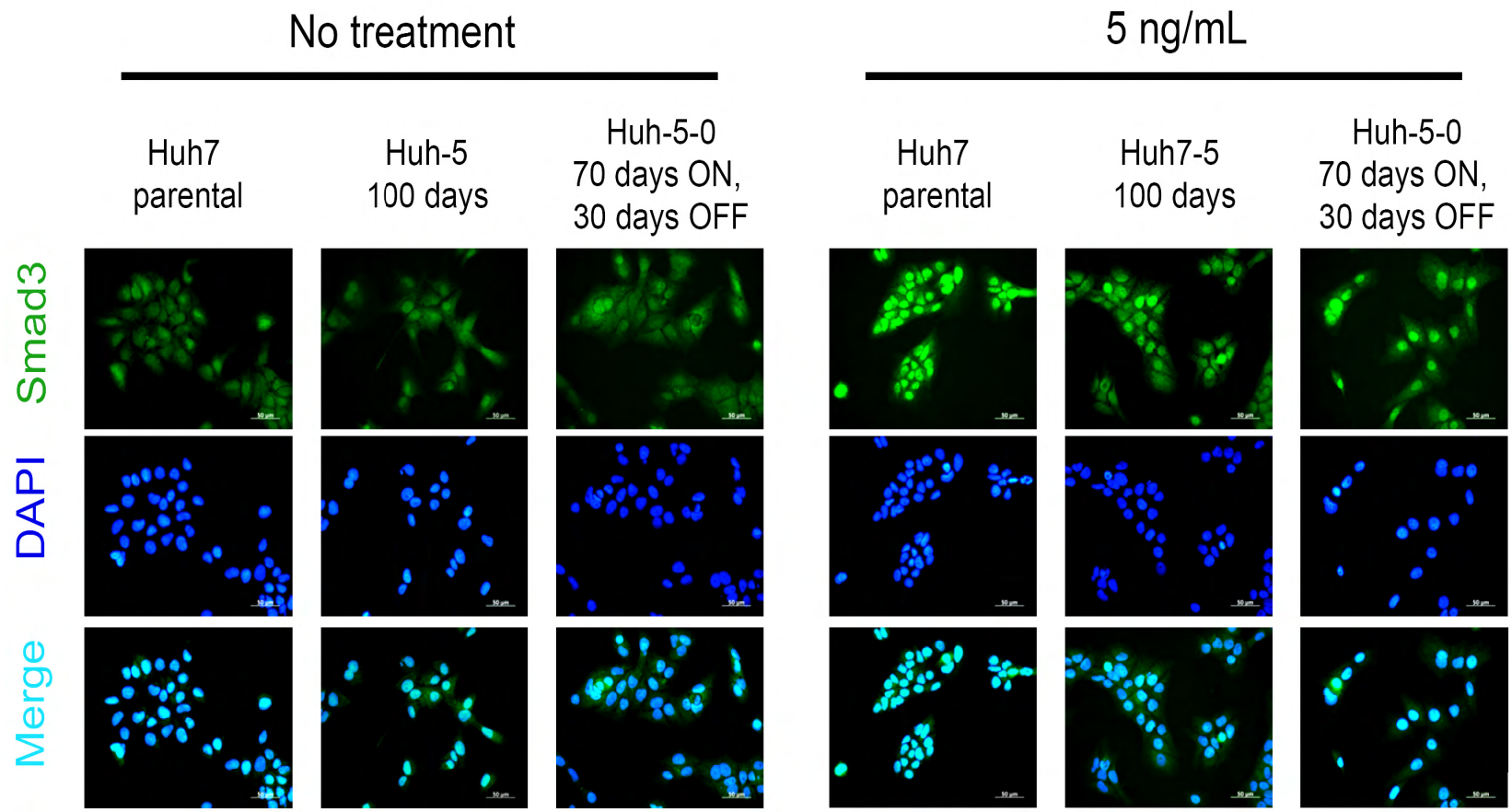

Figure 3.93: Decreased nuclear accumulation of Smad3 in resistant and rescued clones. Cells were treated with 5 ng/mL TGF-β for 60 min under normal culture conditions. Pictures taken at 40X objective lens.

Similar to Smad3, we also performed signal transduction experiments to detect smad2 and smad4 localization. This time we carried out the experiments in a time-based fashion in which we tried to detect cellular localization of Smad2 and Smad4 after 10 min, 30 min and 60 min of TGF-β stimulation. Intracellular localization of Smad2 presented a similar pattern to Smad3 in parental Huh7 and subclones at 60 min (Figure 3.94). Besides, time-dependent Smad2 distribution upon TGF-β stimulation clearly established a delayed Smad2 translocation into the nucleus.

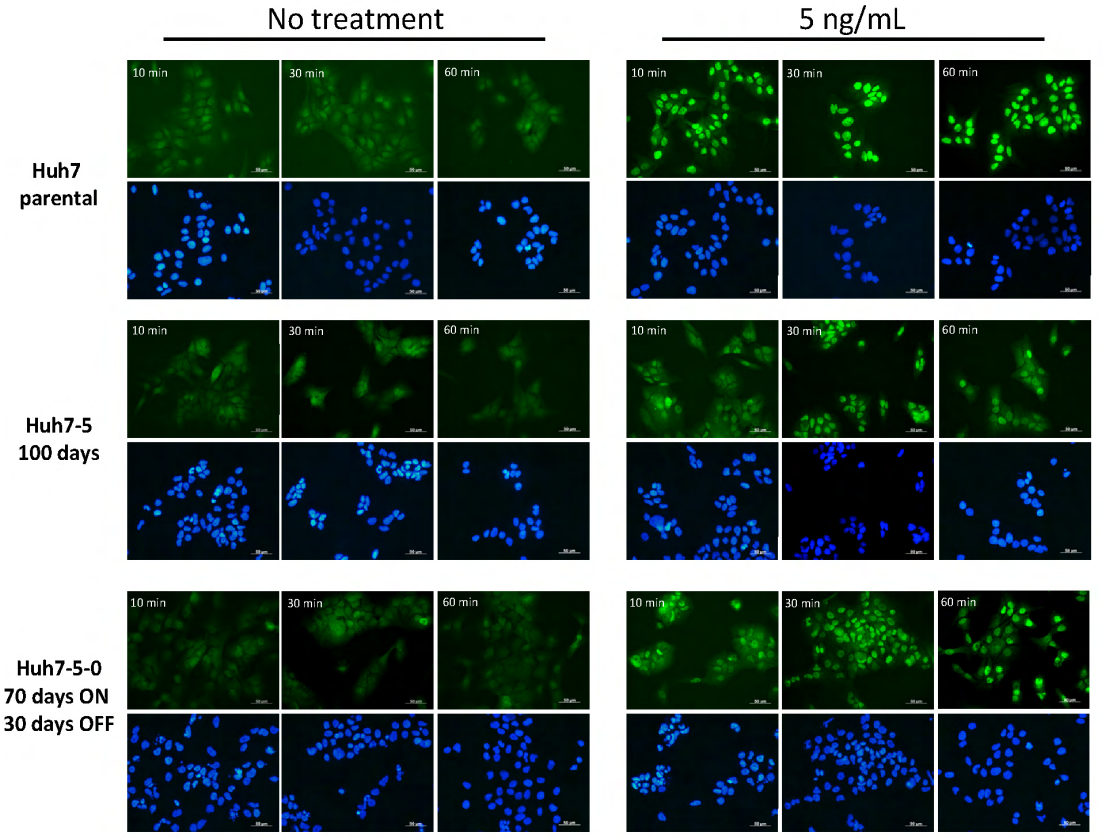

Figure 3.94: Decreased nuclear accumulation and time-dependent delay in Smad2 translocation in resistant Huh7-5 and Huh7-5-0 rescued clones. Cells were treated with 5 ng/mL TGF-β for indicated time frames under normal culture conditions. Pictures taken at 40X objective lens.

Additionally, nuclear smad4 translocation was prohibited in resistant Huh7-5 and rescued Huh7-5-0 subclone cells (Figure 3.95).

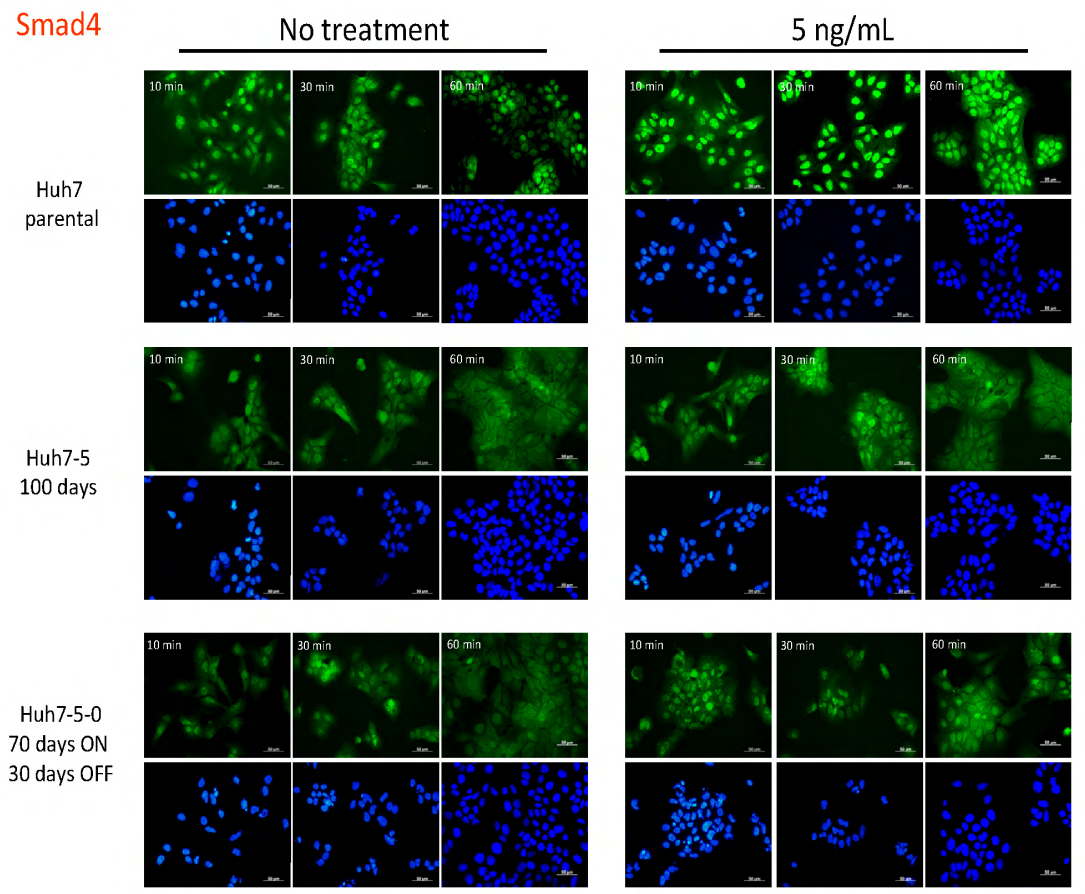

Figure 3.95: Diminished nuclear accumulation of Smad4 in resistant Huh7-5 and rescued Huh7-5-0 clones. Cells were treated with 5 ng/mL TGF-β for indicated time frames under normal culture conditions. Pictures taken at 40X objective lens.

Qualitative analysis with resistant Huh7-5 and rescued Huh7-5-0 subclones demonstrated impairment in transduction of intracellular TGF-β signal transmitting molecules, Smads. In order to have a notion of the degree of this disruption in quantitative terms, we performed western blotting experiments with parental Huh7

and resistant Huh7-5. Both cell clones were treated with 5 ng/mL TGF-β for 60 min and cell lysates were prepared accordingly to have nuclear and cytoplasmic fractions.

Similar to immunofluorescence experiments, we also reported impairment in Smad3 translocation, along with decreased p-Smad3 localization in the nuclei of resistant Huh7-5 subclone (Figure 3.96).

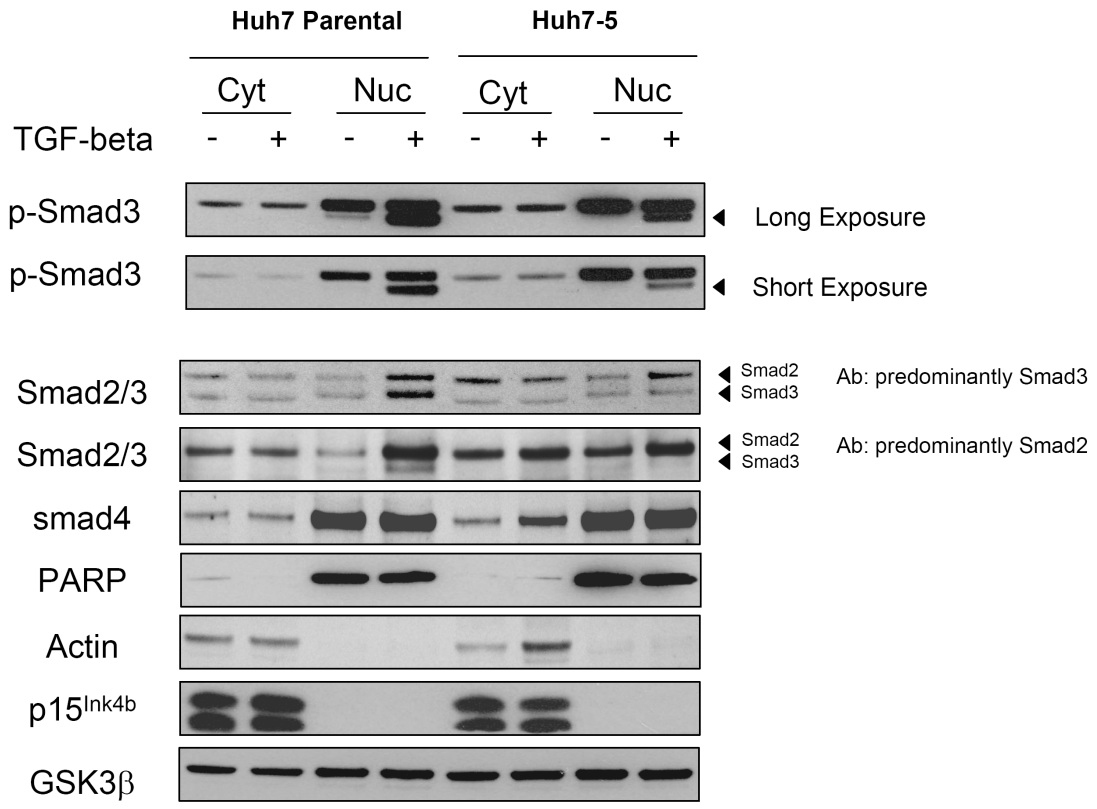

Figure 3.96: Impairment in Smad3 transduction into nucleus. Cells were treated with 5 ng/mL TGF-β for 60 min under normal culture conditions. Cytoplasmic and nuclear fractions were obtained accordingly. PARP and actin were used to test the efficiency of nuclear and cytoplasmic fractionation, respectively.

Nuclear accumulation of Smad3 and p-Smad3 in resistant Huh7-5 clone was substantially inhibited. Whereas, upon TGF-β stimulation, Smad2 was predominantly localized into the nucleus in both parental Huh7 and resistant Huh7-5

subclones. In this experimental set-up, PARP served as nuclear fraction control, while actin and $p15^{Ink4b}$ served as cytoplasmic fraction controls. Please note that, $p15^{Ink4b}$ translocates into the nucleus following 72 hr of incubation (data not shown) where it acts as a senescence inducer, as previously stated. Besides, we used GSK3β as a control for equal loading. Smad2/3 detection was essentially performed with two different antibodies. Both antibodies have different epitopes and preferentially recognize one on another.

Impairment in TGF-β signaling and cytostatic response could be in the form of decreased receptor expression and lack of increase in molecules that control TGF-β-induced growth arrest. We therefore conducted western blotting and real-time PCR analyses to define the expression patterns of genes of our interest, particularly EMT promoting Smad complexes (Fuxe et al., 2010). We initially studied the expression of TGF-β receptors and Smads in parental Huh7, resistant Huh7-5 and rescued Huh7-5-0 subclones in the presence of the ligand.

Surprisingly enough, we detected increased expression of both receptors in parental Huh7 in the presence of TGF-β. TGFβRII expression was substantially increased with increasing doses. However the level of increase in resistant Huh7-5 and rescued Huh7-5-0 was lower (Figure 3.97).

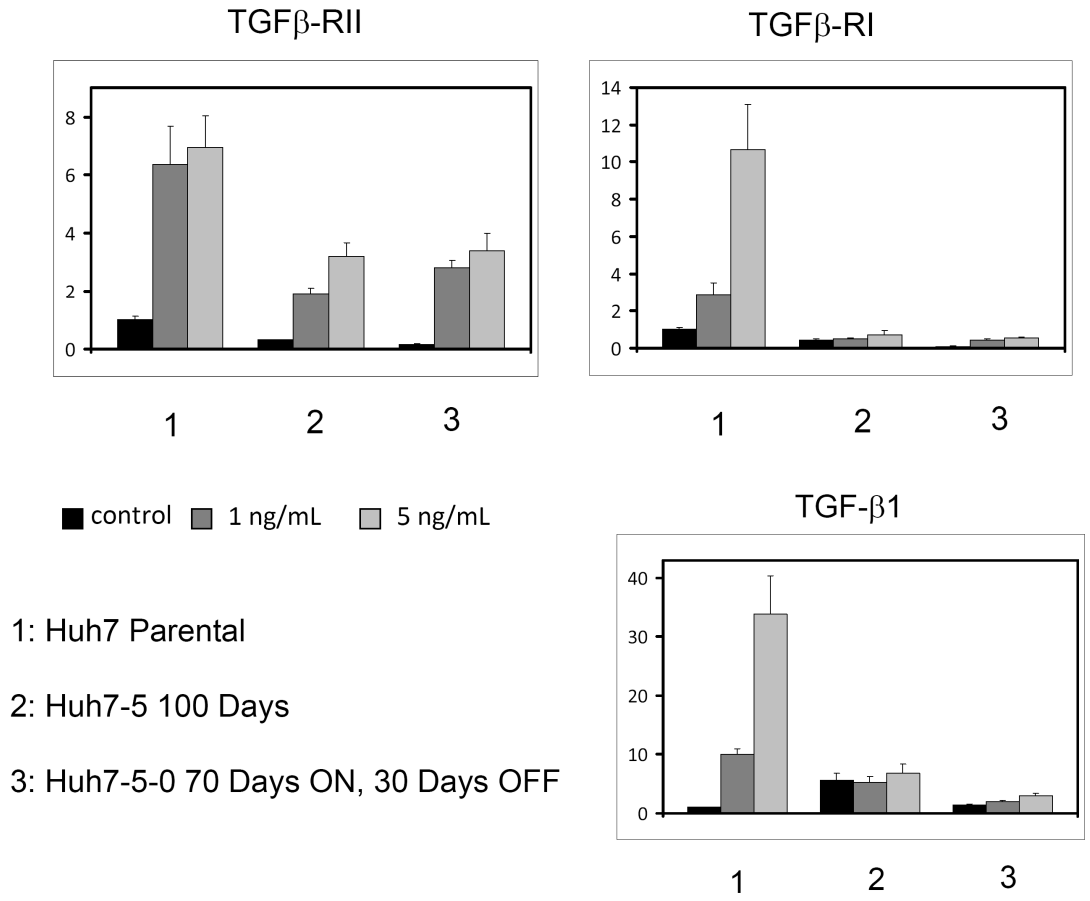

Figure 3.97: Expression of TGF-β1 and its receptors. Cells were treated with 1 ng/mL and 5 ng/mL TGF-β for 72 hr under normal culture conditions. Real-time PCR analysis was performed with corresponding primer pairs. Expression values were normalized with respect to GAPDH. **Y-axis: Fold Difference**

On the other hand, we detected ~10 fold increase in TGFb-RI in parental Huh7 when treated with 5 ng/mL TGF-β, whereas resistant and rescued subclones had diminished expression for this particular receptor both in the absence and presence of TGF-β. Besides, expression levels of TGF-β1 were highly elevated in parental Huh7, and endogenous levels were comparably higher in resistant and rescued subclones (Figure 3.97).

We further studied the expression of intracellular signal transmitting molecules. Smad2 and Smad4 transcript levels were not affected by TGF-β treatment in parental Huh7, resistant Huh7-5 and rescued Huh7-5-0. Whereas, Smad3

expression was elevated in parental Huh7 with TGF-β treatment and stayed almost unaffected in resistant and rescued subclones (Figure 3.98).

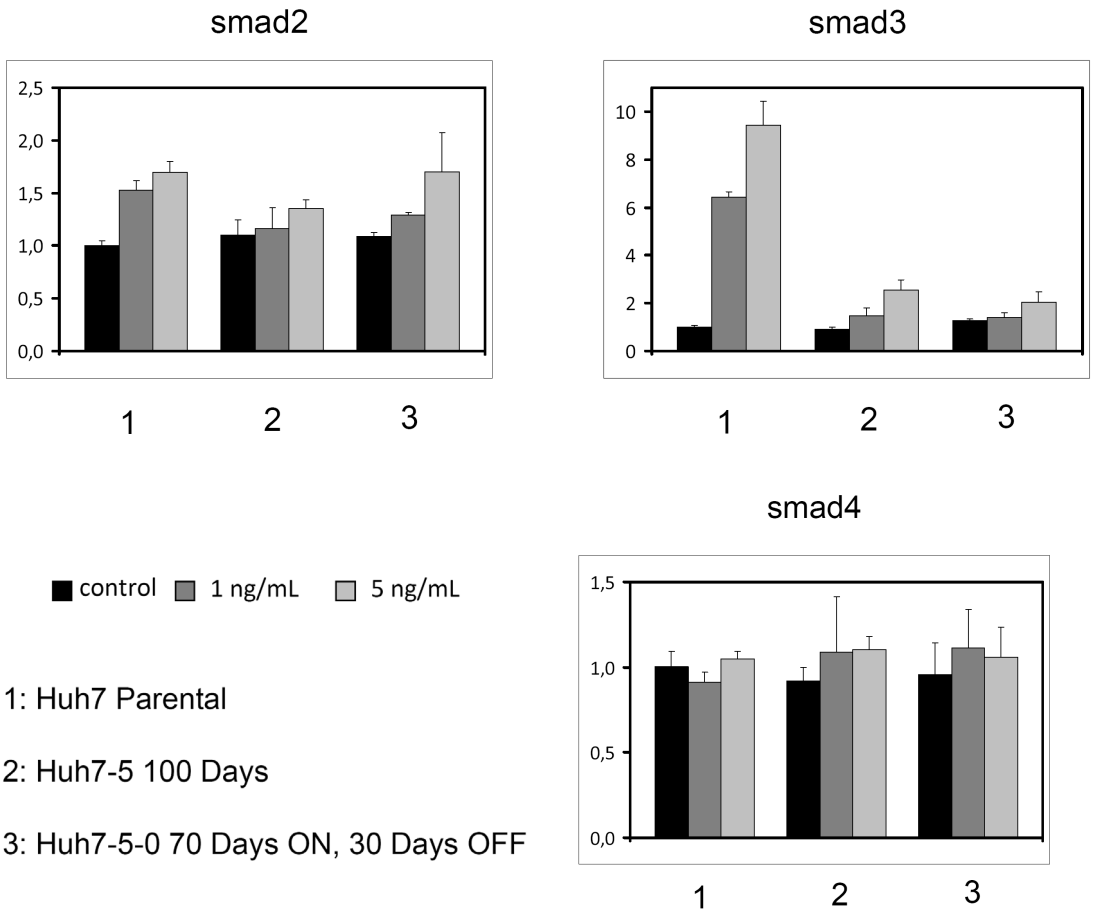

Figure 3.98: Expression of Smads. Cells were treated with 1 ng/mL and 5 ng/mL TGF-β for 72 hr under normal culture conditions. Real-time PCR analysis was performed with corresponding primer pairs. Expression values were normalized with respect to GAPDH. **Y-axis: Fold Difference**

Cytostatic responses controlled by TGF-β in Huh7 cells were mediated through upregulation of $p21^{Cip1}$ and $p15^{Ink4b}$ with a reciprocal decrease in c-myc levels. Besides, nox4 was implicated in TGF-β-induced growth arrest in this study. With this information in mind, we studied the expression of above transcripts and demonstrated substantial increases in $p15^{Ink4b}$, $p21^{Cip1}$ and Nox4 mRNA expression with a reciprocal decrease in c-myc transcript levels in parental Huh7 (Figure 3.99). All these effects were reversed in resistant Huh7-5 and rescued Huh7-5-0 subclones,

suggesting a potential mechanism to explain resistance to TGF-β-induced cytostatic response.

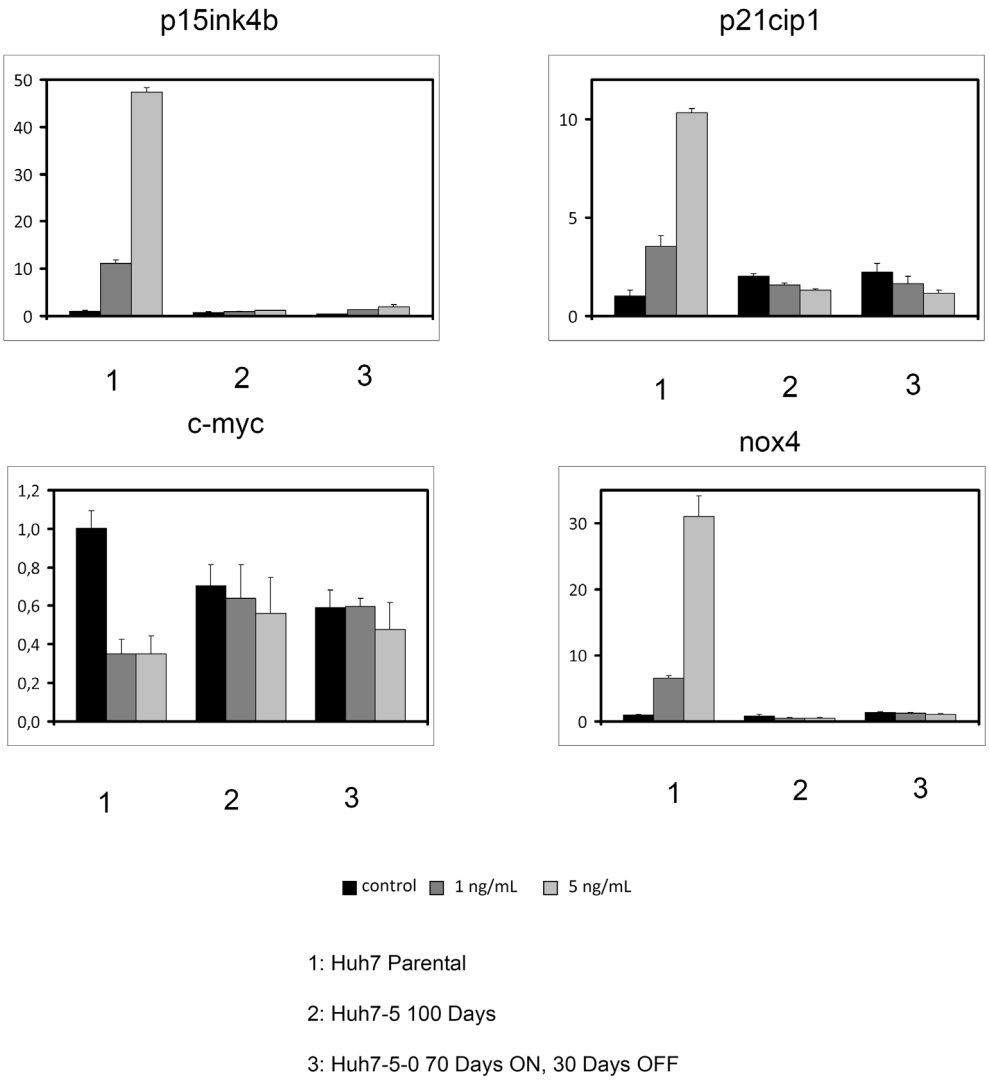

Figure 3.99: Expression of $p15^{Ink4b}$ and $p21^{Cip1}$, Nox4 and c-myc genes in resistant and rescued subclones. Cells were treated with 1 ng/mL and 5 ng/mL TGF-β for 72 hr under normal culture conditions. Real-time PCR analysis was performed with corresponding primer pairs. Expression values were normalized with respect to GAPDH. **Y-axis: Fold Difference**

PAI-1 transcript levels were also unaffected by TGF-β treatment in the established subclones supporting the previous loss of response findings (Figure 3.100).

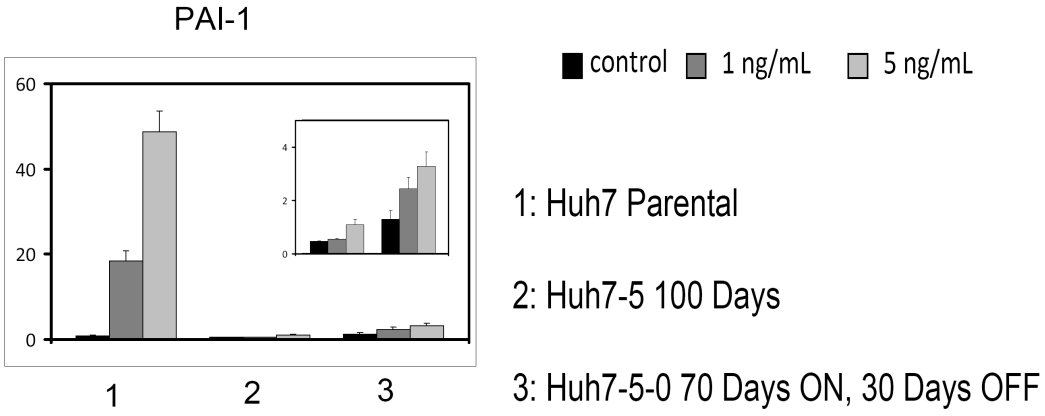

Figure 3.100: Expression of PAI-1 in resistant and rescued subclones. Cells were treated with 1 ng/mL and 5 ng/mL TGF-β for 72 hr under normal culture conditions. Real-time PCR analysis was performed with corresponding primer pairs. Expression values were normalized with respect to GAPDH. Inner box: modified scaling for 2 and 3. **Y-axis: Fold Difference**

Following the work with specific genes at transcript level, we moved on to quantify gene expression at protein level. Phosphorylated–Rb expression was monitored as a positive control in TGF-β-induced growth arrest. As can be seen in Figure 3.101, TGF-β stimulation for 72 hr decreased phospho-Rb levels. Together with that, we also studied $p15^{Ink4b}$ and $p21^{Cip1}$ expression at protein level in parental Huh7, resistant Huh7-5 and rescued Huh7-5-0 subclones and reported substantially increased amounts of protein levels in both cyclin-dependent kinase inhibitors in parental Huh7. Rescued Huh7-5-0 subclone had minor increments in $p15^{Ink4b}$ protein levels but not in $p21^{Cip1}$ expression. This increased expression in $p15^{Ink4b}$ however was not remarkable, hence did not influence ppRb rates. Resistant Huh7-5, on the other hand, was completely unresponsive to TGF-β treatment. Quantitative real-time PCR results were thereby supported by these findings. In addition, PAI-1 and Nox4 protein expression levels were increased in parental Huh7, but not in other subclones (Figure 3.101).

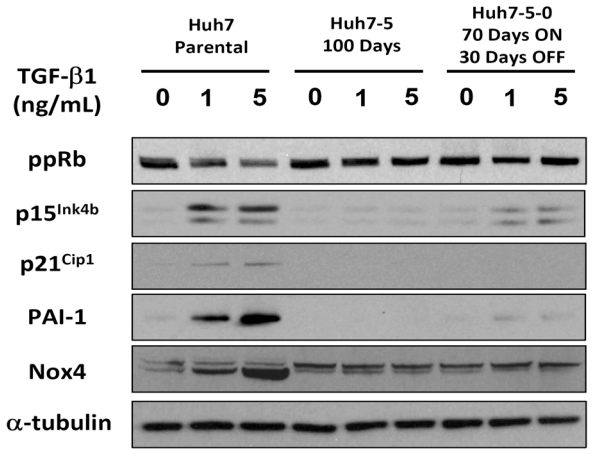

Figure 3.101: Protein expression of target genes in parental Huh7, resistant and rescued subclones. Cells were treated with 1 ng/mL and 5 ng/mL TGF-β for 72 hr under normal culture conditions. Western blotting analysis was performed with corresponding primary antibodies. A-tubuline was monitored as equal loading.

In addition to those targets surveyed above, we also investigated the expression of Smad signaling partners in these cells. Interestingly enough, we observed a dramatic decrease in Smad4 expression in parental Huh7 with increasing doses of TGF-β (Figure 3.102). Quite similar to qRT-PCR results, we detected a substantial increase in Smad3 expression in parental Huh7 cells in the presence of TGF-β.

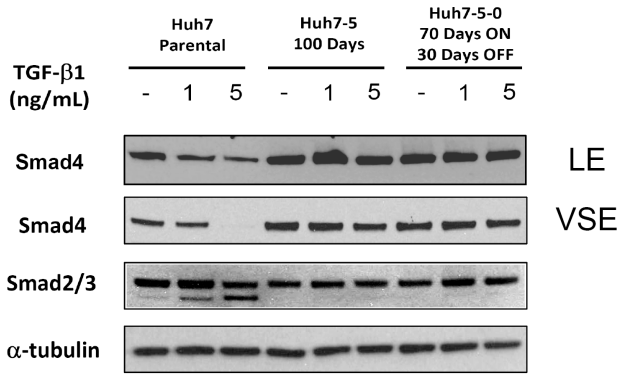

Figure 3.102: Expression of Smads in parental Huh7, resistant and rescued subclones. Cells were treated with 1 ng/mL and 5 ng/mL TGF-β for 72 hr under normal culture conditions. Western blotting analysis was performed with corresponding primary antibodies. A-tubulin was monitored as equal loading. Smad3: lower band in Smad2/3 result. LE: long exposure, VSE: very short exposure.

We further wanted to test the specificity of the decrease in Smad4 expression in parental Huh7 following TGF-β treatment. Therefore we performed a time-scale treatment of parental Huh7 with 5 ng/mL TGF-β. Cell lysates obtained from these treatments were subjected to immunoblotting. Smad4 expression was gradually decreased starting after 72 hr and reaching a maximum at day 5. Smad3 was detected to increase in a time-dependent manner as well, with highest levels at 48 hr and 72 hr (Figure 3.103).

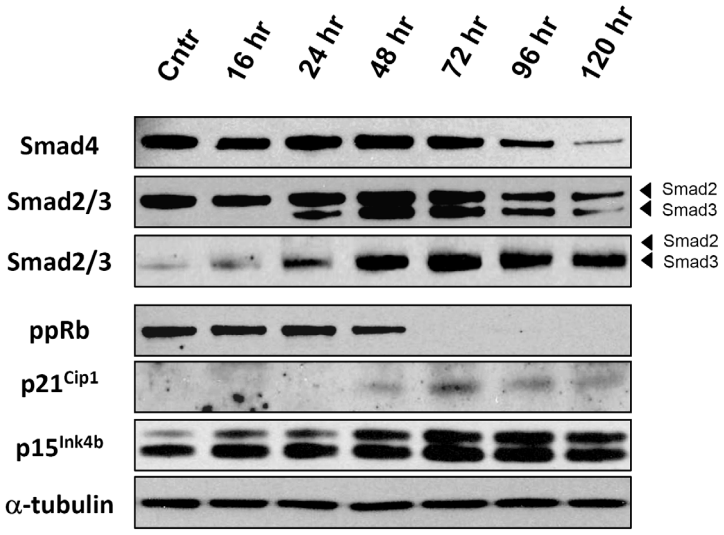

Figure 3.103: Time-dependent expression pattern of Smads and cytostatic response genes in parental Huh7. Cells were treated with 5 ng/mL TGF-β for indicated times. Western blotting analysis was performed with corresponding primary antibodies. A-tubulin was used as equal loading. Control samples were obtained from 120 hr cultured cells in the absence of TGF-β.

Interestingly enough, time-dependent increments in Smad3 levels in parental Huh7 cells overlapped well with decrease in ppRb levels and increases in $p15^{Ink4b}$ and $p21^{Cip1}$ protein levels. Therefore, above results directed our attention much on Smad3. In regard to results which demonstrated lack of induction of Smad3 under TGF-β-treatment conditions in resistant and rescued clones, we hypothesized a potential involvement of TGF-β-induced Smad3 in provoking cytostatic response.

Therefore we decided to transiently overexpress wild-type Smad3 in resistant Huh7-5 and rescued Huh7-5-0 subclones. These experiments were performed with subclones that reached 125 days in culture. Prior to these studies, we again checked the intactness and responsiveness of resistant and rescued clones to TGF-β using pSBE4-luc luciferase reporter assay. Similar to previous results with short-term cultured subclones, we depicted that the subclones at this time-point were still unresponsiveness to TGF-β treatment (Figure 3.104).

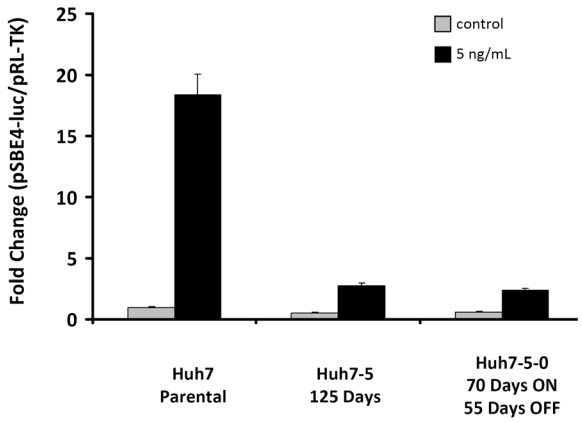

Figure 3.104: Diminished response to TGF-β treatment in Huh7 clones after ~125 days. Cells were co-transfected with pSBE4-Luc and control pRL-TK plasmids, and treated with or without TGF-β1 (5 ng/mL) for 24 hr. The luciferase activity was measured and expressed as fold change of Reporter/pRL-TK (mean ± SD; n=3).

In an effort to assess the contribution of Smad3 to signal transduction and cytostatic responses, we transiently overexpressed wild-type Smad3 in parental Huh7, resistant Huh7-5 and rescued Huh7-5-0 subclones. Cells were co-transfected with pcDNA3.1-Smad3 vector along with p3TP-lux and pRL-TK reporters, and corresponding empty vector pcDNA3.1 for control experiments. Transfected cells were treated with 5 ng/mL TGF-β for 24 hr, and treatment was initiated following 6 hr post-transfection. Results clearly indicated that ectopic expression of Smad3 increased endogenous luciferase reporter signals and enhanced reporter activation in parental Huh7 in the presence of TGF-β. Besides, the effects of TGF-β were

completely reversed in terms of luciferase reporter activation in established subclones as well (Figure 3.105).

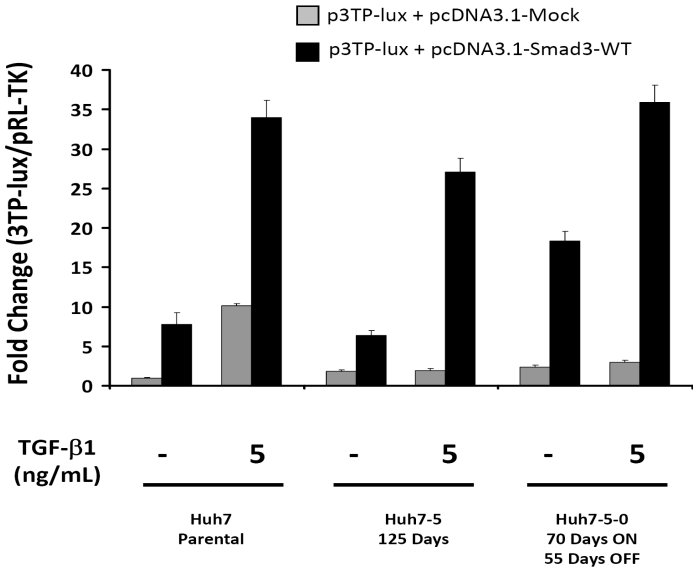

Figure 3.105: Restoring the response of Huh7 subclones to TGF-β treatment following ectopic Smad3 expression. Cells were co-transfected with pcDNA3.1-Smad3-WT and/or pcDNA3.1/p3TP-Lux and control pRL-TK plasmids, and treated with or without TGF-β1 (5 ng/mL) for 24 hr. The luciferase activity was measured and expressed as fold change of Reporter/pRL-TK (mean ± SD; n=3).

Following these encouraging results, we further studied the TGF-β-mediated cytostatic response in the established subclones, in the presence of ectopic Smad3 expression. Initially, we tested proliferation capacity of transfected cells using BrdU incorporation assays. We transiently overexpressed Smad3 in parental Huh7 and resistant subclone Huh7-5. Transfected cells were selected with G418 antibiotic for three days and then seeded in 12-well plates on cover-slips.

One day following seeding, cells were treated with 5 ng/mL TGF-β for 72 hr. Following 24 hr BrdU incorporation, cells were fixed accordingly and stained with anti-BrdU primary antibody. Positive cells were calculated by manual counting with respect to nuclear DAPI staining. Results are shown in Figure 3.106. Ectopic Smad3 expression led to a significant decrease, even in the absence of TGF-β, in BrdU incorporation in parental Huh7 (***, $p < 0.01$) and resistant Huh7-5 (*, $p < 0.005$)

when compared to corresponding empty vector transfected samples. BrdU incorporation in resistant Huh7-5 cells under TGF-β treatment condition decreased by ~50 percent (**, $p < 0.0001$).

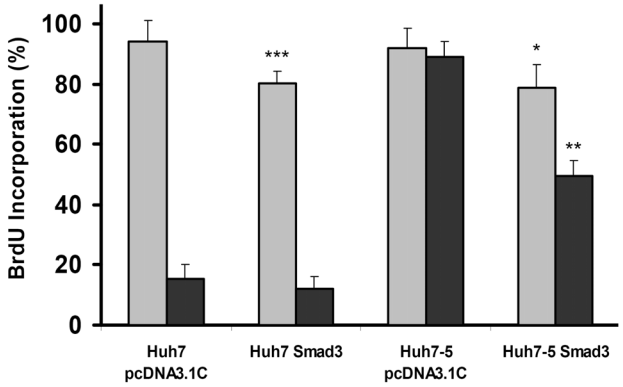

Figure 3.106: BrdU incorporation in parental Huh7 and resistant Huh7-5 subclone after TGF-β treatment following ectopic Smad3 expression. Cells were transfected with pcDNA3.1-Smad3-WT and/or pcDNA3.1 plasmids, selected under antibiotic pressure for three days and then treated with TGF-β1 for 72 hr. Percent BrdU was calculated by manual counting of at least 5 areas from each triplicate experiment. (P value less than, *: 0.005, **: 0.0001, ***: 0.01). Grey bars: 0 ng/mL TGF-β1, black bars: 5 ng/mL TGF-β1.

Using a portion of the same transfected cells, we studied cell-cycle analysis and obtained similar results (Figure 3.107).

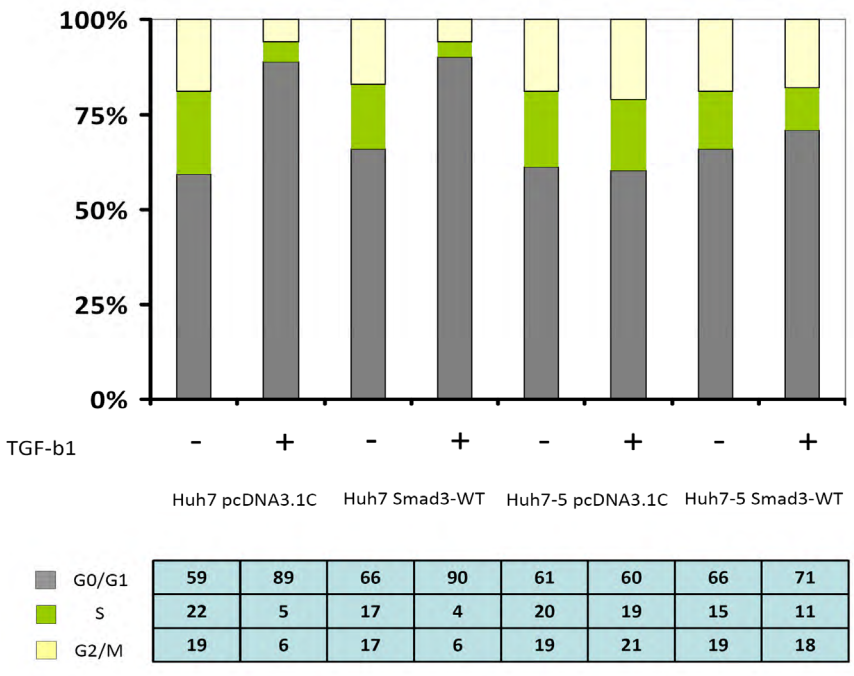

G0/G1	59	89	66	90	61	60	66	71
S	22	5	17	4	20	19	15	11
G2/M	19	6	17	6	19	21	19	18

Figure 3.107: Cell cycle analysis in parental Huh7 and resistant Huh7-5 subclone after TGF-β treatment following ectopic Smad3 expression. TGF-β1: 5 ng/mL

3.17.6. Prolonged TGF-β treatment generates mesenchymal-like Huh7 cells

Epithelial mesenchymal transition is one of the escape mechanisms from TGF-β-induced cytostatic responses (Gal et al., 2008). Recently, EMT has also been implicated in generation of stem-cell like cells with enriched tumorigenicity capacity (Mani et al., 2008). Besides, in liver, CD133+ cancer stem cells were stated to be resistant to TGF-β-induced cytostatic responses (Ding et al., 2009).

Thus, we tested potential EMT transformation in resistant Huh7-5 and rescued Huh7-5-0 along with expression analysis of stem cell markers. We performed qRT-PCR, western blotting and immunofluorescence experiments to determine EMT-like transformation. Initial experiments with qRT-PCR designated increased expression in mesenchymal marker vimentin together with decreased levels in epithelial marker e-cadherin (Figure 3.108).

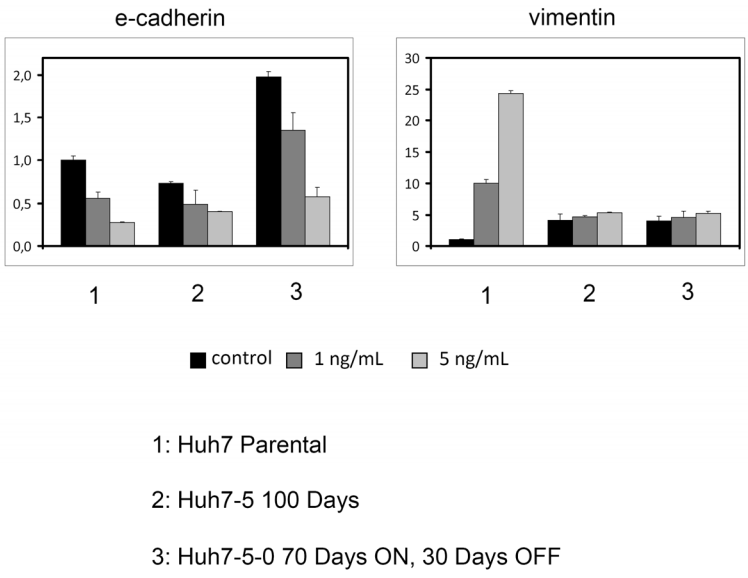

Figure 3.108: Expression of epithelial and mesenchymal markers in resistant and rescued subclones. Cells were treated with 1 ng/mL and 5 ng/mL TGF-β for 72 hr. Real-time PCR analysis was performed with corresponding primer pairs. Expression values were normalized with respect to GAPDH. **Y-axis: Fold Difference**

Endogenous e-cadherin expression was markedly increased in rescued Huh7-5-0 subclone. Moreover, e-cadherin expression is regulated by TGF-β signaling pathway. Zeb2 transcription factor is one of the key players in TGF-β-induced epithelial-mesenchymal transition with particular role in downregulation of e-cadherin expression. Through direct interaction with e-cadherin promoter together with activated Smad molecules, zeb2 downregulates transcription of e-cadherin (Comijn et al., 2001). Besides, recent findings implicated zeb2 in vimentin regulation (Bindels et al., 2006). Therefore, we studied zeb2 expression in established subclones, together with parental Huh7. We demonstrated that zeb2 is also a target of TGF-β signaling pathway in parental Huh7 (Figure 3.109).

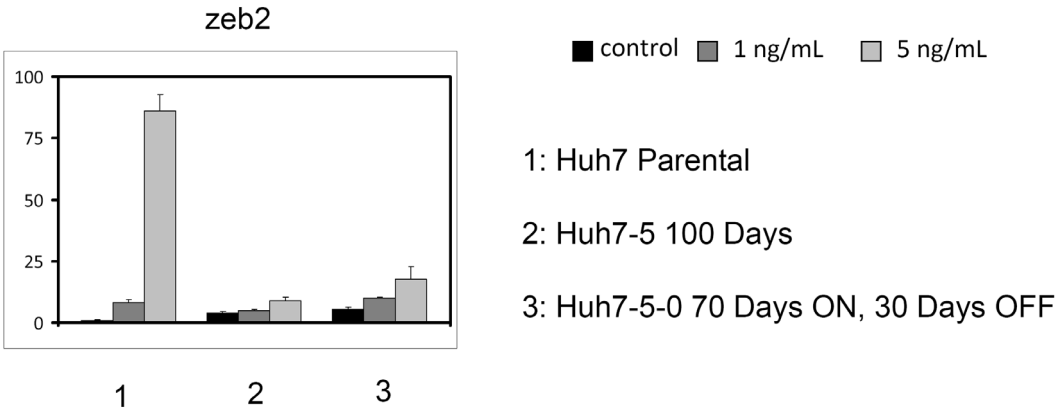

Figure 3.109: Expression of zeb2 in resistant and rescued subclones. Cells were treated with 1 ng/mL and 5 ng/mL TGF-β for 72 hr. Real-time PCR analysis was performed with corresponding primer pairs. Expression values were normalized with respect to GAPDH. **Y-axis: Fold Difference**

We detected substantially high activation of zeb2 expression at transcript level. Likewise, endogenous expression of zeb2 in resistant Huh7-5 and rescued Huh7-5-0 was detected to be ~4 to 6 fold higher than parental Huh7, respectively. Besides these endogenous transcript levels were increased up to ~9 and 17 fold with 5 ng/mL TGF-β treatment in resistant and rescued subclones, respectively. Taken together, these results indicated that zeb2 might have a potential implication in TGF-β-induced EMT-like transformation in HCC cells. Additionally, endogenous vimentin transcript levels were comparably higher in resistant and rescued subclones than parental Huh7. These findings also indicated a possible mesenchymal-like transformation of parental Huh7 during the establishment of the resistant subclone. We also studied the expression of e-cadherin and vimentin at protein level, together with another epithelial marker ZO-1. These results were also in support of qRT-PCR findings (Figure 3.110).

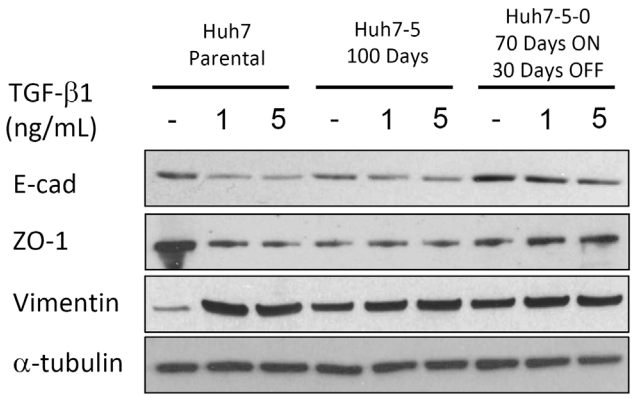

Figure 3.110: Expression of e-cadherin, ZO-1 and vimentin in parental Huh7, resistant and rescued subclones. Cells were treated with 1 ng/mL and 5 ng/mL TGF-β for 72 hr under normal culture conditions. Western blotting analysis was performed with corresponding primary antibodies. A-tubulin was monitored as equal loading.

Endogenous protein levels of vimentin in resistant Huh7-5 and rescued Huh7-5-0 were quite high when compared to parental Huh7. Removal of TGF-β from growth medium during the establishment of rescued Huh7-5-0 did not lead to an escape of resistant Huh7-5 from mesenchymal-like state. Epithelial-mesenchymal transition is usually characterized with cytoskeletal changes depending on diverse stimulating agents (Boyer et al., 1989). We studied localization and staining intensities of selected EMT genes in parental Huh7 and the established clones. Endogenous vimentin expression in parental Huh7 was heterogeneous with a range from completely negative cells to highly positive cells. Whereas, TGF-β treatment induced vimentin expression in parental Huh7 cells similar to qRT-PCR and immunoblotting results (Figure 3.111). Together with that, all of the cells in resistant Huh7-5 and rescued Huh7-5-0 subclones were homogenously positive for vimentin expression with a few exceptional cells that have less but still detectable expression.

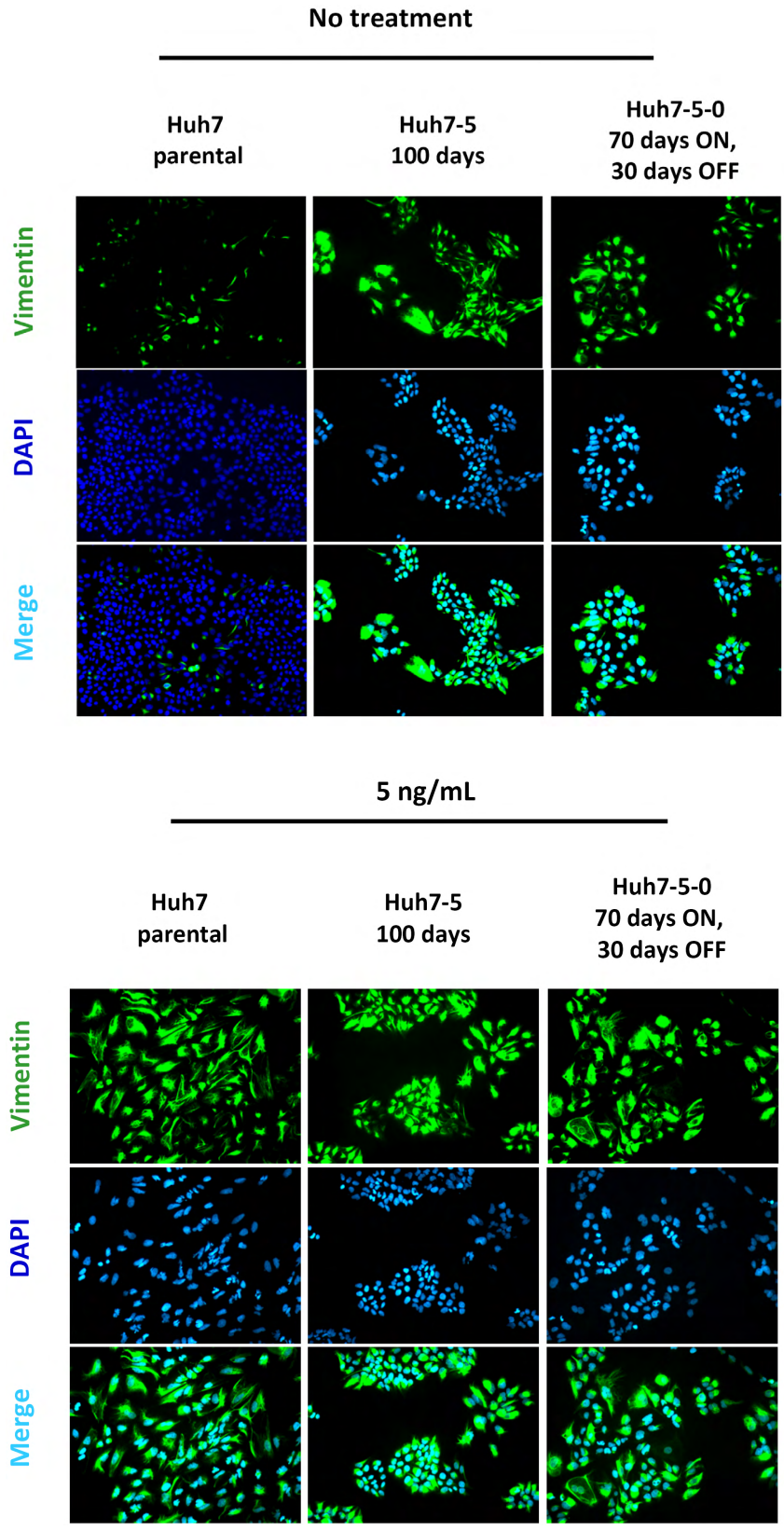

Figure 3.111: Staining pattern of vimentin in parental, resistant and rescued subclones of Huh7. Pictures were obtained at 20X with same exposure time (350 ms).

We next studied the staining pattern of ZO-1 and β-cat at the adherens and tight junctions in TGF-β-treated parental Huh7 and the established subclones. ZO-1 staining pattern changed to a much wider membranous distribution after TGF-β treatment in parental Huh7, indicating the dissolution of tight junctions during EMT (Figure 3.112 and 3.113). Similar distribution was detected with resistant and rescued subclones both in the presence and absence of TGF-β as an indication of a sustained mesenchymal like phenotype.

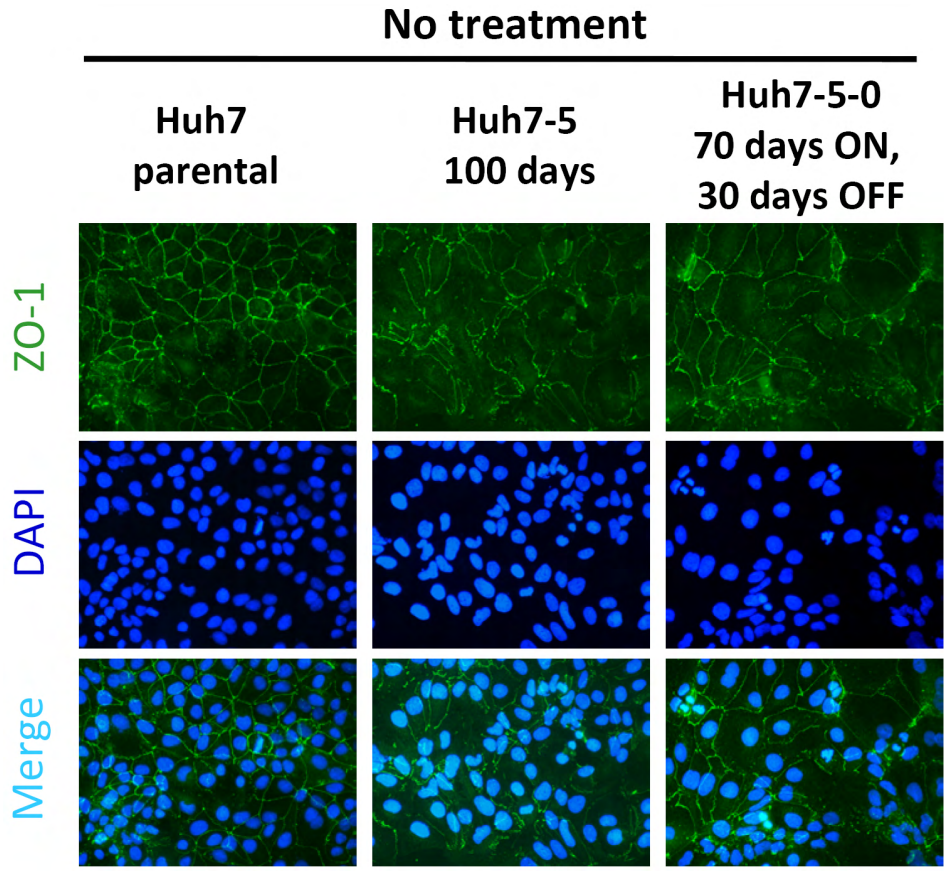

Figure 3.112: Staining pattern of ZO-1 in parental, resistant and rescued subclones of Huh7 in the absence of TGF-β. Pictures were obtained at 20X with same exposure time (350 ms).

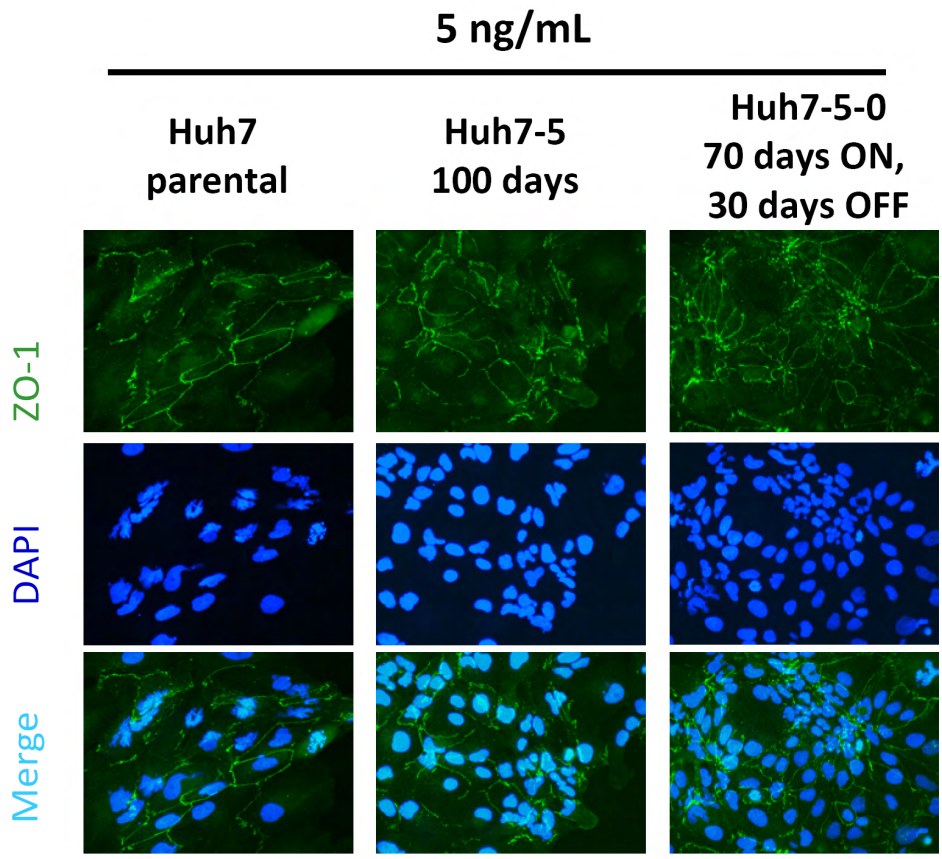

Figure 3.113: Staining pattern of ZO-1 in parental, resistant and rescued subclones of Huh7 in the presence of TGF-β. Pictures were obtained at 40X with same exposure time (350 ms).

The disruption of multiple reciprocal interactions between e-cadherin and b-catenin at adherens junctions promotes EMT transformation (Lecuit and Lenne, 2007). We were not able to detect cell surface staining with the e-cadherin antibody in different fixation methods, therefore decided to study e-cadherin associated β-catenin staining patterns. Cell surface staining of β-catenin demonstrated an even distribution in un-treated controls. However, distribution of β-catenin in parental Huh7 under TGF-β-treatment conditions was diffused on cell surface and more pronounced in the cytoplasm. Nonetheless, similar staining patterns were visible in resistant Huh7-5 and rescued Huh7-5-0 subclones (Figure 3.114). These findings also support alterations in cell surface mechanics in the established subclones.

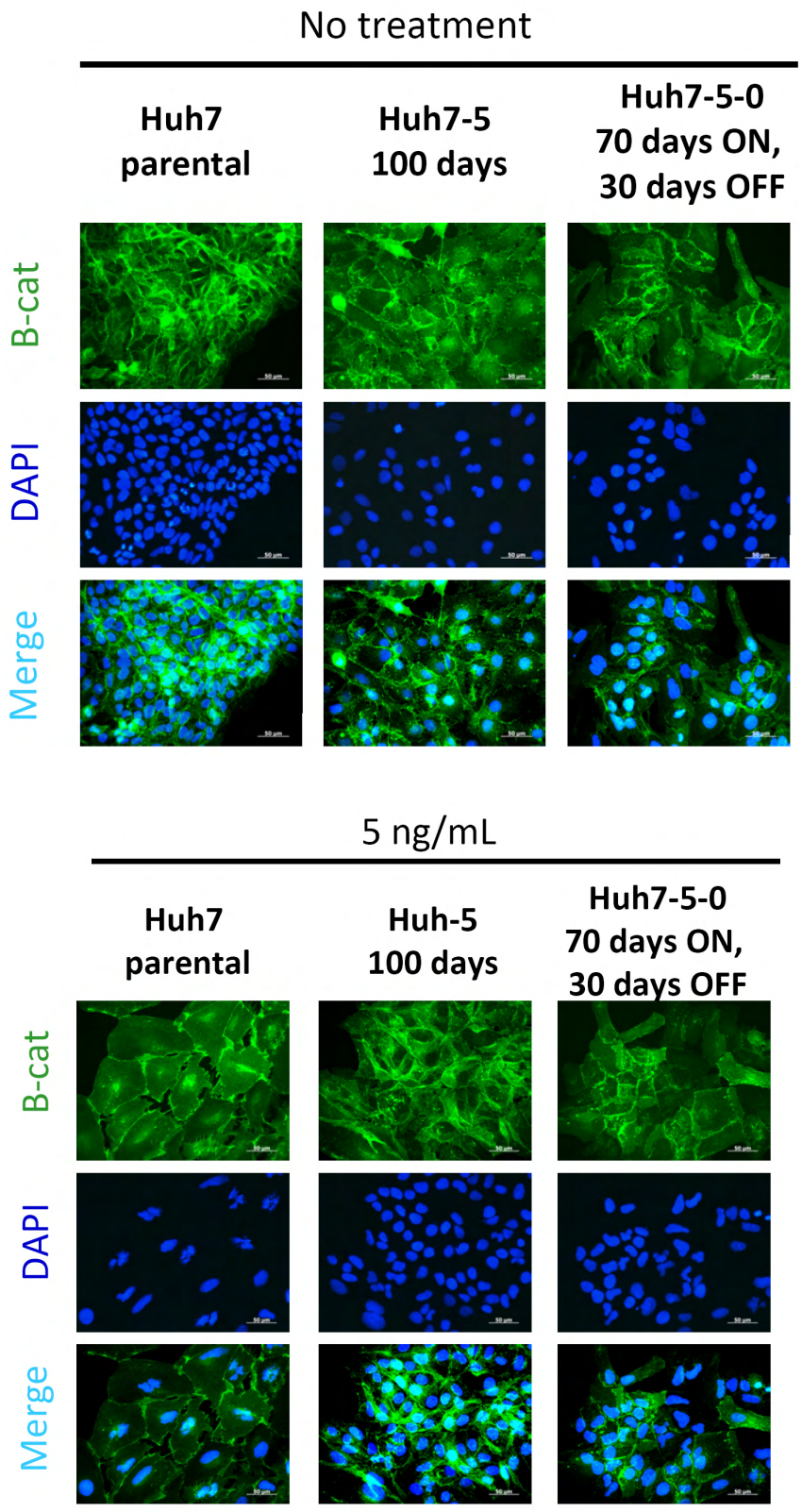

Figure 3.114: Staining pattern of β-catenin in parental, resistant and rescued subclones of Huh7. Pictures were obtained at 40X with same exposure time (650 ms).

Moreover, mesenchymal-like HCC cell lines have higher motility and invasion capacity when compared to epithelial like cells (Yuzugullu et al., 2009). In consideration of such an observation in our lab, we decided to look at motility ratios of the established subclones in the presence of TGF-β, in comparison to parental Huh7. We performed a simple wound healing assay. Cells were seeded in 12-well plates 24 hr prior to wounding, as such to have a 100% monolayer confluence at the time of scratching. Essentially, cells were cultured with growth medium containing 2% FBS after scratching. Results for untreated and treated wells are depicted in Figure 3.115 and Figure 3.116, respectively.

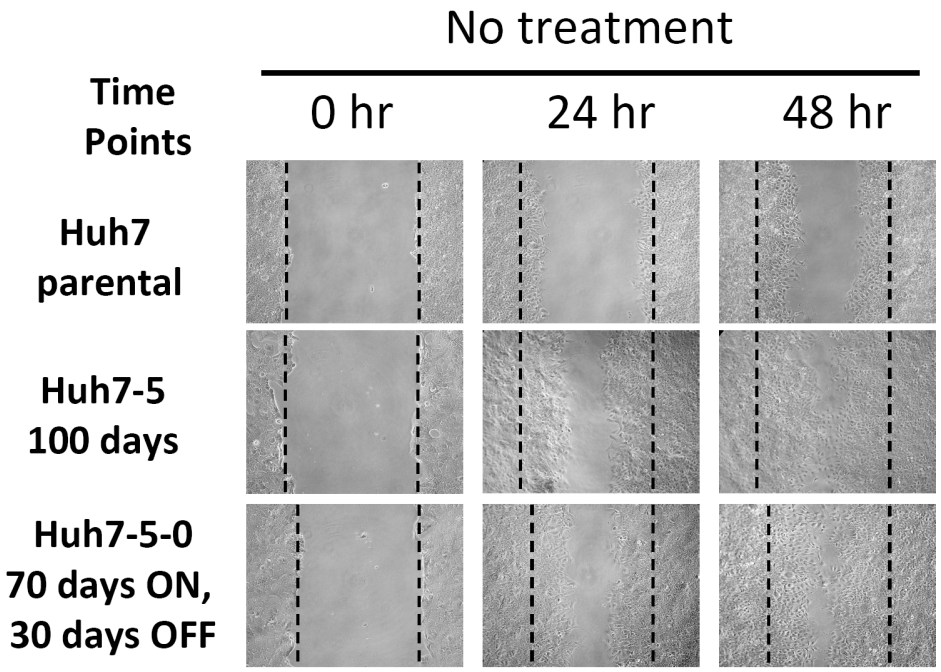

Figure 3.115: Differential motility of parental Huh7, resistant Huh7-5 and rescued Huh7-5-0 subclones in the absence of TGF-β. Cells were cultured in 12-well culture plates, and a single linear wound was made with a pipette tip in confluent monolayer cells. Phase contrast pictures at ×20 magnification. Dashed lanes indicate initial edges after scratching. Experiments were performed in duplicate with two wounds in each well.

The established subclones had enhanced migratory and invasive properties even in the absence of TGF-β. Interestingly enough, none of the samples had significant changes in invasion capacity in the presence of TGF-β.

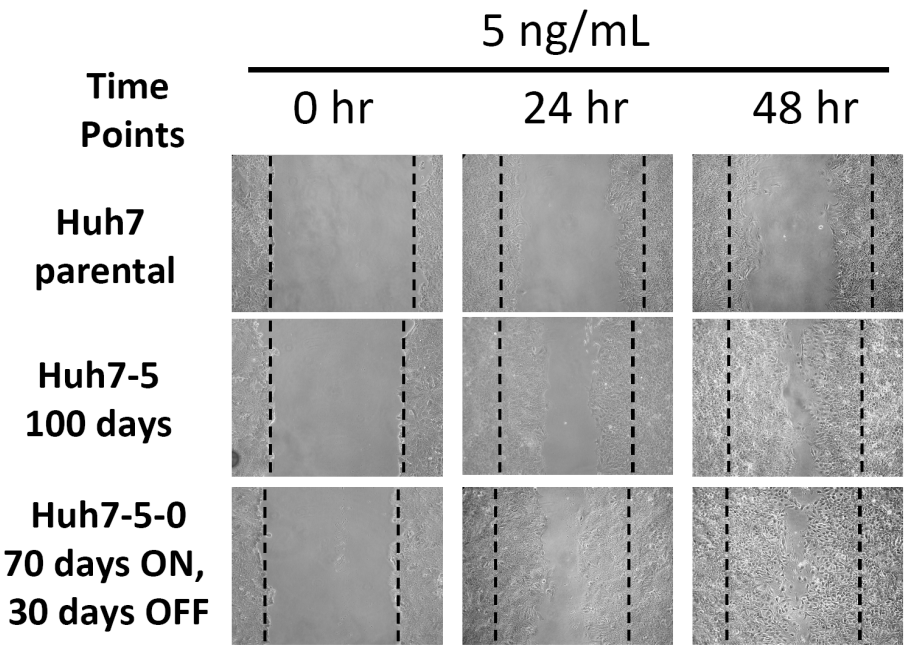

Figure 3.116: Differential motility of parental Huh7, resistant Huh7-5 and rescued Huh7-5-0 subclones in the presence of TGF-β. Cells were cultured in 12-well culture plates, and a single linear wound was made with a pipette tip in confluent monolayer cells. Phase contrast pictures at ×20 magnification. Dashed lanes indicate initial edges after scratching. Experiments were performed in duplicate with two wounds in each well.

Quantitative results obtained through measurement of wound closure demonstrated significant differences between the motility of parental Huh7 and the established subclones (Figure 3.117).

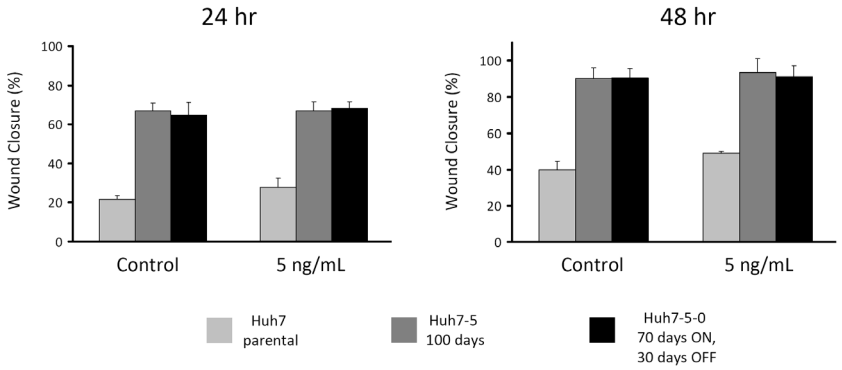

Figure 3.117: Wound closure capacity of parental Huh7, resistant Huh7-5 and rescued Huh7-5-0 subclones. The distances between wound edges were measured at fixed points in each dish according to standardized template. At least three measurements were used in calculation of each wound. Phase contrast pictures at ×20 magnification.

Collectively, these results supported the findings of establishment of a mesenchymal-like phenotype and transformation after prolonged TGF-β exposure. Nonetheless, removal of TGF-β from resistant Huh7-5 did not provoke to a reversion of this established state in rescued Huh7-5-0 subclone.

3.17.7. Lack of increased putative "cancer stem cell" marker expression in resistant Huh7-5 and rescued Huh7-5-0 subclones

A direct link between epithelial-mesenchymal transition and cancer stem cells has been established very recently. Such cell populations were reported to be more refractory to various sources of cellular stresses including DNA-damaging drugs, as well as cytokines including TGF-β (Ding et al., 2009; Trumpp and Wiestler, 2008). Therefore, we decided to study the potential enrichment of this very small putative "cancer stem cell" population, other known as tumor-initiating cells, in Huh7 cells after TGF-β treatment. If this was the case, senescence cells would have been eliminated from the culture and the remaining resistant population might have been enriched with stem cell marker expressing cells.

To test this hypothesis, together with EMT analysis experiments, we screened the expression of known putative cancer stem cell (CSC) markers, namely CD133, CD90 and CD44, in parental Huh7, resistant Huh7-5 and rescued Huh7-5-0 subclone. These markers have been identified to be differentially expressed in a minor subpopulation found in Huh7 cells (Ma et al., 2007).

Quantitative real-time PCR experiments demonstrated that we could exclude this possibility. Interestingly enough, we showed that TGF-β induced the expression of CD133 in parental Huh7 with increasing doses of TGF-β (Figure 3.118). Whereas, endogenous expression of CD133, CD90 and CD44 did not change in resistant Huh7-5 and rescued Huh7-5-0 subclones. Even TGF-β treatment did not alter expression patterns of these selected target genes.

Moreover, recent report has been published suggesting CD133 as a target gene of TGF-β signaling pathway (You et al., 2010), which also supported our findings.

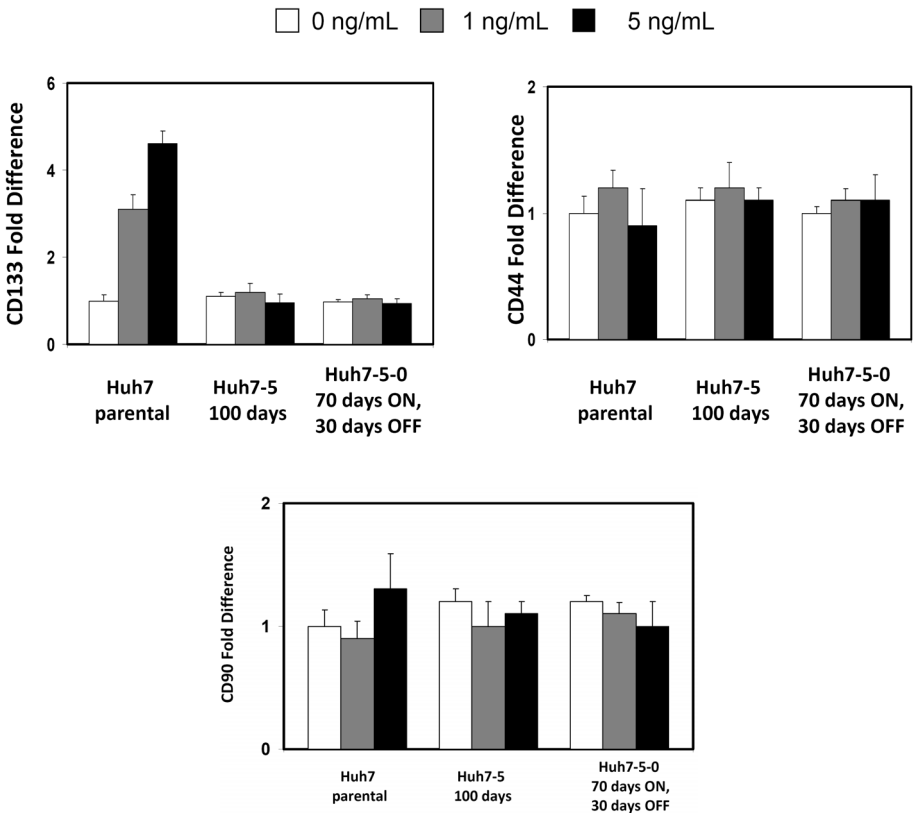

Figure 3.118: Expression of putative CSC markers in parental Huh7, resistant Huh7-5 and rescued Huh7-5-0 cells. All expression values were normalized with GAPDH calues accordingly.

Furthermore, a few others including CK19 and EpCAM/ESA were identified as bipotential hepatic progenitor cell markers in hepatocellular carcinomas (Andersen et al., 2010; Cornella and Villanueva, 2010; Yamashita et al., 2009). With the above information, we therefore studied the expression of CK19 and ESA. Immunohistochemical experiments demonstrated heterogenous staining for both antigens in parental Huh7 without being effected by TGF-β treatment. Likewise, the staining patterns in resistant Huh7-5 and rescued subclone Huh7-5-0 were quite similar to parental Huh7 (Figure 3.119 and 3.120).

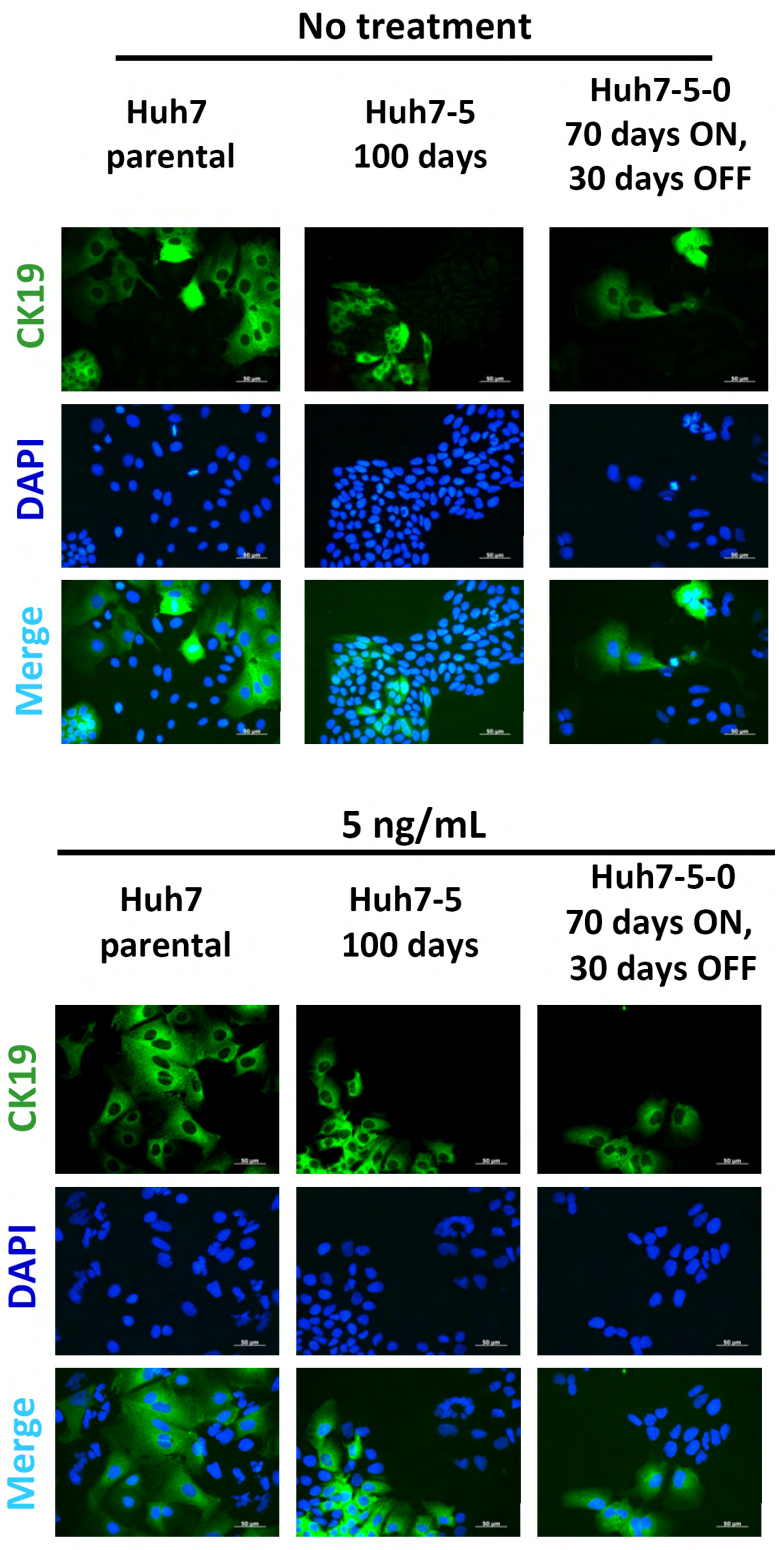

Figure 3.119: Staining pattern of CK19 in parental, resistant and rescued subclones of Huh7. Pictures were obtained at 40X with same exposure time (600 ms).

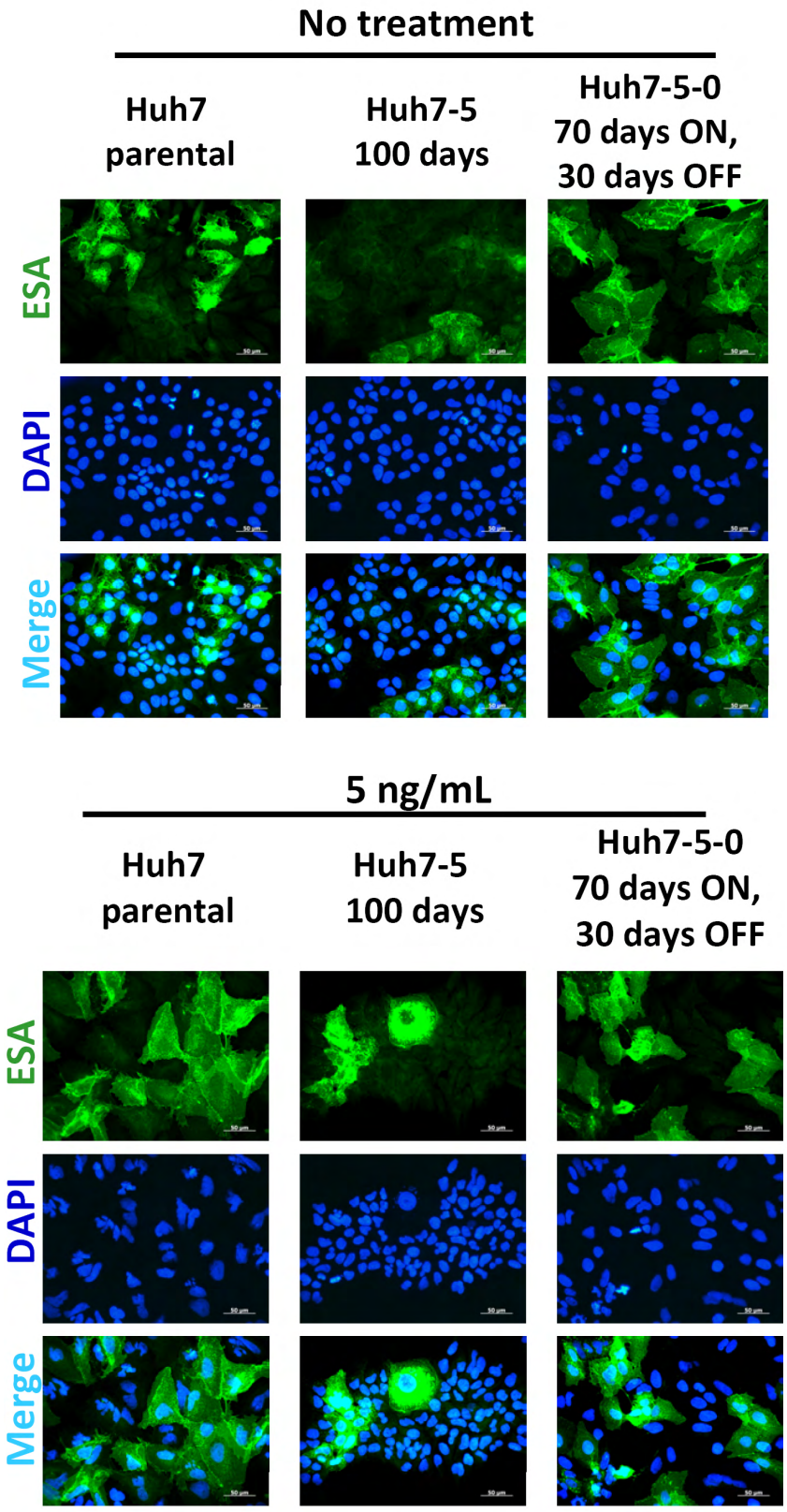

Figure 3.120: Staining pattern of ESA/EpCAM in parental, resistant and rescued subclones of Huh7. Pictures were obtained at 40X with same exposure time (600 ms).

Taken together, these results indicated that there was no increase/enrichment in stem cell/progenitor population in TGF-β treated parental Huh7 and as well as in resistant and rescued subclones.

3.17.8. Implications of epigenetic mechanisms in maintenance of irreversible resistance to TGF-β in the established rescued subclone Huh7-5-0

Remarkably, EMT is an example of cellular plasticity and programming and maintenance of this highly complex process is usually controlled through epigenetic mechanisms including DNA methylations and covalent histone modifications (Vincent and Van Seuningen, 2009). We focused our attention on epigenetic mechanisms mainly histone variations in parental Huh7 and the established subclones after TGF-β treatment to have a better understanding of the molecular mechanisms underlying the intriguing interplays during EMT transformation. Among others, H3K9 and H3K14 acetylations and trimethylation type of H3K4 and H3K36 modifications are generally detected at transcriptionally active gene regions (Barski et al., 2007). Increased levels of such modifications were detected at the INK4 locus and $p21^{Cip1}$ transcription start sites in senescent cells (Egger et al., 2007).

On the other hand, methylation type of modifications detected on H3K9, H3K27 usually mark gene repression (Bannister et al., 2001; Boyer et al., 2006). Loss of these repressive modifications is also observed during the onset of senescence in mouse-embryonic fibroblasts through activation of Arf, p16Ink4a and $p15^{Ink4b}$ (Agherbi et al., 2009). Based on previous findings, we initially studied these particular covalent histone modifications by immunofluorescence technique. Screening of histone variations displayed major differences in a set of modifications. Lysine 9 monomethyl H3 displayed mildly decreased intensity in TGF-β-treated parental Huh7, with no detectable changes in the established subclones (Figure 3.121).

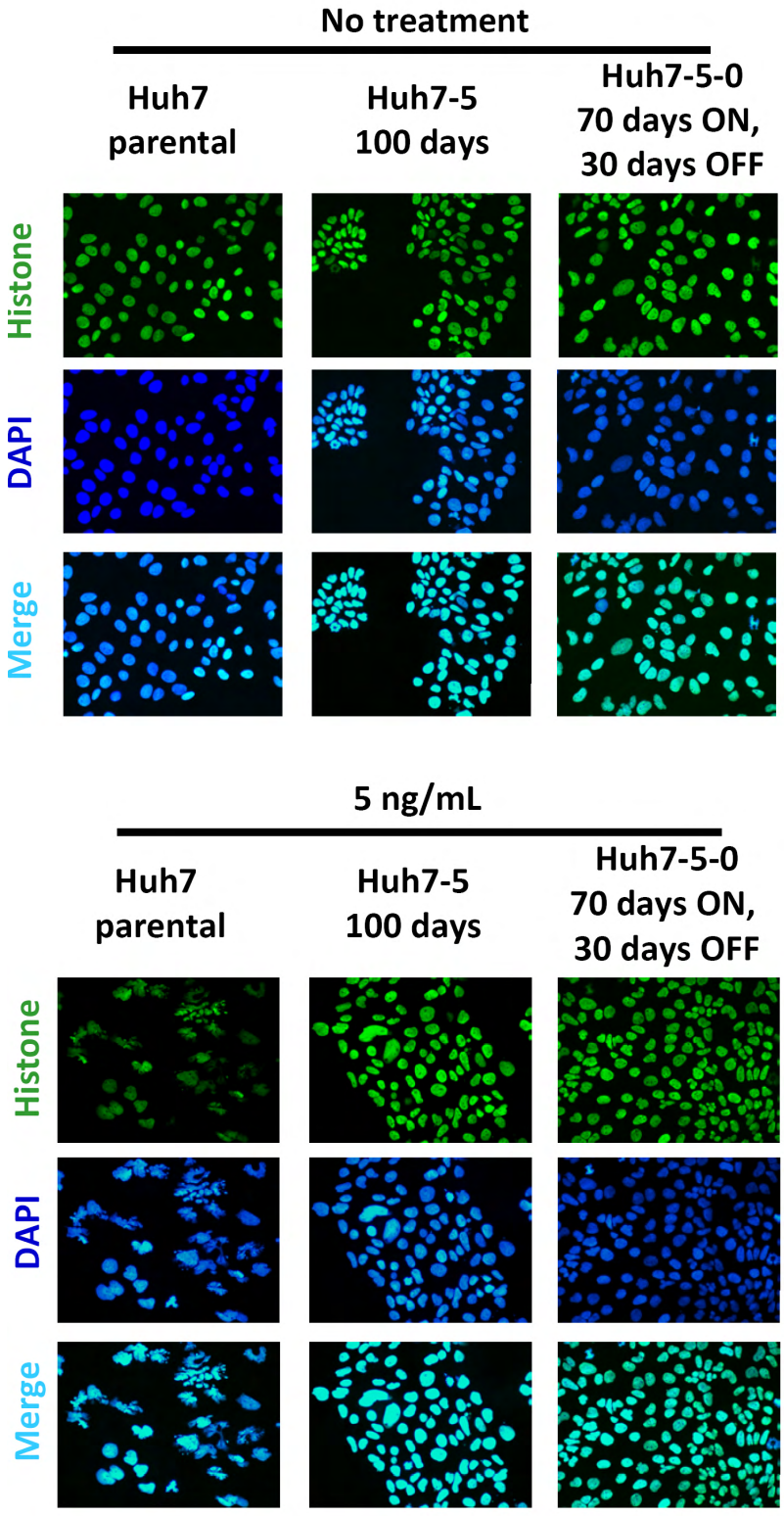

Figure 3.121: Staining pattern of H3K9me1 in parental, resistant and rescued subclones of Huh7. Pictures were obtained at 40X with same exposure time (150 ms).

Nevertheless, Lysine 9 tri-methyl H3 displayed no major differences in TGF-β-treated parental Huh7 and the established subclones (Figure 3.122).

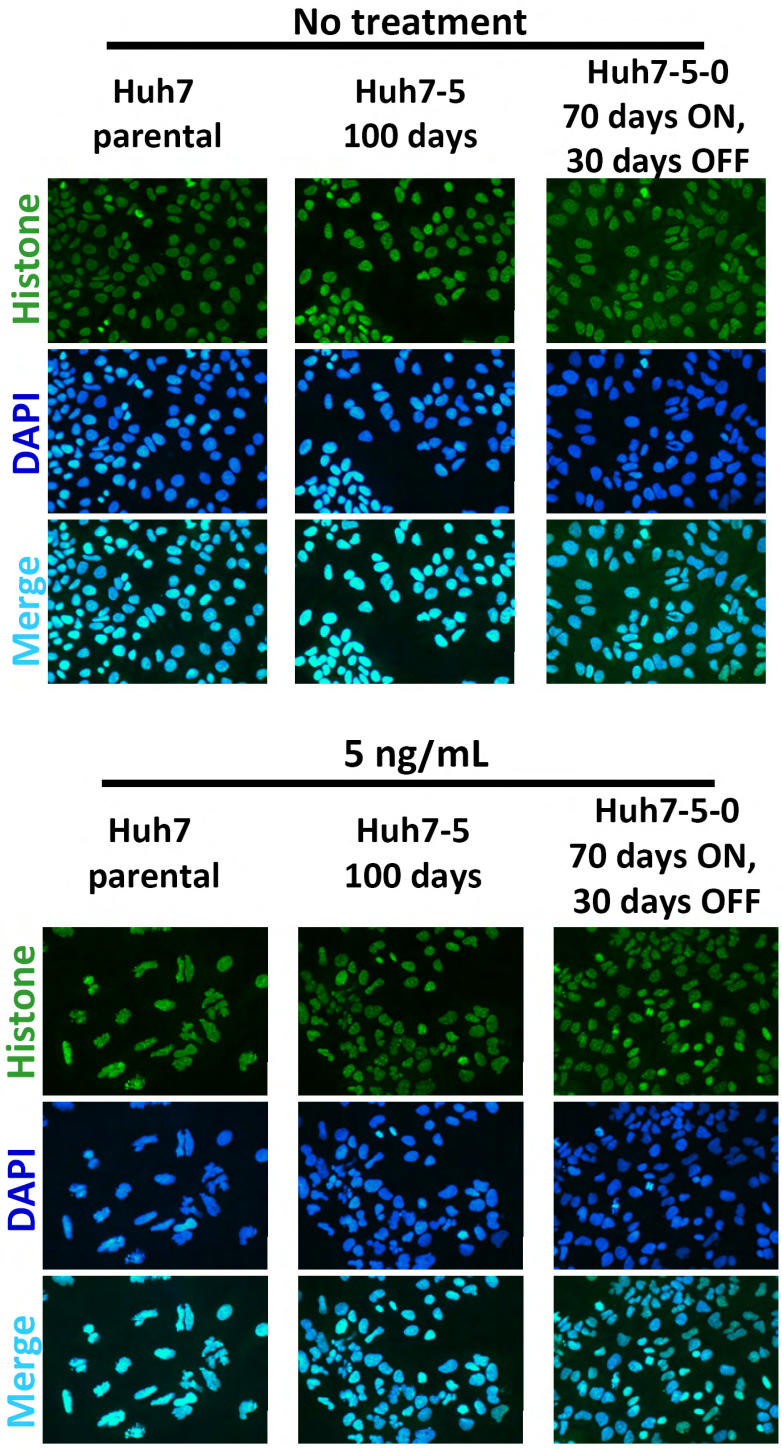

Figure 3.122: Staining pattern of H3K9me3 in parental, resistant and rescued subclones of Huh7. Pictures were obtained at 40X with same exposure time (150 ms).

Moreover, Lysine 27 mono-methyl H3 displayed no major differences in TGF-β-treated parental Huh7 cells, but substantially increased in the established subclones (Figure 3.123).

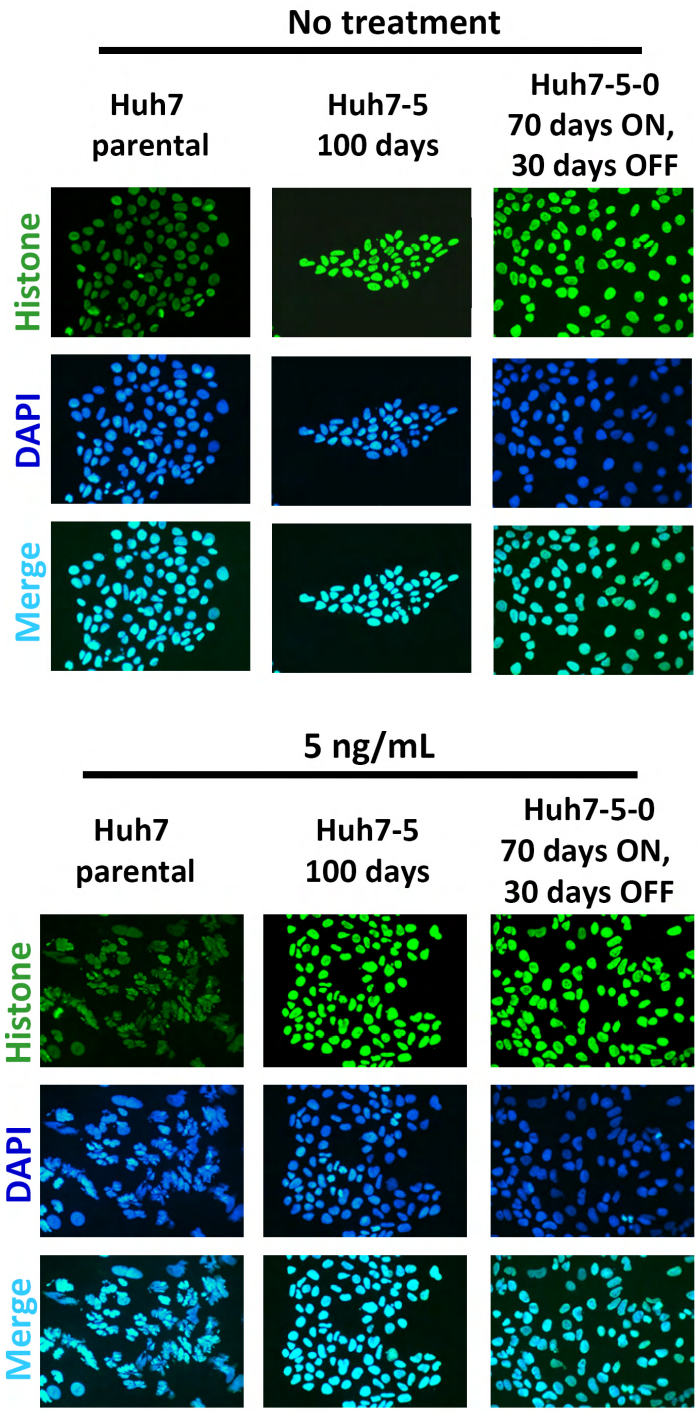

Figure 3.123: Staining pattern of H3K27me1 in parental, resistant and rescued subclones of Huh7. Pictures were obtained at 40X with same exposure time (150 ms).

Additionally, we did not observe any notable differences in H3K27me3 in TGF-β-treated parental Huh7 cells and the established subclones (Figure 3.124).

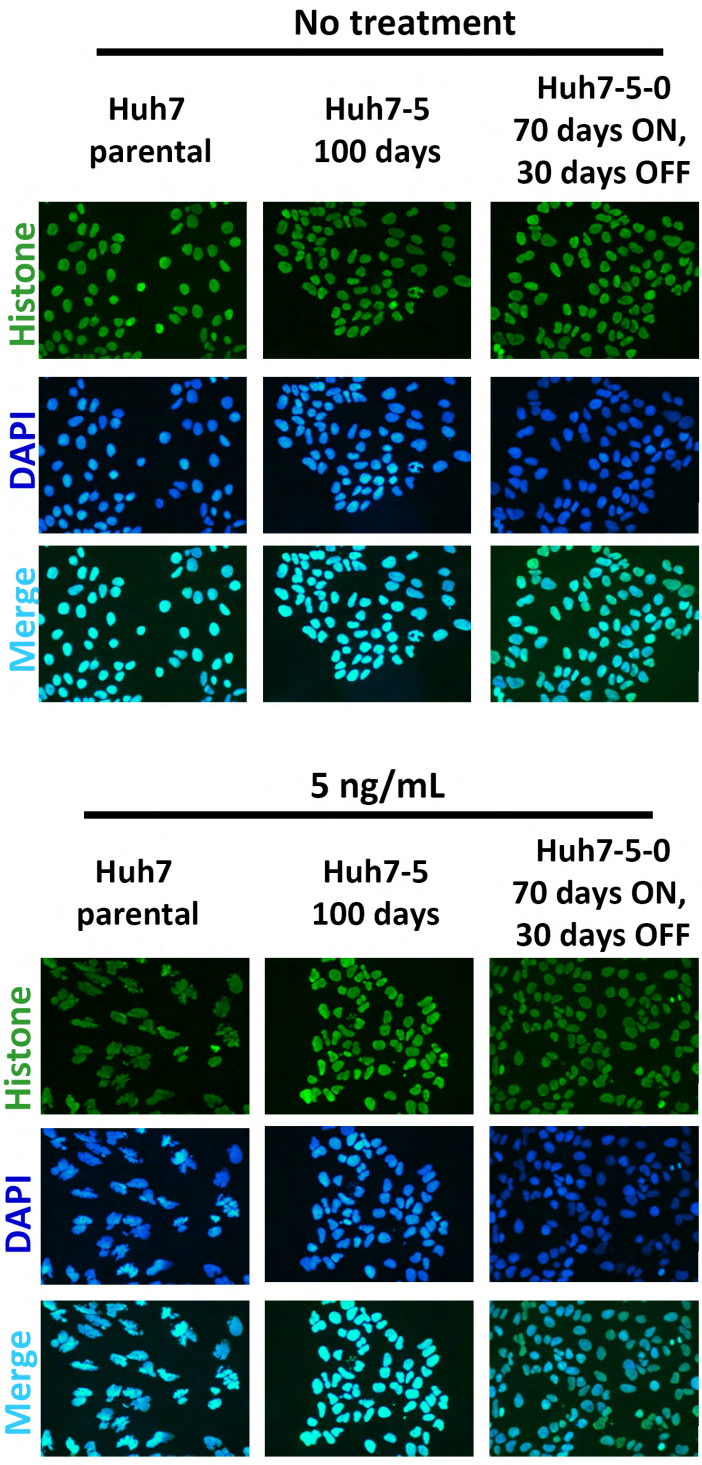

Figure 3.124: Staining pattern of H3K27me3 in parental, resistant and rescued subclones of Huh7. Pictures were obtained at 40X with same exposure time (150 ms).

We detected the most prominent finding with lysine 36 mono-methyl H3 staining. Interestingly enough, H3K36me1 displayed almost a complete loss of expression in TGF-β-treated parental Huh7 cell. However, these modifications were not altered in resistant Huh7-5 and rescued Huh7-5-0 subclones (Figure 3.125).

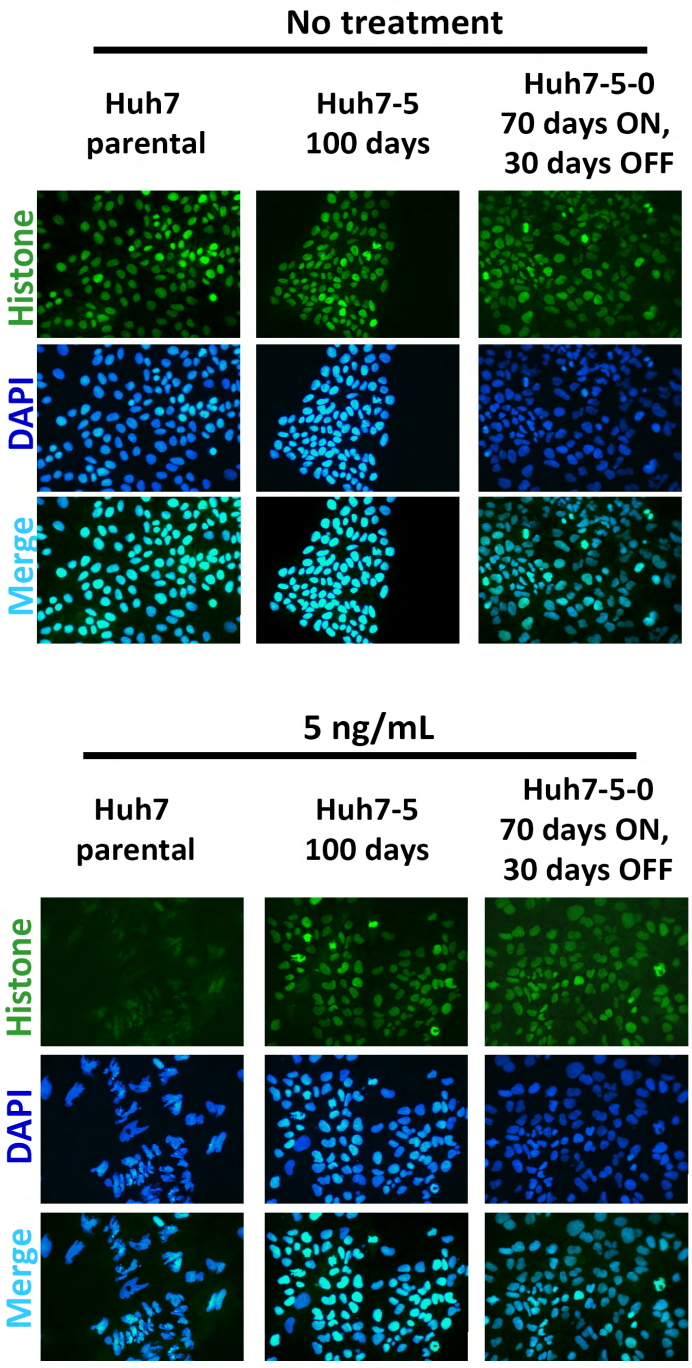

Figure 3.125: Staining pattern of H3K36me1 in parental, resistant and rescued subclones of Huh7. Pictures were obtained at 40X with same exposure time (150 ms).

In summary, deregulated balance in histone modifications may implicate key role in programming of mesenchymal phenotype through epithelial plasticity and maintenance of such a process could be largely relying on epigenetic regulation.

Expression of histone modifying enzymes is usually deregulated in various human cancers (Kassambara et al., 2009). Moreover, histone modifications that presented alterations in our study are basically modulated by WHSC1 and EZH2 for H3K36 and H3K27 methylations, respectively (Martinez-Garcia and Licht, 2010; Nimura et al., 2009). Based on this information, we studied these selected genes in publicly available microarray database, ONCOMINE, to compare the expression data in tumor type with its non-tumor counterpart. Using ONCOMINE, we directed the search in Wurmbach et. al. (Wurmbach et al., 2007) data to display the individual expression values of particular genes in various liver disease stages. According to our query in ONCOMINE, we obtained the following results for WHSC1 (MMSET, NSD2) (Figure 3.126) and EZH2 (Figure 3.127).

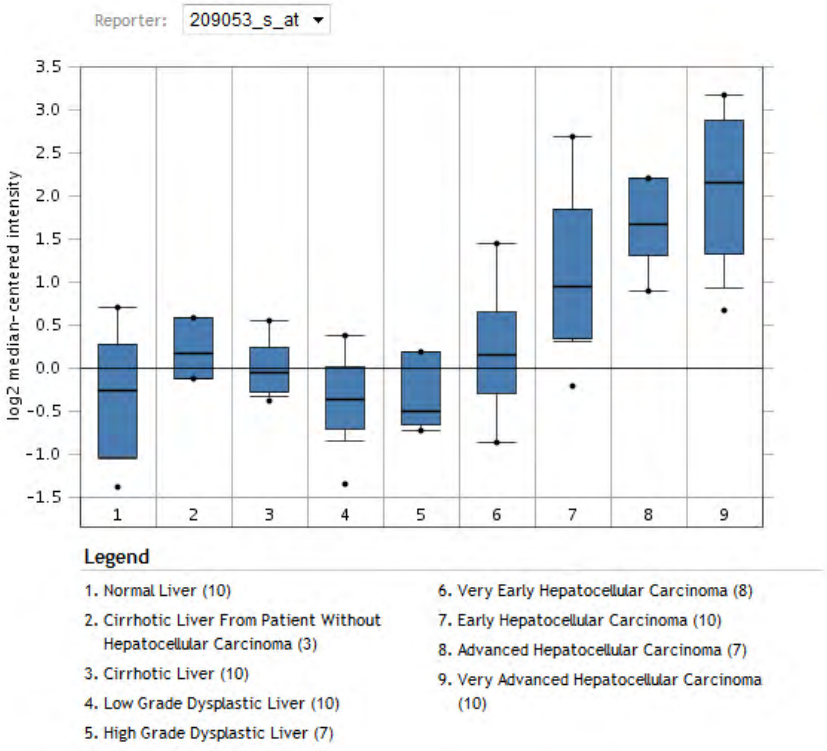

Figure 3.126: Expression analysis of WHSC1 in liver diseases. Distribution of normalized and log(2) transformed WHSC1 signal intensity for each relavant-sample was drawn to scale. Similar results were obtained with other probe-sets as well.

WHSC1 expression was substantially increased with hepatocarcinoma progression as compared to normal liver samples. Similar results were obtained with the query based on Grade comparison (data not shown). Additionally, EZH2 displayed a similar pattern of gene expression data.

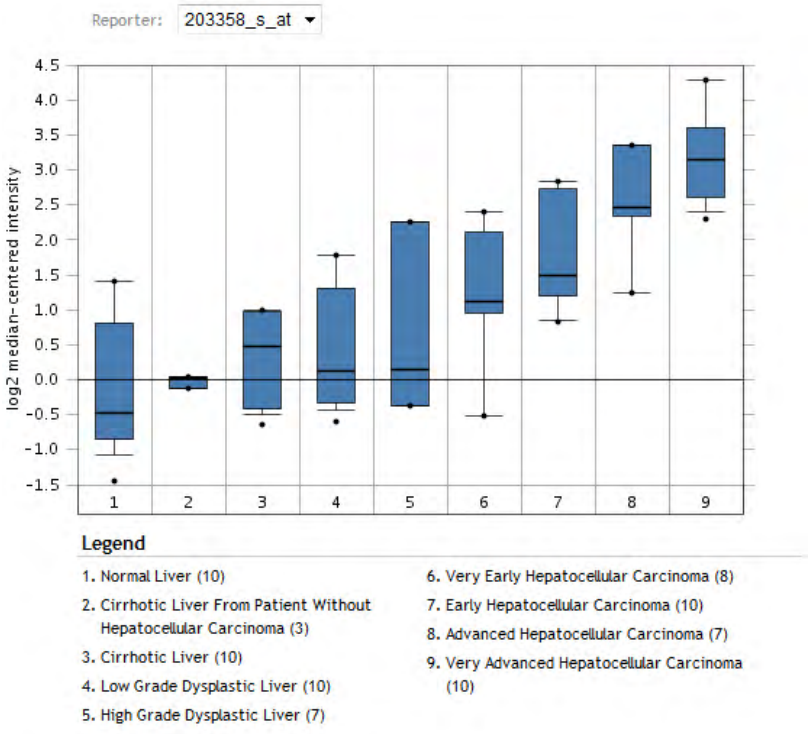

Figure 3.127: Expression analysis of EZH2 in liver diseases. Distribution of normalized and log(2) transformed EZH2 signal intensity for each relavant-sample was drawn to scale. Single probe-set is available for EZH2.

These findings implicated a potential role for WHSC1 and EZH2 in the progression of hepatocarcinogenesis. Of particular importance to mention; aggressive HCCs are less-differentiated with higher invasive and migratory capacity. Similarly, poorly-differentiated HCC cell lines with mesenchymal marker expression displayed higher migratory capacity (Yuzugullu et al., 2009). Conclusively, the resistant Huh7-5 and the rescued Huh7-5-0 subclones resemble in an aspect to poorly-differentiated HCC cell lines. Together with our staining results in parental Huh7, resistant Huh7-5 and rescued Huh7-5-0 subclones, we deduced that these two genes may be further studied to delineate the mechanisms of differential histone modifications upon TGF-

β treatment and maintenance of mesenchymal-phenotype. Therefore, we studied the expression of WHSC1 in parental Huh7 and the established Huh7 subclones. Surprisingly, the gene expression pattern displayed close correlation with H3K36me3 staining. TGF-β treatment substantially decreased the expression of MMSET in parental Huh7, whereas the established subclones had increased expression which was not effected by TGF-β exposure (Figure 3.128).

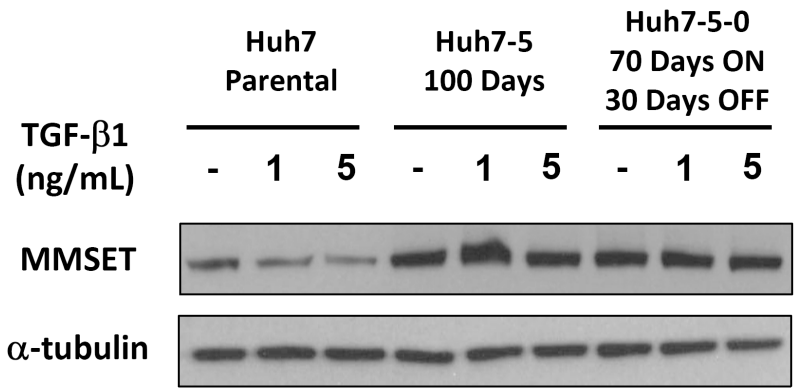

Figure 3.128: Protein expression WHSC1 (MMSet II) in parental Huh7 and the established subclones. Treatment was done for 72 hr. a-tubulin served as equal loading control.

Based on this surprising result we wanted to establish a link between MMSET expression and TGF-β signaling. We studied the expression of MMSET isoforms, I and II, in a time-dependent fashion under TGF-β-treatment conditions. In support of previous findings, we demonstrated diminished expression of MMSET isoforms under TGF-β treatment conditions (Figure 3.129).

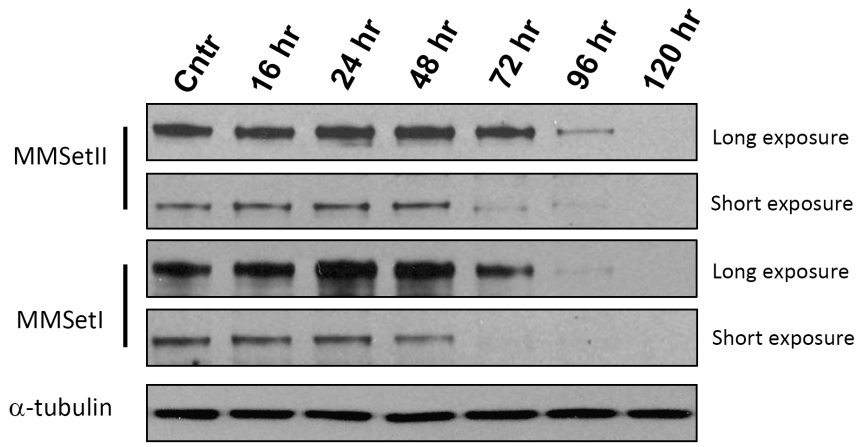

Figure 3.129: Protein expression MMSet isoforms in parental Huh7 and the established subclones. Treatment was done for 72 hr. A-tubulin served as equal loading control.

Taken together, these results established a close link between TGF-β signaling pathway and histone modifications that might be causally associated with TGF-β-mediated gene expression regulation of particular histone modifying enzymes. Obviously, we will have to extend our studies to further delineate the connection mechanisms between the maintenance of mesenchymal transformation and resistance to TGF-β-induced cytostatic response with particular focus on deregulated Smad signaling and involvement of histone modifications.

CHAPTER 4. DISCUSSION AND CONCLUSION

The role of TGF-β signaling in normal hepatocytes and HCC cells remains poorly understood. Here, we provide experimental evidence for a senescence-inducing role of TGF-β in hepatocyte-like well-differentiated HCC cells. Role of TGF-β in hepatocytes and HCC cells have been previously linked to its EMT-inducing, cell cycle inhibitory and apoptotic effects (Fan et al., 1996; Kojima et al., 2008; Lamboley et al., 2000). Our findings indicate that senescence induction is a major component of hepatocellular response to TGF-β exposure. We believe that such an effect has not been noticed before because of the fact that the senescence response to TGF-β observed throughout this study is a late-occurring but permanent event that becomes evident only after 3 days of incubation but still detectable after 12 days in culture. As shown for cell cycle analysis with Huh7 cell line at different time points following TGF-β stimulation, senescence-associated permanent G1-arrest became prominently high after 48 hr of stimulation and reached the peak at 72 hr. Analyses performed at 96 and 120 hr did not display much increase in the percentage of G1-arrested cell population suggesting that the establishment of growth arrest was ensured after 3 days. Taken together, the response of well-differentiated HCC cell lines to TGF-β was manifested by major characteristics of cellular senescence such as flattened morphology, SA-β-gal activity, G1-phase cell cycle arrest with permanent withdrawal from the cell cycle.

Surprisingly enough, we demonstrated that just a very short exposure (less than one minute) was sufficient to trigger a strong senescence response in Huh7, PLC and Hep40 cells. Further analyses presented that such a short TGF-β stimulation of Huh7 cells was also able to induce a sustained nuclear accumulation of Smad molecules. Besides, incubation with TGF-β for 5 min induced luciferase reporter activation similar to continuous treatment.

Nevertheless, TGF-β receptors are continuously degraded and resynthesized through several mechanisms including endosomes and caveolin positive vesicles-mediated internalization (Di Guglielmo et al., 2003). Therefore it is highly possible that TGF-β-mediated senescence is a late-occurring response generated by short exposures. On the other hand, brief TGF-β exposure induced its own expression which was also reported by other studies (Lin et al., 1995; Van Obberghen-Schilling et al., 1988). Thus TGF-β amplifies the autocrine cytokine loop along with pronounced transcriptional activation and release of other senescence related cytokines IL-6 and IL-8. Such dynamic alterations may underlie the sustained senescence response. As a matter of fact, inhibition of autocrine signaling using specific anti-TGF-β1 antibody demonstrated the role of self-produced TGF-β cytokine molecule in spontaneous senescence typically observed in Huh7 cell line (Ozturk et al., 2006).

In contrast to previously published reports with hepatocytes and HCC cell lines performed with TGF-β (Herzer et al., 2005; Lin and Chou, 1992; Oberhammer et al., 1991), we did not detect any apoptotic cell death in our studies with NAPO and activated caspase-3 immunostainings. This could be related to different experimental conditions. Indeed, previously published TGF-β-induced apoptosis responses by hepatocytes and HCC cell lines were obtained under serum-free or low serum conditions. Instead, we used standard culture media (with 10% FCS), but not serum-free conditions in our experiments to test mimicry of relevant TGF-β signaling *in vivo*. It is a well-known fact that serum deprivation sensitizes different types of cells to apoptosis, including HCC cells (Irmak et al., 2003). In addition, although we used well-differentiated cell lines in our experiments the response of these cell lines to TGF-β may be different from that of normal hepatocytes. It would be interesting to know whether TGF-β also induces senescence in normal hepatocytes when tested under serum-containing growth conditions.

The TGF-β and senescence connection that we established here was strongly linked to upregulation of $p21^{Cip1}$ and $p15^{Ink4b}$. Previous studies have demonstrated these two genes as downstream targets of TGF-β signaling pathway

(Datto et al., 1995; Rich et al., 1999). Upregulation of $p21^{Cip1}$ was p53 independent as all these cell lines except HepG2 are devoid of p53 activity. Moreover, possible p53 activation by TGF-β in HepG2 cells was negative as tested by p53 (ser15) specific primary antibody. This finding suggested that the TGF-β-mediated $p21^{Cip1}$ upregulation and the senescence-response was p53-independent. Plus, $p16^{Ink4a}$ protein expression was not modulated by TGF-β treatment indicating that the senescence response was also $p16^{Ink4a}$-independent. Moreover, retinoblastoma protein also appeared to be dispensable for TGF-β-induced senescence, since Hep3B cell line used here is reported to be pRb-deficient (Puisieux et al., 1993). Nevertheless, the p107 'pocket protein' has been shown to be required for initiation of accelerated cellular senescence in the absence of pRb (Lehmann et al., 2008) which may explain the senescence in Hep3B cells.

In addition to above findings, forced ectopic expression of $p21^{Cip1}$, in the absence of TGF-β-treatment resulted in a senescence-like response with flattened morphology, increased SA-β-gal activity, G1-arrest, and inhibition of BrdU incorporation into cellular DNA in Huh7 cells. The overexpression of $p15^{Ink4b}$ also generated a similar response, but to a lesser degree, probably owing to high endogenous expression of $p15^{Ink4b}$.

Another important component of TGF-β-induced senescence in well-differentiated HCC cell lines was accumulation of ROS. As tested by DCFH staining, TGF-β provoked production of intracellular ROS. Mitochondrial ROS generation has been previously implicated in TGF-β-induced senescence arrest in Mv1Lu cells (Yoon et al., 2005). Together with DCFH, we also stained cells with mitochondrial respiration specific dye, namely MitoTracker Red. Unlike DCFH staining pattern, we detected similar endogenous staining with MitoTracker indicating that TGF-β induced ROS production in HCC cells was independent of mitochondrial membrane potential. NADPH oxidase system has been causally linked to TGF-β-induced ROS accumulation in normal and transformed hepatocytes with particular focus on the role of Nox4 protein (Carmona-Cuenca et al., 2006; Hu et al., 2005; Sturrock et al., 2006). Similar to previous findings TGF-β induced Nox4

expression in our study as well. In addition, inhibition of ROS accumulation using a scavenger, N-acetyl-cysteine, inhibited TGF-β-induced growth arrest as well as upregulation of $p15^{Ink4b}$ and $p21^{Cip1}$. Similar results were obtained with Nox4 silencing. Thus both ROS accumulation and Nox4 upregulation were critical steps in TGF-β-mediated senescence in HCC cells (Figure 4.1). A very recent study also provided similar results about the role of Nox4 in ROS accumulation in Huh7 cells with particular interest in the connection of HCV infections and ROS accumulation triggered TGF-β signaling (de Mochel et al., 2010).

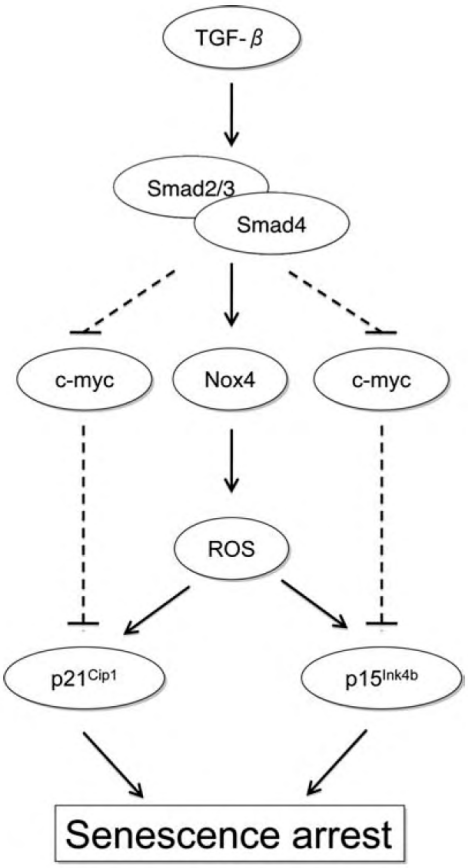

Figure 4.1: A model summarizing major components of TGF-β-induced senescence in HCC cells. (see (Senturk et al., 2010))

Intracellular accumulation of ROS was associated with sustained telomere-independent DNA-damage in chronic liver diseases (Matsumoto et al., 2003), as well

as the onset of cellular senescence (Passos and Von Zglinicki, 2006; Rai et al., 2009). Screening of ATM and 53BP1 foci status demonstrated that TGF-β–induced senescence was also associated with DNA-damage response. However, we were not able to observe supporting results with COMET assay and activation status of H2AX. COMET assay recognizes both double- and single-strand breaks (Olive and Banath, 2006). Activation of H2AX requires double-strand breaks; however it is dispensable for the onset of DNA-damage response (Celeste et al., 2003). Taken together, TGF-β may play a prominent role in ROS-induced DNA-damage response in HCC cells which has never been addressed. Thus, these initial studies require further repeats to be able to establish a link between TGF-β signaling pathway and ROS-induced DNA-damage in hepatocarcinomas.

Two tumor-suppressor mechanisms, one mediated by p53, the other by $p16^{Ink4a}$ are lost frequently in HCC cells. Inactivating p53 mutations were found in a third of HCCs worldwide, but in a great majority of aflatoxin-related HCCs in Africa and China (Ozturk, 1991; Ozturk, 1999). Likewise, more than 50% of HCCs, independent of their geographical origins, display epigenetic or genetic inactivation of INK4 locus gene encoding $p15^{Ink4b}$, ARF and $p16^{Ink4a}$ (Ozturk et al., 2009; Tannapfel et al., 2001). Since our findings indicate that TGF-β is able to induce senescence in p53 mutant HCC cells independent of $p16^{Ink4a}$ induction, candidate therapeutic interventions to induce TGF-β-mediated senescence are likely to be successful in HCC tumors with p53- and/or $p16^{Ink4a}$-deficiency. In support of these *in vitro* findings, we performed *in vivo* studies with subcutaneous Huh7 tumors raised in nude mice. Single intratumoral injection of TGF-β induced local but robust SA-β-Gal activity as tested with resected Huh7 tumors after 7 days. Together with that, peritumoral local injection of TGF-β with four days of intervals in long term follow-up Huh7 tumors provoked a substantial anti-tumor activity together with successful regression in two of six TGF-β-treated tumors.

Senescence-associated secretome including inflammatory cytokines released from senescent cells in mouse model HCC tumors induces immune system activation (Krizhanovsky et al., 2008; Xue et al., 2007). Complete clearance of these

two tumors may be in part due to *in vivo* activation of natural killers and macrophages through known and unknown mechanisms including inflammatory cytokine release as evidenced by *in vitro* studies discussed throughout this study. Nonetheless, HCC cancers constitute a large population estimated to be in the order of several hundred thousands, worldwide. The therapeutic use of TGF-β could be considered at least for early HCCs.

Unlike, well-differentiated cell lines which responded to TGF-β with robust senescence arrest, poorly-differentiated cell lines displayed complete resistance to TGF-β-mediated cytostatic responses. In an effort to delineate the mechanisms of resistance we performed a series of analyses. Such resistance could be implemented by inactivating mutations together with deregulated expression of TGF-β signaling receptors as well as Smad molecules in various cancers (Bae et al., 2009; Kim et al., 2000; Levy and Hill, 2006). The studies of others and our lab demonstrated that inactivating mutations of TGF-β receptors and Smads are infrequent in HCCs (Jong et al., 2002; Yakicier et al., 1999). In this study, we also demonstrated that all cell lines differentially express TGF-β receptor type II and I, except Hep3B-TR (TGF-β resistant) and Snu398, which are devoid of TGF-β receptor type II expression. Our observations were also in support of others which showed TGF-β receptor type II deletion in Hep3B-TR (Hasegawa et al., 1995) and deregulated TGF-β receptor type II expression in Snu398 and Snu475 cell lines (Kitisin et al., 2007). Together with these abnormalities, recent publications highlighted the importance of beta-spectrin ELF, a Smad3/4 adaptor during hepatocarcinogenesis (Baek et al., 2008). Together with decreased TGF-β receptor type II, loss of ELF expression in several Snu398 and Snu475 cell lines has been linked to acquired resistance to TGF-β mediated growth arrest (Kitisin et al., 2007).

Nevertheless, our studies with luciferase reporter analysis in PD cell lines implicated intact TGF-β signaling although comparably less in amplitude than WD cell lines. Unlike previous studies, we showed that all PD cell lines except Snu398 have functional TGF-β receptors as tested by Smad2 activation by phosphorylation. Deregulated translocation of core intracellular signaling cascade has been proposed

as another resistance mechanism in various cancer models with intact TGF-β receptors (Di Guglielmo et al., 2003; Mishra et al., 2004; ten Dijke et al., 2000). In order to test this, we analyzed all PD cell lines for effective Smad3 translocation from cell membrane into nucleus by immunostaining. As evidenced, all cell lines except Snu398 had detectable nuclear Smad3 upon TGF-β stimulation.

Furthermore, PD cell lines lack endogenous Nox4 expression which was not induced by TGF-β either. Together with that we did not detect any sign of ROS accumulation in tested PD cell lines. These results suggested that unknown mechanisms responsible for deregulation in ROS production and Nox4 expression may be partially responsible for resistance to TGF-β-induced senescence arrest. Moreover, we also demonstrated that three cell lines, namely Snu387, Snu449 and SkHep1 are $p15^{Ink4b}$-deficient due to a deletion in INK4 locus. Besides Focus cell line lack pRb expression (Puisieux et al., 1993). Since we closely implicated those genes in growth arrest in WD cell lines, such malformations may also be responsible for TGF-β-resistance in PD cell lines.

Lately, zeb2 overexpression has been associated with TGF-β pathway functions in epithelial-mesenchymal transition and suppression of target gene activation (Kojima et al., 2008; Ohashi et al., 2010; Postigo, 2003). Therefore, we studied potential implications of zeb2 expression in PD cell lines. We demonstrated that mesenchymal-like PD cell lines display high nuclear expression when compared to WD cell lines. Using an epithelial-like cell line A431 with Tet regulatable zeb2 expression, we looked at the expression patterns of $p15^{Ink4b}$ and $p21^{Cip1}$ under TGF-β treatment conditions. These studies pointed the role of zeb2 in inhibition of target gene activation. Together with that we also down regulated zeb2 expression in two selected PD cell lines and reported a slight upregulation in above targets after TGF-β stimulation. Taken together, we concluded that zeb2 overexpression in PD cell lines may also be partially responsible for acquired resistance against TGF-β cytostatic responses. Owing to the genetic and epigenetic heterogeneity of HCC cell lines, it is highly likely that several mechanisms may be involved in resistance to TGF-β.

Interestingly enough, prolonged exposure to TGF-β generated Huh7 subclones with acquired resistance. Complete establishment of these clones occurred in approximately 60 days. We are yet unsure how parental Huh7 cells forced to undergo senescence-arrest after sustained TGF-β exposure acquire proliferative capacity. However we were able to study the mechanisms underlying maintenance of resistance in established subclones. We demonstrated that these cells have substantially lost their responsiveness to TGF-β treatment due to deregulated Smad signaling. Intact TGF-β receptor activity was detectable in resistant and rescued subclones with only slight impairment in the amplitude of Smad phosphorylation. However, it was evident that the timing of nuclear accumulation and exclusion duration was deregulated in both subclones.

According to our data, we also concluded that partial epithelial-mesenchymal like transformation may play a key role in prolonged resistance to TGF-β. Recently, EMT has been proposed as a mechanism to escape from failsafe programs (Ansieau et al., 2008), including resistance to TGF-β-mediated growth arrest (Ohashi et al., 2010). We hypothesize at this point, that EMT may be responsible for the onset and maintenance of TGF-β resistance. Nonetheless, these studies need further clarification to delineate the complete contribution of partial EMT and sustained mesenchymal-like phenotype to persistence of TGF-β unresponsiveness. These encouraging results may also provide further insight into resistance against TGF-β cytostatic responses in other mesenchymal-like cells including poorly-differentiated HCC cell lines. In addition, studying target gene expression patterns in the established subclones after TGF-β treatment revealed interesting results. We observed unchanged or slightly impaired regulations in epithelial and mesenchymal marker gene expressions in both the established subclones. Whereas, those target genes responsible for cytostatic response generation were entirely deregulated. This suggested that the interpretation of TGF-β signal in the established subclones might be somehow altered. The most interesting finding for us was the upregulation of Smad3 in TGF-β-treated parental Huh7 but not in the

established subclones. This led to a hypothesis that upregulation of Smad3 might be essential for the onset of cytostatic responses but not EMT-like transformation.

Another issue that needs to be discussed here is the irreversible resistance to TGF-β treatment in the rescued subclone. Even if this subclone presented a partial responsiveness to TGF-β stimulation in terms of luciferase reporter activation, this was not accompanied by a detectable increase in cytostatic response as tested by proliferation assays. Therefore we decided to look at epigenetic regulations on the maintenance of entire resistance to TGF-β-induced growth suppression. As tested by immunofluorescence analyses, we showed clearly detectable differences in H3K27me3 and H3K36me1 staining patters. These results suggested a potential involvement of epigenetic regulations in TGF-β-mediated senescence arrest in parental Huh7 cells together with an implication in persistent resistance in the established subclones. Such histone modifications were partially correlated with alterations in gene expression patterns of histone modifying enzyme WHSC1 (MMSetI and MMSetII).

Recently, "cancer stem cells" have been demonstrated to have resistance against the effects of DNA-damaging agents (Bao et al., 2006; Gupta et al., 2009; Sabisz and Skladanowski, 2009) and anti-proliferative cytokines, including TGF-β (Ding et al., 2009). In this regard, we looked at the expression pattern of so far identified putative "cancer stem cell" markers. Unfortunately, we were not able to demonstrated a significant change in transcriptional expression as well as immunofluorescence based staining of selected markers. These results therefore suggested that TGF-β does not enrich the population of cancer stem cells found in parental Huh7.

Conclusively, our findings provide in vitro evidence for a strong senescence response of well-differentiated HCC cells to TGF-β. This response was dependent on increased ROS production, sustained DNA damage response, and induction of $p21^{Cip1}$ and $p15^{Ink4b}$ expression leading to G1 phase arrest. TGF-β induced senescence was independent of p53 and $p16^{Ink4a}$ both of which are frequently

inactivated in HCC. Our findings implicate that TGF-β-induced senescence may serve as a tumor-suppressor mechanism in early HCCs, but also promote the decline of hepatocyte proliferation in cirrhosis. We also provide evidence partially shedding light on resistance mechanisms to TGF-β-induced growth arrest in mesenchymal-like HCC cells.

4.1. Future perspectives

Beside growth suppressive effects, TGF-β is a multi functional cytokine that can also modulate cell motility and invasion, epithelial-mesenchymal transition, and immune system regulation that can promote tumor progression (Battaglia et al., 2009; Huang et al., 2008; Yang et al., 2009). In addition, it is yet unclear whether TGF-β activity is increased or decreased during hepatocellular carcinogenesis. In the event that TGF-β activity is increased in HCC tumors, their growth and progression would require the bypass of TGF-β-induced senescence barrier. Interestingly, about 50% of HCCs tested so far displayed SA-β-gal activity, as an indication that the senescence bypass is not fully accomplished in these tumors. It will be informative to know whether the senescence observed in such tumors is related to an increased TGF-β production (Abou-Shady et al., 1999; Dong et al., 2008). Nevertheless, the apparent paucity of senescent cells in other HCC tumors strongly suggests that HCC cells are able to develop a resistance to TGF-β-induced senescence by mechanisms that remain to be uncovered. Further exploration of TGF-β-induced senescence mechanisms in HCC may prove to be highly beneficial for a better understanding of liver malignancy. ROS accumulation after 3 days of TGF-β treatment is mainly responsible for senescence induction in this setting. ROS mediated DNA-damage mechanisms require further investigation to determine the intensity of damage provoked by TGF-β during the onset of senescence induction. It would also be noteworthy to determine the involvement of DNA-damage response in senescence-induction by further studies. Along ROS accumulation during senescence, here we presented data implicating Nox4 upregulation in intriguing interplay of the

mechanisms during the onset of cellular senescence. Silencing of Nox4 established a solid data suggesting Nox4 as one of the key factors responsible for senescence induction. It would be interesting to see the effects of Nox4 overexpression in a regulatable system not only in vitro but also in vivo mouse tumor models.

Liver cirrhosis is a premalignant condition and more than 80% of HCCs take roots in a cirrhosis background. As shown here, well-differentiated HCC cells develop a strong in vitro senescence response to TGF-β even after a minute time of exposure. Together with that, we demonstrated the involvement of autocrine TGF-β signaling in spontaneous senescence observed in Huh7 cells. In confirmation of this hypothesis, we observed that well-differentiated HCC cell lines are not only responsive to TGF-β, but they also produce this senescence-inducing cytokine. The inhibition of senescence in Huh7 cell line by anti-TGF-β antibody treatment provides further evidence for an autocrine or paracrine senescence-inducing role for TGF-β in well-differentiated HCC cells. We observed a net increase in cell proliferation by antibody-mediated blocking of TGF-β activity in Huh7 cells. These observations raise the possibility that the inhibition of TGF-β-induced senescence in cirrhotic liver may help to promote the proliferation of not only normal hepatocytes, but also premalignant or malignant HCC cells. It is therefore very interesting to address how regulatable ectopic TGF-β overexpression would affect senescence onset in Huh7 cells in vitro and in vivo by playing with the released levels of TGF-β, instead of just adding a fixed amount of TGF-β to the growth medium. This way we can more precisely mimic the in vivo conditions.

TGF-β cytokine has been implicated in modulation of tumor microenvironment through autocrine and/or paracrine signaling (Massague, 2008; Padua and Massague, 2009). Oncogene-induced senescence secretome has also been involved in multiple in vivo functions (Coppe et al., 2010). Senescent cells not only stop proliferation but also have adverse effects on the homeostasis tissue microenvironment. In vivo senescence response that we displayed here is probably a reminiscent of oncogene-induced senescence that has been established as a strong barrier against tumor development from preneoplastic lesions in other cancers such

as melanomas (Ozturk et al., 2009). Cytokines such as IL-6 and IL-8 play essential role for oncogene-induced senescence but may also provoke tumor progression. Thus, TGF-β may contribute to the establishment of a senescence barrier against HCC development in cirrhotic liver, by a paracrine or even an autocrine mechanism, however the details of such implications are yet to be determined.

As so far identified, there are many candidate mechanisms which probably contribute to TGF-β resistance in PD cell lines. Among those, it is important that one has to completely shot down the expression of zeb2 and study the cytostatic effects of TGF-β in stable clones.

As we demonstrated here, TGF-β not only induces senescence in such a short notice but also provokes the establishment of resistant clones in prolonged culturing conditions. It is obviously not clear whether short-term effects are reversible under persistent TGF-β exposure conditions by as yet unknown mechanisms. It is noteworthy trying to perform thorough analyses on acquired resistance to TGF-β. Therefore, it becomes essential to perform long term studies with TGF-β *in vivo* tumors. Here we identified deregulated Smad expression as well as impaired signal transduction in the established subclones. One interesting outcome was the upregulation Smad3 expression upon TGF-β exposure in parental Huh7 but not in other clones. Here, we are not sure whether such an observation is a cause or a consequence in the onset of TGF-β-induced senescence. Therefore, we believe silencing each individual Smad partner in parental Huh7 would provide informative insights into the mechanisms of cellular senescence in terms of modulation of signaling molecules during cell cycle arrest triggered by this cytokine. It is also noteworthy saying that, these studies would help defining the downstream signaling cascades by which cells decide to undergo senescence or EMT during the interpretation of TGF-β signal transduction.

Finally, we provide preliminary evidence for partial involvement of epigenetic regulations during senescence induction and in participation of acquired resistance to TGF-β in rescued subclones. Hence it is necessary to draw a broad

picture of gene regulations by starting with RNA and protein array studies to narrow the list of candidate genes by which we can explain the implications of TGF-β signaling pathway in hepatocellular senescence and the mechanisms accountable for irreversible resistance.

REFERENCES

Abou-Shady, M., Baer, H. U., Friess, H., Berberat, P., Zimmermann, A., Graber, H., Gold, L. I., Korc, M., and Buchler, M. W. (1999). Transforming growth factor betas and their signaling receptors in human hepatocellular carcinoma. Am J Surg *177*, 209-215.

Acosta, J. C., O'Loghlen, A., Banito, A., Guijarro, M. V., Augert, A., Raguz, S., Fumagalli, M., Da Costa, M., Brown, C., Popov, N.*, et al.* (2008). Chemokine signaling via the CXCR2 receptor reinforces senescence. Cell *133*, 1006-1018.

Agherbi, H., Gaussmann-Wenger, A., Verthuy, C., Chasson, L., Serrano, M., and Djabali, M. (2009). Polycomb mediated epigenetic silencing and replication timing at the INK4a/ARF locus during senescence. PLoS One *4*, e5622.

Alimonti, A., Nardella, C., Chen, Z., Clohessy, J. G., Carracedo, A., Trotman, L. C., Cheng, K., Varmeh, S., Kozma, S. C., Thomas, G.*, et al.* (2010). A novel type of cellular senescence that can be enhanced in mouse models and human tumor xenografts to suppress prostate tumorigenesis. J Clin Invest *120*, 681-693.

Andersen, J. B., Loi, R., Perra, A., Factor, V. M., Ledda-Columbano, G. M., Columbano, A., and Thorgeirsson, S. S. (2010). Progenitor-derived hepatocellular carcinoma model in the rat. Hepatology (Baltimore, Md *51*, 1401-1409.

Ansieau, S., Bastid, J., Doreau, A., Morel, A. P., Bouchet, B. P., Thomas, C., Fauvet, F., Puisieux, I., Doglioni, C., Piccinin, S.*, et al.* (2008). Induction of EMT by twist proteins as a collateral effect of tumor-promoting inactivation of premature senescence. Cancer cell *14*, 79-89.

Attisano, L., and Wrana, J. L. (2000). Smads as transcriptional co-modulators. Curr

Opin Cell Biol *12*, 235-243.

Attisano, L., and Wrana, J. L. (2002). Signal transduction by the TGF-beta superfamily. Science (New York, NY *296*, 1646-1647.

Azam, F., and Koulaouzidis, A. (2008). Hepatitis B virus and hepatocarcinogenesis. Ann Hepatol *7*, 125-129.

Bae, H. J., Eun, J. W., Noh, J. H., Kim, J. K., Jung, K. H., Xie, H. J., Park, W. S., Lee, J. Y., and Nam, S. W. (2009). Down-regulation of transforming growth factor beta receptor type III in hepatocellular carcinoma is not directly associated with genetic alterations or loss of heterozygosity. Oncol Rep *22*, 475-480.

Baek, H. J., Lim, S. C., Kitisin, K., Jogunoori, W., Tang, Y., Marshall, M. B., Mishra, B., Kim, T. H., Cho, K. H., Kim, S. S., and Mishra, L. (2008). Hepatocellular cancer arises from loss of transforming growth factor beta signaling adaptor protein embryonic liver fodrin through abnormal angiogenesis. Hepatology (Baltimore, Md *48*, 1128-1137.

Balaban, R. S., Nemoto, S., and Finkel, T. (2005). Mitochondria, oxidants, and aging. Cell *120*, 483-495.

Banfi, B., Molnar, G., Maturana, A., Steger, K., Hegedus, B., Demaurex, N., and Krause, K. H. (2001). A Ca(2+)-activated NADPH oxidase in testis, spleen, and lymph nodes. The Journal of biological chemistry *276*, 37594-37601.

Bannister, A. J., Zegerman, P., Partridge, J. F., Miska, E. A., Thomas, J. O., Allshire, R. C., and Kouzarides, T. (2001). Selective recognition of methylated lysine 9 on histone H3 by the HP1 chromo domain. Nature *410*, 120-124.

Bao, S., Wu, Q., McLendon, R. E., Hao, Y., Shi, Q., Hjelmeland, A. B., Dewhirst, M. W., Bigner, D. D., and Rich, J. N. (2006). Glioma stem cells promote radioresistance by preferential activation of the DNA damage response. Nature *444*, 756-760.

Barski, A., Cuddapah, S., Cui, K., Roh, T. Y., Schones, D. E., Wang, Z., Wei, G., Chepelev, I., and Zhao, K. (2007). High-resolution profiling of histone methylations

in the human genome. Cell *129*, 823-837.

Bartosch, B., Thimme, R., Blum, H. E., and Zoulim, F. (2009). Hepatitis C virus-induced hepatocarcinogenesis. Journal of hepatology *51*, 810-820.

Battaglia, S., Benzoubir, N., Nobilet, S., Charneau, P., Samuel, D., Zignego, A. L., Atfi, A., Brechot, C., and Bourgeade, M. F. (2009). Liver cancer-derived hepatitis C virus core proteins shift TGF-beta responses from tumor suppression to epithelial-mesenchymal transition. PLoS One *4*, e4355.

Belbrahem, A., Godden-Kent, D., and Mittnacht, S. (1996). Regulation and activity of the retinoblastoma protein family in growth factor-deprived and TGF(beta)-treated keratinocytes. Exp Cell Res *225*, 286-293.

Ben-Porath, I., and Weinberg, R. A. (2005). The signals and pathways activating cellular senescence. The international journal of biochemistry & cell biology *37*, 961-976.

Bierie, B., Chung, C. H., Parker, J. S., Stover, D. G., Cheng, N., Chytil, A., Aakre, M., Shyr, Y., and Moses, H. L. (2009). Abrogation of TGF-beta signaling enhances chemokine production and correlates with prognosis in human breast cancer. J Clin Invest *119*, 1571-1582.

Bindels, S., Mestdagt, M., Vandewalle, C., Jacobs, N., Volders, L., Noel, A., van Roy, F., Berx, G., Foidart, J. M., and Gilles, C. (2006). Regulation of vimentin by SIP1 in human epithelial breast tumor cells. Oncogene *25*, 4975-4985.

Blanchetot, C., and Boonstra, J. (2008). The ROS-NOX connection in cancer and angiogenesis. Crit Rev Eukaryot Gene Expr *18*, 35-45.

Boyer, B., Tucker, G. C., Valles, A. M., Gavrilovic, J., and Thiery, J. P. (1989). Reversible transition towards a fibroblastic phenotype in a rat carcinoma cell line. Int J Cancer Suppl *4*, 69-75.

Boyer, L. A., Plath, K., Zeitlinger, J., Brambrink, T., Medeiros, L. A., Lee, T. I., Levine, S. S., Wernig, M., Tajonar, A., Ray, M. K.*, et al.* (2006). Polycomb complexes repress developmental regulators in murine embryonic stem cells. Nature

441, 349-353.

Braig, M., Lee, S., Loddenkemper, C., Rudolph, C., Peters, A. H., Schlegelberger, B., Stein, H., Dorken, B., Jenuwein, T., and Schmitt, C. A. (2005). Oncogene-induced senescence as an initial barrier in lymphoma development. Nature *436*, 660-665.

Brechot, C., Gozuacik, D., Murakami, Y., and Paterlini-Brechot, P. (2000). Molecular bases for the development of hepatitis B virus (HBV)-related hepatocellular carcinoma (HCC). Seminars in cancer biology *10*, 211-231.

Bressac, B., Galvin, K. M., Liang, T. J., Isselbacher, K. J., Wands, J. R., and Ozturk, M. (1990). Abnormal structure and expression of p53 gene in human hepatocellular carcinoma. Proc Natl Acad Sci U S A *87*, 1973-1977.

Bressac, B., Kew, M., Wands, J., and Ozturk, M. (1991). Selective G to T mutations of p53 gene in hepatocellular carcinoma from southern Africa. Nature *350*, 429-431.

Bruix, J., and Llovet, J. M. (2009). Major achievements in hepatocellular carcinoma. Lancet *373*, 614-616.

Campisi, J. (2000). Cancer, aging and cellular senescence. In Vivo *14*, 183-188.

Campisi, J., and d'Adda di Fagagna, F. (2007). Cellular senescence: when bad things happen to good cells. Nat Rev Mol Cell Biol *8*, 729-740.

Cao, Y., Liu, X., Zhang, W., Deng, X., Zhang, H., Liu, Y., Chen, L., Thompson, E. A., Townsend, C. M., Jr., and Ko, T. C. (2009). TGF-beta repression of Id2 induces apoptosis in gut epithelial cells. Oncogene *28*, 1089-1098.

Carmona-Cuenca, I., Herrera, B., Ventura, J. J., Roncero, C., Fernandez, M., and Fabregat, I. (2006). EGF blocks NADPH oxidase activation by TGF-beta in fetal rat hepatocytes, impairing oxidative stress, and cell death. J Cell Physiol *207*, 322-330.

Carmona-Cuenca, I., Roncero, C., Sancho, P., Caja, L., Fausto, N., Fernandez, M., and Fabregat, I. (2008). Upregulation of the NADPH oxidase NOX4 by TGF-beta in hepatocytes is required for its pro-apoptotic activity. Journal of hepatology *49*, 965-

976.

Cattan, V., Mercier, N., Gardner, J. P., Regnault, V., Labat, C., Maki-Jouppila, J., Nzietchueng, R., Benetos, A., Kimura, M., Aviv, A., and Lacolley, P. (2008). Chronic oxidative stress induces a tissue-specific reduction in telomere length in CAST/Ei mice. Free Radic Biol Med *44*, 1592-1598.

Cavazza, A., Caballeria, L., Floreani, A., Farinati, F., Bruguera, M., Caroli, D., and Pares, A. (2009). Incidence, risk factors, and survival of hepatocellular carcinoma in primary biliary cirrhosis: comparative analysis from two centers. Hepatology (Baltimore, Md *50*, 1162-1168.

Celeste, A., Fernandez-Capetillo, O., Kruhlak, M. J., Pilch, D. R., Staudt, D. W., Lee, A., Bonner, R. F., Bonner, W. M., and Nussenzweig, A. (2003). Histone H2AX phosphorylation is dispensable for the initial recognition of DNA breaks. Nat Cell Biol *5*, 675-679.

Chen, C. R., Kang, Y., and Massague, J. (2001). Defective repression of c-myc in breast cancer cells: A loss at the core of the transforming growth factor beta growth arrest program. Proc Natl Acad Sci U S A *98*, 992-999.

Chen, C. R., Kang, Y., Siegel, P. M., and Massague, J. (2002). E2F4/5 and p107 as Smad cofactors linking the TGFbeta receptor to c-myc repression. Cell *110*, 19-32.

Chen, Y. F., Chiu, H. H., Wu, C. H., Wang, J. Y., Chen, F. M., Tzou, W. H., Shin, S. J., and Lin, S. R. (2003). Retinoblastoma protein (pRB) was significantly phosphorylated through a Ras-to-MAPK pathway in mutant K-ras stably transfected human adrenocortical cells. DNA Cell Biol *22*, 657-664.

Chochi, Y., Kawauchi, S., Nakao, M., Furuya, T., Hashimoto, K., Oga, A., Oka, M., and Sasaki, K. (2009). A copy number gain of the 6p arm is linked with advanced hepatocellular carcinoma: an array-based comparative genomic hybridization study. The Journal of pathology *217*, 677-684.

Chu, J., and Sadler, K. C. (2009). New school in liver development: lessons from zebrafish. Hepatology (Baltimore, Md *50*, 1656-1663.

Chuang, S. C., La Vecchia, C., and Boffetta, P. (2009). Liver cancer: descriptive epidemiology and risk factors other than HBV and HCV infection. Cancer letters *286*, 9-14.

Classon, M., and Dyson, N. (2001). p107 and p130: versatile proteins with interesting pockets. Exp Cell Res *264*, 135-147.

Colavitti, R., and Finkel, T. (2005). Reactive oxygen species as mediators of cellular senescence. IUBMB Life *57*, 277-281.

Collado, M., Gil, J., Efeyan, A., Guerra, C., Schuhmacher, A. J., Barradas, M., Benguria, A., Zaballos, A., Flores, J. M., Barbacid, M*., et al.* (2005). Tumour biology: senescence in premalignant tumours. Nature *436*, 642.

Comijn, J., Berx, G., Vermassen, P., Verschueren, K., van Grunsven, L., Bruyneel, E., Mareel, M., Huylebroeck, D., and van Roy, F. (2001). The two-handed E box binding zinc finger protein SIP1 downregulates E-cadherin and induces invasion. Mol Cell *7*, 1267-1278.

Conery, A. R., Cao, Y., Thompson, E. A., Townsend, C. M., Jr., Ko, T. C., and Luo, K. (2004). Akt interacts directly with Smad3 to regulate the sensitivity to TGF-beta induced apoptosis. Nat Cell Biol *6*, 366-372.

Coppe, J. P., Desprez, P. Y., Krtolica, A., and Campisi, J. (2010). The senescence-associated secretory phenotype: the dark side of tumor suppression. Annu Rev Pathol *5*, 99-118.

Cornella, H., and Villanueva, A. (2010). Genomic tracing of the elusive liver cancer ancestor. Journal of hepatology.

Coulouarn, C., Factor, V. M., and Thorgeirsson, S. S. (2008). Transforming growth factor-beta gene expression signature in mouse hepatocytes predicts clinical outcome in human cancer. Hepatology *47*, 2059-2067.

Courtois-Cox, S., Genther Williams, S. M., Reczek, E. E., Johnson, B. W., McGillicuddy, L. T., Johannessen, C. M., Hollstein, P. E., MacCollin, M., and Cichowski, K. (2006). A negative feedback signaling network underlies oncogene-

induced senescence. Cancer cell *10*, 459-472.

Courtois-Cox, S., Jones, S. L., and Cichowski, K. (2008). Many roads lead to oncogene-induced senescence. Oncogene *27*, 2801-2809.

Cui, W., Fowlis, D. J., Bryson, S., Duffie, E., Ireland, H., Balmain, A., and Akhurst, R. J. (1996). TGFbeta1 inhibits the formation of benign skin tumors, but enhances progression to invasive spindle carcinomas in transgenic mice. Cell *86*, 531-542.

d'Adda di Fagagna, F. (2008). Living on a break: cellular senescence as a DNA-damage response. Nat Rev Cancer *8*, 512-522.

Danielpour, D., and Song, K. (2006). Cross-talk between IGF-I and TGF-beta signaling pathways. Cytokine Growth Factor Rev *17*, 59-74.

Datto, M. B., Li, Y., Panus, J. F., Howe, D. J., Xiong, Y., and Wang, X. F. (1995). Transforming growth factor beta induces the cyclin-dependent kinase inhibitor p21 through a p53-independent mechanism. Proc Natl Acad Sci U S A *92*, 5545-5549.

Davies, M., Robinson, M., Smith, E., Huntley, S., Prime, S., and Paterson, I. (2005). Induction of an epithelial to mesenchymal transition in human immortal and malignant keratinocytes by TGF-beta1 involves MAPK, Smad and AP-1 signalling pathways. J Cell Biochem *95*, 918-931.

de Mochel, N. S., Seronello, S., Wang, S. H., Ito, C., Zheng, J. X., Liang, T. J., Lambeth, J. D., and Choi, J. (2010). Hepatocyte NAD(P)H oxidases as an endogenous source of reactive oxygen species during hepatitis C virus infection. Hepatology (Baltimore, Md *52*, 47-59.

Derynck, R., Jarrett, J. A., Chen, E. Y., Eaton, D. H., Bell, J. R., Assoian, R. K., Roberts, A. B., Sporn, M. B., and Goeddel, D. V. (1985). Human transforming growth factor-beta complementary DNA sequence and expression in normal and transformed cells. Nature *316*, 701-705.

Derynck, R., Zhang, Y., and Feng, X. H. (1998). Smads: transcriptional activators of TGF-beta responses. Cell *95*, 737-740.

Derynck, R., and Zhang, Y. E. (2003). Smad-dependent and Smad-independent pathways in TGF-beta family signalling. Nature *425*, 577-584.

Dhasarathy, A., Kajita, M., and Wade, P. A. (2007). The transcription factor snail mediates epithelial to mesenchymal transitions by repression of estrogen receptor-alpha. Mol Endocrinol *21*, 2907-2918.

Dhomen, N., Reis-Filho, J. S., da Rocha Dias, S., Hayward, R., Savage, K., Delmas, V., Larue, L., Pritchard, C., and Marais, R. (2009). Oncogenic Braf induces melanocyte senescence and melanoma in mice. Cancer cell *15*, 294-303.

Di Bisceglie, A. M. (2009). Hepatitis B and hepatocellular carcinoma. Hepatology (Baltimore, Md *49*, S56-60.

Di Guglielmo, G. M., Le Roy, C., Goodfellow, A. F., and Wrana, J. L. (2003). Distinct endocytic pathways regulate TGF-beta receptor signalling and turnover. Nat Cell Biol *5*, 410-421.

Di Micco, R., Fumagalli, M., Cicalese, A., Piccinin, S., Gasparini, P., Luise, C., Schurra, C., Garre, M., Nuciforo, P. G., Bensimon, A.*, et al.* (2006). Oncogene-induced senescence is a DNA damage response triggered by DNA hyper-replication. Nature *444*, 638-642.

Diakowska, D., Lewandowski, A., Kopec, W., Diakowski, W., and Chrzanowska, T. (2007). Oxidative DNA damage and total antioxidant status in serum of patients with esophageal squamous cell carcinoma. Hepatogastroenterology *54*, 1701-1704.

Dimri, G. P., Lee, X., Basile, G., Acosta, M., Scott, G., Roskelley, C., Medrano, E. E., Linskens, M., Rubelj, I., Pereira-Smith, O., and et al. (1995). A biomarker that identifies senescent human cells in culture and in aging skin in vivo. Proc Natl Acad Sci U S A *92*, 9363-9367.

Ding, W., Mouzaki, M., You, H., Laird, J. C., Mato, J., Lu, S. C., and Rountree, C. B. (2009). CD133+ liver cancer stem cells from methionine adenosyl transferase 1A-deficient mice demonstrate resistance to transforming growth factor (TGF)-beta-induced apoptosis. Hepatology (Baltimore, Md *49*, 1277-1286.

Dizdaroglu, M. (1992). Oxidative damage to DNA in mammalian chromatin. Mutation research *275*, 331-342.

Dong, Z. Z., Yao, D. F., Yao, M., Qiu, L. W., Zong, L., Wu, W., Wu, X. H., Yao, D. B., and Meng, X. Y. (2008). Clinical impact of plasma TGF-beta1 and circulating TGF-beta1 mRNA in diagnosis of hepatocellular carcinoma. Hepatobiliary Pancreat Dis Int *7*, 288-295.

Droge, W. (2002). Free radicals in the physiological control of cell function. Physiol Rev *82*, 47-95.

Dufour, J. F., and Johnson, P. Liver cancer: from molecular pathogenesis to new therapies: summary of the EASL single topic conference. Journal of hepatology *52*, 296-304.

Edens, W. A., Sharling, L., Cheng, G., Shapira, R., Kinkade, J. M., Lee, T., Edens, H. A., Tang, X., Sullards, C., Flaherty, D. B.*, et al.* (2001). Tyrosine cross-linking of extracellular matrix is catalyzed by Duox, a multidomain oxidase/peroxidase with homology to the phagocyte oxidase subunit gp91phox. J Cell Biol *154*, 879-891.

Edlund, S., Bu, S., Schuster, N., Aspenstrom, P., Heuchel, R., Heldin, N. E., ten Dijke, P., Heldin, C. H., and Landstrom, M. (2003). Transforming growth factor-beta1 (TGF-beta)-induced apoptosis of prostate cancer cells involves Smad7-dependent activation of p38 by TGF-beta-activated kinase 1 and mitogen-activated protein kinase kinase 3. Mol Biol Cell *14*, 529-544.

Egger, G., Aparicio, A. M., Escobar, S. G., and Jones, P. A. (2007). Inhibition of histone deacetylation does not block resilencing of p16 after 5-aza-2'-deoxycytidine treatment. Cancer research *67*, 346-353.

El-Serag, H. B., and Rudolph, K. L. (2007). Hepatocellular carcinoma: epidemiology and molecular carcinogenesis. Gastroenterology *132*, 2557-2576.

Erdal, E., Ozturk, N., Cagatay, T., Eksioglu-Demiralp, E., and Ozturk, M. (2005). Lithium-mediated downregulation of PKB/Akt and cyclin E with growth inhibition in hepatocellular carcinoma cells. Int J Cancer *115*, 903-910.

Ewen, M. E., Oliver, C. J., Sluss, H. K., Miller, S. J., and Peeper, D. S. (1995). p53-dependent repression of CDK4 translation in TGF-beta-induced G1 cell-cycle arrest. Genes Dev *9*, 204-217.

Fan, G., Ma, X., Kren, B. T., and Steer, C. J. (1996). The retinoblastoma gene product inhibits TGF-beta1 induced apoptosis in primary rat hepatocytes and human HuH-7 hepatoma cells. Oncogene *12*, 1909-1919.

Fan, G., Ma, X., Kren, B. T., and Steer, C. J. (2002). Unbound E2F modulates TGF-beta1-induced apoptosis in HuH-7 cells. J Cell Sci *115*, 3181-3191.

Fan, Y., Menon, R. K., Cohen, P., Hwang, D., Clemens, T., DiGirolamo, D. J., Kopchick, J. J., Le Roith, D., Trucco, M., and Sperling, M. A. (2009). Liver-specific deletion of the growth hormone receptor reveals essential role of growth hormone signaling in hepatic lipid metabolism. The Journal of biological chemistry *284*, 19937-19944.

Farazi, P. A., and DePinho, R. A. (2006). Hepatocellular carcinoma pathogenesis: from genes to environment. Nat Rev Cancer *6*, 674-687.

Farrell, G. C., and Larter, C. Z. (2006). Nonalcoholic fatty liver disease: from steatosis to cirrhosis. Hepatology (Baltimore, Md *43*, S99-S112.

Fearon, E. R., and Vogelstein, B. (1990). A genetic model for colorectal tumorigenesis. Cell *61*, 759-767.

Feitelson, M. A., and Lee, J. (2007). Hepatitis B virus integration, fragile sites, and hepatocarcinogenesis. Cancer letters *252*, 157-170.

Ferbeyre, G., de Stanchina, E., Lin, A. W., Querido, E., McCurrach, M. E., Hannon, G. J., and Lowe, S. W. (2002). Oncogenic ras and p53 cooperate to induce cellular senescence. Mol Cell Biol *22*, 3497-3508.

Florenes, V. A., Bhattacharya, N., Bani, M. R., Ben-David, Y., Kerbel, R. S., and Slingerland, J. M. (1996). TGF-beta mediated G1 arrest in a human melanoma cell line lacking p15INK4B: evidence for cooperation between p21Cip1/WAF1 and

p27Kip1. Oncogene *13*, 2447-2457.

Francini, F., Castro, M. C., Gagliardino, J. J., and Massa, M. L. (2009). Regulation of liver glucokinase activity in rats with fructose-induced insulin resistance and impaired glucose and lipid metabolism. Canadian journal of physiology and pharmacology *87*, 702-710.

Fung, J., Lai, C. L., and Yuen, M. F. (2009). Hepatitis B and C virus-related carcinogenesis. Clin Microbiol Infect *15*, 964-970.

Fuxe, J., Vincent, T., and de Herreros, A. G. (2010). Transcriptional crosstalk between TGFbeta and stem cell pathways in tumor cell invasion: Role of EMT promoting Smad complexes. Cell Cycle *9*.

Gal, A., Sjoblom, T., Fedorova, L., Imreh, S., Beug, H., and Moustakas, A. (2008). Sustained TGF beta exposure suppresses Smad and non-Smad signalling in mammary epithelial cells, leading to EMT and inhibition of growth arrest and apoptosis. Oncogene *27*, 1218-1230.

Gao, D., Wei, C., Chen, L., Huang, J., Yang, S., and Diehl, A. M. (2004). Oxidative DNA damage and DNA repair enzyme expression are inversely related in murine models of fatty liver disease. American journal of physiology *287*, G1070-1077.

Geng, Y., and Weinberg, R. A. (1993). Transforming growth factor beta effects on expression of G1 cyclins and cyclin-dependent protein kinases. Proc Natl Acad Sci U S A *90*, 10315-10319.

Giampieri, S., Manning, C., Hooper, S., Jones, L., Hill, C. S., and Sahai, E. (2009). Localized and reversible TGFbeta signalling switches breast cancer cells from cohesive to single cell motility. Nat Cell Biol *11*, 1287-1296.

Gil, J., and Peters, G. (2006). Regulation of the INK4b-ARF-INK4a tumour suppressor locus: all for one or one for all. Nat Rev Mol Cell Biol *7*, 667-677.

Gomis, R. R., Alarcon, C., He, W., Wang, Q., Seoane, J., Lash, A., and Massague, J. (2006). A FoxO-Smad synexpression group in human keratinocytes. Proc Natl Acad

Sci U S A *103*, 12747-12752.

Gonzalez, F. J. (2005). Role of cytochromes P450 in chemical toxicity and oxidative stress: studies with CYP2E1. Mutation research *569*, 101-110.

Gorelik, L., and Flavell, R. A. (2001). Immune-mediated eradication of tumors through the blockade of transforming growth factor-beta signaling in T cells. Nat Med *7*, 1118-1122.

Gouas, D., Shi, H., Hautefeuille, A., Ortiz-Cuaran, S., Legros, P., Szymanska, K., Galy, O., Egevad, L., Abedi-Ardekani, B., Wiman, K.*, et al.* (2010). Effects of the TP53 p.R249S mutant on proliferation and clonogenic properties in human hepatocellular carcinoma cell lines: interaction with Hepatitis B Virus X protein. Carcinogenesis.

Grandori, C., Wu, K. J., Fernandez, P., Ngouenet, C., Grim, J., Clurman, B. E., Moser, M. J., Oshima, J., Russell, D. W., Swisshelm, K.*, et al.* (2003). Werner syndrome protein limits MYC-induced cellular senescence. Genes Dev *17*, 1569-1574.

Gressner, A. M. (1995). Cytokines and cellular crosstalk involved in the activation of fat-storing cells. Journal of hepatology *22*, 28-36.

Gupta, G. P., and Massague, J. (2006). Cancer metastasis: building a framework. Cell *127*, 679-695.

Gupta, P. B., Onder, T. T., Jiang, G., Tao, K., Kuperwasser, C., Weinberg, R. A., and Lander, E. S. (2009). Identification of selective inhibitors of cancer stem cells by high-throughput screening. Cell *138*, 645-659.

Hahn, S. A., Bartsch, D., Schroers, A., Galehdari, H., Becker, M., Ramaswamy, A., Schwarte-Waldhoff, I., Maschek, H., and Schmiegel, W. (1998). Mutations of the DPC4/Smad4 gene in biliary tract carcinoma. Cancer research *58*, 1124-1126.

Han, C. H., Nisimoto, Y., Lee, S. H., Kim, E. T., and Lambeth, J. D. (2001). Characterization of the flavoprotein domain of gp91phox which has NADPH

diaphorase activity. J Biochem *129*, 513-520.

Hanahan, D., and Weinberg, R. A. (2000). The hallmarks of cancer. Cell *100*, 57-70.

Hanyu, A., Ishidou, Y., Ebisawa, T., Shimanuki, T., Imamura, T., and Miyazono, K. (2001). The N domain of Smad7 is essential for specific inhibition of transforming growth factor-beta signaling. J Cell Biol *155*, 1017-1027.

Harley, C. B., Futcher, A. B., and Greider, C. W. (1990). Telomeres shorten during ageing of human fibroblasts. Nature *345*, 458-460.

Hasegawa, K., Wang, Z., Inagaki, M., and Carr, B. I. (1995). Characterization of a human hepatoma cell line with acquired resistance to growth inhibition by transforming growth factor beta 1 (TGF-beta 1). In Vitro Cell Dev Biol Anim *31*, 55-61.

Hashimoto, O., Ueno, T., Kimura, R., Ohtsubo, M., Nakamura, T., Koga, H., Torimura, T., Uchida, S., Yamashita, K., and Sata, M. (2003). Inhibition of proteasome-dependent degradation of Wee1 in G2-arrested Hep3B cells by TGF beta 1. Mol Carcinog *36*, 171-182.

Hassan, M. M., Hwang, L. Y., Hatten, C. J., Swaim, M., Li, D., Abbruzzese, J. L., Beasley, P., and Patt, Y. Z. (2002). Risk factors for hepatocellular carcinoma: synergism of alcohol with viral hepatitis and diabetes mellitus. Hepatology (Baltimore, Md *36*, 1206-1213.

Hayflick, L., and Moorhead, P. S. (1961). The serial cultivation of human diploid cell strains. Exp Cell Res *25*, 585-621.

Herman, J. G., Jen, J., Merlo, A., and Baylin, S. B. (1996). Hypermethylation-associated inactivation indicates a tumor suppressor role for p15INK4B. Cancer research *56*, 722-727.

Hernandez-Alcoceba, R., Sangro, B., and Prieto, J. (2007). Gene therapy of liver cancer. Ann Hepatol *6*, 5-14.

Herrera, B., Murillo, M. M., Alvarez-Barrientos, A., Beltran, J., Fernandez, M., and

Fabregat, I. (2004). Source of early reactive oxygen species in the apoptosis induced by transforming growth factor-beta in fetal rat hepatocytes. Free Radic Biol Med *36*, 16-26.

Herrera, R. E., Makela, T. P., and Weinberg, R. A. (1996). TGF beta-induced growth inhibition in primary fibroblasts requires the retinoblastoma protein. Mol Biol Cell *7*, 1335-1342.

Herzer, K., Ganten, T. M., Schulze-Bergkamen, H., Grosse-Wilde, A., Koschny, R., Krammer, P. H., and Walczak, H. (2005). Transforming growth factor beta can mediate apoptosis via the expression of TRAIL in human hepatoma cells. Hepatology (Baltimore, Md *42*, 183-192.

Hill, C. S. (2009). Nucleocytoplasmic shuttling of Smad proteins. Cell Res *19*, 36-46.

Hirschfield, G. M., and Siminovitch, K. A. (2009). Toward the molecular dissection of primary biliary cirrhosis. Hepatology (Baltimore, Md *50*, 1347-1350.

Hoffmann, A., Xia, Y., and Verma, I. M. (2007). Inflammatory tales of liver cancer. Cancer cell *11*, 99-101.

Hollstein, M., Sidransky, D., Vogelstein, B., and Harris, C. C. (1991). p53 mutations in human cancers. Science (New York, NY *253*, 49-53.

Horie, Y., Yamagishi, Y., Kajihara, M., Kato, S., and Ishii, H. (2003). National survey of hepatocellular carcinoma in heavy drinkers in Japan. Alcoholism, clinical and experimental research *27*, 32S-36S.

Hornsby, P. J. (2007). Senescence as an anticancer mechanism. J Clin Oncol *25*, 1852-1857.

Hov, H., Holt, R. U., Ro, T. B., Fagerli, U. M., Hjorth-Hansen, H., Baykov, V., Christensen, J. G., Waage, A., Sundan, A., and Borset, M. (2004). A selective c-met inhibitor blocks an autocrine hepatocyte growth factor growth loop in ANBL-6 cells and prevents migration and adhesion of myeloma cells. Clin Cancer Res *10*, 6686-6694.

Howe, J. R., Roth, S., Ringold, J. C., Summers, R. W., Jarvinen, H. J., Sistonen, P., Tomlinson, I. P., Houlston, R. S., Bevan, S., Mitros, F. A.*, et al.* (1998). Mutations in the SMAD4/DPC4 gene in juvenile polyposis. Science (New York, NY *280*, 1086-1088.

Hu, T., Ramachandrarao, S. P., Siva, S., Valancius, C., Zhu, Y., Mahadev, K., Toh, I., Goldstein, B. J., Woolkalis, M., and Sharma, K. (2005). Reactive oxygen species production via NADPH oxidase mediates TGF-beta-induced cytoskeletal alterations in endothelial cells. Am J Physiol Renal Physiol *289*, F816-825.

Huang, S., He, X., Ding, J., Liang, L., Zhao, Y., Zhang, Z., Yao, X., Pan, Z., Zhang, P., Li, J.*, et al.* (2008). Upregulation of miR-23a approximately 27a approximately 24 decreases transforming growth factor-beta-induced tumor-suppressive activities in human hepatocellular carcinoma cells. Int J Cancer *123*, 972-978.

Iadonato, S. P., and Katze, M. G. (2009). Genomics: Hepatitis C virus gets personal. Nature *461*, 357-358.

Iavarone, A., and Massague, J. (1997). Repression of the CDK activator Cdc25A and cell-cycle arrest by cytokine TGF-beta in cells lacking the CDK inhibitor p15. Nature *387*, 417-422.

Ikeda, H., Sasaki, M., Sato, Y., Harada, K., Zen, Y., Mitsui, T., and Nakanuma, Y. (2009a). Bile ductular cell reaction with senescent hepatocytes in chronic viral hepatitis is lost during hepatocarcinogenesis. Pathol Int *59*, 471-478.

Ikeda, H., Sasaki, M., Sato, Y., Harada, K., Zen, Y., Mitsui, T., and Nakanuma, Y. (2009b). Large cell change of hepatocytes in chronic viral hepatitis represents a senescent-related lesion. Hum Pathol.

Inagaki, M., Moustakas, A., Lin, H. Y., Lodish, H. F., and Carr, B. I. (1993). Growth inhibition by transforming growth factor beta (TGF-beta) type I is restored in TGF-beta-resistant hepatoma cells after expression of TGF-beta receptor type II cDNA. Proc Natl Acad Sci U S A *90*, 5359-5363.

Irmak, M. B., Ince, G., Ozturk, M., and Cetin-Atalay, R. (2003). Acquired tolerance

of hepatocellular carcinoma cells to selenium deficiency: a selective survival mechanism? Cancer research *63*, 6707-6715.

Ishikawa, K., Takenaga, K., Akimoto, M., Koshikawa, N., Yamaguchi, A., Imanishi, H., Nakada, K., Honma, Y., and Hayashi, J. (2008). ROS-generating mitochondrial DNA mutations can regulate tumor cell metastasis. Science (New York, NY *320*, 661-664.

Itoh, S., Landstrom, M., Hermansson, A., Itoh, F., Heldin, C. H., Heldin, N. E., and ten Dijke, P. (1998). Transforming growth factor beta1 induces nuclear export of inhibitory Smad7. The Journal of biological chemistry *273*, 29195-29201.

Janssen, M. C., and Swinkels, D. W. (2009). Hereditary haemochromatosis. Best practice & research *23*, 171-183.

Jong, H. S., Lee, H. S., Kim, T. Y., Im, Y. H., Park, J. W., Kim, N. K., and Bang, Y. J. (2002). Attenuation of transforming growth factor beta-induced growth inhibition in human hepatocellular carcinoma cell lines by cyclin D1 overexpression. Biochem Biophys Res Commun *292*, 383-389.

Jourdan, T., Djaouti, L., Demizieux, L., Gresti, J., Verges, B., and Degrace, P. (2009). Liver carbohydrate and lipid metabolism of insulin-deficient mice is altered by trans-10, cis-12 conjugated linoleic acid. The Journal of nutrition *139*, 1901-1907.

Kaklamani, V., Baddi, L., Rosman, D., Liu, J., Ellis, N., Oddoux, C., Ostrer, H., Chen, Y., Ahsan, H., Offit, K., and Pasche, B. (2004). No major association between TGFBR1*6A and prostate cancer. BMC Genet *5*, 28.

Kang, Y., Chen, C. R., and Massague, J. (2003). A self-enabling TGFbeta response coupled to stress signaling: Smad engages stress response factor ATF3 for Id1 repression in epithelial cells. Mol Cell *11*, 915-926.

Kaplan, A., and Cosentino, L. Alpha1-antitrypsin deficiency: forgotten etiology. Canadian family physician Medecin de famille canadien *56*, 19-24.

Kassambara, A., Klein, B., and Moreaux, J. (2009). MMSET is overexpressed in cancers: link with tumor aggressiveness. Biochem Biophys Res Commun *379*, 840-

845.

Kavsak, P., Rasmussen, R. K., Causing, C. G., Bonni, S., Zhu, H., Thomsen, G. H., and Wrana, J. L. (2000). Smad7 binds to Smurf2 to form an E3 ubiquitin ligase that targets the TGF beta receptor for degradation. Mol Cell *6*, 1365-1375.

Kawate, S., Takenoshita, S., Ohwada, S., Mogi, A., Fukusato, T., Makita, F., Kuwano, H., and Morishita, Y. (1999). Mutation analysis of transforming growth factor beta type II receptor, Smad2, and Smad4 in hepatocellular carcinoma. Int J Oncol *14*, 127-131.

Kew, M. C. (1986). The development of hepatocellular cancer in humans. Cancer surveys *5*, 719-739.

Kim, H., Oh, B. K., Roncalli, M., Park, C., Yoon, S. M., Yoo, J. E., and Park, Y. N. (2009a). Large liver cell change in hepatitis B virus-related liver cirrhosis. Hepatology *50*, 752-762.

Kim, J., Johnson, K., Chen, H. J., Carroll, S., and Laughon, A. (1997). Drosophila Mad binds to DNA and directly mediates activation of vestigial by Decapentaplegic. Nature *388*, 304-308.

Kim, K. S., Kang, K. W., Seu, Y. B., Baek, S. H., and Kim, J. R. (2009b). Interferon-gamma induces cellular senescence through p53-dependent DNA damage signaling in human endothelial cells. Mech Ageing Dev *130*, 179-188.

Kim, S. J., Im, Y. H., Markowitz, S. D., and Bang, Y. J. (2000). Molecular mechanisms of inactivation of TGF-beta receptors during carcinogenesis. Cytokine Growth Factor Rev *11*, 159-168.

Kim, W. Y., and Sharpless, N. E. (2006). The regulation of INK4/ARF in cancer and aging. Cell *127*, 265-275.

Kirk, G. D., Bah, E., and Montesano, R. (2006). Molecular epidemiology of human liver cancer: insights into etiology, pathogenesis and prevention from The Gambia, West Africa. Carcinogenesis *27*, 2070-2082.

Kishnani, P. S., Chuang, T. P., Bali, D., Koeberl, D., Austin, S., Weinstein, D. A., Murphy, E., Chen, Y. T., Boyette, K., Liu, C. H.*, et al.* (2009). Chromosomal and genetic alterations in human hepatocellular adenomas associated with type Ia glycogen storage disease. Human molecular genetics *18*, 4781-4790.

Kitisin, K., Ganesan, N., Tang, Y., Jogunoori, W., Volpe, E. A., Kim, S. S., Katuri, V., Kallakury, B., Pishvaian, M., Albanese, C.*, et al.* (2007). Disruption of transforming growth factor-beta signaling through beta-spectrin ELF leads to hepatocellular cancer through cyclin D1 activation. Oncogene *26*, 7103-7110.

Klaunig, J. E., and Kamendulis, L. M. (2004). The role of oxidative stress in carcinogenesis. Annu Rev Pharmacol Toxicol *44*, 239-267.

Kojima, T., Takano, K., Yamamoto, T., Murata, M., Son, S., Imamura, M., Yamaguchi, H., Osanai, M., Chiba, H., Himi, T., and Sawada, N. (2008). Transforming growth factor-beta induces epithelial to mesenchymal transition by down-regulation of claudin-1 expression and the fence function in adult rat hepatocytes. Liver Int *28*, 534-545.

Kortlever, R. M., Higgins, P. J., and Bernards, R. (2006). Plasminogen activator inhibitor-1 is a critical downstream target of p53 in the induction of replicative senescence. Nat Cell Biol *8*, 877-884.

Krimpenfort, P., Ijpenberg, A., Song, J. Y., van der Valk, M., Nawijn, M., Zevenhoven, J., and Berns, A. (2007). p15Ink4b is a critical tumour suppressor in the absence of p16Ink4a. Nature *448*, 943-946.

Krimpenfort, P., Quon, K. C., Mooi, W. J., Loonstra, A., and Berns, A. (2001). Loss of p16Ink4a confers susceptibility to metastatic melanoma in mice. Nature *413*, 83-86.

Krizhanovsky, V., Yon, M., Dickins, R. A., Hearn, S., Simon, J., Miething, C., Yee, H., Zender, L., and Lowe, S. W. (2008). Senescence of activated stellate cells limits liver fibrosis. Cell *134*, 657-667.

Kuilman, T., Michaloglou, C., Vredeveld, L. C., Douma, S., van Doorn, R., Desmet,

C. J., Aarden, L. A., Mooi, W. J., and Peeper, D. S. (2008). Oncogene-induced senescence relayed by an interleukin-dependent inflammatory network. Cell *133*, 1019-1031.

Kuilman, T., and Peeper, D. S. (2009). Senescence-messaging secretome: SMS-ing cellular stress. Nat Rev Cancer *9*, 81-94.

Kumar, B., Koul, S., Khandrika, L., Meacham, R. B., and Koul, H. K. (2008). Oxidative stress is inherent in prostate cancer cells and is required for aggressive phenotype. Cancer research *68*, 1777-1785.

Kuniholm, M. H., Lesi, O. A., Mendy, M., Akano, A. O., Sam, O., Hall, A. J., Whittle, H., Bah, E., Goedert, J. J., Hainaut, P., and Kirk, G. D. (2008). Aflatoxin exposure and viral hepatitis in the etiology of liver cirrhosis in the Gambia, West Africa. Environmental health perspectives *116*, 1553-1557.

Lambeth, J. D. (2004). NOX enzymes and the biology of reactive oxygen. Nat Rev Immunol *4*, 181-189.

Lambeth, J. D., Cheng, G., Arnold, R. S., and Edens, W. A. (2000). Novel homologs of gp91phox. Trends Biochem Sci *25*, 459-461.

Lamboley, C., Bringuier, A. F., and Feldmann, G. (2000). Induction of apoptosis in normal cultured rat hepatocytes and in Hep3B, a human hepatoma cell line. Cell Biol Toxicol *16*, 185-200.

Langer, C., Jurgensmeier, J. M., and Bauer, G. (1996). Reactive oxygen species act at both TGF-beta-dependent and -independent steps during induction of apoptosis of transformed cells by normal cells. Exp Cell Res *222*, 117-124.

Lazzerini Denchi, E., Attwooll, C., Pasini, D., and Helin, K. (2005). Deregulated E2F activity induces hyperplasia and senescence-like features in the mouse pituitary gland. Mol Cell Biol *25*, 2660-2672.

Lecuit, T., and Lenne, P. F. (2007). Cell surface mechanics and the control of cell shape, tissue patterns and morphogenesis. Nat Rev Mol Cell Biol *8*, 633-644.

Lee, A. C., Fenster, B. E., Ito, H., Takeda, K., Bae, N. S., Hirai, T., Yu, Z. X., Ferrans, V. J., Howard, B. H., and Finkel, T. (1999). Ras proteins induce senescence by altering the intracellular levels of reactive oxygen species. The Journal of biological chemistry *274*, 7936-7940.

Lee, S. J., and McPherron, A. C. (2001). Regulation of myostatin activity and muscle growth. Proc Natl Acad Sci U S A *98*, 9306-9311.

Lehmann, B. D., Brooks, A. M., Paine, M. S., Chappell, W. H., McCubrey, J. A., and Terrian, D. M. (2008). Distinct roles for p107 and p130 in Rb-independent cellular senescence. Cell Cycle *7*, 1262-1268.

Levayer, R., and Lecuit, T. (2008). Breaking down EMT. Nat Cell Biol *10*, 757-759.

Levy, L., and Hill, C. S. (2006). Alterations in components of the TGF-beta superfamily signaling pathways in human cancer. Cytokine Growth Factor Rev *17*, 41-58.

Liew, C. T., Li, H. M., Lo, K. W., Leow, C. K., Lau, W. Y., Hin, L. Y., Lim, B. K., Lai, P. B., Chan, J. Y., Wang, X. Q.*, et al.* (1999). Frequent allelic loss on chromosome 9 in hepatocellular carcinoma. Int J Cancer *81*, 319-324.

Lin, J. K., and Chou, C. K. (1992). In vitro apoptosis in the human hepatoma cell line induced by transforming growth factor beta 1. Cancer research *52*, 385-388.

Lin, R. Y., Sullivan, K. M., Argenta, P. A., Meuli, M., Lorenz, H. P., and Adzick, N. S. (1995). Exogenous transforming growth factor-beta amplifies its own expression and induces scar formation in a model of human fetal skin repair. Ann Surg *222*, 146-154.

Lindenbach, B. D., Evans, M. J., Syder, A. J., Wolk, B., Tellinghuisen, T. L., Liu, C. C., Maruyama, T., Hynes, R. O., Burton, D. R., McKeating, J. A., and Rice, C. M. (2005). Complete replication of hepatitis C virus in cell culture. Science (New York, NY *309*, 623-626.

Lindor, K. D., Gershwin, M. E., Poupon, R., Kaplan, M., Bergasa, N. V., and Heathcote, E. J. (2009). Primary biliary cirrhosis. Hepatology (Baltimore, Md *50*,

291-308.

Liu, J., Mao, W., Ding, B., and Liang, C. S. (2008). ERKs/p53 signal transduction pathway is involved in doxorubicin-induced apoptosis in H9c2 cells and cardiomyocytes. Am J Physiol Heart Circ Physiol *295*, H1956-1965.

Lu, A. L., Li, X., Gu, Y., Wright, P. M., and Chang, D. Y. (2001). Repair of oxidative DNA damage: mechanisms and functions. Cell biochemistry and biophysics *35*, 141-170.

Lu, K., Yin, X., Weng, T., Xi, S., Li, L., Xing, G., Cheng, X., Yang, X., Zhang, L., and He, F. (2008). Targeting WW domains linker of HECT-type ubiquitin ligase Smurf1 for activation by CKIP-1. Nat Cell Biol *10*, 994-1002.

Lu, T., and Finkel, T. (2008). Free radicals and senescence. Exp Cell Res *314*, 1918-1922.

Lundberg, A. S., Hahn, W. C., Gupta, P., and Weinberg, R. A. (2000). Genes involved in senescence and immortalization. Curr Opin Cell Biol *12*, 705-709.

Ma, S., Chan, K. W., Hu, L., Lee, T. K., Wo, J. Y., Ng, I. O., Zheng, B. J., and Guan, X. Y. (2007). Identification and characterization of tumorigenic liver cancer stem/progenitor cells. Gastroenterology *132*, 2542-2556.

Macera-Bloch, L., Houghton, J., Lenahan, M., Jha, K. K., and Ozer, H. L. (2002). Termination of lifespan of SV40-transformed human fibroblasts in crisis is due to apoptosis. J Cell Physiol *190*, 332-344.

Maclaren, N. K., Gujral, S., Ten, S., and Motagheti, R. (2007). Childhood obesity and insulin resistance. Cell biochemistry and biophysics *48*, 73-78.

Majumder, M., Ghosh, A. K., Steele, R., Ray, R., and Ray, R. B. (2001). Hepatitis C virus NS5A physically associates with p53 and regulates p21/waf1 gene expression in a p53-dependent manner. Journal of virology *75*, 1401-1407.

Mallette, F. A., Gaumont-Leclerc, M. F., and Ferbeyre, G. (2007). The DNA damage signaling pathway is a critical mediator of oncogene-induced senescence. Genes Dev

21, 43-48.

Malumbres, M., and Barbacid, M. (2007). Cell cycle kinases in cancer. Curr Opin Genet Dev *17*, 60-65.

Mani, S. A., Guo, W., Liao, M. J., Eaton, E. N., Ayyanan, A., Zhou, A. Y., Brooks, M., Reinhard, F., Zhang, C. C., Shipitsin, M., *et al.* (2008). The epithelial-mesenchymal transition generates cells with properties of stem cells. Cell *133*, 704-715.

Mani, S. A., Yang, J., Brooks, M., Schwaninger, G., Zhou, A., Miura, N., Kutok, J. L., Hartwell, K., Richardson, A. L., and Weinberg, R. A. (2007). Mesenchyme Forkhead 1 (FOXC2) plays a key role in metastasis and is associated with aggressive basal-like breast cancers. Proc Natl Acad Sci U S A *104*, 10069-10074.

Manning, G., Whyte, D. B., Martinez, R., Hunter, T., and Sudarsanam, S. (2002). The protein kinase complement of the human genome. Science (New York, NY *298*, 1912-1934.

Marcellin, P. (2009). Hepatitis B and hepatitis C in 2009. Liver Int *29 Suppl 1*, 1-8.

Markham, D., Munro, S., Soloway, J., O'Connor, D. P., and La Thangue, N. B. (2006). DNA-damage-responsive acetylation of pRb regulates binding to E2F-1. EMBO Rep *7*, 192-198.

Martinez-Garcia, E., and Licht, J. D. (2010). Deregulation of H3K27 methylation in cancer. Nature genetics *42*, 100-101.

Massague, J. (1998). TGF-beta signal transduction. Annu Rev Biochem *67*, 753-791.

Massague, J. (2008). TGFbeta in Cancer. Cell *134*, 215-230.

Massague, J., and Chen, Y. G. (2000). Controlling TGF-beta signaling. Genes Dev *14*, 627-644.

Massague, J., and Wotton, D. (2000). Transcriptional control by the TGF-beta/Smad signaling system. EMBO J *19*, 1745-1754.

Matsumoto, K., Satoh, Y., Sugo, H., Takamori, S., Kojima, K., Fukasawa, M., Beppu, T., and Futagawa, S. (2003). Immunohistochemical study of the relationship between 8-hydroxy-2'-deoxyguanosine levels in noncancerous region and postoperative recurrence of hepatocellular carcinoma in remnant liver. Hepatol Res *25*, 435-441.

Matsuzaki, K., Date, M., Furukawa, F., Tahashi, Y., Matsushita, M., Sugano, Y., Yamashiki, N., Nakagawa, T., Seki, T., Nishizawa, M.*, et al.* (2000). Regulatory mechanisms for transforming growth factor beta as an autocrine inhibitor in human hepatocellular carcinoma: implications for roles of smads in its growth. Hepatology (Baltimore, Md *32*, 218-227.

Mejlvang, J., Kriajevska, M., Vandewalle, C., Chernova, T., Sayan, A. E., Berx, G., Mellon, J. K., and Tulchinsky, E. (2007). Direct repression of cyclin D1 by SIP1 attenuates cell cycle progression in cells undergoing an epithelial mesenchymal transition. Mol Biol Cell *18*, 4615-4624.

Michaloglou, C., Vredeveld, L. C., Soengas, M. S., Denoyelle, C., Kuilman, T., van der Horst, C. M., Majoor, D. M., Shay, J. W., Mooi, W. J., and Peeper, D. S. (2005). BRAFE600-associated senescence-like cell cycle arrest of human naevi. Nature *436*, 720-724.

Midorikawa, Y., Yamamoto, S., Tsuji, S., Kamimura, N., Ishikawa, S., Igarashi, H., Makuuchi, M., Kokudo, N., Sugimura, H., and Aburatani, H. (2009). Allelic imbalances and homozygous deletion on 8p23.2 for stepwise progression of hepatocarcinogenesis. Hepatology (Baltimore, Md *49*, 513-522.

Miettinen, P. J., Ebner, R., Lopez, A. R., and Derynck, R. (1994). TGF-beta induced transdifferentiation of mammary epithelial cells to mesenchymal cells: involvement of type I receptors. J Cell Biol *127*, 2021-2036.

Minguez, B., Tovar, V., Chiang, D., Villanueva, A., and Llovet, J. M. (2009). Pathogenesis of hepatocellular carcinoma and molecular therapies. Current opinion in gastroenterology *25*, 186-194.

Mishra, B., Tang, Y., Katuri, V., Fleury, T., Said, A. H., Rashid, A., Jogunoori, W.,

and Mishra, L. (2004). Loss of cooperative function of transforming growth factor-beta signaling proteins, smad3 with embryonic liver fodrin, a beta-spectrin, in primary biliary cirrhosis. Liver Int *24*, 637-645.

Mishra, L., Banker, T., Murray, J., Byers, S., Thenappan, A., He, A. R., Shetty, K., Johnson, L., and Reddy, E. P. (2009). Liver stem cells and hepatocellular carcinoma. Hepatology (Baltimore, Md *49*, 318-329.

Miyake, H., Hara, I., Kamidono, S., and Eto, H. (2004). Oxidative DNA damage in patients with prostate cancer and its response to treatment. J Urol *171*, 1533-1536.

Miyazono, K., Hellman, U., Wernstedt, C., and Heldin, C. H. (1988). Latent high molecular weight complex of transforming growth factor beta 1. Purification from human platelets and structural characterization. The Journal of biological chemistry *263*, 6407-6415.

Moutsopoulos, N. M., Wen, J., and Wahl, S. M. (2008). TGF-beta and tumors--an ill-fated alliance. Curr Opin Immunol *20*, 234-240.

Muguruma, M., Unami, A., Kanki, M., Kuroiwa, Y., Nishimura, J., Dewa, Y., Umemura, T., Oishi, Y., and Mitsumori, K. (2007). Possible involvement of oxidative stress in piperonyl butoxide induced hepatocarcinogenesis in rats. Toxicology *236*, 61-75.

Murga, M., Bunting, S., Montana, M. F., Soria, R., Mulero, F., Canamero, M., Lee, Y., McKinnon, P. J., Nussenzweig, A., and Fernandez-Capetillo, O. (2009). A mouse model of ATR-Seckel shows embryonic replicative stress and accelerated aging. Nature genetics *41*, 891-898.

Nagasue, N., Yu, L., Yamaguchi, M., Kohno, H., Tachibana, M., and Kubota, H. (1996). Inhibition of growth and induction of TGF-beta 1 in human hepatocellular carcinoma with androgen receptor by cyproterone acetate in male nude mice. Journal of hepatology *25*, 554-562.

Nam, S. W., Park, J. Y., Ramasamy, A., Shevade, S., Islam, A., Long, P. M., Park, C. K., Park, S. E., Kim, S. Y., Lee, S. H.*, et al.* (2005). Molecular changes from

dysplastic nodule to hepatocellular carcinoma through gene expression profiling. Hepatology (Baltimore, Md *42*, 809-818.

Narita, M., Nunez, S., Heard, E., Lin, A. W., Hearn, S. A., Spector, D. L., Hannon, G. J., and Lowe, S. W. (2003). Rb-mediated heterochromatin formation and silencing of E2F target genes during cellular senescence. Cell *113*, 703-716.

Nevins, J. R. (2001). The Rb/E2F pathway and cancer. Human molecular genetics *10*, 699-703.

Nimura, K., Ura, K., Shiratori, H., Ikawa, M., Okabe, M., Schwartz, R. J., and Kaneda, Y. (2009). A histone H3 lysine 36 trimethyltransferase links Nkx2-5 to Wolf-Hirschhorn syndrome. Nature *460*, 287-291.

Novakova, Z., Hubackova, S., Kosar, M., Janderova-Rossmeislova, L., Dobrovolna, J., Vasicova, P., Vancurova, M., Horejsi, Z., Hozak, P., Bartek, J., and Hodny, Z. (2010). Cytokine expression and signaling in drug-induced cellular senescence. Oncogene *29*, 273-284.

Oberhammer, F., Bursch, W., Parzefall, W., Breit, P., Erber, E., Stadler, M., and Schulte-Hermann, R. (1991). Effect of transforming growth factor beta on cell death of cultured rat hepatocytes. Cancer research *51*, 2478-2485.

Ohashi, S., Natsuizaka, M., Wong, G. S., Michaylira, C. Z., Grugan, K. D., Stairs, D. B., Kalabis, J., Vega, M. E., Kalman, R. A., Nakagawa, M.*, et al.* (2010). Epidermal growth factor receptor and mutant p53 expand an esophageal cellular subpopulation capable of epithelial-to-mesenchymal transition through ZEB transcription factors. Cancer research *70*, 4174-4184.

Olive, P. L., and Banath, J. P. (2006). The comet assay: a method to measure DNA damage in individual cells. Nat Protoc *1*, 23-29.

Ooi, K., Shiraki, K., Sakurai, Y., Morishita, Y., and Nobori, T. (2005). Clinical significance of abnormal lipoprotein patterns in liver diseases. International journal of molecular medicine *15*, 655-660.

Orjalo, A. V., Bhaumik, D., Gengler, B. K., Scott, G. K., and Campisi, J. (2009). Cell

surface-bound IL-1alpha is an upstream regulator of the senescence-associated IL-6/IL-8 cytokine network. Proc Natl Acad Sci U S A *106*, 17031-17036.

Osawa, H., Shitara, Y., Shoji, H., Mogi, A., Kuwano, H., Hagiwara, K., and Takenoshita, S. (2000). Mutation analysis of transforming growth factor beta type II receptor, Smad2, Smad3 and Smad4 in esophageal squamous cell carcinoma. Int J Oncol *17*, 723-728.

Osborne, N. N., Nash, M. S., and Wood, J. P. (1998). Melatonin counteracts ischemia-induced apoptosis in human retinal pigment epithelial cells. Invest Ophthalmol Vis Sci *39*, 2374-2383.

Ozturk, M. (1991). p53 mutation in hepatocellular carcinoma after aflatoxin exposure. Lancet *338*, 1356-1359.

Ozturk, M. (1999). Genetic aspects of hepatocellular carcinogenesis. Seminars in liver disease *19*, 235-242.

Ozturk, M., Arslan-Ergul, A., Bagislar, S., Senturk, S., and Yuzugullu, H. (2009). Senescence and immortality in hepatocellular carcinoma. Cancer letters *286*, 103-113.

Ozturk, N., Erdal, E., Mumcuoglu, M., Akcali, K. C., Yalcin, O., Senturk, S., Arslan-Ergul, A., Gur, B., Yulug, I., Cetin-Atalay, R.*, et al.* (2006). Reprogramming of replicative senescence in hepatocellular carcinoma-derived cells. Proc Natl Acad Sci U S A *103*, 2178-2183.

Padua, D., and Massague, J. (2009). Roles of TGFbeta in metastasis. Cell Res *19*, 89-102.

Paradis, V., Youssef, N., Dargere, D., Ba, N., Bonvoust, F., Deschatrette, J., and Bedossa, P. (2001). Replicative senescence in normal liver, chronic hepatitis C, and hepatocellular carcinomas. Hum Pathol *32*, 327-332.

Parfrey, H., Mahadeva, R., and Lomas, D. A. (2003). Alpha(1)-antitrypsin deficiency, liver disease and emphysema. The international journal of biochemistry

& cell biology *35*, 1009-1014.

Passos, J. F., and Von Zglinicki, T. (2006). Oxygen free radicals in cell senescence: are they signal transducers? Free Radic Res *40*, 1277-1283.

Peinado, H., Olmeda, D., and Cano, A. (2007). Snail, Zeb and bHLH factors in tumour progression: an alliance against the epithelial phenotype? Nat Rev Cancer *7*, 415-428.

Perlman, R., Schiemann, W. P., Brooks, M. W., Lodish, H. F., and Weinberg, R. A. (2001). TGF-beta-induced apoptosis is mediated by the adapter protein Daxx that facilitates JNK activation. Nat Cell Biol *3*, 708-714.

Picco, M., Nesci, A., Barros, G., Cavaglieri, L., and Etcheverry, M. (1999). Aflatoxin B1 and fumosin B1 in mixed cultures of Aspergillus flavus and Fusarium proliferatum on maize. Natural toxins *7*, 331-336.

Pietrangelo, A. (2009). Iron in NASH, chronic liver diseases and HCC: how much iron is too much? Journal of hepatology *50*, 249-251.

Polesel, J., Zucchetto, A., Montella, M., Dal Maso, L., Crispo, A., La Vecchia, C., Serraino, D., Franceschi, S., and Talamini, R. (2009). The impact of obesity and diabetes mellitus on the risk of hepatocellular carcinoma. Ann Oncol *20*, 353-357.

Polyak, K., Lee, M. H., Erdjument-Bromage, H., Koff, A., Roberts, J. M., Tempst, P., and Massague, J. (1994). Cloning of p27Kip1, a cyclin-dependent kinase inhibitor and a potential mediator of extracellular antimitogenic signals. Cell *78*, 59-66.

Postigo, A. A. (2003). Opposing functions of ZEB proteins in the regulation of the TGFbeta/BMP signaling pathway. EMBO J *22*, 2443-2452.

Postigo, A. A., Depp, J. L., Taylor, J. J., and Kroll, K. L. (2003). Regulation of Smad signaling through a differential recruitment of coactivators and corepressors by ZEB proteins. EMBO J *22*, 2453-2462.

Powell, S. M., Harper, J. C., Hamilton, S. R., Robinson, C. R., and Cummings, O. W. (1997). Inactivation of Smad4 in gastric carcinomas. Cancer research *57*, 4221-4224.

Pritchard, K. A., Jr., Ackerman, A. W., Gross, E. R., Stepp, D. W., Shi, Y., Fontana, J. T., Baker, J. E., and Sessa, W. C. (2001). Heat shock protein 90 mediates the balance of nitric oxide and superoxide anion from endothelial nitric-oxide synthase. The Journal of biological chemistry *276*, 17621-17624.

Puisieux, A., Galvin, K., Troalen, F., Bressac, B., Marcais, C., Galun, E., Ponchel, F., Yakicier, C., Ji, J., and Ozturk, M. (1993). Retinoblastoma and p53 tumor suppressor genes in human hepatoma cell lines. FASEB J *7*, 1407-1413.

Puisieux, A., Lim, S., Groopman, J., and Ozturk, M. (1991). Selective targeting of p53 gene mutational hotspots in human cancers by etiologically defined carcinogens. Cancer research *51*, 6185-6189.

Qin, G., Su, J., Ning, Y., Duan, X., Luo, D., and Lotlikar, P. D. (1997). p53 protein expression in patients with hepatocellular carcinoma from the high incidence area of Guangxi, Southern China. Cancer letters *121*, 203-210.

Rai, P., Onder, T. T., Young, J. J., McFaline, J. L., Pang, B., Dedon, P. C., and Weinberg, R. A. (2009). Continuous elimination of oxidized nucleotides is necessary to prevent rapid onset of cellular senescence. Proc Natl Acad Sci U S A *106*, 169-174.

Raoul, J. L. (2008). Natural history of hepatocellular carcinoma and current treatment options. Seminars in nuclear medicine *38*, S13-18.

Ray, R. B., Steele, R., Meyer, K., and Ray, R. (1997). Transcriptional repression of p53 promoter by hepatitis C virus core protein. The Journal of biological chemistry *272*, 10983-10986.

Reaper, P. M., di Fagagna, F., and Jackson, S. P. (2004). Activation of the DNA damage response by telomere attrition: a passage to cellular senescence. Cell Cycle *3*, 543-546.

Rehermann, B., and Nascimbeni, M. (2005). Immunology of hepatitis B virus and hepatitis C virus infection. Nat Rev Immunol *5*, 215-229.

Reimann, M., Lee, S., Loddenkemper, C., Dorr, J. R., Tabor, V., Aichele, P., Stein,

H., Dorken, B., Jenuwein, T., and Schmitt, C. A. (2010). Tumor stroma-derived TGF-beta limits myc-driven lymphomagenesis via Suv39h1-dependent senescence. Cancer cell *17*, 262-272.

Rich, J. N., Zhang, M., Datto, M. B., Bigner, D. D., and Wang, X. F. (1999). Transforming growth factor-beta-mediated p15(INK4B) induction and growth inhibition in astrocytes is SMAD3-dependent and a pathway prominently altered in human glioma cell lines. The Journal of biological chemistry *274*, 35053-35058.

Ritsick, D. R., Edens, W. A., McCoy, J. W., and Lambeth, J. D. (2004). The use of model systems to study biological functions of Nox/Duox enzymes. Biochem Soc Symp, 85-96.

Robson, C. N., Gnanapragasam, V., Byrne, R. L., Collins, A. T., and Neal, D. E. (1999). Transforming growth factor-beta1 up-regulates p15, p21 and p27 and blocks cell cycling in G1 in human prostate epithelium. J Endocrinol *160*, 257-266.

Roncalli, M., Bianchi, P., Bruni, B., Laghi, L., Destro, A., Di Gioia, S., Gennari, L., Tommasini, M., Malesci, A., and Coggi, G. (2002). Methylation framework of cell cycle gene inhibitors in cirrhosis and associated hepatocellular carcinoma. Hepatology (Baltimore, Md *36*, 427-432.

Sabisz, M., and Skladanowski, A. (2009). Cancer stem cells and escape from drug-induced premature senescence in human lung tumor cells: implications for drug resistance and in vitro drug screening models. Cell Cycle *8*, 3208-3217.

Sacco, R., Leuci, D., Tortorella, C., Fiore, G., Marinosci, F., Schiraldi, O., and Antonaci, S. (2000). Transforming growth factor beta1 and soluble Fas serum levels in hepatocellular carcinoma. Cytokine *12*, 811-814.

Sanchez, A., Alvarez, A. M., Benito, M., and Fabregat, I. (1996). Apoptosis induced by transforming growth factor-beta in fetal hepatocyte primary cultures: involvement of reactive oxygen intermediates. J Biol Chem *271*, 7416-7422.

Sandler, M. A., Zhang, J. N., Westerhausen, D. R., Jr., and Billadello, J. J. (1994). A novel protein interacts with the major transforming growth factor-beta responsive

element in the plasminogen activator inhibitor type-1 gene. J Biol Chem *269*, 21500-21504.

Sawitza, I., Kordes, C., Reister, S., and Haussinger, D. (2009). The niche of stellate cells within rat liver. Hepatology (Baltimore, Md *50*, 1617-1624.

Sayan, A. E., Griffiths, T. R., Pal, R., Browne, G. J., Ruddick, A., Yagci, T., Edwards, R., Mayer, N. J., Qazi, H., Goyal, S.*, et al.* (2009). SIP1 protein protects cells from DNA damage-induced apoptosis and has independent prognostic value in bladder cancer. Proc Natl Acad Sci U S A *106*, 14884-14889.

Sayan, B. S., Ince, G., Sayan, A. E., and Ozturk, M. (2001). NAPO as a novel marker for apoptosis. J Cell Biol *155*, 719-724.

Schilder, Y. D., Heiss, E. H., Schachner, D., Ziegler, J., Reznicek, G., Sorescu, D., and Dirsch, V. M. (2009). NADPH oxidases 1 and 4 mediate cellular senescence induced by resveratrol in human endothelial cells. Free Radic Biol Med *46*, 1598-1606.

Schilsky, M. L. (2009). Wilson disease: current status and the future. Biochimie *91*, 1278-1281.

Schlaeger, C., Longerich, T., Schiller, C., Bewerunge, P., Mehrabi, A., Toedt, G., Kleeff, J., Ehemann, V., Eils, R., Lichter, P.*, et al.* (2008). Etiology-dependent molecular mechanisms in human hepatocarcinogenesis. Hepatology (Baltimore, Md *47*, 511-520.

Sekimoto, G., Matsuzaki, K., Yoshida, K., Mori, S., Murata, M., Seki, T., Matsui, H., Fujisawa, J., and Okazaki, K. (2007). Reversible Smad-dependent signaling between tumor suppression and oncogenesis. Cancer research *67*, 5090-5096.

Senturk, S., Mumcuoglu, M., Gursoy-Yuzugullu, O., Cingoz, B., Akcali, K. C., and Ozturk, M. (2010). Transforming growth factor-beta induces senescence in hepatocellular carcinoma cells and inhibits tumor growth. Hepatology (Baltimore, Md.

Seoane, J., Pouponnot, C., Staller, P., Schader, M., Eilers, M., and Massague, J.

(2001). TGFbeta influences Myc, Miz-1 and Smad to control the CDK inhibitor p15INK4b. Nat Cell Biol *3*, 400-408.

Serrano, M., Lin, A. W., McCurrach, M. E., Beach, D., and Lowe, S. W. (1997). Oncogenic ras provokes premature cell senescence associated with accumulation of p53 and p16INK4a. Cell *88*, 593-602.

Sheahan, S., Bellamy, C. O., Harland, S. N., Harrison, D. J., and Prost, S. (2008). TGFbeta induces apoptosis and EMT in primary mouse hepatocytes independently of p53, p21Cip1 or Rb status. BMC Cancer *8*, 191.

Sherr, C. J., and McCormick, F. (2002). The RB and p53 pathways in cancer. Cancer cell *2*, 103-112.

Shi, Y., and Massague, J. (2003). Mechanisms of TGF-beta signaling from cell membrane to the nucleus. Cell *113*, 685-700.

Shi, Y., Wang, Y. F., Jayaraman, L., Yang, H., Massague, J., and Pavletich, N. P. (1998). Crystal structure of a Smad MH1 domain bound to DNA: insights on DNA binding in TGF-beta signaling. Cell *94*, 585-594.

Song, K., Wang, H., Krebs, T. L., and Danielpour, D. (2006). Novel roles of Akt and mTOR in suppressing TGF-beta/ALK5-mediated Smad3 activation. EMBO J *25*, 58-69.

Spender, L. C., O'Brien, D. I., Simpson, D., Dutt, D., Gregory, C. D., Allday, M. J., Clark, L. J., and Inman, G. J. (2009). TGF-beta induces apoptosis in human B cells by transcriptional regulation of BIK and BCL-XL. Cell Death Differ *16*, 593-602.

Stein, G. H. (1985). SV40-transformed human fibroblasts: evidence for cellular aging in pre-crisis cells. J Cell Physiol *125*, 36-44.

Sturrock, A., Cahill, B., Norman, K., Huecksteadt, T. P., Hill, K., Sanders, K., Karwande, S. V., Stringham, J. C., Bull, D. A., Gleich, M.*, et al.* (2006). Transforming growth factor-beta1 induces Nox4 NAD(P)H oxidase and reactive oxygen species-dependent proliferation in human pulmonary artery smooth muscle

cells. Am J Physiol Lung Cell Mol Physiol *290*, L661-L673.

Sugano, Y., Matsuzaki, K., Tahashi, Y., Furukawa, F., Mori, S., Yamagata, H., Yoshida, K., Matsushita, M., Nishizawa, M., Fujisawa, J., and Inoue, K. (2003). Distortion of autocrine transforming growth factor beta signal accelerates malignant potential by enhancing cell growth as well as PAI-1 and VEGF production in human hepatocellular carcinoma cells. Oncogene *22*, 2309-2321.

Sun, P. D., and Davies, D. R. (1995). The cystine-knot growth-factor superfamily. Annu Rev Biophys Biomol Struct *24*, 269-291.

Takahashi, A., Ohtani, N., Yamakoshi, K., Iida, S., Tahara, H., Nakayama, K., Nakayama, K. I., Ide, T., Saya, H., and Hara, E. (2006). Mitogenic signalling and the p16INK4a-Rb pathway cooperate to enforce irreversible cellular senescence. Nat Cell Biol *8*, 1291-1297.

Tanaka, T., Iwasa, Y., Kondo, S., Hiai, H., and Toyokuni, S. (1999). High incidence of allelic loss on chromosome 5 and inactivation of p15INK4B and p16INK4A tumor suppressor genes in oxystress-induced renal cell carcinoma of rats. Oncogene *18*, 3793-3797.

Tannapfel, A., Busse, C., Weinans, L., Benicke, M., Katalinic, A., Geissler, F., Hauss, J., and Wittekind, C. (2001). INK4a-ARF alterations and p53 mutations in hepatocellular carcinomas. Oncogene *20*, 7104-7109.

ten Dijke, P., Miyazono, K., and Heldin, C. H. (2000). Signaling inputs converge on nuclear effectors in TGF-beta signaling. Trends Biochem Sci *25*, 64-70.

Thorgeirsson, S. S., and Grisham, J. W. (2002). Molecular pathogenesis of human hepatocellular carcinoma. Nature genetics *31*, 339-346.

Thuault, S., Valcourt, U., Petersen, M., Manfioletti, G., Heldin, C. H., and Moustakas, A. (2006). Transforming growth factor-beta employs HMGA2 to elicit epithelial-mesenchymal transition. J Cell Biol *174*, 175-183.

Tischendorf, J. J., and Schirin-Sokhan, R. (2009). Primary sclerosing cholangitis:

The importance of treating stenoses and infections. Nature reviews *6*, 691-692.

Trumpp, A., and Wiestler, O. D. (2008). Mechanisms of Disease: cancer stem cells--targeting the evil twin. Nat Clin Pract Oncol *5*, 337-347.

Tsai, W. L., and Chung, R. T. (2010). Viral hepatocarcinogenesis. Oncogene *29*, 2309-2324.

Van Obberghen-Schilling, E., Roche, N. S., Flanders, K. C., Sporn, M. B., and Roberts, A. B. (1988). Transforming growth factor beta 1 positively regulates its own expression in normal and transformed cells. The Journal of biological chemistry *263*, 7741-7746.

Vandewalle, C., Comijn, J., De Craene, B., Vermassen, P., Bruyneel, E., Andersen, H., Tulchinsky, E., Van Roy, F., and Berx, G. (2005). SIP1/ZEB2 induces EMT by repressing genes of different epithelial cell-cell junctions. Nucleic Acids Res *33*, 6566-6578.

Vassilev, L. T., Vu, B. T., Graves, B., Carvajal, D., Podlaski, F., Filipovic, Z., Kong, N., Kammlott, U., Lukacs, C., Klein, C.*, et al.* (2004). In vivo activation of the p53 pathway by small-molecule antagonists of MDM2. Science (New York, NY *303*, 844-848.

Ventura, A., Kirsch, D. G., McLaughlin, M. E., Tuveson, D. A., Grimm, J., Lintault, L., Newman, J., Reczek, E. E., Weissleder, R., and Jacks, T. (2007). Restoration of p53 function leads to tumour regression in vivo. Nature *445*, 661-665.

Vignais, P. V. (2002). The superoxide-generating NADPH oxidase: structural aspects and activation mechanism. Cell Mol Life Sci *59*, 1428-1459.

Vijayachandra, K., Higgins, W., Lee, J., and Glick, A. (2009). Induction of p16ink4a and p19ARF by TGFbeta1 contributes to growth arrest and senescence response in mouse keratinocytes. Mol Carcinog *48*, 181-186.

Vincent, A., and Van Seuningen, I. (2009). Epigenetics, stem cells and epithelial cell fate. Differentiation *78*, 99-107.

von Zglinicki, T. (2002). Oxidative stress shortens telomeres. Trends Biochem Sci *27*, 339-344.

Wang, G., Matsuura, I., He, D., and Liu, F. (2009). Transforming growth factor-{beta}-inducible phosphorylation of Smad3. The Journal of biological chemistry *284*, 9663-9673.

Weinberg, R. A. (2008). Twisted epithelial-mesenchymal transition blocks senescence. Nat Cell Biol *10*, 1021-1023.

Wiegman, E. M., Blaese, M. A., Loeffler, H., Coppes, R. P., and Rodemann, H. P. (2007). TGFbeta-1 dependent fast stimulation of ATM and p53 phosphorylation following exposure to ionizing radiation does not involve TGFbeta-receptor I signalling. Radiother Oncol *83*, 289-295.

Wiemann, S. U., Satyanarayana, A., Tsahuridu, M., Tillmann, H. L., Zender, L., Klempnauer, J., Flemming, P., Franco, S., Blasco, M. A., Manns, M. P., and Rudolph, K. L. (2002). Hepatocyte telomere shortening and senescence are general markers of human liver cirrhosis. FASEB J *16*, 935-942.

Wrana, J. L., Attisano, L., Carcamo, J., Zentella, A., Doody, J., Laiho, M., Wang, X. F., and Massague, J. (1992). TGF beta signals through a heteromeric protein kinase receptor complex. Cell *71*, 1003-1014.

Wu, C. H., van Riggelen, J., Yetil, A., Fan, A. C., Bachireddy, P., and Felsher, D. W. (2007). Cellular senescence is an important mechanism of tumor regression upon c-Myc inactivation. Proc Natl Acad Sci U S A *104*, 13028-13033.

Wu, D., and Cederbaum, A. I. (2003). Alcohol, oxidative stress, and free radical damage. Alcohol Res Health *27*, 277-284.

Wu, D., Zhai, Q., and Shi, X. (2006). Alcohol-induced oxidative stress and cell responses. Journal of gastroenterology and hepatology *21 Suppl 3*, S26-29.

Wu, G., Chen, Y. G., Ozdamar, B., Gyuricza, C. A., Chong, P. A., Wrana, J. L., Massague, J., and Shi, Y. (2000). Structural basis of Smad2 recognition by the Smad

anchor for receptor activation. Science (New York, NY *287*, 92-97.

Wurmbach, E., Chen, Y. B., Khitrov, G., Zhang, W., Roayaie, S., Schwartz, M., Fiel, I., Thung, S., Mazzaferro, V., Bruix, J., *et al.* (2007). Genome-wide molecular profiles of HCV-induced dysplasia and hepatocellular carcinoma. Hepatology *45*, 938-947.

Xiao, Z., Latek, R., and Lodish, H. F. (2003). An extended bipartite nuclear localization signal in Smad4 is required for its nuclear import and transcriptional activity. Oncogene *22*, 1057-1069.

Xiao, Z., Liu, X., Henis, Y. I., and Lodish, H. F. (2000). A distinct nuclear localization signal in the N terminus of Smad 3 determines its ligand-induced nuclear translocation. Proc Natl Acad Sci U S A *97*, 7853-7858.

Xu, B. J., Yan, W., Jovanovic, B., An, A. Q., Cheng, N., Aakre, M. E., Yi, Y., Eng, J., Link, A. J., and Moses, H. L. (2010). Quantitative analysis of the secretome of TGF-beta signaling-deficient mammary fibroblasts. Proteomics.

Xu, J., Lamouille, S., and Derynck, R. (2009). TGF-beta-induced epithelial to mesenchymal transition. Cell Res *19*, 156-172.

Xu, M., Yu, Q., Subrahmanyam, R., Difilippantonio, M. J., Ried, T., and Sen, J. M. (2008). Beta-catenin expression results in p53-independent DNA damage and oncogene-induced senescence in prelymphomagenic thymocytes in vivo. Mol Cell Biol *28*, 1713-1723.

Xue, W., Zender, L., Miething, C., Dickins, R. A., Hernando, E., Krizhanovsky, V., Cordon-Cardo, C., and Lowe, S. W. (2007). Senescence and tumour clearance is triggered by p53 restoration in murine liver carcinomas. Nature *445*, 656-660.

Yakicier, M. C., Irmak, M. B., Romano, A., Kew, M., and Ozturk, M. (1999). Smad2 and Smad4 gene mutations in hepatocellular carcinoma. Oncogene *18*, 4879-4883.

Yam, J. W., Wong, C. M., and Ng, I. O. (2010). Molecular and functional genetics of hepatocellular carcinoma. Front Biosci (Schol Ed) *2*, 117-134.

Yamashita, T., Ji, J., Budhu, A., Forgues, M., Yang, W., Wang, H. Y., Jia, H., Ye, Q., Qin, L. X., Wauthier, E.*, et al.* (2009). EpCAM-positive hepatocellular carcinoma cells are tumor-initiating cells with stem/progenitor cell features. Gastroenterology *136*, 1012-1024.

Yang, M. H., Chen, C. L., Chau, G. Y., Chiou, S. H., Su, C. W., Chou, T. Y., Peng, W. L., and Wu, J. C. (2009). Comprehensive analysis of the independent effect of twist and snail in promoting metastasis of hepatocellular carcinoma. Hepatology (Baltimore, Md *50*, 1464-1474.

Yoon, Y. S., Lee, J. H., Hwang, S. C., Choi, K. S., and Yoon, G. (2005). TGF beta1 induces prolonged mitochondrial ROS generation through decreased complex IV activity with senescent arrest in Mv1Lu cells. Oncogene *24*, 1895-1903.

You, H., Ding, W., and Rountree, C. B. (2010). Epigenetic regulation of cancer stem cell marker CD133 by transforming growth factor-beta. Hepatology (Baltimore, Md *51*, 1635-1644.

Yuzugullu, H., Benhaj, K., Ozturk, N., Senturk, S., Celik, E., Toylu, A., Tasdemir, N., Yilmaz, M., Erdal, E., Akcali, K. C.*, et al.* (2009). Canonical Wnt signaling is antagonized by noncanonical Wnt5a in hepatocellular carcinoma cells. Mol Cancer *8*, 90.

Zavadil, J., and Bottinger, E. P. (2005). TGF-beta and epithelial-to-mesenchymal transitions. Oncogene *24*, 5764-5774.

Zawel, L., Dai, J. L., Buckhaults, P., Zhou, S., Kinzler, K. W., Vogelstein, B., and Kern, S. E. (1998). Human Smad3 and Smad4 are sequence-specific transcription activators. Mol Cell *1*, 611-617.

Zhang, H. S., Postigo, A. A., and Dean, D. C. (1999). Active transcriptional repression by the Rb-E2F complex mediates G1 arrest triggered by p16INK4a, TGFbeta, and contact inhibition. Cell *97*, 53-61.

Zhang, S., Ekman, M., Thakur, N., Bu, S., Davoodpour, P., Grimsby, S., Tagami, S., Heldin, C. H., and Landstrom, M. (2006a). TGFbeta1-induced activation of ATM

and p53 mediates apoptosis in a Smad7-dependent manner. Cell Cycle *5*, 2787-2795.

Zhang, X., Zhang, H., and Ye, L. (2006b). Effects of hepatitis B virus X protein on the development of liver cancer. The Journal of laboratory and clinical medicine *147*, 58-66.

Zimonjic, D. B., Zhou, X., Lee, J. S., Ullmannova-Benson, V., Tripathi, V., Thorgeirsson, S. S., and Popescu, N. C. (2009). Acquired genetic and functional alterations associated with transforming growth factor beta type I resistance in Hep3B human hepatocellular carcinoma cell line. J Cell Mol Med.

Zuckerman, A. J. (1999). More than third of world's population has been infected with hepatitis B virus. BMJ (Clinical research ed *318*, 1213.

APPENDIX

Permissions for reuse Figure 1.1 and Figure 1.2

NATURE PUBLISHING GROUP LICENSE TERMS AND CONDITIONS

Aug 04, 2010

This is a License Agreement between Serif Senturk ("You") and Nature Publishing Group ("Nature Publishing Group") provided by Copyright Clearance Center ("CCC"). The license consists of your order details, the terms and conditions provided by Nature Publishing Group, and the payment terms and conditions.

All payments must be made in full to CCC. For payment instructions, please see information listed at the bottom of this form.

License Number	2482090804000
License date	Aug 04, 2010
Licensed content publisher	Nature Publishing Group
Licensed content publication	Nature Reviews Cancer
Licensed content title	Hepatocellular carcinoma pathogenesis: from genes to environment
Licensed content author	Paraskevi A. Farazi, Ronald A. DePinho
Volume number	
Issue number	
Pages	
Year of publication	2006
Portion used	Figures / tables
Number of figures / tables	2
Requestor type	Student
Type of Use	Thesis / Dissertation

Permissions for reuse Figure 1.3

NATURE PUBLISHING GROUP LICENSE TERMS AND CONDITIONS

Aug 04, 2010

This is a License Agreement between Serif Senturk ("You") and Nature Publishing Group ("Nature Publishing Group") provided by Copyright Clearance Center ("CCC"). The license consists of your order details, the terms and conditions provided by Nature Publishing Group, and the payment terms and conditions.

All payments must be made in full to CCC. For payment instructions, please see information listed at the bottom of this form.

License Number	2482091052427
License date	Aug 04, 2010
Licensed content publisher	Nature Publishing Group
Licensed content publication	Oncogene
Licensed content title	Viral hepatocarcinogenesis
Licensed content author	W-L Tsai, R T Chung
Volume number	
Issue number	
Pages	
Year of publication	2010
Portion used	Figures / tables
Number of figures / tables	1
Requestor type	Student
Type of Use	Thesis / Dissertation
High-res requested	No

Permissions for reuse Figure 1.4

ELSEVIER LICENSE
TERMS AND CONDITIONS

Aug 04, 2010

This is a License Agreement between Serif Senturk ("You") and Elsevier ("Elsevier") provided by Copyright Clearance Center ("CCC"). The license consists of your order details, the terms and conditions provided by Elsevier, and the payment terms and conditions.

All payments must be made in full to CCC. For payment instructions, please see information listed at the bottom of this form.

Supplier	Elsevier Limited The Boulevard,Langford Lane Kidlington,Oxford,OX5 1GB,UK
Registered Company Number	1982084
Customer name	Serif Senturk
Customer address	Bilkent University Sci. B 2nd Floor
	Ankara, other 06800
License number	2482091344189
License date	Aug 04, 2010
Licensed content publisher	Elsevier
Licensed content publication	The International Journal of Biochemistry & Cell Biology
Licensed content title	The signals and pathways activating cellular senescence
Licensed content author	Ittai Ben-Porath, Robert A. Weinberg
Licensed content date	May 2005
Licensed content volume number	37
Licensed content issue number	5
Number of pages	16
Type of Use	reuse in a thesis/dissertation
Requestor type	Not specified
Intended publisher of new work	n/a
Portion	figures/tables/illustrations
Number of figures/tables/illustrations	1
Format	both print and electronic

Permissions for reuse Figure 1.5 and Figure 4.1

ELSEVIER LICENSE
TERMS AND CONDITIONS

Aug 05, 201

This is a License Agreement between Serif Senturk ("You") and Elsevier ("Elsevier") provided by Copyright Clearance Center ("CCC"). The license consists of your order detail the terms and conditions provided by Elsevier, and the payment terms and conditions.

All payments must be made in full to CCC. For payment instructions, please see information listed at the bottom of this form.

Supplier	Elsevier Limited The Boulevard,Langford Lane Kidlington,Oxford,OX5 1GB,UK
Registered Company Number	1982084
Customer name	Serif Senturk
Customer address	Bilkent University Sci. B 2nd Floor
	Ankara, other 06800
License number	2482450670981
License date	Aug 05, 2010
Licensed content publisher	Elsevier
Licensed content publication	Cancer Letters
Licensed content title	Senescence and immortality in hepatocellular carcinoma
Licensed content author	Mehmet Ozturk, Ayca Arslan-Ergul, Sevgi Bagislar, Serif Senturk, Haluk Yuzugullu
Licensed content date	1 December 2009
Licensed content volume number	286
Licensed content issue number	1
Number of pages	11
Type of Use	reuse in a thesis/dissertation
Requestor type	Not specified
Intended publisher of new work	n/a
Portion	figures/tables/illustrations
Number of figures/tables/illustrations	2
Format	both print and electronic

Permissions for reuse Figure 1.6

NATURE PUBLISHING GROUP LICENSE
TERMS AND CONDITIONS

Aug 04, 2010

This is a License Agreement between Serif Senturk ("You") and Nature Publishing Group ("Nature Publishing Group") provided by Copyright Clearance Center ("CCC"). The license consists of your order details, the terms and conditions provided by Nature Publishing Group, and the payment terms and conditions.

All payments must be made in full to CCC. For payment instructions, please see information listed at the bottom of this form.

License Number	2482100080446
License date	Aug 04, 2010
Licensed content publisher	Nature Publishing Group
Licensed content publication	Nature Reviews Cancer
Licensed content title	Living on a break: cellular senescence as a DNA-damage response
Licensed content author	Fabrizio d'Adda di Fagagna
Volume number	
Issue number	
Pages	
Year of publication	2008
Portion used	Figures / tables
Number of figures / tables	1
Requestor type	Student
Type of Use	Thesis / Dissertation

Permissions for reuse Figure 1.7

NATURE PUBLISHING GROUP LICENSE TERMS AND CONDITIONS

Aug 04, 2010

This is a License Agreement between Serif Senturk ("You") and Nature Publishing Group ("Nature Publishing Group") provided by Copyright Clearance Center ("CCC"). The license consists of your order details, the terms and conditions provided by Nature Publishing Group, and the payment terms and conditions.

All payments must be made in full to CCC. For payment instructions, please see information listed at the bottom of this form.

License Number	2482100452373
License date	Aug 04, 2010
Licensed content publisher	Nature Publishing Group
Licensed content publication	Nature Reviews Molecular Cell Biology
Licensed content title	Regulation of the *INK4b–ARF–INK4a* tumour suppressor locus: all for one or one for all
Licensed content author	Jesús Gil, Gordon Peters
Volume number	
Issue number	
Pages	
Year of publication	2006
Portion used	Figures / tables
Number of figures / tables	1
Requestor type	Student
Type of Use	Thesis / Dissertation

Permissions for reuse Figure 1.8

ELSEVIER LICENSE TERMS AND CONDITIONS

Aug 04, 2010

This is a License Agreement between Serif Senturk ("You") and Elsevier ("Elsevier") provided by Copyright Clearance Center ("CCC"). The license consists of your order details, the terms and conditions provided by Elsevier, and the payment terms and conditions.

All payments must be made in full to CCC. For payment instructions, please see information listed at the bottom of this form.

Supplier	Elsevier Limited The Boulevard,Langford Lane Kidlington,Oxford,OX5 1GB,UK
Registered Company Number	1982084
Customer name	Serif Senturk
Customer address	Bilkent University Sci. B 2nd Floor Ankara, other 06800
License number	2482101141775
License date	Aug 04, 2010
Licensed content publisher	Elsevier
Licensed content publication	Cell
Licensed content title	Mechanisms of TGF-β Signaling from Cell Membrane to the Nucleus
Licensed content author	Yigong Shi, Joan Massagué
Licensed content date	13 June 2003
Licensed content volume number	113
Licensed content issue number	6
Number of pages	16
Type of Use	reuse in a thesis/dissertation

Permissions for reuse Figure 1.9

NATURE PUBLISHING GROUP LICENSE TERMS AND CONDITIONS

Aug 04, 2010

This is a License Agreement between Serif Senturk ("You") and Nature Publishing Group ("Nature Publishing Group") provided by Copyright Clearance Center ("CCC"). The license consists of your order details, the terms and conditions provided by Nature Publishing Group, and the payment terms and conditions.

All payments must be made in full to CCC. For payment instructions, please see information listed at the bottom of this form.

License Number	2482101352665
License date	Aug 04, 2010
Licensed content publisher	Nature Publishing Group
Licensed content publication	Nature
Licensed content title	Smad-dependent and Smad-independent pathways in TGF-β family signalling
Licensed content author	Rik Derynck, Ying E. Zhang
Volume number	
Issue number	
Pages	
Year of publication	2003
Portion used	Figures / tables
Number of figures / tables	1
Requestor type	Student
Type of Use	Thesis / Dissertation

Permissions for reuse Figure 1.10

NATURE PUBLISHING GROUP LICENSE TERMS AND CONDITIONS

Aug 04, 2010

This is a License Agreement between Serif Senturk ("You") and Nature Publishing Group ("Nature Publishing Group") provided by Copyright Clearance Center ("CCC"). The license consists of your order details, the terms and conditions provided by Nature Publishing Group, and the payment terms and conditions.

All payments must be made in full to CCC. For payment instructions, please see information listed at the bottom of this form.

License Number	2482110006446
License date	Aug 04, 2010
Licensed content publisher	Nature Publishing Group
Licensed content publication	Cell Research
Licensed content title	Nucleocytoplasmic shuttling of Smad proteins
Licensed content author	Caroline S Hill
Volume number	
Issue number	
Pages	
Year of publication	2008
Portion used	Figures / tables
Number of figures / tables	1
Requestor type	Student
Type of Use	Thesis / Dissertation

Permissions for reuse Figure 1.11

NATURE PUBLISHING GROUP LICENSE
TERMS AND CONDITIONS

Aug 04, 2010

This is a License Agreement between Serif Senturk ("You") and Nature Publishing Group ("Nature Publishing Group") provided by Copyright Clearance Center ("CCC"). The license consists of your order details, the terms and conditions provided by Nature Publishing Group, and the payment terms and conditions.

All payments must be made in full to CCC. For payment instructions, please see information listed at the bottom of this form.

License Number	2482110530071
License date	Aug 04, 2010
Licensed content publisher	Nature Publishing Group
Licensed content publication	Cell Research
Licensed content title	TGF-β-induced epithelial to mesenchymal transition
Licensed content author	Jian Xu, Samy Lamouille, Rik Derynck
Volume number	
Issue number	
Pages	
Year of publication	2009
Portion used	Figures / tables
Number of figures / tables	1
Requestor type	Student
Type of Use	Thesis / Dissertation

Permissions for reuse Table 1.1 and Table 1.2

NATURE PUBLISHING GROUP LICENSE
TERMS AND CONDITIONS

Aug 04, 2010

This is a License Agreement between Serif Senturk ("You") and Nature Publishing Group ("Nature Publishing Group") provided by Copyright Clearance Center ("CCC"). The license consists of your order details, the terms and conditions provided by Nature Publishing Group, and the payment terms and conditions.

All payments must be made in full to CCC. For payment instructions, please see information listed at the bottom of this form.

License Number	2482110675353
License date	Aug 04, 2010
Licensed content publisher	Nature Publishing Group
Licensed content publication	Nature Reviews Immunology
Licensed content title	NOX enzymes and the biology of reactive oxygen
Licensed content author	J. David Lambeth
Volume number	
Issue number	
Pages	
Year of publication	2004
Portion used	Figures / tables
Number of figures / tables	1
Requestor type	Student
Type of Use	Thesis / Dissertation

Journal Publications

1. **Senturk S.**, Mumcuoglu M., Gursoy-Yuzugullu O., Cingoz B., Akcali KC., Ozturk M. Transforming Growth Factor-Beta Induces Senescence Arrest in Hepatocellular Carcinoma Cells and Inhibits Tumor Growth. ***Hepatology,*** DOI: 10.1002/hep.23769; *available online,* 2010

2. Buentempo F., Ersahin T., Missiroli S., **Senturk S.**, Etro D., Ozturk M., Capitani S., Cetin-Atalay R., Neri LM. Inhibition of Akt signaling in hepatoma cells induces apoptotic cell death independent of Akt activation status. ***Investigational New Drugs,*** DOI: 10.1007/s10637-010-9486-3; *available online,* 2010

3. Mumcuoglu M., Bagislar S., Yuzugullu H., Alotaibi H., **Senturk S.**, Telkoparan P., Gur-Dedeoglu B., Cingoz B., Bozkurt B., Tazebay U., Yulug IG., Akcali KC., Ozturk M. The ability to generate senescent progeny as a mechanism underlying breast cancer cell heterogeneity. ***PLoS ONE,*** 5(6) e11288, 2010

4. Yuzugullu H., Benhaj K., Ozturk N., **Senturk S.**, Celik E., Toylu A., Tasdemir N., Yilmaz M., Erdal E., Akcali KC., Atabey N., and Ozturk M. Canonical Wnt signaling is antagonized by noncanonical Wnt5a in hepatocellular carcinoma cells. ***Molecular Cancer*****,** 8(1):90, 2009

5. Ozturk M., Arslan-Ergul A., Bagislar S., **Senturk S.**, Yuzugullu H. Senescence and Immortality in Hepatocellular Carcinoma. ***Cancer Letters,*** 286(1):103-113, 2009

6. Ozturk N., Erdal E., Mumcuoglu M, Akcali KC., Yalcin O., **Senturk S.**, Arslan-Ergul A., Gur B., Yulug I., Cetin-Atalay R., Yakicier C., Yagci T., Tez M., and Ozturk M. Reprogramming of replicative senescence in hepatocellular carcinoma-derived cells. ***Proceedings of National Academy of Sciences USA,*** 103:2178-2183, 2006.

Transforming Growth Factor-Beta Induces Senescence in Hepatocellular Carcinoma Cells and Inhibits Tumor Growth

Serif Senturk,[1] Mine Mumcuoglu,[1] Ozge Gursoy-Yuzugullu,[1,2] Burcu Cingoz,[1] Kamil Can Akcali,[1] and Mehmet Ozturk[1,2]

Senescence induction could be used as an effective treatment for hepatocellular carcinoma (HCC). However, major senescence inducers (p53 and $p16^{Ink4a}$) are frequently inactivated in these cancers. We tested whether transforming growth factor-β (TGF-β) could serve as a potential senescence inducer in HCC. First, we screened for HCC cell lines with intact TGF-β signaling that leads to small mothers against decapentaplegic (Smad)-targeted gene activation. Five cell lines met this condition, and all of them displayed a strong senescence response to TGF-β1 (1-5 ng/mL) treatment. Upon treatment, c-myc was down-regulated, $p21^{Cip1}$ and $p15^{Ink4b}$ were up-regulated, and cells were arrested at G_1. The expression of $p16^{Ink4a}$ was not induced, and the senescence response was independent of p53 status. A short exposure of less than 1 minute was sufficient for a robust senescence response. Forced expression of $p21^{Cip1}$ and $p15^{Ink4b}$ recapitulated TGF-β1 effects. Senescence response was associated with reduced nicotinamide adenine dinucleotide phosphate oxidase 4 (Nox4) induction and intracellular reactive oxygen species (ROS) accumulation. The treatment of cells with the ROS scavenger *N*-acetyl-L-cysteine, or silencing of the *NOX4* gene, rescued $p21^{Cip1}$ and $p15^{Ink4b}$ accumulation as well as the growth arrest in response to TGF-β. Human HCC tumors raised in immunodeficient mice also displayed TGF-β1–induced senescence. More importantly, peritumoral injection of TGF-β1 (2 ng) at 4-day intervals reduced tumor growth by more than 75%. In contrast, the deletion of TGF-β receptor 2 abolished *in vitro* senescence response and greatly accelerated *in vivo* tumor growth. *Conclusion:* TGF-β induces p53-independent and $p16^{Ink4a}$-independent, but Nox4-dependent, $p21^{Cip1}$-dependent, $p15^{Ink4b}$-dependent, and ROS-dependent senescence arrest in well-differentiated HCC cells. Moreover, TGF-β–induced senescence *in vivo* is associated with a strong antitumor response against HCC. (HEPATOLOGY 2010;00:000-000)

Cellular senescence is a permanent withdrawal from the cell cycle in response to diverse stress conditions such as dysfunctional telomeres, DNA damage, strong mitotic signals, and disrupted chromatin. Senescence is considered to be a major cause of aging, but also a strong anticancer mechanism.[1] The relevance of senescence in chronic liver diseases is poorly known, but it may play a central role. Hepatocyte telomeres undergo shortening during chronic liver disease progression,[2] and this is accompanied by a progressive decline of hepatocyte proliferation.[3] Senescence-associated β-galactosidase (SA-β-Gal)-positive cells have been detected in 3%-7% of normal liver, 50% of chronic hepatitis, 70%-100% of cirrhosis, and up to 60% of hepatocellular carcinoma (HCC) tissues.[2,4-7] Highly abundant senescence observed in cirrhosis has been confined to hepatocytes[2] and stellate cells.[8] Because telomere-deficient mice

Abbreviations: BrdU, bromodeoxyuridine; cDNA, complementary DNA; NAC, N-acetyl-L-cysteine; Nox4, NADPH oxidase-4; ROS, reactive oxygen species; SA-β-Gal, senescence-associated-β-galactosidase; siRNA, small interfering RNA; TERT, telomerase reverse transcriptase; TGF-β, transforming growth factor-β; TGF-βR1,TGF-β receptor 1.

From the [1]BilGen Research Center and Department of Molecular Biology and Genetics, Bilkent University, Ankara, Turkey; and [2]Centre de Recherche, Institut National de la Santé et de la Recherche Médicale (INSERM)-Université Joseph Fourrier U823, Institut Albert Bonniot, La Tronche, France.

Received March 16, 2010; accepted May 9, 2010.

This work was supported by grants from the TUBITAK and State Planning Office (Turkey) and the Institut National de Cancer (France). Additional support was provided by the Turkish Academy of Sciences.

Address reprint requests to: Mehmet Ozturk, Ph.D., Centre de Recherche INSERM/UJF U823, Institut Albert Bonniot, Grenoble, France.
E-mail: ozturkm@ujf-grenoble.fr; Fax: +33476549413.

Published online in Wiley InterScience (www.interscience.wiley.com).

DOI 10.1002/hep.23769

Potential conflict of interest: Nothing to report.

Additional Supporting Information may be found in the online version of this article.

develop cirrhosis,[9] and cirrhotic hepatocytes display shortened telomeres, telomere dysfunction was proposed to cause senescence in cirrhosis.[2] It is assumed that HCC tumor cells bypass hepatocellular senescence to become immortalized. Frequent inactivation of *TP53* (encoding the tumor protein p53) and *CDKN2A* (cyclin-dependent kinase inhibitor 2A, encoding $p16^{Ink4a}$ protein) genes in these tumors supports this hypothesis.[10] Nevertheless, the detection of senescent cells in some HCC tumors suggests that transformed and presumably immortal hepatocytes have maintained the capacity to undergo senescence arrest under appropriate conditions.

With this regard, immortal HCC cell lines can spontaneously generate progeny that undergo replicative senescence[11]; murine HCC tumors generated by the expression of a mutant *Ras* gene in p53-deficient hepatoblasts can be cleared by a massive senescence response upon reactivation of p53 expression[12]; c-*myc* oncogene inactivation in murine HCCs results in senescence-mediated tumor regression.[13] One of our goals is to identify novel mechanisms of senescence induction in HCC cells. Here, we identify the transforming growth factor-beta (TGF-β) as a major cytokine that is able to trigger a massive senescence response in well-differentiated HCC cell lines. Reduced nicotinamide adenine dinucleotide phosphate oxidase-4 (Nox4) and reactive oxygen species (ROS) were key intermediates of TGF-β–induced growth arrest that was mediated by $p21^{Cip1}$ and $p15^{Ink4b}$.

Materials and Methods

Detailed materials and methods are described in the Supporting Information Materials and Methods. Cell lines were tested under standard culture conditions in the presence of 10% fetal bovine serum. Total RNA was isolated using a NucleoSpin RNA II Kit (Macherey-Nagel, Duren, Germany), and first-strand complementary DNA (cDNA) was synthesized using RevertAid First Strand cDNA synthesis kit (MBI Fermentas, Leon-Rot, Germany). Genomic DNA was extracted as described,[11] and polymerase chain reaction (PCR) assays were done using appropriate primers. Quantitative PCR was performed using SYBR Green I (Invitrogen, Carlsbad, CA). Glyceraldehyde 3-phosphate dehydrogenase and β-actin were used as internal controls. The SA-β-Gal assay was performed as described.[11] Commercial and homemade antibodies were used. Western blot assays were performed as described,[11] using α-tubulin or calnexin as internal controls. For immunoperoxidase and immunofluorescence assays, cells were fixed with 4% formaldehyde, permeabilized with phosphate-buffered saline supplemented with 0.5% saponin and 0.3% TritonX-100 (Sigma, St. Louis, MO), and subjected to indirect immunofluorescence and immunoperoxidase assays. To test permanent cell cycle arrest, cells were labeled with bromodeoxyuridine (BrdU) for 24 hours in freshly added culture media, and the anti-BrdU immunofluorescence assay was performed as described.[11] Human $p15^{Ink4b}$ and $p21^{Cip1}$ were cloned into pcDNA3.1C/Neo and pcDNA3.1(+)/hygromycin (Invitrogen), respectively. Cells were transfected with Lipofectamine 2000 (Invitrogen) and selected with either Geneticin G418 (Gibco) or hygromycin-B (Roche, Indianapolis, IN) for 8 days. The *NOX4* gene was silenced using previously described Nox4-specific small interfering RNAs (siRNAs).[14] A negative control siRNA was used in parallel experiments. The siRNAs were transfected with Lipofectamine RNAiMAX (Invitrogen). The pSBE4-luc reporter was cotransfected with pRL-TK (plasmid Renilla luciferase, with thymidine kinase promoter; Promega, Madison, WI), using Lipofectamine 2000. The luciferase assay was performed using a Dual-Glo luciferase kit (Promega). For cell cycle studies, fixed cells were labeled with propidium iodide and analyzed using FACSCalibur Flow Cytometer (BD Biosciences, San Jose, CA). Intracellular ROS were detected with 2′,7′-dichlorofluorescein diacetate (DCFH-DA; Sigma), using MitoTracker Red (Invitrogen) as a counterstain. Apoptosis was tested by Negative in Apoptosis (NAPO)[15] and active caspase-3 antibody (Asp-175; Cell Signaling Technology, Danvers, MA) immunoassays. Subcutaneous human HCC tumors were obtained in CD1 *nude* mice using 5×10^6 live cells per injection. All animals received care according to the Guide for the Care and Use of Laboratory Animals. Results were expressed as mean $\pm$ standard deviation from at least three independent experiments. Data between groups were analyzed by one-tailed t test. A P value <0.05 was considered statistically significant. TGF-β1 expression in liver disease was analyzed using a publicly available global gene expression data,[16] which were normalized using JustRMA tool from the Bioconductor group.[17] A two-sample t test with random variance model was used with a 0.05 nominal significance level of each univariate test.

Results

Differential Expression of TGF-β1 in Normal Liver, Cirrhosis, and HCC. We first analyzed TGF-β1 expression in normal liver, cirrhosis, and HCC, using the publicly available clinical data sets.[16] TGF-β1 expression displayed a bell-shaped distribution with

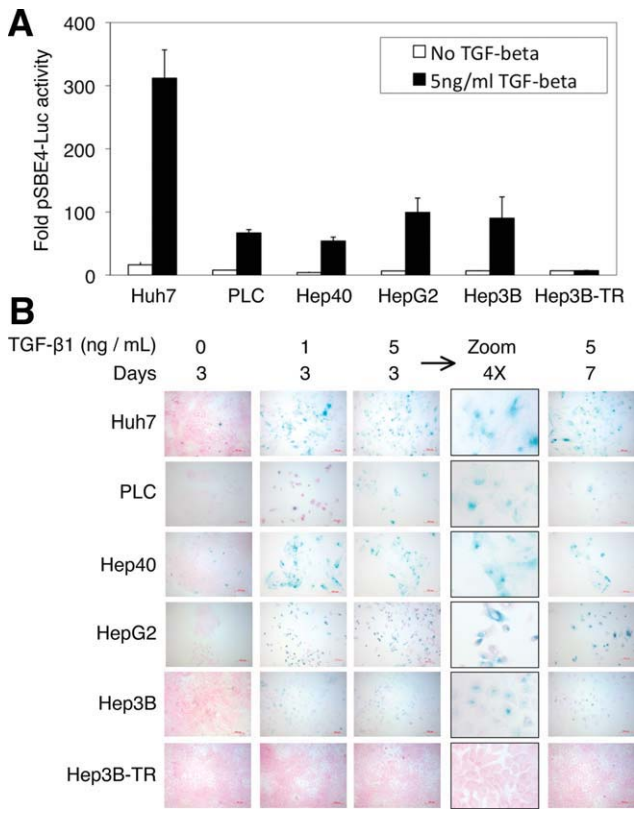

Fig. 1. Well-differentiated HCC cell lines are competent for TGF-β signaling activity and they respond to TGF-β by potent senescence-like growth arrest. (A) Cells were cotransfected with pSBE4-Luc and control pRL-TK plasmids, and treated with or without TGF-β1 (5 ng/mL) for 24 hours. The luciferase activity was measured and expressed as fold-activity of pSBE4-Luc/pRL-TK (mean $\pm$ standard deviation; n = 3). (B) Cells were plated at low density and treated with 1 or 5 ng/mL TGF-β1, and tested for SA-β-Gal activity (blue) at days 3 and 7. Counterstain: Fast Red. TGFBR2-deleted Hep3B-TR cells were used as negative controls in (A) and (B).

a sharp increase in cirrhosis (cirrhosis versus normal liver, $P < 0.001$), followed by a progressive decrease in early HCC (early HCC versus cirrhosis, $P < 0.02$) and advanced HCCs (Supporting Information Fig. 1). This expression pattern closely correlated with reported frequencies of SA-β-Gal activities in normal liver, cirrhosis, and HCC.[2,4-7]

TGF-β Is an Autocrine Cytokine Inducing a Senescence-Like Response in Well-Differentiated HCC Cell Lines. We hypothesized that TGF-β signaling can induce hepatocellular senescence response, because it is a potent inducer of G_1 arrest.[18] To test this hypothesis, we first formed a panel of "well-differentiated" HCC cell lines that display E-cadherin expression, epithelial-like morphology, and hepatocyte-like gene expression.[19] Well-differentiated cell lines also share the same TGF-β early response gene expression patterns with normal hepatocytes.[20] All selected cell lines expressed all critical components of TGF-β signaling including TGF-β1, TGF-β receptor 1 (TGFBR1), TGFBR2, small mothers against decapentaplegic homolog 2 (SMAD2), SMAD3, and SMAD4 (Supporting Information Fig. 2A). Hep3B-TR clone displaying homozygous deletion of *TGFBR2*[21] was used as a negative control (Supporting Information Fig. 2). All cell lines, except Hep3B-TR displayed intact TGF-β signaling activity (Fig. 1A), as tested by pSBE4-Luc reporter activity.[22] Treatment of cells with TGF-β1 (5 ng/mL) yielded 9-fold to 19-fold induction of pSBE4-Luc reporter activity in responsive cell lines. The expression of endogenous plasminogen activator inhibitor-1 (*PAI-1*), a well-known TGF-β target gene,[23] was also induced (Supporting Information Fig. 3). TGF-β1–treated cell lines were kept in culture with medium changes (without TGF-β1) every 3 days, examined morphologically, and subjected to SA-β-Gal assay. All cell lines tested, except Hep3B-TR, displayed growth inhibition associated with flattened cell morphology and >50% positive SA-β-Gal activity, as early as 3 days after TGF-β1 treatment (Fig. 1B).

Expression of TGF-β1 in all tested cell lines suggested that it could act as an autocrine cytokine. Therefore, we exposed Huh7 cells to either anti-TGF-β1 antibody (5 μg/mL) or TGF-β1 (5 ng/mL) and tested for total and SA-β-Gal–positive cells in isolated colonies 10 days later. Cells treated with anti-TGF-β1 antibody displayed two-fold increased colony size ($P < 0.04$) and 50% decreased SA-β-Gal activity ($P < 0.02$; Supporting Information Fig. 4). In contrast, ectopic TGF-β1 treatment caused a seven-fold decrease in colony size ($P < 0.005$) and five-fold increase in SA-β-Gal activity ($P < 0.0001$). Thus, Huh7 cells produced TGF-β1 acting as a weak autocrine senescence-inducing signal that was inhibited by anti-TGF-β1 antibody, and amplified by ectopic TGF-β1.

A Brief Exposure to TGF-β for a Robust Senescence Response. To test the shortest time of exposure to TGF-β1 for a full senescence response, three cell lines were treated with TGF-β1 for durations between <1 minute (~20 seconds) and 72 hours, and subjected to SA-β-Gal staining. To our surprise, <1 minute exposure was sufficient for a robust senescence response (Fig. 2). Thus, the senescence-initiating effect of TGF-β1 was immediate, even though the senescence phenotype (>50% SA-β-Gal–positive and flattened cells) was manifested 3 days later.

Lack of Evidence for TGF-β–Induced Apoptosis. Earlier studies indicated that TGF-β induces apoptosis in hepatocytes and some HCC cell lines under serum-free conditions.[24-27] Under our experimental conditions using 10% fetal bovine serum, all five cell lines tested failed to enter apoptosis following TGF-β

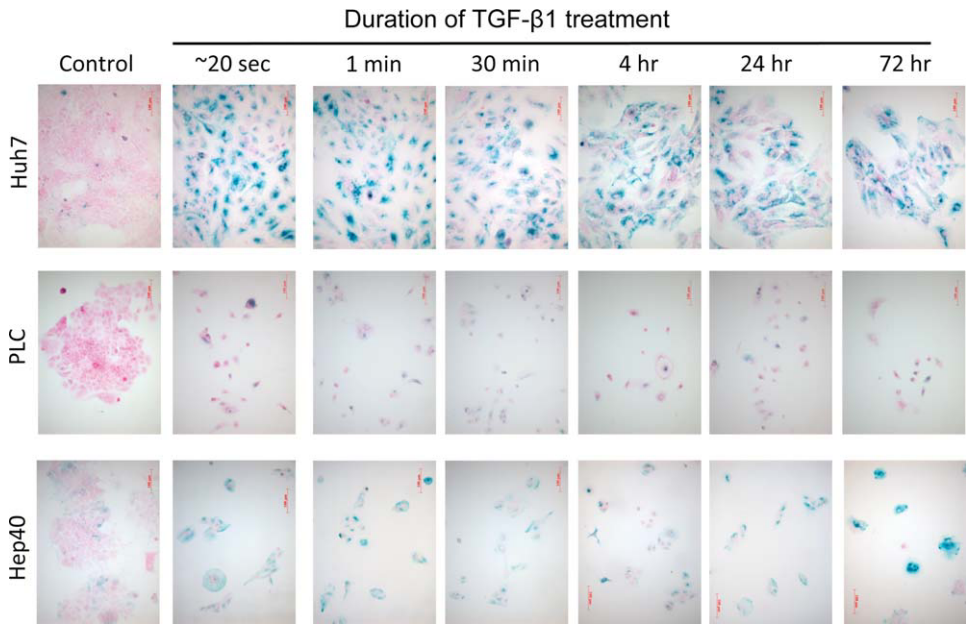

Fig. 2. Induction of a strong senescence-like response by TGF-β after a very short exposure. Cells were treated with TGF-β1 (5 ng/mL) for the indicated times, and SA-β-Gal activity (blue) was tested at 72 hours. Control: no TGF-β1 treatment. Counterstain: Fast Red.

treatment, as examined by NAPO antibody[15] and activated caspase-3–specific antibody tests (Supporting Information Figs. 5 and 6).

TGF-β–Induced Senescence Is Associated with Sustained Induction of $p21^{Cip1}$ and $p15^{Ink4b}$. Cellular senescence is usually associated with cell cycle arrest induced by p53, $p21^{Cip1}$, $p16^{Ink4a}$, and/or $p15^{Ink4b}$.[1,28] TGF-β1 caused c-myc repression and $p15^{Ink4b}$ and $p21^{Cip1}$ induction (Fig. 3; Supporting Information Fig. 7A). Decreased pRb phosphorylation, together with decreased p107 and increased p130 protein levels, was also observed. These changes in retinoblastoma family proteins correlate with exit from the cell cycle.[29] The TGF-β response was independent of p53. All HCC cell lines tested here, except HepG2, display p53 mutations.[30] The levels of total p53 did not change following TGF-β exposure, despite $p21^{Cip1}$ accumulation (Fig. 3; Supporting Information Fig. 7B). Moreover, we observed no phosphorylation of wild-type p53 in HepG2 cells, following TGF-β exposure (Supporting Information Fig. 7B). TGF-β also did not affect $p16^{Ink4a}$ levels (Fig. 3). Indeed, the *CDKN2A* gene is frequently silenced in HCC.[31] Accordingly, $p16^{Ink4a}$ protein levels were extremely low in all tested cell lines, except in pRb-deficient Hep3B and Hep3B-TR cells (Supporting Information Fig. 7C). On the other hand, our

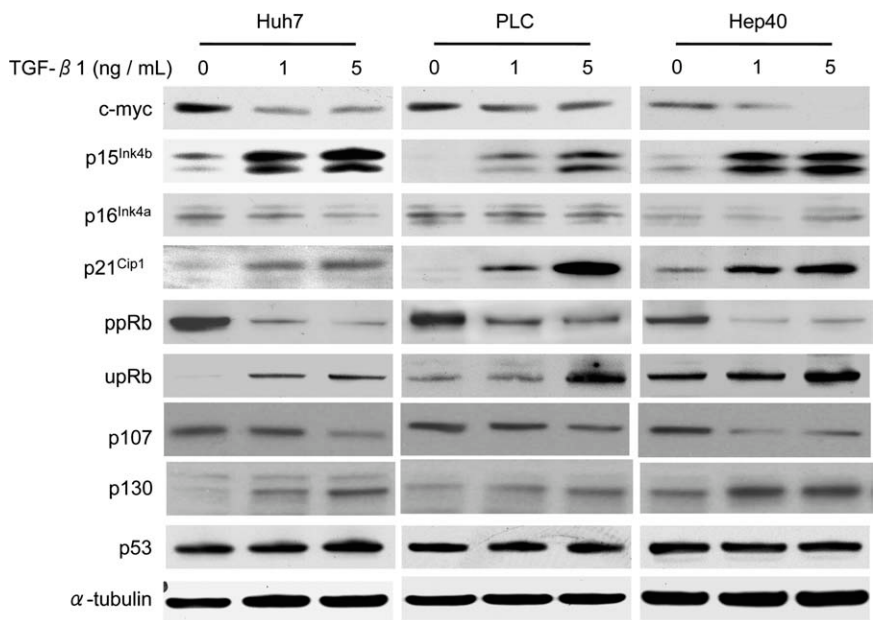

Fig. 3. TGF-β treatment of HCC cell lines causes the induction of $p15^{Ink4b}$ and $p21^{Cip1}$ that is associated with c-myc down-regulation, pRb underphosphorylation, p107 decrease and p130 increase. The levels of p53 and $p16^{Ink4a}$ did not change. Untreated and TGF-β1–treated cells were tested for indicated proteins by western blotting on day 3. ppRb: phospho-Ser^{807}/Ser^{811}-pRb, upRb: underphosphorylated pRb. The α-tubulin served as an internal control. $p16^{Ink4a}$ blots were overexposed to visualize weak expression.

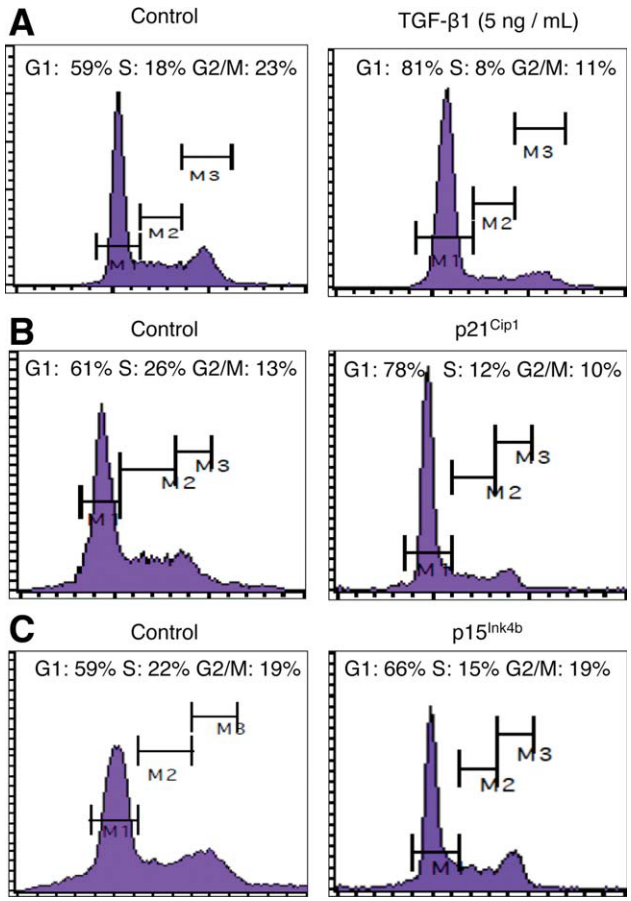

Fig. 4. G_1 arrest induced by TGF-β treatment can be recapitulated by ectopic expression of $p21^{Cip1}$ and $p15^{Ink4b}$. (A) Control and TGF-β1–treated Huh7 cells were subjected to cell cycle analysis after 3 days of culture. (B, C) Huh7 cells were transiently transfected with (B) $p21^{Cip1}$ and (C) $p15^{Ink4b}$ expression vectors, and subjected to cell cycle analysis after 8 days of culture. Control: cells transfected with empty plasmid vectors (B,C). [Color figure can be viewed in the online issue, which is available at www.interscience.wiley.com.]

observation of senescence arrest in Hep3B cells suggests that pRb expression is also dispensable for TGF-β–induced senescence in HCC cells. Taken together, these findings suggested that TGF-β was able to induce senescence in HCC cells independent of p53, $p16^{Ink4a}$, or pRb status.

TGF-β Induces a Permanent G_1 Arrest that Can Be Reproduced Either by $p21^{Cip1}$ or $p15^{Ink4b}$. Cellular senescence is defined as an irreversible arrest of mitotic cells at the G_1 phase, but some cancer cells enter senescence at the G_2 or S phases.[1] Initially, we used Huh7 cells for cell cycle studies. These cells accumulated at G_1 phase (from 59% to 81%) with a concomitant depletion of S phase cells (from 18% to 8%), after TGF-β1 exposure (Fig. 4A). Similar results were obtained with PLC/PRF/5 cells (Fig. 5) and other cell lines (data not shown). These observations suggested that $p21^{Cip1}$ and/or $p15^{Ink4b}$ are involved in TGF-β–mediated G_1 arrest and senescence response. Therefore, we tested respective contributions of $p21^{Cip1}$ and $p15^{Ink4b}$ in these responses, by transient transfection assays using Huh7 cells. The $p21^{Cip1}$-transfected and $p15^{Ink4b}$-transfected cells demonstrated highly increased $p21^{Cip1}$ protein (Supporting Information Fig. 8A) and moderately increased $p15^{Ink4b}$ expression (Supporting Information Fig. 8B), respectively. The $p21^{Cip1}$-overexpressing cells accumulated at G_1 (from 61% to 78%), together with a depletion of S phase cells (from 26% to 13%; Fig. 4B). In association with these changes, SA-β-Gal activity was increased (Supporting Information Fig. 9A) and BrdU

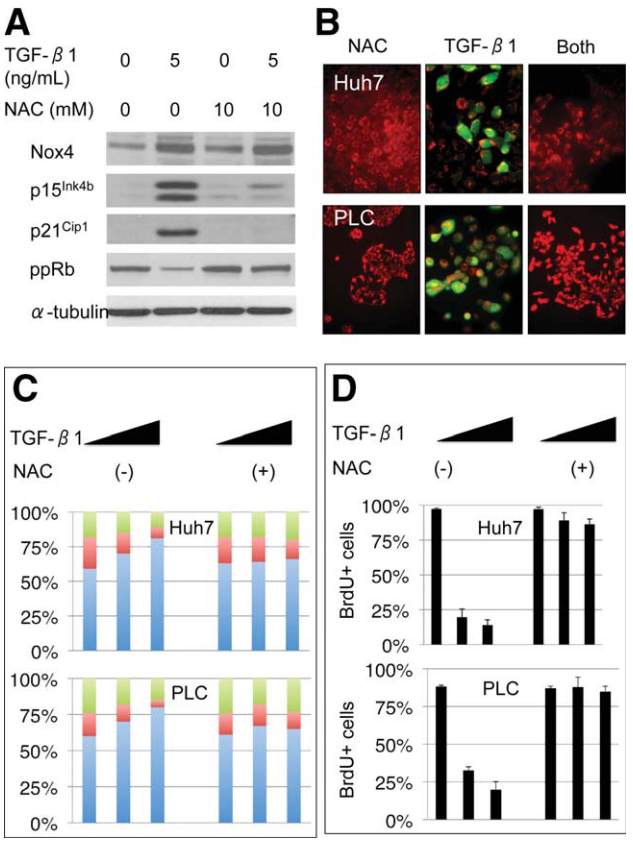

Fig. 5. Implication of Nox4 induction and ROS accumulation in TGF-β-induced growth arrest. (A) TGF-β1 treatement induces the expression of Nox4, $p15^{Ink4b}$, and $p21^{Cip1}$ together with ppRb down-regulation; ROS scavenger NAC inhibits $p15^{Ink4b}$ and $p21^{Cip1}$ induction, and ppRb down-regulation, but not Nox4 accumulation. Cell lysates were collected at day 3, following treatment with TGF-β1 and/or NAC, and tested by western blotting. (B-D) ROS accumulation observed in TGF-β1–treated cells is inhibited by NAC cotreatment (B), and this results in (C) inhibition of G_1 arrest, and (D) restoration of BrdU incorporation into cellular DNA. (A) PLC/PRF/5 cells were treated for 3 days with either 10 mM NAC or 5 ng/mL TGF-β1 alone, or in combination, and tested for Nox4, $p15^{Ink4b}$, $p21^{Cip1}$, and ppRb by western blotting. (B) Huh7 and PLC/PRF/5 (PLC) cells were treated with either 10 mM NAC or 5 ng/mL TGF-β1 alone, or in combination, and tested for ROS accumulation using a green fluorescent ROS indicator, and a red fluorescent mitochondrial marker as counterstain. The effects of 10 mM NAC cotreatment on growth inhibition by TGF-β1 (0, 1, or 5 ng/mL) were tested by (C) cell cycle analysis, and (D) BrdU incorporation assay. Blue, red, and green columns in (C) represent cells at G_1, S, and G_2/M, respectively.

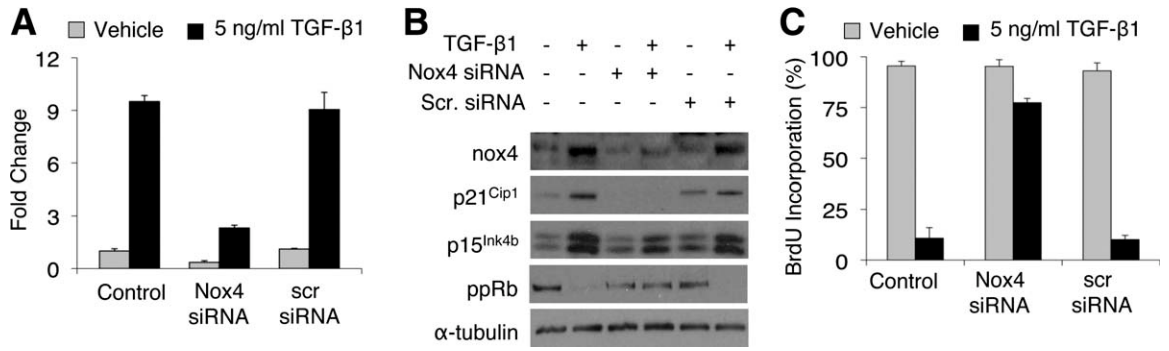

Fig. 6. Rescue of TGF-β-induced $p21^{Cip1}$ and $p15^{Ink4b}$ accumulation and growth arrest by *NOX4* gene silencing. (A) TGF-β-induced accumulation of Nox4 transcripts was strongly inhibited by Nox4 siRNA, but not by control siRNA. Transcript analysis was performed by quantitative reverse transcription PCR. (B) *NOX4* gene silencing rescued TGF-β-induced Nox4, $p21^{Cip1}$, and $p15^{Ink4b}$ protein accumulation, and the inhibition of pRb phosphorylation, as tested by western blotting. Compared to others, the inhibition of $p15^{Ink4b}$ accumulation was modest. (C) *NOX4* gene silencing also rescued TGF-β-induced inhibition of DNA synthesis, as tested by BrdU incorporation. Cells were labeled with BrdU for 24 hours prior to day 3, and percent BrdU-positive cells were counted manually.

incorporation into cellular DNA was inhibited ($P < 0.001$; Supporting Information Fig. 9B). The $p15^{Ink4b}$ overexpression caused a moderate response (G_1 cells rising to 66% from 59%; S phase cells decreasing from 22% from 15%; Fig. 4C). However, $p15^{Ink4b}$ overexpression was also associated with increased SA-β-Gal activity (Supporting Information Fig. 9C) and decreased BrdU incorporation ($P < 0.001$; Supporting Information Fig. 9D).

TGF-β–Induced Senescence Depends on Nox4 Induction and Intracellular Accumulation of ROS. TGF-β induces Nox4 expression and ROS accumulation in hepatocytes.[32-34] Because ROS have been implicated in Ras-induced senescence,[35] we tested whether TGF-β–induced senescence was associated with Nox4 induction and ROS accumulation. TGF-β1 induced Nox4 protein expression (Fig. 5A; Supporting Information Fig. 10A), as well as ROS accumulation (Fig. 5B). First, we used *N*-acetyl-L-cysteine (NAC) as a physiological ROS scavenger[36] to test the role of ROS in TGF-β–induced senescence. The cotreatment of 5 ng/mL TGF-β1–treated cells with 10 mM NAC completely suppressed the accumulation of ROS (Fig. 5B) and TGF-β1 effects on $p15^{Ink4b}$, $p21^{Cip1}$, and pRb, but not Nox4 expression (Fig. 5A). More importantly, NAC cotreatment rescued cells from TGF-β1–induced senescence response (Supporting Information Fig. 10B) and growth arrest (Fig. 5C,D; Supporting Information Fig. 11). Next, we silenced *NOX4* gene in Huh7 cells using a previously described NOX4-specific siRNA.[14] NOX4-specific siRNA inhibited the accumulation of Nox4 transcripts (~75%; Fig. 6A) and protein (Fig. 6B) under TGF-β1 treatment. This resulted in a strong inhibition of $p21^{Cip1}$ accumulation and a moderate inhibition of $p15^{Ink4b}$ accumulation in association with restoration of pRb phosphorylation (Fig. 6B). More importantly, Nox4 inhibition was sufficient to restore cell proliferation under TGF-β treatment (Fig. 6C).

TGF-β–Induced Senescence and Antitumor Activity In Vivo. We tested *in vivo* relevance of TGF-β–induced senescence in human HCC tumors raised in

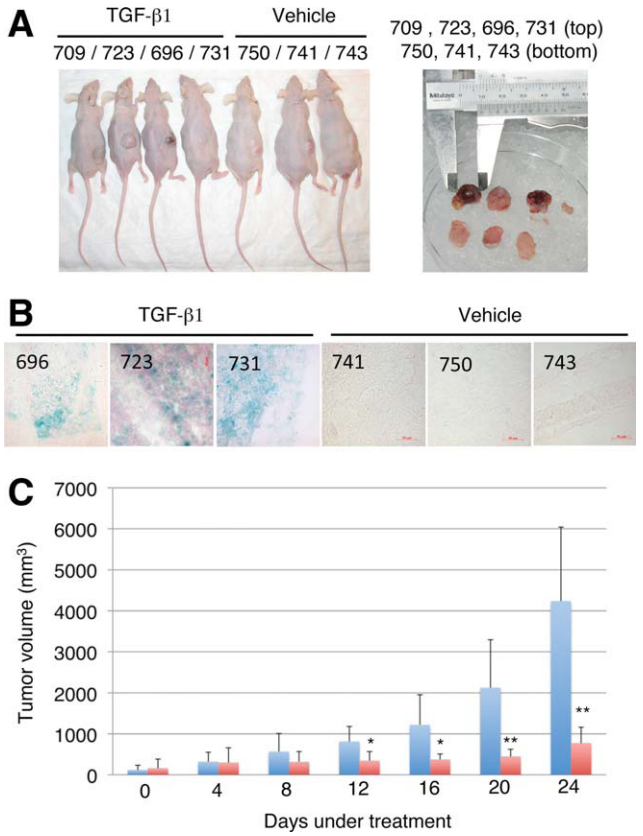

Fig. 7. TGF-β induces senescence and inhibits the growth of Huh7 tumors in *nude* mice. (A,B) TGF-β1–induced SA-β-Gal activity in Huh7 tumors. Huh7 tumors were obtained in *nude* mice and treated with TGF-β1 (~0.5 ng) or a vehicle only. (A) Animals were sacrificed 7 days later to collect tumor tissues. (B) Cryostat sections from freshly frozen tumors were subjected to SA-β-Gal staining (blue). Counterstain: Fast Red. (C) Huh7 tumors were treated with 2 ng TGF-β or vehicle only at 4-day intervals and tumor sizes were measured. TGF-β–treated tumors were growth arrested, resulting in >75% inhibition of tumor growth. *$P < 0.05$; **$P < 0.01$.

immunodeficient mice. TGF-β1 ($\sim$50 μL of a 10 ng/mL solution)-injected Huh7 tumors were removed 1 week later (Fig. 7A) and subjected to SA-β-Gal staining. TGF-β1 induced local but expanded SA-β-Gal activity in three of four tumors tested; three tumors treated with vehicle only were negative (Fig. 7B).

To test antitumor effects of TGF-β, early Huh7 tumors were treated with peritumoral injection of $\sim$2 ng TGF-β at 4 days of intervals. Vehicle-treated tumors displayed exponential growth to reach 4 cm^3 volume on average within 24 days. In contrast, TGF-β–treated tumors were growth arrested throughout the experiment and remained <1 cm^3 on average at the same time period. Tumor inhibition was significant for at least 24 days ($P < 0.01$ to $P < 0.05$). The TGF-β treatment was stopped at day 24 and animals were observed for an additional period of 4 weeks. All vehicle-treated and four TGF-β–treated animals died, whereas complete remission was observed in two TGF-β–treated animals (data not shown). We also compared *TGFBR2*-deleted Hep3B-TR cells[21] with parental Hep3B cells. Hep3B-TR cells formed palpable tumors 2 weeks after subcutaneous injection, and host animals died within 4-6 weeks. In contrast, Hep3B cells formed tumors with a latency of 6-7 weeks (Supporting Information Fig. 12).

Discussion

Our findings provide strong evidence for senescence as a major response of HCC cells to TGF-β. Senescence-associated changes included flattened morphology, $p21^{Cip1}$ and $p15^{Ink4b}$ accumulation, and positive SA-β-Gal activity. This response has not been noticed previously, probably because of its late occurrence, at least 3 days after TGF-β treatment. The primary findings of our mechanistic studies on TGF-β–induced senescence in HCC cells are outlined in Fig. 8. TGF-β-induced senescence response was associated with $p21^{Cip1}$-mediated and $p15^{Ink4b}$-mediated G_1 arrest, independent of p53 or $p16^{Ink4a}$. This correlates with the earlier observations showing that TGF-β uses $p21^{Cip1}$ and $p15^{Ink4b}$, but not $p16^{Ink4a}$ nor p53 to induce G_1 arrest in other cell types.[18] Although TGF-β–induced senescence had been described many years ago,[37] its mechanisms are poorly understood. Here, we show that the overexpression of $p21^{Cip1}$, and $p15^{Ink4b}$ to a lesser degree, recapitulates TGF-β–induced senescence response. Thus, $p21^{Cip1}$ and $p15^{Ink4b}$ are able to induce G_1 arrest and senescence response in HCC cells, as it occurs in other cell types.[10] Our most interesting finding was the implication of both Nox4 and ROS in the induction of $p21^{Cip1}$ and $p15^{Ink4b}$, and

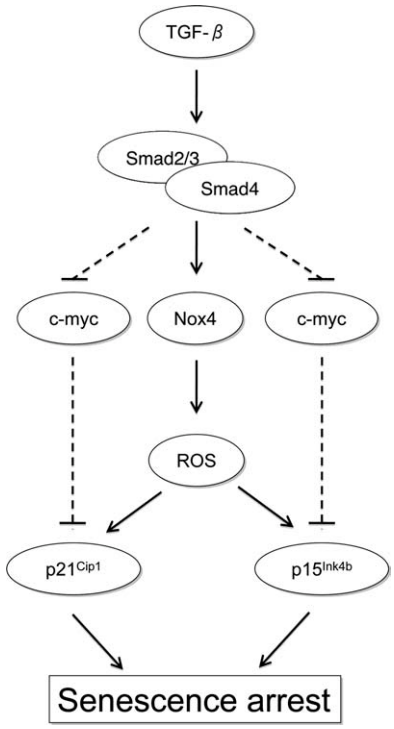

Fig. 8. A hypothetical model summarizing major components of TGF-β–induced senescence in HCC cells.

G_1 arrest by TGF-β. Either *NOX4* gene silencing or ROS scavenging was sufficient to interrupt the TGF-β signaling toward growth arrest mediated by $p21^{Cip1}$ and $p15^{Ink4b}$ induction. Thus, the accumulation of both Nox4 protein and ROS is a critical step for $p21^{Cip1}$ and $p15^{Ink4b}$ accumulation in TGF-β–exposed HCC cells (Fig. 8). Inhibition of $p21^{Cip1}$-mediated ROS accumulation has been previously shown to rescue senescence,[38] and a feedback between $p21^{Cip1}$ and ROS production was necessary for stable growth arrest.[39]

Our findings also provided preliminary evidence for antitumor activity of TGF-β against HCC. This effect was associated with *in vivo* induction of SA-β-Gal activity in tumor cells. Thus,TGF-β–induced senescence in human HCC cells, similar to p53-induced senescence in mouse HCC cells,[12] may be a potent tumor suppressor mechanism. The accelerated tumorigenesis of TGFBR2-deleted Hep3B-TR cells supports this hypothesis. Previous studies indicated that the disruption of TGF-β signaling in mice through dominant-negative Tgfr2 (transforming growth factor receptor 2) accelerates chemically induced hepatocarcinogenesis.[40] A similar disruption in β-spectrin embryonic liver fodrin knockout mice also leads to hepatocellular cancer.[41,42] However, our findings are limited to well-differentiated HCC cells that represent early forms of HCC.[43] Poorly differentiated HCC cell lines appear to

be resistant to TGF-β-induced senescence (S. Senturk and M. Ozturk, unpublished data). Nevertheless, TGF-β treatment might be an attractive therapeutic option for early HCCs.

Acknowledgment: We thank Edward B. Leof (United States) for providing pSBE4-luc and p3TP-lux reporter constructs, and Isabel Fabregat (Spain) for providing *NOX4*-specific siRNA sequence information prior to publication.

References

1. Campisi J, d'Adda di Fagagna F. Cellular senescence: when bad things happen to good cells. Nat Rev Mol Cell Biol 2007;8:729-740.
2. Wiemann SU, Satyanarayana A, Tsahuridu M, Tillmann HL, Zender L, Klempnauer J, et al. Hepatocyte telomere shortening and senescence are general markers of human liver cirrhosis. FASEB J 2002;16: 935-942.
3. Delhaye M, Louis H, Degraef C, Le Moine O, Deviere J, Peny MO, et al. Hepatocyte proliferative activity in human liver cirrhosis. J Hepatol 1999;30:461-471.
4. Paradis V, Youssef N, Dargere D, Ba N, Bonvoust F, Deschatrette J, et al. Replicative senescence in normal liver, chronic hepatitis C, and hepatocellular carcinomas. Hum Pathol 2001;32:327-332.
5. Ikeda H, Sasaki M, Sato Y, Harada K, Zen Y, Mitsui T, et al. Bile ductular cell reaction with senescent hepatocytes in chronic viral hepatitis is lost during hepatocarcinogenesis. Pathol Int 2009;59:471-478.
6. Ikeda H, Sasaki M, Sato Y, Harada K, Zen Y, Mitsui T, et al. Large cell change of hepatocytes in chronic viral hepatitis represents a senescent-related lesion. Hum Pathol 2009;40:1774-1782.
7. Kim H, Oh BK, Roncalli M, Park C, Yoon SM, Yoo JE, et al. Large liver cell change in hepatitis B virus-related liver cirrhosis. Hepatology 2009;50:752-762.
8. Krizhanovsky V, Yon M, Dickins RA, Hearn S, Simon J, Miething C, et al. Senescence of activated stellate cells limits liver fibrosis. Cell 2008;134:657-667.
9. Rudolph KL, Chang S, Millard M, Schreiber-Agus N, DePinho RA. Inhibition of experimental liver cirrhosis in mice by telomerase gene delivery. Science 2000;287:1253-1258.
10. Ozturk M, Arslan-Ergul A, Bagislar S, Senturk S, Yuzugullu H. Senescence and immortality in hepatocellular carcinoma. Cancer Lett 2008; 286:103-113.
11. Ozturk N, Erdal E, Mumcuoglu M, Akcali KC, Yalcin O, Senturk S, et al. Reprogramming of replicative senescence in hepatocellular carcinoma-derived cells. Proc Natl Acad Sci USA 2006;103:2178-2183.
12. Xue W, Zender L, Miething C, Dickins RA, Hernando E, Krizhanovsky V, et al. Senescence and tumour clearance is triggered by p53 restoration in murine liver carcinomas. Nature 2007;445:656-660.
13. Wu CH, van Riggelen J, Yetil A, Fan AC, Bachireddy P, Felsher DW. Cellular senescence is an important mechanism of tumor regression upon c-Myc inactivation. Proc Natl Acad Sci USA 2007;104: 13028-13033.
14. Carmona-Cuenca I, Roncero C, Sancho P, Caja L, Fausto N, Fernandez M, et al. Upregulation of the NADPH oxidase NOX4 by TGF-beta in hepatocytes is required for its pro-apoptotic activity. J Hepatol 2008; 49:965-976.
15. Sayan BS, Ince G, Sayan AE, Ozturk M. NAPO as a novel marker for apoptosis. J Cell Biol 2001;155:719-724.
16. Wurmbach E, Chen YB, Khitrov G, Zhang W, Roayaie S, Schwartz M, et al. Genome-wide molecular profiles of HCV-induced dysplasia and hepatocellular carcinoma. Hepatology 2007;45:938-947.
17. Gentleman RC, Carey VJ, Bates DM, Bolstad B, Dettling M, Dudoit S, et al. Bioconductor: open software development for computational biology and bioinformatics. Genome Biol 2004;5:R80.
18. Siegel PM, Massague J. Cytostatic and apoptotic actions of TGF-beta in homeostasis and cancer. Nat Rev Cancer 2003;3:807-821.
19. Yuzugullu H, Benhaj K, Ozturk N, Senturk S, Celik E, Toylu A, et al. Canonical Wnt signaling is antagonized by noncanonical Wnt5a in hepatocellular carcinoma cells. Mol Cancer 2009;8:90.
20. Coulouarn C, Factor VM, Thorgeirsson SS. Transforming growth factor-beta gene expression signature in mouse hepatocytes predicts clinical outcome in human cancer. Hepatology 2008;47:2059–2067.
21. Inagaki M, Moustakas A, Lin HY, Lodish HF, Carr BI. Growth inhibition by transforming growth factor beta (TGF-beta) type I is restored in TGF-beta-resistant hepatoma cells after expression of TGF-beta receptor type II cDNA. Proc Natl Acad Sci USA 1993;90: 5359-5363.
22. Zawel L, Dai JL, Buckhaults P, Zhou S, Kinzler KW, Vogelstein B, et al. Human Smad3 and Smad4 are sequence-specific transcription activators. Mol Cell 1998;1:611-617.
23. Sandler MA, Zhang JN, Westerhausen DR Jr, Billadello JJ. A novel protein interacts with the major transforming growth factor-beta responsive element in the plasminogen activator inhibitor type-1 gene. J Biol Chem 1994;269:21500-21504.
24. Herzer K, Ganten TM, Schulze-Bergkamen H, Grosse-Wilde A, Koschny R, Krammer PH, et al. Transforming growth factor beta can mediate apoptosis via the expression of TRAIL in human hepatoma cells. Hepatology 2005;42:183-192.
25. Lin JK, Chou CK. In vitro apoptosis in the human hepatoma cell line induced by transforming growth factor beta 1. Cancer Res 1992;52: 385-388.
26. Ponchel F, Puisieux A, Tabone E, Michot JP, Froschl G, Morel AP, et al. Hepatocarcinoma-specific mutant p53-249ser induces mitotic activity but has no effect on transforming growth factor beta 1-mediated apoptosis. Cancer Res 1994;54:2064-2068.
27. Oberhammer F, Bursch W, Parzefall W, Breit P, Erber E, Stadler M, et al. Effect of transforming growth factor beta on cell death of cultured rat hepatocytes. Cancer Res 1991;51:2478-2485.
28. Gil J, Peters G. Regulation of the INK4b-ARF-INK4a tumour suppressor locus: all for one or one for all. Nat Rev Mol Cell Biol 2006;7: 667-677.
29. Classon M, Dyson N. p107 and p130: versatile proteins with interesting pockets. Exp Cell Res 2001;264:135-147.
30. Erdal E, Ozturk N, Cagatay T, Eksioglu-Demiralp E, Ozturk M. Lithium-mediated downregulation of PKB/Akt and cyclin E with growth inhibition in hepatocellular carcinoma cells. Int J Cancer 2005;115:903-910.
31. Roncalli M, Bianchi P, Bruni B, Laghi L, Destro A, Di Gioia S, et al. Methylation framework of cell cycle gene inhibitors in cirrhosis and associated hepatocellular carcinoma. Hepatology 2002;36:427-432.
32. Sanchez A, Alvarez AM, Benito M, Fabregat I. Apoptosis induced by transforming growth factor-beta in fetal hepatocyte primary cultures: involvement of reactive oxygen intermediates. J Biol Chem 1996;271: 7416-7422.
33. Herrera B, Murillo MM, Alvarez-Barrientos A, Beltran J, Fernandez M, Fabregat I. Source of early reactive oxygen species in the apoptosis induced by transforming growth factor-beta in fetal rat hepatocytes. Free Radic Biol Med 2004;36:16-26.
34. Carmona-Cuenca I, Herrera B, Ventura JJ, Roncero C, Fernandez M, Fabregat I. EGF blocks NADPH oxidase activation by TGF-beta in fetal rat hepatocytes, impairing oxidative stress, and cell death. J Cell Physiol 2006;207:322-330.
35. Lee AC, Fenster BE, Ito H, Takeda K, Bae NS, Hirai T, et al. Ras proteins induce senescence by altering the intracellular levels of reactive oxygen species. J Biol Chem 1999;274:7936-7940.
36. Droge W. Free radicals in the physiological control of cell function. Physiol Rev 2002;82:47-95.
37. Lin HK, Bergmann S, Pandolfi PP. Cytoplasmic PML function in TGF-beta signalling. Nature 2004;431:205-211.

38. Macip S, Igarashi M, Fang L, Chen A, Pan ZQ, Lee SW, et al. Inhibition of p21-mediated ROS accumulation can rescue p21-induced senescence. EMBO J 2002;21:2180-2188.
39. Passos JF, Nelson G, Wang C, Richter T, Simillion C, Proctor CJ, et al. Feedback between p21 and reactive oxygen production is necessary for cell senescence. Mol Syst Biol 2010;6:347.
40. Kanzler S, Meyer E, Lohse AW, Schirmacher P, Henninger J, Galle PR, et al. Hepatocellular expression of a dominant-negative mutant TGF-beta type II receptor accelerates chemically induced hepatocarcinogenesis. Oncogene 2001;20:5015-5024.
41. Kitisin K, Ganesan N, Tang Y, Jogunoori W, Volpe EA, Kim SS, et al. Disruption of transforming growth factor-beta signaling through beta-spectrin ELF leads to hepatocellular cancer through cyclin D1 activation. Oncogene 2007;26:7103-7110.
42. Tang Y, Kitisin K, Jogunoori W, Li C, Deng CX, Mueller SC, et al. Progenitor/stem cells give rise to liver cancer due to aberrant TGF-beta and IL-6 signaling. Proc Natl Acad Sci USA 2008;105:2445-2450.
43. Kojiro M. Pathological evolution of early hepatocellular carcinoma. Oncology 2002;62(Suppl. 1):43-47.

Invest New Drugs
DOI 10.1007/s10637-010-9486-3

PRECLINICAL STUDIES

Inhibition of Akt signaling in hepatoma cells induces apoptotic cell death independent of Akt activation status

Francesca Buontempo · Tulin Ersahin · Silvia Missiroli · Serif Senturk · Daniela Etro · Mehmet Ozturk · Silvano Capitani · Rengul Cetin-Atalay · Maria Luca Neri

Received: 1 April 2010 / Accepted: 24 June 2010

Summary The serine/threonine kinase Akt, a downstream effector of phosphatidylinositol 3-kinase (PI3K), is involved in cell survival and anti-apoptotic signaling. Akt has been shown to be constitutively expressed in a variety of human tumors including hepatocellular carcinoma (HCC). In this report we analyzed the status of Akt pathway in three HCC cell lines, and tested cytotoxic effects of Akt pathway inhibitors LY294002, Wortmannin and Inhibitor VIII. In Mahlavu human hepatoma cells Akt was constitutively activated, as demonstrated by its Ser473 phosphorylation, downstream hyperphosphorylation of BAD on Ser136, and by a specific cell-free kinase assay. In contrast, Huh7 and HepG2 did not show hyperactivation when tested by the same criteria. Akt enzyme hyperactivation in Mahlavu was associated with a loss of PTEN protein expression. Akt signaling was inhibited by the upstream kinase inhibitors, LY294002, Wortmannin, as well as by the specific Akt Inhibitor VIII in all three hepatoma cell lines. Cytotoxicity assays with Akt inhibitors in the same cell lines indicated that they were all sensitive, but with different IC50 values as assayed by RT-CES. We also demonstrated that the cytotoxic effect was through apoptotic cell death. Our findings provide evidence for its constitutive activation in one HCC cell line, and that HCC cell lines, independent of their Akt activation status respond to Akt inhibitors by apoptotic cell death. Thus, Akt inhibition may be considered as an attractive therapeutic intervention in liver cancer.

Keywords Akt · PI3K · PTEN · HCC · LY294002 · Inhibitor VIII · Wortmannin · RTCES

Francesca Buontempo and Tulin Ersahin have contributed equally to this work.

Electronic supplementary material The online version of this article (doi:10.1007/s10637-010-9486-3) contains supplementary material, which is available to authorized users.

F. Buontempo · S. Missiroli · D. Etro · S. Capitani · M. L. Neri (✉)
Dipartimento di Morfologia ed Embriologia,
Sezione di Anatomia Umana, Signal Transduction Unit,
Universita' di Ferrara,
via Fossato di Mortara 66,
44100 Ferrara, Italy
e-mail: luca.neri@unife.it

T. Ersahin · S. Senturk · M. Ozturk · R. Cetin-Atalay (✉)
Department of Molecular Biology and Genetics,
Bilkent University,
TR-06800 Ankara, Turkey
e-mail: rengul@bilkent.edu.tr

Introduction

Hepatocellular carcinoma (HCC) is one of the most common cancers worldwide occurs in patients with chronic viral hepatitis and cirrhosis at a high rate (3–5% annually) and is a major cause of morbidity and mortality in patients with advanced liver disease [1]. In healthy individuals, liver is a quiescent organ and adult hepatocytes are nondividing cells under normal physiological conditions. However, chronic liver injury due to viral diseases, exposure to chemicals and other environmental or host factors results in extensive cell death and consequently hepatocyte proliferation [2]. Chronic cell death in liver leads to a state where continuous hepatocyte regeneration is observed as a result of the inflammatory response. Continuous cycles of liver cell death and proliferation induce many cell signaling pathways including cell survival pathways such as Akt [3, 4]. Knowledge on the signaling pathways and the alterations involved in HCC is extending, however their role in molecular targeted therapy still remains to be described.

Published online: 14 July 2010

The most promising molecular targets in the generation of new chemotherapy agents are the protein kinases, including those in the PI3K/Akt pathway. The Akt pathway is involved in many cancers, as well as HCC development, through its activation by EGF or IGF signaling or the constitutive activation of Akt proteins or the inactivation of PTEN tumor suppressor [5–8]. The serine/threonine kinase Akt is a well-characterized downstream target of PI3K and resides within the cytoplasm in an inactive state, but binding of PtdIns (3,4,5)P3 to its pleckstrin homology (PH) domain recruits Akt to the plasma membrane and enables its activation by phosphorylation on the C-terminal hydrophobic tail [9]. Once activated, signaling through Akt can be propagated to a diverse array of substrates. Activated Akt is known to inhibit apoptosis through its ability to phosphorylate several targets, including BAD, FoxO transcription factors, Raf-1 and caspase-9, which are critical for cell survival [9]. Moreover, the tumor suppressor protein PTEN prevents Akt activation by acting as a lipid phosphatase on the PI3K product PtdIns (3,4,5)P3. Akt pathway hyper-activation has been reported due to the loss of tumor suppressor protein PTEN function through mutations, deletions, or epigenetic silencing [10, 11]. The PTEN gene is the second most frequently modified tumor suppressor gene, and is related to many cancers including brain, bladder, breast, prostate, endometrial and liver cancer [10–12].

In primary liver carcinoma, one of the major pathogenic mechanisms resides in the activated intracellular signal transduction caused by oncogenes and the tumor suppressor gene dysfunction that stimulates cell-cycle progression and enhance cell survival [13]. Despite this much information, the behavior and relevance of the Akt pathway in HCC and its therapeutic potential remain to be further elucidated. Since liver cancer usually develops on the background of chronic liver disease, conventional anticancer therapies are not effective. Moreover, the chemotherapeutics currently in use are non-selective cytotoxic drugs that can lead to systemic side effects in HCC patients with compromised liver function. Recently, Sorafenib, a multikinase inhibitor acting through VEGFR and PDGFR of the Raf kinase pathway, was approved for hepatocellular carcinoma treatment [4]. The Sorafenib Hepatocellular Carcinoma Assessment Randomized Protocol (SHARP) three-year clinical trial included 602 advanced-stage HCC patients (ClinicalTrials.gov number, NCT00105443) [4]. The average survival rate for the group taking Sorafenib was 10.7 months, and that for the group taking the placebo was 7.9 months. For the Sorafenib group a one-year survival rate of 44% was observed, whereas it was 33% for the placebo group. FDA- and EU- approved chemotherapeutic Sorafenib thus prolongs median survival and the time to progression by nearly three months in patients with advanced hepatocellular carcinoma. Therefore FDA and EU approved chemotherapeutic Sorafenib prolongs median survival and the time to progression by nearly 3 months in patients with advanced hepatocellular carcinoma. Therefore, there is a need for new liver cancer specific drugs based on the molecular mechanisms involved in liver carcinogenesis.

In this study, we investigated the Akt activation status in HCC cell lines the differential effects of three Akt pathway inhibitors and the extent of the inhibition of Akt signaling as a major molecular mechanism in determining inhibitor-induced apoptosis in these cells. The Akt pathway can be blocked by cell line specific doses of pathway inhibitors. Therefore, our findings suggested that PI3K/Akt could represent an attractive target mitigating in liver cancer.

Materials and methods

Materials

DMEM (cat.12-614F), FCS (cat.DE 14-801F), antibiotics (cat.DE 17-602E), glutamine and non essential amino acids (cat.BE 13-114E) were from Lonza (Milan). Calnexin, β-actin antibody, and Sulforhodamine B (SRB) (cat.86183-5 g) were from Sigma (St. Louis, MO). Lumi-Light detection kit (cat.12 015 196001) was from Roche M.B. (Germany). Akt Inhibitor VIII (cat.124018), Wortmannin (cat. BML-ST415-0005) and LY294002 (cat.440202) were from Calbiochem (La Jolla, CA). The DMSO concentration for drug solubilization was always less than 1% in the cell culture medium.

The Akt Antibody (cat.610861) was from BD Transduction Laboratories (Franklin Lakes, NJ) and anti-p-473Ser Akt (cat.587F11), anti-BAD (cat.185D10), anti-p-BAD (cat.#9292), recGSK3α/β fusion protein (cat.#9237 L), anti-p-GSK3α/β (cat.#9331 L), anti-PTEN and anti-PARP (cat.46D11) antibodies were from Cell Signaling (Danvers, MA). The immunoprecipitation matrix (cat.sc-45042) was from Santa Cruz Biotechnology (Santa Cruz, CA).

Cell culture

Hepatoma cells (Huh7, HepG2, Mahlavu) were cultured at 37°C, 5% CO_2 in standard medium (2 mML-Glutamine, 0.1 mM NEA, 1xPS in DMEM) with 10% FCS.

Western blotting analysis

Proteins, from cells grown to 60–70% confluence, were separated on 10% SDS-PAGE, transferred onto nitrocellulose membranes and visualized as described previously [14].

Akt kinase activity assay

Total homogenates from cells were resuspended in 50 mM Tris-HCl pH 7.4, 1 mM EDTA, 1 mM EGTA, 150 mM NaCl, 1% Triton X-100, 0.1% SDS plus phosphatase and proteases inhibitors. IP was performed according to the manufacturer's instruction. Akt IP was resuspended in 20 mM HEPES pH 7.4, 10 mM $MgCl_2$ and 10 mM $MnCl_2$. The reaction was started by incubating 10 μl IP, 100 μM ATP and 1 μg recGSK3α/β for 40 min at RT, and then stopped by 1 M Tris-HCl pH 6.8, 8% SDS, 40% glycerol, 20% β-ME. GSK3α/β phosphorylation was detected by western blotting.

NCI-60 Sulforhodamine B (SRB) cytotoxicity assay

The cytotoxicities of LY294002, Akt Inhibitor VIII and Wortmannin were tested as previously described [15]. Hepatoma cells (5000) were inoculated into 96 well plates,100 μl/well. Next day, inhibitors with the indicated concentrations were applied in a total of 200 μl of medium. After 72 h of treatment, cells were fixed by cold 10% (w/v) TCA and then the wells were washed and dried. One hundred μl of 0.4% SRB dye was applied to each well and incubated at RT for 10 min then removed and wells were dried. SRB dye was solubilized in 200 μl 10 mM Tris-Base and the absorbance was measured at 515 nm.

Real-time cell growth surveillance by cell electronic sensing

Hepatoma cells (2000cell/well in 150 μl) were inoculated into 96 E-Plates (Roche) containing 50 μl medium/well. Proliferation was monitored in real-time cell electronic sensing RT-CES (xCELLigence-Roche Applied Science), and the cell index (CI) was measured every 30 min for 24 h [16]. Next day, 100 μl medium was discarded and 50 μl fresh medium was added to each well. Inhibitors with indicated concentrations were applied to150 μl of medium. CI values were taken every 10 min for 4 h to visualize the fast drug response and then every 30 min to visualize the long-term drug response. Impedance measurements are displayed as Cell Index (CI) values and the effect of the inhibitors on cell growth is calculated as CI_{DRUG}/CI_{DMSO}. When the cells adhered to electrodes on the bottom of the wells, CI values increased in parallel to the cell growth due to the insulating properties of the cell membrane. As the number of cells covering the electrodes increases the electrical impedance (Z) increased ($Z_0=0$ --->$Z=Z_{cell}$).

Fluorescence microscopy

Cells were seeded at 3×10^4 cells/cm^2 on coverslips, allowed to grow for 24 h, as indicated in the figure legends, then washed twice with PBS and fixed with 4% paraformaldehyde. Subsequently, cells were washed once more with PBS and stained with 0.5 mg/ml DAPI. Preparations were dehydrated with increasing concentrations of ethanol and embedded in glycerol containing the antifading agent to be analyzed with Zeiss Axiophot epifluorescence microscope coupled with a Photometric Cool Snap CCD camera for image acquisition. The percentage of apoptotic cells was determined by counting fragmented nuclei in a minimum of 4 fields containing at least 150 cells. These experiments were performed in triplicate. As a positive control for apoptosis, cells were treated with 100 ng/ml Doxorubicine.

RT-PCR

Total RNA was isolated with NucleoSpin RNA II Kit (MN, Germany). cDNAs synthesized from 4 μg RNA with RevertAid kit (MBI Fermentas, Lithuania) were amplified by PCR with the primers (PTEN: intron-3-F_5′-AAAGATTCAGGCAATGTTTGTT-3′, intron-4-R_5′-TCTCACTCGATAATCTGGATGAC-3′, exon-4-F_5′-GACATTATGACACCGCCAAA-3′, exon-5-R_5′-TTCGTCCCTTTCCAGCTTTA-3′, exon-7-F_5′-CGACGGGAAGACAAGTTCAT-3′, exon-8-R_5′AGGTTTCCTCTGGTCCTGGT-3′, and GAPDH: F-5′-GGCTGAGAACGGGAAGCTTGTCAT-3′ and R-5′CAGCCTTCTCCATGGTGGTGAAGA-3′).

Results

Akt hyperphosphorylation in Mahlavu HCC cells

Hyperactivation of Akt was previously reported in HCC [17]. Therefore, we sought first to analyze the Akt levels and its serine-473 phosphorylation in hepatoma cells. Akt total amount seems comparable albeit a slight higher expression could be observed in Mahlavu cells when compared to Huh7 and HepG2 cells (Fig. 1a). In addition, significant Akt phosphorylation was detectable in Mahlavu cells, whereas only a slight Akt phosphorylation was detectable in HepG2 and Huh7 cells under native conditions.

Therefore, our initial observation suggested that the poorly differentiated Mahlavu cell line might have hyperactivated Akt signaling in comparison to the well-differentiated HCC

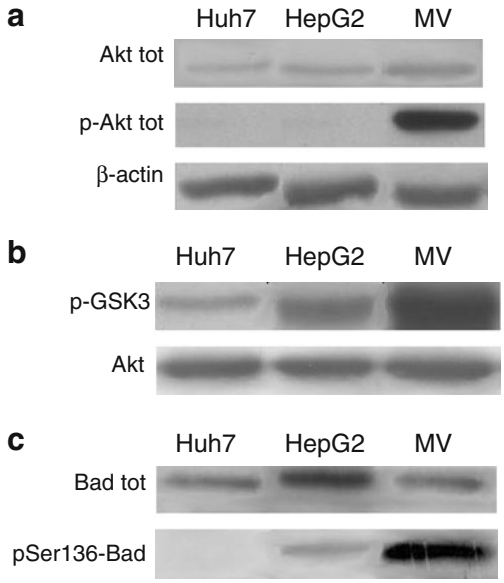

Fig. 1 Akt activity analysis in HCC cell lines. **a** Western blot analysis of untreated Huh7, HepG2, and Mahlavu cell lines, detected with anti Akt antibody or anti-p-Akt antibody. **b** Kinase assay on the fusion protein of GSK3α/β added to the reaction mixture as an exogenous substrate. As a control for equal loading, samples of immunoprecipitated Akt for the kinase assay were used. **c** Western blot analysis of untreated HCC cell lines was performed with anti-total BAD antibody or anti-p-BAD antibody. 20 μg of proteins were loaded for each lane. Data given here are representative of three independent experiments. SDS are less than 10%. The Mahlavu cell line displays high a Akt phosphorylation level and the highest enzymatic activity tested on both exogenous (GSK3α/β) and endogenous (BAD) substrate

cell lines; Huh7 and HepG2 [18]. To further assess whether Akt hyperphosphorylation in Mahlavu cells is related to the hyperactivation of its kinase enzymatic activity, we performed a kinase assay on the fusion protein GSK3 containing Akt target-phosphorylation residues. The results of this assay (Fig. 1b) showed the presence of a very low intrinsic activity in Huh7 cells, an intermediate activity in HepG2 cells but a very high kinase activity in Mahlavu cells. As a control for equal loading, samples of immunoprecipitated total Akt for the kinase assay were used. These data correlate very well with those obtained by western blot data on p-Akt (Fig. 1a).

We sought to further verify Akt pathway activation on a native target of Akt. To this end, we analyzed the phosphorylation status of BAD, a well-known protein downstream of Akt, whose phosphorylation prevents cells from undergoing apoptosis and confers them a proliferative advantage. The p-BAD antibody used in our study was specific to the Ser136 target of Akt kinase. In this way we excluded the possibility of BAD being phosphorylated by other kinases such as Erk-p90RSK kinase, which targets Ser122 [19]. pSer136-BAD was absent in Huh7 cells, and barely detectable in HepG2 cells, whereas a high level of pSer136-BAD was detected in Mahlavu cells (Fig. 1c).

Interestingly, total BAD protein levels were not equal in the cell lines analyzed although each lane contained 20 μg of total cell lysate, in particular Mahlavu showed lower BAD protein levels than HepG2 (Fig. 1c). However, we observed an intense phosphorylation by endogenous BAD in this cell line, which might explain the faint pSer136-BAD band in HepG2.

Determination of IC50 values for the HCC cells with SRB cytotoxicity assay

After the analysis of the hyperphosphorylation state of the Akt protein in well differentiated Huh7, HepG2 cells and poorly differentiated Mahlavu cells under native conditions, we decided to see the effect of PI3K inhibitors (LY294002, Wortmannin) and the specific Akt inhibitor (Inhibitor VIII) on this signaling pathway. Akt Inhibitor VIII selectively prevents Akt1 and Akt2 activity through pleckstrin homology (PH) domain [20, 21].

Initially we assessed their cytotoxicity by NCI-60 conventional Sulforhodamine B assay that was performed in quadruplicate and for 5 different concentrations following the NCI's drug screening protocol. The inhibitory effect of each drug of treatment was plotted (Fig. 2). IC50 values were calculated from these graphs for 24, 48, and 72 h (Fig. 2). IC50 values of LY294002 were 3.65 μM, 25.03 μM and 7.19 μM for 24 h and 3.75 μM, 5.82 μM and 8.71 μM for 72 h in Huh7, HepG2 and Mahlavu cell lines, respectively. For Wortmannin IC50 values in Huh7, HepG2 and Mahlavu cell lines were 26.07 μM, 29.23 μM and 20.19 μM for 24 h and 17.78 μM, 11.27 μM and 36.88 μM for 72 h, respectively. For 24 h, the IC50 values of Inhibitor VIII were 4.42 μM and 17.16 μM for Huh7 and HepG2, while there was not a significant inhibition observed in Mahlavu with NCI-60 assay. For 72 h, the IC50 values of Inhibitor VIII were 5.27 μM, 4.48 μM and 9.04 μM for Huh7, HepG2 and Mahlavu cells, respectively.

Real-time, dynamic monitoring of cell growth in HCC cells treated with the inhibitors

In order to further analyze if the growth inhibition of HCC cells is permanent or temporary, we used a novel cell surveillance system to monitor real-time, dynamic changes in cell growth based on the electrical impedance measurement technique. The RT-CES system allowed us to monitor the effects of LY294002, Wortmannin, and Inhibitor VIII on the hepatoma cells by a label-free and a real-time native approach. The proliferation and cytotoxicity of the inhibitors were followed by real-time through electronic cell sensors, integrated in the bottom of the 96 E-Plates in triplicates with 5 different concentrations (40 μM, 20 μM, 10 μM, 5 μM, 2.5 μM) (Fig. 3). When normalized to

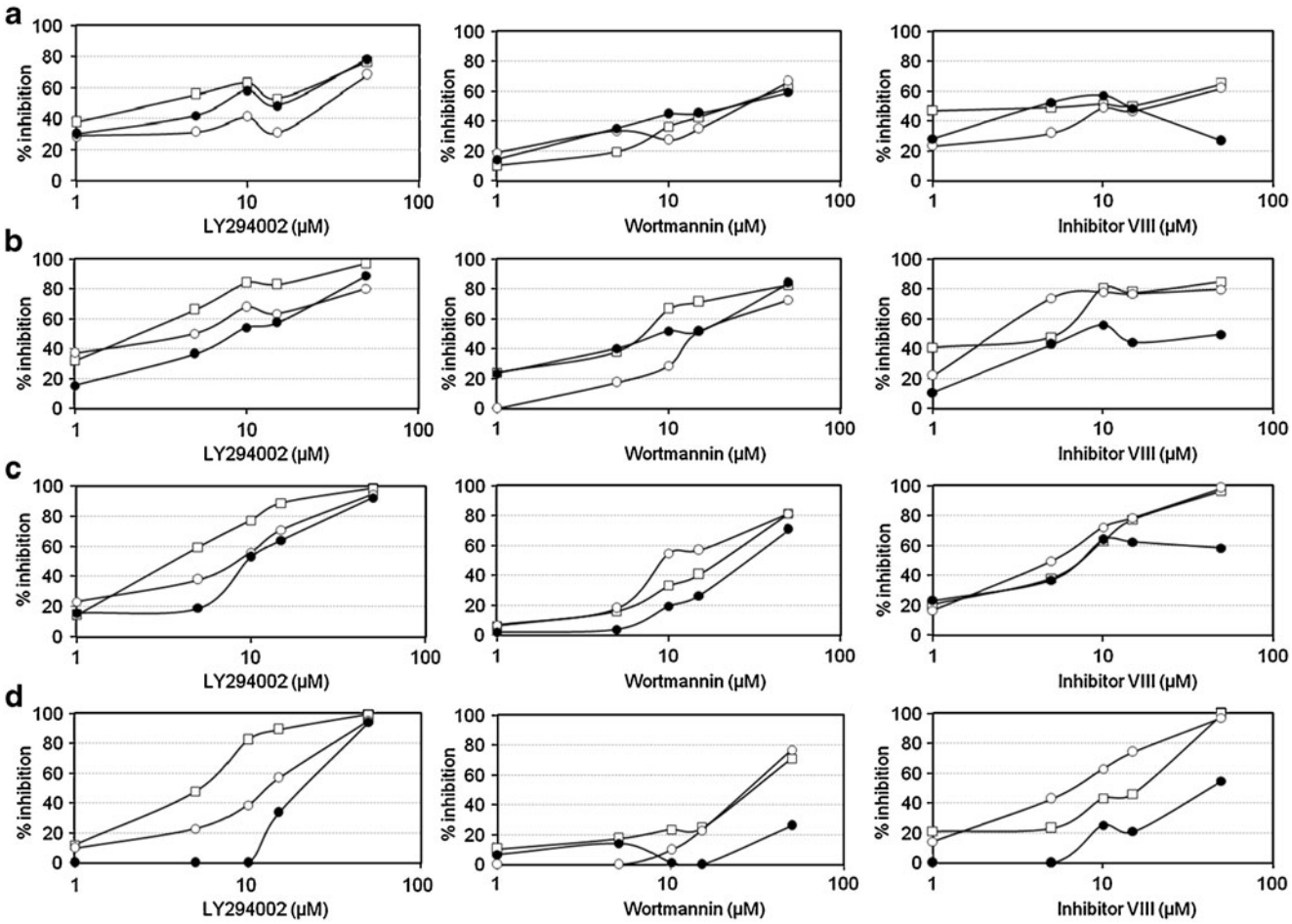

Fig. 2 Inhibitory effects of LY294002, Wortmannin and Akt Inhibitor VIII on HCC cell growth. % inhibition of cell growth after **a** 24, **b** 48, **c** 72 and **d** 96 hours of treatment with the inhibitors. Sulforhodamine B (SRB) colorimetric assay was performed in quadruplets with 5 different concentrations (50 μM, 15 μM, 10 μM, 5 μM, 1 μM) represented with error bars (Supplementary Figs. 1–3). The growth inhibitory effect for shorter exposure is relevant also for low concentrations. At longer exposure times growth inhibition requires higher drug concentrations. IC50 values were calculated based on the logarithmic regression line fitted on the % inhibition vs. log (concentration) graph, Huh7 (—□—), HepG2 (—○—), Mahlavu (—●—)

DMSO treated cell proliferation curves the cell growth plots demonstrated the concentration- and time-dependent cytotoxic effect of the inhibitors. In addition to provide also a visual demonstration of the effects of these drugs on these cells we treated cells with inhibitors and show their morphological changes by light microscope images at 24 and 48 hours in parallel with the RT-CES experiments with IC50 of 24 hours concentrations (Fig. 3b).

High dose treatment of LY294002 (40 μM) suppressed cell growth permanently after 8 h and continuing up to 84 h in Huh7 and Mahlavu cell lines. Lower doses (5 μM, 2.5 μM) of LY294002 had a minor effect on cell growth for up to 48 h but then the cells resumed growth, especially in the case of the Mahlavu cell line. With Inhibitor VIII treatment, cells responded similarly as to LY294002 exposure although Inhibitor VIII appeared more effective at short exposure times. Wortmannin treatment was effective in inhibiting cell growth only for about 24 h and then the cells gradually resumed normal growth. This real-time dynamic continuous analysis of cell growth and toxicity was essential to determine the optimal time points for performing biochemical endpoint assays. The continuous, dynamic analysis of cell growth of LY294002, Wortmannin and Akt Inhibitor VIII treated Huh7 and Mahlavu cells supported the time- and concentration-dependent effects of the three inhibitors on HCC cells as shown in Fig. 2.

We also analyzed Akt enzyme activity in the presence of inhibitors. The IC50 values of 72 h for LY294002, Wortmannin and Akt Inhibitor VIII were used to assess the effects of drug treatments on Akt kinase activity in HCC cell lines by a specific kinase assay using the fusion protein fusion protein of GSK3α/β as substrate similarly to that of Fig. 1b. Our results demonstrated the inhibitory effect of the three drugs on the kinase activity of the Akt protein, when compared to the kinase assay under native conditions. In all cases no Akt phosphorylation activity was

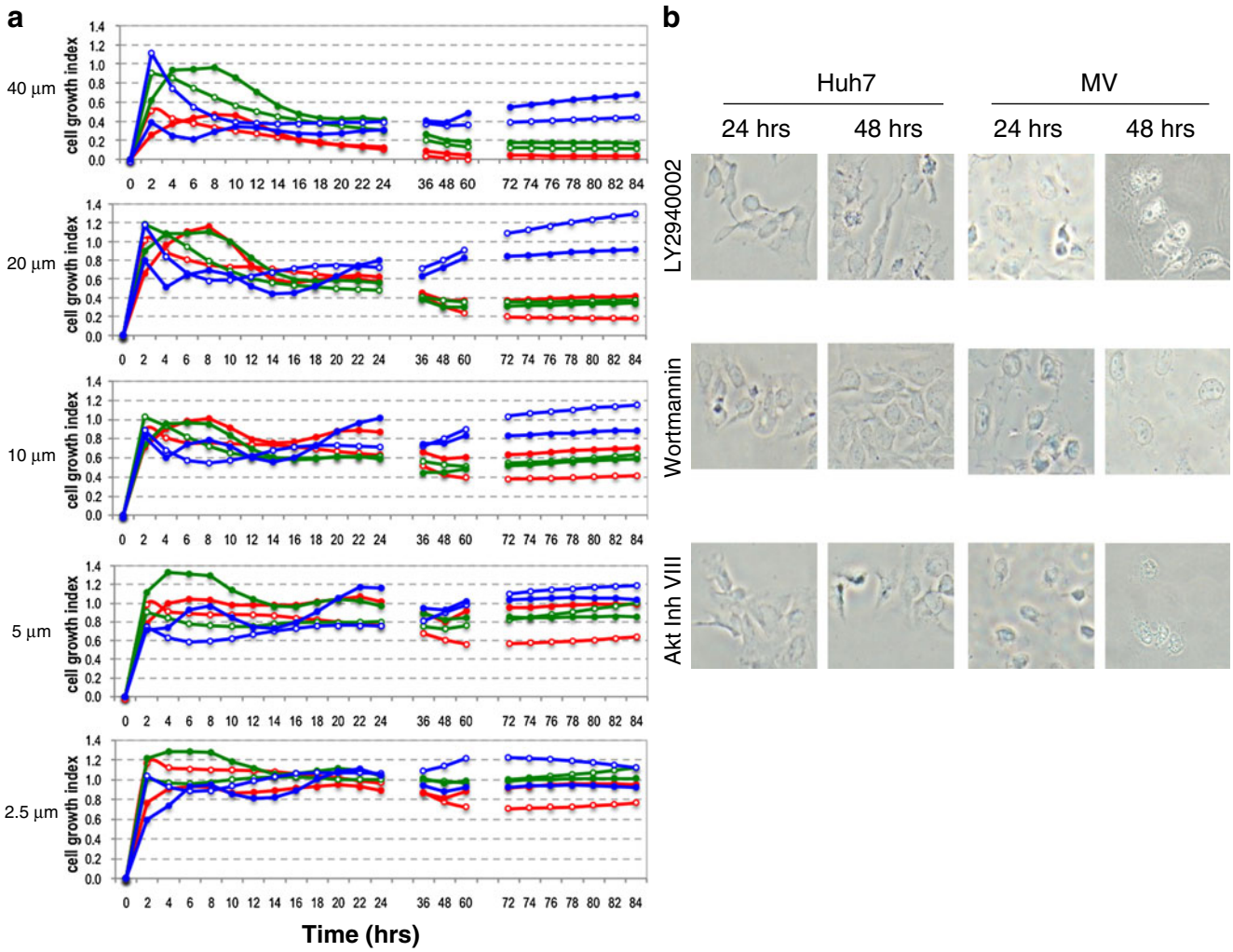

Fig. 3 Cell growth of LY294002, Wortmannin and Akt Inhibitor VIII treated Huh7 and Mahlavu cells. **a** Cell growth is assessed with the xCELLigence system that measures electrical impedance across micro-electrodes integrated on the bottom of tissue culture E-96 plates. Impedance measurements are displayed as Cell Index (CI) values, providing real-time quantitative information on cell growth. The effect of the inhibitors on cell growth is calculated as CI_{DRUG}/CI_{DMSO}. The cell growth assay was performed in triplicates with 5 different concentrations 40 µM, 20 µM, 10 µM, 5 µM, and 2.5 µM. Huh7-LY294002 (), Huh7-Akt Inhibitor VIII (), Huh7-Wortmannin (), Mahlavu-LY294002 (), Mahlavu-Akt Inhibitor VIII (), Mahlavu-Wortmannin (). **b** Analysis of apoptosis associated morphological changes with light microscopy. Huh7 and Mahlavu cells were treated with the indicated inhibitors at 24 and 48 hours. Huh7 cells : LY294002 (4 µM), Wortmannin (26 µM), Akt Inhibitor VIII (4.5 µM) ; Mahlavu cells : LY294002 (7 µM), Wortmannin (20 µM), Akt Inhibitor VIII (10 µM). 20X pictures were taken with OLYMPUS CKX41 microscope with DP72 camera

detected on the fusion protein of GSK3α/β (data not shown). These data indicate a very low Akt activity in each cell line, evidence of a significant inhibition of the pathway by these inhibitory molecules in HCC cells.

Cytotoxic effect of drugs on HCC cells through apoptosis

It is a well-documented fact that the Akt pathway has an important anti-apoptotic role in different cells [22, 23]. Morphological changes specific to apoptosis can be observed quite early after apoptotic stimuli [24, 25]. In order to see the morphological changes in Huh7, HepG2 and Mahlavu cells after treatment with each drug, cells were treated with inhibitors for 24 and 48 h. Each drug was used at its IC50 value obtained after 24 h of treatment. Apoptotic cells usually exhibit extensive DNA cleavage during the early stages of this controlled cell death mechanism. Cleavage may produce double-stranded, low molecular weight DNA fragments as well as single-stranded high molecular weight DNA fragments that manifests themselves as condensed aberrant nuclei, as shown by DAPI (Fig. 4) and the Hoechst 33258 stain (data not shown). This observation demonstrated that those cells displayed the type of cell death that is specific to apoptosis.

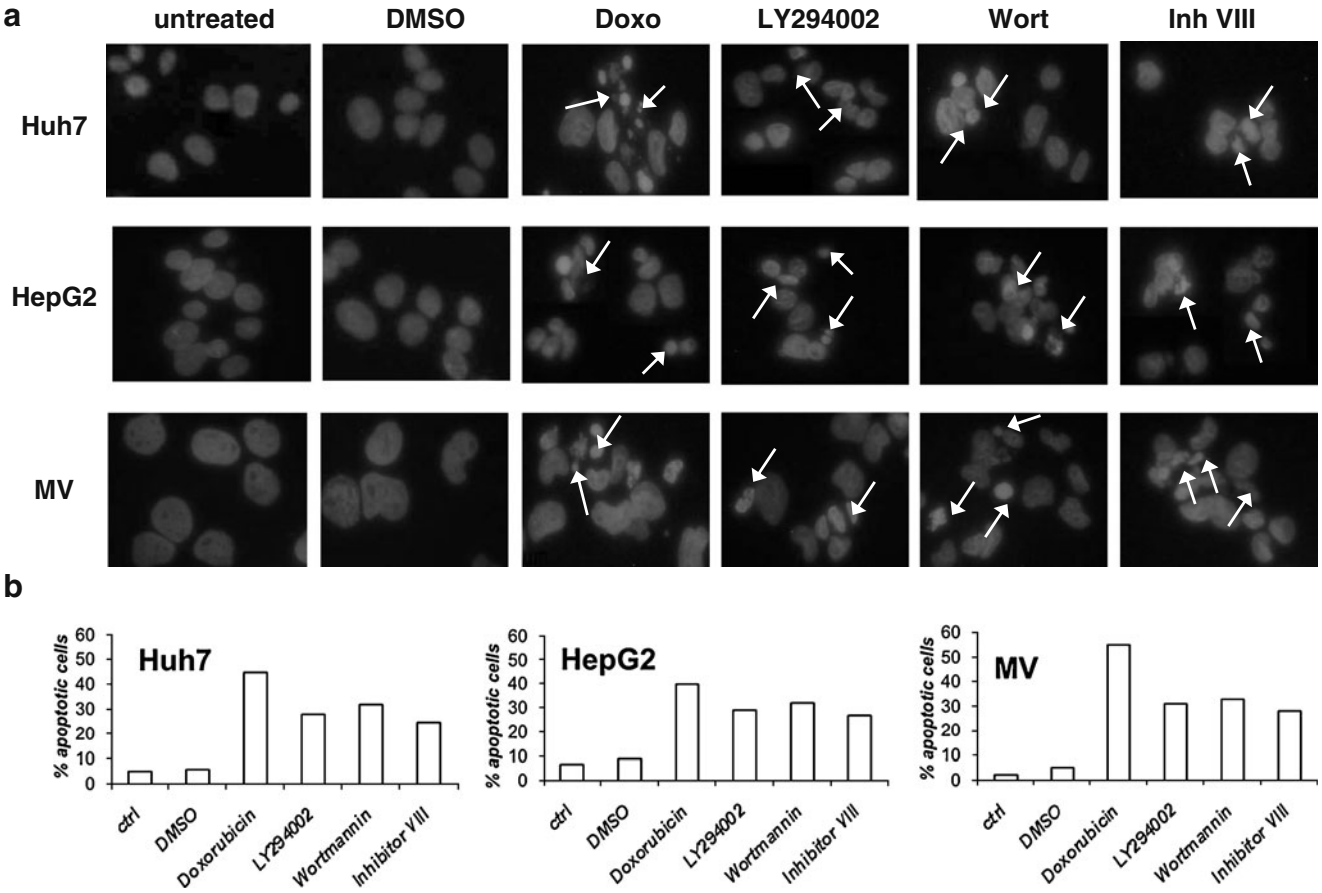

Fig. 4 DAPI staining showing the aberrant nuclear DNA due to the apoptotic cells with condensed nuclei (*white arrows*) in the presence of inhibitors with IC50 concentrations. **a** The pro-apoptotic effect of Akt pathway inhibitors on the morphology of the nuclear chromatin in HCC cells. Cells were treated for 24 h with the IC50 values **(**Huh7 : LY294002 (4 μM), Wortmannin (26 μM), Akt Inhibitor VIII (4.5 μM); HepG2 : LY294002 (25 μM), Wortmannin (29 μM), Akt Inhibitor VIII (18 μM); Mahlavu : LY294002 (7 μM), Wortmannin (20 μM), Akt Inhibitor VIII (10 μM)), then fixed and stained with DAPI. No changes were induced by DMSO. All samples treated with the positive control, Doxorubicine (100 ng/ml) showed evident apoptotic nuclei. Well markable, even if less present, are apoptotic nuclei after apoptosis induction with each drug. The results were from one experiment representative of three experiments. Bar=10 μm **b** Apoptotic cells were quantified by counting a minimum of 4 fields containing at least 150 cells. The results are presented as the mean of three independent experiments. Doxorubicine, an inhibitor of enzyme topoisomerase II progression by intercalation of DNA, induced a marked percentage of apoptosis. The three inhibitors used in this study within each cell line, gave similar results. SD was less then 10%

The pro-apoptotic effect of the drugs was assessed by counting aberrant nuclei in DAPI stained cells. The morphological features of apoptosis, i.e. condensation of chromatin and fragmentation of the nucleus, were examined. Control cells showed rounded and homogeneous nuclei, whereas drug treated-cells showed condensed and fragmented nuclei (Fig. 5a). The percentage of apoptosis ranged from 32% to 25% in Huh7, from 32% to 27% in HepG2 and from 35% to 28% in Mahlavu, (Fig. 4b).

In order to further clarify the type of cell death mechanism and the morphological changes that we observe in Figs. 3b, 4a, in the presence of the inhibitors as apoptosis, we performed Poly ADP-ribosyl polymerase (PARP) cleavage analysis by western blot. Huh7, HepG2 and Mahlavu cells were treated with each drug at the 24hours-IC50. PARP is typically cleaved from 113 kDa to 89 and 24 kDa fragments by caspase-3 during apoptosis. Although cleaved PARP is also detected during necrosis, the cleaved product's molecular size is different (50 kDa). As shown in Fig. 5, the cleaved band (89 kDa) is due to apoptosis, not necrosis [26]. Our observations clearly demonstrated that Akt pathway inhibitors had an apoptosis-dependent cytotoxic effect on HCC cell lines.

Comparative analysis of PTEN in HCC cells

With the aim of identifying differential responses of HCC cells to Akt pathway inhibitors, we further investigated PTEN, another pathway related molecule. PTEN protein expression in HCC cell lines exhibited differential expres-

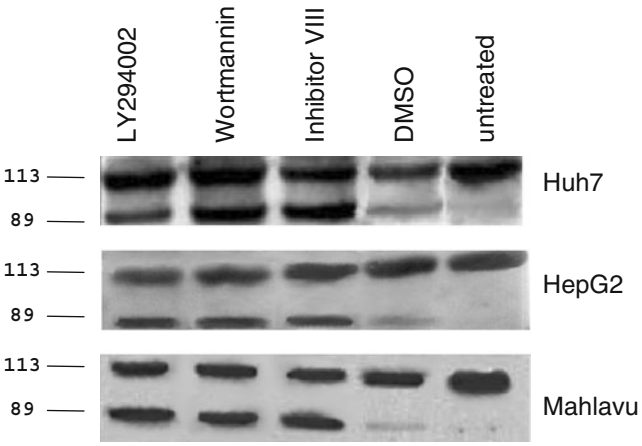

Fig. 5 Investigation of apoptotic cell death in the presence of Akt pathway inhibitors. Apoptosis activation was detected by means of PARP cleavage. The antibodies used recognize both the intact form (113 KDa) and the cleaved one (89 KDa). In each lane 20 μg proteins were loaded. . Almost no cleavage is observable in control and DMSO-treated samples. An evident PARP cleavage is induced by the three inhibitors used. Each cell line induced similar PARP cleavage. Data were representative of three independent experiments

sion patterns, ranging from marked expression in the Huh7 and HepG2 cell lines, to the absence of PTEN expression in Mahlavu cell line. The absence of PTEN protein expression was in correlation with the hyperphosphorylation of Akt, higher kinase activity on exogenous GSK3α/β fusion protein and on endogenous BAD protein in Mahlavu cell line. In correlation with the absence of PTEN protein expression, the Mahlavu cell line had mRNA expression with a partial deletion in the PTEN gene in exon 4 (Fig. 6), which may explain the lack of protein that results in the hyperactivation of the Akt protein in this cell line.

Discussion

In this study, we have shown hyperactivation of the Akt protein in hepatoma cell lines and apoptosis induction in time- and dose- dependent manners after treatment with three specific inhibitors of the PI3K/Akt pathway. The PI3K/Akt signaling pathway plays a significant role in carcinogenesis and drug resistance in different types of cancer including HCC, making Akt a potential target for cancer treatment [28, 29].

Tumors with activated PI3K/Akt signaling have been shown to become more aggressive, and Akt pathway activation has been identified as a significant risk factor for early disease recurrence and poor prognosis in HCC patients [30, 31]. Activated Akt correlates also with local metastasis of tumor cells from the primary liver cancer into the circulatory system and the survival of the circulating cells without cell-substratum interaction [32], showing the significance of this hyperactivated pathway not only in liver tumor aggressiveness but also in tumor diffusion and survival in different environments. Therefore we initially examined total Akt protein and native p-Akt levels in HCC cell lines. Mahlavu cells were previously reported to be poorly differentiated when compared to the well-differentiated "hepatocyte-like" Huh7 and HepG2 cells [18]. Although the cell lines included in this study showed similar total Akt protein expression (Fig. 1a), only Mahlavu cells displayed hyperphosphorylated Akt protein (Fig. 1a), which was determined by anti-p473Ser-Akt antibodies, because Ser473 Akt phosphorylation is a requirement for full Akt enzyme activity [33]. In Mahlavu cells, in parallel to the hyperphosphorylation of Akt, we also observed a lack of PTEN protein expression (Fig. 6) and increased phosphor-

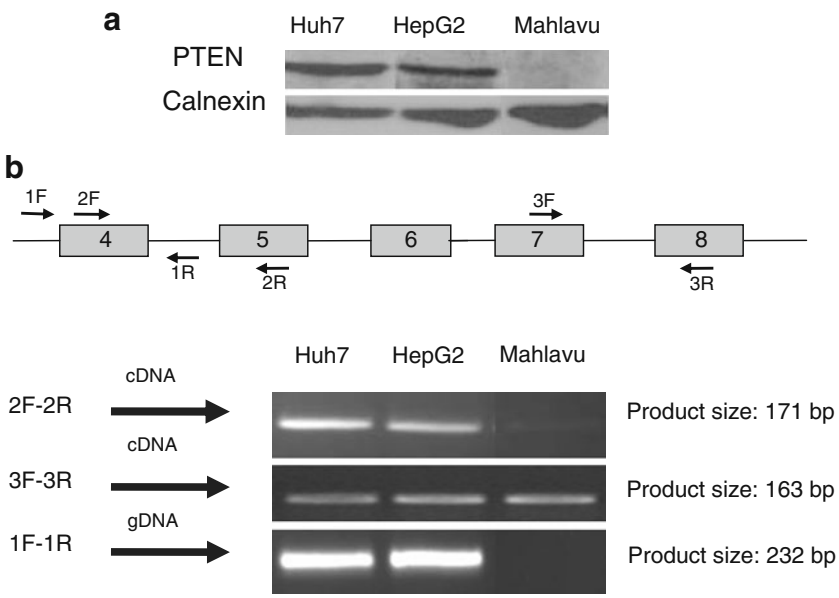

Fig. 6 Differential expression of the PTEN gene in human HCC cell lines. **a** Whole-cell lysates (40 μg) were analyzed by Western blotting using anti-PTEN antibody. Mahlavu cell line has no PTEN expression. **b** PCR analysis of PTEN gene in HCC cell lines. Figure describes the loss of PTEN gene fragment. The gene fragment that is lacking is located within exon 4 and 5

ylation of the downstream protein Bad on Ser136 and of the exogenous GSK3 substrate (Fig. 1b and c).

The activation of PI3K/Akt signaling frequently related to PTEN mutation has also been observed in nearly 50% of HCC [34], suggesting the importance of this pathway, since tumors with hyperactive Akt due to PTEN loss depend on hyperactivated Akt signaling for growth and survival [10]. Indeed, our results support the observations that a PTEN deficient cell line Mahlavu has hyperactivated Akt protein. Moreover Mahlavu has the higher IC50 values for Wortmannin than well differentiated Huh7 and HepG2 cell lines.

The great majority of protein kinase inhibitors that have been developed, bind at or near the ATP binding site [35]. These compounds were recommended for use in a concentration range of 0,1 to 100 μM to assess the roles of particular protein kinases. Depending on concentration, kinase inhibitors may act as multi-kinase inhibitors. Therefore in our study we analyzed the PI3K/Akt signaling inhibitors with concentrations between 40 μM–2.5 μM (Figs. 2 and 3) in order to identify their specific IC50 values on hepatoma cell lines. We think that with the concentration we used LY294002 and Wortmannin exhibit their cytotoxic activity through binding to the proximity of the active sites of their target kinases. Structural analysis of the p110γ isoform of PI3K in the presence of LY294002 demonstrated that this inhibitor binds to the active site. Cell death induced by LY294002 is through GSK3β activity, which is also demonstrated in the presence of lithium, a known inhibitor of GSK3β [36, 37]. Consistent with the structural similarity between the PI3K and mTOR kinase domains, LY294002 and Wortmannin act on both of these kinases with similar IC50 values [38]. Both PI3K and mTORC2 are the upstream proteins of the Akt pathway. Therefore, we focused also on the downstream analysis of Akt protein activation/inhibition regardless of the direct targets of LY294002 and Wortmannin in HCC cells. To stress the importance of Akt pathway signaling inhibition as a potential therapeutic target in liver cancer, we analyzed the effects of the selective Akt inhibitor, Akt Inhibitor VIII on HCC cells [20, 21].

We applied two different cytotoxicity assays, conventional NCI-60 method and novel RT-CES system. Both assays resulted in similar IC50 values for 24, 48, and 72 h for the specific PI3K/Akt signaling inhibitors LY294002, Wortmannin, and Akt inhibitor VIII, although it is possible to calculate IC50 for each time point with RT-CES. As expected, we were able to demonstrate that all three inhibitors had cytotoxic activity. At 24 h all three cells had comparable IC50s but with longer treatment times Mahlavu cells displayed higher IC50s when compared to Huh7 and HepG2 cells. RT-CES analysis demonstrated that normal cell growth has a cell index (CI) of around 1.2 (Fig. 3a). 20 μM inhibitor treatment did not influence the cell proliferation during the initial 10–16 h. The cytotoxic effect of the inhibitors became established toward the end of the 24 h (Fig. 3a, 40–10 μM) as it can be observed by the CI of 0.5. Between 36 h and to 60 h RT-CES data demonstrated whether they inhibit cell proliferation irreversibly or whether cells can survive afterwards. In the case of LY294002 and Akt inhibitor VIII, CI approached to 0.2 at the 60th hour meaning almost no cells attached to the bottom of the cell culture plates to form colonies. We confirmed this data in parallel experiments by direct light microscopy visualization of the cells at 24 and 48 h (Fig. 3b). Cells treated with Wortmannin displayed a similar growth curve with CI during first 24 h to that of LY294002 and Akt inhibitor VIII did. However starting from 36 h both Huh7 and Mahlavu cells continued to proliferate and expanded to cover the bottom of the E-plate parallel to the DMSO treated control cells even with very high (40 μM) concentrations. We confirmed again by microscopy that the cells presented a healthy morphology (Fig. 3b).

Continuous very low Cell Index data (0.2–0.3) with LY294002 and Akt inhibitor VIII treatments on the hepatoma cells were the indications of apoptotic cell death. In addition direct light microscopy visualization of the cell morphology showed that all the inhibitors induced apoptosis on hepatoma cells. From the above evidence the nature of the cell death exhibited in the presence of the PI3K/Akt signaling inhibitors LY294002, Wortmannin, and Akt inhibitor VIII was characterized as apoptosis (Figs. 4 and 5).

The three drugs, generated a PARP cleavage process on the HCC cell lines after being administered (Fig. 5). As shown above, the drugs appear to have similar apoptotic effects in all the cell lines tested. In addition, since PI3K-Class IIIs control autophagic proteolysis, we examined the possibility that the cytotoxic effect of these inhibitors might be through autophagy [27]. After 48 h of incubation with the three inhibitors we performed western blot analysis of autophagy related proteins BECN1 and p62 but did not observe any alterations that could be attributed to autophagy (data not shown).

This study suggests that targeting the PI3K/Akt signaling pathway provides a promising strategy for designing molecular targeted therapy in the case of solid tumors, especially HCC. Our data also suggest that PI3K/Akt activation status serve as a biomarker for identifying candidate patients for treatment with inhibitors of PI3K and/or of its downstream targets. However, it should be noted that drug transporters or IAPs (Inhibitors of Apoptosis Proteins) could contribute to the therapeutic resistance. Likewise, transcription factors, such as NF-κB, can up-regulate transporters like MRP2 to induce multidrug resistance in HCC [39]. Furthermore, we have previously

shown that during liver tumorigenesis HCC cells develop a "survivor phenotype" independent of the cause of oncogenic transformation under oxidative stress conditions [40].

It may also be important to raise questions about the stability of the drugs for longer treatments. We performed experiments, by monitoring cell growth real time, that demonstrated that when drug concentration increases, growth inhibition lasts longer. This observation could be due to a lower a decay rate of active drug molecule concentration. Our results obtained by the three PI3K/Akt pathway inhibitors used clearly demonstrated that the Akt pathway can still be a target when Akt and BAD are hyperphosphorylated and the PTEN protein is impaired, as we show in the Mahlavu cell line. In treatment, chemotherapeutic agents are usually given in a protocol with repeating dosages to target resistant cell populations.

Tumors with hyperactive Akt due to PTEN loss depend on Akt signaling for growth and survival [10]. Activated Akt pathway confers resistance to cancer therapy, making Akt a promising target for cancer treatment [34]. Increasing knowledge in the molecular mechanisms underlying hepatocarcinogenesis and the advent of molecular targeted therapies provide a promising treatment approach for HCC patients. Novel therapeutic targets, molecular oncogenic mechanisms and signaling cascades responsible for tumor growth should be investigated together with potential chemotherapeutic agents to improve clinical efficacy.

Acknowledgement We are indebted to Prof A. Esen (Virgina Tech) and Ms. R. Nelson for editing the English of the final version of our manuscript. This work was supported by The Scientific and Technical Research Council of Turkey, TUBITAK (project # 106 S359), the KANILTEK project Bilkent University local funds and MAE 2008, Fondazione CARIFE, Italian MIUR Cofin 2005, Fondazione CARICENTO, local funds of Ferrara University for Stamina Project (to SC), LMN and DE.

References

1. McGlynn KA, Tsao L, Hsing AW, Devesa SS, Fraumeni JF Jr (2001) International trends and patterns of primary liver cancer. Int J Cancer 94:290–296. doi:10.1002/ijc.1456
2. Ozturk N, Erdal E, Mumcuoglu M, Akcali KC, Yalcin O, Senturk S, Arslan-Ergul A, Gur B, Yulug I, Cetin-Atalay R, Yakicier C, Yagci T, Tez M, Ozturk M (2006) Reprogramming of replicative senescence in hepatocellular carcinoma-derived cells. Proc Natl Acad Sci USA 103:2178–2183. doi:10.1073/pnas.0510877103
3. Osaki M, Oshimura M, Ito H (2004) PI3K-Akt pathway: its functions and alterations in human cancer. Apoptosis 9:667–676. doi:10.1023/B:APPT.0000045801.15585.dd
4. Llovet JM, Ricci S, Mazzaferro V, Hilgard P, Gane E et al (2008) Sorafenib in advanced hepatocellular carcinoma. N Engl J Med 359:378–390. doi:10.1056/NEJMoa0708857
5. Engelman JA (2009) Targeting PI3K signalling in cancer: opportunities, challenges and limitations. Nat Rev Cancer 9:550–562. doi:10.1038/nrc2664
6. Liu P, Cheng H, Roberts TM, Zhao JJ (2009) Targeting the phosphoinositide 3-kinase pathway in cancer. Nat Rev Drug Discov 8:627–644. doi:10.1038/nrd2926
7. Tokunaga E, Oki E, Egashira A, Sadanaga N, Morita M, Kakeji Y, Maehara Y (2008) Deregulation of the Akt pathway in human cancer. Curr Cancer Drug Targets 8:27–36
8. Carnero A, Blanco-Aparicio C, Renner O, Link W, Leal JF (2008) The PTEN/PI3K/AKT signalling pathway in cancer, therapeutic implications. Curr Cancer Drug Targets 8:187–198
9. Hanada M, Feng J, Hemmings BA (2004) Structure, regulation and function of PKB/AKT–a major therapeutic target. Biochim Biophys Acta 1697:3–16. doi:10.1016/j.bbapap.2003.11.009
10. Salvesen HB, Stefansson I, Kretzschmar EI, Gruber P, MacDonald ND, Ryan A, Jacobs IJ, Akslen LA, Das S (2004) Significance of PTEN alterations in endometrial carcinoma: a population-based study of mutations, promoter methylation and PTEN protein expression. Int J Oncol 25:1615–1623
11. Xu G, Zhang W, Bertram P, Zheng XF, McLeod H (2004) Pharmacogenomic profiling of the PI3K/PTEN-AKT-mTOR pathway in common human tumors. Int J Oncol 24:893–900
12. Arcaro A, Guerreiro AS (2007) The phosphoinositide 3-kinase pathway in human cancer: genetic alterations and therapeutic implications. Curr Genomics 8:271–306. doi:10.2174/138920207782446160
13. Ozturk M EE, Ozturk N, Cetin-Atalay R and Irmak B (2005) Molecular Biology of Liver Cancer. In: RA M. Encyclopedia of Molecular Cell Biology and Molecular Medicine, Wiley-VCH, 2ed, vol. 7:323–335
14. Missiroli S, Etro D, Buontempo F, Ye K, Capitani S, Neri LM (2009) Nuclear translocation of active AKT is required for erythroid differentiation in erythropoietin treated K562 erythroleukemia cells. Int J Biochem Cell Biol 41(3):570–577
15. Monks A, Scudiero D, Skehan P, Shoemaker R, Paull K, Vistica D, Hose C, Langley J, Cronise P, Vaigro-Wolff A et al (1991) Feasibility of a high-flux anticancer drug screen using a diverse panel of cultured human tumor cell lines. J Natl Cancer Inst 83:757–766
16. Kirstein SL, Atienza JM, Xi B, Zhu J, Yu N, Wang X, Xu X, Abassi YA (2006) Live cell quality control and utility of real-time cell electronic sensing for assay development. Assay Drug Dev Technol 4(5):545–553
17. LoPiccolo J, Granville CA, Gills JJ, Dennis PA (2007) Targeting Akt in cancer therapy. Anticancer Drugs 18(8):861–874, Review
18. Sayan B, Tolga Emre NC, Irmak MB, Ozturk M, Cetin-Atalay R (2009) Nuclear exclusion of p33ING1b tumor suppressor protein: explored in HCC cells using a new highly specific antibody. Hybridoma 28:1–6. doi:10.1089/hyb.2008.0058
19. del Peso L, Gonzalez-Garcia M, Page C, Herrera R, Nunez G (1997) Interleukin-3-induced phosphorylation of BAD through the protein kinase Akt. Science 278:687–689
20. Barnett SF, Defeo-Jones D, Fu S, Hancock PJ, Haskell KM et al (2005) Identification and characterization of pleckstrin-homology-domain-dependent and isoenzyme-specific Akt inhibitors. Biochem J 385:399–408. doi:10.1042/BJ20041140
21. Zhao Z, Leister WH, Robinson RG, Barnett SF, Defeo-Jones D, Jones RE, Hartman GD, Huff JR, Huber HE, Duggan ME, Lindsley CW (2005) Discovery of 2, 3, 5-trisubstituted pyridine derivatives as potent Akt1 and Akt2 dual inhibitors. Bioorg Med Chem Lett 15:905–909. doi:10.1016/j.bmcl.2004.12.062
22. Manning BD, Cantley LC (2007) AKT/PKB signaling: navigating downstream. Cell 129:1261–1274. doi:10.1016/j.cell.2007.06.009
23. Fabregat I (2009) Dysregulation of apoptosis in hepatocellular carcinoma cells. World J Gastroenterol 15:513–520
24. Kim MJ, Oh SJ, Park SH, Kang HJ, Won MH, Kang TC, Hwang IK, Park JB, Kim JI, Kim J, Lee JY (2007) Hypoxia-induced cell

death of HepG2 cells involves a necrotic cell death mediated by calpain. Apoptosis 12:707–718. doi:10.1007/s10495-006-0002-3
25. Messam CA, Pittman RN (1998) Asynchrony and commitment to die during apoptosis. Exp Cell Res 238:389–398. doi:10.1006/excr.1997.3845
26. Gobeil S, Boucher CC, Nadeau D, Poirier GG (2001) Characterization of the necrotic cleavage of poly(ADP-ribose) polymerase (PARP-1): implication of lysosomal proteases. Cell Death Differ 8:588–594. doi:10.1038/sj.cdd.4400851
27. Blommaart EF, Krause U, Schellens JP, Vreeling-Sindelarova H, Meijer AJ (1997) The phosphatidylinositol 3-kinase inhibitors wortmannin and LY294002 inhibit autophagy in isolated rat hepatocytes. Eur J Biochem 243:240–246
28. Cully M, You H, Levine AJ, Mak TW (2006) Beyond PTEN mutations: the PI3K pathway as an integrator of multiple inputs during tumorigenesis. Nat Rev Cancer 6(3):184–192, Review
29. Schmitz KJ, Wohlschlaeger J, Lang H, Sotiropoulos GC, Malago M et al (2008) Activation of the ERK and AKT signalling pathway predicts poor prognosis in hepatocellular carcinoma and ERK activation in cancer tissue is associated with hepatitis C virus infection. J Hepatol 48:83–90. doi:10.1016/j.jhep.2007.08.018
30. Nakanishi K, Sakamoto M, Yamasaki S, Todo S, Hirohashi S (2005) Akt phosphorylation is a risk factor for early disease recurrence and poor prognosis in hepatocellular carcinoma. Cancer 103(2):307–312
31. Hu TH, Huang CC, Lin PR, Chang HW, Ger LP, Lin YW, Changchien CS, Lee CM, Tai MH (2003) Expression and prognostic role of tumor suppressor gene PTEN/MMAC1/TEP1 in hepatocellular carcinoma. Cancer 97(8):1929–1940
32. Boyault S, Rickman DS, de Reynies A, Balabaud C, Rebouissou S, Jeannot E, Herault A, Saric J, Belghiti J, Franco D (2007) (2008) Transcriptome classification of HCC is related to gene alterations and to new therapeutic targets. Hepatology 45:42–52
33. Recher C, Dos Santos C, Demur C, Payrastre B (2005) mTOR, a new therapeutic target in acute myeloid leukemia. Cell Cycle 4:1540–1549
34. Lindsley CW, Barnett SF, Layton ME, Bilodeau MT (2008) The PI3K/Akt pathway: recent progress in the development of ATP-competitive and allosteric Akt kinase inhibitors. Curr Cancer Drug Targets 8:7–18
35. Bain J, Plater L, Elliott M, Shpiro N, Hastie CJ, McLauchlan H, Klevernic I, Arthur JS, Alessi DR, Cohen P (2007) The selectivity of protein kinase inhibitors: a further update. Biochem J 408:297–315. doi:10.1042/BJ20070797
36. Beurel E, Kornprobst M, Blivet-Van Eggelpoel MJ, Cadoret A, Capeau J, Desbois-Mouthon C (2005) GSK-3beta reactivation with LY294002 sensitizes hepatoma cells to chemotherapy-induced apoptosis. Int J Oncol 27:215–222
37. Erdal E, Ozturk N, Cagatay T, Eksioglu-Demiralp E, Ozturk M (2005) Lithium-mediated downregulation of PKB/Akt and cyclin E with growth inhibition in hepatocellular carcinoma cells. Int J Cancer 115:903–910. doi:10.1002/ijc.20972
38. Ballou LM, Selinger ES, Choi JY, Drueckhammer DG, Lin RZ (2007) Inhibition of mammalian target of rapamycin signaling by 2-(morpholin-1-yl)pyrimido[2, 1-alpha]isoquinolin-4-one. J Biol Chem 282:24463–24470. doi:10.1074/jbc.M704741200
39. Okamoto T, Sanda T, Asamitsu K (2007) NF-kappa B signaling and carcinogenesis. Curr Pharm Des 13:447–462
40. Irmak MB, Ince G, Ozturk M, Cetin-Atalay R (2003) Acquired tolerance of hepatocellular carcinoma cells to selenium deficiency: a selective survival mechanism? Cancer Res 63:6707–6715

OPEN ACCESS Freely available online

PLoS one

The Ability to Generate Senescent Progeny as a Mechanism Underlying Breast Cancer Cell Heterogeneity

Mine Mumcuoglu[1], Sevgi Bagislar[1,2], Haluk Yuzugullu[1,2], Hani Alotaibi[1], Serif Senturk[1], Pelin Telkoparan[1], Bala Gur-Dedeoglu[1], Burcu Cingoz[1], Betul Bozkurt[3], Uygar H. Tazebay[1], Isik G. Yulug[1], K. Can Akcali[1], Mehmet Ozturk[1,2]*

1 BilGen Genetics and Biotechnology Center, Department of Molecular Biology and Genetics, Bilkent University, Ankara, Turkey, **2** INSERM - Université Joseph Fourrier, CRI U823, Grenoble, France, **3** Department of Surgery, Ankara Numune Research and Teaching Hospital, Ankara, Turkey

Abstract

Background: Breast cancer is a remarkably heterogeneous disease. Luminal, basal-like, "normal-like", and ERBB2+ subgroups were identified and were shown to have different prognoses. The mechanisms underlying this heterogeneity are poorly understood. In our study, we explored the role of cellular differentiation and senescence as a potential cause of heterogeneity.

Methodology/Principal Findings: A panel of breast cancer cell lines, isogenic clones, and breast tumors were used. Based on their ability to generate senescent progeny under low-density clonogenic conditions, we classified breast cancer cell lines as senescent cell progenitor (SCP) and immortal cell progenitor (ICP) subtypes. All SCP cell lines expressed estrogen receptor (ER). Loss of ER expression combined with the accumulation of $p21^{Cip1}$ correlated with senescence in these cell lines. $p21^{Cip1}$ knockdown, estrogen-mediated ER activation or ectopic ER overexpression protected cells against senescence. In contrast, tamoxifen triggered a robust senescence response. As ER expression has been linked to luminal differentiation, we compared the differentiation status of SCP and ICP cell lines using stem/progenitor, luminal, and myoepithelial markers. The SCP cells produced CD24+ or ER+ luminal-like and ASMA+ myoepithelial-like progeny, in addition to CD44+ stem/progenitor-like cells. In contrast, ICP cell lines acted as differentiation-defective stem/progenitor cells. Some ICP cell lines generated only CD44+/CD24-/ER-/ASMA- progenitor/stem-like cells, and others also produced CD24+/ER- luminal-like, but not ASMA+ myoepithelial-like cells. Furthermore, gene expression profiles clustered SCP cell lines with luminal A and "normal-like" tumors, and ICP cell lines with luminal B and basal-like tumors. The ICP cells displayed higher tumorigenicity in immunodeficient mice.

Conclusions/Significance: Luminal A and "normal-like" breast cancer cell lines were able to generate luminal-like and myoepithelial-like progeny undergoing senescence arrest. In contrast, luminal B/basal-like cell lines acted as stem/progenitor cells with defective differentiation capacities. Our findings suggest that the malignancy of breast tumors is directly correlated with stem/progenitor phenotypes and poor differentiation potential.

Citation: Mumcuoglu M, Bagislar S, Yuzugullu H, Alotaibi H, Senturk S, et al. (2010) The Ability to Generate Senescent Progeny as a Mechanism Underlying Breast Cancer Cell Heterogeneity. PLoS ONE 5(6): e11288. doi:10.1371/journal.pone.0011288

Editor: Syed A. Aziz, Health Canada, Canada

Received March 16, 2010; **Accepted** June 4, 2010; **Published** June 24, 2010

Funding: This work was supported by TUBITAK (The Scientific and Technological Research Council of Turkey), DPT (State Planning Office of Turkey) and TUBA (Turkish Academy of Sciences). Additional funding was from Institut National de Cancer and INSERM of France. The funders had no role in study design, data collection and analysis, decision to publish, or preparation of the manuscript.

Competing Interests: The authors have declared that no competing interests exist.

* E-mail: ozturkm@ujf-grenoble.fr

Introduction

Human breast tumors are heterogeneous, both in their pathology and in their molecular profiles. Gene expression analyses classify breast tumors into distinct subtypes, such as luminal A, luminal B, ERBB2-positive (ERBB2+) and basal-like [1,2,3]. The prognosis and therapeutic response of each subtype is different. Luminal A cancers are mostly estrogen receptor-α-positive (ER+) and sensitive to anti-estrogen therapy, with the best metastasis-free and overall survival rates. Luminal B tumors have an incomplete anti-estrogen response and lower survival rates. Basal-like and ERBB2+ tumors are ER- and display the worst survival rates [2,3]. The patterns of genetic changes such as chromosomal aberrations and gene mutations observed in breast tumors indicate that breast tumorigenesis does not follow a stepwise linear progression from well-differentiated to poorly differentiated tumors with cumulative genetic aberrations [4]. This suggests that different breast tumor subtypes do not represent different stages of tumor progression, but rather represent the cells from which they initiate [4]. The mammary gland is composed of differentiated luminal and myoepithelial cells that are generated from multi-lineage, luminal-restricted, and myoepithelial-restricted progenitors originating from a hypothetical breast epithelial stem cell. Thus, different types of breast cancers might originate from such stem or progenitor cells at a given stage of commitment and differentiation, as observed in hematological malignancies [4,5]. Without compromising the author's hypothesis, it is also possible that the molecular heterogeneity of breast cancer is due to subtle differences in the ability of tumor-initiating cells to generate differentiated progeny.

Epithelial cells isolated from mammary gland cells undergo two successive senescence states in cell culture, termed "stasis" and "agonescence" [6,7]. In contrast to normal mammary epithelial cells, established breast cancer cells are immortal by definition. They may owe this phenotype of immortalization to genetic and epigenetic inactivation of senescence checkpoints and reactivation of telomerase reverse transcriptase expression [7]. Either in relation to these changes or independently, breast cancer cells may also present a stem/progenitor phenotype that is less subjected or resistant to senescence barriers. However, the abundance of non-tumorigenic and differentiated cells both in breast tumors and cell lines strongly suggests that replicative immortality cannot be assigned to all cells within a tumor or a cancer cell line, and that spontaneous senescence after a limited number of population doublings (PD) is likely to occur. If this hypothesis is correct, then the rate of generation of senescent progeny may reflect the potential of a cancer stem/progenitor cell to produce terminally differentiated progeny. We tested this hypothesis using a panel of luminal and basal-like breast cancer cell lines (Table S1). Although a single cell line is not representative of breast tumor heterogeneity, a panel of cell lines might reproduce the heterogeneity that is observed in primary breast tumors, albeit with some limitations [5,8]. Therefore, we hoped that in vitro studies with a panel of cell lines might help to better understand breast tumor heterogeneity.

Our senescence tests allowed us to classify breast cancer cell lines as senescent cell progenitor (SCP) and immortal cell progenitor (ICP) subtypes. We also show that senescent progeny are observed exclusively in ER-positive cells, as a result of ER inactivation, partly mediated with $p21^{Cip1}$ protein. The ability to produce senescent progeny was associated with the ability to produce luminal-like and myoepithelial-like progeny from stem/progenitor-like cells. In contrast, most of the cell lines lacking senescent progeny were also unable to generate differentiated progeny. Finally, we show that SCP-subtype cells cluster with luminal A and "normal-like" breast tumor types and are less tumorigenic, whereas ICP-subtype cell lines cluster with luminal B and basal-like tumor types and are more tumorigenic.

Materials and Methods

Ethics Statement

We used archival tumor samples remaining from a previous study by BB and IGY described in Gur-Dedeoglu et al. [9], for which the use of the tissue material was approved by the Research Ethics Committee of Ankara Numune Research and Teaching Hospital (decision date: 04/07/2007). The tumor samples in this study were used anonymously. All animals received care according to the Guide for the Care and Use of Laboratory Animals. All animal experiments have been pre-approved by the Bilkent University Animal Ethics Committee (Decision No: 2006/1; Decision date: 10/5/2006).

Clinical samples and cell lines

Freshly frozen tumor specimens were collected at Ankara Numune Hospital. Breast cancer cell lines used in this study were obtained from ATCC (http://www.atcc.org) and listed in Table S1. Cell line authenticity was verified by short tandem repeat profiling, as recommended by ATCC (Dataset S1). Isogenic clones from the T47D (n = 20) cell line were obtained from single cell-derived colonies. Briefly, cells were plated in 96-well plates to obtain single colonies in fewer than 70% of the wells. Isolated colonies were then transferred to progressively larger wells, and to T25 flasks. Clones were subcultivated weekly at 1:4 dilution ratios, and maintained in culture for 25–30 passages to reach >60 PD before testing.

Primary antibodies

The following antibodies were used: anti-CD44 (559046; BD Pharmingen), anti-CD24 (sc53660; Santa Cruz,), anti-ASMA (ab7817; Abcam), anti-CK19 (sc6278; Santa Cruz,), anti-$p21^{Cip1}$ (OP64; Calbiochem), anti-$p16^{Ink4a}$ (NA29, Calbiochem), anti-ERα (sc8002; Santa Cruz).

Low-density clonogenic assays

Cells were seeded as low-density on coverslips in six-well plates (500–2000 cells, according to plating efficiency) and allowed to grow in DMEM supplemented with 10% fetal calf serum (FCS), with medium change every three days, until they formed colonies of a few hundred cells. Depending on the cell line, this took one to two weeks. For bromodeoxyuridine (BrdU) incorporation assays, cells were labeled for 24 h prior to immunocytochemistry, as described previously [10].

Immunocytochemistry

For simple immunoperoxidase assays, cells were fixed with cold methanol for five minutes, then blocked with 10% FCS in phosphate-buffered saline (PBS) for 1 hour. This was followed by incubation with a primary antibody for 1 h. Cells were then washed with PBS three times and subjected to immunostaining using the Dako-Envision-dual-link system and the liquid diaminobenzidine (DAB) substrate chromogen system (Dako, CA, USA), according to the manufacturer's instructions. Hematoxylin was used as a counter-stain when the visualization of cells was necessary. For SABG-immunoperoxidase co-staining studies, unfixed cells were first subjected to SABG assay, and then fixed prior to immunostaining assays. Hematoxylin counter-staining was omitted for co-staining experiments, unless cells were negative for SABG staining.

Immunoblot analyses

Cell pellets were incubated in an NP-40 lysis buffer containing 50 mM Tris–HCl, pH 8.0, 250 mM NaCl, 0.1% Nonidet P-40, and a protease inhibitor cocktail (Roche) for 30 minutes in a cold room. Cell lysates were then cleared by centrifugation, and a Bradford assay was performed to quantify their protein concentration. 30 µg of protein was denatured and resolved by SDS-PAGE using 10% or 12% gels. The proteins were then transferred to the PVDF or nitrocellulose membranes. Membranes were treated for 1 h with a blocking solution of TRIS-buffered saline containing 0.1% Tween-20 and 5% non-fat milk powder (TBS-T) and probed with a primary antibody for 1 h. Next, membranes were washed three times with TBS-T and incubated with an HRP-conjugated secondary antibody for 1 h. Immunocomplexes were then detected by an ECL-plus (Amersham) kit on the membrane. α-tubulin was used as an internal control.

SABG assay and BrdU/SABG co-staining

SABG activity was detected as described [11], except that cells were counterstained with eosin or nuclear fast red following SABG staining. For BrdU/SABG co-staining, cells were first labeled with BrdU (10 µg/ml) for 24 h in a freshly added culture medium as described [10]. Next, cells were subjected to a SABG assay, fixed in 70% methanol, and subjected to BrdU immunostaining.

Estrogen and tamoxifen treatment

Cells were seeded under low-density clonogenic conditions onto coverslips in six-well plates, and cultivated in a standard culture

medium for seven to eight days. Then, cells were fed with phenol red-free DMEM (Gibco) supplemented with 5% charcoal-stripped FCS for 48 h, followed by two successive 48 h treatments with 10^{-9} M estrogen (E2; 17β-estradiol; Sigma), 10^{-6} to 10^{-9} M 4-hydroxytamoxifen (4OHT; Sigma) or an ethanol vehicle, under the same conditions. Colonies were then subjected to a SABG assay. Each experimental condition was conducted in triplicate and experiments were repeated three times.

Generation of estrogen receptor-overexpressing clones

T47D-iso23 cells were transfected with the expression vector pCMV- ERα [12] or an empty vector, using FuGENE-6 (Roche). ER overexpressing and control clones were selected with 500 μg/ml G418 for three weeks. Isolated single cell-derived colonies were picked and expanded in the presence of G418.

Lentiviral infection and generation of $p21^{Cip1}$ knockdown clones

We used mission shRNA plasmid pLKO.1<-puro-p21 (NM_000389.2-640s1c1, Sigma) for $p21^{cip1}$ knockdown experiments. The Control vector shRNA-pGIPz-SCR-puro and a helper packaging mix (Invitrogen) were also used. HEK293T was co-transfected with the appropriate vector and packaging mix, using the CalPhos Mammalian Transfection Kit (Clontech) and following the manufacturer's instructions. After 48 h of culture, virus-containing culture media were collected, filtered, and used to infect T47D-iso23 cells. After 4 h of infection, stable cells were selected with 1 μg/ml puromycin for seven days.

Nude mice tumorigenicity and in vivo senescence assays

T47D and MDA-MB-231 cells (5×10^6) were injected subcutaneously into CD-1 *nude* mice (Charles River). Females (n = 5 for each cell line) and males (n = 4 for each cell line) were used. Tumor sizes were measured up to 47 days post-injection. In addition, four tumors from each cell line were analyzed for the presence of senescent cells by SABG staining, as described previously [10].

Cluster analysis

The two-channel microarray data containing 8102 cDNA genes/clones generated by Sorlie et al. [2] were downloaded from the Stanford Microarray Database (SMD) (http://genome-www.stanford.edu/MicroArray/). In the downloading process, the "log (base 2) of R/G Normalized Ratio (median)" parameter was used for data filtering. We have median-centered expression values for each array. We selected arrays and genes with greater than 75% good data (representing the amount of data passing the spot criteria). Sixty-eight tissue samples were obtained according to this criterion and annotated with the subtypes described by the authors, found in the "Supplementary Information" of the data set in SMD. The expression values of "500 gene signature," defined by the authors, were extracted from the data. Gene expression profiles of 31 breast cancer cell lines performed by Charafe-Jauffret et al. [13], using the whole-genome cDNA microarray Affymetrix HGU-133 plus 2, was obtained from the "Supplementary Table" of the article. The authors filtered genes with low and poorly measured expression, and with low expression variation, retaining 15, 293 genes. After log transformation of the data, we median normalized the data arrays in R language, using the Bioconductor biostatistical package (www.r-project.org/ and www.bioconductor.org/). The "500 gene signature" tumor data [2] and the normalized breast-cancer cell line data [13] were combined with respect to probe IDs using a set of customized perl routines (source codes are available upon request). A set of 175 genes was common. "Median center" normalization of genes was done for the merged data set for the total samples. We performed unsupervised hierarchical clustering with the 99 samples (the 31 breast cell line [13] and 68 breast tumor [2] samples) by the pair-wise complete-linkage hierarchical clustering parameter, using the Gene-Pattern program. The Pearson correlation method was used for distance measurements. Clustering was visualized by java treeview, again using Gene-Pattern (http://www.broad.mit.edu/cancer/software/genepattern/).

Statistical analyses

Significant differences were evaluated using unpaired Student's t test for compared samples sizes of 10 or higher. Otherwise, one-tailed Fisher's exact test was used with 2×2 tables; $P<0.05$ was considered statistically significant. On the graphical representation of the data, y-axis error bars indicate the standard deviation for each point on the graph.

Results

Classification of breast cancer cell lines as senescent-cell progenitor and immortal-cell progenitor subtypes

Clonogenic assays have been successfully used to test the generation and self-renewal abilities of phenotypically distinct progeny of mammary stem/progenitor cells [14]. We previously applied this technique to test the ability of cancer cells to produce progeny with replication-dependent senescence arrest [10]. Cells were plated under low-density clonogenic conditions and cultivated for one to two weeks until individual cells performed eight to ten PDs and generated isolated colonies composed of several hundred cells. This method permits tracing progeny generated by a few hundred cells under the same experimental conditions. We explored a panel of 12 breast cancer cell lines, composed of luminal (n = 7) and basal (n = 5) subtypes (Table S1). Cell lines formed two groups, according to the presence of senescent cells in isolated colonies. One group of cell lines generated colonies with high rates of senescence, while others did not produce appreciable amounts of senescent cells. Representative pictures of colonies subjected to the SABG assay are shown in Fig. 1A. The percent of SABG+ progeny was calculated by manual counting of at least 10 different colonies for each cell line. Colonies derived from five cell lines generated SABG+ cells at high rates (means: 5-40%) Senescence rates were negligible (means <5%) in the progeny of the remaining seven cell lines. The first group, the senescent cell progenitor subtype, included T47D, BT-474, ZR-75-1, MCF-7, and CAMA-1 cell lines. The second group, the immortal cell progenitor subtype, included MDA-MB-453, BT-20, SK-BR-3, MDA-MB-468, HCC1937, MDA-MB-231 and MDA-MB-157 (Fig. 1B).

In order to verify whether the occurrence of senescent cells in the SCP group was intrinsic to each cell line or due to the presence of a side population, we generated clones from the T47D (n = 20) cell line, and subjected them to the SABG assay at different intervals. All clones acted similarly to the parental T47D cell line with similar rates of SABG+ progeny. No clone gained the ICP phenotype. More importantly, none of the clones tested over a long period of time (>60 PDs) entered full senescence (data not shown), unlike normal mammary epithelial cells that undergo two stages of senescence arrest over a period of ~20 PDs [7]. The SABG assay can provide false-positive responses, especially when cells remain under confluence for a long period [15]. Although all our tests used low-density clonogenic conditions, we wanted to confirm the senescence arrest by a long-term (24 h) BrdU labeling assay under mitogenic

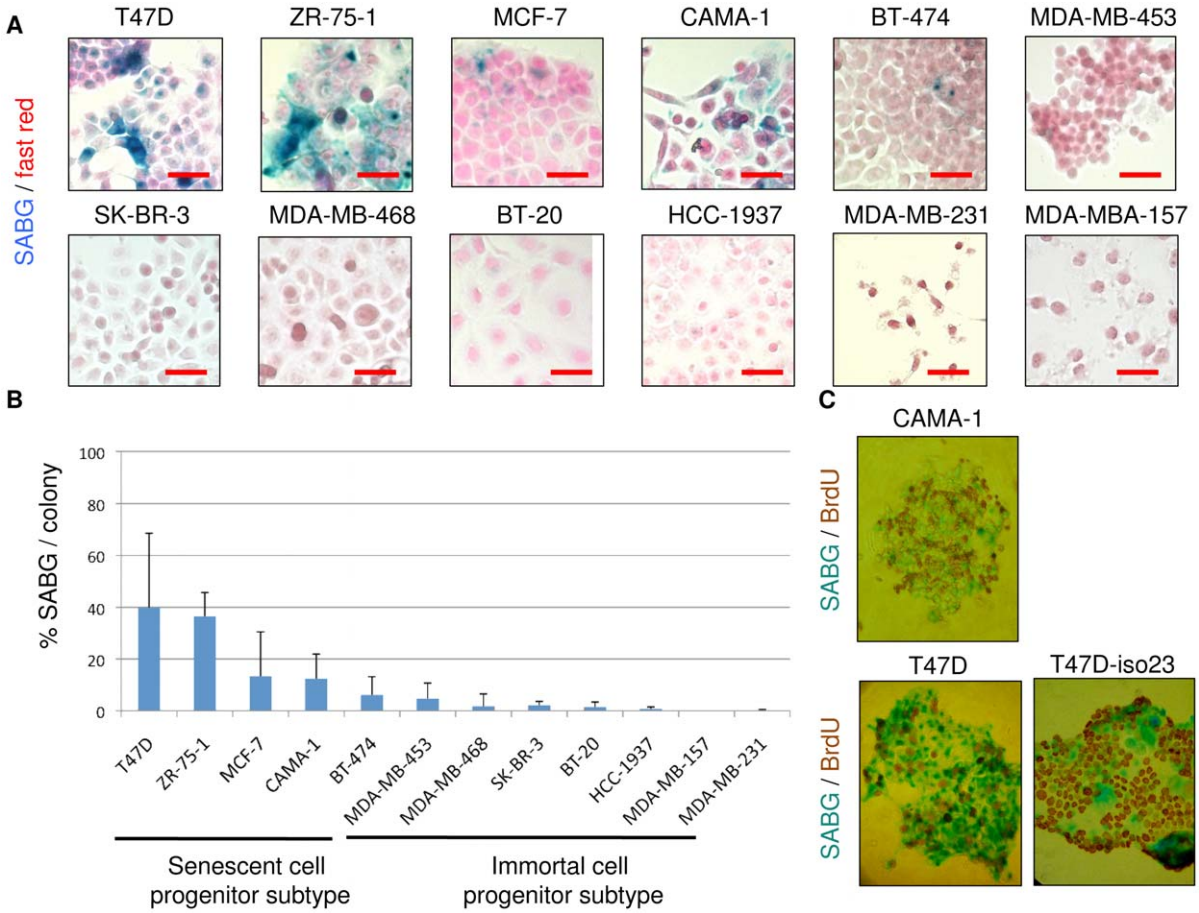

Figure 1. Classification of breast cancer cell lines as senescent cell progenitor and immortal cell progenitor subtypes. (**A**) Examples of SABG staining for senescence of breast cancer cell line colonies obtained after plating at low-density clonogenic conditions. Breast cancer cell lines (Table S1) were plated to obtain a few hundred colonies with 1–2 weeks of cell culturing and were subjected to SABG assay, followed by counterstaining with nuclear fast red. T47D, ZR-75-1, MCF-7, CAMA-1 and BT-474 generated heterogeneous colonies composed of with SABG+ and SABG- cells (shown here), but also fully negative and/or fully positive colonies. All other cell lines produced only SABG- colonies (<5% SABG+ cells). Scale bar: 50 μm. (**B**) Classification of breast cancer cell lines as senescent cell progenitor (SCP) and immortal cell progenitor (ICP) subtypes by quantification of the ability to generate senescent progeny. Cell lines with a mean of SABG+ cells higher than 5% were termed SCP, and the other cell lines as ICP. Colonies that were generated and stained as described in (**A**) were counted manually to calculate % SABG+ cells. At least 10 colonies were counted for each cell line. Error bars represent mean ± SD. (**C**) SABG+ senescent cells displayed terminal growth arrest. CAMA-1, T47D and T47D-iso23 colonies were generated as described in (**A**), labeled with BrdU for 24 h in the presence of freshly added culture medium, and subjected to SABG/BrdU double-staining. SABG+ cells are BrdU-, and *vice versa*. T47D-iso23 is a clone derived from T47D. Note that parental T47D and T47D-iso23 clones displayed similar staining features.
doi:10.1371/journal.pone.0011288.g001

conditions, as senescent cells in permanent cell cycle arrest cannot incorporate BrdU under these conditions [16]. Co-staining of cells for SABG and BrdU from CAMA-1, T47D, and T47D-iso23 colonies provided clear indication that the great majority of SABG+ senescent cells were BrdU-, whereas non-senescent BrdU+ cells were usually SABG- (Fig. 1C). These findings indicated that SABG+ senescent cells were at the terminal differentiation stage with an irreversible loss of DNA synthesis ability. Our observations also indicated that SABG and BrdU tests could be used alternatively to identify senescent (SABG+/BrdU-) and immortal (SABG-/BrdU+) cells under our experimental conditions.

Senescent cell progenitor phenotype association with $p21^{Cip1}$ expression

$p16^{Ink4a}$ and $p21^{Cip1}$ (in a p53-dependent manner or independently) have been shown to be mediators of senescence arrest in different cells, including mammary epithelial cells [6,15,17,18,19]. We therefore analyzed the expression of $p16^{Ink4a}$ and $p21^{Cip1}$ in the cell line panel. Heterogeneously positive nuclear $p21^{Cip1}$ immunoreactivity was observed in four of the five SCP cell lines, but not in any of the seven ICP cell lines (Fig. 2A). The association of $p21^{Cip1}$ expression with the SCP subtype was statistically significant ($P = 0.01$). We also compared the expression of $p16^{Ink4a}$. Three of five SCP cell lines displayed heterogeneously positive immunostaining, whereas three of seven ICP cell lines displayed homogenously positive staining (Fig. S1). The difference of $p16^{Ink4a}$ expression between the two groups was not significant ($P = 1$). These observations indicated that the SCP phenotype was associated with $p21^{Cip}$ expression in breast cancer cell lines.

To test whether $p21^{Cip1}$ was directly involved in the senescence observed in SCP cells, we first performed $p21^{Cip1}$/SABG staining in T47D-iso23 cells (hereafter termed T47D). $p21^{Cip1}$, but not $p16^{Ink4a}$ staining, was associated with SABG staining (Fig. S2). Next, we generated two derivative cell lines following infection of T47D with lentiviral vectors encoding $p21^{Cip1}$ shRNA (T47D-p21sh) or a scrambled control (T47D-scr). Following the

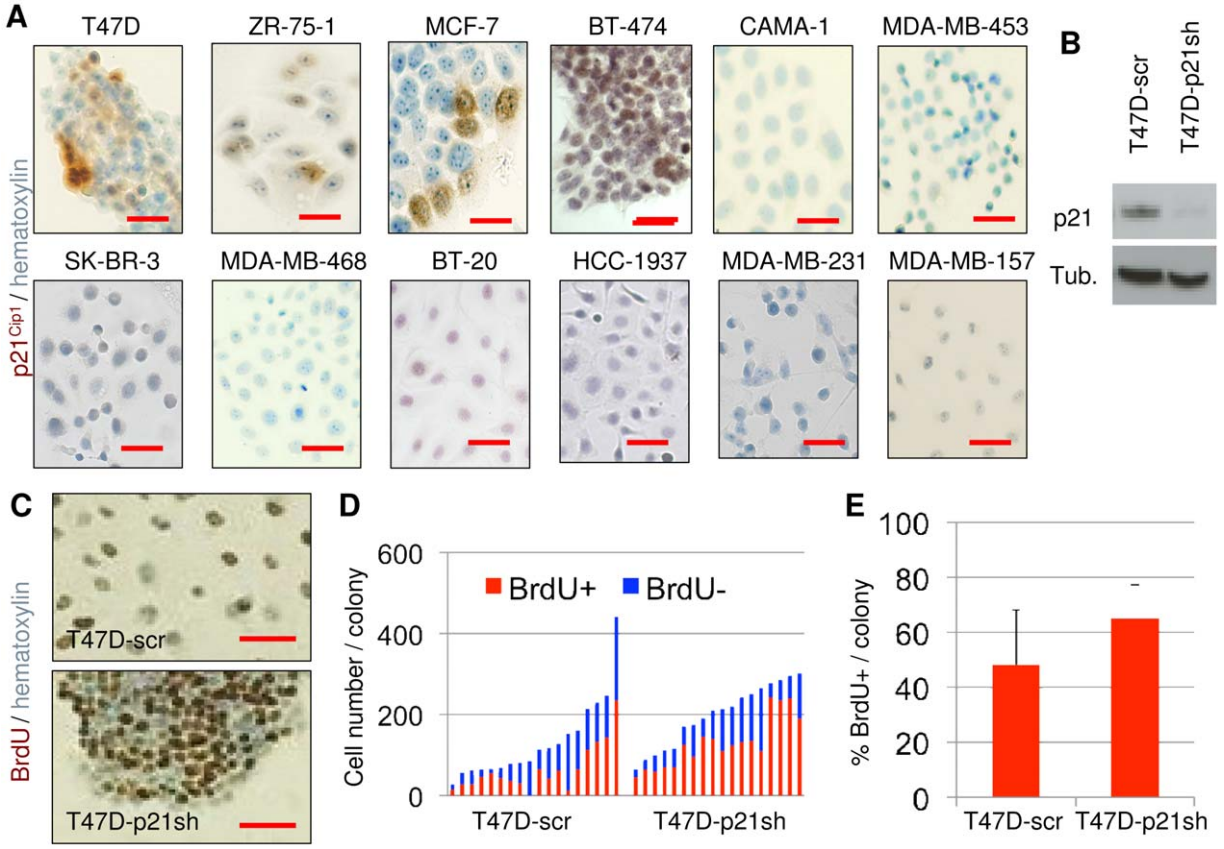

Figure 2. Growth arrest observed in senescent cell progenitors was inhibited by $p21^{Cip1}$ silencing. (**A**) Four of five senescent SCP cell lines (top four from left) generated colonies with heterogeneous expression of $p21^{Cip1}$; in contrast none of seven ICP cell lines generated $p21^{Cip1}$ cells. Colonies were immunostained for $p21^{Cip1}$, with hematoxylin used as counterstain. Scale bar: 50 μm. (**B–E**) $p21^{Cip1}$ silencing inhibited the production of the terminally arrested progeny of SCP cells. (**B**) shRNA-mediated inhibition of $p21^{Cip1}$ expression. T47D cells were infected with lentiviral vectors encoding $p21^{Cip1}$ shRNA or scrambled shRNA to generate T47D-p21sh and T47D-scr stable cell lines, and tested for $p21^{Cip1}$ knockdown by western blotting. (**C–E**) The ability to generate growth-arrested cells was inhibited by $p21^{Cip1}$ knockdown. Colonies were generated from respective cell lines, labeled with BrdU for 24 h, immunostained for BrdU, and slightly counterstained with hematoxylin to visualize BrdU+ and negative cells. Scale bar: 50 μm. (**C**). Individual colonies were manually counted for quantification of % BrdU cells. Each bar represents one colony (**D**). The silencing of $p21^{Cip1}$ caused a significant increase ($P = 0.0043$) in % ratios of BrdU+ cells (**E**). Mean % BrdU+ cells (± SD) values were calculated from data presented in (**D**). Error bars represent mean ± SD. Tub.; α-tubulin.
doi:10.1371/journal.pone.0011288.g002

demonstration of $p21^{Cip1}$ knockdown in T47D-p21sh cells by western blot assay (Fig. 2B), both cell lines were plated under low-density plating conditions, colonies were grown for 10 days, and subjected to SABG and BrdU staining. It was not possible to quantify SABG+ cells in T47D-p21sh cells because they formed tight clusters in culture (data not shown). We therefore used BrdU staining as an alternative method for senescent cell quantification (Fig. 2C). Randomly selected colonies were counted for the number of BrdU+ and BrdU- cells (Fig. 2D). The T47D-scr cell line generated BrdU+ progeny at a rate of 48±20% per colony (n = 18). Under the same conditions, T47D-p21sh cells displayed BrdU+ progeny at a rate of 65±12% per colony (n = 18), with a significant ($P = 0.0043$) increase in the number of cells escaping terminal arrest (Fig. 2E). These results indicated that $p21^{Cip1}$ was responsible, at least partly, for inducing the senescence observed in the progeny of T47D cells.

The control of senescent cell progeny generation by an estrogen receptor

As stated above, $p21^{Cip1}$ is a downstream target of p53 for senescence, but T47D cells do not express wild-type p53 (Table S1). Estrogen inhibits $p21^{Cip1}$ expression [20] by c-Myc-mediated repression [21], *MYC* gene being a direct target of ER complex [22]. We therefore tested whether ER could be involved in the senescence observed in T47D cells. The data shown in Fig. 3A indicates that T47D cells displayed nuclear ER immunoreactivity in their great majority, but some progeny was ER-. More interestingly, these ER- cells tended to be SABG+, suggesting that senescence occurred in T47D cells as a result of ER loss. Next, we tested whether experimentally modifying ER activity in T47D cells had any effect on senescence response. After plating at low-density clonogenic conditions, cells were grown in a regular cell culture medium that contained weakly estrogenic phenol red [23] for seven days in order to obtain visible colonies. The culture medium was then changed with phenol-free DMEM complemented with charcoal-treated FCS, grown for two more days, and then cultivated for four more days in the presence of E2 (10^{-9} M), OHT (10^{-9} M to 10^{-6} M), or an ethanol vehicle as control. Colonies were subjected to SABG staining (Fig. 3B). Total and SABG+ cells were counted from 20 randomly selected colonies for each treatment (Fig. 3C). Colonies grown in a phenol-free charcoal-treated control medium complemented with an ethanol vehicle only displayed 31±13% SABG+ cells. Complementing this medium with 10^{-9} M

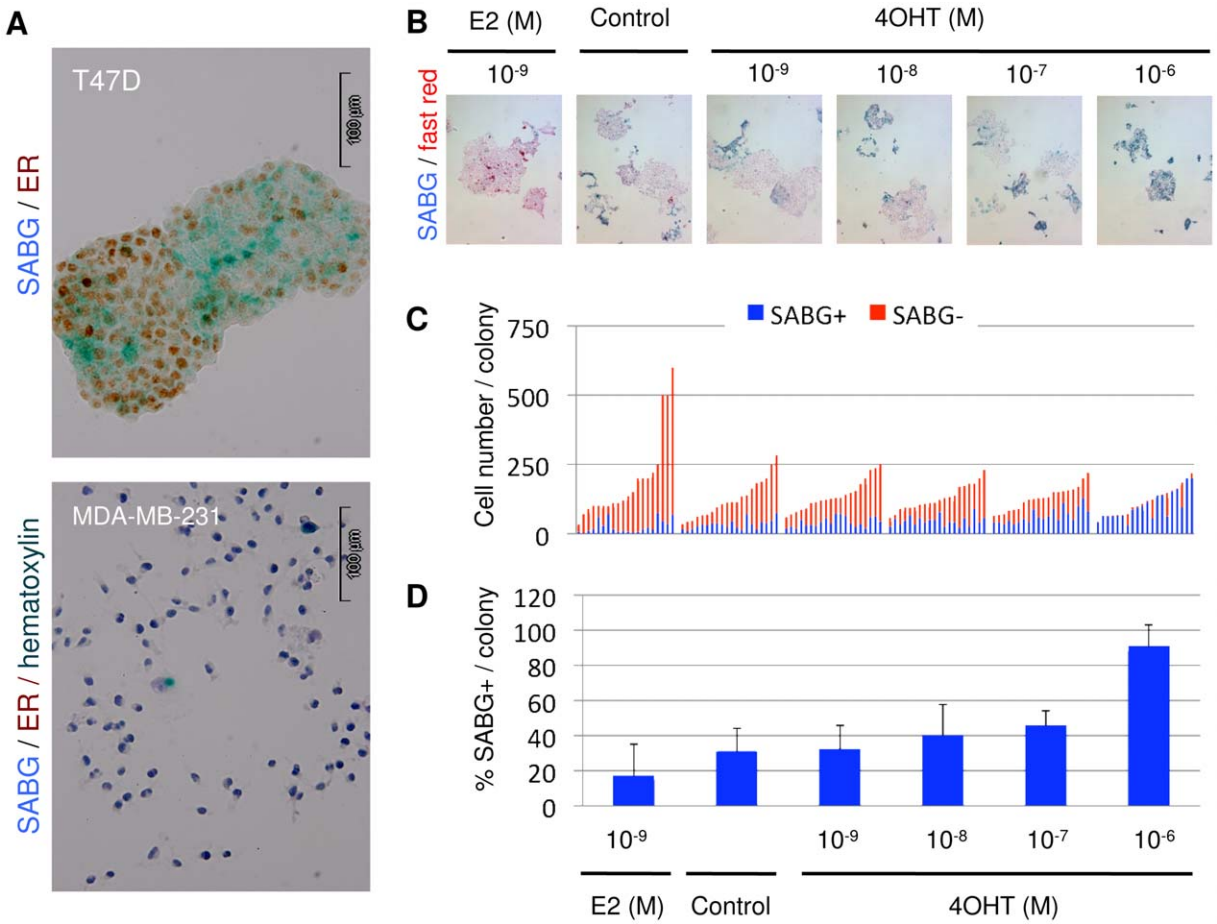

Figure 3. Generation of senescent cell progeny was controlled by the estrogen receptor-α. (**A**) SCP cells (T47D) expressed nuclear ER. Colonies were co-stained for senescence by SABG and for ER expression by immunoperoxidase. The MDA-MB-231 cell line was used as a negative control. (**B–D**) The production of senescent progeny in SCP cells was inhibited by estrogen (E2), but enhanced by tamoxifen (4OHT) treatment. After plating in low-density clonogenic conditions, T47D cells were grown in standard cell culture medium for seven days, followed by phenol-free DMEM complemented with charcoal-treated fetal calf serum for two days, and then cultivated for four days in the presence of E2, OHT, or an ethanol vehicle (control). Colonies were subjected to SABG staining (**B**). Total and SABG+ and SABG- cells were counted from 20 randomly selected colonies (**C**), and mean % SABG+ cells (± SD) values were calculated (**D**). Error bars represent mean ± SD. The inhibition of senescence by E2 and its activation by OHT was statistically significant when compared to ethanol-complemented control cells (*P* values 0.0093, 0.0002 and <0.0001 for 10^{-9} M E2, 10^{-7} M OHT and 10^{-6} M OHT, respectively).
doi:10.1371/journal.pone.0011288.g003

E2 generated colonies with 17±18% SABG+ cells. Senescence inhibition by E2 was nearly 50% and statistically significant when compared to the ethanol-complemented control cells ($P=0.0093$). In contrast to E2, OHT provoked a dose-dependent increase in the proportion of SABG+ cells. At the maximum dose used (10^{-6} M OHT), 90±13% of colony-forming cells displayed a SABG+ signal (Fig. 3D), indicating that tamoxifen-mediated inactivation of ER can induce almost a complete senescence response in these cells ($P<0.0001$). The increase in senescence rate was also significant with 10^{-7} M OHT ($P=0.0002$).

Our findings strongly suggested that the senescence observed in the SCP T47D cell line was due to a loss of expression and/or function of ER in a subpopulation of the progeny of these cells. For confirmation, we constructed ER-overexpressing stable clones from T47D cells. The thhree clones with the highest ER expression were selected. In addition, three clones with endogenous expressions of ER were selected from stable clones obtained with an empty vector (Fig. 4A). Progeny obtained from these six clones were tested by BrdU assay (Fig. S3). Randomly selected colonies (n = 10) from each clone were evaluated for total and BrdU+ number of cells (Fig. 4B). Consistently higher levels of BrdU+ cells were observed with clones ectopically expressing the ER protein (Fig. 4C). Overexpression of ER resulted in a significant increase in the BrdU+ progeny ($P=0.034$). The protective effect of ER overexpression was not as important as the senescence-promoting effects of ER inhibition. This was not unexpected, since the parental cells used for the ER overexpression studies were already expressing high levels of endogenous ER (Fig. 4A), displaying a baseline anti-senescence activity due to the serum estrogen and phenol red found in the cell culture medium.

The close relationship between ER and senescence in the ER+ T47D cell line, and the highly effective treatment of ER+ breast tumors with tamoxifen, which induced senescence in our experimental model, suggested that senescence induction might be a relevant mechanism involved in anti-estrogen treatments. As fresh tumor tissues cannot be obtained from tamoxifen-treated patients for obvious ethical reasons, we analyzed untreated ER+ breast tumor samples for evidence of spontaneously occurring in vivo senescence. We screened a panel of 12 snap-frozen ER+ breast tumor tissues from 11 patients for senescence by an SABG

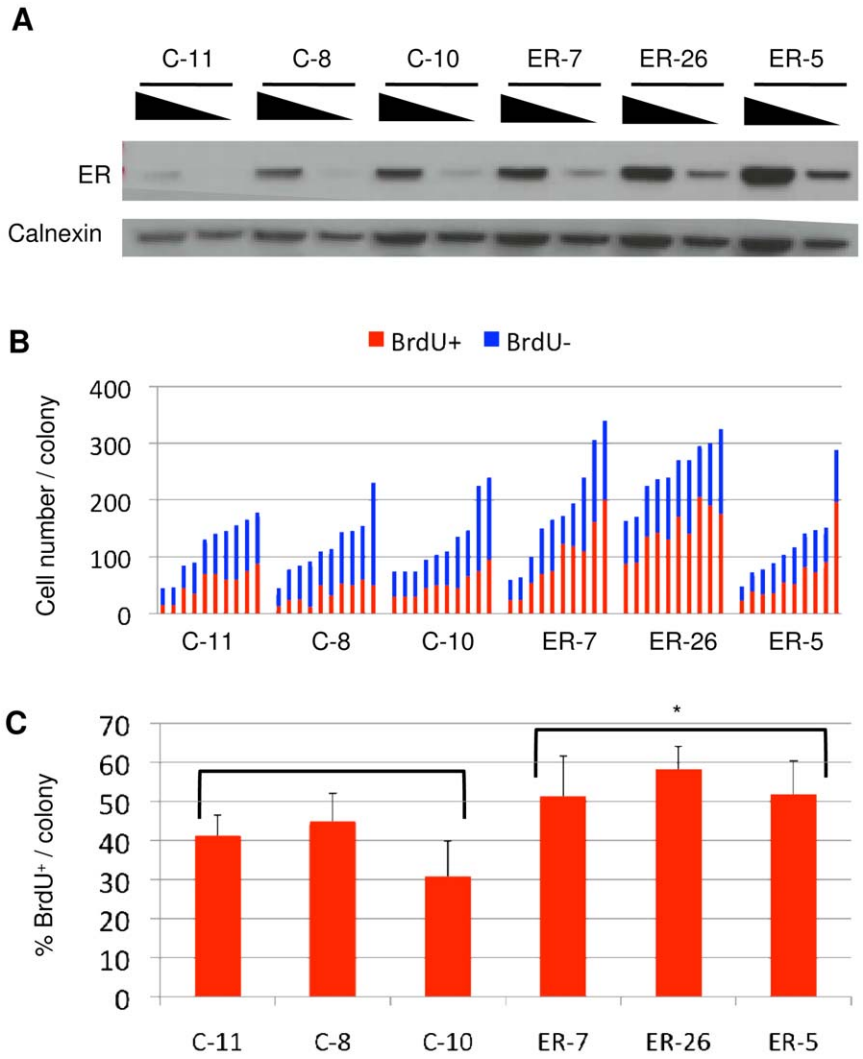

Figure 4. Overexpression of estrogen receptor-α inhibited the production of terminally arrested progeny. (**A**) ER-overexpressing (ER-5, ER-7, ER-26) and control (C-8, C-10, C-11) clones were established from T47D cells and tested for ER expression by western blotting using decreasing amounts of total proteins. Calnexin was used as loading control. (**B–C**). Colonies were generated, labeled with BrdU for 24 h and immunostained for BrdU (shown in Fig. S3). Individual colonies were manually counted for quantification of % BrdU cells (**B**), and mean % BrdU+ cells values were calculated (**C**). Error bars represent mean ± SD. ER overexpression caused a significant increase in % ratio of BrdU+ cells (*three ER clones *versus* three controls; $P = 0.034$).
doi:10.1371/journal.pone.0011288.g004

assay. The mean age of the patients was 58±12 yrs, with a mixed menopause status (Table S2). Two tumors (17%) displayed SABG+ cells that were scattered within the tumor area (Fig. S4). Thus, ER+ breast tumors also produced senescent progeny in vivo, but at a lower rate.

Senescent cell progenitor and immortal cell progenitor subtypes' abilities to differentiate into luminal and myoepithelial cell types

The cellular specificity of ER expression in the mammary epithelial cell hierarchy is poorly understood. Previous data suggests that normal ER+ cells may represent either relatively differentiated luminal cells with limited progenitor capacity or primitive progenitors with stem cell properties in the luminal cell compartment [4,24,25]. Based on the close association between senescence (which can be considered a manifestation of terminal differentiation) and loss of ER positivity, we hypothesized that ER+ SCP cells may differ from ER- ICP cells by their differentiation potential. We surveyed a few hundred single-cell-derived colonies from each of the 12 cell lines for production of stem/progenitor-like, luminal-like, and myoepithelial-like cells. We used CD44 as a positive stem/progenitor cell marker [26,27], CD24, ER, and CK19 as luminal lineage markers [27,28,29], and ASMA as a myoepithelial lineage marker [29].

Representative examples of marker studies by immunoperoxidase staining in SCP and ICP cell lines are shown in Fig. 5. All five SCP cell lines displayed a heterogeneous pattern of positivity for CD44; some colonies were fully positive, some fully negative, and others were composed of both positive and negative cells. CD44/CD24 double immunofluorescence studies with the T47D cell line indicated that SCP cells produce also CD44+/CD24- stem/progenitor cells, as expected (data not shown). In sharp contrast, five of the seven ICP cell lines generated only fully positive CD44 colonies, indicating they do not produce CD44- cells. One cell line was totally CD44-. Only one cell line displayed

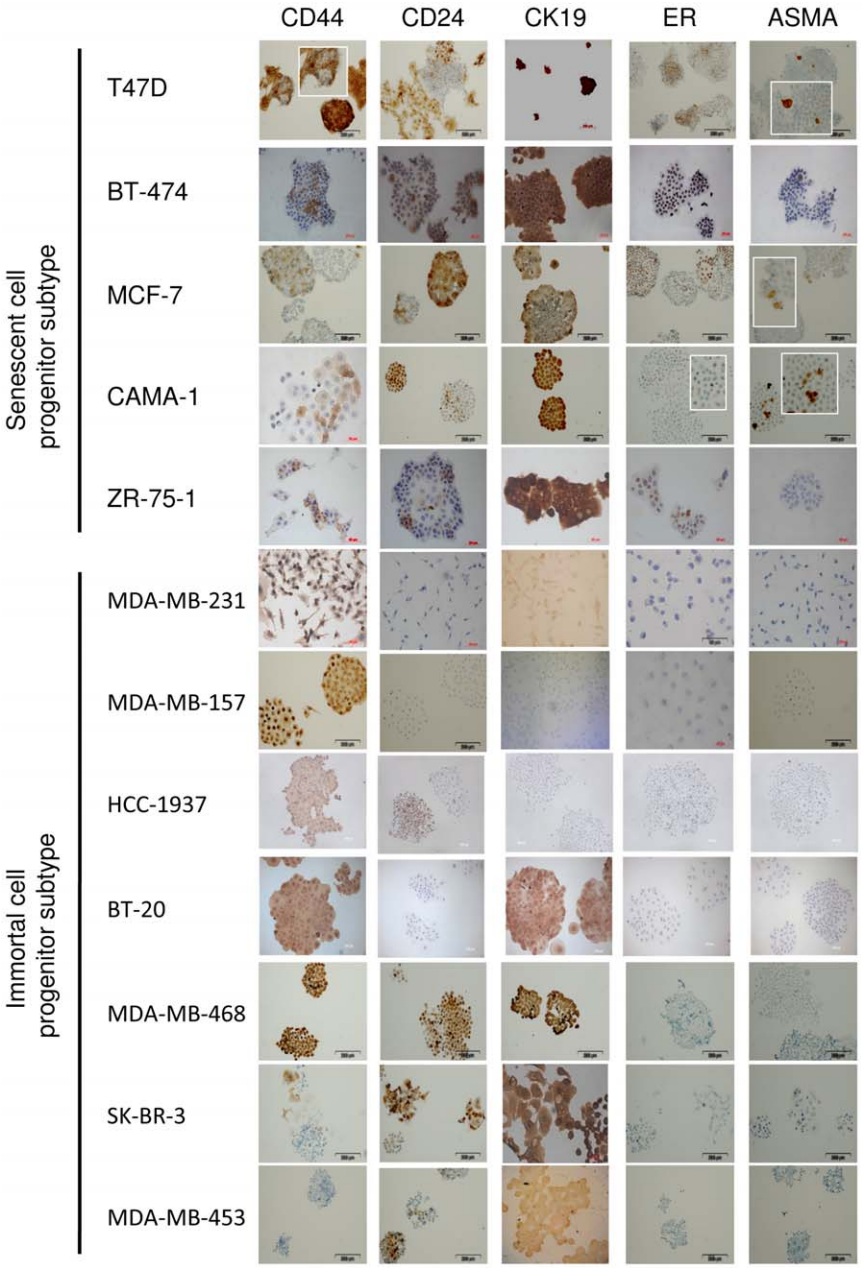

Figure 5. Senescent cell progenitor and immortal cell progenitor subtypes greatly differed in their ability to differentiate into luminal and myoepithelial lineage cells. Senescent cell progenitor and immortal cell progenitor subtype cell lines were studied by immunoperoxidase staining using CD44 and markers for luminal epithelial (CD24, CK19, ER) and myoepithelial (ASMA) lineages. Insets: magnified views of positive cells. Both subtypes have CD44+ cells. Senescent cell progenitor cell lines produced both progenitor-like (CD44+; CD24−), as well as ER+ luminal-like and ASMA+ myoepithelial-like cells (except ZR-75-1 for myoepithelial-like cells). Immortal cell progenitor cell lines were defective for generation of ER+ luminal-like or ASMA+ myoepithelial-like cells. Moreover, five of seven cell lines could not generate CD44- cells. The expression of CD24 and CK19 markers did not differ significantly between the two subgroups, except that some immortal cell progenitor subtype cell lines did not express CD24 or CK19.
doi:10.1371/journal.pone.0011288.g005

a pattern similar to that of SCP cell lines. A comparison of the two subtypes indicated that the ability to generate both CD44+ and CD44- progeny was significantly associated with the SCP phenotype ($P = 0.0046$). All five SCP cell lines displayed heterogeneous, but mostly positive ER immunostaining, whereas all seven ICP cell lines never generated ER+ cells. The expression of ER was also significantly associated with the SCP subtype ($P = 0.0012$), as well as the ability to produce ASMA+ progeny ($P = 0.0046$). The ICP cell lines did not generate ASMA+ cells, while four out of five SCP cell lines generated rare ASMA+ cells under low-density clonogenic conditions. Interestingly, the abundance of ASMA+ cells was much higher in the two SCP cell lines that were tested at high cell density (Fig. S5). This suggests that either the production of ASMA+ cells is enhanced at high cell density, or these myoepithelial-like cells display limited survival under long-term culture conditions. We did not find a strong association between the expression of CD24 and CK19 markers and cell subtype. All five SCP cell lines and three ICP cell lines

generated heterogeneously staining colonies for CD24 expression. Similarly, all five SCP cell lines, as well as three ICP cell lines, expressed CK19, but homogenously.

Typical features of senescent progenitor and immortal progenitor breast cancer cell lines

As summarized in Fig. 6, SCP and ICP subtype cell lines displayed several subtype-specific features. All SCP cell lines produced differentiated and senescent cells, in addition to putative CD44+/CD24− stem/progenitor cells. Indeed, all of them produced ER+ and CD24+ luminal-like cells and most of them (n = 4/5) also produced ASMA+ myoepithelial-like cells. In contrast, five of the seven ICP cell lines never produced CD44- cells, suggesting they cannot generate differentiated progeny under the experimental conditions tested. In confirmation of this hypothesis, four ICP cell lines only produced CD44+/CD24−/ER-/CK19-/ASMA- stem/progenitor-like, but never differentiated cells. Furthermore, all seven ICP cell lines were unable to produce ASMA+ myoepithelial-like, ER+ luminal-like or SABG+ senescent cells. CD24 and CD19 luminal lineage markers were expressed in three cell lines, one of which was fully positive for the CD44 stem/progenitor marker.

SCP and ICP subtype cell lines correlate with distinct breast tumor subtypes

Distinct cell-type features associated with SCP and ICP subtypes suggest that they may be phenocopies of molecularly defined breast tumor subtypes [1,2,3,30]. As the prognosis and therapeutic response of each subtype is different [2,3], we questioned whether we could assign SCP and ICP cell lines to known molecular subtypes of breast tumors. Using cell line and primary tumor gene expression datasets, we conducted a hierarchical clustering analysis. The "intrinsic gene set" data generated by Sorlie et al. [2] to classify breast tumors into five molecular subtypes was used to filter cell line data generated by Charafe-Jauffret et al. [13]. A set of 175 genes was common between the two data sets. Sixty-eight tumors and 31 cell lines were subjected to pair-wise complete-linkage hierarchical clustering and distance measurements. This tumor–cell line combined analysis produced two major clusters. One cluster was composed of basal and luminal B subtype tumors and five of six ICP cell lines. The other cluster included luminal A, ERBB2+, and "normal-like" subtype tumors and all five SCP subtype cells. Four cell lines clustered with the luminal A tumor subclass. Finally. one cell line clustered with the "normal-like" subclass (Fig. 7A). A full list of clustered tumors and cell lines is provided in Fig. S6.

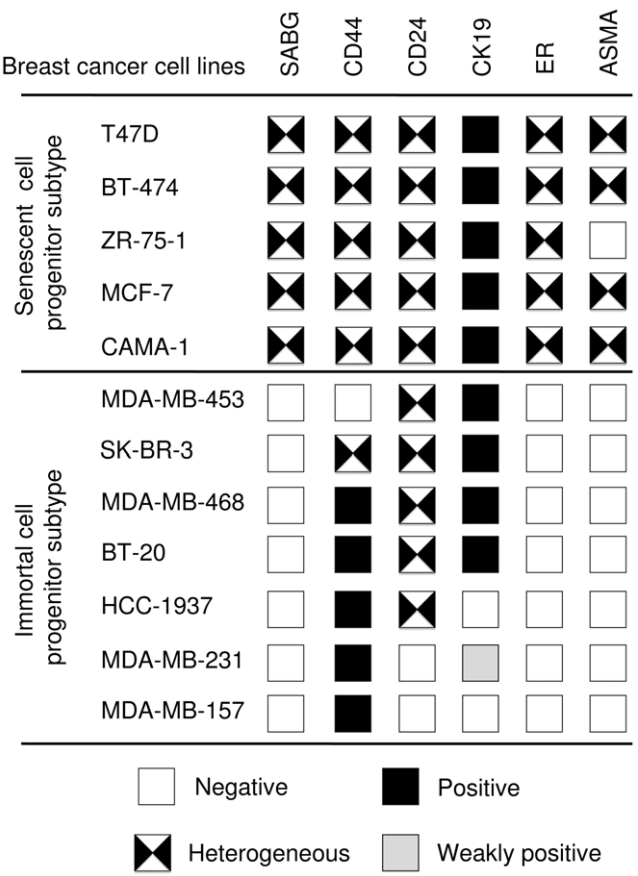

Figure 6. Typical features of senescent progenitor and immortal progenitor breast cancer cell lines.
doi:10.1371/journal.pone.0011288.g006

Luminal A tumors clustering with our SCP subtype cell lines displayed the longest tumor-free, distant metastasis-free, and overall survival rates. In contrast, basal and luminal B tumors clustering with our ICP subtype cell lines had the worst prognosis, with shorter tumor-free, distant metastasis-free, and overall survival times [2]. Our cluster analysis suggested that the ability to generate differentiated and senescent progeny characterized breast cancers with poor tumorigenicity, and that resistance to differentiation and senescence was indicative of more aggressive tumorigenicity. We compared in vivo intrinsic tumorigenic behaviors of the SCP cell line T47D and the ICP cell line MDA-MB-231 in female (n = 5 for each cell line) and male (n = 4 for each cell line) CD1 *nude* mice Fig. 7B). MDA-MB-231 cells displayed higher tumorigenicity than T47D cells. In total, we observed progressively growing tumors in five of nine animals injected with MDA-MB-231. In contrast, T47D formed smaller and regressing tumors in nine of nine animals ($P<0.03$). Interestingly, the difference in tumorigenicity between these two cell lines was more pronounced in male animals ($P<0.05$ after 20 days post-injection). To test whether the difference in tumorigenicity between MDA-MB-231 and T47D cells was correlated with spontaneous in vivo senescence, we analyzed four tumors from each cell line. Two T47D tumors displayed positive SABG staining, whereas no positive staining was observed with all four MDA-MB-231 tumors (Fig. S7).

Discussion

In recent years, phenotypic heterogeneity of breast cancers has been correlated with genetic and molecular heterogeneity [1,3]. Breast cancer subtypes may represent cancers originating from different progenitor cells. Molecular and phenotypic heterogeneity and associated clinical manifestations of breast tumor subtypes have been related to the type of hypothetical tumor progenitor cells originating from a hypothetical mammary epithelial stem cell or from downstream progenitor cells [4,5]. This hypothesis has not been fully validated, mainly because a hierarchical map of cells involved in mammary epitheliogenesis has not yet been established.

To better understand phenotypic differences between breast cancer subtypes, we applied senescence as a surrogate marker for the potential to generate terminally differentiated progeny. We completed these studies with markers for breast stem/progenitor and differentiated luminal and myoepithelial lineage cells. The use of low-density clonogenic conditions allowed us to follow the fate

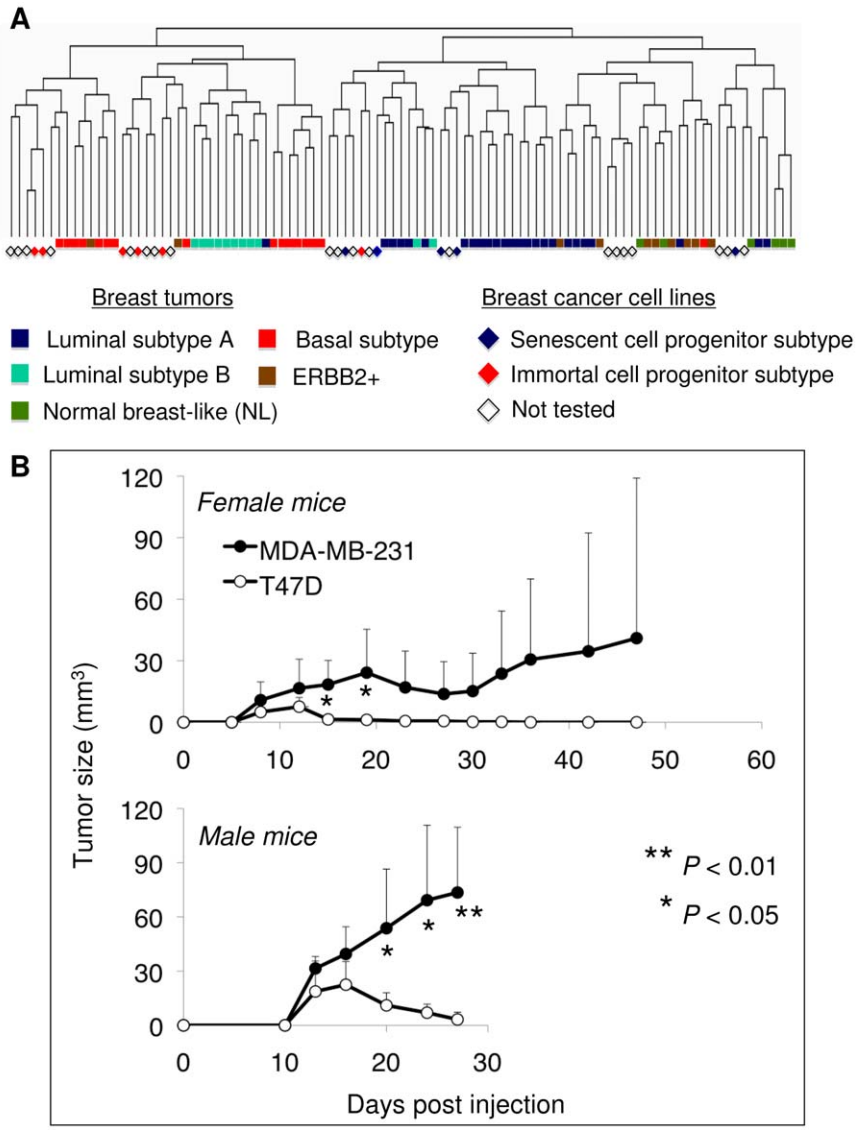

Figure 7. Senescence cell progenitor and immortal cell progenitor subtype cell lines correlate with distinct breast tumor subtypes. (**A**) Unsupervised hierarchical clustering of breast tumor and cell line gene expression data were obtained from Sorlie et al [2] and Charafe-Jauffret et al [25]. Dendrogram displaying the relative organization of tumor and cell line data demonstrated that ICP cell lines cluster with basal and luminal A tumors in the same branch, except for MDA-MB-453. In contrast, SCP cell lines clustered with luminal A (BT-474, CAMA-1, MCF-7, T47D) and "normal-like" tumors (ZR-75-1). No data was available for MDA-MB-468. A dendrogram with sample IDs was provided in Fig. S6. The "intrinsic gene set" data generated by Sorlie et al. [2] was used to filter cell line data generated by Charafe-Jauffret et al. [13]. A set of 175 genes was common between the two data sets. Sixty-eight tumors and 31 cell lines were subjected to pair-wise complete-linkage hierarchical clustering and distance measurements. (**B**) Immortal cell progenitor MDA-MB-231 was more tumorigenic than the SCP type T47D cell line. Female (n = 5 per cell line) and male (n = 4 per cell line) CD1*nude* mice received 5×10^6 cells by subcutaneous injection and observed up to 47 days for tumor formation. Chart displays mean tumor sizes (± S.D.) generated by MDA-MB-231 and T47D cell lines, respectively in female (top) and mala (bottom) mice. T47D cells formed smaller tumors that regressed and completely resolved within 30 days. Tumors formed by MDA-MB-231 were larger in size and did not show total resolution. Note that this cell line was more tumorigenic in male mice.
doi:10.1371/journal.pone.0011288.g007

of a large number of progeny for each cell line studied. From these approaches, we draw several important conclusions. First, breast cancer cell lines form two distinct groups: SCP and ICP subtypes. The SCP cell lines produce non-senescent and senescent progeny, whereas the ICP cell lines produce only non-senescent progeny. Second, SCP and ICP cell lines are exclusively ER+ and ER- cell lines, respectively. Senescence occurs as a result of ER loss associated with $p21^{Cip1}$ induction in SCP cells. Inversely, experimental activation of ER by E2 protects from senescence, whereas its inactivation by tamoxifen aggravates it. Thus, senescence in ER-dependent cells appears to result from the loss of survival signals generated by transcriptional activity of ER. A similar type of senescence has been reported for lymphoma, osteosarcoma, and hepatocellular carcinoma tumors upon c-*MYC* inactivation [31]. Third, SCP cells generate ER+, CD24+, or CK19+ luminal-like, as well as ASMA+ myoepithelial-like progeny. These findings strongly suggest that most, if not all, SCP cells have the capacity to give rise to two major types of differentiated cells that are found in normal mammary epithelium. In sharp contrast, ICP cells never produce ER+ luminal-like or

ASMA+ myoepithelial-like cells. Indeed, some ICP cells generate only CD44+ stem/progenitor-like cells and never CD44−, CD24+, CK19+, ER+, or ASMA+ cells. These findings indicate that ICP cells have limited differentiation ability, at least under in vitro conditions. The differentiation ability of ICP cells appears to be lost completely or partially, so that they do not differentiate fully while they self-renew as stem/progenitor-like cells. Fourth, SCP cell lines form the same molecular cluster with luminal A and "normal-like" breast tumors. This suggests that SCP cell lines are phenocopies of these relatively benign and/or anti-estrogen-responsive tumors. The poor tumorigenicity of SCP cells in *nude* mice correlates with better tumor-free and metastasis-free survival of patients with luminal A type tumors. In contrast, ICP cell lines cluster with luminal B and basal-like breast tumor subtypes, and they are more tumorigenic, as expected for luminal B and basal-like tumor cells. It is presently unknown whether breast tumor subtypes that cluster with SCP or ICP cell lines are also composed of either differentiating or mostly self-renewing stem/progenitor cells. Recent studies reported that breast tumors may contain only CD44+, or only CD24+ cells, as well as mixed cell populations, and that CD44+ tumor cells express many stem-cell markers [27,32]. In addition, an association between basal-like breast cancer and the presence of CD44+/CD24− cells has been established [32].

The mechanisms of the differentiation block observed in ICP cell lines are not known. One might argue that cell lines that produce only CD44+, but never differentiation marker-positive cells, cannot be defined as stem/progenitor cells. However, such cell lines are not completely inert to differentiation stimuli, and may undergo differentiation under special conditions. For example, MDA-MB-231 and MDA-MB-468 cells (identified as ICP cell lines here) can be induced to differentiate into ER+ cells by Wnt5a treatment, and MDA-MB-231 cells then become sensitive to tamoxifen [33].

Most of the findings reported here are derived from in vitro studies performed with established cancer cell lines. Presently, it is unknown to what extent these findings are also relevant for breast tumors. We provide here some promising data that supports in vivo relevance of our conclusions. First, our cluster analyses associated SCP cell types with luminal A and "normal-like" breast tumors, whereas ICP cell types shared similar gene expression profiles with luminal B and basal-like breast tumors. Second, ICP-type MDA-MB-231 cells were more tumorigenic than SCP-type T47D cells. T47D cells formed smaller tumors in some animals, and all tumors displayed regression between 10 and 15 days post-injection. Accordingly, we observed positive SABG staining in two out of four T47D tumors, but not in MDA-MB-231 tumors. Obviously, ICP-like and SCP-like tumors in affected women may or may not display similar tumorigenic potentials, depending on the women's hormonal status and treatment conditions. However, as most SCP-like luminal A or ER+ tumors are successfully treated with tamoxifen [34], their less aggressive behavior could be related to their highly effective senescence response to tamoxifen treatment, as shown here with T47D cells under in vitro conditions (Fig. 3). It will be interesting to examine whether the success of anti-estrogenic treatments is indeed associated with senescence induction in breast tumors. If this is the case, senescence-inducing treatments could be considered for breast cancer.

In conclusion, our analyses reveal that the in vitro ability to generate senescent progeny permits discrimination between cells that share molecular and tumorigenic similarities with luminal A subtype breast tumors from cells related to basal/luminal B subtype tumors. We also provide in vitro evidence for classifying breast cancers into two major groups based on the ability to generate differentiated progeny. Less-tumorigenic SCP cell lines generate both luminal- and myoepithelial-like cells. In contrast, more-tumorigenic ICP cell lines are defective in their ability to generate differentiated progeny. Our findings may have prognostic relevance and serve as a basis for therapeutically inducing differentiation and senescence in breast cancer.

Supporting Information

Dataset S1 STR analysis data that shows the authenticity of breast cancer cell lines used in this study.
Found at: doi:10.1371/journal.pone.0011288.s001 (1.50 MB XLS)

Table S1 Gene clusters, genetic mutations and epigenetic changes of breast cancer cell lines used in this study.
Found at: doi:10.1371/journal.pone.0011288.s002 (0.05 MB DOC)

Table S2 Estrogen receptor (ER) status, main pathological features of senescence staining (SABG) of breast tumors used in this study.
Found at: doi:10.1371/journal.pone.0011288.s003 (0.05 MB DOC)

Figure S1 p16Ink4a expression in colonies obtained from breast cancer cell lines. There was no correlation between p16Ink4a expression and progenitor subtype.
Found at: doi:10.1371/journal.pone.0011288.s004 (3.39 MB TIF)

Figure S2 Co-staining experiments indicate that SABG staining is associated with p21Cip1, but with p16Ink4a expression in SCP cells. Colonies were generated from T47D and MB-MDA-231 cells and subjected to SABG staining, followed by p21Cip1 or p16Ink4a immunoperoxidase (brown) staining. MDA-MB-231 cells were used as negative control.
Found at: doi:10.1371/journal.pone.0011288.s005 (2.74 MB TIF)

Figure S3 Effect of estrogen receptor-overexpression on the production of BrdU-negative terminally arrested cell progeny. ER-overexpressing (ER-5, ER-7, ER-26) and control (C-8, C-10, C-11) stable clones were established from T47D cells. Following transfection with ER expression and control vectors, colonies were generated from respective cell lines, labeled with BrdU for 24 h, immunostained for BrdU (brown), and slightly counterstained with hematoxylin to visualize BrdU+ and BrdU- cells.
Found at: doi:10.1371/journal.pone.0011288.s006 (6.57 MB TIF)

Figure S4 Detection of SABG+ senescent cells in estrogen receptor-positive breast tumors. Snap-frozen tumors were used to obtain 6 μ thick sections and used directly to detect SABG+ cells. H&E: hematoxylin-eosin staining.
Found at: doi:10.1371/journal.pone.0011288.s007 (9.45 MB TIF)

Figure S5 ASMA+ myoepithelial-like cells are produced frequently in senescent cell progenitor T47D and MCF-7 cell lines under confluent conditions. ASMA was tested by immunoperoxidase.
Found at: doi:10.1371/journal.pone.0011288.s008 (4.08 MB TIF)

Figure S6 Unsupervised hierarchical clustering of breast tumor and cell line gene expression data that is described in Fig. 7A. Dendrogram shown here includes tumor and cell line sample IDs.
Found at: doi:10.1371/journal.pone.0011288.s009 (1.05 MB TIF)

Figure S7 Tumors derived from T47D but not from MDA-MB-231 display SABG (+) senescent cells. Two of four T47D tumors

displayed SABG+ cells. All four MDA-MB-231 tumors lacked SABG+ cells.
Found at: doi:10.1371/journal.pone.0011288.s010 (7.97 MB TIF)

Acknowledgments

We thank Rana Nelson for editorial help.

Author Contributions

Conceived and designed the experiments: MO. Performed the experiments: MM SB HY HA SS PT BGD BC. Analyzed the data: MM UHT IGY CA MO. Contributed reagents/materials/analysis tools: BB. Wrote the paper: MM MO.

References

1. Perou CM, Sorlie T, Eisen MB, van de Rijn M, Jeffrey SS, et al. (2000) Molecular portraits of human breast tumours. Nature 406: 747–752.
2. Sorlie T, Tibshirani R, Parker J, Hastie T, Marron JS, et al. (2003) Repeated observation of breast tumor subtypes in independent gene expression data sets. Proc Natl Acad Sci U S A 100: 8418–8423.
3. Sotiriou C, Pusztai L (2009) Gene-expression signatures in breast cancer. N Engl J Med 360: 790–800.
4. Stingl J, Caldas C (2007) Molecular heterogeneity of breast carcinomas and the cancer stem cell hypothesis. Nat Rev Cancer 7: 791–799.
5. Vargo-Gogola T, Rosen JM (2007) Modelling breast cancer: one size does not fit all. Nat Rev Cancer 7: 659–672.
6. Romanov SR, Kozakiewicz BK, Holst CR, Stampfer MR, Haupt LM, et al. (2001) Normal human mammary epithelial cells spontaneously escape senescence and acquire genomic changes. Nature 409: 633–637.
7. Stampfer MR, Yaswen P (2003) Human epithelial cell immortalization as a step in carcinogenesis. Cancer Lett 194: 199–208.
8. Neve RM, Chin K, Fridlyand J, Yeh J, Baehner FL, et al. (2006) A collection of breast cancer cell lines for the study of functionally distinct cancer subtypes. Cancer Cell 10: 515–527.
9. Gur-Dedeoglu B, Konu O, Kir S, Ozturk AR, Bozkurt B, et al. (2008) A resampling-based meta-analysis for detection of differential gene expression in breast cancer. BMC Cancer 8: 396.
10. Ozturk N, Erdal E, Mumcuoglu M, Akcali KC, Yalcin O, et al. (2006) Reprogramming of replicative senescence in hepatocellular carcinoma-derived cells. Proc Natl Acad Sci U S A 103: 2178–2183.
11. Dimri GP, Lee X, Basile G, Acosta M, Scott G, et al. (1995) A biomarker that identifies senescent human cells in culture and in aging skin in vivo. Proc Natl Acad Sci U S A 92: 9363–9367.
12. Alotaibi H, Yaman EC, Demirpence E, Tazebay UH (2006) Unliganded estrogen receptor-alpha activates transcription of the mammary gland Na+/I− symporter gene. Biochem Biophys Res Commun 345: 1487–1496.
13. Charafe-Jauffret E, Ginestier C, Monville F, Finetti P, Adelaide J, et al. (2006) Gene expression profiling of breast cell lines identifies potential new basal markers. Oncogene 25: 2273–2284.
14. Stingl J (2009) Detection and analysis of mammary gland stem cells. J Pathol 217: 229–241.
15. Campisi J, d'Adda di Fagagna F (2007) Cellular senescence: when bad things happen to good cells. Nat Rev Mol Cell Biol 8: 729–740.
16. Wei W, Sedivy JM (1999) Differentiation between senescence (M1) and crisis (M2) in human fibroblast cultures. Exp Cell Res 253: 519–522.
17. Kiyono T, Foster SA, Koop JI, McDougall JK, Galloway DA, et al. (1998) Both Rb/p16INK4a inactivation and telomerase activity are required to immortalize human epithelial cells. Nature 396: 84–88.
18. Beausejour CM, Krtolica A, Galimi F, Narita M, Lowe SW, et al. (2003) Reversal of human cellular senescence: roles of the p53 and p16 pathways. EMBO J 22: 4212–4222.
19. Garbe JC, Holst CR, Bassett E, Tlsty T, Stampfer MR (2007) Inactivation of p53 function in cultured human mammary epithelial cells turns the telomere-length dependent senescence barrier from agonescence into crisis. Cell Cycle 6: 1927–1936.
20. Cariou S, Donovan JC, Flanagan WM, Milic A, Bhattacharya N, et al. (2000) Down-regulation of p21WAF1/CIP1 or p27Kip1 abrogates antiestrogen-mediated cell cycle arrest in human breast cancer cells. Proc Natl Acad Sci U S A 97: 9042–9046.
21. Mukherjee S, Conrad SE (2005) c-Myc suppresses p21WAF1/CIP1 expression during estrogen signaling and antiestrogen resistance in human breast cancer cells. J Biol Chem 280: 17617–17625.
22. Dubik D, Shiu RP (1992) Mechanism of estrogen activation of c-myc oncogene expression. Oncogene 7: 1587–1594.
23. Berthois Y, Katzenellenbogen JA, Katzenellenbogen BS (1986) Phenol red in tissue culture media is a weak estrogen: implications concerning the study of estrogen-responsive cells in culture. Proc Natl Acad Sci U S A 83: 2496–2500.
24. Booth BW, Smith GH (2006) Estrogen receptor-alpha and progesterone receptor are expressed in label-retaining mammary epithelial cells that divide asymmetrically and retain their template DNA strands. Breast Cancer Res 8: R49.
25. Shyamala G, Chou YC, Cardiff RD, Vargis E (2006) Effect of c-neu/ErbB2 expression levels on estrogen receptor alpha-dependent proliferation in mammary epithelial cells: implications for breast cancer biology. Cancer Res 66: 10391–10398.
26. Al-Hajj M, Wicha MS, Benito-Hernandez A, Morrison SJ, Clarke MF (2003) Prospective identification of tumorigenic breast cancer cells. Proc Natl Acad Sci U S A 100: 3983–3988.
27. Shipitsin M, Campbell LL, Argani P, Weremowicz S, Bloushtain-Qimron N, et al. (2007) Molecular definition of breast tumor heterogeneity. Cancer Cell 11: 259–273.
28. Sleeman KE, Kendrick H, Ashworth A, Isacke CM, Smalley MJ (2006) CD24 staining of mouse mammary gland cells defines luminal epithelial, myoepithelial/basal and non-epithelial cells. Breast Cancer Res 8: R7.
29. Yeh IT, Mies C (2008) Application of immunohistochemistry to breast lesions. Arch Pathol Lab Med 132: 349–358.
30. Sotiriou C, Neo SY, McShane LM, Korn EL, Long PM, et al. (2003) Breast cancer classification and prognosis based on gene expression profiles from a population-based study. Proc Natl Acad Sci U S A 100: 10393–10398.
31. Wu CH, van Riggelen J, Yetil A, Fan AC, Bachireddy P, et al. (2007) Cellular senescence is an important mechanism of tumor regression upon c-Myc inactivation. Proc Natl Acad Sci U S A 104: 13028–13033.
32. Honeth G, Bendahl PO, Ringner M, Saal LH, Gruvberger-Saal SK, et al. (2008) The CD44+/CD24− phenotype is enriched in basal-like breast tumors. Breast Cancer Res 10: R53.
33. Ford CE, Ekstrom EJ, Andersson T (2009) Wnt-5a signaling restores tamoxifen sensitivity in estrogen receptor-negative breast cancer cells. Proc Natl Acad Sci U S A 106: 3919–3924.
34. (1998) Tamoxifen for early breast cancer: an overview of the randomised trials. Early Breast Cancer Trialists' Collaborative Group. Lancet 351: 1451–1467.

Cancer Letters 286 (2009) 103–113

Contents lists available at ScienceDirect

Cancer Letters

journal homepage: www.elsevier.com/locate/canlet

Mini-review

Senescence and immortality in hepatocellular carcinoma

Mehmet Ozturk [a,b,*], Ayca Arslan-Ergul [a], Sevgi Bagislar [a,b], Serif Senturk [a], Haluk Yuzugullu [a,b]

[a] Department of Molecular Biology and Genetics, Bilkent University, 06800 Ankara, Turkey
[b] Centre de Recherche INSERM-Université Joseph Fourrier U823, Institut Albert Bonniot, 38042 Grenoble, France

ARTICLE INFO

Article history:
Received 26 March 2008
Received in revised form 23 June 2008
Accepted 29 October 2008

Keywords:
Liver cancer
Senescence
Telomeres
DNA damage
p53
$p16^{INK4a}$
$p21^{Cip1}$
Retinoblastoma
Cirrhosis
Hepatocytes
Telomerase reverse transcriptase

ABSTRACT

Cellular senescence is a process leading to terminal growth arrest with characteristic morphological features. This process is mediated by telomere-dependent, oncogene-induced and ROS-induced pathways, but persistent DNA damage is the most common cause. Senescence arrest is mediated by $p16^{INK4a}$- and $p21^{Cip1}$-dependent pathways both leading to retinoblastoma protein (pRb) activation. p53 plays a relay role between DNA damage sensing and $p21^{Cip1}$ activation. pRb arrests the cell cycle by recruiting proliferation genes to facultative heterochromatin for permanent silencing. Replicative senescence that occurs in hepatocytes in culture and in liver cirrhosis is associated with lack of telomerase activity and results in telomere shortening. Hepatocellular carcinoma (HCC) cells display inactivating mutations of p53 and epigenetic silencing of $p16^{INK4a}$. Moreover, they re-express telomerase reverse transcriptase required for telomere maintenance. Thus, senescence bypass and cellular immortality is likely to contribute significantly to HCC development. Oncogene-induced senescence in premalignant lesions and reversible immortality of cancer cells including HCC offer new potentials for tumor prevention and treatment.

1. Introduction

Senescence is an evolutionary term meaning "the process of becoming old"; the phase from full maturity to death characterized by accumulation of metabolic products and decreased probability of reproduction or survival [1]. The term "cellular senescence" was initially used by Hayflick and colleagues to define cells that ceased to divide in culture [2]. Today, cellular senescence is recognized as a response of proliferating somatic cells to stress and damage from exogenous and endogenous sources. It is characterized by permanent cell cycle arrest. Senescent cells also display altered morphology and an altered pattern of gene expression, and can be recognized by the presence of senescence markers such as senescence-associated β-galactosidase (SABG), $p16^{INK4A}$, senescence-associated DNA-damage foci and senescence-associated heterochromatin foci (for a review see Ref. [3]). This cellular response has both beneficial (anti-cancer) and probably deleterious (such as tissue aging) effects on the organism. Most of our knowledge of cellular senescence is derived from in vitro studies performed with fibroblasts, and some epithelial cells such as mammary epithelial cells. Animal models are increasingly being used to study cellular senescence in vivo. Telomerase-deficient mouse models lacking RNA subunit (TERC−/−) have been very useful in demonstrating the critical role of telomeres in organ aging and tumor susceptibility [4]. Other mouse models including tumor suppressor gene-deficient and oncogene-expressing mice were also used extensively.

Compared to other tissues and cancer models, the role of senescence in liver cells and its implications in hepatocellular carcinogenesis have been less explored. One of

* Corresponding author. Address: Centre de Recherche INSERM-Université Joseph Fourrier U823, Institut Albert Bonniot, Grenoble 38000, France. Tel.: +33 (0) 4 76 54 94 10; fax: +33 (0) 4 76 54 94 54.
E-mail address: ozturkm@ujf-grenoble.fr (M. Ozturk).

0304-3835/$ - see front matter © 2008 Elsevier Ireland Ltd. All rights reserved.
doi:10.1016/j.canlet.2008.10.048

the main obstacles is the lack of adequate in vitro systems. As hepatocytes can not divide in cell culture, the study of their replicative senescence mechanisms is not easy. Nevertheless, these cells are able to quit their quiescent state in vivo and proliferate massively in response to partial hepatectomy or liver injury [5]. This capacity can be explored to study in vivo senescence of hepatocytes using rodent models. Studies with clinical samples indicate that hepatocyte senescence occurs in vivo in patients with chronic hepatitis, cirrhosis and HCC [6–8]. In contrast to the paucity of studies directly addressing cellular senescence, the critical role of telomere shortening (as a feature associated with replicative senescence) in cirrhosis and HCC development is well established [9]. Telomeres in normal liver show a consistent but slow shortening during aging. In contrast, hepatocyte DNA telomere shortening is accelerated in patients with chronic liver disease with shortest telomeres described in cirrhotic liver and HCC. Telomerase-deficient mice have also been used elegantly to demonstrate the critical roles of telomerase and telomeres in liver regeneration and experimentally induced cirrhosis [10,11]. A major accomplishment in recent years was the demonstration of critical role played by senescence for the clearance of ras-induced murine liver carcinomas following p53 restoration [12].

Despite a relatively important progress, the mechanisms of hepatocellular senescence and the role of cellular immortality in HCC remain ill-known issues. As one of the rare tissues with ample clinical data on senescence-related aberrations, liver may serve as an excellent model to further explore the relevance of cellular senescence in human biology. Moreover, a better understanding of senescence and immortality in hepatic tissues may help to develop new preventive and therapeutic approaches for severe liver diseases such as cirrhosis and HCC. Here we will review recent progress on senescence and immortality mechanisms with a specific emphasis on hepatocellular carcinogenesis.

2. Senescence pathways

Cellular senescence has long been considered as a mechanism that limits the number of cell divisions (or population doublings) in response to progressive telomere shortening. Most human somatic cells are telomerase-deficient because of the repression of telomerase reverse transcriptase (TERT) expression. Therefore, proliferating somatic cells undergo progressive telomere DNA erosion as a function of their number of cell divisions. This form of senescence is now called as replicative or telomere-dependent senescence (Fig. 1).

Human chromosome telomere ends are composed of TTAGGG repeats (5–20 kb) in a DNA-protein complex formed by six telomere-specific proteins, called "shelterin" [13]. Telomeric DNA has a structure called "t-loop" which is formed as a result of invasion of the single stranded G-rich sequence into the double-stranded telomeric tract. Since the 1930s, it has been known that telomeres, with telomere-binding proteins, prevent genomic instability and the loss of essential genetic information by "capping" chromosome ends. They are also indispensable for proper recombination and chromosomal segregation during cell division. Telomeres become shorter with every cell division in somatic cells, because of replication complex's inability to copy the ends of linear DNA, which also makes them a "cell cycle counter" for the cell [14]. Telomeres are added to the end of chromosomes with a complex containing the RNA template TERC and the reverse transcriptase TERT [15]. Most somatic cells lack telomerase activity because the expression of TERT is repressed, in contrast to TERC expression. The lack of sufficient TERT expression in somatic cells is the main cause of telomere shortening during cell replication. This telomerase activity also helps to maintain telomere integrity by telomere capping [15].

The loss of telomeres has long been considered to be the critical signal for senescence induction. It is now well known that telomere-dependent senescence is induced by a change in the protected status of shortened telomeres, whereby the loss of telomere DNA contributes to this change [16]. The loss of telomere protection or any other cause of telomere dysfunction results in inappropriate chromosomal end-to-end fusions through non-homologous end joining or homologous recombination DNA repair pathways [17]. These DNA repair pathways are used principally to repair double-strand DNA breaks (DSBs). Thus, it is highly likely that the open-ended telomere DNA is sensed as a DSB by the cell machinery when telomere structure becomes dysfunctional. Accordingly, dysfunctional telomeres elicit a potent DSB type DNA damage response by recruiting phosphorylated H2AX, 53BP1, NBS1 and MDC1 [18].

Telomere-dependent senescence is not the only form of senescence. At least two other forms of telomere-independent senescence are presently known: (1) oncogene-induced senescence; and (2) reactive oxygen species (ROS)-induced senescence (Fig. 1).

Oncogene-induced senescence had initially been identified as a response to expression of Ras oncogene in normal cells ([19], for a recent review see [20]). The expression of oncogenic Ras in primary human or rodent cells results in permanent G1 arrest. The arrest was accompanied by accumulation of p53 and $p16^{INK4a}$, and was phenotypically indistinguishable from cellular senescence. This landmark observation suggested that the onset of cellular senescence does not simply reflect the accumulation of cell divisions, but can be prematurely activated in response to an oncogenic stimulus [19]. In 10 years following this important discovery, telomere-independent forms of senescence have become a new focus of extensive research leading to the recognition of senescence as a common form of stress response. Moreover, oncogene-induced senescence is now recognized as a novel mechanism contributing to the cessation of growth of premalignant or benign neoplasms to prevent malignant cancer development [21]. In addition to Ras, other oncogenes including Raf, Mos, Mek, Myc and Cyclin E also induce senescence [20]. Conversely, the loss of PTEN tumor suppressor gene also leads to senescence [22]. Similar to telomere-dependent senescence, oncogene-induced senescence is also primarily a DNA damage response (Fig. 1). Experimental inactivation of DNA damage response abrogates Ras-induced senescence

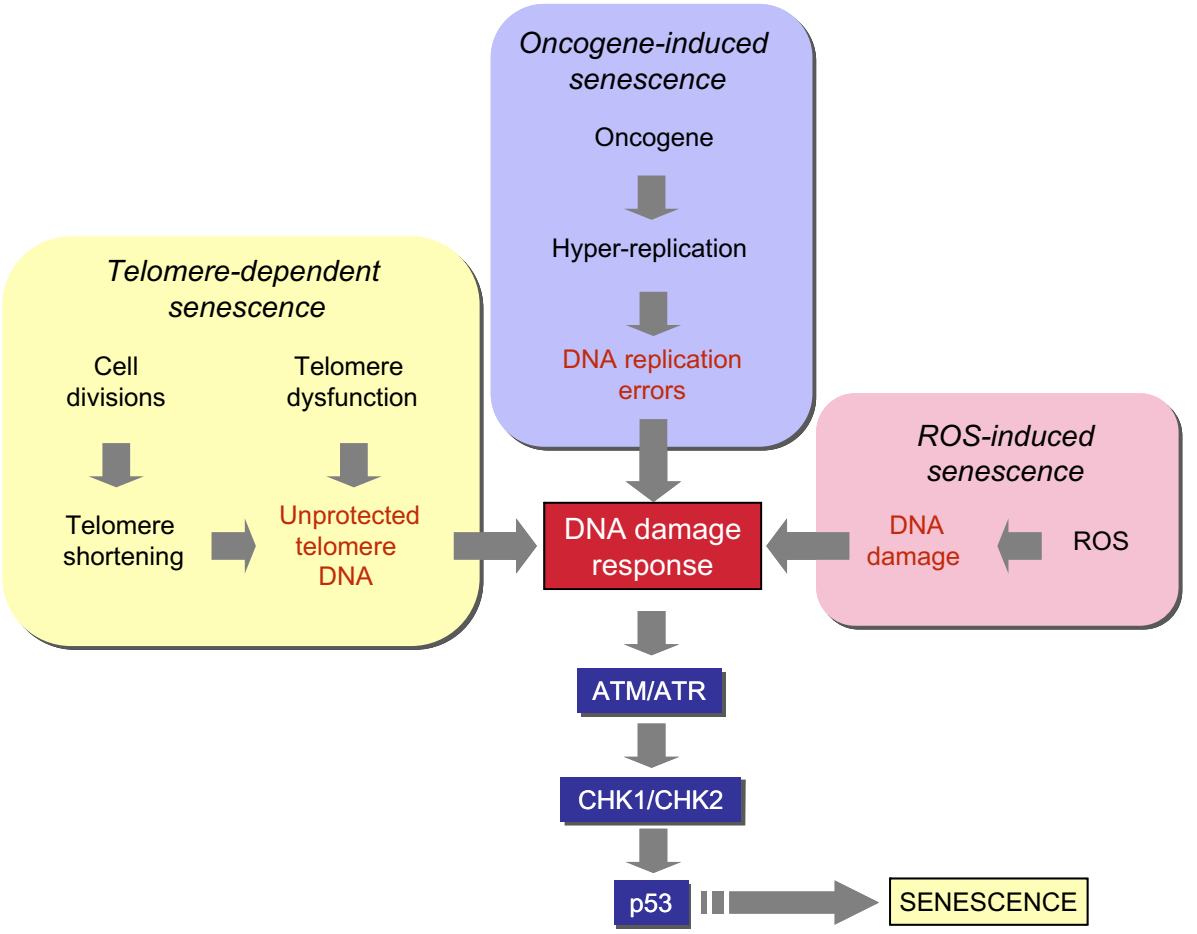

Fig. 1. DNA damage and p53 activation play a central role in different senescence pathways. DNA damage (often in the form of double-strand breaks) activate upstream kinases (ATM and ATR) leading to p53 phosphorylation by CHK1 and CHK2 kinases. Phosphoryated p53 is released from MDM, and stabilized in order to induce senescence arrest or apoptosis (not shown here).

and promotes cell transformation. DNA damage response and oncogene-induced senescence are established following DNA hyper-replication immediately after oncogene expression. Senescent cells arrest with partly replicated DNA, where DNA replication origins have fired multiple times, prematurely terminated DNA replication forks and DNA double-strand breaks are present [23,24].

ROS-induced senescence, the other telomere-independent senescence pathway is gaining importance (for a recent review see Ref. [25]). Mitochondria are the major intracellular sources of ROS which are mainly generated at the respiratory chain. Therefore, ROS have been suspected for many years as cellular metabolites involved in organismal aging [26]. ROS are also generated in the cytoplasm by the NOX family of enzymes [27]. Experimental induction of ROS accumulation in cells (for example by mild H2O2 treatment or glutathione depletion) induces senescence-like growth arrest in different cell types, whereas anti-oxidant treatment can inhibit senescence [25]. More importantly, ROS have been identified as critical mediators of both telomere-dependent and oncogene-induced senescence. Telomere-dependent senescence arrest is accelerated in cells grown under high O_2 conditions. Inversely, cells grown under low O_2 conditions display increased lifespan ([28], see Ref. [25]). ROS also play a critical role in Ras-induced senescence [29,30].

Currently, mechanisms of ROS-induced senescence are not fully understood. It is generally accepted that oxidative stress and ROS eventually cause DNA damage, whereby DNA damage response may contribute to senescence induction. The relationship between mitochondrial dysfunction, ROS, DNA damage and telomere-dependent senescence has recently been demonstrated [31]. However, ROS may also induce modifications in the cellular signaling pathways resulting in senescence arrest. For example, ROS induce senescence in hematopoietic stem cells by activating p38 MAPK [32].

Whether induced by telomere dysfunction, DNA replication stress following oncogene activation, or ROS accumulation, DNA damage is one of the common steps in the generation of senescence arrest via p53 activation (Fig. 1). Upstream checkpoint kinases, such as ATM or ATR are activated in response to DNA damage in the form of double-stand breaks. These kinases phosphorylate

downstream factors including CHK1 and CHK2 that in turn phosphorylate p53. Phosphorylation of p53 results in its activation by the displacement of the MDM2 protein. Critical involvement of this p53 activating pathway has been reported for both telomere-dependent [33], and oncogene-induced senescence [34].

Other mechanisms of senescence that are apparently not driven by DNA damage should also be discussed here. Of particular interest is the INK4 locus encoding two inhibitors of cyclin-dependent kinases ($p16^{INK4a}$, $p15^{INK4b}$), and ARF, a p53 regulatory protein (for a review see Ref. [35]). $p16^{INK4a}$ and $p15^{INK4b}$ connect some senescent initiating signals to the retinoblastoma (Rb) pathway, independent of p53 activation. These proteins are easily activated in cell culture and induce senescence arrest. Cells that escape senescence often display inactivation of $p16^{INK4a}$, and sometimes $p15^{INKb}$ and ARF either by homozygous deletion or by shutting-down gene expression. A prominent role for $p16^{INK4a}$ in senescence and tumor suppression in humans has emerged, despite some confusion due to the fact that a relatively small DNA segment encodes the 3 proteins of the INK4 locus. $p16^{INK4a}$ is activated during telomere-dependent and oncogene-induced senescence [19,36]. Moreover, its expression is induced in aging tissues [37]. The mechanisms of regulation of $p16^{INK4a}$ expression are not well known. Although individual components of INK4 locus can respond independently to positively – (for example to Ras) or negatively – (for example c-Myc) acting signals, the entire INK4 locus might be coordinately regulated by epigenetic mechanisms (reviewed in Ref. [35]).

A very recent addition to the list of senescence mechanisms is to be qualified as "senescence induced by secreted proteins". It was reported many years ago that TGF-β is a mediator of oncogene-induced senescence [38]. This mechanism of induction is of particular interest, because it suggests that not only intrinsic cellular factors, but also extracellular or secreted proteins can induce senescence. Recent discovery of several other secreted proteins, including IGFBP7 and IL6 as autocrine/paracrine mediators of oncogene-induced senescence arrest, provide strong support for an extracellularly induced form of senescence [39–41]. This new form of senescence regulation is reminiscent of the so called active apoptosis induction by death ligands. Thus, an active form of cellular senescence induced by "aging ligands" could be a major physiological regulator of tissue/organism aging.

3. Cyclin-dependent inhibitors as common mediators of senescence arrest

We have already stated that senescence and apoptosis share interesting similarities. Another similarity between these cellular processes is the convergence of different pathways in a common place to induce the same cell fate, independent of the initial signal. Similarly to caspase activation, prior to apoptosis induction by different stimuli, most if not all senescence pathways result in the activation of cyclin-dependent kinase inhibitors (CDKIs) in order to induce permanent cell cycle arrest. Senescent cells accumulate at G1 phase of the cell cycle due to an inability to enter into S phase in order to initiate DNA synthesis. The transition of proliferating cells from G1 to S phase requires the release of E2F factors from their inhibitory partner retinoblastoma protein (pRb) following phosphorylation by cyclin-dependent kinases (CDKs), in particular by CDK4/CDK6 and CDK2 at this stage of the cycle [35]. The senescence arrest is mediated by inhibition of pRb phosphorylation by CDK4 and CDK2. The activities of these enzymes are controlled by different mechanisms, but the major proteins involved in the control of senescence arrest are CDKIs. Almost all known CDKIs have been reported to be implicated in senescence arrest, but three of them are best characterized: $p16^{INK4a}$ and $p15^{INK4b}$ which inhibit CDK4/CDK6, and $p21^{Cip1}$ which inhibits CDK2 (Fig. 2).

$p21^{Cip1}$ is one of the main targets of p53 for the induction of cell cycle arrest following DNA damage [42]. Pathways that generate DNA damage response and p53 activation use $p21^{Cip1}$ as a major mediator of cellular senescence to control pRb protein [43]. Exceptionally, $p21^{Cip1}$ can be activated by p53-independent pathways to induce senescence [44].

The Rb protein plays two important and complementary roles that are necessary to initiate and to permanently maintain the cell cycle arrest in senescent cells. pRb proteins firstly contribute to the exit from the cell cycle by arresting cells at G1 phase, as expected [45]. In senescent cells, this exit is complemented with a dramatic remodeling of chromatin through the formation of domains of facultative heterochromatin called SAHF [46–48]. SAHF contain modifications and associated proteins characteristic of transcriptionally silent heterochromatin. Proliferation-promoting genes, such as E2F target genes are recruited into SAHF in a pRb protein-dependent manner. This recruitment is believed to contribute to irreversible silencing of these proliferation-promoting genes [49].

4. Senescence of hepatocytes and chronic liver disease

Hepatocytes in the adult liver are quiescent cells, they are renewed slowly, approximately once a year, as estimated by telomere loss which is 50–120 bp per year in healthy individuals [50,51]. However, the liver has an extremely powerful regenerative capacity, as demonstrated experimentally in rodents, and as observed in patients with chronic liver diseases [5]. This regenerative capacity is due mostly to the ability of mature hepatocytes to proliferate in response to a diminution of total liver mass either experimentally, or following exposure to viral and non viral hepatotoxic agents. In addition, the adult liver seems to harbor hepatocyte-progenitor cells (<0.10% of total hepatocyte mass) that are able to restore liver hepatocyte populations [52]. However, hepatocytes, like any other somatic cells, do not have unlimited replicative capacity, due to the lack of telomerase activity that is needed to avoid telomere shortening during successive cell divisions. This is best exemplified by decreased hepatocyte proliferation in liver cirrhosis stage of chronic liver diseases [53], providing in vivo evidence for the exhaustion of hepatocyte proliferation capacity. Senescence mechanisms in hepatocytes and in liver tissue are not well known. However, a limited

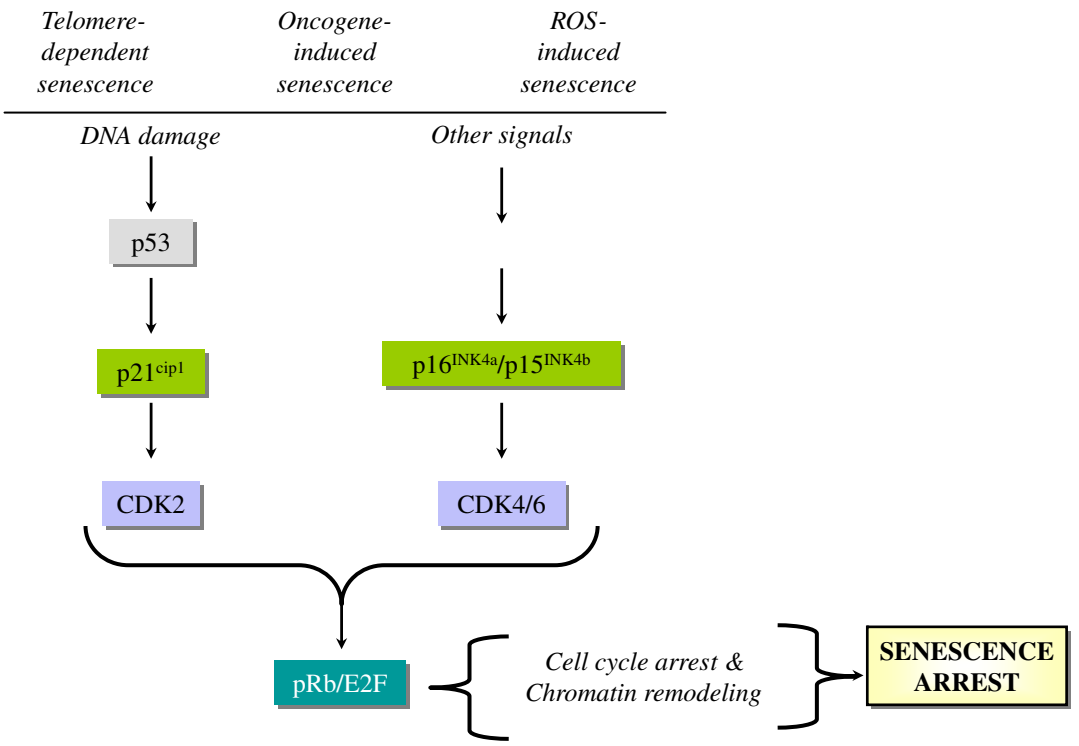

Fig. 2. All known senescence pathways converge at the level of activation of CDKIs ($p15^{INK4b}$, $p16^{INK4a}$ and $p21^{Cip1}$) that keep the pRb protein under the active form. The pRb protein inhibits E2F action and prevents the expression of growth-promoting genes for cell cycle exit. Furthermore, pRb recruits growth-promoting genes into a facultative chromatin structure for permanent silencing and growth arrest.

number of in vitro studies with hepatocytes, as well as numerous descriptive in vivo studies in liver tissue provide sufficient evidence that hepatocytes can undergo senescence type changes.

In vitro senescence in hepatocytes: as stated earlier, limited proliferative capacity of somatic cells is controlled by replicative senescence. The experimental study of replicative senescence is done traditionally by serial culture of primary cells. Initially observed in fibroblasts, this phenomenon has also been well understood in some epithelial cells, mammary epithelial cells in particular [54]. On the other hand, our knowledge of hepatocyte replicative senescence is highly limited. In contrast to in vivo conditions, mature hepatocytes are extremely resistant to cell proliferation in cell culture. Usually, more than 99.9% of adult liver hepatocytes do not divide and can only be maintained in culture for a few weeks at most. A small progenitor-type cell population (so called small hepatocytes) has been shown to proliferate in vitro, but they usually stop growing at passages 5–7, with an ill-defined senescence-like phenotype [55].

Fetal hepatocytes display better proliferation capacity in culture. A few studies have shown that these fetal cells enter replicative senescence, as shown by senescence-associated β-galactosidase assay (SABG) at population doubling (PD) 30–35 [55]. This is accompanied by progressive shortening of telomeres down to ~6 kbp, as these cells like adult hepatocytes lack telomerase activity. However, it was possible to immortalize these fetal hepatocytes by stable expression of TERT [55]. Such immortalized cells have been expanded beyond known senescence barriers (>300 PD).

In vivo senescence in liver tissue: in contrast to in vitro studies, in vivo senescence of human hepatocytes is better known. Indeed, the liver is one of the rare tissues where in vivo evidence for senescence has been convincingly and independently demonstrated by different investigators [6–9]. Replicative senescence (as tested by SABG assay) displayed a gradual increase from 10% in normal liver, to 84% in cirrhosis ([6,7]. It was also detected in 60% HCCs [6]. It has also been demonstrated that telomere shortening in cirrhosis is restricted to hepatocytes and this hepatocyte-specific shortening was correlated with SABG staining [7].

Potential mechanisms of senescence in hepatocytes and the liver: as presented in detail in the previous section, multiple pathways of senescence have been described in different experimental systems. Key molecules that are already involved in senescence arrest have also been summarized. The published data on different senescence pathways in the liver is fragmented and control mechanisms involved in hepatocyte senescence are not completely understood. Therefore, existing data on hepatocellular senescence together with potential mechanisms that may be involved in this process will be presented.

For reasons previously described, almost nothing is known about molecular mechanisms involved in replicative senescence and immortalization of hepatocytes in cul-

ture. There are only a few demonstrations of hepatocyte immortalization in vitro. Thus, ectopically expressed TERT may induce hepatocyte immortalization. However, as the published data using TERT immortalization is scarce, it is highly likely that the immortalization of hepatocytes is not an easy task even with a well-established protocol that works with other epithelial cell types such as mammary epithelial cells. The mechanisms of in vitro senescence induction in hepatocytes are also mostly unknown. Rapid induction of a senescence arrest in cultured hepatocytes suggests that these cells display robust telomere-independent senescence-inducing systems that are functional in vitro. However, they remain to be discovered. It is highly likely that, similar to other somatic cells, p53 and RB pathways in general, and some CDKIs in particular are also involved in hepatocyte senescence, but the evidence is lacking for the time being.

Telomere shortening during aging is slow (55–120 base pairs per year) and stabilizes at mid age in healthy liver, so that the loss of telomeric DNA does not reach a level to induce telomere dysfunction and DNA damage response [50,51]. Other forms of telomere-independent senescence such as ROS-induced senescence may also be rare under normal physiological conditions. On the other hand, telomere loss is accelerated in chronic liver disease to reach lowest levels in the cirrhotic liver [7,51]. Therefore, one plausible mechanism involved in cirrhosis is probably telomere-dependent senescence, or replicative senescence. The relevance of replicative senescence to liver tissue aging has been demonstrated experimentally using telomerase-deficient mice. Late generation telomerase-deficient mice display critically shortened telomeres and an impaired liver growth response to partial hepatectomy. A subpopulation of telomere-shortened hepatic cells displayed impaired proliferative capacity that is associated with SABG activity [11,56]. On the other hand, it has been reported that mouse liver cells are highly resistant to extensive telomere dysfunction. Conditional deletion of the telomeric protein TRF2 in hepatocytes resulted in telomeric accumulation of phospho-H2AX and frequent telomere fusions, indicating loss of telomere protection. However, there was no induction of p53 and liver function appeared unaffected. The loss of TRF2 did not compromise liver regeneration after partial hepatectomy. Liver regeneration occurred without cell division involving endoreduplication and cell growth, thereby circumventing the chromosome segregation problems associated with telomere fusions. Thus, it appears that hepatocytes display intrinsic resistance to telomere dysfunction, although they are apparently vulnerable to severe telomere loss [57].

Hepatocyte senescence that is observed in severe chronic liver diseases such as cirrhosis may also be induced by telomere-independent pathways. Chronic liver injury observed under such conditions is accompanied with inflammation, cell death, and oxidative stress [58–60]. Some of the etiological factors such as HCV and alcohol induce mitochondrial dysfunction may result in ROS accumulation [61,62]. Thus, ROS-induced senescence may also occur during cirrhosis, although this has not yet been reported. The status of DNA damage in chronic liver disease is less well-known. 8-Hydroxydeoxyguanosine, an indicator of DNA lesions produced by ROS, was reported to be increased in chronic liver disease [63]. On the other hand, the upregulation of DNA repair enzymes in cirrhosis has also been reported [64]. Increased DNA repair activity in cirrhosis which may reflect increased DNA damages as a consequence of chronic liver injury, but also inhibition of DNA damage responses such as senescence were observed. Taken together, these observations suggest that the primary cause of senescence in cirrhotic patients is telomere dysfunction and that ROS may also play additional roles.

Among senescence-related proteins, $p16^{INK4a}$ and $p21^{Cip1}$ expression was found to be high in cirrhosis, as compared to normal liver and tumor tissues [65], suggesting that these major senescence-inducing proteins accumulate in the cirrhotic liver. Promoter methylation of these CDKIs was also studied. Chronic liver disease samples displayed lower levels of methylation as compared to HCCs [66]. Thus, the progression of chronic liver disease towards cirrhosis is accompanied with a progressive activation of different CDKIs, as expected.

5. Senescence pathway aberrations and telomerase reactivation in hepatocellular carcinoma

As stated earlier, p53 and retinoblastoma (Rb) pathways play a critical role in senescence arrest as observed in different in vitro and in vivo models. Indirect evidence suggests that these pathways may also be important in hepatocellular senescence. The accumulation of p21 and p16 in cirrhotic liver tissues has been reported independently by different reports. On the other hand, HCC rarely develops in liver tissues absent of chronic liver disease. More than 80% of these cancers are observed in patients with cirrhosis [9]. As the appearance of proliferating malignant cells from this senescence stage requires the bypass of senescence, the status of both p53 and RB pathways in HCC is of great importance in terms of molecular aspects of hepatocellular carcinogenesis.

HCC is one of the major tumors displaying frequent p53 mutations [67,68]. The overall p53 mutation frequency in HCC is around 30%. Both the frequency and the spectrum of p53 mutations show great variations between tumors from different geographical areas of the World. A hotspot mutation (codon 249 AGG → AGT) has been linked to exposure to aflatoxins which are known to be potent DNA damaging agents (for a review see Ref. [67]). Although, it is unknown whether aflatoxins are able to generate a DNA damage-dependent senescence response in hepatocytes, their association with DNA damage and p53 mutation provides indirect evidence for such an ability. Other p53 mutations described in HCCs from low aflatoxin areas may similarly be correlated with other DNA damaging agents, such as ROS which are known to accumulate in the livers of patients with chronic liver diseases, including cirrhosis.

Another player of senescence arrest, the p16 gene is rarely mutated in HCC, but its epigenetic silencing by promoter methylation is highly frequent in this cancer. More than 50% of HCCs display de novo methylation of the promoter of CDKN2A gene, encoding p16 protein, resulting in

loss of gene expression [67]. Major components of p53 and Rb pathways in the same set of HCCs with different etiologies have been analyzed [69]. Retinoblastoma pathway alterations (p16 ^{INK4a}, p15^{INK4b} or RB1 genes) were present in 83% of HCCs, whereas p53 pathway alterations (p53 or ARF genes) were detected in only 31% of tumors. Alterations in both Rb and p53 pathways were present in 30% of HCCs. Thus, it appears that either the Rb and/or the p53 pathway are affected in the great majority of HCCs, and that both pathways are affected in at least one third of these tumors. Unfortunately, p53 and p16^{INK4a} aberrations observed in HCC have not yet been studied in relation to senescence aberrations. However, these observations provide supporting evidence on the critical role of senescence-controlling pathways in the development of HCC.

The lack of telomerase activity in normal and cirrhotic liver correlates with progressive loss of telomere sequences ending up with a senescence arrest. The emergence of malignant hepatocytes from this senescence-dominated cirrhotic milieu would require not only the bypass of senescence, but also a way of survival despite critically shortened telomeres. Additionally, the proliferative expansion of neoplastic cells in order to form sustained tumor masses would require telomeres at a minimal length required to maintain intact chromosomal structures.

Many studies showed that telomerase activity is a hallmark of all human cancers, including 80–90% of HCCs [70–72]. It is currently unclear how the TERT expression is repressed and released in normal hepatocytes and HCC cells, respectively. The integration of HBV DNA sequences into TERT gene provides evidence for a virus-induced deregulation of TERT expression, but this appears to rarely occur, as only four cases have been reported thus far [73–75]. Hbx and PreS2 proteins may upregulate TERT expression [76,77]. The molecular mechanisms involved in TERT suppression in somatic cells and its reactivation in cancer cells are ill-known. The TERT promoter displays binding sites for a dozen of transcriptional regulators: estrogen receptor, Sp1, Myc and ER81 acting positively, and vitamin D receptor, MZF-2, WT1, Mad, E2F1 and SMAD interacting protein-1 (SIP1, also called ZEB-2 or ZFHX1B) acting negatively [78]. Despite high telomerase activity, telomeres in HCC were repeatedly found to be highly shortened [65,79,80]. However, 3′ telomere overhangs were found to be increased in nearly 40% HCCs [80]. Moreover, the expression of several telomeric proteins is increased in HCC [80,81].

Another ill-known aspect of TERT activity in HCC cells is the cellular origin of these malignant cells. It is presently unclear whether HCC arises from mature hepatocytes which lack telomerase activity, or stem/progenitor cell-like cells that may already express TERT at sufficient levels to maintain telomere integrity. In the non-tumor area surrounding the cancer tissue, telomerase activity could not be detected, or was detected at very low levels.

The importance of telomerase activity in HCC development has been studied experimentally using telomerase-deficient mouse model. These mice show increased susceptibility to adenoma development (tumor initiation), but they are quite resistant to fully malignant tumor development [82]. Likewise, telomerase deletion limits the progression of p53-mutant HCCs with short telomeres [83]. These observations suggest that the aberrations affecting telomerase activity and senescence controlling genes such as p53 may cooperate during hepatocellular carcinogenesis.

In summary, HCC is characterized by mutational inactivation of p53, a major player in DNA damage-induced senescence. In addition, p15^{INK4b}, p16^{INK4a}, p21^{Cip1} CDKIs are often inactivated in this cancer mostly by epigenetic mechanisms involving promoter methylation. These changes may play a critical role in the bypass of senescence that is observed in most cirrhosis cases, allowing some initiated cells to escape senescence control and proliferate. In the absence of telomerase activity such cells would probably not survive due to telomere loss. However, since more than 80% of HCCs display telomerase activity, it is highly likely that the telomerase reactivation, together with the inactivation of major CDKIs, plays a critical role in HCC development by conferring premalignant or malignant cells the ability to proliferate indefinitely (Fig. 3). However, cellular immortality is not sufficient for full malignancy [84]. Thus, senescence-related aberrations that are observed in HCC cells, may confer a partial survival advantage that would need to be complemented by other genetic or epigenetic alterations.

6. Senescence as an anti-tumor mechanism in hepatocellular carcinoma

Senescence in normal somatic cells and tissues is expected. How about cancer cells and tumors? Initial studies using different cancer cell lines provided ample evidence for the induction of senescence by different genetic as well as chemical or biological treatments [85]. Thus, it appeared that cancer cells, immortalized by definition, do have a hidden senescence program that can be revealed by different senescence-inducing stimuli. These studies provided preliminary evidence for considering senescence induction as an anti-cancer therapy. The in vivo relevance of these observations and expectations became evident only very recently. Senescence was observed in tumors or pre-neoplastic lesions. SABG activity as well as several other senescence markers were detected in lung adenomas, but not in adenocarcinomas observed in oncogenic Ras "knock-in" mice [86]. Ras-driven mouse T-cell lymphomas entered senescence after drug therapy, when apoptosis was blocked [87]. The first direct evidence of cellular senescence in humans was reported for the melanocytic nevus [88].

Senescence response of HCC cells was not the subject of intensive study until very recently. Therefore the potential role of senescence in these tumors is less well understood. Treatment of HCC cell lines with 5-aza-2-deoxycytidine induced the expression of p16^{INK4a}, hypophosphorylation of pRb and G1 arrest associated with positive SABG staining [89]. Recent findings indicate that senescence induction is a powerful mechanism of HCC regression. Xue et al. expressed H-ras oncogene and suppressed endogenous p53 expression in mouse hepatoblasts which produced massive

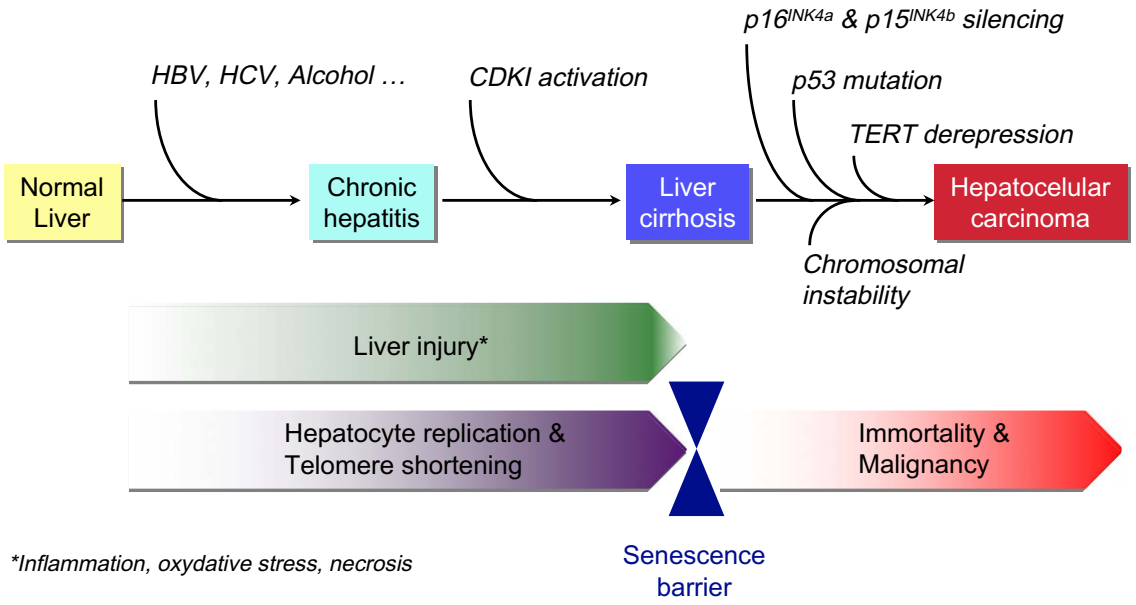

Fig. 3. Role of cellular senescence and immortalization in hepatocellular carcinogenesis. Chronic liver injury (triggered by major etiological factors HBV, HCV and alcohol) leading to cirrhosis is a common cause of HCC. Hepatocytes having no telomerase activity undergo progressive telomere shortening and DNA damage during this process. Consequently, CDKIs (primarily $p16^{INK4a}$ and $p21^{Cip1}$) are activated gradually to induce senescence in the preneoplastic cirrhosis stage. Mutation and expression analyses in HCC strongly suggest that neoplastic cells bypass the senescence barrier by inactivating major senescence-inducing genes (p53, $p16^{INK4a}$ and $p15^{INK4b}$). Moreover, they acquire the ability of unlimited proliferation (immortality) by re-expressing the TERT enzyme. Chromosomal instability that is generated by telomere erosion may contribute to additional mutations necessary for tumor progression.

HCCs upon implantation into livers of athymic mice [12]. However, these tumors regressed rapidly upon restoration of p53 expression. Tumor regression was due to differentiation and massive senescence induction, followed by immune-mediated clearance of senescent cells. These observations may indicate that oncogene-induced senescence is also involved in HCC. On the other hand, HCCs induced by tet-regulated c-Myc activation in mouse liver cells differentiate into mature hepatocytes and biliary cells or undergo senescence [90]. Thus, senescence induction may also be relevant to oncogene inactivation in HCC. In this regard, c-Myc down-regulation and senescence induction in several HCC cell lines as a response to TGF-β was observed (S. Senturk, M. Ozturk, unpublished data).

So far, all the reported examples of senescence induction in HCC cells are in the form of a telomere-independent permanent cell cycle arrest. Until recently, it was unknown whether replicative senescence could also be induced in immortal cancer cells. Ozturk et al. reported recently that immortal HCC cells can revert spontaneously to a replicative senescence phenotype [91]. Immortal HCC cells generated progeny that behaved, in vitro, similar to normal somatic cells. Such senescence-programmed progeny lacked telomerase activity due to TERT repression (probably mediated by SIP1 gene), and displayed progressive telomere shortening in cell culture, resulting in senescence arrest. It will be interesting to test whether such spontaneous reversal of replicative immortality is involved in well known tumor dormancy and/or spontaneous tumor regression.

7. Concluding remarks

Cellular senescence has gained great interest in recent years following the demonstration that it also occurs in vivo. It is also highly interesting that senescence can be mediated by a large number of pathways and molecules, as is the case for apoptosis. Recent findings that implicate secreted molecules in senescence induction strongly suggest that cellular senescence is not just a cellular event, but also a physiologically relevant process for the whole organism. In terms of tumor biology, oncogene-induced senescence that may serve as anti-tumor mechanism in pre-neoplastic lesions underlines its clinical relevance. On the other hand, induced or spontaneous senescence that is observed in cancer cells is promising to explore new approaches for tumor prevention and treatment. The role of senescence bypass and cellular immortality in hepatocellular carcinogenesis is not well defined. But, many findings (inactivation of senescence-mediator genes such as p53, $p16^{INK4a}$ and $p15^{INK4b}$, as well as reactivation of TERT) indicate that senescence mechanisms and their aberrations are critically involved in HCC. We may expect that this field will attract more attention in coming years for a better definition of senescence implications in hepatocellular carcinogenesis.

AcknowledgmentS

Authors' research is supported by grants from TUBITAK, DPT and TUBA (Turkey), and InCA (France). We thank D. Ozturk for language editing.

References

[1] D.E. Crew (Ed.), Human senescence-evolutionary and biocultural perspectives, Cambridge University Press, Cambridge, 2003.
[2] L. Hayflick, The limited in vitro lifetime of human diploid cell strains, Exp. Cell Res. 37 (1965) 614–636.
[3] J. Campisi, F. d'Adda di Fagagna, Cellular senescence: when bad things happen to good cells, Nat. Rev. Mol. Cell Biol. 8 (2007) 729–740.
[4] K.L. Rudolph, S. Chang, H.W. Lee, M. Blasco, G.J. Gottlieb, C. Greider, R.A. DePinho, Longevity, stress response, and cancer in aging telomerase-deficient mice, Cell 96 (1999) 701–712.
[5] G.K. Michalopoulos, Liver regeneration, J. Cell Physiol. 213 (2007) 286–300.
[6] V. Paradis, N. Youssef, D. Dargere, N. Ba, F. Bonvoust, J. Deschatrette, P. Bedossa, Replicative senescence in normal liver, chronic hepatitis C, and hepatocellular carcinomas, Hum. Pathol. 32 (2001) 327–332.
[7] S.U. Wiemann, A. Satyanarayana, M. Tsahuridu, H.L. Tillmann, L. Zender, J. Klempnauer, P. Flemming, S. Franco, M.A. Blasco, M.P. Manns, K.L. Rudolph, Hepatocyte telomere shortening and senescence are general markers of human liver cirrhosis, FASEB J. 16 (2002) 935–942.
[8] V. Trak-Smayra, J. Contreras, F. Dondero, F. Durand, S. Dubois, D. Sommacale, P. Marcellin, J. Belghiti, C. Degott, V. Paradis, Role of replicative senescence in the progression of fibrosis in hepatitis C virus (HCV) recurrence after liver transplantation, Transplantation 77 (2004) 1755–1760.
[9] H.B. El-Serag, K.L. Rudolph, Hepatocellular carcinoma: epidemiology and molecular carcinogenesis, Gastroenterology 132 (2007) 2557–2576.
[10] K.L. Rudolph, S. Chang, M. Millard, N. Schreiber-Agus, R.A. DePinho, Inhibition of experimental liver cirrhosis in mice by telomerase gene delivery, Science 287 (2000) 1253–1258.
[11] A. Satyanarayana, S.U. Wiemann, J. Buer, J. Lauber, K.E. Dittmar, T. Wüstefeld, M.A. Blasco, M.P. Manns, K.L. Rudolph, Telomere shortening impairs organ regeneration by inhibiting cell cycle re-entry of a subpopulation of cells, EMBO J. 22 (2003) 4003–4013.
[12] W. Xue, L. Zender, C. Miething, R.A. Dickins, E. Hernando, V. Krizhanovsky, C. Cordon-Cardo, S.W. Lowe, Senescence and tumour clearance is triggered by p53 restoration in murine liver carcinomas, Nature 445 (2007) 656–660.
[13] T. de Lange, Shelterin: the protein complex that shapes and safeguards human telomeres, Genes Dev. 19 (2005) 2100–2110.
[14] E.H. Blackburn, Structure and function of telomeres, Nature 350 (1991) 569–573.
[15] Y.S. Cong, W.E. Wright, J.W. Shay, Human telomerase and its regulation, Microbiol. Mol. Biol. Rev. 66 (2002) 407–425.
[16] J. Karlseder, A. Smogorzewska, T. de Lange, Senescence induced by altered telomere state, Not telomere loss, Science 295 (2002) 2446–2449.
[17] R.E. Verdun, J. Karlseder, Replication and protection of telomeres, Nature 447 (2007) 924–931.
[18] F. d'Adda di Fagagna, P.M. Reaper, L. Clay-Farrace, H. Fiegler, P. Carr, T. Von Zglinicki, G. Saretzki, N.P. Carter, S.P. Jackson, A DNA damage checkpoint response in telomere-initiated senescence, Nature 426 (2003) 194–198.
[19] M. Serrano, A.W. Lin, M.E. McCurrach, D. Beach, S.W. Lowe, Oncogenic ras provokes premature cell senescence associated with accumulation of p53 and p16INK4a, Cell 88 (1997) 593–602.
[20] R. Di Micco, M. Fumagalli, d'Adda F. di Fagagna, Breaking news: high-speed race ends in arrest-how oncogenes induce senescence, Trends Cell Biol. 17 (2007) 529–536.
[21] W.J. Mooi, D.S. Peeper, Oncogene-induced cell senescence-halting on the road to cancer, N. Engl. J. Med. 355 (2006) 1037–1046.
[22] Z. Chen, L.C. Trotman, D. Shaffer, H.K. Lin, Z.A. Dotan, M. Niki, J.A. Koutcher, H.I. Scher, T. Ludwig, W. Gerald, C. Cordon-Cardo, P.P. Pandolfi, Crucial role of p53-dependent cellular senescence in suppression of Pten-deficient tumorigenesis, Nature 436 (2005) 725–730.
[23] R. Di Micco, M. Fumagalli, A. Cicalese, S. Piccinin, P. Gasparini, C. Luise, C. Schurra, M. Garre', P.G. Nuciforo, A. Bensimon, R. Maestro, P.G. Pelicci, F. d'Adda di Fagagna, Oncogene-induced senescence is a DNA damage response triggered by DNA hyper-replication, Nature 444 (2006) 638–642.
[24] J. Bartkova, N. Rezaei, M. Liontos, P. Karakaidos, D. Kletsas, N. Issaeva, L.V. Vassiliou, E. Kolettas, K. Niforou, V.C. Zoumpourlis, M. Takaoka, H. Nakagawa, F. Tort, K. Fugger, F. Johansson, M. Sehested, C.L. Andersen, L. Dyrskjot, T. Ørntoft, J. Lukas, C. Kittas, T. Helleday, T.D. Halazonetis, J. Bartek, V.G. Gorgoulis, Oncogene-induced senescence is part of the tumorigenesis barrier imposed by DNA damage checkpoints, Nature 444 (2006) 633–637.
[25] T. Lu, T. Finkel, Free radicals and senescence, Exp. Cell Res. 314 (2008) 1918–1922.
[26] M. Giorgio, M. Trinei, E. Migliaccio, P.G. Pelicci, Hydrogen peroxide: a metabolic by-product or a common mediator of ageing signals?, Nat Rev. Mol. Cell Biol. 8 (2007) 722–728.
[27] C. Blanchetot, J. Boonstra, The ROS-NOX connection in cancer and angiogenesis, Crit. Rev. Eukaryot. Gene Expr. 18 (2008) 35–45.
[28] T. von Zglinicki, G. Saretzki, W. Döcke, C. Lotze, Mild hyperoxia shortens telomeres and inhibits proliferation of fibroblasts: a model for senescence?, Exp Cell Res. 220 (1995) 186–193.
[29] A.C. Lee, B.E. Fenster, H. Ito, K. Takeda, N.S. Bae, T. Hirai, Z.X. Yu, V.J. Ferrans, B.H. Howard, T. Finkel, Ras proteins induce senescence by altering the intracellular levels of reactive oxygen species, J. Biol. Chem. 274 (1999) 7936–7940.
[30] S. Courtois-Cox, S.L. Jones, K. Cichowski, Many roads lead to oncogene-induced senescence, Oncogene 27 (2008) 2801–2809.
[31] J.F. Passos, G. Saretzki, S. Ahmed, G. Nelson, T. Richter, H. Peters, I. Wappler, M.J. Birket, G. Harold, K. Schaeuble, M.A. Birch-Machin, T.B. Kirkwood, T. von Zglinicki, Mitochondrial dysfunction accounts for the stochastic heterogeneity in telomere-dependent senescence, PLoS Biol. 5 (2007) e110.
[32] K. Ito, A. Hirao, F. Arai, K. Takubo, S. Matsuoka, K. Miyamoto, M. Ohmura, K. Naka, K. Hosokawa, Y. Ikeda, T. Suda, Reactive oxygen species act through p38 MAPK to limit the lifespan of hematopoietic stem cells, Nat. Med. 12 (2006) 446–451.
[33] U. Herbig, W.A. Jobling, B.P. Chen, D.J. Chen, J.M. Sedivy, Telomere shortening triggers senescence of human cells through a pathway involving ATM, p53, and p21(CIP1), but not p16(INK4a) but not p16(INK4a), Mol. Cell. 14 (2004) 501–513.
[34] F.A. Mallette, M.F. Gaumont-Leclerc, G. Ferbeyre, The DNA damage signaling pathway is a critical mediator of oncogene-induced senescence, Genes Dev. 21 (2007) 43–48.
[35] J. Gil, G. Peters, Regulation of the INK4b-ARF-INK4a tumour suppressor locus: all for one or one for all, Nat. Rev. Mol. Cell Biol. 7 (2006) 667–677.
[36] D.A. Alcorta, Y. Xiong, D. Phelps, G. Hannon, D. Beach, J.C. Barrett, Involvement of the cyclin-dependent kinase inhibitor p16 (INK4a) in replicative senescence of normal human fibroblasts, Proc. Natl. Acad. Sci. U S A 93 (1996) 13742–13747.
[37] F. Zindy, D.E. Quelle, M.F. Roussel, C.J. Sherr, Expression of the p16INK4a tumor suppressor versus other INK4 family members during mouse development and aging, Oncogene 15 (1997) 203–211.
[38] R. Tremain, M. Marko, V. Kinnimulki, H. Ueno, E. Bottinger, A. Glick, Defects in TGF-beta signaling overcome senescence of mouse keratinocytes expressing v-Ha-ras, Oncogene 19 (2000) 1698–1709.
[39] N. Wajapeyee, R.W. Serra, X. Zhu, M. Mahalingam, M.R. Green, Oncogenic BRAF induces senescence and apoptosis through pathways mediated by the secreted protein IGFBP7, Cell 132 (2008) 363–374.
[40] J.C. Acosta, A. O'Loghlen, A. Banito, M.V. Guijarro, A. Augert, S. Raguz, M. Fumagalli, M. Da Costa, C. Brown, N. Popov, Y. Takatsu, J. Melamed, F. d'Adda di Fagagna, D. Bernard, E. Hernando, J. Gil, Chemokine signaling via the CXCR2 receptor reinforces senescence, Cell 133 (2008) 1006–1018.
[41] T. Kuilman, C. Michaloglou, L.C. Vredeveld, S. Douma, R. van Doorn, C.J. Desmet, L.A. Aarden, W.J. Mooi, D.S. Peeper, Oncogene-induced senescence relayed by an interleukin-dependent inflammatory network, Cell 133 (2008) 1019–1031.
[42] W.S. el-Deiry, T. Tokino, V.E. Velculescu, D.B. Levy, R. Parsons, J.M. Trent, D. Lin, W.E. Mercer, K.W. Kinzler, B. Vogelstein, WAF1, a potential mediator of p53 tumor suppression, Cell 75 (1993) 817–825.
[43] Y. Deng, S.S. Chan, S. Chang, Telomere dysfunction and tumor suppression: the senescence connection, Nat. Rev. Cancer 8 (2008) 450–458.
[44] L. Fang, M. Igarashi, J. Leung, M.M. Sugrue, S.W. Lee, S.A. Aaronson, p21Waf1/Cip1/Sdi1 induces permanent growth arrest with markers

of replicative senescence in human tumor cells lacking functional p53, Oncogene 18 (1999) 2789–2797.
[45] C. Giacinti, A. Giordano, RB and cell cycle progression, Oncogene 25 (2006) 5220–5227.
[46] M. Narita, S. Nunez, E. Heard, A.W. Lin, S.A. Hearn, D.L. Spector, G.J. Hannon, S.W. Lowe, Rb-mediated heterochromatin formation and silencing of E2F target genes during cellular senescence, Cell 113 (2003) 703–716.
[47] R. Zhang, M.V. Poustovoitov, X. Ye, H.A. Santos, W. Chen, S.M. Daganzo, J.P. Erzberger, I.G. Serebriiskii, A.A. Canutescu, R.L. Dunbrack, J.R. Pehrson, J.M. Berger, P.D. Kaufman, P.D. Adams, Formation of MacroH2A-containing senescence-associated heterochromatin foci and senescence driven by ASF1a and HIRA, Dev. Cell 8 (2005) 19–30.
[48] M. Narita, M. Narita, V. Krizhanovsky, S. Nunez, A. Chicas, S.A. Hearn, M.P. Myers, S.W. Lowe, A novel role for high-mobility group a proteins in cellular senescence and heterochromatin formation, Cell 126 (2006) 503–514.
[49] P.D. Adams, Remodeling of chromatin structure in senescent cells and its potential impact on tumor suppression and aging, Gene 397 (2007) 84–93.
[50] K. Takubo, N. Izumiyama-Shimomura, N. Honma, M. Sawabe, T. Arai, M. Kato, M. Oshimura, K. Nakamura, Telomere lengths are characteristic in each human individual, Exp. Gerontol. 37 (2002) 523–531.
[51] H. Aikata, H. Takaishi, Y. Kawakami, S. Takahashi, M. Kitamoto, T. Nakanishi, Y. Nakamura, F. Shimamoto, G. Kajiyama, T. Ide, Telomere reduction in human liver tissues with age and chronic inflammation, Exp. Cell Res. 256 (2000) 578–582.
[52] R. Utoh, C. Tateno, C. Yamasaki, N. Hiraga, M. Kataoka, T. Shimada, K. Chayama, K. Yoshizato, Susceptibility of chimeric mice with livers repopulated by serially subcultured human hepatocytes to hepatitis B virus, Hepatology 47 (2008) 435–446.
[53] M. Delhaye, H. Louis, C. Degraef, O. Le Moine, J. Devière, B. Gulbis, D. Jacobovitz, M. Adler, P. Galand, Relationship between hepatocyte proliferative activity and liver functional reserve in human cirrhosis, Hepatology 23 (1996) 1003–1011.
[54] M.R. Stampfer, P. Yaswen, Human epithelial cell immortalization as a step in carcinogenesis, Cancer Lett. 194 (2003) 199–208.
[55] H. Wege, H.T. Le, M.S. Chui, L. Lui, J. Wu, G. Giri, H. Malhi, B.S. Sappal, V. Kumaran, S. Gupta, M.A. Zern, Telomerase reconstitution immortalized human fetal hepatocytes without disrupting their differentiation potential, Gastroenterology 124 (2003) 432–444.
[56] A. Lechel, A. Satyanarayana, Z. Ju, R.R. Plentz, S. Schaetzlein, C. Rudolph, L. Wilkens, S.U. Wiemann, G. Saretzki, N.P. Malek, M.P. Manns, J. Buer, K.L. Rudolph, The cellular level of telomere dysfunction determines induction of senescence or apoptosis in vivo, EMBO Rep. 6 (2005) 275–281.
[57] E. Lazzerini Denchi, G. Celli, T. de Lange, Hepatocytes with extensive telomere deprotection and fusion remain viable and regenerate liver mass through endoreduplication, Genes Dev. 20 (2006) 2648–2653.
[58] G. Szabo, P. Mandrekar, A. Dolganiuc, Innate immune response and hepatic inflammation, Semin. Liver Dis. 27 (2007) 339–350.
[59] H. Malhi, G.J. Gores, Cellular and molecular mechanisms of liver injury, Gastroenterology 134 (2008) 1641–1654.
[60] D. Schuppan, N.H. Afdhal, Liver cirrhosis, Lancet 371 (2008) 838–851.
[61] F. Farinati, R. Cardin, M. Bortolami, P. Burra, F.P. Russo, M. Rugge, M. Guido, A. Sergio, R. Naccarato, Hepatitis C virus: from oxygen free radicals to hepatocellular carcinoma, J. Viral Hepat. 14 (2007) 821–829.
[62] A. Reuben, Alcohol and the liver, Curr. Opin. Gastroenterol. 24 (2008) 328–338.
[63] R. Shimoda, M. Nagashima, M. Sakamoto, N. Yamaguchi, S. Hirohashi, J. Yokota, H. Kasai, Increased formation of oxidative DNA damage, 8-hydroxydeoxyguanosine, in human livers with chronic hepatitis, Cancer Res. 54 (1994) 3171–3172.
[64] P. Zindy, L. Andrieux, D. Bonnier, O. Musso, S. Langouët, J.P. Campion, B. Turlin, B. Clément, N. Théret, Upregulation of DNA repair genes in active cirrhosis associated with hepatocellular carcinoma, FEBS Lett. 579 (2005) 95–99.
[65] R.R. Plentz, Y.N. Park, A. Lechel, H. Kim, F. Nellessen, B.H. Langkopf, L. Wilkens, A. Destro, B. Fiamengo, M.P. Manns, M. Roncalli, K.L. Rudolph, Telomere shortening and inactivation of cell cycle checkpoints characterize human hepatocarcinogenesis, Hepatology 45 (2007) 968–976.
[66] M. Roncalli, P. Bianchi, B. Bruni, L. Laghi, A. Destro, S. Di Gioia, L. Gennari, M. Tommasini, A. Malesci, G. Coggi, Methylation framework of cell cycle gene inhibitors in cirrhosis and associated hepatocellular carcinoma, Hepatology 36 (2002) 427–432.
[67] M. Ozturk, Genetic aspects of hepatocellular carcinogenesis, Semin. Liver Dis. 19 (1999) 235–242.
[68] T. Soussi, p53 alterations in human cancer: more questions than answers, Oncogene 26 (2007) 2145–2156.
[69] Y. Edamoto, A. Hara, W. Biernat, L. Terracciano, G. Cathamos, H.M. Riehle, M. Matsuda, H. Fuji, J.M. Scoazec, H. Ohgaki, Alterations of RB1, p53 and Wnt pathways in Hepatocellular carcinomas associated with HCV, HBV and alcoholic liver cirrhosis, Int. J. Cancer 106 (2003) 334–341.
[70] H. Tahara, T. Nakanishi, M. Kitamoto, R. Nakashio, J.W. Shay, E. Tahara, G. Kajiyama, T. Ide, Telomerase activity in human liver tissues: Comparison between chronic liver disease and hepatocellular carcinomas, Cancer Res. 55 (1995) 2734–2736.
[71] H. Kojima, O. Yokosuka, F. Imazeki, H. Saisho, M. Omata, Telomerase activity and telomere length in hepatocellular carcinoma and chronic liver disease, Gastroenterology 112 (1997) 493–500.
[72] J. Nakayama, H. Tahara, E. Tahara, M. Saito, K. Ito, H. Nakamura, T. Nakanishi, E. Tahara, T. Ide, F. Ishikawa, Telomerase activation by hTERT in human normal fibroblasts and hepatocellular carcinomas, Nat. Genet. 18 (1998) 65–68.
[73] D. Gozuacik, Y. Murakami, K. Saigo, M. Chami, C. Mugnier, D. Lagorce, T. Okanoue, T. Urashima, C. Bréchot, P. Paterlini-Bréchot, Identification of human cancer-related genes by naturally occurring Hepatitis B Virus DNA tagging, Oncogene 20 (2001) 6233–6240.
[74] I. Horikawa, JC. Barrett, Transcriptional regulation of the telomerase hTERT gene as a target for cellular and viral oncogenic mechanisms, Carcinogenesis 24 (2003) 1167–1176.
[75] Y. Murakami, K. Saigo, H. Takashima, M. Minami, T. Okanoue, C. Bréchot, P. Paterlini-Bréchot, Large scaled analysis of hepatitis B virus (HBV) DNA integration in HBV related hepatocellular carcinomas, Gut 54 (2005) 1162–1168.
[76] Z.L. Qu, S.Q. Zou, N.Q. Cui, X.Z. Wu, M.F. Qin, D. Kong, Z.L. Zhou, Upregulation of human telomerase reverse transcriptase mRNA expression by in vitro transfection of hepatitis B virus X gene into human hepatocarcinoma and cholangiocarcinoma cells, World J. Gastroenterol. 11 (2005) 5627–5632.
[77] H. Liu, F. Luan, Y. Ju, H. Shen, L. Gao, X. Wang, S. Liu, L. Zhang, W. Sun, C. Ma, In vitro transfection of the hepatitis B virus PreS2 gene into the human hepatocarcinoma cell line HepG2 induces upregulation of human telomerase reverse transcriptase, Biochem. Biophys. Res. Commun. 355 (2007) 379–384.
[78] R. Janknecht, On the road to immortality: hTERT upregulation in cancer cells, FEBS Lett. 564 (2004) 9–13.
[79] N. Miura, I. Horikawa, A. Nishimoto, H. Ohmura, H. Ito, S. Hirohashi, J.W. Shay, M. Oshimura, Progressive telomere shortening and telomerase reactivation during hepatocellular carcinogenesis, Cancer Genet. Cytogenet. 93 (1997) 56–62.
[80] J.E. Lee, B.K. Oh, J. Choi, Y.N. Park, Telomeric 3' overhangs in chronic HBV-related hepatitis and hepatocellular carcinoma, Int. J. Cancer 123 (2008) 264–272.
[81] B.K. Oh, Y.J. Kim, C. Park, Y.N. Park, Up-regulation of telomere-binding proteins, TRF1, TRF2, and TIN2 is related to telomere shortening during human multistep hepatocarcinogenesis, Am. J. Pathol. 166 (2005) 73–80.
[82] A. Satyanarayana, M.P. Manns, K.L. Rudolph, Telomeres and Telomerase: a Dual role in hepatocarcinogenesis, Hepatology 40 (2004) 276–283.
[83] A. Lechel, H. Holstege, Y. Begus, A. Schienke, K. Kamino, U. Lehmann, S. Kubicka, P. Schirmacher, J. Jonkers, K.L. Rudolph, Telomerase deletion limits progression of p53-mutant hepatocellular carcinoma with short telomeres in chronic liver disease, Gastroenterology 132 (2007) 1465–1475.
[84] W.C. Hahn, C.M. Counter, A.S. Lundberg, R.L. Beijersbergen, M.W. Brooks, R.A. Weinberg, Creation of human tumor cells with defined genetic elements, Nature 400 (1999) 464–468.
[85] J.W. Shay, I.B. Roninson, Hallmarks of senescence in carcinogenesis and cancer therapy, Oncogene 23 (2004) 2919–2933.
[86] M. Collado, J. Gil, A. Efeyan, C. Guerra, A.J. Schuhmacher, M. Barradas, A. Benguría, A. Zaballos, J.M. Flores, M. Barbacid, D. Beach, M. Serrano, Tumour biology: senescence in premalignant tumours, Nature 436 (2005) 642.
[87] M. Braig, S. Lee, C. Loddenkemper, C. Rudolph, A.H. Peters, B. Schlegelberger, H. Stein, B. Dörken, T. Jenuwein, C.A. Schmitt, Oncogene-induced senescence as an initial barrier in lymphoma development, Nature 436 (2005) 660–665.

[88] C. Michaloglou, L.C. Vredeveld, M.S. Soengas, C. Denoyelle, T. Kuilman, C.M. van der Horst, D.M. Majoor, J.W. Shay, W.J. Mooi, D.S. Peeper, BRAFE600-associated senescence-like cell cycle arrest of human naevi, Nature 436 (2005) 720–724.
[89] S.I. Suh, H.Y. Pyun, J.W. Cho, W.K. Baek, J.B. Park, T. Kwon, J.W. Park, M.H. Suh, D.A. Carson, 5-Aza-2'-deoxycytidine leads to down-regulation of aberrant p16 RNA transcripts and restores the functional retinoblastoma protein pathway in hepatocellular carcinoma cell lines, Cancer Lett. 160 (2000) 81–88.
[90] C.H. Wu, J. van Riggelen, A. Yetil, A.C. Fan, P. Bachireddy, D.W. Felsher, Cellular senescence is an important mechanism of tumor regression upon c-Myc inactivation, Proc. Natl. Acad. Sci. USA 104 (2007) 13028–13033.
[91] N. Ozturk, E. Erdal, M. Mumcuoglu, K.C. Akcali, O. Yalcin, S. Senturk, A. Arslan-Ergul, B. Gur, I. Yulug, R. Cetin-Atalay, C. Yakicier, T. Yagci, M. Tez, M. Ozturk, Reprogramming of replicative senescence in hepatocellular carcinoma-derived cells, Proc. Natl. Acad. Sci. USA 103 (2006) 2178–2183.

Molecular Cancer

BioMed Central

Research

Open Access

Canonical Wnt signaling is antagonized by noncanonical Wnt5a in hepatocellular carcinoma cells

Haluk Yuzugullu†[1,2], Khemais Benhaj†[1,3], Nuri Ozturk[1], Serif Senturk[1], Emine Celik[4], Asli Toylu[4], Nilgun Tasdemir[1], Mustafa Yilmaz[1], Esra Erdal[1,4], Kamil Can Akcali[1], Nese Atabey[4] and Mehmet Ozturk*[1,2]

Address: [1]Department of Molecular Biology and Genetics, Faculty of Science, Bilkent University, 06800, Ankara, Turkey, [2]Centre de Recherche INSERM-Université Joseph Fourrier U823, Institut Albert Bonniot, 38706 La Tronche Cedex, France, [3]Centre de Biotechnologie de Sfax, B.P "1177", 3038 Sfax, Tunisia and [4]Department of Medical Biology and Genetics, Dokuz Eylul University School of Medicine, Izmir, 35340 Turkey

Email: Haluk Yuzugullu - yuzugulh@ujf-grenoble.fr; Khemais Benhaj - bilhaj@alumni.bilkent.edu.tr; Nuri Ozturk - nuri_ozturk@med.unc.edu; Serif Senturk - serif@bilkent.edu.tr; Emine Celik - emine.celik@gmail.com; Asli Toylu - asli.toylu@deu.edu.tr; Nilgun Tasdemir - tasdemir@cshl.edu; Mustafa Yilmaz - myilmaz@ug.bilkent.edu.tr; Esra Erdal - esra.erdal@deu.edu.tr; Kamil Can Akcali - akcali@fen.bilkent.edu.tr; Nese Atabey - nese.atabey@deu.edu.tr; Mehmet Ozturk* - ozturkm@ujf-grenoble.fr

* Corresponding author †Equal contributors

Published: 22 October 2009

Molecular Cancer 2009, **8**:90 doi:10.1186/1476-4598-8-90

Received: 4 March 2009
Accepted: 22 October 2009

This article is available from: http://www.molecular-cancer.com/content/8/1/90

Abstract

Background: β-catenin mutations that constitutively activate the canonical Wnt signaling have been observed in a subset of hepatocellular carcinomas (HCCs). These mutations are associated with chromosomal stability, low histological grade, low tumor invasion and better patient survival. We hypothesized that canonical Wnt signaling is selectively activated in well-differentiated, but repressed in poorly differentiated HCCs. To this aim, we characterized differentiation status of HCC cell lines and compared their expression status of Wnt pathway genes, and explored their activity of canonical Wnt signaling.

Results: We classified human HCC cell lines into "well-differentiated" and "poorly differentiated" subtypes, based on the expression of hepatocyte lineage, epithelial and mesenchymal markers. Poorly differentiated cell lines lost epithelial and hepatocyte lineage markers, and overexpressed mesenchymal markers. Also, they were highly motile and invasive. We compared the expression of 45 Wnt pathway genes between two subtypes. TCF1 and TCF4 factors, and LRP5 and LRP6 co-receptors were ubiquitously expressed. Likewise, six Frizzled receptors, and canonical Wnt3 ligand were expressed in both subtypes. In contrast, canonical ligand Wnt8b and noncanonical ligands Wnt4, Wnt5a, Wnt5b and Wnt7b were expressed selectively in well- and poorly differentiated cell lines, respectively. Canonical Wnt signaling activity, as tested by a TCF reporter assay was detected in 80% of well-differentiated, contrary to 14% of poorly differentiated cell lines. TCF activity generated by ectopic mutant β-catenin was weak in poorly differentiated SNU449 cell line, suggesting a repressive mechanism. We tested Wnt5a as a candidate antagonist. It strongly inhibited canonical Wnt signaling that is activated by mutant β-catenin in HCC cell lines.

Conclusion: Differential expression of Wnt ligands in HCC cells is associated with selective activation of canonical Wnt signaling in well-differentiated, and its repression in poorly differentiated cell lines. One potential mechanism of repression involved Wnt5a, acting as an antagonist of canonical Wnt signaling. Our observations support the hypothesis that Wnt pathway is selectively activated or repressed depending on differentiation status of HCC cells. We propose that canonical and noncanonical Wnt pathways have complementary roles in HCC, where the canonical signaling contributes to tumor initiation, and noncanonical signaling to tumor progression.

Background

Hepatocellular carcinoma (HCC) is an epithelial cancer that originates from hepatocytes or their progenitors. It is the fifth most frequent neoplasm worldwide (>500,000 deaths/year), and its incidence is steadily increasing in the West [1]. Hepatocellular carcinoma is graded into four stages as well-differentiated, moderately differentiated, poorly differentiated and undifferentiated tumors, respectively. HCC arises as a very well differentiated cancer and proliferates with a stepwise process of dedifferentiation. Indeed, well-differentiated histology is exclusively seen in early stage and is rare in advanced HCC. Well-differentiated and moderately differentiated HCC cells are morphologically similar to hepatocytes, and are distinguished only by their smaller size and architectural organization as irregular trabecular or pseudoglandular patterns. In contrast, poorly differentiated and undifferentiated HCC cells are characterized with scanty cytoplasms and pleomorphism [2]. Like in other epithelial tumors, in HCC the progenitors evolve during tumor progression and become more and more autonomous. In this process, the tumor cells change their morphology and behavior; they loose cuboidal shape and polarity, and become more independent from neighboring tissues. Finally, they acquire the capacity to invade the underlying tissue and form distant metastases. These morphological changes are usually associated with progressive loss of biochemical and morphological features of hepatocytes, hence the process is qualified as "dedifferentiation" [3]. Portal venous invasion is significantly associated with poorly differentiated and undifferentiated HCCs and the tumor invasiveness is the most crucial factor in determining the long-term outcome for the patient [4].

Molecular changes involved in HCC dedifferentiation and invasiveness are known only partially. Epithelial markers such as hepatocyte nuclear factors and E-cadherin were reported to be down-regulated in HCC [3,5] and their loss is closely related to tumor invasion and metastasis [5]. In contrast, mesenchymal cell markers such as snail [6], twist [7] and vimentin [8] display positive correlation with HCC invasiveness and/or metastasis. These changes have been considered to represent the epithelial-mesenchymal transition (EMT) in HCC, based on in vitro studies [9-15]. Hepatocyte nuclear factor-4α (Hnf-4α) is essential for morphological and functional differentiation of hepatocytes [16,17], and its expression is downregulated during HCC progression in mice [18]. HCC dedifferentiation process is associated with a progressive accumulation of genomic changes including chromosomal gains and losses, as well as p53 mutations [19]. A rare exception to this picture is the status of the *CTNNB1* gene that encodes β-catenin, a key component of the Wnt/β-catenin (canonical Wnt) signaling pathway.

Independent studies showed that β-catenin mutations are associated with a subset of low grade (well-differentiated) HCCs with a favorable prognosis and chromosome stability [20-25]. Among 366 unifocal HCCs studied by Hsu et al. [20], β-catenin mutations were associated with grade I histogoly. Another study with similarly high number of tumors (n = 372) also indicated that mutant nuclear β-catenin correlated positively with non-invasive tumor and inversely with portal vein tumor thrombi [23]. In addition, β-catenin mutations were associated with significantly better 5-year patient survival in these large cohorts. Direct study of canonical Wnt signaling activity in primary tumors is not possible. However, this can be studied indirectly by using target genes [22]. Using glutamine synthetase (encoded by canonical Wnt signaling target *GLUL* gene) as a sensitive and specific marker, Audard et al. [22] showed that 36% HCCs displayed canonical Wnt activation. These tumors exhibited significant features associated with well-differentiated morphology. The association of β-catenin mutation and nuclear translocation with well-differentiated tumor grade was also reported during hepatocellular carcinogenesis, using several transgenic mouse models [26]. Activation of β-catenin was most frequent in liver tumors from c-myc and c-myc/TGF-β1 transgenic mice. However, it was very rare in faster growing and histologically more aggressive HCCs developed in c-myc/TGF-α mice. Taken together, these studies suggest that nuclear translocation of β-catenin and activation of canonical Wnt signaling are early events in liver carcinogenesis, mostly affecting well-differentiated HCCs.

Mutations of β-catenin gene initially identified in colorectal cancers, cause constitutive activation of canonical Wnt signaling, as a result of aberrant β-catenin protein accumulation. Inactivating mutations of APC gene in colorectal cancer and AXIN1 in HCC also activate canonical Wnt signaling by the same mechanism. Therefore, tumors displaying β-catenin, APC or AXIN1 mutation are considered to display active or constitutive canonical Wnt signaling [27] Activation of canonical Wnt signaling appears to be a common event for colorectal cancer, as opposed to HCC with mutations limited to a subset of these cancers. Interestingly, transgenic mice expressing oncogenic β-catenin in hepatocytes develop only hepatomegaly [28,29], in contrast to intestinal polyposis and microadenoma when expressed in intestinal cells [30].

Taken together, published data indicate that Wnt pathway and β-catenin mutations may play a complex role in HCC. Close association of β-catenin mutation with low tumor grade suggests that canonical Wnt signaling has a dual role in HCC cells, depending on their differentiation state. As an initial attempt to characterize differentiation-dependent functions of Wnt pathway and canonical Wnt signaling in HCC, we used a panel of HCC-derived cell lines. We

first performed gene expression and in vitro cell migration analyses to classify HCC cell lines into two distinct subtypes. The first subtype that we named here as "well-differentiated" was formed by epithelial cell lines with limited motility and invasiveness. Mesenchymal-like cell lines that have lost their epithelial-, hepatocyte-like features clustered into a second subtype named as "poorly differentiated". Next, we compared these two subtypes for the expression of 45 Wnt pathway genes, as well as for the activity of canonical Wnt signaling. Our findings provided evidence for the constitutive activation of canonical Wnt signaling in well-differentiated, but not in poorly differentiated cell lines. We also report the upregulation canonical Wnt3 ligand in the majority of HCC cell lines. Canonical Wnt8b was selectively expressed in well-differentiated cell lines. In contrast, noncanonical Wnt4, Wnt5a, Wnt5b and Wnt7b ligands were expressed selectively in poorly differentiated HCC cell lines. In addition, ectopic expression of noncanonical Wnt5a inhibited canonical Wnt signaling in two different cell lines. Our findings support the differential involvement of canonical and noncanonical Wnt signaling in HCC, depending on tumor cell differentiation state.

Results

Classification of hepatocellular carcinoma cell lines into "well-differentiated" and "poorly differentiated" subtypes

Fuchs et al. [12] have recently classified HCC cell lines into "epithelial" and "mesenchymal" types based on E-cadherin and vimentin expression. We performed a similar analysis using our cell line panel. Initially, we analyzed 15 cell lines (Figure 1). The expression of α-fetoprotein (AFP) was limited to six cell lines (Huh7, Hep40, HepG2, Hep3B, Hep3B-TR, PLC/PRF/5); the other cell lines being either not expressing (SNU182, SNU387, SNU398, SNU423, SNU449, SK-Hep1, Mahlavu, FOCUS) or weakly expressing (SNU475). All AFP-positive (AFP+) cell lines also expressed E-cadherin, whereas only 3/9 (33%) of AFP- cell lines expressed this epithelial marker. Mesenchymal cell markers including vimentin, slug, snail, twist-1 and twist-2 were also positive in most AFP- cell lines. These markers also displayed weakly positive expression in some AFP+ cell lines. For confirmation, we performed immunocytochemical analysis of vimentin protein expression in five AFP+ and five AFP- cell lines (Figure 2). We observed strong and homogenous immunostaining with all five AFP- cell lines. In contrast AFP+ cell lines were either negative or displayed heterogeneously positive immunoreactivity. These findings suggested that all AFP+ HCC cell lines were epithelial-like based on E-cadherin expression, but they also expressed some mesenchymal cell markers at variable degrees. In contrast, AFP- cell lines were usually negative for E-cadherin, and most of them were strongly positive for mesenchymal cell markers. The expression patterns of these mesenchymal markers showed marked heterogeneity. For example, SNU182 was positive for all five markers tested, whereas FOCUS was positive only for vimentin expression.

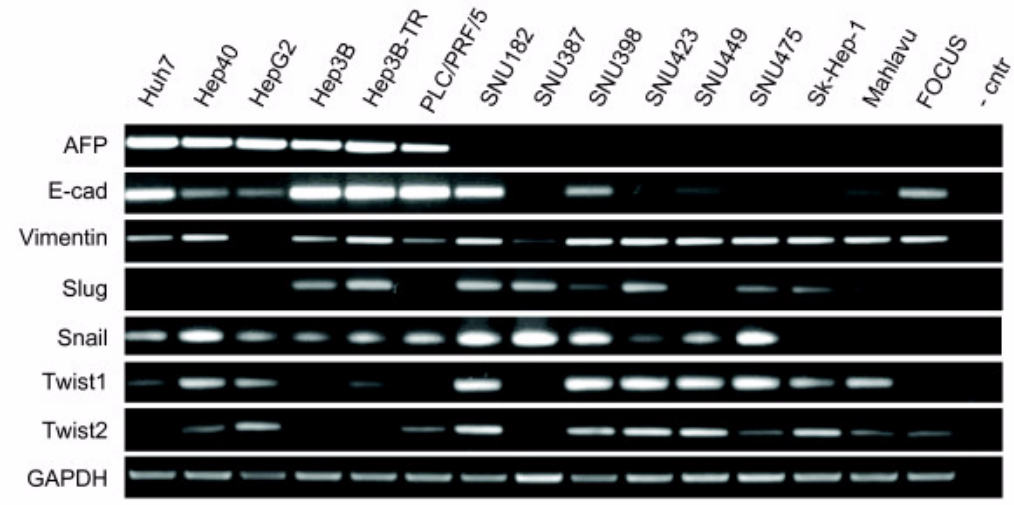

Figure 1

Expression analysis of a-fetoprotein (AFP), E-cadherin and five mesenchymal cell markers in HCC cell lines. Total RNAs were extracted from cell lines and used to detect gene expression by RT-PCR assay. GAPDH was used as a control for expression analyses shown here and in figures 4 to 7.

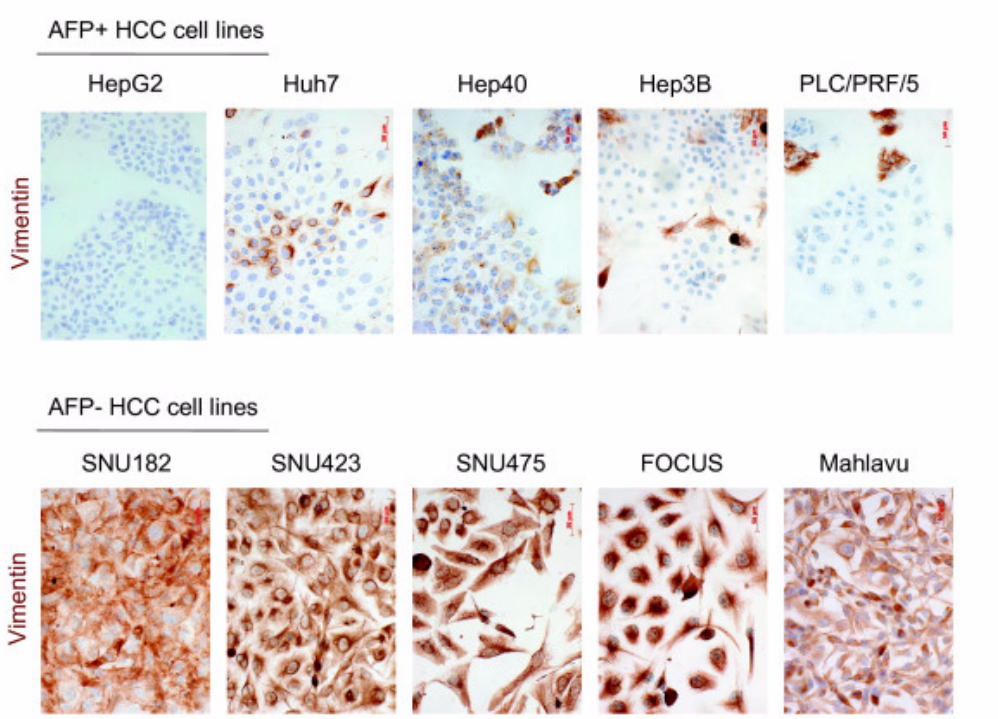

Figure 2
Immunocytochemical analysis of mesenchymal marker vimentin protein in AFP+ and AFP- HCC cell lines. Cells grown on coverslips were subjected to immunoperoxidase assay using anti-vimentin antibody (brown), and counter-stained with hematoxylin (blue).

We selected four AFP+, and seven AFP- cell lines for further analysis. HNF-4α and its downstream target HNF-1α are best known hepatocyte-associated epithelial cell markers [3]. These two genes that are involved in liver development and hepatocyte specification have previously been identified as specific markers for HCC cells with well-differentiated function and morphology [31]. The expression of these HNFs displayed perfect correlation with the expression of AFP (Figure 3a): four AFP+ cell lines (Huh7, Hep3B, HepG2, Hep40) were also highly positive for both HNF-4α and HNF-1α. In contrast, seven AFP- cell lines (SNU398, SNU475, SNU449, SNU387, FOCUS, Mahlavu, SNU182) did not express these factors. SNU449, another AFP- cell line displayed only weak HNF-4α expression. Epithelial cells including hepatocytes show low motility, in contrast to mesenchymal cells that display high motility and invasive behavior. To test whether epithelial and mesenchymal gene expression patterns of HCC cells correlated with their in vitro motility, we used wound-healing assay. After 24 hours of wounding, AFP- HCC cells (Mahlavu, SNU449, SNU475, SNU182) moved through the wound, whereas AFP+ HCC cells (Huh7, Hep3B, Hep G2, Hep40) cells did not (Figure 3b; Hep40 and SNU182 data not shown). A quantitative analysis of this data confirmed that poorly differentiated cell lines display higher motility (Figure 3c).

Based on expression analysis, together with in vitro motility and previously published invasiveness data, we classified our panel of HCC cell lines into two subtypes (Table 1). We qualified HepG2, Huh7, Hep3B and Hep40 as "well-differentiated" HCC cell lines, because they express AFP, E-cadherin, HNF-4α and HNF-1α, and they display low motility and/or low invasiveness. Most of these features are confined to "well-differentiated" HCC tumors ([2,18,32,33]. We qualified the remaining seven cell lines (SNU398, SNU475, SNU449, SNU387, FOCUS, Mahlavu, SNU182) as "poorly-differentiated" HCC cell lines, based on the lack of expression of both hepatocyte lineage and epithelial cell markers analyzed here. In addition, these poorly differentiated cell lines shared many features with mesenchymal cells including the expression of mesenchymal markers (vimentin, slug, snail, twist-1, and twist-2), high motility and invasiveness. These expression

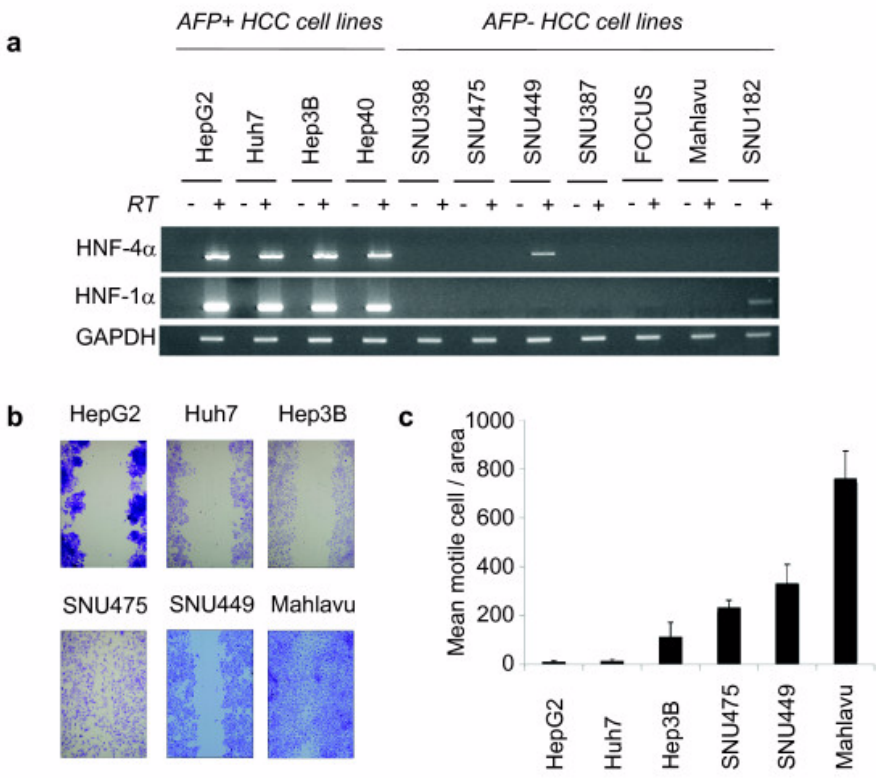

Figure 3

Expression of hepatocyte lineage markers HNF-4α and HNF-1α in HCC cell line correlate with low motility. (**a**)Selective expression of HNF-4α and HNF-1α in AFP+ HCC cell lines. Total RNAs were extracted from cells and used for RT-PCR analysis of HNF-4α and HNF-1α expression. GAPDH RT-PCR was used as a loading control. (**b. c**) Differential motility of AFP+ and AFP- HCC cell lines. Cells were cultured in six-well culture plates, and a single linear wound was made with a pipette tip in confluent monolayer cells. The distances between wound edges were measured at fixed points in each dish according to standardized template. After 24 hours migration, cell migration into the wound was visualized using phase contrast microscopy at ×20 magnification (**b**). The number of cells migrating beyond the wound edge was counted (**c**). Assays in six replicates, error bars; SD. SNU475 cells are larger cells giving rise to visual overestimation of migrating cell number in the picture shown in **b**.

and migratory features are associated with tumor dedifferentiation and confined to poorly differentiated HCCs [6-8,14,34].

Expression TCF/LEF family of transcription factors

Following the identification of well-differentiated and poorly differentiated HCC cell lines, we analyzed the expression of 45 Wnt pathway genes by RT-PCR assay. We first investigated the expression profile of TCF/LEF factors. The TCF-1 and TCF-4 were highly expressed in all HCC cell lines, while TCF-3 expression was limited to a subset of cell lines (Figure 4). LEF-1 transcript expression was weak, except for SNU398 cells. These findings indicated that at least two different nuclear factors mediating canonical Wnt signaling were expressed in any of HCC cell lines tested.

Expression of Frizzled receptors and LRP co-receptors

Next we analyzed the expression of 10 Frizzled receptors and their two co-receptors. Two canonical (Fzd1, Fzd5) and three noncanonical (Fzd3, Fzd4, Fzd6) Frizzled receptors were expressed in all cell lines tested. Also, Fzd2, Fzd7 and Fzd8 were expressed in most cell lines independent of their differentiation status (Figure 5-top). Lrp-5 and Lrp-6 co-receptors also were consistently expressed in all cell lines (Figure 5-bottom). These findings indicated that HCC cell lines were equipped with the expression of several canonical and noncanonial Wnt signaling receptors,

Table 1: Well-differentiated and poorly differentiated HCC cell lines according to hepatocyte lineage, epithelial and mesenchymal markers, and in vitro motility and invasiveness assays

Cell Lines	Fetal Hepatocyte Marker	Epithelial & Hepatocyte Markers			Mesenchymal markers					Motility	Invasiveness
	AFP	**HNF4a**	**HNF1a**	**E-cadherin**	**vimentin**	**slug**	**Snail**	**Twist-1**	**Twist-2**		
Well-differentiated											
HepG2	High	High	High	Low	(-)	Low	Low	Low	High	Low	Low [14]
Huh7	High	High	High	High	Low	(±)	Low	Low	(-)	Low	Low [14]
Hep3B	High	High	High	High	Low	High	Low	(-)	(-)	Low	Low ([74]
Hep40	High	High	High	Low	High	(-)	High	High	Low	Low	n.t.
Poorly differentiated											
SNU398	(-)	(-)	(-)	Low	High	Low	High	High	High	Low	n.t.
SNU475	(±)	(-)	(-)	(-)	High	High	High	High	Low	High	n.t.
SNU449	(-)	Low	(-)	(±)	High	Low	Low	High	High	High	n.t.
SNU387	(-)	(-)	(-)	(-)	Low	High	High	(-)	(±)	n.t.	n.t.
FOCUS	(-)	(-)	(-)	Low	High	Low	(-)	(-)	Low	n.t.	n.t.
Mahlavu	(-)	(-)	(-)	(±)	High	Low	(-)	High	Low	High	High [74]
SNU182	(-)	(-)	(±)	High	high	High	High	High	High	High	n.t.

(-); not detected; ±; traces; n.t.; not tested.

so that each HCC cell line was likely to respond to both canonical and noncanonical Wnt signals.

Differential expression of canonical and noncanonical Wnt ligands

In humans, there are 19 known genes encoding canonical and noncanonical Wnt ligands [35]. We studied the expression profile of the complete list of human Wnt ligands (Figures 6 and 7). From the group of eight known canonical Wnt ligands, only Wnt3 was strongly and uniformly expressed in all cell lines tested. Wnt10b was also strongly expressed, but not in all cell lines (Figure 6). We observed selective expression of canonical Wnt8b in well differentiated cell lins. In contrast, among seven noncanonical Wnt ligands, Wnt4, Wnt5a, Wnt5b and Wnt7b were expressed in almost all poorly differentiated cell lines tested. This contrasted with their poor expression in well differentiated cell lines (Figure 7-top). Signaling specificity of four other Wnt ligands have not yet been clearly established [35]. Among these ligands, Wnt9a expression was detectable in nearly all cell lines tested. In contrast, Wnt9b and Wnt2b expressions were associated to well differentiated and poorly differentiated cell lines, respectively (Figure 7-bottom).

Our comprehensive analysis of Wnt signaling molecules in HCC cell lines revealed several features. First, with the exception of Wnt ligands, most of the major components of Wnt signaling pathway were expressed redundantly in HCC cell lines, independent of their differentiation status. In contrast, Wnt ligand expression displayed two types of selectivity. First, out of eight known canonical only Wnt3 and Wnt10b displayed strong expression in most cell lines, independent of differentiation status. Second, out of seven noncanonical Wnt ligands, four were expressed in HCC cell lines with a high selectivity for poorly differentiated ones. Well-diffferentiated cell lines displayed selective expression of Wnt8b. These findings may have several

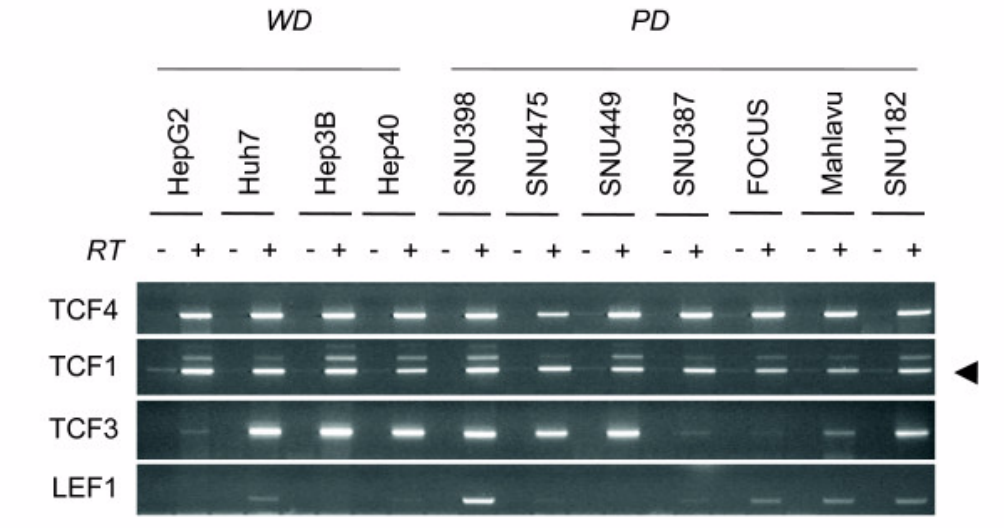

Figure 4
Comparative analysis of TCF/LEF transcription factors in hepatocellular carcinoma cell lines. Total RNAs were extracted from cell lines and used to detect gene expression by RT-PCR assay of four members of TCF/LEF family. See Figure 1 for GAPDH loading control.

implications. Most, in not all HCC cell lines were equipped with an autocrine/paracrine canonical Wnt signaling system, as reported previously for breast and ovarian cancer cell lines [36]. In contrast, because of selective expression of noncanonical Wnt ligands, only poorly differentiated cell lines could serve from an autrocrine noncanonical Wnt signaling system. In addition, poorly differentiated HCC cells could also provide noncanonical Wnt signals to other cells by a paracrine mechanism. Finally, noncanonical Wnt ligands such as Wnt5a might inhibit canonical Wnt signaling in HCC cells, as previously reported in other cell types [37-39].

Autocrine canonical Wnt signaling in well differentiated hepatocellular carcinoma cell lines

Canonical Wnt signaling activates TCF/LEF-dependent transcription, which can be monitored by reporters containing TCF/LEF-responsive elements [27,40]. We surveyed canonical Wnt signaling in HCC cell lines using TCF/LEF reporter pGL3-OT plasmid, as described previously [41]. First, we compared TCF/LEF (TCF) activity in three cell lines with known mutations in canonical Wnt signaling pathway (Figure 8a). Well-differentiated HepG2 cell line displays β-catenin mutation. Poorly-differentiated SNU398 and SNU475 cell lines display β-catenin and AXIN1 mutations, respectively [42,43]. Normalized TCF activity was the highest in HepG2 cells. Compared to HepG2, SNU398 cells displayed 50% less activity. More interestingly, despite a homozygous deletion leading to a loss of Axin1 expression (data not shown; [42,43], there was no detectable TCF activity in SNU475 cells. This contrasted sharply with another well-differentiated AXIN1 mutant HCC cell line, namely PLC/PRF/5 (Alexander) that displayed high TCF activity [42] (additional data not shown).

Next, we compared TCF activity of eight other cell lines that displayed wild-type β-catenin and AXIN1 status [41-43]. Hep40 cells that harbor a missense AXIN1 mutation/polymorphism (R454H) was included in this group, since functional significance of this mutation is unknown [41]. We detected weak, but significant (3-4 fold) TCF activity in well-differentiated Huh7 and Hep3B cell lines. On the other hand, all five poorly differentiated cell lines, as well as well-differentiated Hep40 cells displayed no detectable activity under our experimental conditions (Figure 8b).

Taken together, we collected TCF activity data from 12 HCC cell lines. Independent of β-catenin or AXIN1 status, TCF activity was detected in four out of five (80%) well-differentiated cell lines, whereas only one out of seven (14%) poorly differentiated cell lines had constitutive TCF activity [$P < 0.046$ (one-tailed), 0.071(two-tailed); Fisher Exact Probability Test]. This data supports the hypothesis that well-differentiated HCC cells display an autocrine/paracrine canonical Wnt signaling, probably because they co-express Wnt3 and several canonical Frizzled receptors. However, the great majority of poorly differentiated cell lines failed to generate canonical Wnt signaling activity, although they similarly co-expressed Wnt3 and canonical Frizzled receptors.

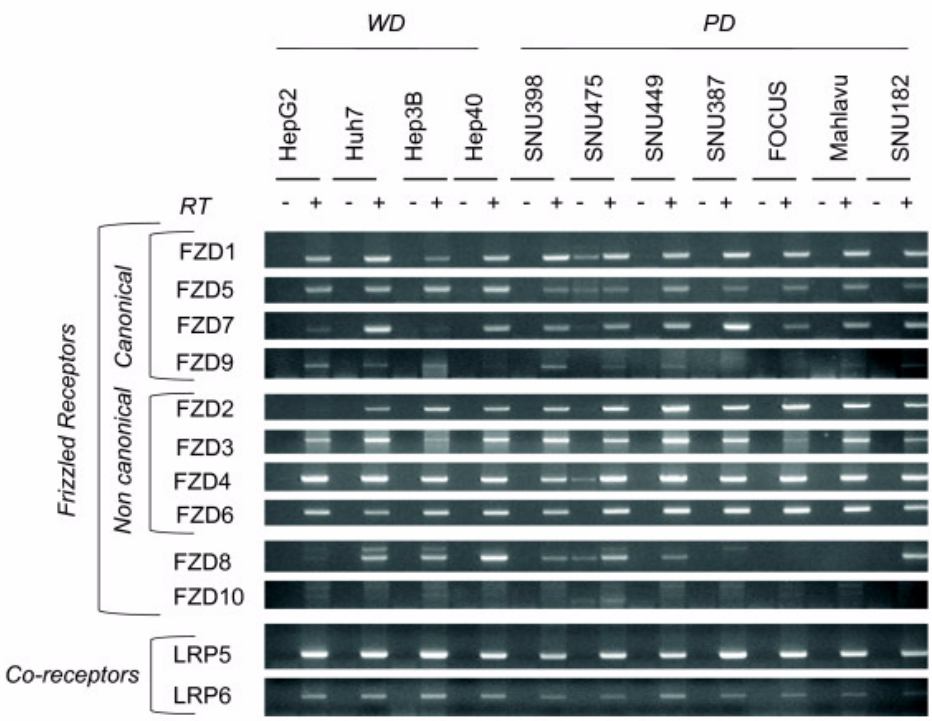

Figure 5

Comparative analysis of Frizzled receptors and LRP co-receptors in hepatocellular carcinoma cell lines. Frizzled receptors involved in canonical and noncanonical Wnt signaling were tested for expression by RT-PCR assay (Top). The expression of LRP co-receptors was analyzed similarly (bottom). Total RNAs were extracted from cell lines and used to detect gene expression by RT-PCR assay. See Figure 1 for GAPDH loading control.

Canonical Wnt signaling is repressed in poorly differentiated hepatocellular carcinoma cells

The lack of canonical Wnt activity in poorly differentiated cells could be due to either lack of sufficient Wnt ligand activity. Alternatively, canonical Wnt signaling could be repressed in these cell lines. A number of proteins downstream to β-catenin such as Axin2, HTLE family, hAES, Chibby, CTBP and ICAT are known to display inhibitory activity on canonical Wnt signaling [44]. We compared the expression of genes encoding these inhibitory proteins, but found no correlation with TCF activity or differentiation state (Figure 9).

Next, we compared TCF activity in Huh7, SNU449 and SNU182 cell lines following transient expression of a mutant (S33Y)-β-catenin (Figure 10). Transfection with S33Y-β-catenin resulted in an increase in total β-catenin protein in Huh7 and SNU449. This increase was less evident in SNU182 cells (Figure 10a). Well-differentiated Huh7 cells responded to S33Y-β-catenin expression by a strong activation of TCF/LEF reporter (130 folds). Under the same experimental conditions, the response of SNU449 cells was minimal (5 folds). More importantly, SNU182 cells were totally unresponsive (Figure 10b). These important differences between well-differentiated Huh7 and two different poorly differentiated cell lines (SNU449 and SNU182) are apparently not due to differences in transient transfection efficiencies, since the measured activities have been corrected for such differences (see material and methods section).

In order to confirm the data on weakened response in poorly differentiated cell lines, we generated a clone from SNU449 cells (SNU449-cl8) with Tet repressor controlled expression of N-terminally truncated β-catenin (aa 98-781). N-terminally truncated β-catenin forms are frequently detected in cancer cells including HCC cells. They lack Ser/Thr phosphorylation sites (aa Ser23, Ser29, Ser33, Ser37, Thr41, Ser45) that are critically involved in its ubiquitin-mediated degradation, and they accumulate in the cell nucleus leading to oncogenic activation canonical Wnt signaling [27]. As shown in figure 11a, SNU449-cl8 cells expressed only wild-type β-catenin in the presence of tetracycline (Tet-on conditions), while expressing both wild-type and truncated β-catenin at comparable levels in Tet-off conditions. The induced expression of truncated β-catenin resulted in only a weak activation (3-4 fold) of TCF reporter activity, similar to data obtained by

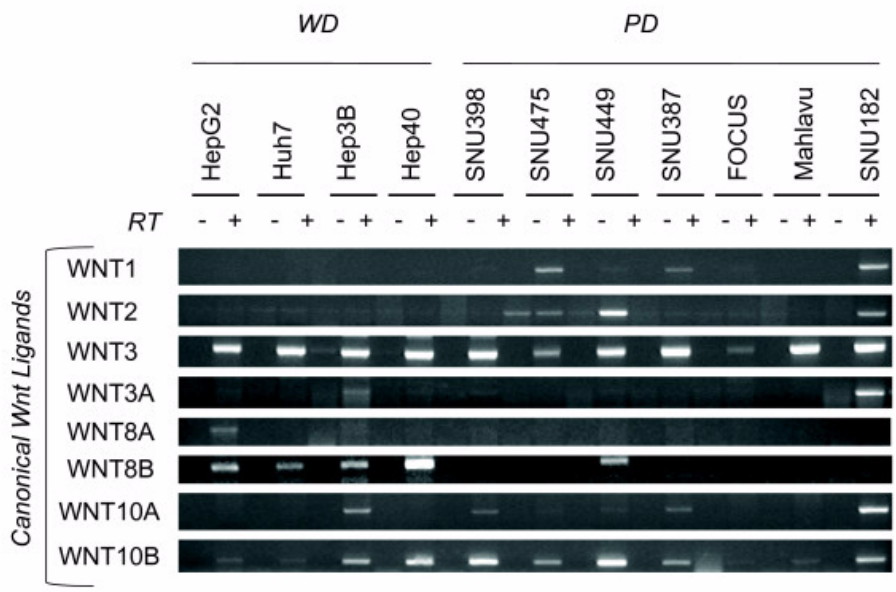

Figure 6
Comparative analysis of canonical Wnt ligands in hepatocellular carcinoma cell lines. Canonical Wnt ligands were tested for expression by RT-PCR assay. Total RNAs were extracted from cell lines and used to detect gene expression by RT-PCR assay. See Figure 1 for GAPDH loading control.

transient transfection experiments (Figure 11b). This low level of activation was similar to that seen in well-differentiated HCC cells in the absence of β-catenin or Axin-1 mutation (Fig. 8b), and strongly suggests that canonical Wnt signaling is actively repressed in this poorly differentiated HCC cell line. For comparison, well-differentiated HepG2 cells expressing wild-type and a similar N-terminally truncated β-catenin (Δ25-140 aa) activated TCF reporter gene by more than 60-fold (Figure 8a). In other words, although both Tet-off SNU449-cl8 and HepG2 cells displayed a heterozygous truncating β-catenin mutation, TCF activation was 15-fold less in poorly differentiated SNU449 background. To test whether this repression was related to cellular localization of β-catenin, we performed immunofluorescence detection using confocal microscopy (Figure 11c). Wild-type β-catenin was localized at the cell membrane with weak nuclear localization. The induction of truncated β-catenin in Tet-off SNU449-cl8 cells did not change this distribution significantly. We observed only weak cytoplasmic accumulation, with slight increases in both membrane and nuclear localization. In sharp contrast with these observations, in colorectal cancer cells (APC-mutated), used as a positive control [45], we detected strong nuclear accumulation of β-catenin by the same technique.

WNT5A inhibits canonical Wnt signaling in HCC cells

Presently, the mechanism of repression of canonical Wnt signaling in poorly differentiated HCC cells is unknown, but it is associated with a lack of nuclear accumulation of β-catenin. Among noncanonical Wnt ligands, Wnt5a is best known for its antagonistic effect on canonical Wnt signaling [46]. Therefore, we tested the effect of ectopic Wnt5a expression on mutant-β-catenin-induced TCF activity in Huh7 cell line. In the absence of Wnt5a, TCF activity was induced more than 160-fold by mutant β-catenin in this cell line. Co-expression of Wnt5a resulted in three-fold repression of TCF activity (Figure 12a). To confirm our observations, we also tested the effects of Wnt5a on TCF activity induced by endogenous mutant β-catenin using HepG2 cell line. The expression of Wnt5a in this cell line caused a significant inhibition of TCF activation mediated by endogenous β-catenin ($P < 0.05$; Figure 12b). We concluded that Wnt5a that is selectively expressed in poorly differentiated HCC cell lines, and probably similarly acting noncanonical Wnt ligands are involved, at least partly, in the repression of canonical Wnt signaling in these cells.

Discussion

Since the initial description of β-catenin mutations in HCCs in 1998 [33], Wnt signaling became a center of interest for these tumors. A large set of Wnt ligands and a large array of receptors are implicated in different cell processes by initiating canonical, but also noncanonical Wnt signals [35]. The antagonism between canonical and noncanonical Wnt pathways has also been reported [37,38,46]. Thus, both β-catenin and Wnt signaling are

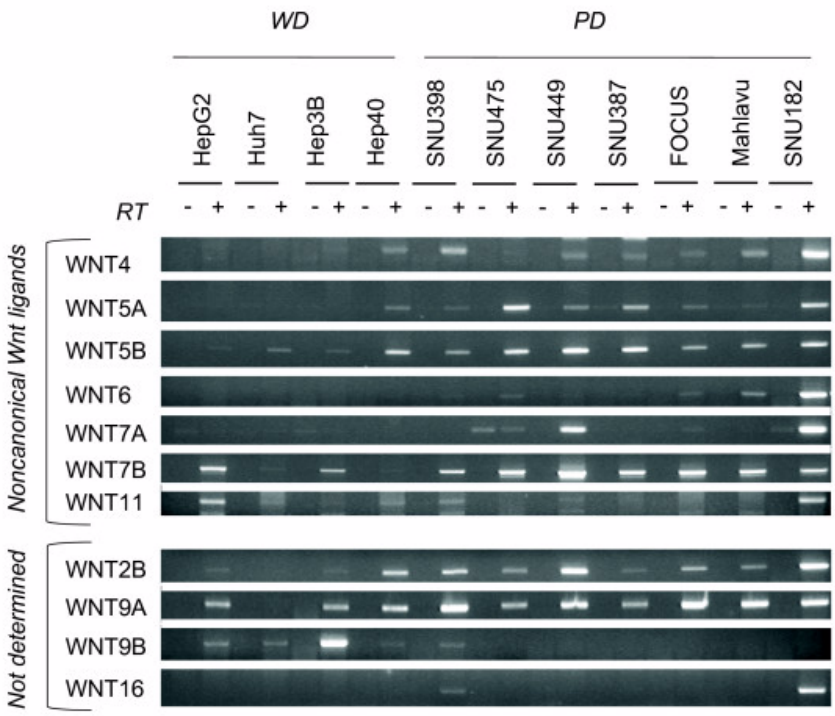

Figure 7
Comparative analysis of noncanonical (top) and unclassified (bottom) Wnt ligands in hepatocellular carcinoma cell lines. Noncanonical and unclassified Wnt ligands were tested for expression by RT-PCR assay. Total RNAs were extracted from cell lines and used to detect gene expression by RT-PCR assay. See Figure 1 for GAPDH loading control.

involved in highly complex cellular events of which only some are mediated by canonical Wnt pathway. This complexity is also observed during liver development and as well as in adult liver homeostatic events. Canonical Wnt signaling contributes to liver growth and regeneration, but also to liver "zonation" by controlling some liver-specific metabolic programs. ([47]). In addition, it contributes to the activation of liver stem or progenitor cells, as well as HCC-initiating cells [48-51].

Mutational activation of canonical Wnt signaling is not a frequent event in HCC, in contrast to hepatoblastoma displaying very high rates [52]. Mutations of β-catenin were restricted to a group of HCCs associated with low p53 mutation rate, negative HBV status and chromosomal stability, as stated earlier. These mutations were also associated with lower histological grade and better patient survival. Unexpectedly, β-catenin mutations are rare in more advanced and poorly differentiated HCCs [20,23]. Therefore, although considered to play an active role in HCC malignancy, the activation of canonical Wnt signaling may not be necessary for, or even repressed in advanced HCCs. Thus, β-catenin mutation and constitutive activation of canonical Wnt signaling may be differentiation-dependent events with mechanistic implications in HCC initiation and progression. We attempted to address this issue by using HCC-derived cell lines.

We first classified 11 HCC cell lines into "well-differentiated" and "poorly differentiated" subtypes using hepatocyte lineage, epithelial and mesenchymal cell markers, and in vitro migration assays. Well-differentiated HCC cell lines shared many features with hepatocytes such as expression of HNF-1α, HNF-4α, and E-cadherin, and epithelial morphology. Poorly differentiated cell lines were usually deficient in the expression of hepatocyte lineage and epithelial markers, but they expressed different mesenchymal markers strongly. These two types of HCC cell lines were also distinguished from each other by their in vitro behaviors. Poorly differentiated cell lines were usually more motile and more invasive than well-differentiated cell lines (Table 1). A global expression profiling study classified HCC cell lines in Group I and Group II [51]. Our well-differentiated and poorly differentiated cell line subtypes showed perfect correlation with Group I and Group II, respectively. Well-differentiated Group I was characterized by the activation of oncofetal promoters leading to increased expression of AFP and IGF-II, whereas poorly differentiated Group II was characterized by overexpression of genes involved in metastasis and

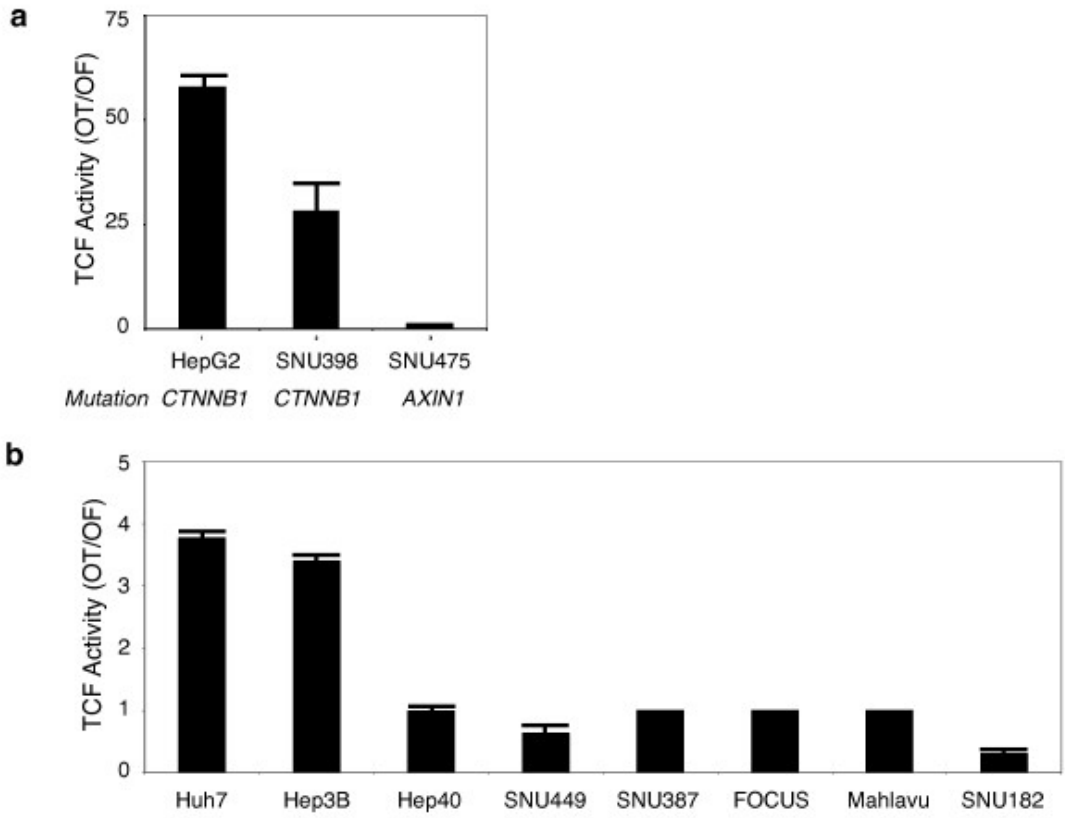

Figure 8

Frequent constitutive activation of canonical Wnt signaling in well-differentiated, but not in poorly differentiated hepatocellular carcinoma cell lines. (**a**) Comparative analysis of the canonical Wnt signaling in hepatoma cell lines with known mutations of β-catenin or Axin-1 genes. TCF reporter assay shows that well-differentiated HepG2 cells display high signaling activity. In contrast, canonical Wnt signaling is attenuated in poorly differentiated SNU398, and undetectable in poorly differentiated SNU475 cell line. Assays in triplicate, error bars; SD. (**b**) Comparative analysis of the canonical Wnt signaling in HCC cell lines with wild-type β-catenin and Axin-1 genes. Huh7 and Hep3B cell lines (both well-differentiated) display weak but significantly increased TCF reporter activity. Other cell lines (all poorly differentiated, except Hep40) display no detectable TCF reporter activity. TCF activity denotes the ratio of signals detected with pGL3-OT (OT) and pGL3-OF (OF) plasmids, respectively. Assays in triplicate, error bars; S. D. Cells were transfected with the reporter gene pGL3-OT (OT) harboring LEF-1/TCF binding sites for β-catenin and the corresponding pGL3-OF (OF) without these sites.

invasion. Our well-differentiated and poorly differentiated subtypes were also in perfect correlation with respectively epithelial and mesenchymal HCC cell line types that have been identified very recently [12]. Mesenchymal cancer cells are considered as the products of EMT that is believed to be a key mechanism for the acquisition of invasive and metastatic capabilities by tumor cells [53]. Higher motility of poorly differentiated HCC cell lines reported here is in line with this concept. Thus, our two classes of cell lines share many similarities with well-differentiated and poorly differentiated HCC tumors. We used this model to compare the status of Wnt pathway according to HCC differentiation status.

A comprehensive analysis of Wnt signaling components in liver or hepatocytes is lacking. However, the expression of Wnt ligands and Frizzled receptors in mouse hepatocytes has been published [54]. Mouse hepatocytes expressed canonical receptors Fzd7 and Fzd9, as well as noncanonical Fzd2, Fzd3, Fzd4 and Fzd6. We observed highly similar pattern of expression in HCC cell lines with the exception of Fzd9 that showed weak expression. In addition, we detected increased expression of canonical Fzd1 and Fzd5 in most HCC cell lines. The expression frequency of these receptors was not associated with HCC cell differentiation status. Mouse hepatocytes expressed canonical Wnt1 and Wnt2, and noncanonical Wnt4, Wnt5a, Wnt5b and Wnt11. All or most HCC cell lines

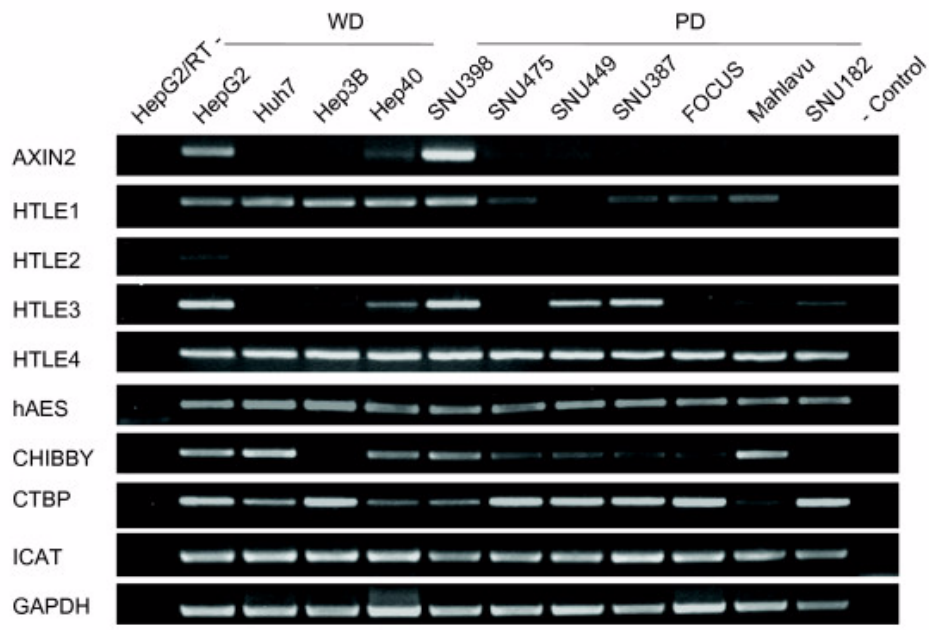

Figure 9
Expression analysis of genes inhibiting canonical Wnt signaling downstream to β-catenin in HCC cells. Total RNAs were extracted from cell lines and used to detect gene expression by RT-PCR assay. GAPDH RT-PCR was used as a loading control.

have lost the expression of canonical Wnt1 and Wnt2, but they displayed increased expression of canonical Wnt3 and Wnt10b ligands. Another canonical ligand, Wnt8b was expressed selectively in well-differentiated cell lines. In contrast, noncanonical Wnt4, Wnt5a and Wnt5b ligands were expressed in the majority of poorly differentiated cell lines, but not in most of well-differentiated cell lines. In addition, most HCC cell lines (poorly differentiated cell lines in particular) also displayed increased expression of noncanonical Wnt7b. Among Wnt ligands and Frizzled receptors that we found to be expressed or upregulated in HCC cell lines, Wnt3, Wnt4, Wnt5a, Fzd3, Fzd6 and Fzd7 have been previously reported to be overexpressed also in primary HCC tumors [55-57]. Overexpression of Wnt10b was also reported in HCC cels [58]. Increased levels of Wnt5a transcripts were detected in chronic hepatitis, cirrhosis and HCC [59]. A C-terminally mutated HBV X protein was shown to upregulate Wnt5a expression in HCC cells [60]. Thus, Wnt5a upregulation observed in clinical samples might be related to HBV at least in HBV-related liver diseases. Based on our observations that associate noncanonical Wnt ligand expression to poorly differentiated HCC cell lines, it will be interesting to test the predictive value of noncanonical Wnt expression for HCC prognosis.

Another important finding of this study is the differential activity of canonical Wnt signaling in different HCC subtypes. Well-differentiated cell lines displayed active canonical Wnt signaling at variable degrees. In addition to strong signaling activity associated to β-catenin and Axin1 mutations in two well differentiated cell lines, we also observed autocrine canonical Wnt signaling in two other well differentiated cell lines, as reported for some other cancer cell lines [36]. The functional significance of autocrine canonical Wnt signaling in these cell lines is not known.

However, small molecule antagonists of Tcf4/beta-catenin complex were shown to inhibit TCF reporter activity and down-regulate the endogenous Tcf4/β-catenin target genes c-Myc, cyclin D1, and survivin in Huh7 cells [61]. This observation strongly suggests that the autocrine canonical Wnt signaling is functional in well-differentiated HCC cell lines. Canonical Wnt signaling has been linked to both stem cell and cancer cell self-renewal in other cancer types. It was proposed that some adult cancers derive from stem/progenitor cells and that canonical Wnt signaling in stem and progenitor cells can be subverted in cancer cells to allow malignant proliferation [62]. Indeed, well-differentiated-HCC cell lines identified

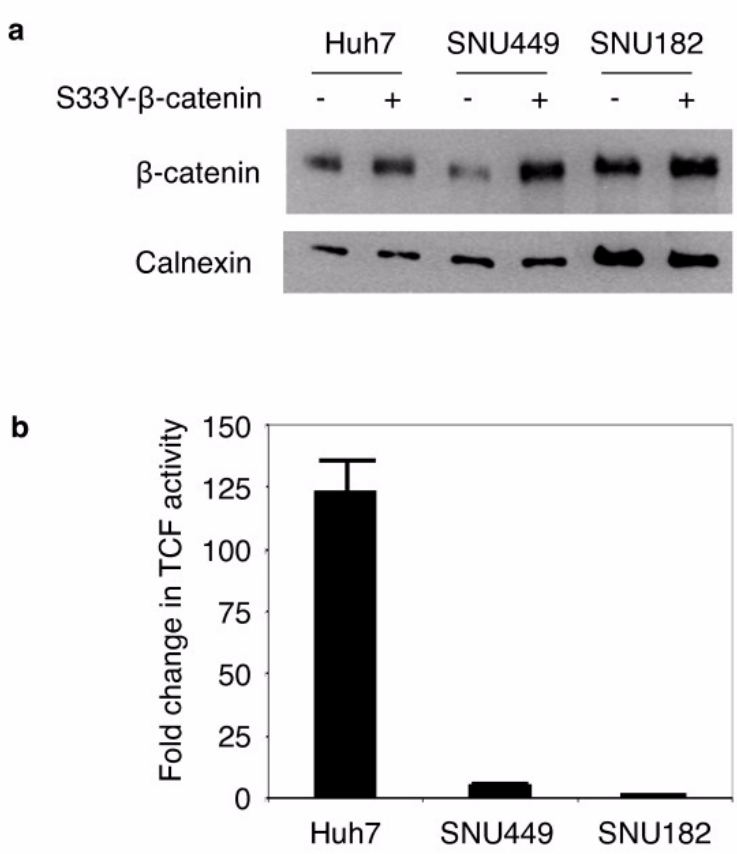

Figure 10

Ectopic expression of mutant β-catenin induces high canonical Wnt activity in well-differentiated, but not in poorly differentiated hepatocellular carcinoma cells. (**a**) Well-differentiated Huh7, and poorly differentiated SNU449 and SNU182 cell lines have been co-transfected with either pCI-neo-mutant β-catenin (S33Y) plasmid (S33Y-β-catenin +) or empty pCI-neo plasmid (S33Y-β-catenin -), and cellular β-catenin levels at post-transfection 48 h were tested by immunoblotting. Calnexin was used as a loading control. (**b**) Cell lines were treated as described, then pCI-neo-mutant β-catenin (S33Y)-transfected cells were subjected to TCF reporter assay. TCF activity denotes the ratio of signals detected with pGL3-OT (OT) and pGL3-OF (OF) plasmids, respectively. Assays in triplicate, error bars; SD. Co-transfections included pGL-OT or pGL-OF, in addition to pCI-neo plasmids in both (a) and (b).

here such as HepG2, Huh7 and PLC/PRF/5 have been reported to harbor HCC stem cells [63]

Our third noteworthy observation was the lack of detectable canonical Wnt signaling activity in six out of seven poorly differentiated cell lines. Even a poorly differentiated cell line with a deleterious Axin1 mutation (SNU475) lacked detectable signaling activity. Thus, most probably, the canonical Wnt signaling was not only inactive, but also repressed in poorly differentiated HCC cell lines. In confirmation of this expectation, transient or Tet-regulated expression of mutant β-catenin failed to generate significant canonical Wnt signaling activity in two different poorly differentiated cell lines. Furthermore, we linked this weak activity to poor nuclear accumulation of β-catenin protein in SNU449.cl8 cell line. Thus, unlike well-differentiated cell lines, poorly differentiated HCC cells displayed strong resistance to canonical Wnt signal activation.

The mechanisms of resistance to canonical Wnt signal activation in poorly differentiated HCC cells are presently unknown. We provide here one potential mechanism. Wnt5a has been previously implicated in canonical Wnt signaling as an antagonist and regulator of β-catenin levels in other cell types [48,49]. Using both ectopic and endogenous mutant β-catenin expression systems in two different cell lines, we demonstrated that co-transfections with Wnt5a-expressing plasmid can significantly inhibit canonical Wnt signaling in HCC cells. The mechanism of Wnt5a antagonism on canonical Wnt signaling in HCC cells is not known. In breast cancer cells, the loss of Wnt5a

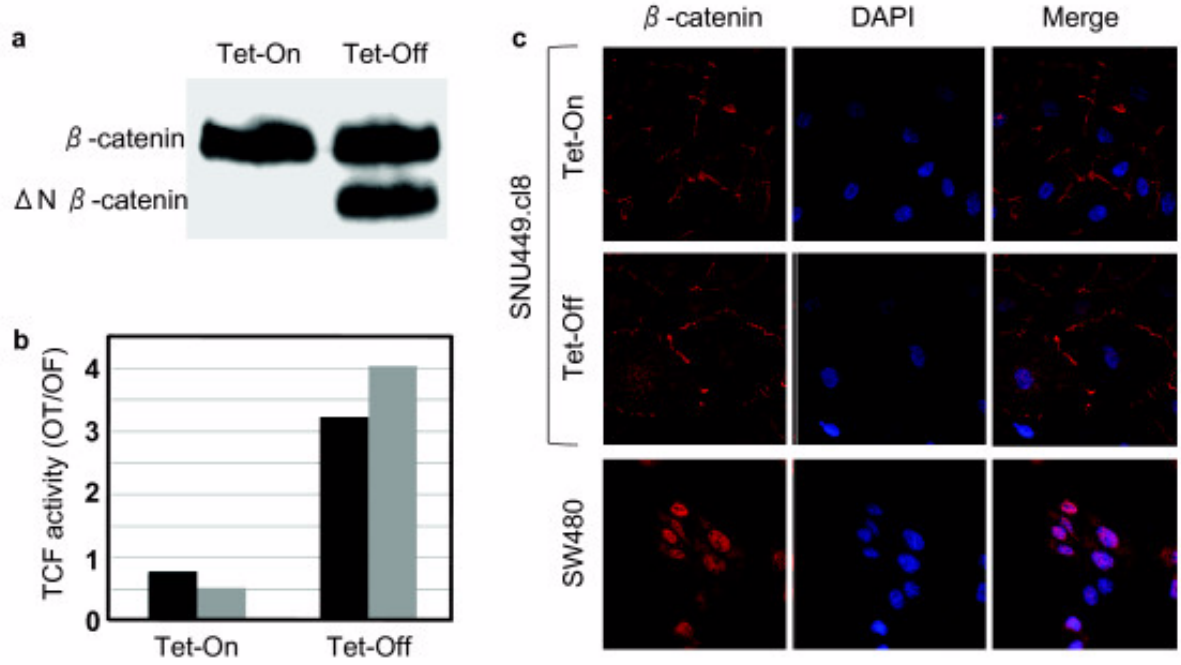

Figure 11
Minimal TCF reporter activity and lack of nuclear accumulation of mutant β-catenin in poorly differentiated SNU449.cl8 cells. SNU449 cells were stably transfected with Tet-responsive ΔN-β-catenin expression vector to obtain SNU448.cl8 cells. (**a**) Induced expression of N-terminally truncated ΔN-β-catenin protein in the Tet-Off conditions, as tested by western blot assay. Total cell lysates were extracted from cells and subjected to western blot assay using anti-β-catenin antibody. (**b**) TCF activity is only weakly induced in Tet-off conditions, as tested by duplicate experiments. (**c**) SNU449.cl8 cells at Tet-On state express wild-type endogenous β-catenin protein principally located at cell membrane. Under Tet-Off conditions the staining pattern remains almost identical despite ΔN-β-catenin expression. Note lack of nuclear accumulation. SW480 cells used as positive control display strong nuclear β-catenin staining. Cells were grown on coverslips, subjected to indirect immunofluorescence assay using anti-β-catenin antibody (red), counterstained with DAPI (blue) and examined by confocal microscopy.

signaling resulted in stabilization of nuclear beta-catenin and expression of Wnt/beta-catenin target genes [64]. However, both ectopically and endogenously expressed mutant β-catenins used in our experiments were N-terminally truncated devoid of their Ser/Thr phosphorylation motifs. Thus, Wnt5a appears to inhibit canonical Wnt signaling in HCC cells, downstream to β-catenin, independent of its glycogen synthase 3-β- and bTrCO-dependent degradation. Wnt5a has been shown to inhibit canonical Wnt signaling either by bTrCP-independent proteasomal degradation [65], or, by downregulating β-catenin-induced reporter gene expression without influencing β-catenin levels [37] in kidney epithelial cells. Wnt5a may use similar mechanisms in Huh7 and HepG2 cells. Further studies with downregulation of noncanonical Wnt ligands in poorly differentiated HCC cell lines may help to better define the implications of such ligands in liver cancer biology.

The role of Wnt5a in cancer is complex. It may play tumor-promoting or tumor-suppressing functions depending on cellular context. Wnt5a has been described as a tumor promoter in melanoma, gastric, pancreas, prostate cancer, but as a tumor suppressor in HCC, neuroblastoma, leukemia, colon, and thyroid cancers [46]. The inability of Wnt5a to transform cells or signal through the canonical β-catenin pathway pointed that it cannot promote tumorigenesis by upregulation of canonical Wnt signaling, unlike canonical Wnt ligands [66]. Our results suggest that Wnt5a, upregulated in poorly differentiated highly motile mesenchymal-like HCC cells may play a role in tumor progression by inducing EMT. Upregulation of Wnt5a expression during EMT has been reported [67]. Furthermore, the Wnt5A/Protein kinase C pathway was shown to mediate motility in melanoma cells via of an EMT [68]. Similarly, CUTL1-upregulated Wnt5a significantly enhanced migration, proliferation and invasiveness

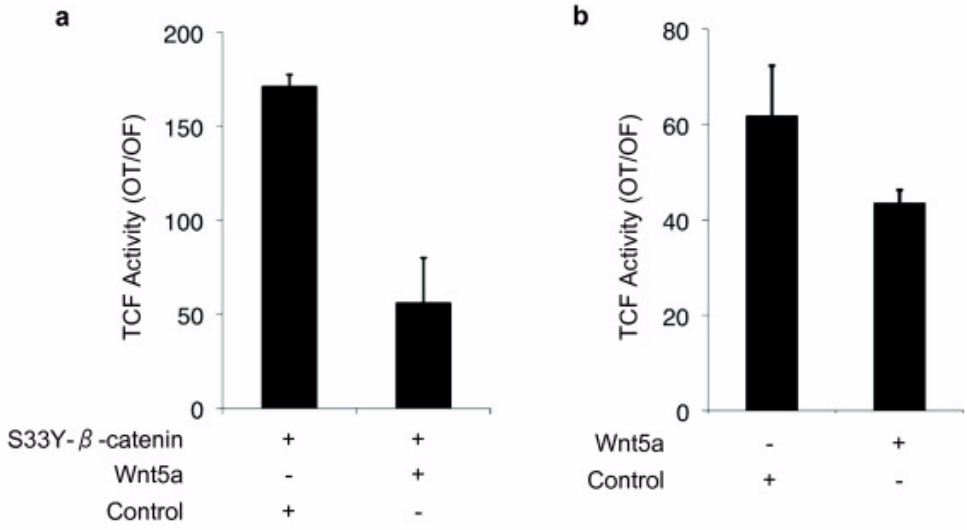

Figure 12

Wnt5a inhibits canonical Wnt signaling activity in Huh7 and HepG2 cells. (**a**) Huh7 cells were co-transfected with either pCI-neo-mutant β-catenin (S33Y) plasmid (S33Y-β-catenin +) along with pShuttle-IRES-WNT5a or empty pShuttle-IRES vector. 48 hours post transfection; cells were subjected to TCF reporter assay. TCF activity denotes the ratio of signals detected with pGL3-OT (OT) and pGL3-OF (OF) plasmids, respectively. Assays in triplicate, error bars; SD. Co-transfections included pGL-OT or pGL-OF, in addition to pCI-neo-S33Y-β-catenin and pIRES plasmids. (**b**) HepG2 experiments were performed under similar conditions, except that pCI-neo-mutant β-catenin (S33Y) plasmid was omitted.

in pancreas cancer cellls [69]. These effects were accompanied by a marked modulation of marker genes associated with EMT. Wnt5a may promote EMT in HCC cells by a similar mechanism.

The expression status of Wnt5a in HCC is not well known. To our knowledge, only one report addressed this issue [59]. Compared to normal tissue, Wnt5a mRNA expression was strongly induced in HCC, as well as in chronic hepatitis and cirrhosis. However, immunostaining of Wnt5a protein showed a bell-shaped pattern: low to undetectable levels were present in normal tissue and in tumor samples, whereas strong immunostaining was seen in chronic hepatitis, cirrhosis and dysplastic liver cells. The reasons of the discrepancy between transcript and protein expression in HCC tissues are not known presently. However, it appears that peritumoral liver tissues express high levels of Wnt5a protein that could trigger noncanonical Wnt signaling in adjacent tumor cells. It will be important to further investigate the role of Wnt5a in HCC tumor progression.

Taken together, our studies demonstrate that canonical Wnt activity is active in well-differentiated, but repressed in poorly differentiated HCC cell lines. This correlates with in vivo tumor studies indicating that β-catenin mutations are prevelant in well-differentiated, but not in poorly differentiated tumors. In addition, we showed that poorly differentiated cell lines express noncanonical Wnt ligands such as Wnt5a acting as an antagonist of canonical Wnt signaling. Thus, it appears that HCC cells may activate or repress their canonical Wnt signaling, using autocrine/paracrine systems based on selective use of canonical and noncanonical Wnt ligands.

We hypothesize that the active canonical Wnt signaling observed in well-differentiated HCC cells contributes to tumor initiation, but not necessarily to tumor progression. Instead, noncanonical Wnt signaling may be used by poorly differentiated HCC tumors to promote cell motility and invasion. Selective use of canonical and noncanonical Wnt signaling at different stages may be a key mechanism involved in hepatocellular carcinogenesis. Recent studies showed that canonical Wnt signaling contributes to the self-renewal and expansion of HCC-initiating cells with stem/progenitor cell features [50,70]. However, the lack of HCC development in β-catenin transgenic mice strongly suggests that canonical Wnt signaling activation has limited tumorigenic potential in liver tissue. Indeed, recent studies showed that canonical Wnt signaling plays a major role in the specification of mature hepatocytes for perivenous-specific gene expression ([71,72]. Such a hepatocyte differentiation function of canonical Wnt signaling may not be compatible with cellular dedifferentiation that goes along with HCC development. Therefore, alternative pathways such as Wnt5a-

mediated noncanonical Wnt signaling may be necessary for sustained growth and progression of HCC tumors. Melanoma may serve as a demonstrated model to our hypothesis. Similar to HCC, canonical Wnt signaling activation is an early event and nuclear β-catenin accumulation is associated with better patient survival in melanoma. Nuclear β-catenin is lost in more aggressive melanomas that express Wnt5a that promotes EMT, cell motility and metastasis[46]. Chien et al. [73] have recently demonstrated that canonical Wnt signaling induces growth inhibition and differentiation in melanoma cells, whereas Wnt5a can antagonize some of these effects. These findings clearly establish a dual function of Wnt signaling in melanoma. In light of these recent developments, our findings call for further investigations on respective roles of canonical and noncanonical Wnt signaling in HCC.

Conclusion

Our observations support the hypothesis that Wnt pathway is selectively activated or repressed depending on differentiation status of HCC cells. We propose that canonical and noncanonical Wnt pathways have complementary roles in HCC, where the canonical signaling contributes to tumor initiation, and noncanonical signaling to tumor progression.

Methods

Cell lines

Hepatocellular carcinoma cell lines Huh7, Hep40, Hep3B, Hep3B-TR, FOCUS, Mahlavu, SNU182, SNU 387, SNU 398, SNU423, SNU 449, SNU 475, PLC/PRF/5, SK-Hep-1, hepatoblastoma cell line HepG2 and colorectal cancer cell line SW480 were cultivated as described previously [41].

Reverse transcription-polymerase chain reaction (RT-PCR) analysis

Total RNAs were extracted from cultured cells using NucleoSpin RNA II Kit (MN Macherey-Nagel, Duren, Germany) according to the manufacturer's protocol. The cDNAs were prepared from total RNA (2 μg) using RevertAid First Strand cDNA Synthesis Kit (MBI-Fermentas, Vilnius, Lithuania). A negative control without reverse transcriptase (1 μl ddH2O instead) was also prepared for each sample. All PCR reactions were carried out using 1 μl cDNA from the reverse transcription mix, for 35 cycles except GAPDH, which was amplified for 24 cycles. Negative controls without reverse transcriptase were included for each set of primers (primer sequence information is available upon request). PCR products were analyzed on a 2% (w/v) agarose gel.

Wound-healing assay

Cells were cultured in six-well culture plates in RPMI 1640 or DMEM with 10% FBS. A single linear wound was made with a p200 pipette tip in confluent monolayer cells. The distances between wound edges were measured at fixed points in each dish according to standardized template. Debris were removed by washing the cells twice with PBS and then cells were incubated in RPMI 1640 or DMEM with 2% FBS. After 24 hours migration, cells were fixed with methanol and stained with 0.2% crystal violet. Cell migration into the wound was visualized using phase contrast microscopy (x20 magnification). The number of cells migrating beyond the wound edge was quantified microscopically in the randomly selected fields for each triplicate well.

Immunocytochemistry

Cells were grown on coverslips, fixed in 4% formaldehyde, permeated with 0.5% saponin/0.1% Triton X-100, and stained with mouse monoclonal anti-human vimentin antibody (Dako) using Envision kit (Dako), developed with diaminobenzidine, and counterstained with hematoxylin.

Confocal microscopy

Cells were grown on slides in 6 well plates and were fixed in 3.5% paraformaldehyde (PFA) for 15 minutes, and permealized using 0,25% Triton-X-100 for 10 min. Non specific protein binding was blocked by 30 minutes of incubation with 5% bovine serum albumin (BSA) in phosphate-buffered saline (PBS) at room temperature. Cells were then incubated 2 hours with monoclonal anti-β-catenin antibody M5.2 (1:200 dilution) in 1% BSA in PBS at room temperature in a moist chamber. Immunofluorescence staining was obtained by incubating for 1 hour with Alexa Fluor® 594 F(ab')2 fragment of rabbit anti-mouse IgG (H+L) (Invitrogen) (dilution 1:750). Cells were counterstained with DAPI (dilution 1:750), slides were mounted using ProLong® Gold antifade reagent (Invitrogen) and examined under Zeiss LSM 510 Meta laser scanning confocal microscope (MPI Freibourg, Germany) using 488 nm and 543 nm laser excitation lines, and photographed.

Plasmids

The pShuttle-IRES-Wnt5a expression plasmid was constructed by subcloning of an EcoRI-cut Wnt5a cDNA fragment from plasmid pGEMTz-Wnt5a vector (a gift from R. Kemler) into BglII site of the pShuttle-IRES-hrGFP-1 vector (Stratagene, USA). pCI-Neo-mutant β-catenin (S33Y) expression plasmid, and pGL3-OT and pGL3-OF reporter plasmids were kindly provided by B. Vogelstein. Other plasmids were pCI-Neo (Promega) and pEGFP-N2 (Clontech, Palo Alto, CA). The pAUCT-ΔN-β-catenin plasmid expressing N-terminally truncated β-catenin (aa 98-781)

under the control of Tet repressor was constructed using pAUCT-CCW vector (gift from Ali Fattaey, USA). A cDNA fragment of XhoI-NotI digestion from pCI-Neo-mutant β-catenin (S33Y) plasmid was inserted into XhoI-NotI site of pAUCT-CCW vector.

Transfections

Endogenous TCF/LEF-dependent transcriptional activity was tested by using pGL3-OT and pGL3-OF reporter plasmids, as described previously [41], except that cells were transfected using Lipofectamin 2000 reagent (Invitrogen), following instructions provide by the supplier. Mutant β-catenin-induced TCF/LEF-dependent transcriptional activity was tested after co-transfection of cells with pCI-Neo-mutant β-catenin (S33Y) expression plasmid (1.75 μg/well) together with the reporter plasmids. pCI-Neo (1.75 μg/well) was used as negative control. The effect of Wnt5a expression on TCF/LEF-dependent transcriptional activity was tested using Huh7 and HepG2 cell lines. Huh7 cell line was co-transfected with pCI-Neo-mutant β-catenin (S33Y) expression plasmid (1 μg/well) together with either pShuttle-IRES-Wnt5a (0.75 μg/well) or the empty vector pShuttle-IRES-hrGFP-1 (0.75 μg/well) and pGL3-OT/pGL3-OF reporter plasmids (0.75 μg/well for each). At 48 h following transfection, luciferase assay was performed by using Luciferase Reporter Gene Assay, constant light signal kit (Roche Diagnostics GmbH., Mannheim, Germany). Luciferase activity was read with The Reporter® Microplate Luminometer (Turner BioSystems Inc., Sunnyvale, CA) and data was normalized according to transfection efficiency obtained with each transfection, as described previously [41]. HepG2 cell line was co-transfected with either pShuttle-IRES-Wnt5a (0.5 μg/well) or the empty vector pShuttle-IRES-hrGFP-1 (0.5 μg/well) and pGL3-OT/pGL3-OF reporter plasmids (0.5 μg/well for each), with an internal control (0.05 μg/well pRL-TK Renilla luciferase vector) in a 12-well plate, using Lipofectamine 2000 Transfection Reagent. Forty-eight hours post-transfection, the cells were washed with PBS, and lysed in passive lysis buffer (Dual Luciferase kit; Promega). The cell lysates were transferred into an Opti-Plate 96-well plate (Perkin-Elmer) and assayed in a 1420-Multilabel counter luminometer, VICTOR3 (Perkin-Elmer) using the Dual-Luciferase kit (Promega). Relative TOP-FLASH luciferase units were measured and normalized against Renilla luciferase activity and further normalized luciferase activity against FOP-FLASH activity. All transfection experiments were performed in triplicate and data were expressed as mean of triplicate values (±S. D.) and p values were calculated. TCF/LEF activity was reported as the ratio of normalized luciferase activities obtained with pGL-OT and pGL-OF plasmids, respectively (mean ± S. D.).

Generation of mutant β-catenin expressing SNU449-cl8 cell line

SNU449 cell line clone ectopically expressing N-terminally truncated (aa 98-781) β-catenin, under the control of Tet repressor was generated by stable transfection with pAUCT-ΔN-β-catenin plasmid. Briefly, SNU449 cells were plated onto 6-well plate and transfected with 2 μg of plasmid DNA using Lipofectamin 2000 reagent (Invitrogen). 24 hours post transfection, cells were transferred to 90 mm dishes and subjected to G418 (0.6 μg/ml) selection in the presence of tetracycline (1 μg/ml) until resistant cell colonies became visible. Several clones were tested by Western blot for the expression of N-terminally truncated (aa 98-781) β-catenin after withdrawing tetracycline from the culture medium to induce the expression of the transgene. Only one clone (SNU449-cl8) displayed Tet-dependent expression of mutant β-catenin, and it was used for further studies.

Western blotting

Detergent-soluble cell lysates were prepared at 48 h post-transfection and used for western blot analysis, as described previously [41]. Antibodies to β-catenin (Santa Cruz Biotechnology, Inc., CA) and calnexin (Sigma) were obtained commercially. ECL kit (Amersham Life Science, Inc., Piscataway, NJ) was used for detection of antigen-antibody complexes. Equal protein loading was verified by Western blot assay with calnexin antibody.

Statistical analysis

The statistical significance of the active TCF reporter activity between well-differentiated and poorly differentiated HCC cell lines was tested by Fisher Exact Probability Test using an on-line tool http://faculty.vassar.edu/lowry/VassarStats.html.

List of abbreviations

AFP: α-fetoprotein; EMT: epithelial to mesenchymal transition; FZD: Frizzled; HCC: hepatocellular carcinoma; HBV: hepatitis B virus; HNF: hepatocyte nuclear factor; PD: poorly differentiated; RT-PCR: reverse transcriptase-polymerase chain reaction; WD: well differentiated

Competing interests

The authors declare that they have no competing interests.

Authors' contributions

HY, KB, SS and EE carried our RT-PCR analyses. HY carried out confocal microscopy and western blot analyses. SS and MY carried out the immunocytochemistry. HY, HB, NO and NT carried out TCF reporter activity assays. KB constructed SNU440.cl8 cell line. EC, AT and NA carried out wound-healing and cell migration assays. KCA contributed to the design of the study. M.O. conceived of, designed and coordinated the study. MO., HY and KB

drafted the manuscript. All authors read and approved the final manuscript.

Authors' information

Nuri Ozturk - present address: Department of Biochemistry and Biophysics, University of North Carolina School of Medicine, Chapel Hill, North Carolina 27599. USA.

Nilgun Tasdemir - present address: Cold Spring Harbor Laboratory, One Bungtown Road, Cold Spring Harbor, NY 11724, USA.

Acknowledgements

This work was supported by a grant from TUBITAK. Additional support was provided by Terry Fox Fund of the Turkish Association for Research and Fight against Cancer, Turkish Academy of Sciences (Turkey), and Institut National de Cancer (France). H.Y. has performed confocal microscopy studies at MPI (Ralf Kemler's Lab, Freibourg, Germany), and was supported by an EMBO Short-term Fellowship. We thank B. Vogelstein for providing pCI-Neo-mutant β-catenin (S33Y), pGL3-OT and pGL3-OF plasmids, and A. Fattaey for the gift of pAUCT-CCW plasmid. We also thank R. Kemler for guidance in confocal microscopy analyses and for providing pGEMTz-Wnt5a plasmid and anti-β-catenin M5.2 antibody.

References

1. Bruix J, Boix L, Sala M, Llovet JM: **Focus on hepatocellular carcinoma.** *Cancer Cell* 2004, **5:**215-219.
2. Kojiro M: **Histopathology of liver cancers.** *Best Pract Res Clin Gastroenterol* 2005, **19:**39-62.
3. Abelev GI, Lazarevich NL: **Control of differentiation in progression of epithelial tumors.** *Adv Cancer Res* 2006, **95:**61-113.
4. Hsu HC, Wu TT, Wu MZ, Sheu JC, Lee CS, Chen DS: **Tumor invasiveness and prognosis in resected hepatocellular carcinoma. Clinical and pathogenetic implications.** *Cancer* 1988, **61:**2095-2099.
5. Osada T, Sakamoto M, Ino Y, Iwamatsu A, Matsuno Y, Muto T, Hirohashi S: **E-cadherin is involved in the intrahepatic metastasis of hepatocellular carcinoma.** *Hepatology* 1996, **24:**1460-1467.
6. Sugimachi K, Tanaka S, Kameyama T, Taguchi K, Aishima S, Shimada M, Tsuneyoshi M: **Transcriptional repressor snail and progression of human hepatocellular carcinoma.** *Clin Cancer Res* 2003, **9:**2657-2664.
7. Lee TK, Poon RT, Yuen AP, Ling MT, Kwok WK, Wang XH, Wong YC, Guan XY, Man K, Chau KL, Fan ST: **Twist overexpression correlates with hepatocellular carcinoma metastasis through induction of epithelial-mesenchymal transition.** *Clin Cancer Res* 2006, **12:**5369-5376.
8. Hu L, Lau SH, Tzang CH, Wen JM, Wang W, Xie D, Huang M, Wang Y, Wu MC, Huang JF, *et al.*: **Association of Vimentin overexpression and hepatocellular carcinoma metastasis.** *Oncogene* 2004, **23:**298-302.
9. Cicchini C, Filippini D, Coen S, Marchetti A, Cavallari C, Laudadio I, Spagnoli FM, Alonzi T, Tripodi M: **Snail controls differentiation of hepatocytes by repressing HNF4alpha expression.** *J Cell Physiol* 2006, **209:**230-238.
10. Giannelli G, Bergamini C, Fransvea E, Sgarra C, Antonaci S: **Laminin-5 with transforming growth factor-beta1 induces epithelial to mesenchymal transition in hepatocellular carcinoma.** *Gastroenterology* 2005, **129:**1375-1383.
11. Lee HC, Tian B, Sedivy JM, Wands JR, Kim M: **Loss of Raf kinase inhibitor protein promotes cell proliferation and migration of human hepatoma cells.** *Gastroenterology* 2006, **131:**1208-1217.
12. Fuchs BC, Fujii T, Dorfman JD, Goodwin JM, Zhu AX, Lanuti M, Tanabe KK: **Epithelial-to-mesenchymal transition and integrin-linked kinase mediate sensitivity to epidermal growth factor receptor inhibition in human hepatoma cells.** *Cancer Res* 2008, **68:**2391-2399.
13. Lahsnig C, Mikula M, Petz M, Zulehner G, Schneller D, van Zijl F, Huber H, Csiszar A, Beug H, Mikulits W: **ILEI requires oncogenic Ras for the epithelial to mesenchymal transition of hepatocytes and liver carcinoma progression.** *Oncogene* 2009, **28:**638-650.
14. Matsuo N, Shiraha H, Fujikawa T, Takaoka N, Ueda N, Tanaka S, Nishina S, Nakanishi Y, Uemura M, Takaki A, *et al.*: **Twist expression promotes migration and invasion in hepatocellular carcinoma.** *BMC Cancer* 2009, **9:**240.
15. Miyoshi A, Kitajima Y, Sumi K, Sato K, Hagiwara A, Koga Y, Miyazaki K: **Snail and SIP1 increase cancer invasion by upregulating MMP family in hepatocellular carcinoma cells.** *Br J Cancer* 2004, **90:**1265-1273.
16. Parviz F, Matullo C, Garrison WD, Savatski L, Adamson JW, Ning G, Kaestner KH, Rossi JM, Zaret KS, Duncan SA: **Hepatocyte nuclear factor 4alpha controls the development of a hepatic epithelium and liver morphogenesis.** *Nat Genet* 2003, **34:**292-296.
17. Battle MA, Konopka G, Parviz F, Gaggl AL, Yang C, Sladek FM, Duncan SA: **Hepatocyte nuclear factor 4alpha orchestrates expression of cell adhesion proteins during the epithelial transformation of the developing liver.** *Proc Natl Acad Sci USA* 2006, **103:**8419-8424.
18. Lazarevich NL, Cheremnova OA, Varga EV, Ovchinnikov DA, Kudrjavtseva EI, Morozova OV, Fleishman DI, Engelhardt NV, Duncan SA: **Progression of HCC in mice is associated with a downregulation in the expression of hepatocyte nuclear factors.** *Hepatology* 2004, **39:**1038-1047.
19. Thorgeirsson SS, Grisham JW: **Molecular pathogenesis of human hepatocellular carcinoma.** *Nat Genet* 2002, **31:**339-346.
20. Hsu HC, Jeng YM, Mao TL, Chu JS, Lai PL, Peng SY: **Beta-catenin mutations are associated with a subset of low-stage hepatocellular carcinoma negative for hepatitis B virus and with favorable prognosis.** *Am J Pathol* 2000, **157:**763-770.
21. Taniguchi K, Roberts LR, Aderca IN, Dong X, Qian C, Murphy LM, Nagorney DM, Burgart LJ, Roche PC, Smith DI, *et al.*: **Mutational spectrum of beta-catenin, AXIN1, and AXIN2 in hepatocellular carcinomas and hepatoblastomas.** *Oncogene* 2002, **21:**4863-4871.
22. Audard V, Grimber G, Elie C, Radenen B, Audebourg A, Letourneur F, Soubrane O, Vacher-Lavenu MC, Perret C, Cavard C, Terris B: **Cholestasis is a marker for hepatocellular carcinomas displaying beta-catenin mutations.** *J Pathol* 2007, **212:**345-352.
23. Mao TL, Chu JS, Jeng YM, Lai PL, Hsu HC: **Expression of mutant nuclear beta-catenin correlates with non-invasive hepatocellular carcinoma, absence of portal vein spread, and good prognosis.** *J Pathol* 2001, **193:**95-101.
24. Wong CM, Fan ST, Ng IO: **beta-Catenin mutation and overexpression in hepatocellular carcinoma: clinicopathologic and prognostic significance.** *Cancer* 2001, **92:**136-145.
25. Laurent-Puig P, Zucman-Rossi J: **Genetics of hepatocellular tumors.** *Oncogene* 2006, **25:**3778-3786.
26. Calvisi DF, Factor VM, Loi R, Thorgeirsson SS: **Activation of beta-catenin during hepatocarcinogenesis in transgenic mouse models: relationship to phenotype and tumor grade.** *Cancer Res* 2001, **61:**2085-2091.
27. Barker N, Clevers H: **Mining the Wnt pathway for cancer therapeutics.** *Nat Rev Drug Discov* 2006, **5:**997-1014.
28. Cadoret A, Ovejero C, Terris B, Souil E, Levy L, Lamers WH, Kitajewski J, Kahn A, Perret C: **New targets of beta-catenin signaling in the liver are involved in the glutamine metabolism.** *Oncogene* 2002, **21:**8293-8301.
29. Harada N, Miyoshi H, Murai N, Oshima H, Tamai Y, Oshima M, Taketo MM: **Lack of tumorigenesis in the mouse liver after adenovirus-mediated expression of a dominant stable mutant of beta-catenin.** *Cancer Res* 2002, **62:**1971-1977.
30. Harada N, Tamai Y, Ishikawa T, Sauer B, Takaku K, Oshima M, Taketo MM: **Intestinal polyposis in mice with a dominant stable mutation of the beta-catenin gene.** *EMBO J* 1999, **18:**5931-5942.
31. Ishiyama T, Kano J, Minami Y, Iijima T, Morishita Y, Noguchi M: **Expression of HNFs and C/EBP alpha is correlated with immunocytochemical differentiation of cell lines derived from human hepatocellular carcinomas, hepatoblastomas and immortalized hepatocytes.** *Cancer Sci* 2003, **94:**757-763.
32. Du GS, Wang JM, Lu JX, Li Q, Ma CQ, Du JT, Zou SQ: **Expression of P-aPKC-iota, E-cadherin, and beta-catenin related to invasion and metastasis in hepatocellular carcinoma.** *Ann Surg Oncol* 2009, **16:**1578-1586.

33. Wang W, Hayashi Y, Ninomiya T, Ohta K, Nakabayashi H, Tamaoki T, Itoh H: **Expression of HNF-1 alpha and HNF-1 beta in various histological differentiations of hepatocellular carcinoma.** *J Pathol* 1998, **184:**272-278.
34. Niu RF, Zhang L, Xi GM, Wei XY, Yang Y, Shi YR, Hao XS: **Up-regulation of Twist induces angiogenesis and correlates with metastasis in hepatocellular carcinoma.** *J Exp Clin Cancer Res* 2007, **26:**385-394.
35. Staal FJ, Luis TC, Tiemessen MM: **WNT signalling in the immune system: WNT is spreading its wings.** *Nat Rev Immunol* 2008, **8:**581-593.
36. Bafico A, Liu G, Goldin L, Harris V, Aaronson SA: **An autocrine mechanism for constitutive Wnt pathway activation in human cancer cells.** *Cancer Cell* 2004, **6:**497-506.
37. Mikels AJ, Nusse R: **Purified Wnt5a protein activates or inhibits beta-catenin-TCF signaling depending on receptor context.** *PLoS Biol* 2006, **4:**e115.
38. Nemeth MJ, Topol L, Anderson SM, Yang Y, Bodine DM: **Wnt5a inhibits canonical Wnt signaling in hematopoietic stem cells and enhances repopulation.** *Proc Natl Acad Sci USA* 2007, **104:**15436-15441.
39. Ishitani T, Kishida S, Hyodo-Miura J, Ueno N, Yasuda J, Waterman M, Shibuya H, Moon RT, Ninomiya-Tsuji J, Matsumoto K: **The TAK1-NLK mitogen-activated protein kinase cascade functions in the Wnt-5a/Ca(2+) pathway to antagonize Wnt/beta-catenin signaling.** *Mol Cell Biol* 2003, **23:**131-139.
40. Morin PJ, Sparks AB, Korinek V, Barker N, Clevers H, Vogelstein B, Kinzler KW: **Activation of beta-catenin-Tcf signaling in colon cancer by mutations in beta-catenin or APC.** *Science* 1997, **275:**1787-1790.
41. Erdal E, Ozturk N, Cagatay T, Eksioglu-Demiralp E, Ozturk M: **Lithium-mediated downregulation of PKB/Akt and cyclin E with growth inhibition in hepatocellular carcinoma cells.** *Int J Cancer* 2005, **115:**903-910.
42. Satoh S, Daigo Y, Furukawa Y, Kato T, Miwa N, Nishiwaki T, Kawasoe T, Ishiguro H, Fujita M, Tokino T, *et al.*: **AXIN1 mutations in hepatocellular carcinomas, and growth suppression in cancer cells by virus-mediated transfer of AXIN1.** *Nat Genet* 2000, **24:**245-250.
43. Cagatay T, Ozturk M: **P53 mutation as a source of aberrant beta-catenin accumulation in cancer cells.** *Oncogene* 2002, **21:**7971-7980.
44. Brantjes H, Roose J, Wetering M van De, Clevers H: **All Tcf HMG box transcription factors interact with Groucho-related co-repressors.** *Nucleic Acids Res* 2001, **29:**1410-1419.
45. Munemitsu S, Albert I, Souza B, Rubinfeld B, Polakis P: **Regulation of intracellular beta-catenin levels by the adenomatous polyposis coli (APC) tumor-suppressor protein.** *Proc Natl Acad Sci USA* 1995, **92:**3046-3050.
46. McDonald SL, Silver A: **The opposing roles of Wnt-5a in cancer.** *Br J Cancer* 2009, **101:**209-214.
47. Nejak-Bowen K, Monga SP: **Wnt/beta-catenin signaling in hepatic organogenesis.** *Organogenesis* 2008, **4:**92-99.
48. Hu M, Kurobe M, Jeong YJ, Fuerer C, Ghole S, Nusse R, Sylvester KG: **Wnt/beta-catenin signaling in murine hepatic transit amplifying progenitor cells.** *Gastroenterology* 2007, **133:**1579-1591.
49. Apte U, Thompson MD, Cui S, Liu B, Cieply B, Monga SP: **Wnt/beta-catenin signaling mediates oval cell response in rodents.** *Hepatology* 2008, **47:**288-295.
50. Yang W, Yan HX, Chen L, Liu Q, He YQ, Yu LX, Zhang SH, Huang DD, Tang L, Kong XN, *et al.*: **Wnt/beta-catenin signaling contributes to activation of normal and tumorigenic liver progenitor cells.** *Cancer Res* 2008, **68:**4287-4295.
51. Lee JS, Thorgeirsson SS: **Functional and genomic implications of global gene expression profiles in cell lines from human hepatocellular cancer.** *Hepatology* 2002, **35:**1134-1143.
52. Armengol C, Cairo S, Fabre M, Buendia MA: **Wnt signaling and hepatocarcinogenesis: The hepatoblastoma model.** *Int J Biochem Cell Biol* 2009 in press.
53. Kalluri R, Weinberg RA: **The basics of epithelial-mesenchymal transition.** *J Clin Invest* 2009, **119:**1420-1428.
54. Zeng G, Awan F, Otruba W, Muller P, Apte U, Tan X, Gandhi C, Demetris AJ, Monga SP: **Wnt'er in liver: expression of Wnt and frizzled genes in mouse.** *Hepatology* 2007, **45:**195-204.
55. Merle P, Kim M, Herrmann M, Gupte A, Lefrancois L, Califano S, Trepo C, Tanaka S, Vitvitski L, de la Monte S, Wands JR: **Oncogenic role of the frizzled-7/beta-catenin pathway in hepatocellular carcinoma.** *J Hepatol* 2005, **43:**854-862.
56. Kim M, Lee HC, Tsedensodnom O, Hartley R, Lim YS, Yu E, Merle P, Wands JR: **Functional interaction between Wnt3 and Frizzled-7 leads to activation of the Wnt/beta-catenin signaling pathway in hepatocellular carcinoma cells.** *J Hepatol* 2008, **48:**780-791.
57. Bengochea A, de Souza MM, Lefrancois L, Le Roux E, Galy O, Chemin I, Kim M, Wands JR, Trepo C, Hainaut P, *et al.*: **Common dysregulation of Wnt/Frizzled receptor elements in human hepatocellular carcinoma.** *Br J Cancer* 2008, **99:**143-150.
58. Yoshikawa H, Matsubara K, Zhou X, Okamura S, Kubo T, Murase Y, Shikauchi Y, Esteller M, Herman JG, Wei Wang X, Harris CC: **WNT10B functional dualism: beta-catenin/Tcf-dependent growth promotion or independent suppression with deregulated expression in cancer.** *Mol Biol Cell* 2007, **18:**4292-4303.
59. Liu XH, Pan MH, Lu ZF, Wu B, Rao Q, Zhou ZY, Zhou XJ: **Expression of Wnt-5a and its clinicopathological significance in hepatocellular carcinoma.** *Dig Liver Dis* 2008, **40:**560-567.
60. Liu X, Wang L, Zhang S, Lin J, Feitelson MA, Gao H, Zhu M: **Mutations in the C-terminus of the X protein of hepatitis B virus regulate Wnt-5a expression in hepatoma Huh7 cells: cDNA microarray and proteomic analyses.** *Carcinogenesis* 2008, **29:**1207-1214.
61. Wei W, Chua MS, Grepper S, So S: **Small molecule antagonists of Tcf4/beta-catenin complex inhibit the growth of HCC cells in vitro and in vivo.** *Int J Cancer* 2009 in press.
62. Reya T, Clevers H: **Wnt signalling in stem cells and cancer.** *Nature* 2005, **434:**843-850.
63. Chiba T, Kita K, Zheng YW, Yokosuka O, Saisho H, Iwama A, Nakauchi H, Taniguchi H: **Side population purified from hepatocellular carcinoma cells harbors cancer stem cell-like properties.** *Hepatology* 2006, **44:**240-251.
64. Roarty K, Baxley SE, Crowley MR, Frost AR, Serra R: **Loss of TGF-beta or Wnt5a results in an increase in Wnt/beta-catenin activity and redirects mammary tumour phenotype.** *Breast Cancer Res* 2009, **11:**R19.
65. Topol L, Jiang X, Choi H, Garrett-Beal L, Carolan PJ, Yang Y: **Wnt-5a inhibits the canonical Wnt pathway by promoting GSK-3-independent beta-catenin degradation.** *J Cell Biol* 2003, **162:**899-908.
66. Shimizu H, Julius MA, Giarre M, Zheng Z, Brown AM, Kitajewski J: **Transformation by Wnt family proteins correlates with regulation of beta-catenin.** *Cell Growth Differ* 1997, **8:**1349-1358.
67. Taki M, Kamata N, Yokoyama K, Fujimoto R, Tsutsumi S, Nagayama M: **Down-regulation of Wnt-4 and up-regulation of Wnt-5a expression by epithelial-mesenchymal transition in human squamous carcinoma cells.** *Cancer Sci* 2003, **94:**593-597.
68. Dissanayake SK, Wade M, Johnson CE, O'Connell MP, Leotlela PD, French AD, Shah KV, Hewitt KJ, Rosenthal DT, Indig FE, *et al.*: **The Wnt5A/protein kinase C pathway mediates motility in melanoma cells via the inhibition of metastasis suppressors and initiation of an epithelial to mesenchymal transition.** *J Biol Chem* 2007, **282:**17259-17271.
69. Ripka S, Konig A, Buchholz M, Wagner M, Sipos B, Kloppel G, Downward J, Gress T, Michl P: **WNT5A--target of CUTL1 and potent modulator of tumor cell migration and invasion in pancreatic cancer.** *Carcinogenesis* 2007, **28:**1178-1187.
70. Yamashita T, Ji J, Budhu A, Forgues M, Yang W, Wang HY, Jia H, Ye Q, Qin LX, Wauthier E, *et al.*: **EpCAM-positive hepatocellular carcinoma cells are tumor-initiating cells with stem/progenitor cell features.** *Gastroenterology* 2009, **136:**1012-1024.
71. Benhamouche S, Decaens T, Godard C, Chambrey R, Rickman DS, Moinard C, Vasseur-Cognet M, Kuo CJ, Kahn A, Perret C, Colnot S: **Apc tumor suppressor gene is the "zonation-keeper" of mouse liver.** *Dev Cell* 2006, **10:**759-770.
72. Burke ZD, Reed KR, Phesse TJ, Sansom OJ, Clarke AR, Tosh D: **Liver zonation occurs through a beta-catenin-dependent, c-Myc-independent mechanism.** *Gastroenterology* 2009, **136:**2316-2324. e2311-2313
73. Chien AJ, Moore EC, Lonsdorf AS, Kulikauskas RM, Rothberg BG, Berger AJ, Major MB, Hwang ST, Rimm DL, Moon RT: **Activated Wnt/beta-catenin signaling in melanoma is associated with decreased proliferation in patient tumors and a murine melanoma model.** *Proc Natl Acad Sci USA* 2009, **106:**1193-1198.

74. Riou P, Saffroy R, Chenailler C, Franc B, Gentile C, Rubinstein E, Resink T, Debuire B, Piatier-Tonneau D, Lemoine A: **Expression of T-cadherin in tumor cells influences invasive potential of human hepatocellular carcinoma.** *FASEB J* 2006, **20:**2291-2301.

Reprogramming of replicative senescence in hepatocellular carcinoma-derived cells

Nuri Ozturk*, Esra Erdal*†, Mine Mumcuoglu*, Kamil C. Akcali*, Ozden Yalcin*‡, Serif Senturk*, Ayca Arslan-Ergul*, Bala Gur*, Isik Yulug*, Rengul Cetin-Atalay*, Cengiz Yakicier*, Tamer Yagci*, Mesut Tez§, and Mehmet Ozturk*¶‖

*Department of Molecular Biology and Genetics, Bilkent University, Bilkent, Ankara 06800, Turkey; and §Department of 5th Surgery, Numune Training and Research Hospital, Sihhiye, Ankara 06100, Turkey

Communicated by Aziz Sancar, University of North Carolina, Chapel Hill, NC, December 18, 2005 (received for review October 10, 2005)

Tumor cells have the capacity to proliferate indefinitely that is qualified as replicative immortality. This ability contrasts with the intrinsic control of the number of cell divisions in human somatic tissues by a mechanism called replicative senescence. Replicative immortality is acquired by inactivation of p53 and $p16^{INK4a}$ genes and reactivation of hTERT gene expression. It is unknown whether the cancer cell replicative immortality is reversible. Here, we show the spontaneous induction of replicative senescence in p53-and $p16^{INK4a}$-deficient hepatocellular carcinoma cells. This phenomenon is characterized with hTERT repression, telomere shortening, senescence arrest, and tumor suppression. SIP1 gene (*ZFHX1B*) is partly responsible for replicative senescence, because short hairpin RNA-mediated SIP1 inactivation released hTERT repression and rescued clonal hepatocellular carcinoma cells from senescence arrest.

immortality | liver cancer | SIP1 | telomerase | p53

Tumor cells are clonal (1), and tumorigenesis usually requires three to six independent mutations in the progeny of precancerous cells (2). For this to occur, preneoplastic somatic cells would need to breach the replicative senescence barriers. Replicative senescence is a telomere-dependent process that sets a limit to the successive rounds of cell division in human somatic cells (3). Progressive telomere shortening is observed in almost all dividing normal cells. This phenomenon is linked to the lack of efficient *hTERT* expression that is observed in most human somatic cells (3). Replicative senescence (permanent growth arrest also called M_1 stage) is believed to be initiated by a DNA damage-type signal generated by critically shortened telomeres, or by the loss of telomere integrity, leading to the activation of cell cycle checkpoint pathways involving p53, $p16^{INK4a}$, and/or retinoblastoma (pRb) proteins (4, 5). In the absence of functional p53 and $p16^{INK4a}$/pRb pathway responses, telomeres continue to shorten resulting in crisis (also called M2 stage). Cells that bypass the M_2 stage by reactivating *hTERT* expression gain the ability for indefinite cell proliferation, also called immortality (3, 4, 6). There is accumulating evidence that cancer cells undergo a similar process during carcinogenesis to acquire immortality. Telomerase activity associated with *hTERT* reexpression is observed in ≈80% of human tumors (7), and senescence controlling *p53* and $p16^{INK4A}$ genes are commonly inactivated in the majority of human cancers (8). Moreover, experimental transformation of normal human cells to tumor cells requires hTERT-mediated immortalization, as well as inactivation of *p53* and *pRb* genes (9).

Aberrant expression of hTERT, together with the loss of p53 and $p16^{INK4a}$/pRb control mechanisms, suggests that the replicative immortality is a permanent and irreversible characteristic of cancer cells. Although some cancer cells may react to extrinsic factors by a senescence-like stress response, this response is immediate, telomere-independent, and cannot be qualified as replicative senescence (10). Experimental inactivation of telomerase activity in cancer cells mostly results in cell death (11), whereas ectopic expression of p53, $p16^{INK4a}$, or pRb provokes an immediate senescence-like growth arrest or cell death (10). Thus, to date there is no experimental evidence for spontaneous reprogramming of replicative senescence in immortalized cancer cells. Using hepatocellular carcinoma (HCC)-derived Huh7 cells as a model system, here we show that cancer cells with replicative immortality are able to spontaneously generate progeny with replicative senescence. Thus, we provide preliminary evidence for the reversibility of cancer cell immortality. The replicative senescence of cancer cells shares many features with normal cell replicative senescence such as repression of *hTERT* expression, telomere shortening, and permanent growth arrest with morphological hallmarks of senescence. However, the *p53* gene is mutated, whereas $p16^{INK4a}$ promoter is hypermethylated in these cells. Thus, we show that fully malignant and tumorigenic HCC cells that display aberrant hTERT expression and lack functional *p53* and $p16^{INK4a}$ genes are able to revert from replicative immortality to replicative senescence by an intrinsic mechanism. Furthermore, we demonstrate that the *SIP1* gene, encoding a zinc-finger homeodomain transcription factor protein involved in TGF-β signaling (12, 13) and *hTERT* regulation (14), serves as a molecular switch between replicative immortality and replicative senescence fates in HCC cells.

Results

When analyzing clones from established cancer cell lines, we observed that some clones change morphology and cease proliferation at late passages with features reminiscent of cellular senescence (data not shown). We reasoned that this could be an indication for generation of progeny programmed for replicative senescence. We surveyed a panel of HCC and breast carcinoma cell lines and hTERT-immortalized human mammary epithelial cells (hTERT-HME). Plated at low clonogenic density, cells were maintained in culture until they performed 6–10 population doublings (PD), and tested for senescence-associated β-galactosidase (SABG) activity (15). Different cancer cell lines generated progeny with greatly contrasting SABG staining patterns. The first group, represented here by HCC-derived Huh7 and breast cancer-derived T-47D and BT-474 cell lines, generated heterogeneously staining colonies. Cells of some colonies were mostly positive for SABG, but others displayed significantly diminished or complete lack of staining (Fig. 1*A*). The second group, represented by HCC-derived Hep3B and Mahlavu, and hTERT-HME generated only SABG-negative colonies (Fig. 1*B*). Manual counting of randomly selected colonies demonstrated that mean SABG-labeling indexes for Huh7,

Conflict of interest statement: No conflicts declared.

Abbreviations: HCC, hepatocellular carcinoma; PD, population doubling; SABG, senescence-associated β-galactosidase; shRNA, short hairpin RNA.

†Present address: Department of Medical Biology and Genetics, Faculty of Medicine, Dokuz Eylul University, 35210 Izmir, Turkey.

‡Present address: Swiss Institute for Experimental Cancer Research, Ch. des Boveresses 155, CH-1066 Epalinges, Lausanne, Switzerland.

¶To whom correspondence should be addressed. E-mail: ozturk@fen.bilkent.edu.tr.

www.pnas.org/cgi/doi/10.1073/pnas.0510877103

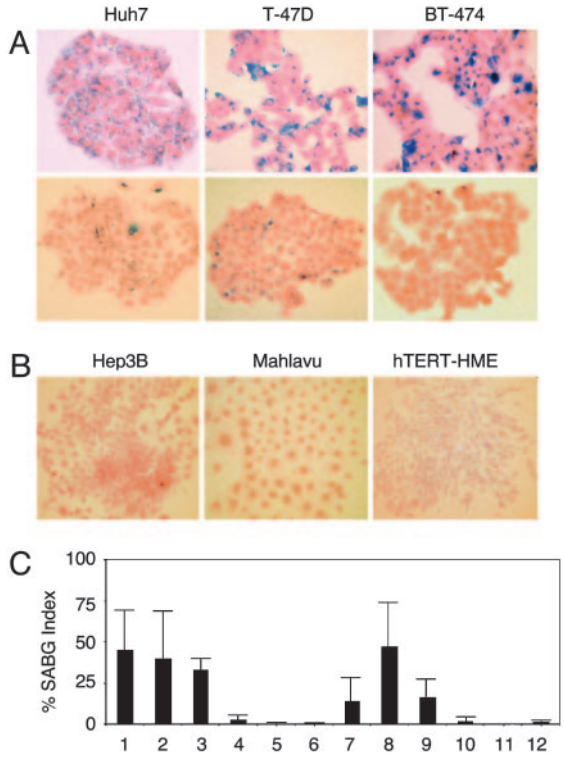

Fig. 1. Established human cancer cell lines generate senescence-associated β-galactosidase (SABG)-expressing progeny. (*A*) Representative pictures of HCC (Huh7) and breast cancer (T-47D and BT-474) cell lines that generate both SABG-positive (*Upper*) and SABG-negative (*Lower*) colonies. (*B*) Representative pictures of HCC (Hep3B and Mahlavu) and telomerase-immortalized mammary epithelial (hTERT-HME) cell lines that generate only SABG-negative colonies. Cells were plated at clonogenic density to generate colonies with 6–10 population doublings, and stained for SABG activity (blue), followed by eosin counterstaining (red). (*C*) Quantification of SABG-positive cells in colonies. Randomly selected colonies ($n \geq 10$) obtained from parental (lanes 1–6) cell lines and expanded clones (lanes 7–12) were counted to calculate the average % SABG positive cells per colony (% SABG index). Lanes 1–6 designate Huh7, T-47D, BT-474, Hep3B, Mahlavu, and hTERT-HME, respectively. Lanes 7–9 are Huh7-derived C1, C3, and C11 clones, and lanes 10–12 are Hep3B-derived 3B-C6, 3B-C11, and 3B-C13 clones. Error bars indicate SD.

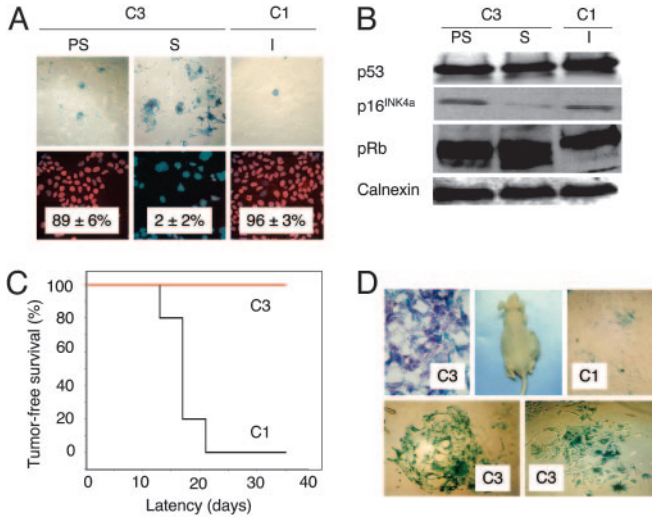

Fig. 2. p53-and p16^{INK4a}-deficient Huh7 cells generate progeny that undergo *in vitro* and *in vivo* replicative senescence resulting in loss of tumorigenicity. (*A*) Huh7-derived clones C3 and C1 were tested for replicative senescence arrest by SABG and BrdUrd staining at different passages. Presenescent C3 and immortal C1 cells display low SABG staining (*Upper*) and high BrdUrd incorporation (*Lower*), whereas senescent C3 cells are fully positive for SABG (*Upper*) and fail to incorporate BrdUrd into DNA after mitogenic stimuli (*Lower*). (*B*) p53 and p16^{INK4a} protein levels show no increase in senescent C3 cells, compared to presenescent C3 and immortal C1 cells, but senescent C3 cells display partial hypophosphorylation of pRb. Calnexin was used as a loading control. Proteins were tested by Western blotting. PS, presenescent (PD 57); S, senescent (PD 80); I, immortal (PD 179). (*C*) C1 cells (black line) were fully tumorigenic, but C3 cells (red line) were not in *nude* mice. (*D*) C1 tumors displayed low SABG staining (*Upper Right*), whereas implanted C3 cells remaining at the injection site are fully positive for SABG *in situ* (*Upper Left*), as well as after short-term *in vitro* selection (*Lower*). Animals were injected with presenescent C3 (PD 59) and immortal C1 (PD 119) cells, and tumors and nontumorigenic cell samples were collected at day 35 and analyzed.

T-47D and BT-474 progenies were 45 ± 23%, 40 ± 29%, and 33 ± 7%, respectively (Fig. 1*C*, lanes 1–3). In contrast, Hep3B, Mahlavu, and hTERT-HME progenies displayed <3 ± 3% mean SABG-labeling indexes (Fig. 1*C*, lanes 4–6). Clones from representative cell lines were expanded and subjected to the same analysis. SABG-staining patterns of all clones tested were closely similar to the patterns of their respective parental cell lines. For example, mean SABG staining indexes of Huh7-derived clones were 14 ± 15%, 47 ± 27%, and 17 ± 11% (Fig. 1*C*, lanes 7–9), whereas Hep3B-derived clones generated <2 ± 3% SABG-positive progenies (Fig. 1*C*, lanes 10–12). We speculated that the first group of cell lines comprised progenies in different stages of replicative senescence process at the time of analysis, whereas the second group of cell lines were composed mostly of immortal cells. The results obtained with the first group were unexpected. These cell lines have been established >20 years ago (16–18) and expanded in culture over many years, with PD well beyond the known senescence barriers for normal human cells (3), but they were still capable of generating presumably senescent progeny.

The study of a potentially active replicative senescence program in the progeny of immortal cancer cell lines requires the long-term follow up of single cell-derived clones. To this end, we chose to focus our investigations on Huh7 cell line. We expanded different Huh7-derived clones in long-term culture and examined their potential to undergo replicative senescence. Some clones performed >100 PD in culture with stable proliferation rates and heterogeneous SABG staining, whereas others sustained a limited number of PD, then entered a growth arrest phase with full SABG staining patterns. For example, C3 clone performed only 80 PD, whereas C1 clone replicated >150 PD. Permanently arrested C3 cells (PD 80) displayed enlarged size, flattened shape, and fully positive SABG staining, whereas early passage C3 (PD 57) and C1 (PD 179) cells displayed normal morphology with heterogeneous SABG staining (Fig. 2*A Upper*). Normal human cells at replicative senescence (M_1) are refractory to mitotic stimulation and display <5% BrdUrd index (19). Growth-arrested C3 cells displayed very low BrdUrd staining (2 ± 2%), in contrast to early passage C3 and late passage C1 cells, which exhibited 89 ± 6%, and 96 ± 3% BrdUrd indexes, respectively (Fig. 2*A Lower*). Senescent C3 cells remained growth arrested, but alive when maintained in culture for at least 3 months, with no emergence of immortal clones (data not shown).

Biological mechanisms of replicative senescence observed here are of particular interest, because senescence-regulatory *p53* is inactivated (20–22) and *p16^{INK4a}* promoter is hypermethylated (23) in Huh7 cells. Accordingly, there was no change in p53 levels, whereas the low level p16^{INK4a} expression did not increase, but decreased in senescent C3 (PD 80) cells, when compared to presenescent C3 (PD 57) or immortal C1 (PD 179) cells. Retinoblastoma protein (pRb) displayed partial hypophos-

phorylation in senescent C3 cells, apparently in a p53- and $p16^{INK4a}$-independent manner (Fig. 2*B*). Cyclin E and A levels were also decreased, but $p21^{cip1}$ levels were elevated in both presenescent and senescent C3 cells (Fig. 5*A*, which is published as supporting information on the PNAS web site). Cyclin D1, CDK4, and CDK2 protein levels (Fig. 5*A*) and $p14^{ARF}$ transcript levels (Fig. 5*B*) did not change.

Cancer cell senescence that we characterized here shared many features with normal cell replicative senescence (3), except that it was not accompanied with wild-type *p53* or *p16*^{INK4a} induction. However, *in vivo* relevance of the replicative senescence observed in cell culture is debated (6). Therefore, we compared *in vivo* replicative potentials of C3 (PD 59) and C1 (PD 119) cells in CD-1 *nude* mice. C3 cells did not form visible tumors, whereas C1 cells were fully tumorigenic in the same set of animals (Fig. 2*C*), like parental Huh7 cells (data not shown; ref. 24). C1 tumors collected at day 35 displayed scattered but low-rate SABG-positive staining, but remnant C3 cell masses collected from their injection sites were fully SABG-positive (Fig. 2*D Upper*). For confirmation, these remnants were removed from two different animals, passaged twice in cell culture for selection, and examined. Nearly all cells displayed senescence features including enlarged size, flattened shape, and highly positive SABG staining (Fig. 2*D Lower*). We concluded that loss of C3 tumorigenicity was due to replicative senescence *in vivo*.

Replicative senescence, also called telomere-dependent senescence is associated with progressive telomere shortening due to inefficient telomerase activity (3). When compared to parental Huh7 cells, presenescent C3 cells at PD 57 had telomeres that have already been shortened to ≈7 kbp from ≈12 kbp. These cells eroded their telomeres to <5 kbp at the onset of senescence. In contrast, immortal C1 clone (PD 179) telomeres did not shorten (Fig. 3*A*). These observations showed a perfect correlation with telomerase activity and *hTERT* expression. Immortal C1 cells displayed robust telomerase activity, whereas both presenescent and senescent C3 cells had no detectable telomerase activity (Fig. 3*B*). Accordingly, the expression of *hTERT* gene was high in C1, but barely detectable in C3 cells (Fig. 3*C*). Thus, senescence observed with C3 cells was characterized with the loss of *hTERT* expression and telomerase activity, associated with telomere shortening.

Mechanisms of *hTERT* expression are presently unclear, but several genes including *SIP1*, *hSIR2*, *c-myc*, *Mad1*, *Menin*, *Rak*, and *Brit1* have been implicated (14, 25). Therefore, we analyzed their expression in C1 and C3 clones. All tested genes, except *SIP1*, were expressed at similar levels in both C1 and C3 clones, independent of *hTERT* expression (Fig. 6, which is published as supporting information on the PNAS web site). SIP1 transcripts were undetectable in C1 cells, but elevated in C3 cells, moderately in presenescent, but strongly in senescent stages (Fig. 3*C*). We verified these findings with another Huh7-derived clone (G12) that displayed replicative senescence resulting in permanent cell proliferation arrest. Like C3, presenescent G12 cells that displayed low SABG staining with high BrdUrd index (98 ± 1%), became fully positive for SABG, and nearly negative for BrdUrd (3 ± 2%) at the onset of senescence (Fig. 7, which is published as supporting information on the PNAS web site). Presenescent G12 cells displayed only a weak *hTERT* repression associated with a slight increase in *SIP1* expression, whereas SIP1 was strongly elevated in hTERT-negative senescent cells (Fig. 3*D*). Thus, there was a close correlation between *SIP1* expression and *hTERT* repression in all Huh7 clones tested. The analysis of *SIP1* and *hTERT* expression in primary HCCs and their corresponding nontumor liver tissues confirmed this relationship. SIP1 transcript levels were high, but *hTERT* expression was low in nontumor liver tissues, whereas respective HCC tumors displayed diminished *SIP1* expression associated with up-regulated *hTERT* expression (Fig. 3*E*).

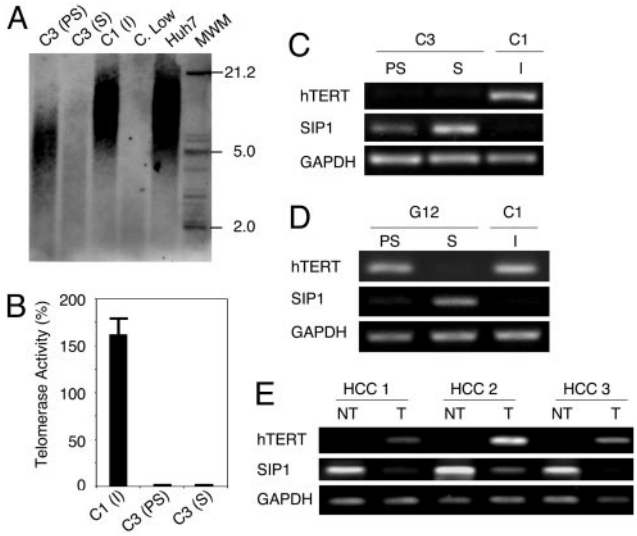

Fig. 3. C3 clonal cells undergo telomere-dependent replicative senescence associated with SIP1 expression and hTERT repression. SIP1 expression is lost, whereas hTERT is induced in primary HCC tumors. (*A*) Genomic DNAs from parental Huh7 and immortal C1 cells display long telomeres, whereas C3 telomeres are progressively shortened in presenescent and senescent stages, respectively. Equal amounts of genomic DNAs were blotted with a telomere repeat probe. C. Low, short telomere control DNA. (*B*) Presenescent and senescent C3 cells have lost telomerase activity, as measured by TRAP assay. Telomerase activity was shown as % value of test samples (± SD) compared to ''high positive'' control sample. (*C*) hTERT expression as tested by RT-PCR was high in immortal C1, but decreased to weakly detectable levels in C3 cells. Inversely, SIP1 expression tested by RT-PCR was undetectable in C1 cells, but showed a progressive increase in presenescent and senescent C3 cells. (*D*) Inverse relationship between SIP1 and hTERT expression was confirmed with another senescence-programmed Huh7 clone named G12 (for SABG and BrdUrd assays, see Fig. 7). hTERT expression in G12 showed a slight decrease in presenescent stage, followed by a loss at the onset of senescence. Inversely, the expression of SIP1 gene was weakly positive in presenescent G12, but highly positive in senescent G12 cells. C1 was used as control. PS, presenescent; S, senescent; I, immortal. (*E*) Negative correlation between hTERT and SIP1 expression in primary tumors (T) and nontumor liver tissues (NT).

The *SIP1* gene (Zinc finger homeobox 1B; *ZFHX1B*) encodes a transcriptional repressor protein that interacts with SMAD proteins of the TGF-β signaling pathway and CtBP corepressor (12, 13). This gene has recently been implicated in TGF-β-dependent regulation of *hTERT* expression in breast cancer cells (14). Our observations implicated *SIP1* gene as a candidate regulator of replicative senescence in HCC cells. To investigate whether *SIP1* expression constitutes a protective barrier against hTERT expression and senescence bypass, we constructed SIP1 short hairpin RNA (shRNA)-expressing plasmids, based on a reported effective SIP1 siRNA sequence (14). SIP1 shRNA was expressed by using either G-418-resistance plasmid pSuper.retro.neo+GFP or puromycin-resistance plasmid pSUPER.puro (see *shRNA* in *Methods*). Presenescent C3 cells at PD 75 were used for transfections, 3–4 weeks before expected senescence arrest stage. pSuper.retro.neo+GFP-based SIP1 shRNA suppressed the accumulation in SIP1 when expressed transiently (Fig. 4*A*, day 5). This resulted in a weak increase in *hTERT* expression. Transfected cells were maintained in culture in the presence of 500 μg/ml G-418 and observed for 30 days. At this period, C3 cells transfected with a control plasmid reached senescence-arrested stage with further up-regulation of *SIP1* expression (Fig. 4*A*, day 30) and resistance to BrdUrd incorporation after mitogenic stimuli (BrdUrd index = 3 ± 1%; Fig. 4*B Upper Left*). In sharp contrast, SIP1 shRNA-transfected cells lost

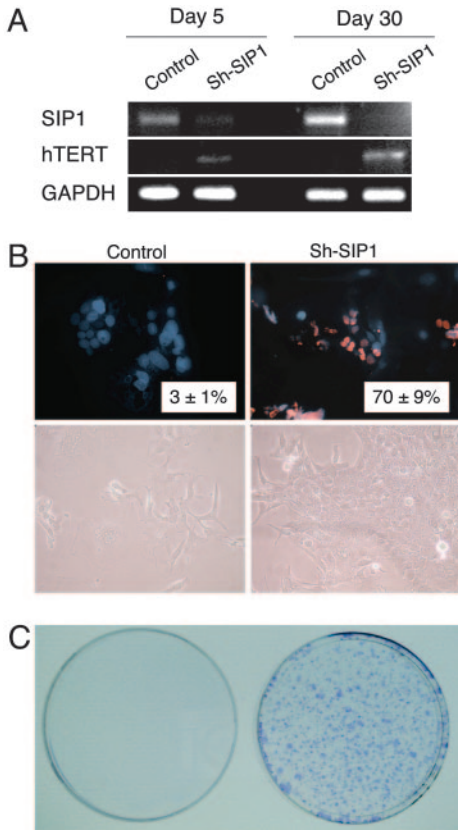

Fig. 4. ShRNA-mediated down-regulation of endogeneous SIP1 transcripts releases hTERT repression and rescues C3 cells from senescence arrest. (*A*) At day 5 after transfection, SIP1 shRNA-transfected cells (Sh-SIP1) show decreased expression of SIP1 and weak up-regulation of hTERT expression. At day 30, the expression of SIP1 is lost completely, and hTERT expression is stronger. (*B*) Cells transfected with empty vector (Control) are senescence-arrested as evidenced by resistance to BrdUrd incorporation (*Upper Left*) and morphological changes (*Lower Left*), but cells transfected with SIP1 shRNA vector (Sh-SIP1) escaped senescence arrest as indicated by high BrdUrd index (*Upper Right*) and proliferating cell clusters (*Lower Right*). (*C*) Colony-forming assay shows that C3 cells formed large number of colonies following puromycin selection after transfection with a puromycin-resistant SIP1-shRNA-expressing plasmid (*Right*), whereas cells transfected with empty vector did not survive (*Left*). SIP1 shRNA was expressed by using either G-418-resistance plasmid pSuper.retro.neo+GFP (*A* and *B*) or puromycin-resistance plasmid pSUPER. puro (*C*). Presenescent C3 cells at PD 75 were transfected with either SIP1 shRNA-expressing or empty plasmid vectors, maintained in culture in the presence of appropriate selection media and tested at days 5 (*A*) and 30 (*A–C*).

SIP1 expression and up-regulated *hTERT* transcripts (Fig. 4*A*, day 30). Furthermore, *SIP1*-inactivated cells escaped senescence, as evidenced with 70 ± 9% BrdUrd index (Fig. 4*B Upper Right*). Morphologically, SIP1 shRNA-transfected cells formed proliferating clusters, whereas cells transfected with control plasmid displayed hallmarks of senescence such as scattering, enlargement, and multiple nuclei (Fig. 4*B Lower*). Twelve independent clones were selected from SIP1 shRNA-transfected C3 cells. All but one of these clones have performed so far >15 PD beyond the expected senescence barrier (data not shown). As an additional confirmatory assay, C3 cells were transfected with the puromycin-selectable *pSUPER.puro-based* SIP1 shRNA vector and subjected to puromycin selection. SIP1 shRNA-transfected cells survived and formed large number of colonies after 30 days of puromycin selection. In contrast, no surviving colony was obtained from cells transfected with the control plasmid, as expected (Fig. 4*C*).

Discussion

Our observations provide experimental evidence for the generation of senescence-arrested clones from immortal HCC and breast cancer cell lines. Detailed analysis of clones from HCC-derived Huh7 cell line further indicates that what we observe is a replicative senescence, but not a stress-induced premature senescence-like arrest. Clonal C3 cells displayed telomerase repression, progressive telomere shortening, and permanent growth arrest after ≈80 PD with senescence-associated morphological changes and positive SABG staining. Similar changes have also been observed with G12, another independently derived clone. Thus, we demonstrate that immortal cancer cells have the intrinsic ability to reprogram the replicative senescence. As expected, this shift in cell fate results in a complete loss of tumorigenicity. The replicative senescence arrest that we identified with clonal C3 cells was not accompanied with the induction of the *p53*, $p16^{INK4a}$, $p14^{ARF}$, or $p21^{Cip1}$ gene. The nonparticipation of *p53* and $p16^{INK4a}$ to the senescence arrest described here was expected, in the light of published observations showing that Huh7 cells express a mutant p53 protein (20–22) and they are deficient in $p16^{INK4a}$ expression (23). Although the levels of $p21^{Cip1}$ protein displayed a slight increase in C3 cells, this was not related to senescence arrest, as early passage proliferating C3 cells also displayed this slight increase (Fig. 5). The early loss of *hTERT* expression in this clone could contribute to early $p21^{Cip1}$ up-regulation, because hTERT is known to down-regulate $p21^{Cip1}$ promoter activity (26). *p53*, $p16^{INK4a}$, $p14^{ARF}$, and $p21^{Cip1}$ form a group of replicative senescence-related cell cycle checkpoint genes. The lack of induction of these genes in senescence-arrested C3 cells clearly indicates that there are additional genes involved in senescence arrest in these tumor-derived cells.

The loss of *hTERT* expression in senescence programmed clones prompted us to analyze the expression of genes that have been implicated in *hTERT* regulation. Among seven candidate genes studied, only one, the *SIP1* gene, displayed a differential expression between immortal and senescence-programmed clones. This gene has been identified as a mediator of TGF-β-regulated repression of *hTERT* expression in a breast cancer cell line, although it was not effective in an osteosarcoma cell line (14). In our studies, SIP1 was not expressed in immortal hTERT-expressing C1 clone, but expressed in senescence-programmed hTERT-repressed C3 and G12 clones (Fig. 3 *B* and *C*). Furthermore, experimental depletion of SIP1 transcripts resulted in hTERT up-regulation in C3 clonal cells (Fig. 4*A*). This effect has been confirmed by using SKHep1, another HCC cell line (data not shown). Thus, we demonstrate that the *SIP1* gene acts as an hTERT repressor in HCC cells. More importantly, we also showed the bypass of senescence arrest after functional inactivation of SIP expression by shRNA in senescence-programmed C3 clonal cells. In contrast to C3 cells transfected with a control plasmid, SIP1 shRNA-treated cells displayed continued proliferation beyond PD ≈80 as evidenced by 70% BrdUrd incorporation index, and formation of large number of colonies. Selected shRNA-transfected clones from these experiments have already performed >15 PD beyond the senescence barrier. Thus, our findings indicate that the functional inactivation of *SIP1* in senescence-programmed cancer cells is sufficient to bypass senescent arrest.

SIP1 is a zinc finger and homeodomain containing transcription factor that exerts a repressive activity by binding to CACCT sequences in regulatory elements of target genes (12, 27). The *SIP1* gene is expressed at high levels in almost all human somatic tissues tested, including liver (28). Therefore, we also performed comparative analysis of hTERT and *SIP1* expression in nontumor liver and primary HCC tissues. *SIP1*

was strongly positive in nontumor liver samples, but its expression was significantly decreased in corresponding HCC samples. Inversely, *hTERT* expression was negative or low in nontumor liver samples, but highly positive in HCC tumors (Fig. 3*E*). We also detected complete loss of *SIP1* expression in 5 of 14 (36%) of HCC cell lines (data not shown). Taken together with *in vitro* studies, these observations strongly suggest that *SIP1* acts as a tumor suppressor gene in HCC. Although SIP1, as a repressor of *E-cadherin* promoter, has been suggested to be a promoter of invasion in malignant epithelial tumors (29), a tumor suppressive activity by the repression of *hTERT* and inhibition of senescence arrest is not precluded.

Hepatocellular carcinoma is one of the most common cancers worldwide. Liver cirrhosis is the major etiology of this tumor with limited therapeutic options (30, 31). Telomere shortening and senescence play a major role in liver cirrhosis, from which the neoplastic HCC cells emerge with high rates of telomerase reactivation (32). Furthermore, *p53* and $p16^{INK4a}$ are the most frequently inactivated genes in these tumors. This fact enhances the importance of our findings for potential therapeutic applications of replicative senescence programming in HCC.

Methods

Tissues, Cells, and Clones. Snap-frozen HCC and nontumor liver tissues were used. HCC and breast cancer cell lines T-47D (ATCC) and BT-474 (ATCC) were cultivated as described (33). hTERT-HME cells (Clontech) were cultivated in DMEM/Ham's F-12 (Biochrom) containing insulin (3.5 μg/ml), EGF (0.1 ng/ml), hydrocortison (0.5 μg/ml), and 10% FBS (Biochrom). Huh7- and Hep3B-derived isogenic clones were obtained by either G-418 selection after transfection with neomycin-resistance pcDNA3.1 (Invitrogen) or pEGFP-N2 (Clontech) plasmids, or by low-density cloning. Huh7-derived isogenic clones C1 and C3 were obtained with pCDNA3.1, and G12 with pEGFP-N2. Huh7-derived C11, and Hep3B-derived 3B-C6, 3B-C11 and 3B-C13 were obtained by low-density cloning. Cells transfected with calcium phosphate/DNA-precipitation method were cultivated in the presence of geneticin G-418 sulfate (500 μg/ml; GIBCO), and isolated single cell-derived colonies were picked up by using cloning cylinders and expanded in the presence of 200 μg/ml geneticin G-418 sulfate. For low-density cloning, cells were plated at 30 cells per cm^2 and single-cell derived colonies were expanded. Initial cell stocks were prepared when total number of cells became 1–3 $\times$ 10^7, and the number of accumulated population doubling (PD) at this stage was estimated to be 24, assuming that the progeny of the initial colony-forming cells performed at least 24 successive cell divisions until that step. Subsequent passages were performed every 4–7 days, and the number of additional PD was determined by using a described protocol (34).

Low-Density Clonogenic Assay. Cells (30–50 per cm^2) were plated in six-well plates and grown 1–3 weeks to obtain isolated colonies formed with 100–1,000 cells. The medium was changed every 4 days, and colonies were subjected to SABG staining (see below).

***In Vivo* Studies.** Cells were injected s.c. into CD-1 *nude* mice (Charles River Breeding Laboratory). Tumors and nontumorigenic cells at the injection sites were collected at day 35 and analyzed directly or after *in vitro* culture by SABG assay (see below). These experiments have been approved by the Bilkent University Animal Ethics Committee.

SABG Assay. SABG activity was detected by using a described protocol (15). After DAPI or eosin counterstaining, SABG-positive and negative cells were identified and counted.

BrdUrd Incorporation Assay. Subconfluent cells were labeled with BrdUrd for 24 h in freshly added culture medium and tested as described (33), using anti-BrdUrd antibody (Dako) followed by tetramethylrhodamine B isothiocyanate-labeled secondary antibody (Sigma). DAPI (Sigma) was used for counterstaining.

Immunoblotting. Antibodies against cyclin D1, CDK4, CDK2, $p21^{Cip1}$, pRb (all from Santa Cruz Biotechnology), cyclin E (Transduction), cyclin A (Abcam), $p16^{INK4a}$ (Abcam), p53 (clone 6B10; ref. 35), and calnexin (Sigma) were used for immunoblotting as described (33).

RT-PCR. RT-PCR expression analysis was performed as described (33), using primers listed in Table 1, which is published as supporting information on the PNAS web site.

TRAP and Telomere Length Assays. Telomerase activity and telomere length assays were performed by using Telo*TAGGG* Telomerase PCR $ELISA^{PLUS}$ and Telo*TAGGG* Telomere Length Assay (Roche Diagnostics), following kit instructions.

shRNA. SIP1-directed shRNA was designed according to a previously described effective siRNA sequence (14) using the pSUPER RNAi system instructions (Oligoengine) and cloned into pSuper.retro.neo+GFP and pSUPER.puro (Oligoengine), respectively. SIP1 shRNA-encoding sequence was inserted by using 5′-GATCCCCCTGCCATCTGATCCGCTCTTTCAAGAGAAGAGCGGATCAGATGGCAGTTTTTA-3′ (sense) and 5′-AGCTTAAAAACTGCCATCTGATCCGCTCTTCTCTTGAAAG AGCGGATCAG ATGGCAGGGG-3′ (antisense) oligonucleotides.

The integrity of the inserted shRNA-coding sequence has been confirmed by nucleic acid sequencing of recombinant plasmids. Clone C3 cells were transfected with calcium phosphate precipitation method, using either pSuper.retro.neo+GFP-based or pSUPER.puro-based SIP1 shRNA expression plasmid, and cells were maintained in the presence of 500 μg/ml geneticin G-418 sulfate and 2 μg/ml puromycin (Sigma), respectively. Empty vectors were used as control. Media changed every 3 days, and cells were tested at days 5 and 30.

We thank E. Galun, G. Hotamisligil, F. Saatcioglu, and A. Sancar for reading the manuscript and helpful suggestions. This work was supported by Grant SBAG-2774/104S045 from the Scientific and Technological Research Council of Turkey (TUBITAK) and funds from Bilkent University and Turkish Academy of Sciences (TUBA).

1. Nowell, P. C. (1976) *Science* **194,** 23–28.
2. Vogelstein, B. & Kinzler, K. W. (1993) *Trends. Genet.* **9,** 138–141.
3. Shay, J. W. & Wright, W. E. (2005) *Carcinogenesis* **26,** 867–874.
4. Campisi, J. (2005) *Cell* **120,** 513–522.
5. Dimri, G. P. (2005) *Cancer Cell* **7,** 505–512.
6. Ben-Porath, I. & Weinberg, R. A. (2004) *J. Clin. Invest.* **113,** 8–13.
7. Shay, J. W. & Bacchetti, S. (1997) *Eur. J. Cancer* **33,** 787–791.
8. Sherr, C. J. & McCormick, F. (2002) *Cancer Cell* **2,** 103–112.
9. Boehm, J. S. & Hahn, W. C. (2005) *Curr. Opin. Genet. Dev.* **15,** 13–17.
10. Roninson, I. B. (2003) *Cancer Res.* **63,** 2705–2715.
11. Shay, J. W. & Roninson, I. B. (2004) *Oncogene* **23,** 2919–2933.
12. Verschueren, K., Remacle, J. E., Collart, C., Kraft, H., Baker, B. S., Tylzanowski, P., Nelles, L., Wuytens, G., Su, M. T., Bodmer, R., *et al.* (1999) *J. Biol. Chem.* **274,** 20489–20498.
13. Postigo, A. A., Depp, J. L., Taylor, J. J. & Kroll, K. L. (2003) *EMBO J.* **22,** 2453–2462.
14. Lin, S. Y. & Elledge, S. J. (2003) *Cell* **113,** 881–889.
15. Dimri, G. P., Lee, X., Basile, G., Acosta, M., Scott, G., Roskelley, C., Medrano, E. E., Linskens, M., Rubelj, I., Pereira-Smith, O., *et al.* (1995) *Proc. Natl. Acad. Sci. USA* **92,** 9363–9367.
16. Lasfargues, E. Y., Coutinho, W. G. & Redfield, E. S. (1978) *J. Natl. Cancer Inst.* **61,** 967–978.

17. Keydar, I., Chen, L., Karby, S., Weiss, F. R., Delarea, J., Radu, M., Chaitcik, S. & Brenner, H. J. (1979) *Eur. J. Cancer* **15,** 659–670.
18. Nakabayashi, H., Taketa, K., Miyano, K., Yamane, T. & Sato, J. (1982) *Cancer Res.* **42,** 3858–3863.
19. Wei, W. & Sedivy, J. M. (1999) *Exp. Cell Res.* **253,** 519–522.
20. Bressac, B., Galvin, K. M., Liang, T. J., Isselbacher, K. J., Wands, J. R. & Ozturk, M. (1990) *Proc. Natl. Acad. Sci. USA* **87,** 1973–1977.
21. Volkmann, M., Hofmann, W. J., Muller, M., Rath, U., Otto, G., Zentgraf, H. & Galle, P. R. (1994) *Oncogene* **9,** 195–204.
22. Kubica, S., Trauwein, C., Niehof, M. & Manns, M. (1997) *Hepatology* **25,** 867–873.
23. Roncalli, M., Bianchi, P., Bruni, B., Laghi, L., Destro, A., Di Gioia, S., Gennari, L., Tommasini, M., Malesci, A. & Coggi, G. (2002) *Hepatology* **36,** 427–432.
24. Kaneko, S., Hallenbeck, P., Kotani, T., Nakabayashi, H., McGarrity, G., Tamaoki, T., Anderson, W. F. & Chiang, Y. L. (1995) *Cancer Res.* **55,** 5283–5287.
25. Wang, J., Xie, L. Y., Allan, S., Beach, D. & Hannon, G. J. (1998) *Genes Dev.* **12,** 1769–1774.
26. Young, J. I., Sedivy, J. M. & Smith, J. R. (2003) *J. Biol. Chem.* **278,** 19904–19908.
27. Remacle, J. E., Kraft, H., Lerchner, W., Wuytens, G., Collart, C., Verschueren, K., Smith, J. C. & Huylebroeck, D. (1999) *EMBO J.* **18,** 5073–5084.
28. Cacheux, V., Dastot-Le Moal, F., Kaariainen, H., Bondurand, N., Rintala, R., Boissier, B., Wilson, M., Mowat, D. & Goossens, M. (2001) *Hum. Mol. Genet.* **10,** 1503–1510.
29. Comijn, J., Berx, G., Vermassen, P., Verschueren, K., van Grunsven, L., Bruyneel, E., Mareel, M., Huylebroeck, D. & van Roy, F. (2001) *Mol. Cell* **7,** 1267–1278.
30. Thorgeirsson, S. S. & Grisham, J. W. (2002) *Nat. Genet.* **31,** 339–346.
31. Bruix, J., Boix, L., Sala, M. & Llovet, J. M. (2004) *Cancer Cell* **5,** 215–219.
32. Satyanarayana, A., Manns, M. P. & Rudolph, K. L. (2004) *Hepatology* **40,** 276–283.
33. Erdal, E., Ozturk, N., Cagatay, T., Eksioglu-Demiralp, E. & Ozturk, M. (2005) *Int. J. Cancer* **115,** 903–910.
34. Masutomi, K., Yu, E. Y., Khurts, S., Ben-Porath, I., Currier, J. L., Metz, G. B., Brooks, M. W., Kaneko, S., Murakami, S., DeCaprio, J. A., *et al.* (2003) *Cell* **114,** 241–253.
35. Yolcu, E., Sayan, B. S., Yagci, T., Cetin-Atalay, R., Soussi, T., Yurdusev, N. & Ozturk, M. (2001) *Oncogene* **15,** 1398–1401.